

- **Evidence that viral antigen alone is not the target for T cell-mediated immunity**
 - Zinkernagel & Doherty, Nature 248:701-702. 1974
 - Zinkernagel & Doherty J. Exp. Med. 141:1427-1436. 1975
- **T cell subsets, antigen-presenting cells, antigen presentation AND antigen cross-presentation**
 - Rock et al. Trends Immunol. 37:724-737. 2016.
 - Blum, J.S. et al. Annual Rev. Immunol. 31:443-73. 2013.
- **Engagement of TCR is not sufficient to activate a T cell: co-stimulatory (and inhibitory) molecules**
 - Linsley, P. S., Clark, E.A. and Ledbetter, J.A. Proc. Natl. Acad. Sci USA 87: 5031-5035. 1990 T cell antigen CD28 mediates adhesion with B cells by interacting with activation antigen B7/BB-1 (cell-cell interaction through surface antigens CD28 and B7)
- **Co-stimulatory vs inhibitory molecules affecting T cell response/function**
 - Linsley, P.S. J. Exp. Med. 182: 289. 1995 (commentary). JEM commentary Distinct roles for CD28 and Cytotoxic T Lymphocyte-associated Molecule-4 Receptors during T Cell Activation?
 - Krummel, M.F. and Allison, J. P. J. Exp. Med. 182: 459. 1995. CD28 and CTLA-4 have opposing effects on the response of T cells to stimulation
- **Blockade therapy for cancer**
 - James P. Allison – Nobel Lecture. <https://www.nobelprize.org/prizes/medicine/2018/allison/lecture>
 - Sharma, P. and Allison, J.P. Immune checkpoint targeting in cancer therapy: toward combination strategies with curative potential. Cell 161: 205. 2015
 - Leach, D.R., Krummer, M.F., and Allison, J.P. Enhancement of antitumor immunity by CTLA-4 blockade. Science 271: 1734. 1996.
 - Hodi, F.S., O'Day, S.J., McDermott, D.F., Weber, R.W., Sosman, J.A., Haanen, J.B., Gonzalez, R., Robert, C., Schadendorf, D., Hassel, J.C., et al. (2010). Improved survival with ipilimumab in patients with metastatic melanoma. N. Engl. J. Med. 363, 711-723
 - Zamora, A.E., Crawford, J.C., Thomas, P.G. Hitting the target: how T cells detect and eliminate tumors. J. Immunol. 200:392. 2018.
- **Constantly-arising tumor “neo-antigens” due to genomic instability of cancer cells**
 - Snyder, A., Makarov, V., Merghoub, T., Yuan, J., Zaretsky, J.M., Desrichard, A., Walsh, L.A., Postow, M.A., Wong, P., Ho, T.S., et al. Genetic basis for clinical response to CTLA-4 blockade in melanoma. N. Engl. J. Med. 371: 2189. 2014.
 - Tran, E., Turcotte, S., Gros, A., Robbins, P.F., Lu, Y-C, Dudley, M., Wunderlich, J.R., Somerville, R.P., Hogan, K., Hinrichs, C., Parkhurst, M.R., Yang, J.C., Rosenberg, S.A. Cancer immunotherapy based on mutation-specific CD4+ T cells in a patient with epithelial cancer. Science 344: 641. 2014
- **PD-1 AND PD-L1 – another “brake” system affecting T cell function**
 - LaFleur, MW et al., Inhibitors of the PD-1 pathway in tumor therapy. J. Immunol. 200: 375. 2018
 - Tasuku Honjo Nobel lecture: <https://www.nobelprize.org/prizes/medicine/2018/honjo/lecture/>
 - Iwai, Y. et al. Involvement of PD-L1 on tumor cells in the escape from host immune system and tumor immunotherapy by PD-L1 blockade. Proc. Natl. Acad. Sci. (USA) 99:12293. 2002
- **PD-1 and PD-L1 use in cancer blockade therapy. The good and the bad.**
 - S. Topalian et al., Safety, activity, and immune correlates of anti-PD-1 antibody in cancer. N. Engl. J. Med 366: 2443. 2012.
 - Miyajima, M. et al. Metabolic shift induced by systemic activation of T cells in PD-1-deficient mice perturbs brain monoamines and emotional behavior Nat. Immunol. 18: 1432. 2017.
- **A modified TCR for tumor antigens (Chimeric antigen receptors = CARs)**
 - Srivastava, S. and Riddell, S.R. Chimeric Antigen Receptor T cell therapy: challenges to bench-to-bedside efficacy. J. Immunol. 200:459. 2018.
 - Eshhar, Z., Waks, T., Gross, G., and Schindler, D.G. Specific activation and targeting of cytotoxic lymphocytes through chimeric single chains consisting of antibody-binding domains and the gamma or zeta subunits of the immunoglobulin and T-cell receptors. Proc. Natl. Acad. Sci USA 90:720. 1993.
 - Maher, J., Brentjens, R. J., Gunset, G., Riviere, and Sadelain, M. Human T-lymphocyte cytotoxicity and proliferation directed by a single chimeric TCR-zeta/CD28 receptor. Nature Biotechnology 20:70. 2002
 - Maude, S.L., Frey, N., Shaw, P.A., Aplenc, R., Barrett, D.M., Bunin, N.J., Chew, A., Gonzalez, V.E., Zheng, Z., Lacey, S.F. et al. Chimeric antigen receptor T cells for sustained remissions in leukemia N. Engl. J. Med. 371: 1507. 2014.
- **Metabolic “checkpoint” for T cell responses to tumors: Formal presentation by MASTERS/PhD students in class**
 - Sukumar, M. Roychoudhuri, R. and Restifo, N.P. Nutrient Competition: a new axis of tumor immunosuppression. Cell 162: 1206. 2015
 - MacIver, NJ and Rathmell, JC Editorial overview: metabolism of T cells: integrating nutrients, signals, and cell fate. Curr. Opin. Immunol. 46:viii-xi. 2017
 - Ho, P.-C., Bihuniak, J.D., Macintyre, A.N., Staron, M., Liu, X., Amezquita, R., Tsui, Y.-C., Cui, G., Micevic, G., Perales, J.C., et al. Phosphoenolpyruvate is a metabolic check-point of anti-tumor T cell responses. Cell 162: 1217. 2015

Received December 17, 1973.

- ¹ Andersson, J., Sjöberg, O., and Möller, G., *Transplantn. Rev.*, **11**, 131 (1972).
- ² Greaves, M. F., and Janossy, G., *Transplantn. Rev.*, **11**, 87 (1972).
- ³ Smith, R. T., *Transplantn. Rev.*, **11**, 178 (1972).
- ⁴ Meuwissen, H. J., Stutman, O., and Good, A., *Sem. Haemat.*, **6**, 28 (1969).
- ⁵ Janossy, G., and Greaves, M. F., *Clin. exp. Immun.*, **10**, 525 (1972).
- ⁶ Piquet, P.-F., and Vassalli, P., *Eur. J. Immun.*, **3**, 477 (1973).
- ⁷ Greaves, M. F., Bauminger, S., and Janossy, G., *Clin. exp. Immun.*, **10**, 537 (1972).
- ⁸ Möller, G., Anderson, J., Pohlitz, H., and Sjöberg, O., *Clin. exp. Immun.*, **13**, 89 (1973).
- ⁹ Stobo, J. D., Rosenthal, A., and Paul, W. E., *J. Immun.*, **108**, 1 (1972).
- ¹⁰ Greaves, M. F., and Bauminger, S., *Nature new Biol.*, **235**, 67 (1972).
- ¹¹ Andersson, J., Edelman, G. M., Möller, G., and Sjöberg, O., *Eur. J. Immun.*, **2**, 233 (1972).
- ¹² Vischer, T. L., *Clin. exp. Immun.*, **11**, 551 (1972).
- ¹³ Phillips, B., and Roitt, I. M., *Nature new Biol.*, **241**, 254 (1973).
- ¹⁴ Thomas, D. B., and Phillips, B., *J. exp. Med.*, **138**, 64 (1973).
- ¹⁵ Douglas, S. D., *Transplantn. Rev.*, **11**, 39 (1972).
- ¹⁶ Janossy, G., and Greaves, M. F., *Clin. exp. Immun.*, **9**, 483 (1971).
- ¹⁷ Möller, G. (Editor), *Transplantn. Rev.*, **16** (1973).
- ¹⁸ Greaves, M. F., *Current Titles in Immunology: Transplantation and Allergy*, **1**, 193 (1973).
- ¹⁹ Greaves, M. F., and Brown, G., *J. Immun.*, **112**, 420 (1974).
- ²⁰ Aiuti, F., Wigzell, H., *Clin. exp. Immun.*, **14**, 171 (1973).
- ²¹ Bobrovec, A. M., Strober, S., Herzenberg, L. A., and De Pamphilis, J. D., *J. Immun.* (in the press).
- ²² Gajl-Peczalska, K. J., Park, B. H., Biggar, W. D., and Good, R. A., *J. clin. Invest.*, **52**, 919 (1973).
- ²³ August, C. S., Rosen, F. S., Filler, R. M., Janeway, C. A., Markowski, B., and Kay, H. E. M., *Lancet*, ii, 1210 (1968).
- ²⁴ Gery, I., and Waksman, B., *J. exp. Med.*, **136**, 143 (1972).
- ²⁵ Andersson, J., Möller, G., and Sjöberg, O., *Eur. J. Immun.*, **2**, 99 (1972).
- ²⁶ Katz, D. H., and Unanue, E. R., *J. Immun.*, **109**, 1022 (1972).
- ²⁷ Möller, G., *Immunology*, **19**, 583 (1970).
- ²⁸ Janossy, G., Greaves, M. F., Doenhoff, M. J., and Snajdr, J., *Clin. exp. Immun.*, **14**, 581 (1973).
- ²⁹ Brown, G., and Greaves, M. F., *Eur. J. Immun.* (in the press).
- ³⁰ Greaves, M. F., and Brown, G., *Nature new Biol.*, **246**, 116 (1973).
- ³¹ Eisen, S. A., Wedner, H. J., Parker, C. W., *Immun. Commun.*, **1**, 571 (1972).
- ³² Julius, M. H., Simpson, E., and Herzenberg, L. A., *Eur. J. Immun.*, **3**, 645 (1973).
- ³³ Huber, H., and Fudenberg, H. H., *Int. Archs. Allergy appl. Immun.*, **34**, 18 (1968).

Restriction of *in vitro* T cell-mediated cytotoxicity in lymphocytic choriomeningitis within a syngeneic or semiallogeneic system

RECENT experiments¹⁻³ indicate that cooperation between thymus derived lymphocytes (T cells) and antibody-forming cell precursors (B cells) is restricted by the H-2 gene complex. Helper activity *in vivo* operates only when T cells and B cells share at least one set of H-2 antigenic specificities. Evidence is presented here that the interaction of cytotoxic T cells with other somatic cells budding⁴⁻⁵ lymphocytic choriomeningitis (LCM) virus is similarly restricted.

Both the cytotoxic assay used and the characteristics of the cells involved have been described previously⁶⁻⁸. Briefly, monolayers of C3H mouse fibroblasts (L cells) are grown in plastic tissue culture trays, infected with a high multiplicity of the WE3 strain of LCM virus and the cells labelled with ⁵¹Cr and overlaid (40:1) with the spleen cell preparation to be tested. Supernatants are removed between 15 and 16 h later and % ⁵¹Cr release calculated⁷. Results are expressed as mean \pm s.e.m. for four replicates. Cytolysis of

TABLE 1 Cytotoxic activity of spleen cells from various strains of mice injected i.c. 7 d previously with 300 LD₅₀* of WE3 LCM virus for monolayers of LCM-infected or normal C3H (H-2^k) mouse L cells.

Experiment	Mouse strain	H-2 type	% ⁵¹ Cr release†	
			Infected	Normal
1	CBA/H	<i>k</i>	65.1 \pm 3.3	17.2 \pm 0.7
	Balb/C	<i>d</i>	17.9 \pm 0.9	17.2 \pm 0.6
	C57Bl	<i>b</i>	22.7 \pm 1.4	19.8 \pm 0.9
	CBA/H \times C57Bl	<i>k/b</i>	56.1 \pm 0.5	16.7 \pm 0.3
	C57Bl \times Balb/C	<i>b/d</i>	24.8 \pm 2.4	19.8 \pm 0.9
	nu/+ or +/+		42.8 \pm 2.0	21.9 \pm 0.7
2	nu/nu		23.3 \pm 0.6	20.0 \pm 1.4
	CBA/H	<i>k</i>	85.5 \pm 3.1	20.9 \pm 1.2
	AKR	<i>k</i>	71.2 \pm 1.6	18.6 \pm 1.2
3	DBA/2	<i>d</i>	24.5 \pm 1.2	21.7 \pm 1.7
	CBA/H	<i>k</i>	77.9 \pm 2.7	25.7 \pm 1.3
	C3H/HeJ	<i>k</i>	77.8 \pm 0.8	24.5 \pm 1.5

* Other mice were injected with 2×10^6 LD₅₀, but levels of specific release were invariably lower due to the high dose immune paralysis^{9,20} associated with viscerotropic (WE3) LCM virus.

† % ⁵¹Cr release by normal spleen cells on infected targets ranged from: (experiment 1) 17.1 \pm 0.3 to 20.0 \pm 0.7; (experiment 2) 20.0 \pm 1.4 to 25.3 \pm 0.7; (experiment 3) 27.2 \pm 2.0.

infected L cells by CBA/H immune spleen cells has been shown to be a property of specifically sensitised thymus-derived lymphocytes, which act in the absence of both macrophages and substances secreted into the medium at large⁶⁻⁸.

Various strains of mice were injected intracerebrally (i.c.) with 300 mouse LD₅₀ of WE3 LCM virus. Mice were sampled 7 d later when, in CBA/H mice, maximal cytotoxic activity is found in lymphoid tissue^{6,7}. Only spleen preparations⁶ from mice sharing at least one set of H-2 antigenic specificities with the target monolayer caused high levels (40% to 50%) of specific lysis (Table 1). Spleen cells from nude control (nu/+ or +/+) mice, derived locally from CBA and Balb/C stock (Dr J. B. Smith, personal communication), were less active and lymphocytes from histoincompatible mice caused minimal specific release (< 5%) of ⁵¹Cr.

Spleen preparations from mice immunised 10 and 13 d previously were also assayed, as Marker and Volkert⁹ have reported that maximal cytotoxicity of C3H lymphocytes for L cells infected with the Traub strain of LCM virus occurs at 11 d after inoculation. High levels of specific ⁵¹Cr release were again recognised only in the histocompatible system (Table 2) activity declining, as has been shown previously⁷, from a peak on day 7.

Demonstration of reciprocal exclusion of cytosis was essential to establish that mice possessing other than H-2* antigenic specificities are capable of generating cytotoxic T cells. Comparisons were thus made using similar targets from allogeneic mouse strains. Peritoneal macrophages were obtained¹⁰ from normal Balb/C and CBA/H mice, cultured in plastic tissue culture trays and infected¹¹ with WE3 LCM virus. Specific lysis was restricted to the syngeneic system

TABLE 2 % ⁵¹Cr release* from infected C3H L cells overlaid with spleen cells from mice sampled at 7, 10 and 13 d after intravenous inoculation with 2,000 LD₅₀ of WE3 LCM virus.

Mouse strain	Days after inoculation		
	7	10	13
CBA/H	72.0 \pm 2.0	66.4 \pm 1.4	27.5 \pm 0.5
Balb/C	26.1 \pm 0.7	28.0 \pm 1.6	22.7 \pm 1.8
C57Bl	27.3 \pm 1.1	24.3 \pm 1.8	24.0 \pm 0.4

* Levels of ⁵¹Cr release due to overlaying normal L cells with immune spleen cells, infected L cells with control spleen cells or with medium alone ranged from 17.1 \pm 0.4 to 24.0 \pm 1.4. Other mice were injected with 2×10^6 LD₅₀, but levels of specific release were invariably lower.

TABLE 3 % ^{51}Cr release from normal and infected peritoneal macrophages by spleen cells from control mice and from mice injected i.e. with 300 LD₅₀ of WE3 LCM virus 7 d previously.

		Macrophage source	% ^{51}Cr release from macrophages			
			Infected	Experiment 1 Normal	Infected	Experiment 2 Normal
Spleen cells		Balb/C				
Balb/C	Immune Anti- θ^* N ascitic*	Balb/C	61.8 \pm 4.2 ^c ND ND	27.6 \pm 1.9 ^e ND ND	77.5 \pm 4.2 ^d 40.6 \pm 2.5 ^e 90.0 \pm 2.7	47.0 \pm 3.5 ^d ND ND
CBA/H	Control		42.0 \pm 4.8 ^a	40.5 \pm 5.2 ^a	49.6 \pm 2.5	43.5 \pm 1.6
CBA/H	Immune		42.7 \pm 6.7 ^a	33.7 \pm 5.4 ^a	32.9 \pm 3.0 ^a	48.6 \pm 3.9 ^a
CBA/H	Control		28.0 \pm 4.1	40.5 \pm 5.2	46.5 \pm 3.7	39.7 \pm 4.3
Balb/C	Immune Anti- θ^* N ascitic	CBA/H	69.1 \pm 2.8 ^e ND ND	30.9 \pm 3.4 ^e ND ND	72.5 \pm 5.2 ^d 44.0 \pm 2.5 ^d 74.3 \pm 8.4	40.0 \pm 2.9 ^d ND ND
Balb/C	Control		34.2 \pm 1.1	35.1 \pm 3.7	46.5 \pm 3.6	44.4 \pm 6.2
Balb/C	Immune		46.2 \pm 3.3 ^a	30.4 \pm 3.8 ^b	44.0 \pm 2.9 ^a	41.0 \pm 2.4 ^a
Balb/C	Control		34.9 \pm 5.7	33.7 \pm 5.6	40.5 \pm 2.5	41.0 \pm 2.4

* Treated with AKR anti- θ (C3H) ascitic fluid and guinea pig complement, or normal AKR ascitic fluid and guinea pig complement.

^a, ^b, ^c, ^d, ^e, Differences by Student's *t* test between values for immune spleen cells treated with anti- θ ascitic fluid or normal ascitic fluid, immune and control spleen cells overlaid on infected macrophages (infected column), or immune spleen cells overlaid on infected and normal macrophages (normal column). ^a, *P* > 0.05; ^b, *P* < 0.05; ^c, *P* < 0.02; ^d, *P* < 0.01; ^e, *P* < 0.001.

ND, Not done.

(Table 3). Comparable levels of specific ^{51}Cr release from isologous infected macrophages were caused by Balb/C and CBA/H spleen cells (overlaid at 20:1) from mice infected at the same time with the same dose of LCM virus, whereas histoincompatible macrophages were not damaged. Lysis was completely abrogated by treatment with AKR anti- θ ascitic fluid and guinea pig complement, but not by normal AKR ascitic fluid and complement. Though levels of ^{51}Cr release from macrophages were more variable than for L cells, probably because of inconsistencies in target cell concentrations and the higher background of non-specific lysis, the effect was both highly significant and repeatable.

The ability of T cells to cause lysis across an allogeneic barrier, when lymphocytes are sensitised to antigens specified by the H-2 gene complex, is well established^{12,13}. This also applies to L cells (H-2^k), which are readily lysed by spleen cells from C57Bl (H-2^b) mice stimulated in mixed lymphocyte culture by CBA/H (H-2^k) but not by Balb/C (H-2^d) lymph node cells. Sufficiently close association for lysis to occur is possible if the T cells is sensitised to alloantigens present on the surface of the target. Interaction between immune lymphocytes and cells expressing antigens expressed by LCM virus is, however, apparently confined to a histocompatible system, perhaps because it is only in this situation that the necessary intimacy of contact is achieved.

This restriction may possibly be overcome by previous treatment of the target population with trypsin. Balb/C (H-2^d) immune spleen cells will lyse recently trypsinised L cells (H-2^k) infected with the E-350 strain of LCM virus, the effect being completely abrogated by treatment with a rabbit anti-mouse brain serum cytotoxic for T cells¹⁴. Our experiments with previously trypsinised WE3-infected L cells have, to date, given equivocal results because of the high background of non-specific ^{51}Cr release.

An alternative possibility that must be considered in LCM is that the process of virus maturation⁵⁻⁶ through the cell membrane causes changes in self components, which are recognised only within the syngeneic or semi-allogeneic system. There is ample evidence¹⁵⁻¹⁶, for instance, that concentrations of H-2 antigens in the cell membrane are decreased in cells productively infected with budding viruses. The cytotoxic T cell may thus be recognising altered self, the implication being that LCM is essentially an autoimmune phenomenon.

These results impose a possible constraint on attempts to demonstrate cytotoxic T cells in infections of man and domestic mammals, where histocompatible cell lines and inbred strains are not available. Perhaps isologous macrophages or lectin-transformed peripheral blood leukocytes may prove

suitable targets in at least some disease states. Restriction of cell-mediated cytotoxicity within a syngeneic or semiallogeneic system may prove a reliable index of T cell involvement in species where the θ marker is not available, lysis across this barrier indicating an antibody-associated process¹⁷⁻¹⁹.

Dr Zinkernagel is supported by the Schweizerische Stiftung Fuer Biologisch-Medizinische Stipendien.

R. M. ZINKERNAGEL
P. C. DOHERTY

Department of Microbiology,
John Curtin School of Medical Research,
Australian National University,
Canberra

Received December 10, 1973.

- ¹ Kindred, B., and Shreffler, D. C., *J. Immun.*, **109**, 940 (1972).
- ² Katz, D. H., Hamaoka, T., and Benacerraf, B., *J. exp. Med.*, **137**, 1405 (1973).
- ³ Katz, D. H., Hamaoka, T., Dorf, M. E., and Benacerraf, B., *Proc. natn. Acad. Sci., U.S.A.*, **70**, 2624 (1973).
- ⁴ Abelson, H. T., Smith, G. H., Hoffman, H. A., and Rowe, W. P., *J. natn. Cancer Inst.*, **42**, 497 (1969).
- ⁵ Kajima, M., and Majde, J., *Naturwissenschaften*, **57**, 93 (1970).
- ⁶ Zinkernagel, R. M. and Doherty, P. C., *J. exp. Med.*, **138**, 1266 (1973).
- ⁷ Doherty, P. C., Zinkernagel, R. M., and Ramshaw, I. A., *J. Immun.* (in the press).
- ⁸ Doherty, P. C., and Zinkernagel, R. M., *Transpln. Rev.*, **18** (in the press).
- ⁹ Marker, O., and Volkert, M., *J. exp. Med.*, **137**, 1511 (1973).
- ¹⁰ Blanden, R. V., Mackaness, G. B., and Collins, F. M., *J. exp. Med.*, **124**, 585 (1966).
- ¹¹ Mims, C. A., and Subrahmanyam, T. P., *J. Path. Bact.*, **91**, 403 (1966).
- ¹² Cerottini, J.-C., Nordin, A. A., and Brunner, K. T., *Nature*, **228**, 1308, (1970).
- ¹³ Cerottini, J.-C., and Brunner, K. T., *Adv. Immun.* (in the press).
- ¹⁴ Cole, G. A., Prendergast, R. A., and Henney, C. S., *Fedn. Proc.*, **32**, 964 (1973).
- ¹⁵ Hecht, T. T., and Summers, D. F., *J. Virol.*, **10**, 578 (1972).
- ¹⁶ Lengerova, A., *Adv. Cancer Res.*, **16**, 235 (1972).
- ¹⁷ Perlmann, P., Perlmann, H., and Wigzell, H., *Transpln. Rev.*, **13**, 91 (1972).
- ¹⁸ MacLennan, I. C. M., *Transpln. Rev.*, **13**, 67 (1972).
- ¹⁹ Steele, R. W., Hensen, S. A., Vincent, M. M., Fuccillo, D. A., and Bellanti, J. A., *J. Immun.*, **110**, 1502 (1973).
- ²⁰ Hotchin, J., *Monogr. Virol.*, **3**, 1 (1971).

H-2 COMPATIBILITY REQUIREMENT FOR T-CELL-MEDIATED LYSIS OF TARGET CELLS INFECTED WITH LYMPHOCYTIC CHORIOMENINGITIS VIRUS

Different Cytotoxic T-Cell Specificities are Associated with Structures
Coded for in *H-2K* or *H-2D*

By ROLF M. ZINKERNAGEL AND PETER C. DOHERTY

(From the Department of Microbiology, The John Curtin School of Medical Research, Australian National University, Canberra City, A. C. T. 2601, Australia)

Compatibility at the *H-2*-gene complex is essential for interaction of sensitized thymus-derived lymphocytes (T cells) and target cells infected with either lymphocytic choriomeningitis (LCM)¹ virus or with ectromelia virus. This constraint has been demonstrated both in vitro (1-4), by the use of ⁵¹Cr-release assays, and in vivo in adoptive transfer experiments (5, 6). Similar restrictions have also been described for T-cell-mediated lysis of trinitrophenyl-modified spleen cells (7), for the T-cell helper effect (8-10), for the transfer of cell-mediated immunity to *Listeria monocytogenes* (11) and for the proliferation of sensitized guinea pig lymphocytes exposed to antigen-pulsed macrophages (12). Furthermore, in vitro cell-mediated lysis of Rous sarcoma virus-transformed cells appears to be restricted in the same way (13).

Two mutually exclusive hypotheses have been proposed to explain these phenomena (1, 2, 14). Firstly, that genes in the *H-2*-gene complex, perhaps located in the *Ir* region, code for products involved in recognition of other somatic cells by T cells. This implies the existence of a dual recognition system, requiring both presence of structures involved in physiologic interaction and an antigen-specific T-cell receptor. The second possibility is that cell surface components specified in the *H-2K* or *H-2D* regions are involved in antigen presentation. T cells are sensitized to "altered-self," either modified *H-2* antigens or structures coded for by the *H-2*-gene complex that are not normally expressed on the cell surface, or to some complex of viral and *H-2* antigens.

Evidence presented here supports the second hypothesis, by establishing that distinct cytotoxic T-cell specificities are associated with each parental haplotype in *F₁* mice, or with either the *H-2K* or *H-2D* region as demonstrated with *H-2* recombinant strains.

Materials and Methods

Mice. CBA/H, BALB/c, CBA/H × BALB/c *F₁*, and A/J mice were from colonies at the Australian National University, Canberra City, Australia. The C3H.OH mice were originally obtained from

¹Abbreviations used in this paper: FCS, Fetal calf serum; L cells, L929 fibroblasts (*H-2^a*); LCM, lymphocytic choriomeningitis; LU, lytic units (19); P-815, DBA/2 mastocytoma cells (*H-2^d*).

Doctors D. C. Shreffler and C. S. David, Department of Human Genetics, the University of Michigan Medical School, Ann Arbor, Mich., and were then bred locally. The H-2 genotypes (15) of the mouse strains used throughout these experiments are shown in Table I.

Immunization. 7- to 10-wk old mice were injected intracerebrally (i.c.) with 300 LD₅₀, or intravenously (i.v.) with a mean lethal dose (LD₅₀) of the WE3 strain of LCM virus.

Target cells. C3H (H-2^a) mouse L929 fibroblasts (L cells) were grown in Eagle's minimal essential medium (F-15; Grand Island Biological Co., Grand Island, N. Y.) plus 10% fetal calf serum (FCS) in 250-ml Falcon plastic tissue culture flasks (Falcon Plastics, Div. of BioQuest, Oxnard, Calif.). When confluent, the monolayer was infected with supernates of a 10% suspension of LCM-infected guinea pig lung for 1 h at 37°C. After one wash with 20 ml of prewarmed medium the cells were incubated for 24 h at 37°C. After trypsinization, normal or infected L cells were transferred into spinner flasks, at a density of 2-5 × 10⁵/ml, and maintained as spinner cultures for a further 24 h before being used as ⁵¹Cr-labeled targets, or as unlabeled competitor cells.

Mastocytoma cells of DBA/2 (H-2^d) (P-815) origin were cultured in Dulbecco's modified Eagle's medium (H-16, GIBCO) plus 10% FCS. LCM-infected P-815 cells were maintained as a continuously infected line.

Peritoneal Macrophages. Peritoneal macrophages were obtained from mice killed by cervical

TABLE I
H-2 Genotypes of the Mouse Strains Used (15)

Strain	H-2 genotype					
	K	IA	IB	IC	Ss-Slp	D
BALB/c	d	d	d	d	d	d
	d	d	d	d	d	d
CBA/H	k	k	k	k	k	k
	k	k	k	k	k	k
CBA/H × BALB/c	k	k	k	k	k	k
	d	d	d	d	d	d
A/J	k	k	k	d	d	d
	k	k	k	d	d	d
C3H.OH	d	d	d	d	d	k
	d	d	d	d	d	k

dislocation. The abdominal skin was reflected and 10-15 ml of cold (4°C) Puck's saline A (16) were injected vigorously into the abdominal cavity, aspirated, and reinjected twice more. Between 2 × 10⁶ to 2 × 10⁷ viable large nucleated cells were recovered from each mouse. These cells were plated at a density of 2 × 10⁵ large cells per well of 96-hole tissue culture trays (Linbro Chemical Co., New Haven, Conn.). Cell losses during infection, ⁵¹Cr labeling, and washings left about 5 × 10⁴ cells per well.

Cytotoxicity Assay. The assay for measuring T-cell-mediated virus-specific ⁵¹Cr release was performed, with some modification, as described previously (17). LCM virus-infected or normal target cells were labeled with ⁵¹Cr and washed. Target cells in suspension were dispensed in 50-μl aliquots, containing 5 × 10⁴ cells, into individual flat-bottomed wells of 96-hole plastic trays.

Targets were overlayed at a ratio of 20:1, except where otherwise stated. After incubation for 8-10 h at 37°C, the supernates were pipetted and the remaining ⁵¹Cr was recovered by water lysis. Results are expressed as the mean ± SEM percent ⁵¹Cr release for four replicates (17). The cytotoxic activity per spleen was calculated by determining the total amount of arbitrary lytic units (LU), defined as numbers of nucleated spleen cells necessary to specifically lyse 33% of the target cells in one well (19).

Competing unlabeled target cells were added, at appropriate concentrations, in 50-μl vol to wells containing ⁵¹Cr-labeled targets. Spleen cells were then added in a further 200 μl, using a tuberculin syringe fitted with a 26 gauge needle to achieve good mixing.

Results

Assay on F_1 and $H-2$ Recombinant Target Cells. Compatibility of immune spleen cells and target cells at one $H-2$ haplotype, or at $H-2K$ or $H-2D$, was sufficient for the lytic interaction to occur (Table II). Providing that this degree of identity was achieved, presence of foreign $H-2$ specificities on T cells or target cells did not cause impairment of cytotoxicity, establishing that the requirement for $H-2$ compatibility in no way reflects allogeneic inhibition (18).

Relative Cytotoxic Activity Generated by F_1 and $H-2$ Recombinant Mice. The capacity of immune F_1 and $H-2$ recombinant spleen cells to lyse $H-2^k$ or $H-2^d$ virus-infected targets was determined firstly as LU (19), secondly as LU per spleen, and thirdly as percent of cytotoxic activity for syngeneic $H-2^k$ or $H-2^d$ combinations (Table III). Comparisons of absolute LU values can only be made

TABLE II
LCM-Specific Cytotoxic Activity of Spleen Cells Assayed on F_1 and $H-2$ Recombinant Macrophage Target Cells*

Mouse strain	Spleen cells [§]	⁵¹ Cr release† from target macrophages							
		CBA/H		BALB/c		CBA/H × BALB/c F_1		A/J	
		LCM	Normal	LCM	Normal	LCM	Normal	LCM	Normal
CBA/H	Immune	% 61.0±1.3	% 28.3±1.1	% 34.6±2.4	% 36.4±1.3	% 55.1±0.8	% 31.9±0.9	% 57.5±1.2	% 37.0±2.6
	Normal	31.4±2.1	27.5±0.6	38.4±3.3	34.6±0.7	34.7±2.8	31.3±2.5	36.3±0.3	38.0±2.2
BALB/c	Immune	35.2±1.4	32.2±1.3	68.0±2.8	35.2±1.9	71.7±2.0 [#]	29.3±0.4	69.3±3.9	38.2±1.2
	Normal	34.0±1.5	31.9±1.3	36.6±2.6	38.9±1.6	36.9±3.3	31.3±2.5	33.6±4.2	38.4±3.4
CBA/H × BALB/c F_1	Immune	56.4±1.5 [#]	29.2±2.0	69.9±2.7	39.6±2.3	73.1±1.2	29.3±0.4	NT	NT
	Normal	33.4±4.3	28.7±2.1	33.3±1.3	37.5±2.5	35.8±2.6	31.6±1.7	NT	NT
A/J	Immune	50.0±2.8#	32.4±2.2	67.8±0.2	32.5±0.6	63.0±1.0	31.4±0.7	68.7±4.8	38.7±2.3
	Normal	28.5±0.7	31.2±0.4	43.8±6.4	39.8±3.7	36.8±1.5	29.3±2.3	31.4±4.8	40.1±1.7

* Peritoneal macrophages were infected 12 h after plating and assayed 24 h later.

† Spleen cells were overlayed at 30:1 for 9 h at 37°C. Mean ± SEM of four replicates.

§ Donor mice were infected i.v. with 2,000 LD₅₀ WE3 9 days previously.

Significantly greater than control values ($P < 0.001$).

within the same target system, as the P-815 are apparently more readily lysed than are the L cells. In both systems T cells from F_1 mice showed from 70 to 100% of the activity of parental strain lymphocytes, depending on the method of comparison. Recombinant T cells were relatively more effective when there was compatibility at $H-2D$ (Tables I and III), an observation indicating that there may be at least two specificities of cytotoxic T cells, those associated with the D end being the more potent.

Cold Target Competition In Vitro. Further evidence for more than one specificity of cytotoxic T cells in LCM-immune mice was found from cold target competitive inhibition experiments in vitro (20). The cytotoxic activity of immune T cells for ⁵¹Cr-labeled, virus-infected target cells could only be inhibited specifically by mixture with unlabeled, syngeneic virus-infected cells (Fig. 1). Syngeneic normal cells, or virus-infected allogeneic cells, had no effect.

TABLE III
Relative Activity of Immune Spleen Cells from Parent, F₁, and H-2 Recombinant Mice*

Mouse strain	Total N cells per spleen	H-2 ^a LCM target			H-2 ^d LCM target		
		LU‡	LU/ spleen	CBA/H (H-2 ^a) activity	LU	LU/ spleen	BALB/c (H-2 ^d) activity
CBA/H	4.2×10^7	5.5	77	100	$>10^7$	<5	<2
BALB/c	6.8×10^7	$>10^7$	<7	<9	2.0×10^8	340	100
CBA/H × BALB/c F ₁	3.0×10^7	5.5×10^8	55	72	1.1×10^8	268	79
A/J	3.7×10^7	1.1×10^8	35	46	1.6×10^8	237	70
C3H.OH	6.1×10^7	1.0×10^8	59	77	4.0×10^8	153	45

* All mice were sampled on day 7. The kinetics of the cytotoxic T-cell response is comparable in different mouse strains (3).

‡ LU, i.e., number of nucleated (N) cells necessary to specifically lyse 33% of the LCM-infected targets (19).

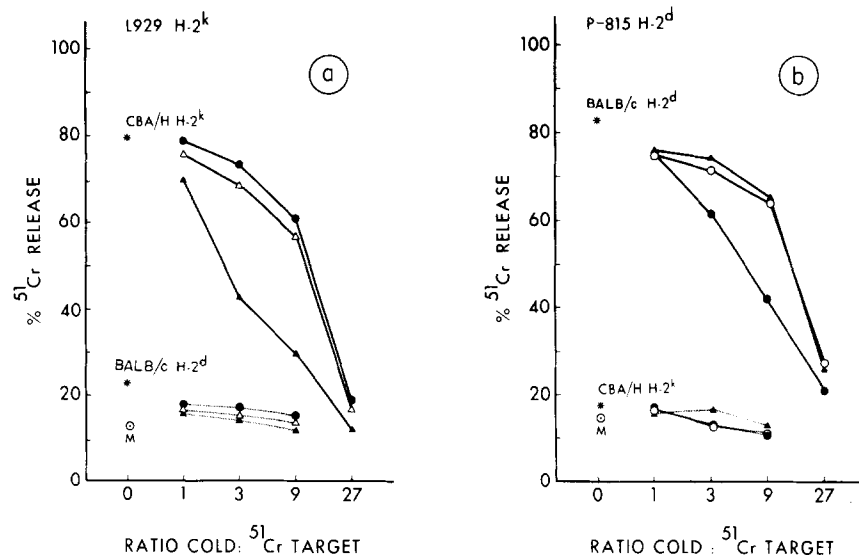


FIG. 1. Competitive inhibition with unlabeled targets, LCM-P-815 (●), normal P-815 (○), LCM-L cells (▲), or normal L cells (Δ), added at various ratios of the LCM-specific ⁵¹Cr release (*) by 7 day immune CBA/H (H-2^a) and BALB/c (H-2^d) spleen cells assayed on (a) LCM-L cells (H-2^a) and (b) LCM-P-815 (H-2^d). Spontaneous ⁵¹Cr release (○) was not significantly different from that observed for normal target cells.

Competition was most apparent when cold targets were at from three to nine times in excess. Use of higher concentrations resulted in nonspecific steric hindrance.

Cytolytic capacity of immune spleen cells from H-2^{k/d} F₁ mice was inhibited only when the competing virus-infected cells were syngeneic with the target cells (Fig. 2). Presence of excess H-2^{d/d} virus-infected mastocytoma cells caused no specific decrease in killing of H-2^{k/k} virus-infected L-cells, and the converse was also true. This finding is most readily interpreted as indicating that there are at least two specificities of LCM-immune cytotoxic T cells in H-2^{k/d} F₁ mice, each associated with altered-self characteristics of one parental H-2 type (14).

ROLF M. ZINKERNAGEL AND PETER C. DOHERTY

Essentially similar results were recorded for recombinant mice (Table I and Fig. 3). Cytotoxic activity of immune lymphocytes for $H-2K$ or $H-2D$ compatible virus-infected targets was specifically inhibited only when there was $H-2$ identity between target and competing cells, and was not diminished by presence of

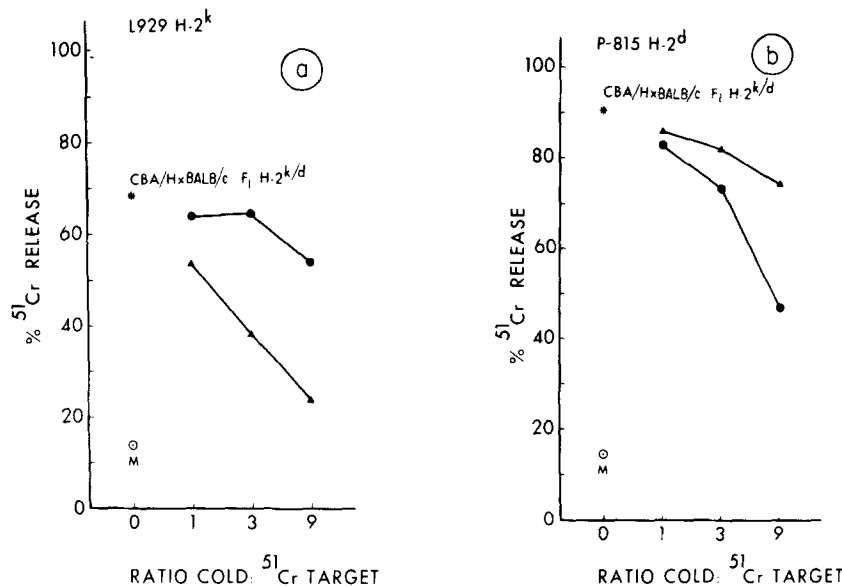


FIG. 2. Competitive inhibition with various ratios of unlabeled LCM-P-815 (●), or with LCM-L cells (▲), of the LCM-specific ^{51}Cr release by 7 day immune CBA/H \times BALB/c F_1 ($H-2^{k/d}$) spleen cells (*) assayed on LCM-L cells ($H-2^k$) or LCM-P-815 ($H-2^d$) target cells.

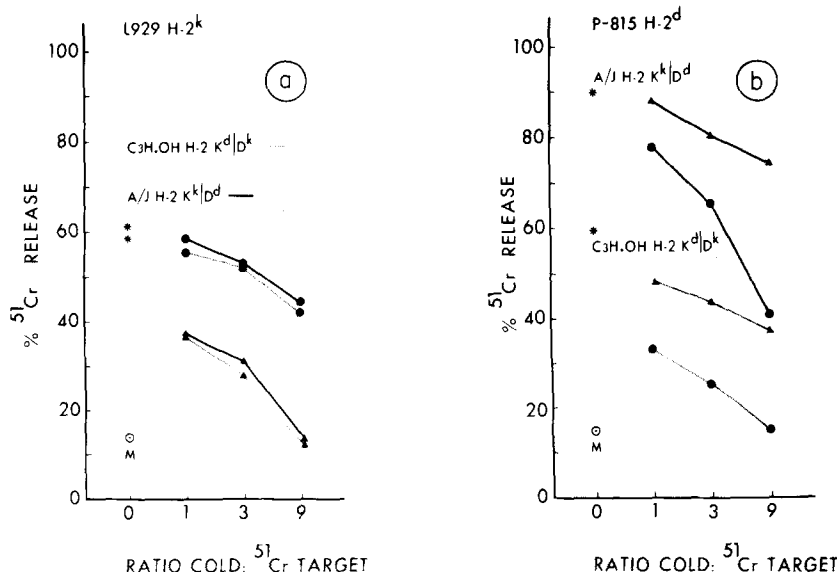


FIG. 3. Competitive inhibition by different ratios of unlabeled LCM-L cells (▲) or LCM-P-815 (●) of the LCM-specific ^{51}Cr release from labeled LCM-L cells or LCM-P-815 by 7 day immune A/J ($H-2K^k/D^d$) or C3H.OH ($H-2K^k/D^k$) (*) spleen cells.

virus-infected cells compatible with the T cell at the irrelevant *H-2* locus. Again, these experiments indicate that there are at least two specificities of cytotoxic T cells in recombinant mice, one associated with *H-2K* and the other with *H-2D*.

Selective Proliferation In Vivo. Evidence for cytotoxic T cells of more than one specificity was also found from in vivo experiments. The system used has been described previously (14). Briefly, donors are killed at 7 days after i.v. inoculation with 2,000 LD₅₀ of WE3 LCM virus. Recipients are irradiated (850 R) 24 h before adoptive transfer, dosed with 10⁶ LD₅₀ of WE3 LCM virus 18 h later, inoculated with 10⁸ immune donor lymphoid cells, and cytotoxic activity in pooled spleen and lymph nodes determined after a further 3 days. Donor cells (14) proliferate in the recipient throughout this interval, as shown by failure of irradiated (850 R) spleen cells to multiply further (Table IV). Replication depends on continued exposure to histocompatible, virus-infected recipient cells

TABLE IV
Failure of Irradiated (850 R) LCM-Immune CBA/H × C57BL F₁ Immune T Cells to Show Cytotoxic Activity at 72 h after Transfer to Irradiated, Virus-Infected CBA/H Recipients

Cell population	Treatment	⁵¹ Cr release from L cells	
		Infected	Normal
Before transfer*	None	53.9 ± 3.2	15.3 ± 1.2
	850 R	54.6 ± 4.2	14.7 ± 2.1
72 h after transfer‡	None	98.2 ± 1.9	18.8 ± 1.9
	850 R	19.1 ± 0.5	16.9 ± 3.1
Control LCM immune‡		93.9 ± 2.3	18.4 ± 0.9
Control normal spleen		18.9 ± 1.4	17.7 ± 1.7

* Assayed for 4 h at 37°C.

‡ Assayed for 15 h at 37°C.

(5, 14). Presence of alloantigens, in an F₁ donor or recipient, has no inhibitory effect (5, 14), providing one haplotype is shared.

T cells from 7 day immune F₁ (*H-2^{k/d}*) mice readily lyse virus-infected targets of both parental *H-2* types (Table II). However passage through *H-2^k* recipients results in selective proliferation of lymphocytes with significant cytotoxic activity only for *H-2^k* virus-infected fibroblasts (Table V). The converse applies after transfer through *H-2^d* recipients. These results are best explained as representing preferential multiplication of cytotoxic T cells of two distinct specificities, each associated with one parental *H-2* type (14).

Similar observations have also been made for T cells from recombinants (Table I). Spleen cells from immune A/J or C3H.OH mice lyse both *H-2^k* and *H-2^d* virus-infected targets (Fig. 3). Passage through *H-2^k* recipients selects a population(s) of T cells which preferentially kill *H-2^k* targets, i.e., specific for altered *H-2K* in the A/J mice or altered *H-2D* in the C3H.OH mice (Table V).

TABLE V

*Cytotoxic T-Cell Activity in Lymphoid Tissue of Irradiated LCM-Infected Recipients Dosed with LCM-Immune Spleen Cells 3 days Previously**

Recipients	⁵¹ Cr release‡				
	L-929		P-815		
	Infected	Normal	Infected	Normal	
Donors	%	%	%	%	
CBA/H × BALB/c F ₁	BALB/c	21.2 ± 1.2	18.5 ± 1.2	78.0 ± 1.2	26.9 ± 3.1
CBA/H × BALB/c F ₁	CBA/H	84.9 ± 0.9	25.5 ± 2.1	29.8 ± 0.8	22.7 ± 2.1
C3H.OH	CBA/H	48.3 ± 0.3	21.9 ± 1.2	25.8 ± 1.5	23.8 ± 3.1
A/J	CBA/H	63.3 ± 1.1	21.0 ± 1.1	32.9 ± 1.5	28.9 ± 3.3
Controls					
BALB/c immune		24.9 ± 1.0	18.6 ± 0.6	70.2 ± 3.9	20.5 ± 1.0
BALB/c normal		18.6 ± 1.5	15.6 ± 1.6	19.9 ± 1.8	23.6 ± 0.6
CBA/H immune		85.7 ± 1.6	22.7 ± 2.9	23.6 ± 0.6	23.4 ± 0.7
CBA/H normal		18.3 ± 0.5	23.8 ± 1.4	22.1 ± 3.2	21.6 ± 1.1
Medium		18.6 ± 0.5	17.8 ± 0.7	18.7 ± 0.3	22.4 ± 2.7

* Donor mice were injected i.v. with 2,000 LD₅₀ of WE3 LCM virus and killed after 7 days. Recipient mice were irradiated (850 R) 24 h previously and dosed with 10⁶ LD₅₀ of WE3 LCM 6 h before cell transfer. Activity of donor cells in Table III and Figs. 1-3.

† Target cells were overlayed at a ratio of 30:1 and incubated for 10 h at 37°C. Means ± SEM of four replicates.

Discussion

LCM-immune mice apparently possess cytotoxic T cells of at least two broad specificities, associated with either *H-2K* or *H-2D*. The evidence for this is derived from a variety of separate approaches. Genetic mapping studies, using recombinant mice, have rigorously shown that T cells and virus-infected targets need be compatible only in the region of either the *H-2K* or the *H-2D* locus.² The same is true for the ectromelia model.² Identity at *Ir-Ss/Slp* is neither essential, nor is it sufficient, for successful interaction to occur.² It must be stressed that there is no indication that this *H-2* compatibility requirement for cytotoxic T-cell killing of virus-infected cells reflects presence of a physiological interaction mechanism coded for by genes in the *Ir* region (9, 10, 12, 21).

Even so, existence of two separate self-recognition systems, specified by genes in either the *H-2K* or *H-2D* regions, may still be invoked, e.g., in this case the observation that compatibility at *H-2D* results in greater killing could indicate that the physiological interaction mechanism coded for at the *D* end is more effective. The apparent separation of two distinct T-cell specificities in F₁ mice, one associated with either parental haplotype, might be explained by allelic exclusion in this hypothetical physiological interaction mechanism (22,

^aBlanden, R. V., P. C. Doherty, M. B. C. Dunlop, I. D. Gardner, R. M. Zinkernagel, and C. S. David. 1975. Genes required for T-cell-mediated cytotoxicity against virus-infected target cells are in the *K* and *D* regions of the *H-2*-gene complex. Manuscript submitted for publication.

23). Such an argument cannot, however, be applied to the comparable results obtained for *H-2* recombinant mice, as they are homozygous. It would thus be necessary to postulate that only one, or other, of the self-recognition structures coded for at *H-2K* or *H-2D* could be expressed in any one T cell, i.e., some form of *H-2K* or *H-2D* receptor exclusion. Furthermore, the results of the selective proliferation experiments indicate that any such exclusion is clonal.

This complex mechanism is, to our knowledge, without precedent. We therefore favor the simpler postulate that the T cell is sensitized to altered self (1-3, 14), the self antigens involved being coded for at, or near to, either *H-2K* or *H-2D*. Altered self is interpreted broadly as reflecting either short- or long-range virus-induced modification of *H-2* antigens, perhaps associated with the *H-2* private specificities or products of genes linked closely to them. Such a concept accommodates recognition of alloantigens, or of changes induced by viruses, intracellular bacteria or chemicals, within the same model (14). Furthermore, it is in general agreement with Bodmer's modification (24) of Jerne's argument for generation of immunological diversity (25). In the present model all T-cell specificities may be considered to have arisen by somatic mutation from genes originally coding for recognition of histocompatibility antigens.

The altered-self concept is also in accord with Burnet's immunological surveillance theory, broadened somewhat to include response to infectious agents as an essential part (26). Viruses and bacteria may, in evolutionary terms, be considered as potent selective forces, affecting young animals particularly. The T-cell-mediated response to such agents is, in the great majority of cases, protective. The realization that T cells in virus-infected mice are sensitized to either altered *H-2K* or *H-2D* thus provides a reason for gene duplication in the *H-2*-gene complex (27). The overall T-cell response is, as numerically analyzed here, considerably augmented by the presence of two distinct cytotoxic T-cell specificities. An identical argument may be used to explain selective advantage of heterozygosity of the *H-2*-gene complex, four specificities are more effective than two. The extreme polymorphism of histocompatibility antigen systems (24) may thus, on a purely mechanistic basis, be considered to have developed in response to selective pressure exerted by infectious agents.

Summary

Use of syngeneic, allogeneic, *F₁*, and *H-2* recombinant mice has shown that animals injected with lymphocytic choriomeningitis (LCM) virus generate T cells which are cytotoxic for *H-2K* or *H-2D* compatible, but not *H-2* different, virus-infected target cells. Three separate lines of evidence are presented which indicate that these immune T cells are sensitized to "altered-self," the self antigens involved being coded for in the *H-2K* or *H-2D* regions. Firstly, cytotoxic activity associated with mutuality at *H-2D* is greater than that observed when T cells and targets are identical at *H-2K*. Secondly, lysis mediated by immune T cells from *F₁* or *H-2* recombinant mice is specifically inhibited only by presence of unlabeled, virus-infected cells that are *H-2* compatible with the targets. Thirdly, LCM-immune *F₁* and *H-2* recombinant T cells inoculated into irradiated, virus-infected recipients proliferate only to kill target cells that are *H-2* compatible with both the donor and the recipient.

All of these experiments establish that there is a dissociation of T-cell activities between parental haplotypes in F_1 mice, and between $H-2K$ and $H-2D$ in recombinants. It would thus seem that there are at least two specificities of LCM-immune T cells in homozygotes, associated with either $H-2K$ or $H-2D$, and four specificities in F_1 hybrids. The significance of these findings, with respect both to gene duplication and to the marked polymorphism in the $H-2$ system, is discussed.

We wish to thank Dr. M. H. R. MacDonald for helpful discussions, Doctors D. C. Shreffler and C. S. David for the original breeding pairs of C3H.OH mice, and Miss Gail Essery for her capable technical assistance.

Received for publication 3 February 1975.

References

1. Zinkernagel, R. M., and P. C. Doherty. 1974. Restriction of *in vitro* T cell-mediated cytotoxicity in lymphocytic choriomeningitis within a syngeneic or semiallogeneic system. *Nature (Lond.)*. **248**:701.
2. Doherty, P. C., and R. M. Zinkernagel. 1974. T cell-mediated immunopathology in viral infections. *Transplant. Rev.* **19**:89.
3. Doherty, P. C., and R. M. Zinkernagel. 1975. $H-2$ compatibility is required for T-cell-mediated lysis of target cells infected with lymphocytic choriomeningitis virus. *J. Exp. Med.* **141**:502.
4. Gardner, I., N. A. Bowern, and R. V. Blanden. 1974. Cell-mediated cytotoxicity against ectromelia virus-infected target cells. III. Role of the $H-2$ gene complex. *Eur. J. Immunol.* **4**:63.
5. Doherty, P. C., and R. M. Zinkernagel. 1975. Capacity of sensitized thymus derived lymphocytes to induce fatal lymphocytic choriomeningitis is restricted by the $H-2$ gene complex. *J. Immunol.* **114**:30.
6. Blanden, R. V. 1975. Mechanisms of cell-mediated immunity in viral infection. In Proceedings of the Second International Congress of Immunology. Brighton, England. L. Brent and J. Holborow, editors. **2**(4):17.
7. Shearer, G. M. 1974. Cell-mediated cytotoxicity to trinitrophenyl-modified syngeneic lymphocytes. *Eur. J. Immunol.* **4**:527.
8. Kindred, B., and D. C. Shreffler. 1972. $H-2$ dependence of co-operation between T and B cells *in vivo*. *J. Immunol.* **109**:940.
9. Katz, D. H., T. Hamaoka, and B. Benacerraf. 1973. Cell interactions between histoincompatible T and B lymphocytes. II. Failure of physiologic cooperative interactions between T and B lymphocytes from allogeneic donor strains in humoral response to hapten-protein conjugates. *J. Exp. Med.* **137**:1405.
10. Katz, D. H., T. Hamaoka, M. E. Dorf, and B. Benacerraf. 1973. Cell interactions between histoincompatible T and B lymphocytes. The $H-2$ gene complex determines successful physiologic lymphocyte interactions. *Proc. Natl. Acad. Sci. U. S. A.* **70**:2624.
11. Zinkernagel, R. M. 1974. Restriction by the $H-2$ gene complex of the transfer of cell-mediated immunity to *Listeria monocytogenes*. *Nature (Lond.)* **251**:230.
12. Rosenthal, A. S., and E. M. Shevach. 1973. Function of macrophages in antigen recognition by guinea pig T lymphocytes. I. Requirement for histocompatible macrophages and lymphocytes. *J. Exp. Med.* **138**:1194.
13. Wainberg, M. A., Y. Markson, D. W. Weiss, and F. Donjanski. 1974. Cellular immunity against Rous sarcomas of chickens. Preferential reactivity against autoch-

- thorous target cells as determined by lymphocyte adherence and cytotoxicity tests *in vitro*. *Proc. Natl. Acad. Sci. U. S. A.* **71**:3565.
14. Zinkernagel, R. M., and P. C. Doherty. 1974. Immunological surveillance against altered self by sensitized thymus derived lymphocytes in lymphocytic choriomeningitis. *Nature (Lond.)*. **251**:547.
 15. Shreffler, D. C. and C. S. David. 1974. The H-2 major histocompatibility complex and the I immune response region: genetic variation, function, and organization. *Adva. Immunol.* In press.
 16. Blanden, R. V., and R. E. Langman. 1972. Cell-mediated immunity to bacterial infection in the mouse. Thymus-derived cells as effectors of acquired resistance to *Listeria monocytogenes*. *Scand. J. Immunol.* **1**:379.
 17. Zinkernagel, R. M., and P. C. Doherty. 1974. Characteristics of the interaction *in vitro* between cytotoxic thymus-derived lymphocytes and target monolayers infected with lymphocytic choriomeningitis virus. *Scand. J. Immunol.* **3**:287.
 18. Hellström, K. E., and G. Möller. 1965. Immunological and immunogenetic aspects of tumor transplantation. *Prog. Allergy*. **9**:158.
 19. Cerottini, J. C., and K. T. Brunner. 1974. Cell-mediated cytotoxicity, allograft rejection, and tumor immunity. *Adv. Immunol.* **18**:67.
 20. Ortiz de Landazuri, M., and R. B. Herberman. 1972. Specificity of cellular immune reactivity to virus-induced tumors. *Nat. New Biol.* **238**:18.
 21. Katz, D. H., and B. Benacerraf. 1974. The function and interrelationship of T cell receptors, Ir genes and other histocompatibility gene products. *Transplant. Rev.* In press.
 22. Pernis, B., G. Chiappino, A. S. Kelus, and P. G. H. Gell. 1965. Cellular localization of immunoglobulins with different allotypic specificities in rabbit lymphoid tissue. *J. Exp. Med.* **122**:853.
 23. Gell, P. G. H. 1967. Restriction on antibody production by single cells. *Cold Spring Harbor Symp. Quant. Biol.* **32**:441.
 24. Bodmer, W. F. 1972. Evolutionary significance of the HL-A system. *Nature (London.)*. **237**:139.
 25. Jerne, N. K. 1971. The somatic generation of immune recognition. *Eur. J. Immunol.* **1**:1.
 26. Burnet, M. 1970. Immunological Surveillance. Pergamon Press (Australia) Pty. Ltd., Sydney, Australia.
 27. Klein, J., and D. C. Shreffler. 1971. The H-2 model for the major histocompatibility systems. *Transplant. Rev.* **6**:3.



HHS Public Access

Author manuscript

Trends Immunol. Author manuscript; available in PMC 2017 November 01.

Published in final edited form as:

Trends Immunol. 2016 November ; 37(11): 724–737. doi:10.1016/j.it.2016.08.010.

Present Yourself! By MHC Class I and MHC Class II Molecules

Kenneth L. Rock¹, Eric Reits², and Jacques Neefjes³

¹Department of Pathology, UMass Medical School, Worcester

²Department of Cell Biology & Histology, Amsterdam Medical Center, University of Amsterdam NL

³Department of Cell Biology, the Netherlands Cancer Institute, Amsterdam and Department of Chemical Immunology, Leiden University Medical Center LUMC, Leiden NL

Abstract

Since the discovery of major histocompatibility complex (MHC) molecules, it took some 40 years to arrive at a coherent picture of how MHC class I and MHC class II molecules really work. This is a story of proteases and MHC-like chaperones that support the MHC class I and II molecules in presenting peptides to the immune system. We now understand that the MHC system shapes both the repertoire of presented peptides and the subsequent T cell responses, with important implications ranging from transplant rejection to tumor immunotherapies. Here we present an illustrated review on the ins and outs of MHC class I and MHC class II antigen presentation.

Keywords

Antigen Presentation; MHC class I; MHC class II; tumor immunology; transplantation; autoimmune diseases

Why Do We Need to Present Antigens?

T cells help eliminate pathogens present in infected cells and also help B cells make better and different kinds of antibodies to protect against extracellular microbes and toxic molecules. To accomplish these important functions, T cells have to interact intimately with other cells and then find and instruct or eliminate the ones that are harbouring or have been exposed to these pathogenic threats. However, T cells are unable to peek beneath the surface of cells to identify ones that have ingested bacteria or are synthesizing viral or mutant proteins. Instead, antigen presentation systems have evolved, that display on the cell surface information about the various antigens that cells are synthesizing or have ingested. These antigen presentation pathways monitor the major subcellular compartments wherein pathogens could be lurking and report their findings to the appropriate kinds of T cells. Endogenously synthesized antigens in the cytosol of all cells are presented to CD8+ T cells

Correspondence to JN: J.J.C.Neefjes@lumc.nl.

Publisher's Disclaimer: This is a PDF file of an unedited manuscript that has been accepted for publication. As a service to our customers we are providing this early version of the manuscript. The manuscript will undergo copyediting, typesetting, and review of the resulting proof before it is published in its final citable form. Please note that during the production process errors may be discovered which could affect the content, and all legal disclaimers that apply to the journal pertain.

as peptides bound to MHC I molecules, thereby allowing the CD8+ lymphocytes to identify and eliminate virally infected cells or cancers. Antigens ingested into endocytic compartments of macrophages, dendritic cells or B cells are presented to CD4+ T cells as peptides bound to MHC II molecules. T cells have antigen receptors that recognize antigenic peptide, but only in the context of MHC I or MHC II molecules that are displaying the antigen on the cell surface. Consequently, T cells are directed to work with cells, while not being ‘distracted’ by free antigen, to which they would not be able to do anything. Moreover, the pattern of expression of MHC I and II molecules directs T cells to interact with exactly the right kind of cells. Here, we review the current understanding of the mechanisms of antigen presentation, as well as their implications in health and disease. The studies discussed here have paved the way for increasingly refined analyses of the biology of antigen presentation – in different physiologic or clinical contexts, different cells, different organs – that are the focus of this special issue.

The MHC Scaffold or How Did MHC-I and MHC-II Molecules Evolve?

MHC I and II molecules present protein fragments to CD8+ and CD4+ T cells, respectively. These molecules are essential for cell-mediated immunity and therefore appeared at the inception of the adaptive immune system, some 500 million years ago[1]. For their construction they used two Ig-domains topped by two parallel alpha helices resting on a platform of beta-pleated sheets. This capital structure generated a peptide-binding groove between the alpha helices[2, 3], which is ‘evolutionarily speaking’ likely borrowed from earlier chaperone structures. There are arguments for this: a. chaperones bind unfolded stretches of proteins and the prototypic unfolded structure is a peptide; b. various phylogenetically older chaperones have a somewhat similar structure[4]; c. there are various MHC molecule look-a-likes that act as specific chaperones in the process of MHC-restricted antigen presentation. These include tapasin[5], tapasin binding protein-related (TAPBPR)[6] [7], DM [8,9] and DO[10] molecules, as we discuss later. Yet MHC I and MHC II molecules are unique in the proteome because of their extreme polymorphism (>10,000 different alleles of MHC I molecules have been identified thus far!). This has interesting consequences. Polymorphic residues on the top alpha helices interact with the TCR and are the basis for the specificity of TCRs for both an antigen peptide plus a particular allelic form of an MHC molecule (a phenomenon called MHC restriction). Polymorphic residues in the MHC peptide binding groove change the nature and location of so-called pockets. These variable pockets are filled by complementary variable amino acid side chains of peptides (so-called anchor residues), with the effect that different fragments from a defined antigen are presented by different polymorphic MHC molecules[11,12] (Figure 1). Yet, next to the anchor residues, most other amino acids in a peptide fill a free space and can be (almost) any of the 20 amino acids[13,14]. By having pockets with specificity for only a few side chains and allowing the remaining 6–10 amino acids to vary between all possibilities, each kind of MHC molecules can present a very large repertoire of peptides. Moreover, by having 3 to 6 different MHC I as well as 3 to 12 different MHC II molecules (the exact number depending on how many different MHC alleles were inherited from one’s parents and how the MHC II subunits paired), cells can present a large fraction of the universe of peptides, although not all sequences. In theory then, MHC I molecules can present a peptidome of around $6 \times$

20^(6–7) different peptides, and MHC II can display up to 12 × 20⁽¹⁰⁾ peptides. In actuality, such a large array of peptides cannot all be presented because there are only around 200,000 MHC I and 20,000 MHC II molecules on cells such as B and T cells[15]. Moreover, since some peptides are present in high number (from highly expressed proteins), the real number of different peptides presented by one cell is likely less than 10,000. Importantly, when a pathogen alters a critical anchor residue in one of its antigenic epitopes, it may prevent presentation of this antigen in one individual but not in another person with different MHC molecules that will simply select different peptides from the same pathogen.[16] Therefore, MHC polymorphism is good for the survival of the population and not necessarily the individual. How is this extensive polymorphism maintained in the species? One possibility is based on evidence that females can distinguish by smell MHC allele differences in males and prefer as mates individuals with whom they do not share MHC alleles. The attendant consequence of such a preference would be to promote maximal expression of polymorphic MHC alleles in offspring and maintenance of diverse alleles in the population [17]. Perfumes may then mask natural scent of this basis of partner choice, with unknown effects in human species. The obvious modern disadvantage of MHC polymorphism is transplant rejection, but even this may serve a useful function in nature by preventing the seeding of cancer cells between individuals. This is illustrated by the fact that MHC-deficient oral cancers are currently being transferred between Tasmanian Devils through bites and decimating the population of these animals in the wild [18,19].

How to Present Your Inner Self? MHC Class I Molecules

MHC I molecules present peptides from the proteins that are synthesized by cells. In healthy cells, all of these proteins are autologous ones to which CD8+ T cells are tolerant. However, when cells are expressing mutant sequences (e.g. in cancers), microbial genes (e.g. from viral infections) or foreign polymorphic genes (e.g. from transplants), these ‘non-self’ antigenic peptides are included in the presented peptidome, allowing CD8+ T cells to detect and destroy these abnormal cells. How MHC I manages to present a blueprint of the intracellular proteome has been established over the last 25 years[20] (Figure 2). Briefly, normal and pathogenic proteins are degraded by the proteasome into peptide fragments [21] [22]. These fragments are further trimmed and to a large extent destroyed by cytosolic peptidases[23] but some survive by escaping into the ER through a peptide transporter called transporter associated with antigen processing (TAP) that is embedded in the ER membrane[20]. In the ER, TAP forms the centre of a peptide loading complex that includes a dedicated chaperone, tapasin, empty MHC I molecules awaiting peptides and two common chaperones, calreticulin and protein disulfide isomerase ERp57[24]. TAP translocates peptides that then are considered for binding by MHC I molecules. These empty MHC I molecules are held in a peptide-receptive state by the chaperone tapasin and tapasin also promotes MHC I-binding of peptides with a slow-off rate, thereby helping to shape the repertoire of presented peptides[25]. In this reaction, MHC-I molecules test the binding of many peptides and subsequently release most of these until a proper (low off-rate) peptide is bound[26]. These are usually peptides of a very specific length of 8–10 amino acids with appropriate anchor residues. Peptides that are too long can be trimmed by an ER resident aminopeptidase, ERAP1 (and ERAP 2 in some species)[27–29] before consideration by

MHC I molecules that are either in the peptide-loading complex or associating with another tapasin look-alike chaperone in the ER called TAPBPR. Like tapasin, TAPBPR also shapes the peptide repertoire on MHC I molecules [30,31]. Very interestingly, binding of peptides longer than 8–9 residues, but not shorter ones, triggers a conformational change in ERAP1 that activates its hydrolysis [32–34]. Through this mechanism, ERAP1 trims most peptides only down to 8–9 residues, corresponding to the size needed for optimal binding to MHC I molecules. In the end, the peptides that are available to be presented are the ones that have been cleaved to the right size and have somehow escaped further hydrolysis to a size that is too small to stably bind to MHC I molecules (Figure 3). Peptides that are unable to bind an MHC I molecule are ultimately translocated back into the cytosol for degradation[35]. Whether there are mechanisms that help to protect some of these peptides from destruction or release from the ER during the time before they bind MHC I molecules, is not entirely clear.

Peptides should be considered the third subunit of MHC I molecules as they are required to stabilize these complexes when the MHC I molecules are not bound to chaperones in the ER[36]. Peptides also allow the MHC I molecules to be released from the ER quality control system (the various chaperones) for transport to the cell surface for presentation to CD8+ T cells[37,38]. This system of low off-rate peptide selection, exporting only peptide-loaded MHC I complexes may help prevent healthy cells from easily replacing their bound endogenous peptides for exogenous antigenic peptides, an event that would lead to the presentation of peptides that do not reflect the status of a given cell and possible execution by CD8+ T cells.

Complexity in the MHC Class I Antigen Presentation Pathway

The general scheme outlined above, is somewhat more complex when taking into consideration the diversity of the MHC I family. Indeed, the different loci expressed (in humans, HLA-A, -B and –C) and the many polymorphic allelic forms behave somewhat differently with respect to expression, peptide binding and stability[39,40]. Peptides may also be generated from multiple sources. This is because the proteasome not only degrades proteins as part of normal protein turn over, but also degrades abnormal ones that arise from errors in translation, folding and/or pairing. The degradation of these disabled proteins prevents their aggregation and also potentially more directly couples protein translation to antigen presentation[41–43]. Such antigens are called defective ribosomal products (DRiPs) and may be produced in greater amounts during high protein synthesis conditions, such as occur during viral infection. The degradation of DRiPs would quickly generate peptides after initial translation of the antigen and this may allow rapid detection of infected cells [44,45].

While the source of antigens can be different, so can be the cleavage of these antigens by different proteasomes. Many presented peptides can be generated through the phylogenetically older ‘conventional’ proteasome. However, the development of the immune system coincided with the evolution of alternate forms of active site subunits for this particle, leading to the assembly of an immunoproteasome. A set of these subunits (β 1i, β 2i, β 5i) [46] is constitutively expressed in dendritic cells and lymphocytes and can be induced

Author Manuscript
Author Manuscript
Author Manuscript
Author Manuscript

in all other cells by interferons, for example during viral infections [47,48]. When these subunits are expressed, they preferentially incorporate into newly assembling particles to form immunoproteasomes, that generate a distinct set of peptides during protein degradation[49]. This shift from constitutive to immunoproteasome in cells often enhances the generation of peptides presented by MHC I molecules, including many unique ones[50]. Generation of new peptides will be at the cost of other peptide fragments that are cleaved to make the new fragment [51]. Another set of alternate active site subunits ($\beta 1i$, $\beta 2i$, $\beta 5t$) are expressed uniquely only in cortical thymic epithelial cells (cTECs), where they incorporate into thymoproteasome particles[52]. Among the peptides generated by thymoproteasomes, a number are unique and these play a critical role in the auditioning of developing CD8+ T cells during positive selection and also in allowing many of these cells to avoid subsequent negative selection [50]. Proteasomes but also the cytosolic and ER associated peptidases are variable in content and numbers. From this stew of proteolytic activities an estimated 0.02% of the peptides generated by the proteasome survive for presentation to the immune system [53](Figure 3).

Not How to Present... but What to Present

MHC I molecules present peptides from a cell's expressed genes and thereby allow the immune system to monitor the proteins synthesized in a cell. Yet, cells may also alter signalling in response to transformation or infection, resulting in an altered phosphoproteome[54], acetylome, glycome[55] or any other (small) post-translational modifications[56–58]. The peptide transporter TAP allows peptides with these small modifications to enter the ER and some of these can bind to MHC I molecules for presentation to CD8+ T cells. These modified peptides are in fact not genetically-encoded but neo-epitopes to which the immune system may not be tolerant[59,60]. This can allow the immune system to detect cells in abnormal states (e.g. transformed ones) for elimination. Other non-genetically encoded antigenic peptides arise by peptide splicing by the proteasome, where the proteasome in fact performs the opposite reaction, linking two peptide fragments into a new one[61]. Whether this is just a consequence of the reverse proteolysis reaction of the proteasome or is influenced by particular cellular states is unclear, but these peptides can be presented and stimulate CD8+ T cell responses. Through these various mechanisms the repertoires of MHC I-presented peptide (the “presentome”) is expanded beyond the genetically-encoded sequences and add additional options for the detection of abnormal cells, but also provide risks for auto-immune reactions.

How to Hide One's Inner Self? Pathogen and Tumor Escape of Antigen Presentation

While the MHC class I pathway evolved to allow detection and elimination of the nidi of viruses in an infected host, some viruses have co-evolved cloaking mechanisms to avoid such detection (Figure 4). A large majority of the human species – for example- is chronically infected with cytomegalovirus (CMV) and Herpes Simplex Virus (HSV). It is clear that these viruses have evolved ways to tamper with the process of antigen presentation [62]. CMV encodes proteins that inhibit the peptide transporter TAP or that induce the degradation of MHC I molecules in the ER or plasma membrane[63,64]. Other viruses shut down genomic MHC class I expression[65], produce a peptide mimic that blocks TAP or block the transport of MHC I molecules to the cell surface[66]. In fact, any step in the MHC

Author Manuscript
Author Manuscript
Author Manuscript
Author Manuscript

class I antigen presentation pathway not interfering with cell viability can be expected to be manipulated by viruses to prevent their presentation.

Since most of the steps in the MHC class I pathway are not essential for viability and because cancer cells are often genetically unstable, tumors can, under the selection pressure imposed by CD8+ T cells, generate variants that have lost key components of the MHC class I pathway and escape control by CD8+ T cells [67]. In fact, a reduction of MHC I molecule expression in human tumors is often detected by pathologists[68]. This is one of the reasons for assuming an important role of the immune system in the control of particular tumors, especially those with more neo-antigens (from mutated proteins) such as melanoma and lung cancer[69,70]. Understanding how a given tumor can evade detection by CD8+ T cells could help determine the immunotherapies that are most likely to succeed against that tumor.

Some Exceptions on Self-Presentation by MHC Class I Molecules

The MHC class I antigen presentation system is constructed in such a way that most cells exclusively present their own antigens. Because of this, it was thought that CD8+ T cells selectively eliminate infected cells without destroying neighbouring ‘innocent bystanders’. However, this concept is challenged by the fact that the cytosol of many healthy cells (unlike cancer cells) are connected by so-called gap junctions. These gap junctions allow peptide fragments to pass into their direct connected neighbouring cells for entry in their antigen presentation pathway and presentation through the neighbour’s MHC I molecules to CD8+ T cells[71,72]. It is likely that cytosolic peptidases will limit the spread of such peptides beyond the most proximal neighbouring cells. However, since the proximal cells are at high risk of viral invasion, gap junctions may allow their elimination even before real entry of the pathogen.

A more intensely studied system where the MHC-I presents antigens are different than those made by the cell itself is cross-presentation[73,74] (Figure 5). This pathway operates in dendritic cells and other phagocytes and is quite important because it plays a central role in immune surveillance 74–76]. It allows dendritic cells to acquire antigens from other infected cells and cancers in the periphery and then report their presence to naive CD8+ T cells in lymphoid organs in ways that initiate an immune response. Phagocytes acquire these antigens when they ingest them by phagocytosis (e.g. eating cell debris [77–79] or possibly even by taking a “bite” of living cells[80]) or via receptor-mediated endocytosis (e.g. of glycan modified proteins through lectin receptors or of antibody-bound antigens through Fc-receptors[81,82]). There is more than one mechanism by which ingested antigens can be cross-presented but one likely involves cytosolic transfer of antigen from the phagosome into the cytosol for degradation by the proteasome[83,84]. The fragments may then be loaded on MHC I molecules in the ER or translocated back into the phagosome for local MHC class I peptide loading[78]. In another mechanism, some antigens are degraded by lysosomal proteases and loaded onto recycling MHC class I molecules in a pathway similar to MHC class II molecules[85–87]. TLR signalling can induce the accumulation of MHC I in recycling endosomes to promote cross-presentation[88]. A potential limitation of this latter mechanism is that it could result in priming CD8+ T cells to different peptides than the ones the T cells will encounter in infected cells (as the priming peptides are generated by

Author Manuscript

Author Manuscript

Author Manuscript

Author Manuscript

proteases different from the proteasome). However, this may also be a problem in the phagosome-to-cytosol mechanism of cross presentation because in the absence of inflammation, immunoproteasomes in dendritic cells may also generate different fragments than the constitutive proteasome in most peripheral (and notably, tumor) cells [89]. Thus, whether and how cross-presentation allows activation of CD8+ T cells recognizing the full range of antigenic peptides presented by peripheral cells is unclear. Regardless of the exact mechanism, cross-presentation allows MHC I molecules to present peptides from antigens that usually are handled by MHC II molecules. The system employed by MHC II molecules for antigen presentation is understood in considerable more molecular detail and may share elements used for cross-presentation by MHC I molecules.

MHC class II Molecules

MHC II molecules are both similar and different from MHC I molecules, and so are their mechanisms of presentation. MHC II molecules are expressed on immune cells such as B cells, monocytes, macrophages and dendritic cells and on epithelial cells following inflammatory signals, while MHC I molecules are expressed more ubiquitously. MHC II molecules on dendritic cells present antigen to naïve CD4+ T cells to activate them, and later MHC II molecules participate in the interaction of B cells and macrophages with these specific CD4+ effector T cells[90]. This is a critical function as exemplified by patients with deficits in MHC class II expression (bare lymphocyte syndrome), which results in extreme susceptibility to infections to a variety of microorganisms and death at young age[91]. The structure of MHC class II resembles that of MHC class I and they are both polymorphic proteins (and thus transplantation antigens)[90, 92]. Interestingly, *Gadus morhua* fish (atlantic cod) lack MHC II but express an MHC I molecule containing endocytosis signals, that effectively takes over MHC II function, illustrating the strong relationship and conserved function of these two MHC classes [93]. However, the nature of the presented peptides usually differ and so does the underlying biology of MHC class II antigen presentation.

How to Present the Outside World?

MHC class II presents peptide fragments that are generally larger than those presented by MHC class I, because the peptide-binding groove of MHC class II is open, allowing peptides to extend out of this site[94]. The MHC class II associated peptides are derived from extracellular proteins and from self-proteins that are degraded in the endosomal pathway (Figure 6)[95]. MHC II molecules associate during their assembly in the ER with the invariant chain Ii that acts as a pseudopeptide by filling the MHC class II peptide-binding groove and in addition targets MHC II molecules into the endosomal pathway through its cytosolic dileucine motif[20, 96]. In a compartment commonly named MIIC[97], MHC II molecules then meet antigenic fragments generated by resident proteases. In order for these peptides to bind MHC II molecules, the invariant chain has to be degraded by the same mix of proteases, especially cathepsin L and S[90]. This leaves an invariant chain fragment (called CLIP) inaccessible for proteases and remaining in the peptide-binding groove of MHC II molecules[98]. This CLIP fragment has to be exchanged for higher affinity peptides with the help of a dedicated MHC class II-like chaperone called DM (in human, HLA-DM)

[99]. The structure of HLA-DM in association with MHC-II (HLA-DR1) reveals that DM locally opens the groove to release low-affinity peptides such as CLIP. DM release from MHC class II then locks the proper peptide fragments in the MHC class II peptide-binding groove[100]. After some residence in MIIC, MHC II molecules move to the plasma membrane either via vesicular transport or in the form of tubules[101–103]. Since the targeting information in the invariant chain has been removed after its degradation in MIIC, MHC II molecules can stably reside on the plasma membrane.

Variations in MHC class II presentation

Like for MHC I molecules, there are also different MHC II loci in most species (in man three named HLA-DR, HLA-DQ and HLA-DP). Also, MHC II molecules are polymorphic (>3,000 alleles known) [90] and their polymorphic amino acids similarly cluster in and around the peptide-binding groove, shaping the peptide-binding pockets. Consequently, different MHC II alleles bind different peptides by virtue of their different anchor residues[104]. This likely explains why different MHC II alleles link strongly to defined auto-immune diseases [105] and immune responses against external environmental and food antigens[90]. This is well illustrated for the link between gluten sensitivity (Celiac disease) and the MHC class II allele HLA-DQ2. HLA-DQ2 is able to present a peptide from gluten after de-amination by tissue transglutaminase to activate CD4+ T cells and drives the disease[106]. The dominant antigens for auto-immune diseases are often not clear but there are some suggestions. For example, insulin has been suspected to mediate HLA-DR3/4 associated Type I Diabetes and myelin basic protein to participate in HLA-DR1 related Multiple Sclerosis[107, 108]. One additional mechanism involves the presentation of an atypical conformation of a peptide [109] as the result of peptide-loading of MHC II molecules in compartments that lack DM molecules, such as may occur in recycling endocytic compartments [110] or in the ER [111,112]. In the absence of DM's function, the non-optimal peptide conformation bound to MHC II is not corrected. A different conformation of a self-peptide can be recognized as non-self by the CD4+ T cells that may drive the induction of auto-antibodies[109]. Yet, the fact that many people with these MHC class II alleles never develop auto-immune diseases and that for most of these conditions well less than half of identical twins are concordant for disease, indicates that epigenetic and other factors must also be involved and these are as of yet unclear.

Next to genetic variation resulting in polymorphism of MHC II molecules, another variation in the life of MHC class II lies with the associated invariant chain, that is actually not so invariant. In fact, there are multiple splice variants including one (p44) that contains an additional protease inhibitor (cystatin) domain[90]. This variant can be expected to modify the protease activities involved in antigen preparation for MHC II molecules. The proteases (cathepsins in the endosomal pathway) also vary in the different MHC class II-expressing immune cells, as do natural inhibitors for these cathepsins (called cystatins)[90,96]. Likely, antigens are degraded after denaturation (which involves the reduction of their disulphide bonds by the enzyme GILT[113], and acidic pH[114]) by a swarm of proteases that will generate and destroy potential peptides for a defined MHC II allele.

Author Manuscript

Author Manuscript

Author Manuscript

Author Manuscript

Peptides are selected for presentation by MHC II with the help of the chaperone DM. DM can be further controlled by a dedicated co-chaperone called DO (HLA-DO in man) that strongly pairs with DM[115]. DO associates to DM at the same interface as occupied by MHC II molecules [100] and thus inhibits DM-assisted peptide loading of MHC II molecules unless the DM-DO complex enters very acidic endosomes along with MHC II molecules[116,117]. DO thus shapes the peptide repertoire by preventing peptide binding in earlier vesicular compartments. Deleting DO induces type I diabetes in mouse models and possibly other autoimmune diseases[118].

Other variations entail the transport and surface half-life of MHC II molecules. MHC II transport from MIIC to the plasma membrane is not constitutive but controlled in dendritic cells, monocytes and B cells. Activation of dendritic cells promotes MHC II transport to the cell surface and strongly enhances the half-life of these molecules on the plasma membrane[119, 120]. As a result, activated dendritic cells have high numbers (around 2 million per cell) of MHC II molecules on the cell surface that continue to present antigens for long periods. However, there are also other ways to control MHC II expression. For example, in human monocytes IL-10 increases the expression of an ubiquitin ligase membrane associated RING-CH1 (MARCH-1) that ubiquitinates the tail of cell surface MHC II molecules initiating their rapid internalization and destruction[121]. Genome-wide analyses have identified many factors that control the complex process of control of MHC II expression and transport in dendritic cells[122]. Many pathogens, especially those residing in MHC II-containing phagosomes, also inhibit MHC II expression or peptide loading[123, 124]. Such immune evasion by pathogens may be caused by manipulation of DM interactions with MHC II molecules, manipulation of pH levels, alteration of protein networks, and induction of MHC ubiquitination by MARCH homologs [125], or other processes required for optimal antigen presentation by MHC II molecules.

Concluding Remarks and Future Perspectives

The work of many labs over the last decades has informed our understanding of the function of MHC class I and MHC class II molecules at the immunological, cell biological, genetic and atomic level. Many of the major mechanisms of both the MHC I and MHC II pathways are understood and we can look forward to an even more comprehensive understanding of the antigen presentation mechanisms in the coming years. With such knowledge, we can look forward to better understanding how these processes help to maintain health and/or contribute to disease pathogenesis. We anticipate that there will be the strong potential to translate this knowledge into clinical medicine. One important area is in cancer immunotherapy. While the role of MHC class I and -II antigen presentation in tumor immunology was initially restricted to curing cancer in mouse models, the recent development of checkpoint inhibitor antibodies has translated this into clinical responses in human melanoma, lung cancer and other tumors[126]. Characterizing the defects in antigen presentation in such tumors might in theory help identify patients who can or cannot respond to such interventions. Moreover, if methods can be developed to reverse such defects, they might be able to improve efficacy of these immunotherapies. Similarly, manipulating antigen presentation pathways might overcome the inhibition of antigen presentation induced by certain microbes, and then help eliminate these chronic infections. The rules for antigen

presentation by MHC I molecules can be used to predict neo-epitopes detected by CD8+ T cells[127] and this information might be exploited to actively immunize cancer patients in conjunction with removal of checkpoint control and also to monitor patient responses.

Targeting antigens into dendritic cells and in particular into specific presentation pathways has the potential to generate more robust and effective kinds of responses to vaccines and immunotherapies. On the other hand, antigen presentation might be manipulated in the opposite way to dampen autoimmune diseases, e.g. with tolerogenic peptides or tolerogenic antigen presenting cells. Despite the remarkable advances in our knowledge about antigen presentation, the picture is still incomplete but should continue to improve. For example, forward genetic screens are uncovering unsuspected new components in the pathways [122,128]. Filling in these gaps (see Outstanding Questions) should provide a higher resolution understanding of the pathways and their contribution to disease pathogenesis, as well as increasing the opportunities to exploit these pathways to develop better immunotherapies to prevent and/or treat disease.

Supplementary Material

Refer to Web version on PubMed Central for supplementary material.

Acknowledgments

The work was supported by grants from NWO-TOP and an ERC Advanced grant to JN and NIH grants RO1AI114495 and RO1AI110374 to KLR

References

- Flajnik MF, Kasahara M. Origin and evolution of the adaptive immune system: genetic events and selective pressures. *Nature reviews Genetics*. 2010; 11:47–59.
- Brown JH, et al. Three-dimensional structure of the human class II histocompatibility antigen HLA-DR1. *Nature*. 1993; 364:33–39. [PubMed: 8316295]
- Bjorkman PJ, et al. The foreign antigen binding site and T cell recognition regions of class I histocompatibility antigens. *Nature*. 1987; 329:512–518. [PubMed: 2443855]
- Zhang P, et al. Crystal structure of the stress-inducible human heat shock protein 70 substrate-binding domain in complex with peptide substrate. *PloS one*. 2014; 9:e103518. [PubMed: 25058147]
- Dong G, et al. Insights into MHC class I peptide loading from the structure of the tapasin-ERp57 thiol oxidoreductase heterodimer. *Immunity*. 2009; 30:21–32. [PubMed: 19119025]
- Teng MS, et al. A human TAPBP (TAPASIN)-related gene, TAPBP-R. *European journal of immunology*. 2002; 32:1059–1068. [PubMed: 11920573]
- Boyle LH, et al. Tapasin-related protein TAPBPR is an additional component of the MHC class I presentation pathway. *Proc Natl Acad Sci U S A*. 2013; 110:3465–3470. [PubMed: 23401559]
- Mosyak L, et al. The structure of HLA-DM, the peptide exchange catalyst that loads antigen onto class II MHC molecules during antigen presentation. *Immunity*. 1998; 9:377–383. [PubMed: 9768757]
- Fremont DH, et al. Crystal structure of mouse H2-M. *Immunity*. 1998; 9:385–393. [PubMed: 9768758]
- Guce AI, et al. HLA-DO acts as a substrate mimic to inhibit HLA-DM by a competitive mechanism. *Nature structural & molecular biology*. 2013; 20:90–98.
- Falk K, et al. Pool sequencing of natural HLA-DR, DQ, and DP ligands reveals detailed peptide motifs, constraints of processing, and general rules. *Immunogenetics*. 1994; 39:230–242. [PubMed: 8119729]

- Author Manuscript
- Author Manuscript
- Author Manuscript
- Author Manuscript
12. Falk K, et al. Allele-specific motifs revealed by sequencing of self-peptides eluted from MHC molecules. *Nature*. 1991; 351:290–296. [PubMed: 1709722]
 13. Madden DR, et al. The antigenic identity of peptide-MHC complexes: a comparison of the conformations of five viral peptides presented by HLA-A2. *Cell*. 1993; 75:693–708. [PubMed: 7694806]
 14. Smith KJ, et al. Bound water structure and polymorphic amino acids act together to allow the binding of different peptides to MHC class I HLA-B53. *Immunity*. 1996; 4:215–228. [PubMed: 8624812]
 15. Walz S, et al. The antigenic landscape of multiple myeloma: mass spectrometry (re)defines targets for T-cell-based immunotherapy. *Blood*. 2015; 126:1203–1213. [PubMed: 26138685]
 16. Schmid BV, et al. Quantifying how MHC polymorphism prevents pathogens from adapting to the antigen presentation pathway. *Epidemics*. 2010; 2:99–108. [PubMed: 21352780]
 17. Chaix R, Cao C, Donnelly P. Is mate choice in humans MHC-dependent? *PLoS Genet*. 2008; 4:e1000184. [PubMed: 18787687]
 18. Siddle HV, et al. Characterization of major histocompatibility complex class I and class II genes from the Tasmanian devil (*Sarcophilus harrisii*). *Immunogenetics*. 2007; 59:753–760. [PubMed: 17673996]
 19. Siddle HV, et al. Reversible epigenetic down-regulation of MHC molecules by devil facial tumour disease illustrates immune escape by a contagious cancer. *Proc Natl Acad Sci U S A*. 2013; 110:5103–5108. [PubMed: 23479617]
 20. Neefjes J, et al. Towards a systems understanding of MHC class I and MHC class II antigen presentation. *Nature reviews Immunology*. 2011; 11:823–836.
 21. Michalek MT, et al. A role for the ubiquitin-dependent proteolytic pathway in MHC class I-restricted antigen presentation. *Nature*. 1993; 363:552–554. [PubMed: 8389422]
 22. Rock KL, et al. Inhibitors of the proteasome block the degradation of most cell proteins and the generation of peptides presented on MHC class I molecules. *Cell*. 1994; 78:761–771. [PubMed: 8087844]
 23. Reits E, et al. Peptide diffusion, protection, and degradation in nuclear and cytoplasmic compartments before antigen presentation by MHC class I. *Immunity*. 2003; 18:97–108. [PubMed: 12530979]
 24. Cresswell P, et al. The nature of the MHC class I peptide loading complex. *Immunological reviews*. 1999; 172:21–28. [PubMed: 10631934]
 25. Wearsch PA, Cresswell P. Selective loading of high-affinity peptides onto major histocompatibility complex class I molecules by the tapasin-ERp57 heterodimer. *Nature immunology*. 2007; 8:873–881. [PubMed: 17603487]
 26. Garstka MA, et al. The first step of peptide selection in antigen presentation by MHC class I molecules. *Proc Natl Acad Sci U S A*. 2015; 112:1505–1510. [PubMed: 25605945]
 27. Saveanu L, et al. Concerted peptide trimming by human ERAP1 and ERAP2 aminopeptidase complexes in the endoplasmic reticulum. *Nature immunology*. 2005; 6:689–697. [PubMed: 15908954]
 28. Saric T, et al. An IFN-gamma-induced aminopeptidase in the ER, ERAP1, trims precursors to MHC class I-presented peptides. *Nature immunology*. 2002; 3:1169–1176. [PubMed: 12436109]
 29. Serwold T, et al. ERAAP customizes peptides for MHC class I molecules in the endoplasmic reticulum. *Nature*. 2002; 419:480–483. [PubMed: 12368856]
 30. Morozov GI, et al. Interaction of TAPBPR, a tapasin homolog, with MHC-I molecules promotes peptide editing. *Proc Natl Acad Sci U S A*. 2016; 113:E1006–E1015. [PubMed: 26869717]
 31. Hermann C, et al. TAPBPR alters MHC class I peptide presentation by functioning as a peptide exchange catalyst. *eLife*. 2015; 4
 32. Chang SC, et al. The ER aminopeptidase, ERAP1, trims precursors to lengths of MHC class I peptides by a "molecular ruler" mechanism. *Proc Natl Acad Sci U S A*. 2005; 102:17107–17112. [PubMed: 16286653]
 33. York IA, et al. The ER aminopeptidase ERAP1 enhances or limits antigen presentation by trimming epitopes to 8–9 residues. *Nature immunology*. 2002; 3:1177–1184. [PubMed: 12436110]

34. Nguyen TT, et al. Structural basis for antigenic peptide precursor processing by the endoplasmic reticulum aminopeptidase ERAP1. *Nature structural & molecular biology*. 2011; 18:604–613.
35. Roelse J, et al. Trimming of TAP-translocated peptides in the endoplasmic reticulum and in the cytosol during recycling. *J. Exp. Med.* 1994; 180:1591–1597. 127. [PubMed: 7964447]
36. Elliott T, et al. Peptide-induced conformational change of the class I heavy chain. *Nature*. 1991; 351:402–406. [PubMed: 2034289]
37. Schumacher TN, et al. Direct binding of peptide to empty MHC class I molecules on intact cells and in vitro. *Cell*. 1990; 62:563–567. [PubMed: 2199065]
38. Kelly A, et al. Assembly and function of the two ABC transporter proteins encoded in the human major histocompatibility complex. *Nature*. 1992; 355:641–644. [PubMed: 1538751]
39. Neefjes JJ, Ploegh HL. Allele and locus-specific differences in cell surface expression and the association of HLA class I heavy chain with beta 2-microglobulin: differential effects of inhibition of glycosylation on class I subunit association. *European journal of immunology*. 1988; 18:801–810. [PubMed: 2967765]
40. Rammensee H, et al. SYFPEITHI: database for MHC ligands and peptide motifs. *Immunogenetics*. 1999; 50:213–219. [PubMed: 10602881]
41. Schubert U, et al. Proteasome inhibition interferes with gag polyprotein processing, release, and maturation of HIV-1 and HIV-2. *Proc Natl Acad Sci U S A*. 2000; 97:13057–13062. [PubMed: 11087859]
42. Princiotta MF, et al. Quantitating protein synthesis, degradation, and endogenous antigen processing. *Immunity*. 2003; 18:343–354. [PubMed: 12648452]
43. Reits EA, et al. The major substrates for TAP in vivo are derived from newly synthesized proteins. *Nature*. 2000; 404:774–778. [PubMed: 10783892]
44. Yewdell JW. DRiPs solidify: progress in understanding endogenous MHC class I antigen processing. *Trends in immunology*. 2011; 32:548–558. [PubMed: 21962745]
45. Rock KL, et al. Re-examining class-I presentation and the DRiP hypothesis. *Trends in immunology*. 2014; 35:144–152. [PubMed: 24566257]
46. Monaco JJ, Nandi D. The genetics of proteasomes and antigen processing. *Annual review of genetics*. 1995; 29:729–754.
47. Gaczynska M, et al. Gamma-interferon and expression of MHC genes regulate peptide hydrolysis by proteasomes. *Nature*. 1993; 365:264–267. [PubMed: 8396732]
48. Groettrup M, et al. A third interferon-gamma-induced subunit exchange in the 20S proteasome. *European journal of immunology*. 1996; 26:863–869. [PubMed: 8625980]
49. Toes RE, et al. Discrete cleavage motifs of constitutive and immunoproteasomes revealed by quantitative analysis of cleavage products. *The Journal of experimental medicine*. 2001; 194:1–12. [PubMed: 11435468]
50. Kincaid EZ, et al. Specialized proteasome subunits have an essential role in the thymic selection of CD8(+) T cells. *Nat. Immunol.* 2016; 17:938–945. [PubMed: 27294792]
51. Ossendorp F, et al. A single residue exchange within a viral CTL epitope alters proteasome-mediated degradation resulting in lack of antigen presentation. *Immunity*. 1996; 5:115–124. [PubMed: 8769475]
52. Tomaru U, et al. Exclusive expression of proteasome subunit beta5t in the human thymic cortex. *Blood*. 2009; 113:5186–5191. [PubMed: 19289856]
53. Yewdell JW, Reits E, Neefjes J. Making sense of mass destruction: quantitating MHC class I antigen presentation. *Nat. Rev. Immunol.* 2003; 3:952–961. [PubMed: 14647477]
54. Meyer VS, et al. Identification of natural MHC class II presented phosphopeptides and tumor-derived MHC class I phospholigands. *Journal of proteome research*. 2009; 8:3666–3674. [PubMed: 19415920]
55. Haurum JS, et al. Presentation of cytosolic glycosylated peptides by human class I major histocompatibility complex molecules in vivo. *The Journal of experimental medicine*. 1999; 190:145–150. [PubMed: 10429679]
56. Petersen J, et al. Post-translationally modified T cell epitopes: immune recognition and immunotherapy. *Journal of molecular medicine*. 2009; 87:1045–1051. [PubMed: 19763524]

57. Gromme M, et al. The rational design of TAP inhibitors using peptide substrate modifications and peptidomimetics. *European journal of immunology*. 1997; 27:898–904. [PubMed: 9130642]
58. Andersen MH, et al. Phosphorylated peptides can be transported by TAP molecules, presented by class I MHC molecules, and recognized by phosphopeptide-specific CTL. *Journal of immunology*. 1999; 163:3812–3818.
59. Mohammed F, et al. Phosphorylation-dependent interaction between antigenic peptides and MHC class I: a molecular basis for the presentation of transformed self. *Nature immunology*. 2008; 9:1236–1243. [PubMed: 18836451]
60. Zarling AL, et al. Phosphorylated peptides are naturally processed and presented by major histocompatibility complex class I molecules in vivo. *The Journal of experimental medicine*. 2000; 192:1755–1762. [PubMed: 11120772]
61. Berkers CR, et al. Definition of Proteasomal Peptide Splicing Rules for High-Efficiency Spliced Peptide Presentation by MHC Class I Molecules. *Journal of immunology*. 2015; 195:4085–4095.
62. Ploegh HL. Viral strategies of immune evasion. *Science*. 1998; 280:248–253. [PubMed: 9535648]
63. Ploegh HL. Trafficking and assembly of MHC molecules: how viruses elude the immune system. *Cold Spring Harbor symposia on quantitative biology*. 1995; 60:263–266. [PubMed: 8824399]
64. van Hall T, et al. The varicellovirus-encoded TAP inhibitor UL49.5 regulates the presentation of CTL epitopes by Qa-1b1. *Journal of immunology*. 2007; 178:657–662.
65. Lichtenstein DL, Wold WS. Experimental infections of humans with wild-type adenoviruses and with replication-competent adenovirus vectors: replication, safety, and transmission. *Cancer gene therapy*. 2004; 11:819–829. [PubMed: 15359291]
66. Ziegler H, et al. The luminal part of the murine cytomegalovirus glycoprotein gp40 catalyzes the retention of MHC class I molecules. *The EMBO journal*. 2000; 19:870–881. [PubMed: 10698929]
67. Mittal D, et al. New insights into cancer immunoediting and its three component phases-- elimination, equilibrium and escape. *Current opinion in immunology*. 2014; 27:16–25. [PubMed: 24531241]
68. Garcia-Lora A, et al. MHC class I antigens, immune surveillance, and tumor immune escape. *Journal of cellular physiology*. 2003; 195:346–355. [PubMed: 12704644]
69. Snyder A, et al. Genetic basis for clinical response to CTLA-4 blockade in melanoma. *The New England journal of medicine*. 2014; 371:2189–2199. [PubMed: 25409260]
70. Smit EF, Baas P. Lung cancer in 2015: Bypassing checkpoints, overcoming resistance, and honing in on new targets. *Nature reviews Clinical oncology*. 2016; 13:75–76.
71. Saccheri F, et al. Bacteria-induced gap junctions in tumors favor antigen cross-presentation and antitumor immunity. *Science translational medicine*. 2010; 2:44ra57.
72. Neijissen J, et al. Cross-presentation by intercellular peptide transfer through gap junctions. *Nature*. 2005; 434:83–88. [PubMed: 15744304]
73. Bevan MJ. Cross-priming for a secondary cytotoxic response to minor H antigens with H-2 congenic cells which do not cross-react in the cytotoxic assay. *The Journal of experimental medicine*. 1976; 143:1283–1288. [PubMed: 1083422]
74. Rock KL, et al. Presentation of exogenous antigen with class I major histocompatibility complex molecules. *Science*. 1990; 249:918–921. [PubMed: 2392683]
75. Kurts C, et al. Cross-priming in health and disease. *Nature reviews Immunology*. 2010; 10:403–414.
76. Amigorena S. Y in X priming. *Nature immunology*. 2003; 4:1047–1048. [PubMed: 14586419]
77. Segura E, Amigorena S. Cross-Presentation in Mouse and Human Dendritic Cells. *Advances in immunology*. 2015; 127:1–31. [PubMed: 26073982]
78. Guermonprez P, et al. ER-phagosome fusion defines an MHC class I cross-presentation compartment in dendritic cells. *Nature*. 2003; 425:397–402. [PubMed: 14508489]
79. Zitvogel L, et al. Immunological aspects of anticancer chemotherapy. *Bulletin de l'Academie nationale de medecine*. 2008; 192:1469–1487.
80. Kovacsics-Bankowski M, et al. Efficient major histocompatibility complex class I presentation of exogenous antigen upon phagocytosis by macrophages. *Proc Natl Acad Sci U S A*. 1993; 90:4942–4946. [PubMed: 8506338]

81. Matheoud D, et al. Cross-presentation by dendritic cells from live cells induces protective immune responses in vivo. *Blood*. 2010; 115:4412–4420. [PubMed: 20308597]
82. Amigorena S. Fc gamma receptors and cross-presentation in dendritic cells. *The Journal of experimental medicine*. 2002; 195:F1–F3. [PubMed: 11781374]
83. Schuette V, Burgdorf S. The ins-and-outs of endosomal antigens for cross-presentation. *Current opinion in immunology*. 2014; 26:63–68. [PubMed: 24556402]
84. Joffre OP, et al. Cross-presentation by dendritic cells. *Nature reviews Immunology*. 2012; 12:557–569.
85. Kovacsovics-Bankowski M, Rock KL. A phagosome-to-cytosol pathway for exogenous antigens presented on MHC class I molecules. *Science*. 1995; 267:243–246. [PubMed: 7809629]
86. Gromme M, et al. Recycling MHC class I molecules and endosomal peptide loading. *Proc Natl Acad Sci U S A*. 1999; 96:10326–10331. [PubMed: 10468607]
87. Dorsey BD, et al. Discovery of a potent, selective, and orally active proteasome inhibitor for the treatment of cancer. *Journal of medicinal chemistry*. 2008; 51:1068–1072. [PubMed: 18247547]
88. Shen L, et al. Important role of cathepsin S in generating peptides for TAP-independent MHC class I crosspresentation in vivo. *Immunity*. 2004; 21:155–165. [PubMed: 15308097]
89. Nair-Gupta P, et al. TLR signals induce phagosomal MHC-I delivery from the endosomal recycling compartment to allow cross-presentation. *Cell*. 2014; 158:506–521. [PubMed: 25083866]
90. Unanue ER, et al. Variations in MHC Class II Antigen Processing and Presentation in Health and Disease. *Annual review of immunology*. 2016; 34:265–297.
91. Waldburger JM, et al. Lessons from the bare lymphocyte syndrome: molecular mechanisms regulating MHC class II expression. *Immunological reviews*. 2000; 178:148–165. [PubMed: 11213800]
92. Jones EY. MHC class I and class II structures. *Current opinion in immunology*. 1997; 9:75–79. [PubMed: 9039778]
93. Malmstrom M, et al. Unraveling the Evolution of the Atlantic Cod's (*Gadus morhua* L.) Alternative Immune Strategy. *PLoS ONE*. 2013; 8:e74004. [PubMed: 24019946]
94. Stern LJ, et al. Crystal structure of the human class II MHC protein HLA-DR1 complexed with an influenza virus peptide. *Nature*. 1994; 368:215–221. [PubMed: 8145819]
95. Suri A, et al. The wide diversity and complexity of peptides bound to class II MHC molecules. *Current opinion in immunology*. 2006; 18:70–77. [PubMed: 16316750]
96. Cresswell P, Roche PA. Invariant chain-MHC class II complexes: always odd and never invariant. *Immunology and cell biology*. 2014; 92:471–472. [PubMed: 24777311]
97. Neefjes J. CIV, MIIC and other compartments for MHC class II loading. *European journal of immunology*. 1999; 29:1421–1425. [PubMed: 10359095]
98. Ghosh P, et al. The structure of an intermediate in class II MHC maturation: CLIP bound to HLA-DR3. *Nature*. 1995; 378:457–462. [PubMed: 7477400]
99. Denzin LK, Cresswell P. HLA-DM induces CLIP dissociation from MHC class II alpha beta dimers and facilitates peptide loading. *Cell*. 1995; 82:155–165. [PubMed: 7606781]
100. Pos W, et al. Crystal structure of the HLA-DM-HLA-DR1 complex defines mechanisms for rapid peptide selection. *Cell*. 2012; 151:1557–1568. [PubMed: 23260142]
101. Wubbolts R, et al. Direct vesicular transport of MHC class II molecules from lysosomal structures to the cell surface. *The Journal of cell biology*. 1996; 135:611–622. [PubMed: 8909537]
102. Boes M, et al. T-cell engagement of dendritic cells rapidly rearranges MHC class II transport. *Nature*. 2002; 418:983–988. [PubMed: 12198548]
103. Kleijmeer M, et al. Reorganization of multivesicular bodies regulates MHC class II antigen presentation by dendritic cells. *The Journal of cell biology*. 2001; 155:53–63. [PubMed: 11581285]
104. Nielsen M, et al. NetMHCIIpan-2.0 - Improved pan-specific HLA-DR predictions using a novel concurrent alignment and weight optimization training procedure. *Immunome research*. 2010; 6:9. [PubMed: 21073747]
105. Fernando MM, et al. Defining the role of the MHC in autoimmunity: a review and pooled analysis. *PLoS genetics*. 2008; 4:e1000024. [PubMed: 18437207]

106. Solid LM, Jabri B. Celiac disease and transglutaminase 2: a model for posttranslational modification of antigens and HLA association in the pathogenesis of autoimmune disorders. *Current opinion in immunology*. 2011; 23:732–738. [PubMed: 21917438]
107. Steck AK, Rewers MJ. Genetics of type 1 diabetes. *Clinical chemistry*. 2011; 57:176–185. [PubMed: 21205883]
108. Pette M, et al. Myelin autoreactivity in multiple sclerosis: recognition of myelin basic protein in the context of HLA-DR2 products by T lymphocytes of multiple-sclerosis patients and healthy donors. *Proc Natl Acad Sci U S A*. 1990; 87:7968–7972. [PubMed: 1700423]
109. Wan X, Thomas JW, Unanue ER. Class-switched anti-insulin antibodies originate from unconventional antigen presentation in multiple lymphoid sites. *J. Exp. Med.* 2016; 213:967–978. [PubMed: 27139492]
110. Sinnathamby G, Eisenlohr LC. Presentation by recycling MHC class II molecules of an influenza hemagglutinin-derived epitope that is revealed in the early endosome by acidification. *J Immunol*. 2003; 170:3504–3513. [PubMed: 12646611]
111. Tewari MK, et al. A cytosolic pathway for MHC class II-restricted antigen processing that is proteasome and TAP dependent. *Nat Immunol*. 2005; 6:287–294. [PubMed: 15711549]
112. van Luijn MM, et al. Alternative Ii-independent antigen-processing pathway in leukemic blasts involves TAP-dependent peptide loading of HLA class II complexes. *Cancer Immunol Immunother*. 2010; 59:1825–1838. [PubMed: 20820776]
113. Maric M, et al. Defective antigen processing in GILT-free mice. *Science*. 2001; 294:1361–1365. [PubMed: 11701933]
114. Ziegler HK, Unanue ER. Decrease in macrophage antigen catabolism caused by ammonia and chloroquine is associated with inhibition of antigen presentation to T cells. *Proc Natl Acad Sci U S A*. 1982; 79:175–178. [PubMed: 6798568]
115. Liljedahl M, et al. HLA-DO is a lysosomal resident which requires association with HLA-DM for efficient intracellular transport. *The EMBO journal*. 1996; 15:4817–4824. [PubMed: 8890155]
116. Denzin LK, et al. Negative regulation by HLA-DO of MHC class II-restricted antigen processing. *Science*. 1997; 278:106–109. [PubMed: 9311912]
117. van Ham SM, et al. HLA-DO is a negative modulator of HLA-DM-mediated MHC class II peptide loading. *Current biology*. 1997; 7:950–957. [PubMed: 9382849]
118. Yi W, et al. Targeted regulation of self-peptide presentation prevents type I diabetes in mice without disrupting general immunocompetence. *The Journal of clinical investigation*. 2010; 120:1324–1336. [PubMed: 20200448]
119. Cella M, et al. Inflammatory stimuli induce accumulation of MHC class II complexes on dendritic cells. *Nature*. 1997; 388:782–787. [PubMed: 9285591]
120. Pierre P, et al. Developmental regulation of MHC class II transport in mouse dendritic cells. *Nature*. 1997; 388:787–792. [PubMed: 9285592]
121. Thibodeau J, et al. Interleukin-10-induced MARCH1 mediates intracellular sequestration of MHC class II in monocytes. *European journal of immunology*. 2008; 38:1225–1230. [PubMed: 18389477]
122. Paul P, et al. A Genome-wide multidimensional RNAi screen reveals pathways controlling MHC class II antigen presentation. *Cell*. 2011; 145:268–283. [PubMed: 21458045]
123. Mitchell EK, et al. Inhibition of cell surface MHC class II expression by Salmonella. *European journal of immunology*. 2004; 34:2559–2567. [PubMed: 15307188]
124. Zwart W, et al. Spatial separation of HLA-DM/HLA-DR interactions within MIIC and phagosome-induced immune escape. *Immunity*. 2005; 22:221–233. [PubMed: 15723810]
125. van Niel G, et al. Dendritic cells regulate exposure of MHC class II at their plasma membrane by oligoubiquitination. *Immunity*. 2006; 25:885–894. [PubMed: 17174123]
126. Pennock GK, Chow LQ. The Evolving Role of Immune Checkpoint Inhibitors in Cancer Treatment. *The oncologist*. 2015; 20:812–822. [PubMed: 26069281]
127. Schumacher TN, Schreiber RD. Neoantigens in cancer immunotherapy. *Science*. 2015; 348:69–74. [PubMed: 25838375]

128. Jongsma ML, Berlin I, et al. An ER-Associated Pathway Defines Endosomal Architecture for Controlled Cargo Transport. *Cell*. 2016; 166:152–166. [PubMed: 27368102]
129. Saveanu L, et al. IRAP identifies an endosomal compartment required for MHC class I cross-presentation. *Science*. 2009; 325:213–217. [PubMed: 19498108]

Author Manuscript

Author Manuscript

Author Manuscript

Author Manuscript

Outstanding questions

While antigen presentation by MHC molecules has been intensively studied for over almost 40 years, many aspects are still unclear. For example (and note that this is only a partial listing):

- Why can peptides presented by MHC molecules not be more accurately predicted? What are we missing?
- What are the many proteases involved in generating and destroying presented peptides, and what is their relative contribution and specificity?
- How do the antigen presentation pathways so successfully present a broad peptidome from very large numbers of different proteins of very different abundances and in the face of robust peptide destruction?
- Are there mechanisms that protect peptides from destruction before they bind to MHC molecules?
- The components in the MHC antigen presentation pathway have remarkable heterogeneity in expression and activity in different tissues. Does that lead to different presentation of self-antigens and contribute to auto-immune responses?
- Why do we have three different proteasomes?
- Why do we express only three MHC I and three MHC II locus products and not more to cover all possible peptides for presentation?
- What is the major mechanism(s) that generate DRIPS? - Inaccurate transcription, translation, folding or assembly?
- Is antigen cross-presentation the result of many different systems or are there dominant systems?
- For cross-presentation, how are antigens transported from endosomes into the cytosol?
- For cross-presentation, how are MHC I molecules kept stable during transport to and after arrival in endosomes?
- Are there mechanisms that promote the loading of peptides in endosomes for cross presentation?
- Do dendritic cells or specific subsets of dendritic cells have unique components that promote cross presentation?
- How are hydrophobic peptides delivered in the peptide binding groove of MHC I and MHC II molecules? Are there unique chaperones for such peptides?
- Is there an MHC class II Peptide-Loading Complex?

Author Manuscript

Author Manuscript

Author Manuscript

Author Manuscript

Trends

MHC molecules are critical in transplantation, auto-immunity, infections and tumor immunotherapy.

The biology of antigen presentation by MHC I and MHC II molecules provides targets for manipulation of these diseases.

This biology also explains the fragments presented to the immune system and the cellular evolutionary race to escape immune control of infected and transformed cells.

Many of the players determining antigen degradation and subsequent peptide-loading on MHC molecules are defined and are helping to improve the accuracy of predicting presented fragments.

The combined understanding of antigen presentation by MHC molecules allows exploitation to improve the responses of the cellular arm of the immune system to vaccinations and immunotherapies.

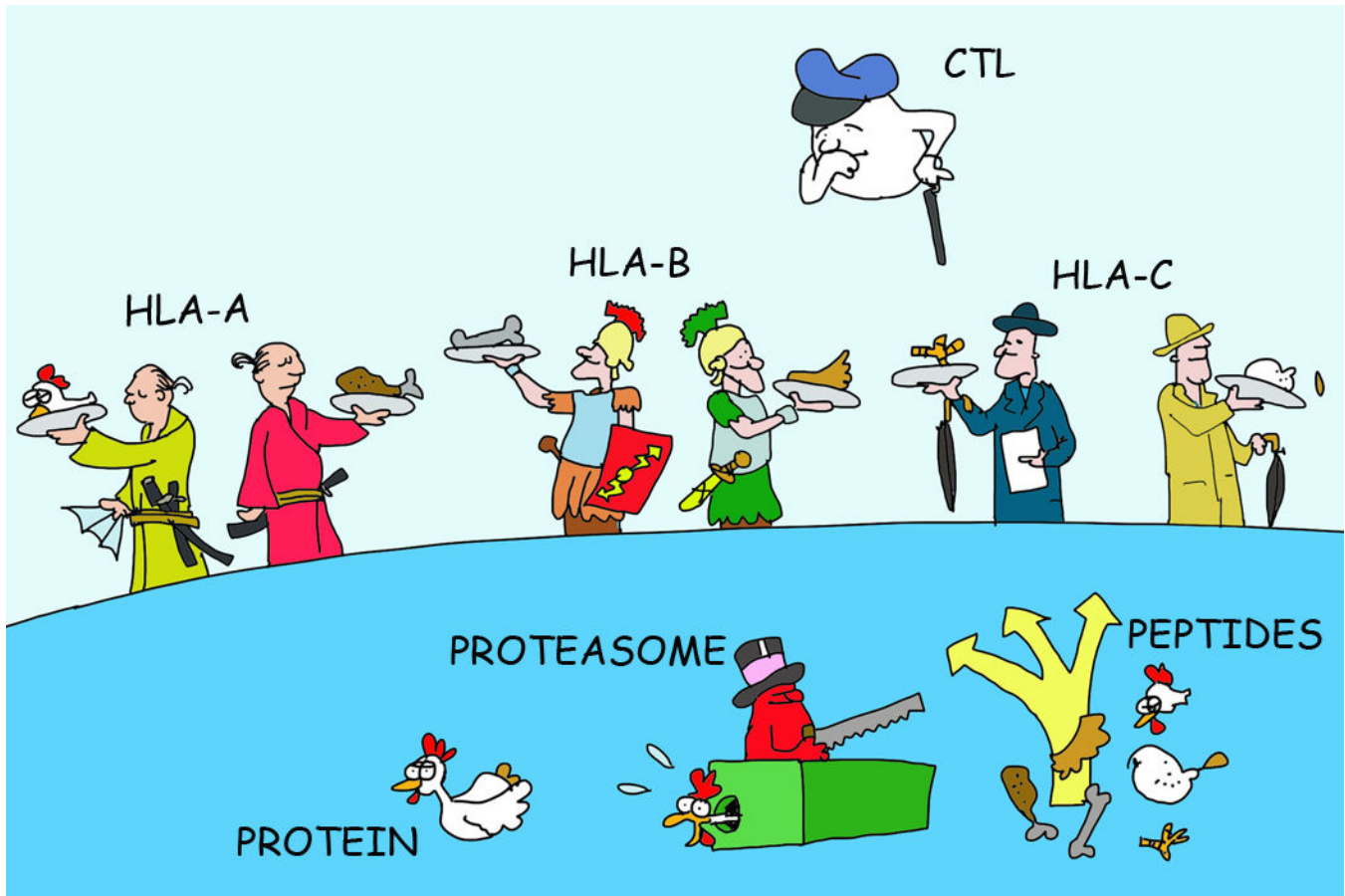


Figure 1. Of MHC Locus and Allelic Products with Polymorphism

Most mammalian species express three different MHC I and three different MHC II molecules (shown here for the human MHC I HLA-A, HLA-B and HLA-C locus products). Since these are polymorphic and genetically encoded, a total of somewhere between 3 and 6 (depending on the differences between the inherited genes) alleles will be expressed on cells. These are polymorphic in the peptide-binding groove region of MHC molecules to present different peptides of a defined antigen.

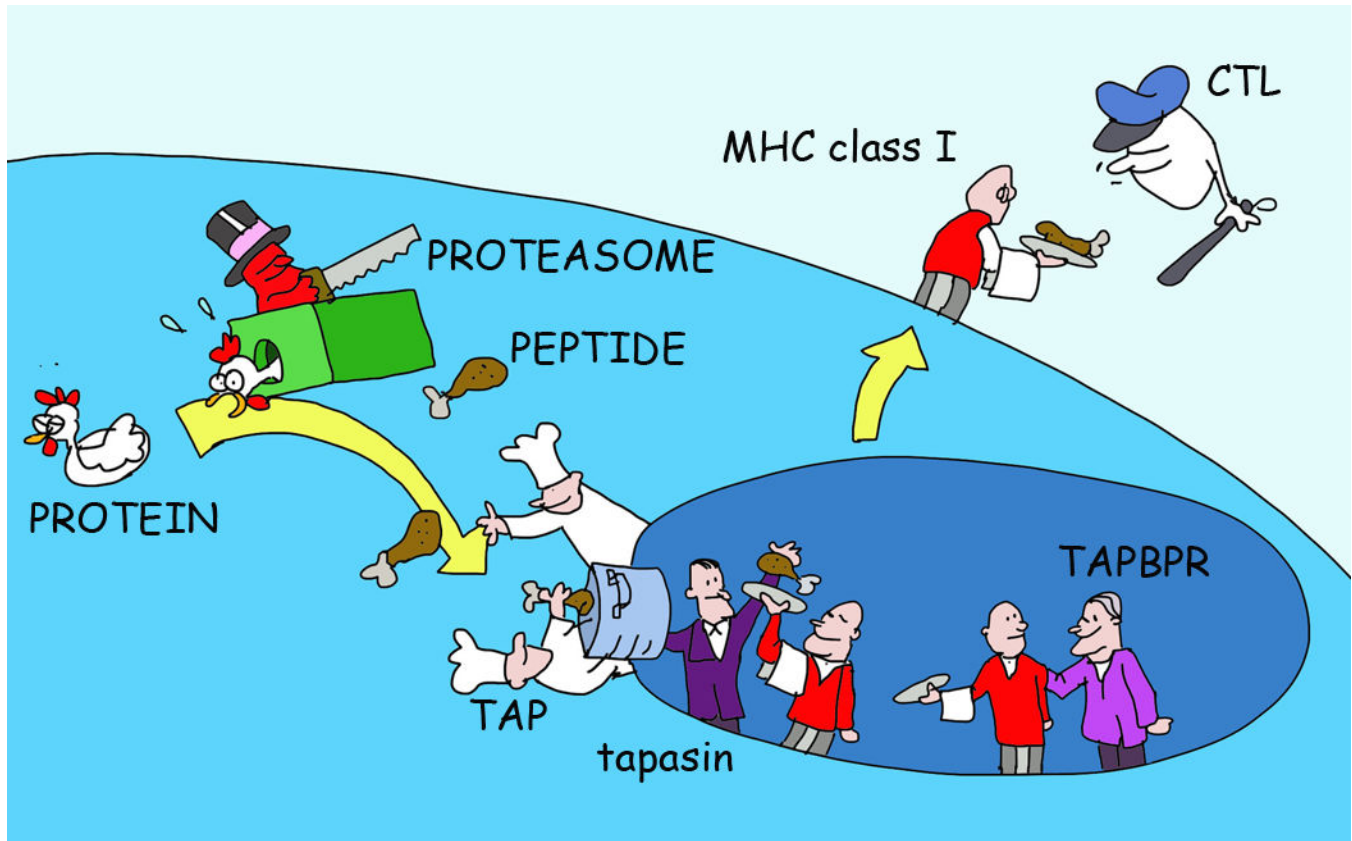


Figure 2. A Simple Illustration of MHC I Antigen Presentation

Antigens are degraded by the proteasome to yield peptide fragments. These peptides are then translocated from the cytosol into the endoplasmic reticulum (ER) lumen where MHC I is waiting for peptides is retained by a series of chaperones including a dedicated chaperone tapasin in the peptide-loading complex. A second dedicated chaperone (TAPBPR) can further optimize the peptides in MHC I. Only MHC I with optimal peptides is allowed to leave the ER to present the peptide fragments at the cell surface to CD8⁺ T cells.

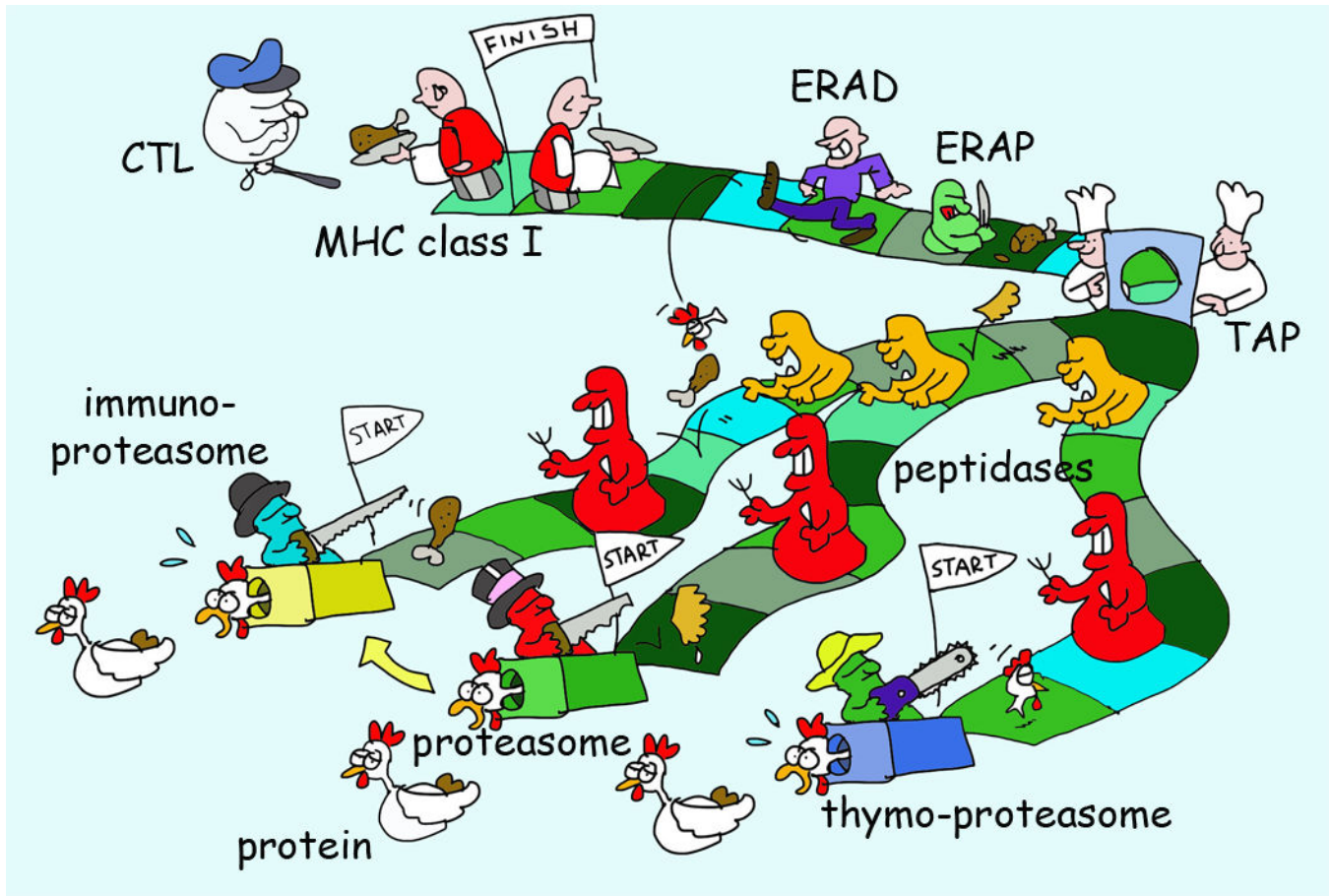


Figure 3. Survival of The Fittest for MHC I Presentation and The Many Proteasomes

There are three types of proteasomes with unique tissue expression. These proteasomes have an altered cleavage specificity yielding (in part) different degradation fragments. These fragments are released in the hostile environment of the cytosol where the majority of peptides will be destroyed by peptidases. Few peptides survive this massacre through translocation in the ER by transporter associated with antigen processing (TAP). Here they can be further trimmed by ER resident aminopeptidase (ERAP) or translocated back into the cytosol by the ER associated degradation (ERAD) system. Only few peptides survive the chaperone-mediated survival selection for low off-rate peptides for a defined MHC I allele and these are ultimately presented.

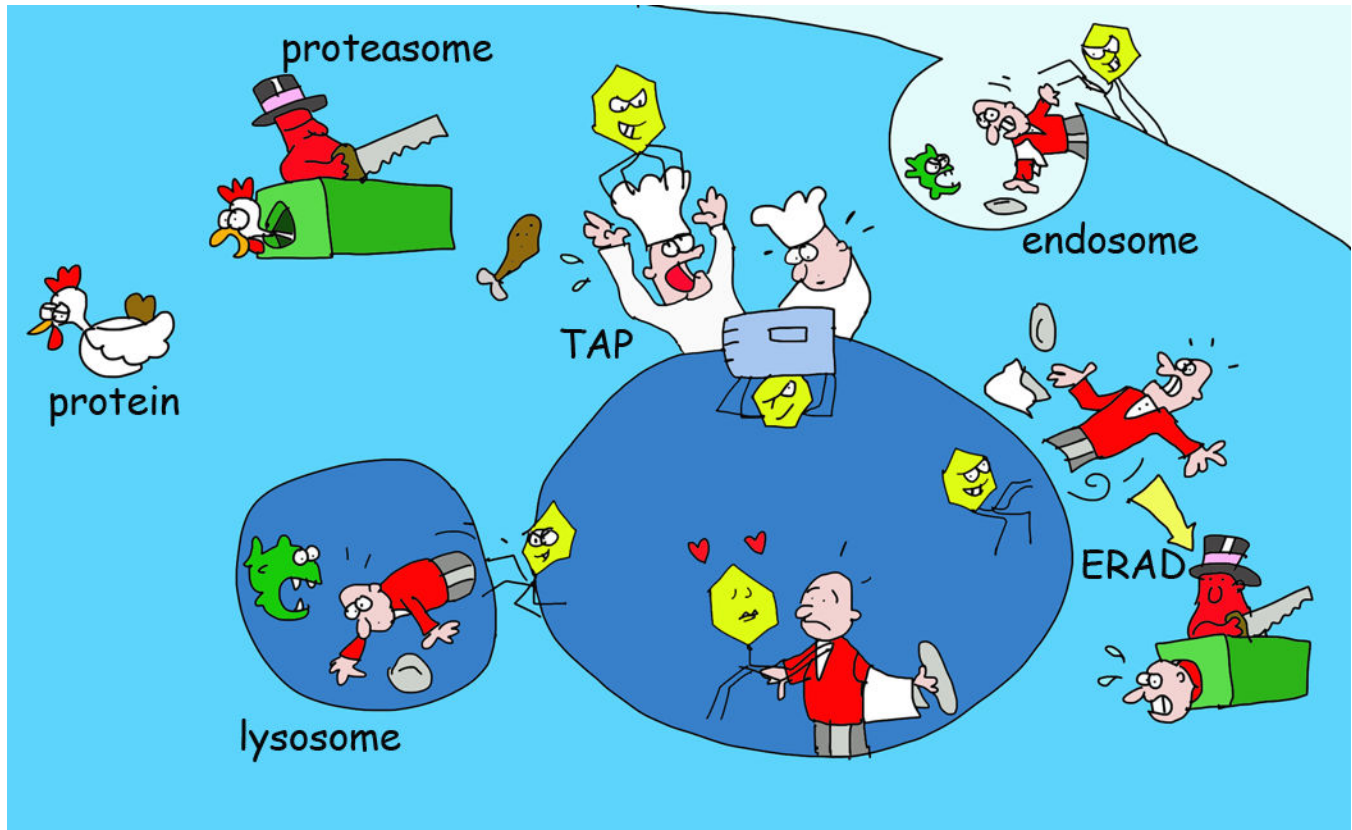


Figure 4. Various Viral Immune Evasion Strategies for MHC I Antigen Presentation

Pathogens have evolved different ways to obstruct processes selective in the antigen presentation pathway. Examples include viral proteins inhibiting peptide transport by TAP, retaining MHC I in the ER or recognizing MHC I in the ER for targeting these back into the cytosol for degradation by the proteasome (the ERAD system). Other viral proteins recognize MHC I at the cell surface for internalization and destruction in lysosomes.

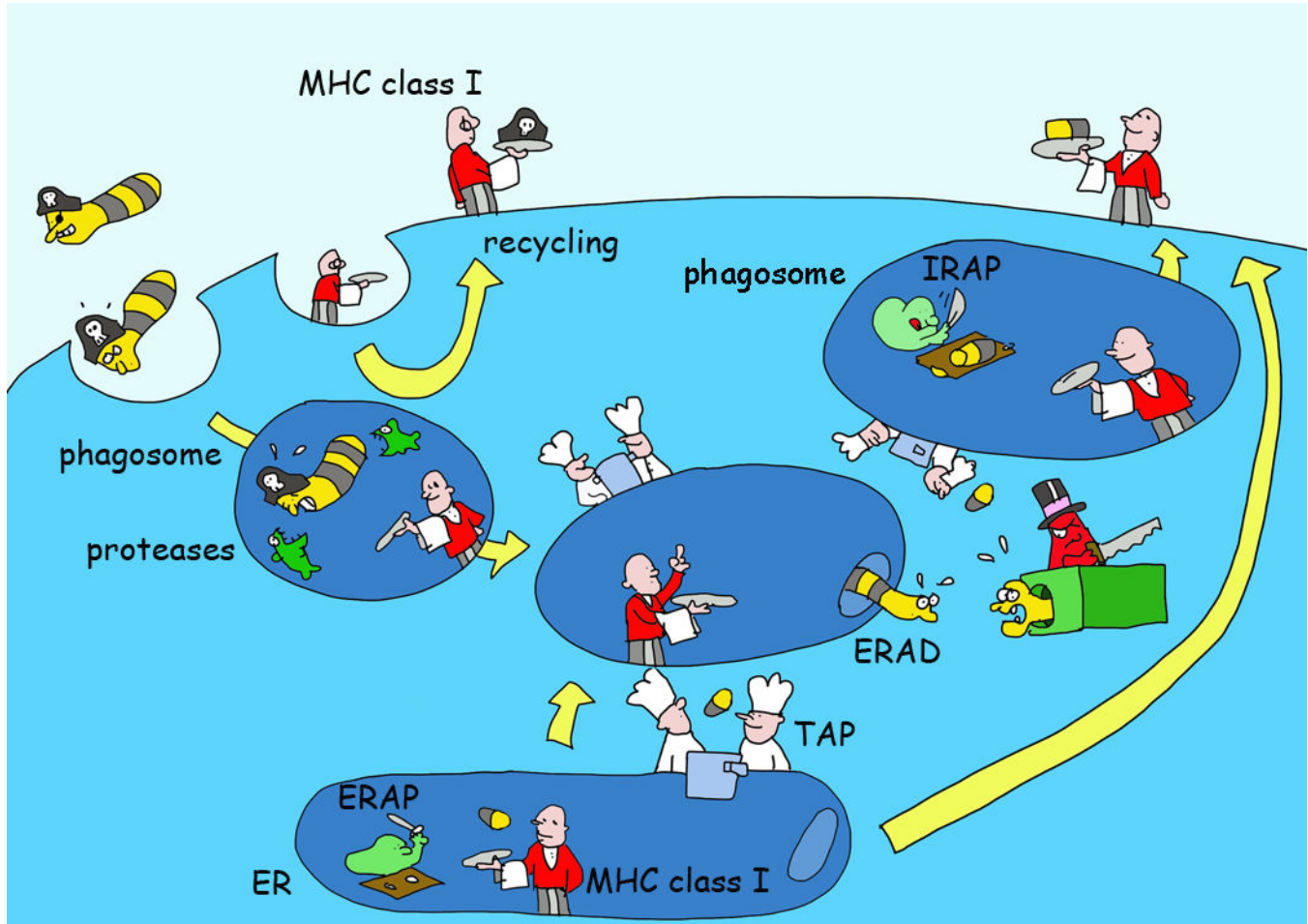


Figure 5. Crossing Boundaries; Various Models of Cross-Presentation by MHC I

MHC I molecules can present exogenous antigens and antigens delivered in apoptotic bodies and other types of cell debris. For dendritic cells, this process can result in cross-priming of CD8+ T cells. MHC I can recycle through the endosomal pathway to acquire antigen fragments made by proteases such as insulin regulated aminopeptidase (IRAP)[129] for cross-presentation. Endosomes may also acquire TAP and other ER molecules that may help export antigens into the cytosol for proteasomal hydrolysis and the resulting peptides may be reimported into the endosomes for MHC I loading and recycling and/or be delivered in the normal antigen presentation pathway as shown in Figure 2.

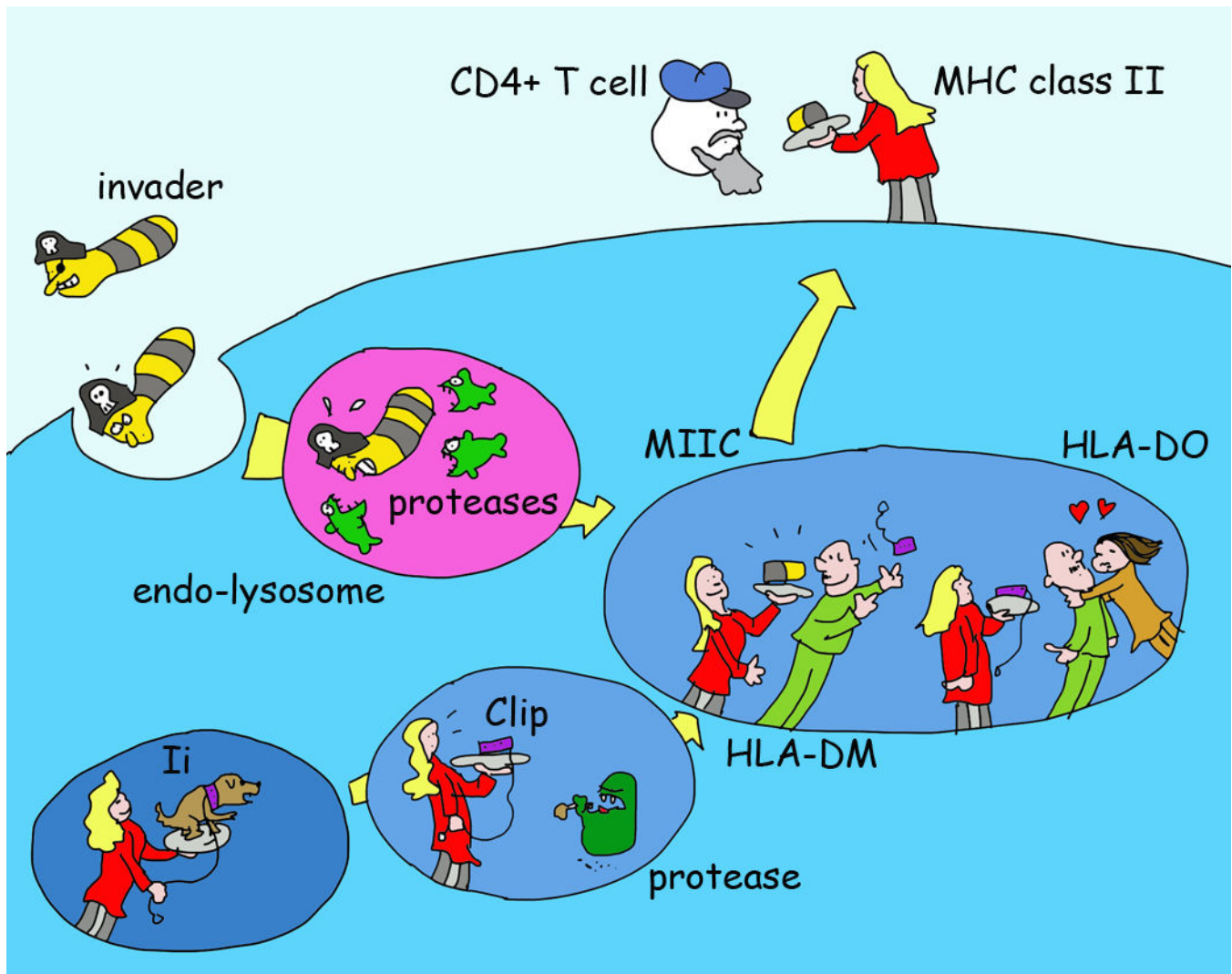


Figure 6. A Simple Illustration of MHC II Antigen Presentation

MHC II proteins are made in the ER where they pair with a third chain, the invariant chain or Ii. Ii fills (through a peptide sequence called CLIP) the MHC II peptide-binding groove and allows efficient exit of MHC II from the ER. Ii also guides MHC II through the cells to a late endosomal compartment, MIIC. Ii is degraded by endosomal proteases, as are antigens taken up by endocytosis or phagocytosis. The CLIP segment is protected from destruction and exchanged for an antigenic peptide with the help of a dedicated chaperone called DM (HLA-DM in human). Another chaperone expressed in a few immune cell types (immature B cells, some DC forms), called DO (HLA-DO) can compete for DM binding to MHC II and thereby affect the peptide repertoire on MHC II that is ultimately presented at the cell surface to CD4+ T cells.

Pathways of Antigen Processing

Janice S. Blum,¹ Pamela A. Wearsch,²
and Peter Cresswell³

¹Department of Microbiology and Immunology, Indiana University School of Medicine, Indianapolis, Indiana 46202; email: jblum@iupui.edu

²Department of Pathology, Case Western Reserve University School of Medicine, Cleveland, Ohio 44106; email: paw28@case.edu

³Howard Hughes Medical Institute, Department of Immunobiology, Yale University School of Medicine, New Haven, Connecticut 06520; email: peter.cresswell@yale.edu

Ann. Rev. Immunol. 2013. 31:443–73

First published online as a Review in Advance on January 3, 2013

The *Annual Review of Immunology* is online at immunol.annualreviews.org

This article's doi:
10.1146/annurev-immunol-032712-095910

Copyright © 2013 by Annual Reviews.
All rights reserved

Keywords

cross-presentation, MHC class I, MHC class II, proteolysis, peptide

Abstract

T cell recognition of antigen-presenting cells depends on their expression of a spectrum of peptides bound to major histocompatibility complex class I (MHC-I) and class II (MHC-II) molecules. Conversion of antigens from pathogens or transformed cells into MHC-I- and MHC-II-bound peptides is critical for mounting protective T cell responses, and similar processing of self proteins is necessary to establish and maintain tolerance. Cells use a variety of mechanisms to acquire protein antigens, from translation in the cytosol to variations on the theme of endocytosis, and to degrade them once acquired. In this review, we highlight the aspects of MHC-I and MHC-II biosynthesis and assembly that have evolved to intersect these pathways and sample the peptides that are produced.

INTRODUCTION

The T cell arm of the adaptive immune response has evolved to recognize the products of partial intracellular proteolysis. CD8⁺ T cells recognize protein-derived peptides in association with major histocompatibility complex (MHC) class I (MHC-I) molecules, whereas CD4⁺ T cells recognize peptides bound to MHC class II (MHC-II) molecules. There

are also T cells that recognize lipid antigens associated with CD1 molecules (1), but CD1 functions and the processing mechanisms that regulate their interaction with lipids are not considered here.

All vertebrates possess an MHC, a large multigenic region with many conserved genes in addition to MHC-I and MHC-II molecules. Some of these encode products essential to MHC-I and MHC-II function. In many species, the MHC encodes multiple MHC-I and MHC-II molecules, which are presumed to have arisen by gene duplication. For example, in mice, depending on the strain, there are two to three genes encoding so-called classical MHC-I molecules, called H2-D, -K, and -L, within the H2 complex, and most strains have two MHC-II molecules, called I-A and I-E. Humans have three genes encoding classical MHC-I molecules within the HLA complex, called HLA-A, -B, and -C, and there are three MHC-II molecules, called HLA-DR, -DQ, and -DP. In both mice and humans, there are other class I genes present in the MHC. These are known as class Ib genes and are discussed elsewhere in this volume (2).

Multiple structures of MHC-I and MHC-II molecules have been determined, and a schematic structure of each is presented in **Figure 1**. MHC-I and MHC-II genes exhibit enormous allelic polymorphism, and amino acid sequence variation is heavily concentrated in the part of each structure that interacts with peptides, allowing different alleles to bind a different range of peptides. The peptide-binding structure consists of a membrane-distal groove formed by two antiparallel α -helices overlaying an eight-strand β -sheet. In the case of MHC-I, the groove corresponds to a contiguous amino acid sequence formed by the N-terminal region of the single MHC-encoded subunit, or heavy chain, whereas for MHC-II it is formed by the juxtaposition of the N-terminal regions of two MHC-encoded α - and β -chains. For both molecules, the membrane-proximal region consists of two conserved domains that are homologous to immunoglobulin (Ig) constant region domains. For MHC-I, one is provided by

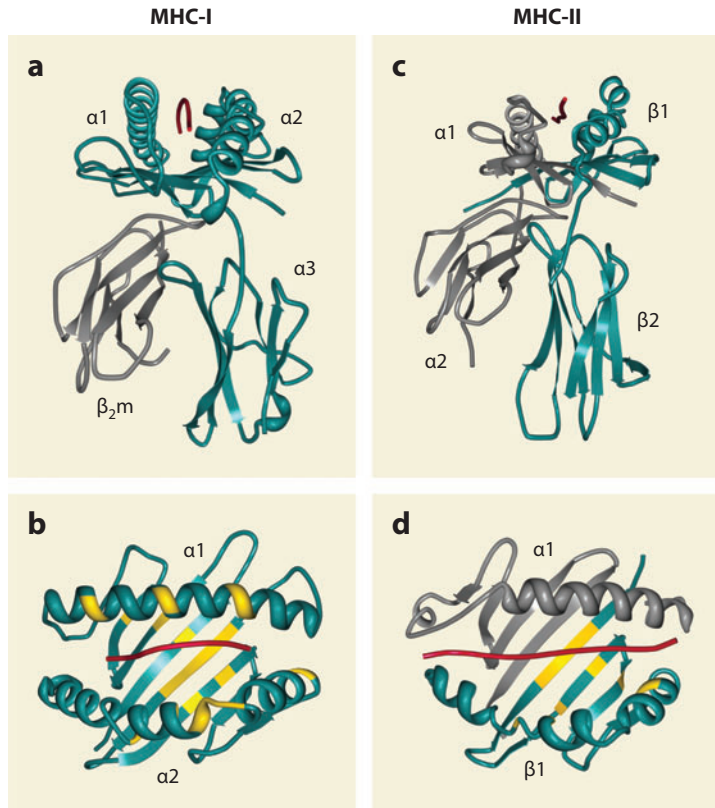


Figure 1

Three-dimensional structures of MHC-I and MHC-II molecules with peptide ligands. (a,b) Structure of the MHC-I molecule: HLA-A2 complexed with residues 58–66 of the influenza matrix protein (232) (teal, MHC-I heavy chain; gray, β_2 -microglobulin; red, peptide). (c,d) Structure of the MHC-II molecule: HLA-DR1 complexed with residues 306–318 of influenza hemagglutinin (233) (gray, MHC-II α chain; teal, MHC-II β chain; red, peptide). Ribbon diagrams were generated with the Protein Workshop software available from the RCSB Protein Data Bank (<http://www.rcsb.org>). Highly polymorphic residues of HLA-A (b) and HLA-DR (d) proximal to the peptide binding groove (<http://hla.alleles.org>) are highlighted in yellow. Note that the polymorphism of the MHC-II α chains is limited; HLA-DR α chains are essentially nonpolymorphic.

the heavy chain and the other is a separate protein, β_2 -microglobulin (β_2 m), a soluble product of a non-MHC-linked gene. For MHC-II, one conserved domain is part of the α -subunit and the other is part of the β -subunit. The MHC-I heavy chain and the MHC-II α - and β -subunits are transmembrane glycoproteins with short cytoplasmic domains. The theme that emerges is that MHC-I and MHC-II molecules each have a structurally homologous platform capable of binding peptides with very high affinity that can engage the T cell receptor. A significant difference is that for MHC-I the peptide is confined by binding groove interactions at both the N and C termini, whereas for MHC-II each end of the peptide can overhang the binding groove.

Peptides are the products of proteolysis, and there are two major proteolytic systems operating within the cell that contribute to MHC-dependent T cell recognition (Figure 2). In the cytosol, most proteolysis is mediated by the proteasome. The proteasome (reviewed in 3) is not discussed extensively here, but in brief its core is a barrel-shaped 20S structure consisting of four stacked rings of seven subunits each. The outer rings are composed of α -subunits and the middle two of β -subunits, three of which, $\beta 1$, $\beta 2$, and $\beta 5$, constitute the active proteolytic components. Variants of the active β -subunits are induced by interferon- γ (IFN- γ) and replace the constitutive versions. These were historically called LMP1, LMP2, and MECL1, and the genes encoding LMP1 and LMP2 are MHC-linked. Commonly, the IFN- γ -inducible subunits are now called $\beta 1i$, $\beta 2i$, and $\beta 5i$, and proteasomes that contain them are called immunoproteasomes. The cleavage specificities of standard proteasomes and immunoproteasomes differ. The 20S core is capped at each end by an additional 19S multisubunit complex that recognizes ubiquitin-conjugated proteins targeted for degradation. The 19S component has deubiquitinase activity and an unfoldase activity that allows the targeted proteins to enter the channel in the center of the barrel where the β -subunit active sites reside. The unfolding function, in particular,

necessitates that proteolysis by the capped (26S) proteasome is ATP-dependent. There is an alternative capping structure (11S) composed of a different set of IFN- γ -inducible proteins that allow a level of ATP-independent proteolysis of peptides but not of folded proteins. The end products of proteolysis by the 26S proteasome (20S plus 19S) form the dominant source of peptides for MHC-I binding.

Proteins that are internalized by a cell from exogenous sources are degraded by lysosomal proteolysis (Figure 2). In brief, endocytosed proteins enter a vesicular pathway consisting of progressively more acidic and proteolytically active compartments classically referred to as early endosomes, late endosomes, and lysosomes (4). Particles internalized by phagocytosis follow a similar path, terminating in phagolysosomes that are formed by the fusion of phagosomes and lysosomes. Lysosomes and phagolysosomes have a pH of 4 to 4.5 and contain a number of acid pH-optimum proteases generically called cathepsins (5). In highly degradative cells such as macrophages, successive cleavages by these enzymes result in very short peptides and free amino acids that are translocated into the cytosol to replenish tRNAs for new protein synthesis, but in less proteolytically active antigen-presenting cells (APCs), larger intermediates form the dominant source of peptides for MHC-II binding.

The trafficking of exogenous and endogenous proteins for antigen processing and presentation are summarized in Figure 2. In general, MHC-I molecules bind peptides generated by proteasomal proteolysis, and they bind them in the endoplasmic reticulum (ER) after the peptides are translocated from the cytosol. Peptide binding by MHC-I is integrated into the assembly pathway of the heavy chain- β_2 m dimer. MHC-II molecules generally bind peptides generated by lysosomal proteolysis in the endocytic and phagocytic pathways. However, both can access peptides from endogenous and exogenous antigens. For example, MHC-II binds peptides derived from endogenous

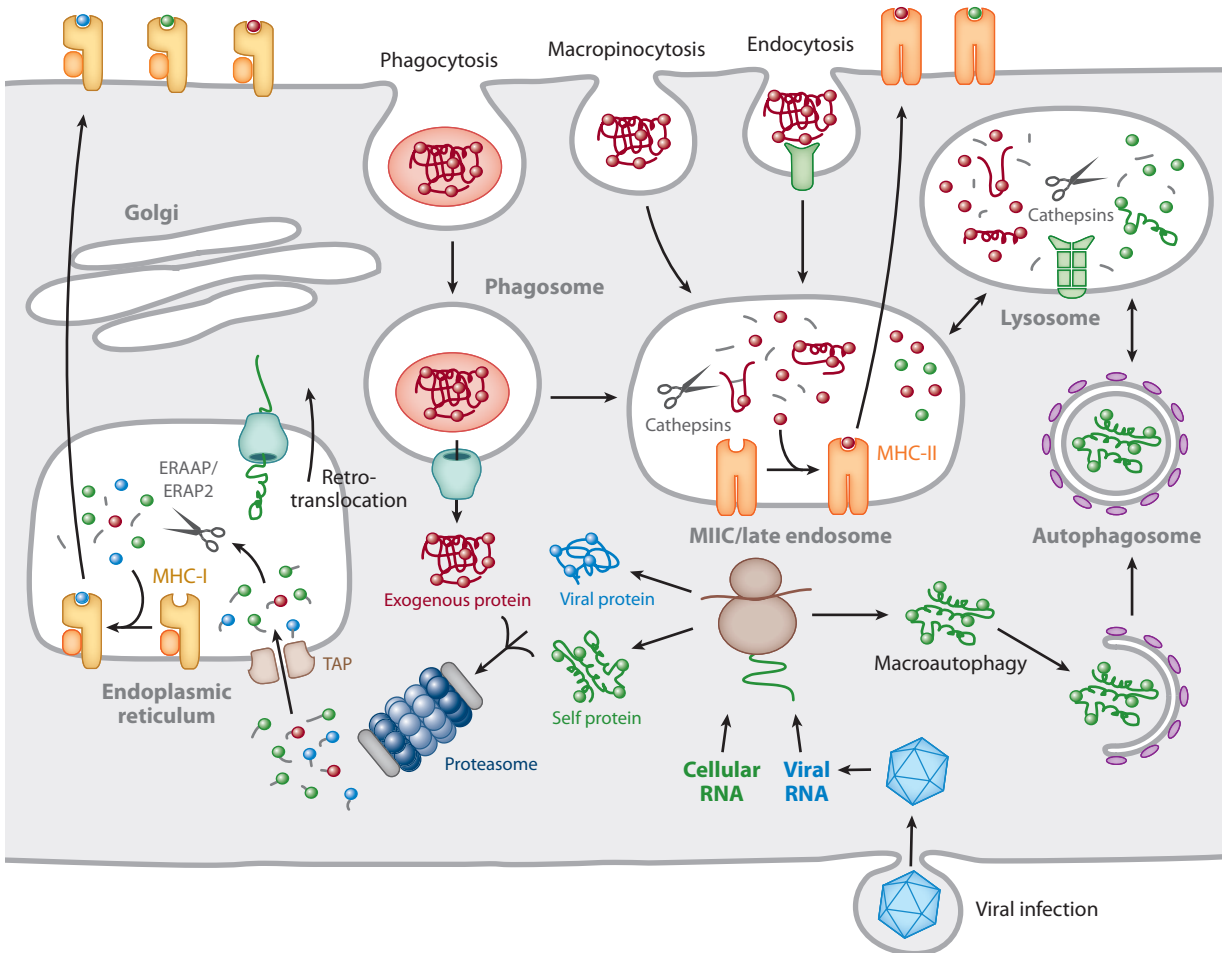


Figure 2

Trafficking of antigens for processing and presentation with major histocompatibility complex (MHC) molecules: basic pathways and exceptions to the “rules.” Cytosolic proteins are processed primarily by the action of the proteasome. The short peptides are then transported into the endoplasmic reticulum (ER) by the transporter associated with antigen processing (TAP) for subsequent assembly with MHC-I molecules. In certain antigen-presenting cells, particularly dendritic cells, exogenous proteins can also be fed into this pathway by retrotranslocation from phagosomes, a phenomenon known as cross-presentation. The retrotranslocation channels may be recruited from the ER, where they are used for ER-associated degradation, or ERAD, of misfolded transmembrane or secretory proteins. Exogenous proteins are primarily presented by MHC-II molecules. Antigens are internalized by several pathways, including phagocytosis, macropinocytosis, and endocytosis, and eventually traffic to a mature or late endosomal compartment, often called the MHC-II compartment, or MIIc, where they are processed and loaded onto MHC-II molecules. Cytoplasmic/nuclear antigens can also be trafficked into the endosomal network via autophagy for subsequent processing and presentation with MHC-II molecules.

membrane proteins that are degraded in the lysosome. In addition, MHC-I can bind peptides derived from exogenous proteins internalized by endocytosis or phagocytosis, a phenomenon called cross-presentation.

Specific subsets of dendritic cells (DCs) are particularly adept at mediating this process, which is critically important for the initiation of a primary response by naive CD8⁺ T cells when it is termed cross-priming.

PEPTIDE BINDING TO MHC-I MOLECULES

Peptides generated in the cytosol are translocated into the ER by the transporter associated with antigen processing (TAP), which is a member of the ATP-binding cassette (ABC) family of transporters (6). TAP is a heterodimeric protein, and the TAP1 and TAP2 subunits are encoded by closely linked genes in the MHC. These are widely distributed in both prokaryotes and eukaryotes and transfer a variety of molecules across membranes. Biochemical evidence combined with molecular modeling suggests that each TAP subunit consists of a central core domain of six transmembrane α -helices, which constitute the channel, that is immediately N-terminal to the nucleotide-binding domain (NBD) (7). The NBD structure is known for TAP1 and it is similar to that of other ABC family members, with the classical Walker A and B motifs present in many ATPases (8). Cytosolic loops in the core domains that are proximal to the NBDs constitute the peptide recognition site, and ATP hydrolysis mediates the translocation event (7). Both subunits have additional N-terminal domains (N-domains), comprising four transmembrane segments for TAP1 and three for TAP2, which have no counterparts in other members of the ABC family of transporters (7).

The TAP heterodimer associates with a number of other proteins to form the peptide-loading complex, or PLC (Figure 3). The transmembrane glycoprotein tapasin, which is encoded by an MHC-linked gene (9), interacts within the membrane with the N-domains (10–13). Tapasin has a bridging function, recruiting MHC-I- β_2 m dimers and the chaperone calreticulin (CRT) to the PLC (14). Recent experiments have confirmed that there are two tapasin molecules in the PLC, one associated with each TAP subunit (13, 15). Tapasin in turn is stably linked via a disulfide bond to a second molecule, the protein disulfide isomerase homolog ERp57, and the structure of the luminal region of human tapasin conjugated to ERp57 has been solved (16). The N-domain of

tapasin consists of a β barrel fused to an Ig-like domain, and, as for the MHC-I and MHC-II proteins, the membrane proximal domain is Ig-like. ERp57 has a slightly twisted U-shaped structure, and tapasin is inserted into the U in a way that results in extensive protein-protein interactions with ERp57, particularly with the α and α' domains, each of which contains a double cysteine “CXXC” motif that constitutes its two redox active sites. As predicted by earlier biochemical experiments (17), a disulfide bond connects cysteine 95 of tapasin with cysteine 57 of ERp57, which is the N-terminal cysteine residue of the α domain CXXC motif. Normally, disulfide bonds involving cysteine 57 are transiently formed during the reduction of a disulfide-containing ERp57 substrate protein, and reduction of this enzyme-substrate bond by the second cysteine in the motif releases the substrate. The interactions of tapasin with the α and α' domains appear to trap the disulfide-linked species, explaining the stability of the tapasin-ERp57 disulfide bond.

ERp57 assists the folding of newly synthesized glycoproteins in the ER by mediating disulfide bond isomerization. Its specificity for glycoproteins results from its ability to associate via its β' domain with CRT and a second lectin-like ER chaperone, the transmembrane CRT homolog calnexin (CNX). Both CNX and CRT are important in MHC-I assembly (Figure 3). CNX and CRT normally function in a quality-control cycle that depends on their interactions with the N-linked glycans of the glycoproteins (18). They then recruit ERp57, which mediates proper disulfide bond formation in the folding glycoprotein. Glycan binding to CNX or CRT is dependent on the precise structure of the N-linked glycan, which must bear a single terminal glucose residue and is a biosynthetic intermediate maintained in this form by the competing actions of two enzymes. One, glucosidase II, removes the glucose and the other, UDP-glucose glycoprotein transferase-1 (UGT1), replaces the glucose only if the glycoprotein bearing the glycan is partially unfolded (19–21). This cycle plays a role in MHC-I-peptide loading

Transporter associated with antigen processing (TAP): an ATP-dependent transporter composed of two subunits, TAP1 and TAP2, that translocates peptides from the cytosol into the endoplasmic reticulum

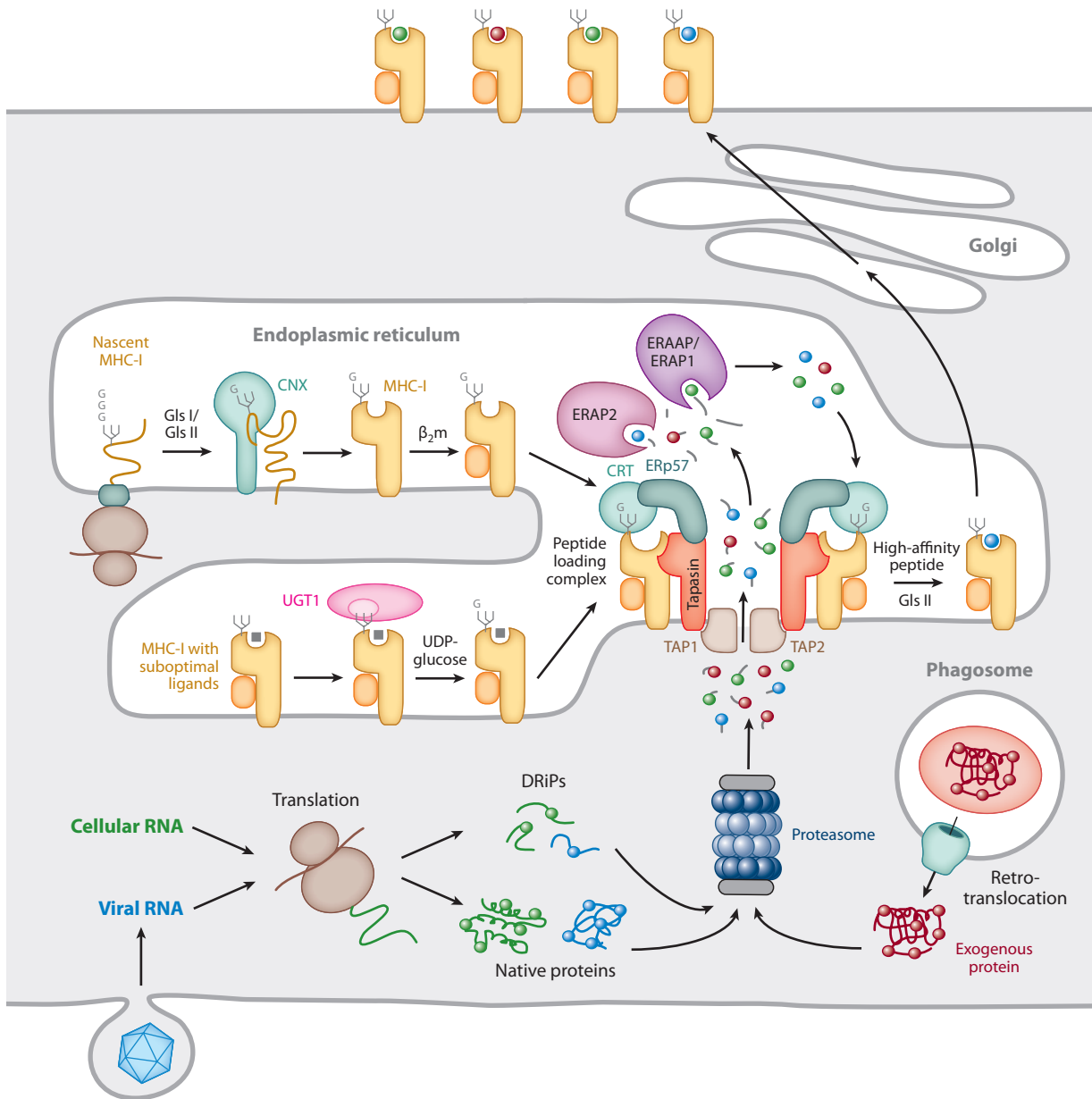
Peptide-loading complex (PLC): protein complex consisting of the MHC-I heavy chain and β_2 -microglobulin, TAP, tapasin, calreticulin, and ERp57 that facilitates MHC-I-peptide loading

ERp57: an endoplasmic reticulum-resident homolog of protein disulfide isomerase

(Figure 3), but the one step that does not appear to be involved is the reduction-oxidation cycle mediated by ERp57 (see below).

Cells that lack TAP1 or TAP2 do not form MHC-I-peptide complexes because no peptides are imported into the ER. There are a few published exceptions to this rule, some of which lead to CD8⁺ T cell recognition (22, 23),

but the only major one, in terms of quantitative effects on MHC-I assembly, is the unusual and specific ability of HLA-A2 molecules to bind peptides derived from signal sequences of certain ER-targeted molecules (24). Because of the inherent instability of so-called empty MHC-I molecules, and because they do not fold into a transport-competent structure in the ER,



TAP-negative cells express very little surface MHC-I. Cells that lack tapasin also exhibit reduced surface MHC-I, but the defect is much less drastic than in TAP-negative cells, and the magnitude of the effect depends on the individual MHC-I allele expressed (25–28). Data from tapasin knockout mice showed an essential function for tapasin in generating CD8⁺ T cell responses. Furthermore, data based on T cell recognition demonstrated that tapasin plays a peptide-editing role, mediating the binding of high-affinity peptides at the expense of peptides with lower but still significant affinity and that, for this reason, surface MHC-I molecules on tapasin-negative cells are less stable than those on tapasin-positive cells (27–30). Subsequently, *in vitro* data produced using recombinant tapasin-ERp57 conjugates confirmed that tapasin facilitates high-affinity peptide binding and further showed that its association with ERp57 is essential (31). The addition of tapasin-ERp57 conjugates to extracts of human tapasin-negative cells expressing HLA-B8 was found to facilitate the binding of added high-affinity peptides to HLA-B8- β_2 m dimers. Lower-affinity peptides were much less successful competitors for binding in the presence of the conjugate than in its absence, indicative of a peptide-editing effect. The tapasin-ERp57 conjugate was also found to mediate peptide binding to purified, soluble, recombinant

HLA-B8- β_2 m dimers, provided that the HLA-B8 molecules expressed a monoglycosylated N-linked glycan (32). Although this reaction depended on the addition of recombinant CRT, presumably to provide a bridge between MHC-I and the tapasin-associated ERp57, no other components were required. In a more simplified *in vitro* system, neither CRT nor tapasin-associated ERp57 were needed for peptide binding when the MHC-I heavy chain and tapasin were artificially coupled by the addition of leucine zippers to their C termini (33).

ERp57-negative cells, as well as CRT-negative cells, also have reduced numbers of MHC-I molecules on the cell surface (34, 35). The initial identification of ERp57 in the PLC led to considerable speculation that its redox activity was important for generating stable MHC-I-peptide complexes. However, the structural data indicated that tapasin obstructs both of the ERp57 active sites, rendering this unlikely. In fact, when the second active site cysteine in the α domain and both active site cysteine residues in the α' domain were mutated to serine residues, the combined substitutions had no effect on the ability of tapasin to reconstitute MHC-I cell surface expression when it was introduced into an ERp57-deficient cell line (36). This triply mutated ERp57 was still disulfide-linked to tapasin. However, further analysis in both cell-free systems and intact

Figure 3

MHC-I biosynthesis and antigenic peptide binding in the endoplasmic reticulum (ER). Trimming of the N-linked glycan by glucosidases I and II (GlsI/GlsII) to a single terminal glucose residue (G) permits the interaction of the MHC-I heavy chain with lectin-like chaperones at several stages during folding and assembly. The initial folding events involve the chaperone calnexin (CNX) and allow subsequent assembly with β_2 -microglobulin (β_2 m). The empty heterodimer, which is inherently unstable, is then recruited by calreticulin (CRT) via the monoglycosylated N-linked glycan to the peptide loading complex (PLC). The association of MHC-I/ β_2 m heterodimers with the PLC both stabilizes the empty MHC-I molecule and maintains the binding groove in a conformation that favors high-affinity peptide loading. These functions are mediated by direct interactions between the MHC-I heavy chain and tapasin and are supported by coordinating interactions with CRT and ERp57 in the PLC. MHC-I molecules with suboptimal peptides are substrates for UGT1, which reglucosylates the heavy chain glycan, allowing reentry of the MHC-I into the PLC and exchange for high-affinity peptides. Peptides translocated into the ER by the transporter associated with antigen processing (TAP) originate primarily from the proteasomal degradation of endogenous proteins or DRiPs. These proteins may arise from the translation of either self or foreign (i.e., viral) RNA or, in the case of cross-presentation, by translocation into the cytosol from endosomes or phagosomes. Many of the peptides that are delivered into the ER are longer than the 8–10 residues preferred by MHC-I molecules and undergo trimming by ER aminopeptidases known as ERAAP/ERAP1 and ERAP2. Finally, high-affinity peptides bind preferentially to MHC-I molecules in the PLC by a tapasin-mediated editing process; MHC-I-peptide complexes are released and then transit to the cell surface for T cell recognition by CD8⁺ T cells.

Endoplasmic reticulum-associated degradation (ERAD):

pathway that promotes the translocation of misfolded ER proteins into the cytoplasm for proteolysis

ERAAP: endoplasmic reticulum aminopeptidase associated with antigen processing (murine); in humans, known as ER aminopeptidase-1 (ERAP1)

cells using ERp57 mutated in the β' domain showed that the ability of ERp57 to bind CRT is essential for MHC-I recruitment to the PLC and normal MHC-I-peptide loading (32). In addition to the CRT-dependent interactions with the MHC-I glycan and ERp57 that mediate MHC-I binding to the PLC, there is also a direct interaction between MHC-I and tapasin. Mutagenesis of specific tapasin residues and expression of the mutants as recombinant tapasin-ERp57 conjugates revealed a patch on the surface of tapasin that binds to the MHC-I molecule, and there was a positive correlation between the relative abilities of different mutants to bind MHC-I and their efficiency in mediating peptide binding to MHC-I *in vitro* (16). In addition, a tapasin mutant that was nonfunctional in cell-free assays also failed to function when expressed as a full-length protein in a tapasin-negative cell.

The PLC consists of the TAP heterodimer and two tapasin-ERp57 conjugates, and up to two CRT molecules and MHC-I- β_2m dimers can be recruited (**Figure 3**). The MHC-I heavy chain glycan must be in the monoglycosylated form, consistent with the CRT requirement (32). Cellular expression of UGT1 is essential for optimal MHC-I-peptide loading, and *in vitro* the enzyme can discriminate between MHC-I molecules bound to high-affinity peptides and those associated with lower-affinity peptides (37). This suggests a mechanism that resembles the normal CRT/CNX quality-control cycle. A plausible model is that there are two discriminatory events that regulate peptide editing (**Figure 3**). First, after peptide-free MHC-I- β_2m dimers bearing a monoglycosylated N-linked glycan are recruited to the PLC by CRT, there is a direct interaction of the MHC-I molecule with tapasin. This interaction is sensitive to the peptide occupancy of the MHC-I molecule such that, when a peptide is bound, the affinity of the MHC-I interaction with tapasin is reduced, perhaps by a conformational change in the MHC-I heavy chain similar to that proposed to explain the ability of HLA-DM/H2-DM molecules to regulate peptide binding to MHC-II (see

below). Thus, peptide binding induces dissociation of the MHC-I molecule from tapasin, and because the affinity of the CRT interaction with the monoglycosylated MHC-I glycan is low, the glucose residue becomes accessible to the enzyme glucosidase II, which removes it. If the peptide affinity is sufficiently high, the MHC-I molecule can be transported from the ER through the Golgi apparatus and ultimately to the cell surface. If the affinity of the peptide is low, there are two possible scenarios for the second stage. Either the peptide dissociates and the transiently empty MHC-I molecule now becomes a substrate for UGT1 and glucose is added back to the N-linked glycan, or the UGT1 can recognize that the conformation of the MHC-I-peptide complex is in some way imperfect and reglucosylates the glycan. In either case, the consequence of the addition of the glucose residue is that the MHC-I molecule reassociates with CRT, reintegrates completely into the PLC, and is subjected to further rounds of tapasin-mediated peptide binding and selection. Ultimately, the MHC-I molecule will escape with a high-affinity peptide, or, in common with other glycoproteins that are subject to the CRT/CNX/ERp57 quality-control cycle, enzymatic removal of mannose residues from the N-linked glycan will render it unsusceptible to reglucosylation by UGT1. This acts as a timer, leading to irreversible dissociation of the MHC-I from the PLC and its degradation by the ER-associated degradation (ERAD) pathway (38).

One other ER luminal component that is critical for the proper generation of MHC-I-peptide complexes is an aminopeptidase; in the mouse it is called ER aminopeptidase associated with antigen processing (ERAAP) and in humans it is called ER aminopeptidase-1 (ERAP1) (**Figure 3**) (39, 40). A second aminopeptidase, ERAP2, is present in humans but not in mice and can also play a role (41). Peptides associated with MHC-I are generally 8–10 amino acids in length, but TAP can translocate peptides into the ER that are significantly longer (42). These peptides can be amino-terminally trimmed in the ER by ERAAP/ERAP1 to yield peptides

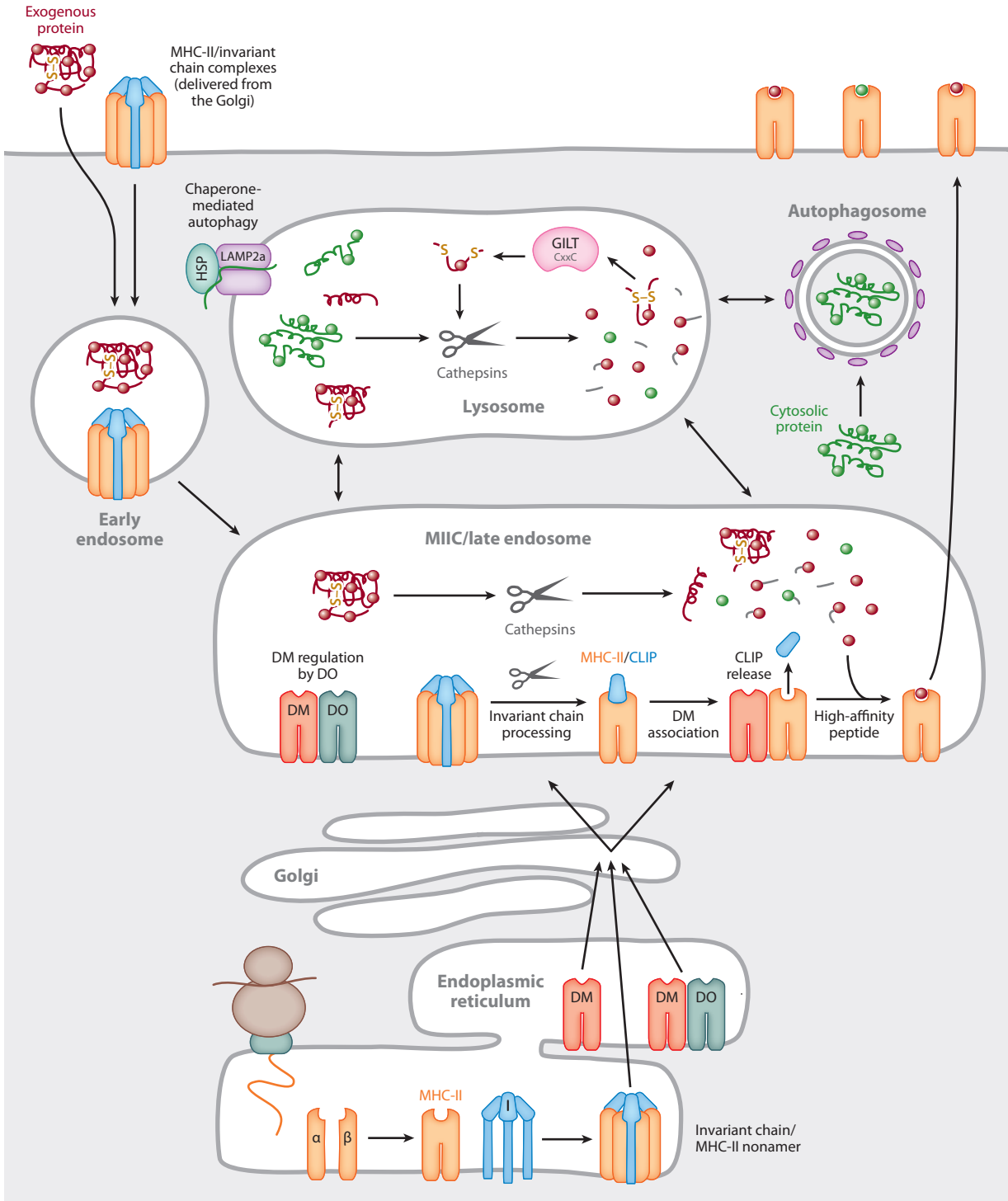
of the appropriate length for MHC-I binding. A structural change required for cleavage that can only be induced by a longer peptide prevents ERAAP1 from so-called over-trimming TAP-translocated peptides to a length that would eliminate their ability to bind MHC-I (43). Many of the peptides associated with MHC-I molecules expressed on cells derived from ERAAP knockout mice are elongated, and the MHC-I molecules are relatively unstable (44–46). The absence of ERAAP results in such a severe alteration in the range of bound peptides that wild-type and knockout mice on the same background are actually histoincompatible, with wild-type mice able to generate CD8⁺ T cell responses, and even antibody responses, against knockout cells (45). The antibodies generated recognize the MHC-I molecules complexed with elongated peptides and can block recognition of ERAAP-negative cells by the ERAAP-positive CD8⁺ T cells.

PEPTIDE BINDING TO MHC-II MOLECULES

MHC-II molecules assemble within the ER, followed by functional maturation in endosomal compartments rich in antigenic peptides. Upon ER translocation, MHC-II α and β subunits associate in a process facilitated by a specific chaperone, the invariant chain (I chain), or CD74 (**Figure 4**). Studies using I chain-deficient cells and animals have shown that I chain promotes MHC-II $\alpha\beta$ folding, protects the MHC-II ligand binding groove, and directs MHC-II molecules to endosomal compartments for ligand capture. I chain is a nonpolymorphic type II transmembrane glycoprotein not encoded in the MHC. Several forms of I chain exist due to alternative splicing and the use of alternate start codons (47). Nomenclature for the variants is based on their molecular mass, with the shortest form, p33, being most abundantly expressed. A larger splice variant, p41, contains a glycosylated domain, homologous to domains present in thyroglobulin, which can inhibit the activity of the protease cathepsin L (48). All forms of

I chain contain a conserved di-leucine motif in the N-terminal cytoplasmic domain required for targeting I chain and associated MHC-II to late endosomal compartments (49, 50). In humans, an alternate upstream translational start site gives rise to two additional forms of I chain, p35 and p43, each with an N-terminal 16 amino acid extension. This extended cytoplasmic domain encodes an ER retention motif, which may facilitate ER accumulation and the folding of nascent MHC-II $\alpha\beta$. A limited number of I chain molecules are also modified via linkage of a chondroitin sulfate chain; these molecules reach the cell surface and facilitate cell-cell adhesion (51, 52). Several other molecules involved in antigen presentation or transport have been reported to associate with I chain, including CD1, MHC-I, and the neonatal Fc γ receptor (53–55). Although I chain expression is not required for the function of CD1 or MHC-I, it may enhance antigen presentation by these molecules (56, 57). I chain expression negatively regulates DC motility in vitro, but it is unknown whether this facilitates antigen presentation or if it is related to the role of I chain as a receptor for the macrophage and stem cell chemoattractant migration inhibitory factor (55, 56).

Newly synthesized I chain variants form homo- or mixed trimers, involving p33, p35, p41, and p43 in humans, which accumulate in the ER (58). These multimers act as nuclei for MHC-II α and β assembly, giving rise to nonamers with three α , three β , and three I chains (**Figure 4**) (59). Distinct MHC-II alleles have different affinities and requirements for I chain binding that can influence their expression and function. In the absence of I chain, some MHC-II $\alpha\beta$ complexes are unstable, resulting in their aggregation, retention in the ER, and failure to reach the cell surface (60–62). Association of I chain with MHC-II $\alpha\beta$ dimers prevents antigenic peptide binding, consistent with minimal peptide acquisition early in MHC-II biosynthesis (63, 64). After assembly, the MHC-II-I chain complexes leave the ER and are routed to the endocytic pathway by the I chain di-leucine motifs (47). This may occur by direct



targeting from the trans-Golgi network (TGN) or by endocytosis from the plasma membrane (**Figure 4**) (65).

I chain release is initiated by progressive proteolysis in acidic endosomes (66). This culminates in a variably extended peptide of roughly 20 residues that is associated with the MHC-II binding groove (**Figure 4**). This is called CLIP, for class II-associated invariant chain peptide (67, 68). The structure of CLIP bound to HLA-DR3 is virtually identical to the structure of MHC-II bound to antigenic peptides indicated in **Figure 1**. (69). There are some MHC-II alleles with a low affinity for CLIP, and they are genetically associated with the development of autoimmunity (70). This may reflect a role for MHC-II-CLIP complexes in regulating thymic selection or skewing of T helper cell subset differentiation (71, 72). Alternatively, premature release of CLIP from these disease-associated MHC-II alleles may favor the selection of epitopes from autoantigens or the capture of self-peptides within distinct endosomal compartments (73, 74).

CLIP release from MHC-II is facilitated by another MHC-encoded heterodimeric glycoprotein, DM, which is highly homologous to conventional MHC-II (**Figure 4**) (75, 76). In humans DM is known as HLA-DM and in mice as H2-DM. The DM α and β subunits display limited genetic polymorphism, and the assembled dimer lacks an open or accessible ligand binding groove (77, 78). The cytoplasmic domain of the DM β chain contains a tyrosine motif that is responsible for sorting assembled DM molecules to late endosomes; DM may also bind I chain, which may facilitate but is not required

for DM assembly and stability (79–81). DM interaction with MHC-II-CLIP complexes occurs in late endosomes, where DM acts to promote a conformational change that induces CLIP dissociation (**Figure 4**). This reaction can be replicated using purified MHC-II-CLIP and DM, and it displays Michaelis-Menten kinetics and an acidic pH optimum (76, 82, 83). CLIP removal facilitates MHC-II loading with antigenic peptides, which influences the repertoire of CD4 $^{+}$ T cells selected in the thymus (84, 85). DM can remove any low-affinity peptides from MHC-II, and analogous to the role of tapasin in MHC-I peptide editing discussed above (**Figure 3**), repetitive interactions with DM lead to the accumulation of MHC-II complexes with high-affinity peptides (86). Whereas MHC-II binding to peptides derived from endocytosed antigens is inefficient in the absence of DM, there is a slow release of CLIP from MHC-II even in DM-negative APCs. As a consequence, synthetic peptides bind efficiently to surface MHC-II in these cells and presentation of endogenous antigens can be detected, whereas in B cells BCR-mediated targeting of antigens can overcome the loss of DM, presumably by increasing the amount internalized over a critical threshold (87–89).

The function of DM is modulated by another MHC-encoded MHC-II-like $\alpha\beta$ heterodimer, DO, and it is generally accepted that DO inhibits DM function (90, 91). DO is expressed in B cells and thymic epithelium and at low levels in select DC subsets, where there is evidence that it is regulated by Toll-like receptor (TLR) agonists (92–95). DO $\alpha\beta$ dimers associate tightly with DM molecules

CLIP: class II-associated invariant chain peptide

BCR: B cell receptor for antigen

Figure 4

Major histocompatibility complex (MHC)-II biosynthesis and antigenic peptide binding in the endocytic pathway. MHC-II α and β associate with invariant chain (I chain) trimers to form nonamers. These complexes transit to mature endosomes either via the trans-Golgi network (TGN) or by recycling from the cell surface. Within endosomes, I chain is sequentially proteolyzed to yield the residual I chain fragment, class II-associated invariant chain peptide (CLIP). Displacement of CLIP from the ligand groove of MHC-II $\alpha\beta$ is mediated by the MHC-II-related chaperone HLA-DM (DM) and blunted by HLA-DO (DO). Expression of DO and regulation of DM function involves the assembly of DM-DO complexes in the endoplasmic reticulum and cotransport to endocytic compartments. Antigens delivered to late endosomes by phagocytosis, pinocytosis, endocytosis, and autophagy are processed by cathepsins and the thiol oxidoreductase GILT (γ -interferon-inducible lysosomal thiol), and acquisition of high-affinity peptides by MHC-II is facilitated by DM. The MHC-II-peptide complexes are subsequently transported to the cell surface for T cell recognition by CD4 $^{+}$ T cells.

and are retained in the ER in the absence of DM, suggesting that in DO-positive cells DM and DO move in concert to endosomes (**Figure 4**) (96). Studies using Förster (fluorescence) resonance energy transfer (FRET) and mutational analysis that defined the DM/DR interface suggested that DO and DR bind to the same region of DM (97). Recently, the crystal structure of the DO/DM complex confirmed this and demonstrated an apparent displacement of a segment of the DO α -chain α -helix compared with that of the α -chain α -helix in MHC-II-peptide complexes, which may reflect the conformational alteration that DM imparts to induce the dissociation of low-affinity peptides (98).

A precise biological function for DO has been hard to define. Studies in mice deficient in DO have revealed subtle defects in MHC-II antigen presentation, although the effects observed were influenced by the genetic background of the mice and the MHC-II allele examined (91, 99). In vivo, overexpression of DO in DCs can impair MHC-II presentation of antigenic epitopes and, presumably because of this, reduce type I diabetes development in NOD mice (100, 101).

ANTIGEN INTRODUCTION AND PROTEOLYSIS IN THE ENDOCYTIC PATHWAY

Exploiting conserved pathways established for nutrient and growth factor uptake, APCs sample soluble and particulate matter from extracellular fluids. Many pathogens, including viruses, bacteria, and fungi, use these same pathways as conduits into cells, favoring immune recognition and antigen presentation. Pathogen-driven disruption of these pathways allows immune evasion (102–104). Among these transport pathways, three routes—clathrin-mediated endocytosis, phagocytosis, and macropinocytosis—efficiently promote antigen internalization and sorting to vesicular organelles for processing and presentation by MHC molecules (**Figure 2**). During clathrin-mediated endocytosis, cell surface receptor-

ligand complexes, membrane proteins, and soluble macromolecules are internalized. Regulated capture of particulate antigens and pathogens is mediated by phagocytosis, a process that synchronizes engulfment with delivery into a microenvironment containing reactive oxygen species, proteases, and antimicrobial agents to promote pathogen destruction. The nonselective process of macropinocytosis captures larger quantities of extracellular material, including proteins, bacteria, and viruses, via plasma membrane ruffling and folding. All these pathways exist in DCs, macrophages, and B lymphocytes, although there are variations in efficiency and regulation. For example, B cells are less efficient at fluid-phase endocytosis than are DCs or macrophages (105). However, soluble antigen uptake and MHC-II presentation by B cells can be detected *in vivo* using antibodies recognizing specific MHC-II-peptide complexes (50). Surface Ig as a component of the BCR promotes rapid and efficient internalization of antigens, enhancing the potency of antigen-specific B cells 10³- to 10⁴-fold as stimulators of CD4⁺ T cells (106).

APCs in general display multiple cell surface receptors that can capture antigens or intact pathogens to promote internalization and processing. Enhanced antigen presentation by MHC-II has been observed following antigen uptake via several receptors that cluster in clathrin-coated domains, including the BCR, Fc receptors, and the C-type lectin family receptor DEC205, as well as mannose and transferrin receptors (107–111). MHC-I cross-presentation was also increased following the internalization of ovalbumin (OVA) via the mannose receptor on DCs and macrophages (112). DEC205 can promote efficient antigen internalization and presentation by both MHC-I and MHC-II, and conjugation of antigens to antibodies recognizing DEC205 has been used to induce tolerance (109). APCs also express receptors for self and microbial heat shock proteins such as Hsp70, Hsp90, and gp96, which promote endocytic uptake of these chaperones and associated ligands (including peptides and

antigens) for MHC-I and MHC-II presentation (113–116).

Receptors on the surface of APCs promote the phagocytosis of bacteria, fungi, select viruses, and apoptotic or necrotic cells (117–119). Macrophages and DCs are well-established phagocytes, but this process can also be observed in B cells, which can present phagocytosed antigens to CD4⁺ T cells (120–122). MHC-I cross-presentation as well as MHC-II presentation of opsonized antigens is enhanced by receptor engagement upon phagocytosis, which may reflect intracellular receptor signaling rather than simply enhanced uptake of these particles. Thus, IgG-coated bacteria were effectively presented to CD8⁺ T cells while complement C3 opsonization of bacteria facilitated phagocytosis but not antigen presentation (123). Signaling by receptors such as the C-type lectin family receptor DNGR-1 promotes MHC-I and MHC-II presentation of antigens from phagocytosed necrotic cells (124, 125). Internalization and presentation of self-antigens associated with necrotic cells may contribute to autoimmunity or allograft rejection. Indeed, while all the above pathways promote uptake of extracellular antigens by APCs, internalization and recycling of the plasma membrane also delivers endogenous proteins for processing; peptides derived from membrane proteins, such as transferrin receptor and MHC-I heavy chain, are abundantly associated with MHC-II molecules (126).

Endocytic Compartments in Antigen Processing and Presentation

Internalized antigens enter organelles with microenvironments favoring protein denaturation and proteolysis. Although these pathways permit MHC-II access to exogenous antigens, MHC-I molecules also use these routes to acquire antigens for cross-presentation (**Figure 2**). Electron microscopy initially revealed an abundance of MHC-II molecules distributed in the endocytic pathway, concentrated in late endosomal vesicles, originally defined as MHC-II compartments, or MIICs

(**Figure 2**), in contrast to only limited amounts of MHC-I (127–129). The role for endosomal MHC-I in cross-presentation has been debated. Disrupting expression of HS-1, a modulator of endocytic invaginations, demonstrated that endocytosis delivers extracellular antigens for presentation by MHC-I as well as by MHC-II in DCs (130). However, in DCs antigens can transit from within endosomes to the cytoplasm or the ER, raising questions about the role of endocytosed MHC-I in antigen cross-presentation (131). A tyrosine motif in the cytoplasmic tail of MHC-I heavy chain facilitates recycling of low levels of these molecules from the cell surface into endosomes, but direct delivery of immature MHC-I from the ER may also occur in DCs, possibly facilitated by associated I chain (57, 132–135).

Early endosomes mature into late endosomes and lysosomes driven in part by processes such as increased luminal acidification and fusion with TGN-derived vesicles delivering enzymes that promote antigen denaturation and proteolysis. Low temperature (18°C) can block the maturation step and disrupt the presentation of several exogenous antigens by MHC-II (136). However, MHC-II presentation of select antigenic epitopes processed within early endosomes can be detected (137, 138). MHC-I-restricted cross-presentation via the mannose receptor was favored by its delivery of antigen into early endosomes (112). Whether this is due to limited antigen processing in these vesicles, favoring epitope recovery by endocytic MHC-I, or to enhanced translocation of antigens into the cytoplasm for redirection via TAP to MHC-I is not clear. Colocalization of MHC-I in endosomes with the insulin-regulated aminopeptidase (IRAP), potentially a substitute for ERAP1, also promoted antigen cross-presentation (139). MHC-I presentation was also facilitated by liposome-mediated antigen delivery into early but not late endosomes, and neutralization of the acidic pH in the latter enhanced antigen presentation by MHC-I. By contrast, antigens delivered via liposomes into early or late endosomes were processed for MHC-II presentation (140).

GILT:

γ -interferon-inducible lysosomal thiolreductase

Mature or late endosomal vesicles are heterogeneous in morphology and content and include translucent and electron dense vesicles, multivesicular bodies containing intraluminal vesicles, multilamellar vesicles, and prelysosomes. Antigen processing in these vesicles is influenced by their pH, which regulates the activity of resident proteases and other relevant enzymes, such as γ -interferon-inducible lysosomal thiolreductase (GILT) (Figure 4) (141–143). Differences in the ability of distinct APCs to regulate endocytic processing have also been documented. For example, the limited protease content and higher pH of DC endocytic compartments may enhance their capacity for presenting antigens via MHC-I and MHC-II compared with macrophages (144). The precise steps in I chain processing vary between APC types, consistent with their differential expression of cathepsins. Studies using protease inhibitors and protease-deficient mice revealed that several enzymes, including cathepsins (S, L, F) and asparaginyl endopeptidase (AEP), mediate I chain cleavage (5). Although cathepsin S plays a key role in the late stages of I chain processing in DCs and B cells, in macrophages cathepsin F is required. Cathepsin L or V is necessary for terminal I chain proteolysis in cortical thymic epithelial cells. Disruptions in I chain processing can impede MHC-II binding to peptides as well as the transit of the complexes to the cell surface (145).

Although it is well established that I chain guides MHC-II to endosomes, the regulation of MHC-II transport within and out of endosomal compartments is not well understood and may differ between APC types. Myosin II, an actin-based motor, may modulate this process in B cells, whereas in DCs MHC-II internalization is mediated by ubiquitination of the cytoplasmic tail of the β chain; DC maturation promotes the expression of MHC-II-peptide complexes on the cell surface (146, 147). Recently, downregulation of the MIR (modulator of immune recognition) family ubiquitin ligase MARCH-1 has been implicated in the reduction of MHC-II ubiquitination and retention of surface expression (148, 149). Subcompartments

within mature endosomes may also regulate MHC-II acquisition of peptides. In multivesicular bodies, the interaction of DM and DO favors their colocalization with HLA-DR in the outer or limiting membrane of these endosomes, whereas DM without DO migrates into internal vesicles that can be shed from cells as exosomes (150, 151). At the cell surface, MHC-II-peptide presentation is greatly enhanced by the clustering in lipid raft microdomains (152).

Phagocytosis, Macropinocytosis, and Antigen Presentation

MHC-I and MHC-II are both detectable within phagosomes (132, 153, 154). Phagosomal antigen processing and MHC-II presentation are well established, and newly formed MHC II-peptide complexes can be detected in these organelles (155). In contrast with endocytosed antigens, MHC-II presentation of phagocytosed antigens is impaired in DCs lacking the cytoplasmic adaptor AP-3 owing to defective transit of MHC-II-peptide complexes to the cell surface (156). Recent studies have revealed the importance of phagocytosis in cross-presentation (117), which typically leads to antigen translocation into the cytoplasm for processing and subsequent delivery for presentation by MHC-I (Figure 2). Processing of phagocytosed antigen by cathepsins has been observed to promote MHC-I cross-presentation, in some cases by a vacuolar peptide exchange pathway (117, 157). In DCs, antigen cross-presentation by MHC-I is enhanced within newly formed phagosomes, which maintain a neutral pH by regulated delivery of NADPH oxidase to the phagosomal membrane (157). In contrast, phagosome maturation and acidification can facilitate MHC-II presentation of pathogen-associated antigens (158).

Exposure of APCs to TLR ligands and proinflammatory cytokines can influence the microenvironment within phagosomes by reducing protease content, controlling luminal pH, and modulating the binding of cytoplasmic

regulatory proteins such as LC3 and GTPases, which mediate phagosome maturation (159–162). In macrophages, phagosome maturation was found to be independent of TLR2 or TLR4 signaling (163), whereas in DCs, TLR4 activation within a specific phagosome drives maturation and MHC-II-restricted antigen presentation within the organelle (164). The pH is higher and the protease content lower within DC endosomes and phagosomes than in macrophages, which preserves epitopes and favors antigen presentation (144). Macrophages, however, are more proficient in killing engulfed pathogens, at least partly because of their higher phagosomal protease content and more acidic phagosomal pH (165).

Macropinocytosis does not rely on receptors (**Figure 2**) but nevertheless captures large antigens and extracellular material into vesicles termed pinosomes (166). These vesicles share features with early and late endosomes but are distinct, although pinosomes eventually fuse with lysosomes (167). TLR ligands can promote a rapid burst of macropinocytosis in DCs that then abruptly halts, stimulating preferential MHC-I and MHC-II presentation of the bolus of internalized antigen (168). A lack of specific inhibitors has limited analysis of macropinocytosis in APCs, although studies suggest a role for this pathway in MHC-II presentation of the autoantigen type II collagen and liposome-coupled antigen presentation via MHC-I (169, 170).

Although TLR signals clearly influence antigen-processing functions, studies in macrophages suggest that intracellular MHC-II molecules help sustain TLR signaling, whereas phosphorylation of intracellular MHC-I molecules promotes SHP-2 inhibition of TLR activation (171, 172). Conceivably, these effects could influence antigen processing and presentation, although whether they do so remains unknown.

Autophagy and Antigen Presentation

Between 10% and 30% of the peptides bound to MHC-II are derived from cytoplasmic and

nuclear proteins (173). Within APCs, three routes of autophagy promote the delivery of proteins and peptides from the cytoplasm and nucleus into the endosomal network (173, 174). In macroautophagy, nuclear and cytoplasmic material, including mitochondria, peroxisomes, and some intracellular bacteria, are engulfed by isolation membranes to form autophagosomes. These fuse with endosomes and lysosomes, facilitating antigen presentation by MHC-II (**Figure 4**) as well as the delivery of nucleic acids to TLRs. MHC-II presentation of Epstein-Barr virus (EBV) nuclear antigen I as well as ectopically expressed recombinant viral and bacterial antigens were perturbed in APCs deficient in macroautophagy (175). Macroautophagy is readily detected in thymic epithelial cells, and disruption of Atg5, a regulator of this process, perturbed the selection of thymic CD4⁺ but not CD8⁺ T cells, implying an effect on MHC-II but not on MHC-I processing (176). The induction of macroautophagy in macrophages and DCs also enhanced MHC-II presentation of mycobacteria, likely owing to more efficient phagosome maturation (177). In B cells, chaperone-mediated autophagy also promoted MHC-II presentation of autoantigens to CD4⁺ T cells (173). In this pathway, cytoplasmic chaperones such as Hsc70 and Hsp90, together with the lysosomal transmembrane protein LAMP-2A, selectively deliver epitopes to MHC-II (**Figure 4**). Proteins may also be captured by microautophagy for delivery into endosomes via Hsc70 and the ESCRT system, although whether this contributes to antigen presentation is unclear (174).

APCs readily acquire and present antigens from target or dying cells for MHC-I and MHC-II, promoting graft rejection and autoimmunity as well as immune responses to pathogens. In APCs, MHC-II presentation of cytoplasmic antigens derived from target cells with diminished TAP, ERAAP, and proteasome activity was enhanced, suggesting a role for these molecules in subverting cross-presentation of cytoplasmic antigens (178). In addition, induction of macroautophagy in tumor or target cells can enhance their

phagocytosis and MHC-I cross-presentation to CD8⁺ T cells (179). By contrast, in DCs, MHC-II direct presentation of membrane antigens from influenza virus required TAP and proteasome activity (180). A requirement for proteasomal processing of some cytoplasmic antigens in MHC-II presentation, as well as a role for ERAAP, has been reported, but the mechanisms by which these components influence the MHC-II pathway remain unclear (178, 181–183).

Epitope Selection and Guided Antigen Processing

Proteins can contain multiple sequences capable of binding MHC molecules, but only a handful of peptides are selected for presentation to T cells. T cell responses are influenced by the diversity of the T cell repertoire, but the steps in antigen processing and presentation play a major role. The concept that a hierarchy of antigenic epitopes is recognized by the immune system is well established; the strongest are called immunodominant, and there are subdominant and cryptic epitopes. Immunodominant epitopes are important for immunity to tumors and pathogens, whereas a shift in the hierarchy of T cell responses to subdominant epitopes is associated with autoimmune disorders (184, 185). Multiple factors contribute to the process of epitope selection by MHC-I and MHC-II molecules. In the case of MHC-I, the specificity of the proteasome, ERAAP/ERAP1, tapasin, and TAP can influence epitope generation and transport to receptive MHC-I molecules (184). For MHC-II, antigen unfolding and proteolysis influence processing and epitope presentation (186, 187). Multiple endocytic proteases have been implicated in processing antigens for MHC-II, including cathepsins B, D, L, and S and AEP, and several of these enzymes also function in I chain processing (5). Antigen reduction facilitates protease access for processing, influencing the generation of antigenic epitopes, and GILT is the key enzyme implicated in this process (142). In melanoma cells, the hierarchy of

epitopes presented by MHC-II is GILT dependent (143). GILT expression also influences autoantigen processing and the development of experimental autoimmune encephalomyelitis and tolerance development to melanocyte antigens (188, 189). MHC-I and MHC-II epitopes can also be destroyed by proteases, which may result in differential epitope presentation by different APC types as well as tissue-specific differences in presentation (5, 190).

The open groove of MHC-II allows large fragments of antigen to bind (**Figure 1**) (191). This led to the concept of guided antigen processing, in which MHC-II binding to epitopes within antigens shapes proteolytic cleavage (192, 193). In B cells, the specific interaction of antigens with the Ig component of the BCR also influences processing and presentation by MHC-II (194). An *in vitro* system reconstituting antigen binding to the BCR followed by digestion with the enzyme AEP favored epitope capture by proximal MHC-II (193). Similarly, MHC-II binding to immunodominant epitopes from an intact protein was reconstituted *in vitro* using soluble purified components, including cathepsins to yield peptides and DM to promote editing of the resulting MHC-II-peptide complexes (195). Epitopes may bind MHC-II in an unstable conformation, and editing of these complexes by DM alters the hierarchy of peptides displayed to CD4⁺ T cells (196). Notably, DM-independent epitope conformations can persist, particularly when the antigen is available to APCs as a peptide rather than an intact protein, and may induce unusual CD4⁺ T cells (so-called Type B T cells) that can lead to autoimmunity (74, 197). Far less is known about the endosomal factors that influence epitope selection for MHC-I cross-presentation, although GILT expression is required for cross-presentation of a disulfide-containing glycoprotein antigen from herpes simplex virus 1 (198). Notably, innate signaling via TLRs during cross-presentation appears to influence antigen presentation, as suggested by a shift in the dominant CD8⁺ T cell epitopes during lymphocytic choriomeningitis virus infection (199).

ANTIGEN INTRODUCTION AND PROTEOLYSIS IN THE CYTOSOL

Protein antigens are conventionally introduced into the cytosol by the cellular protein synthetic machinery. When a virus infects a cell the viral genes are transcribed into mRNAs and these are translated on host ribosomes to generate viral proteins. Although autophagic mechanisms can give them access to the MHC-II pathway, cytosolic antigens are the prime source of MHC-I-associated peptides. Their proteolysis generates peptides that are translocated into the ER by TAP and ultimately bind to MHC-I molecules (**Figure 3**). If they are too long, they are trimmed in the ER by ERAAP/ERAP1/2 as described above. This process is not specific to viral proteins; host proteins are similarly degraded and generate peptides that bind to MHC-I. In fact, in the case of autoimmunity or tumor immunity, MHC-I-associated host protein-derived peptides can be recognized by CD8⁺ T cells. For example, CD8⁺ T cell-mediated killing of melanoma cells, which is exploited for immunotherapy, often involves the recognition of MHC-I-associated peptides derived from melanocyte-specific glycoproteins (200). These proteins are found in melanosomes, the pigment-containing organelles of melanocytes from which melanomas originate. In an infected cell, viral proteins must compete with host proteins for representation in the peptide profile presented to CD8⁺ T cells.

Protein Sources of MHC-I-Associated Peptides

Epitopes from viral glycoproteins, as well as from melanosomal glycoproteins, can be recognized by CD8⁺ T cells. These peptides are generally derived from parts of the antigen that are luminal, not cytosolic (201, 202). Nevertheless, the generation of these MHC-I-peptide complexes is virtually always TAP and proteasome dependent. This implies that, in spite of the presence of a signal sequence and the potential for translocation into the

ER, the processing mechanisms at work are no different from those involved in the generation of peptides from exclusively cytosolic antigens. These observations have contributed to the hypothesis that intact, folded, cytosolic proteins are not the major source of peptides that bind to MHC-I. Instead, the sources are proteins that are either incomplete, perhaps because of premature termination, or misfolded because cytosolic chaperones are not 100% effective in mediating the folding of newly synthesized proteins. In mammalian cells, approximately 30% of total proteins are degraded extremely rapidly following synthesis (**Figure 3**) (203). Yewdell has been a strong advocate of the hypothesis that this rapidly degraded pool is the primary source of MHC-I-associated peptides, coining the acronym DRiP (defective ribosomal product) to describe them, and has recently reviewed the evidence supporting the hypothesis (204). Briefly, very early experiments showed that expression in cells of truncated proteins, which are unstable, generated MHC-I-peptide complexes as effectively as full-length proteins. In fact, the experiments that mapped and defined the first MHC-I-restricted epitope, an influenza nucleoprotein-derived peptide that binds to H2-D^b, relied on the expression of truncated proteins (205). Work by Neefjes and coworkers (206) suggested that newly synthesized proteins are the primary source of TAP-translocated peptides. They showed by FRAP (fluorescence recovery after photobleaching) analysis that the lateral mobility of TAP in the ER membrane decreases when active peptide translocation is occurring and that inhibiting protein synthesis by cycloheximide addition rapidly enhanced TAP mobility. Kinetic analysis of the synthetic rates of cytosolic antigens versus the rates at which complexes of MHC-I and peptide, which are derived from them, are generated confirmed a general principle that the accumulation of the protein lags considerably behind the acquisition of the complexes (207). Using the SILAC (stable isotope labeling with amino acids in cell culture) technique, in which cellular proteins, and the peptides derived from them, are labeled with specific

Defective ribosomal product (DRiP):
misfolded cytosolic protein or truncated protein that arises as a result of premature termination of translation in host cells

isotopic variants of amino acids upon synthesis and identified by mass spectrometry, investigators have observed that there is no clear relationship between the abundance of MHC-I-bound peptides and the abundance of the proteins from which they derive (208). In fact, some MHC-I-associated peptides are derived from proteins that are undetectable in the cell.

Exactly what mechanisms drive DRiP formation are still not entirely clear, although one component may involve modifications to normal translational processes. Work by Fähraeus and coworkers (209, 210) adapted the phenomenon of nonsense-mediated decay, in which mRNA with a premature stop codon is degraded after only a single round of translation, to show that an epitope encoded by such an mRNA is produced with high efficiency for T cell recognition. More recently, Granados et al. (211) used the SILAC method to analyze MHC-I-associated peptides in human EBV-transformed B cell lines and made the intriguing observations that, first, many of the peptides were derived from proteins associated with B cell differentiation rather than more abundant housekeeping proteins and, second, the peptides were preferentially derived from proteins encoded by transcripts that were the targets of microRNAs, which are known to regulate transcript stability. Analysis of data covering multiple epitopes and their sources determined that this is a general phenomenon, not specific to transformed B cell lines. The precise mechanistic connection between mRNA instability and the generation of MHC-I-associated peptides remains unknown.

Chaperones and Cytosolic Peptide Generation

Although DRiPs are a significant and perhaps major source, MHC-I-associated peptides can be derived from intact proteins. Proteins introduced directly into the cytosol of a cell—for example, listeriolysin and other proteins secreted by *Listeria monocytogenes* after its internalization by macrophages (212)—can be processed and recognized by CD8⁺ T cells. What, then, are the intracellular processing

steps that proteins, or DRiPs, follow before they degenerate into the peptides that are translocated into the ER by TAP? Shastri and coworkers (213) developed exceptionally clever techniques to identify the cytosolic precursors of MHC-I-binding peptides and have shown that they are associated with cytosolic chaperones. The approach draws on the ability of exogenous MHC-I-binding peptides to sensitize cells for recognition by CD8⁺ T cells. In the most refined version of the method, the epitope, derived from OVA, is flanked with lysine residues and embedded in a protein that is then expressed in cells. The precise epitope (SIINFEHL, a modification of the classical H2-K^b-associated SIINFEKL epitope with histidine substituted for the normal internal lysine residue) is released from any cytosolic precursor of the peptide by digestion with trypsin, which produces the correct N-terminal amino acid, and carboxypeptidase B, which removes the C-terminal lysine. The exceptional sensitivity of a T cell hybridoma recognizing this epitope allowed the identification of precursors that coimmunoprecipitated with antichaperone antibodies, assaying the proteolytically released epitope by sensitization of an H2-K^b-positive target cell. Large intermediate degradation fragments of the protein were found in association with the chaperone Hsp90 α (213). shRNA-mediated knockdown of Hsp90 α inhibited accumulation of the fragments and processing of the antigen, as well as its recognition by CD8⁺ T cells, as did knockdown of a cochaperone, CHIP (carboxyl terminus of Hsp70-interacting protein), which ubiquitinates Hsp70 or Hsp90 α -associated proteins and delivers them to proteasomes for degradation. This suggests that these fragments are pre-proteasomal. Consistent with this, the addition of a proteasome inhibitor to the cell increased the amounts of the fragments, and they were extended at the C terminus beyond the actual epitope; the C-terminal residue of peptides translocated by TAP and associated with MHC-I is usually generated by proteasomal cleavage (214). Other fragments were associated with another chaperone, the

tailless complex polypeptide-1 (TCP-1) ring complex, or TRiC (215). These fragments were N-terminally extended but not C-terminally extended; i.e., all of them ended with the precise epitope sequence that was originally embedded in the protein. This indicates that they are postproteasomal. Thus, the pathway that has emerged is that a cytosolic protein, usually a recently synthesized or somehow defective one (a DRiP), associates with Hsp90 α , is ubiquitinated by CHIP, and is degraded by the proteasome to yield truncated fragments, which then associate with TRiC. Cytosolic amino terminal trimming, for example, by leucine aminopeptidase (216), can then reduce them to an appropriate size for TAP-mediated transport into the ER. For individual epitopes, cytosolic peptidases, including leucine aminopeptidase and/or tripeptidyl peptidase II, may facilitate or inhibit their generation (217).

Nonconventional Sources of MHC-I-Associated Peptides

The extraordinary sensitivity of T cell recognition is well established. Very low numbers of MHC-I-peptide complexes are required; even a single complex may be sufficient to trigger a T cell (218). Possibly because of this, some MHC-I-associated peptides have origins that do not depend on conventional translation. There are examples of antigenic peptides that are out of frame with regard to their proteins of origin and others derived from sequences embedded in introns (219). There are peptides that derive from translation initiated at codons other than the conventional methionine codon, ATG. Shastri and coworkers (220) have identified a novel translational mechanism that involves leucine-tRNA-mediated initiation of translation at a CUG codon and suggest that other codons may be functional. These experiments constitute recent examples of a historically common phenomenon: Immunological studies often enhance our understanding of molecular biological processes.

There are also examples of peptide epitopes derived from noncontiguous sequences in proteins. Many of these derive from studies of

human epitopes recognized by patient-derived tumor-specific CD8 $^{+}$ T cells. Vigneron et al. (221) described an HLA-A32-associated epitope derived from the melanosomal glycoprotein gp100 (or pmel17) that was a nonamer but was derived from a 13 amino acid precursor by removal of four internal residues. They showed that this excision/splicing event was mediated by the proteasome and involved a mechanism in which the hydrolysis of a bond between the peptide and the active site threonine residue of the proteolytic proteasome β -subunit, normally the final step of proteolysis, is replaced by reaction with the N-terminal amino group of a second peptide instead of water. Several other examples of this have been described, including one peptide in which the N-terminal sequence of the peptide is actually C-terminal to the N-terminal peptide sequence in the intact protein (222).

Another example of an epitope that does not represent the primary sequence of a protein also involves a melanosomal glycoprotein. In this case, an asparagine residue present in the melanosomal enzyme tyrosinase was replaced by an aspartic acid residue in a tyrosinase-derived HLA-A2.1-associated nonameric peptide (223). This occurs because the peptide is generated from the protein after its signal sequence-mediated entry into the ER and subsequent degradation following retrotranslocation into the cytosol. This is the conventional mechanism for disposal of misfolded proteins and glycoproteins and is known as ERAD (224). The proteasome is the normal destination for such retrotranslocated proteins. A component of the pathway for glycoproteins involves their cytosolic deglycosylation by an N-glycanase that converts the glycan-bearing asparagine residue to an aspartic acid (225); the epitope encompassed a glycosylated sequence in tyrosinase that was deglycosylated in the cytosol.

Implications of ERAD for Cross-Presentation

A pathway in which proteins that enter the ER are retrotranslocated into the cytosol and

generate peptides that are potentially available for MHC-I-restricted T cell recognition has a clear parallel to the dominant mechanism involved in cross-presentation. Here, the compartment is an endosome or phagosome rather than the ER, but the underlying principle is the same (**Figure 3**). A luminal protein internalized by a DC must enter the cytosol and be degraded by the proteasome to generate the relevant peptide, in principle the same peptide that would be generated by a normal cell expressing the protein as an endogenously translated protein. Thus, a CD8⁺ T cell induced by cross-presentation of a viral protein would recognize the epitope generated in the infected cell, allowing its destruction. The seductive logic of this argument has led to a considerable body of work suggesting, although not without controversy, that the mechanisms responsible for cross-presentation are an adaptation of ERAD (**Figure 2**). This was first suggested by the work of Desjardin and coworkers, who identified ER-derived proteins in phagosomes purified from a macrophage cell line (226), with the implication that the ERAD retro-translocation machinery could be recruited to phagosomes from the ER. Experimental evidence supporting this rapidly followed. DCs and DC-like cell lines were found to be capable of transferring proteins into the cytosol from endosomes or phagosomes, including enzymes such as luciferases, as well as cytochrome *c* (227–229). The addition of cytochrome *c* to DCs and its entry into the cytosol caused apoptosis, mimicking the effect of cytochrome *c* released from mitochondria in conventionally induced apoptosis (228). Processing and presentation of soluble, exogenous OVA by H2-K^b expressed in a human DC-like cell line, KG-1, could be blocked by a cytosolically expressed, dominant-negative, ATPase-defective, mutant version of the AAA-ATPase p97, which normally mediates the extraction of proteins from the ER during ERAD. In addition, phagosomes derived from KG-1 were capable of extruding luciferases that were internalized along with the phagocytic substrate, a latex bead, into the external milieu, which is topologically

equivalent to the cytosol (227). This was ATP dependent, could be enhanced by recombinant p97, and could be inhibited by recombinant dominant-negative p97, all of which are consistent with an ERAD-like mechanism. TAP and other PLC components were also identified in purified phagosomes, and they were capable of internalizing peptides via TAP and assembling them with MHC-I molecules present in the phagosome (132, 154). This led to the concept that phagosomes in DCs are compartments specialized for MHC-I-restricted antigen processing, and this concept was later extended to endosomes (230). This is an interesting but not essential element of a coherent hypothesis involving ER recruitment to phagosomes. The critical step is the role of ERAD in mediating cytosolic access; after that, proteolytic degradation and TAP-mediated transport of peptides into the ER would be sufficient. However, as mentioned earlier, the ERAP1-like aminopeptidase IRAP is present in DC phagosomes and can facilitate cross-presentation, which is consistent with the idea that they may be dedicated cross-presenting organelles (139).

Vesicular fusion events in cells are regulated by the interactions of SNARE proteins present on the vesicles involved. Recently, it has been shown that recruitment of ER-resident proteins to the phagosome and cross-presentation in DCs is dependent on Sec22b, a SNARE protein localized to the ER-Golgi intermediate compartment (ERGIC), that interacts with a partner SNARE, syntaxin 4, normally present on the plasma membrane but present on phagosomes in DCs (231). This appears to have resolved some of the controversies surrounding the connection of ERAD and cross-presentation, although the nature of the channel that mediates the translocation of internalized antigens into the cytosol of the cross-presenting cell remains unknown.

CONCLUDING REMARKS

The study of antigen processing is now over three decades old, yet novel findings continue to surprise and delight those of us working

in the field. For MHC-I, the mechanisms of cross-presentation and the precise mechanisms that regulate DRiP formation and the cytosolic generation of peptides are areas in need of clarification. For MHC-II, the mechanisms that regulate the formation of the peptide complexes recognized by Type A and Type B CD4⁺ T cells, in particular the role of DM in the process, and the precise function of DO still need to be uncovered. In addition, recent demonstrations of phagocytosis in B cells underlines the need for additional work

to determine how this modulates MHC-I and MHC-II functions in these cells, given the clear differences in the process between B cells, DCs, and macrophages. Applications of mechanistic insights to vaccine development are likely to be important. For example, how do we best incorporate immunogenic epitopes into recombinant vaccines and how can they be moved into the cytosol for effective sensitization of CD8⁺ T cells? Over the next few years, many of these problems will be solved, and questions not yet asked will undoubtedly be answered.

DISCLOSURE STATEMENT

The authors are not aware of any affiliations, memberships, funding, or financial holdings that might be perceived as affecting the objectivity of this review.

ACKNOWLEDGMENTS

This review is an attempt to synthesize the antigen processing field into a semicoherent whole. As a result, we have been forced to focus on some aspects and give short shrift to others. We apologize to our many colleagues who may disagree with our points of emphasis and to those who will no doubt believe their work is inadequately cited. We thank Nancy Dometios for assistance with manuscript preparation. Work by the authors has been supported by grants from the National Institutes of Health (P01 AI056097, R01AI079065, P01AI084853, U01DK085505, RO1AI069085, R01AI059167, R01AI097206) and by the Howard Hughes Medical Institute.

LITERATURE CITED

1. Cohen NR, Garg S, Brenner MB. 2009. Antigen presentation by CD1 lipids, T cells, and NKT cells in microbial immunity. *Adv. Immunol.* 102:1–94
2. Adams EJ, Luoma AM. 2013. The adaptable major histocompatibility complex (MHC) fold: structure and function of nonclassical and MHC-like class I molecules. *Annu. Rev. Immunol.* 31:529–61
3. Maupin-Furlow J. 2012. Proteasomes and protein conjugation across domains of life. *Nat. Rev. Microbiol.* 10:100–11
4. Huotari J, Helenius A. 2011. Endosome maturation. *EMBO J.* 30:3481–500
5. Watts C. 2004. The exogenous pathway for antigen presentation on major histocompatibility complex class II and CD1 molecules. *Nat. Immunol.* 5:685–92
6. Oancea G, O'Mara ML, Bennett WF, Tielemans DP, Abele R, Tampe R. 2009. Structural arrangement of the transmission interface in the antigen ABC transport complex TAP. *Proc. Natl. Acad. Sci. USA* 106:5551–56
7. Hinz A, Tampe R. 2012. ABC transporters and immunity: mechanism of self-defense. *Biochemistry* 51:4981–89
8. Gaudet R, Wiley DC. 2001. Structure of the ABC ATPase domain of human TAP1, the transporter associated with antigen processing. *EMBO J.* 20:4964–72
9. Ortmann B, Copeman J, Lehner PJ, Sadasivan B, Herberg JA, et al. 1997. A critical role for tapasin in the assembly and function of multimeric MHC class I-TAP complexes. *Science* 277:1306–9

10. Tan P, Kropshofer H, Mandelboim O, Bulbuc N, Hammerling GJ, Momburg F. 2002. Recruitment of MHC class I molecules by tapasin into the transporter associated with antigen processing-associated complex is essential for optimal peptide loading. *J. Immunol.* 168:1950–60
11. Procko E, Raghuraman G, Wiley DC, Raghavan M, Gaudet R. 2005. Identification of domain boundaries within the N-termini of TAP1 and TAP2 and their importance in tapasin binding and tapasin-mediated increase in peptide loading of MHC class I. *Immunol. Cell Biol.* 83:475–82
12. Koch J, Guntrum R, Heintke S, Kyritsis C, Tampe R. 2004. Functional dissection of the transmembrane domains of the transporter associated with antigen processing (TAP). *J. Biol. Chem.* 279:10142–47
13. Leonhardt RM, Keusekotten K, Bekpen C, Knittler MR. 2005. Critical role for the tapasin-docking site of TAP2 in the functional integrity of the MHC class I-peptide-loading complex. *J. Immunol.* 175:5104–14
14. Sadasivan B, Lehner PJ, Ortmann B, Spies T, Cresswell P. 1996. Roles for calreticulin and a novel glycoprotein, tapasin, in the interaction of MHC class I molecules with TAP. *Immunity* 5:103–14
15. Panter MS, Jain A, Leonhardt RM, Ha T, Cresswell P. 2012. Dynamics of major histocompatibility complex class I association with the human peptide-loading complex. *J. Biol. Chem.* 287:31172–84
16. Dong G, Wearsch PA, Peaper DR, Cresswell P, Reinisch KM. 2009. Insights into MHC class I peptide loading from the structure of the tapasin-ERp57 thiol oxidoreductase heterodimer. *Immunity* 30:21–32
17. Dick TP, Bangia N, Peaper DR, Cresswell P. 2002. Disulfide bond isomerization and the assembly of MHC class I-peptide complexes. *Immunity* 16:87–98
18. Hebert DN, Garman SC, Molinari M. 2005. The glycan code of the endoplasmic reticulum: asparagine-linked carbohydrates as protein maturation and quality-control tags. *Trends Cell Biol.* 15:364–70
19. Caramelo JJ, Castro OA, de Prat-Gay G, Parodi AJ. 2004. The endoplasmic reticulum glucosyltransferase recognizes nearly native glycoprotein folding intermediates. *J. Biol. Chem.* 279:46280–85
20. Ritter C, Quirin K, Kowarik M, Helenius A. 2005. Minor folding defects trigger local modification of glycoproteins by the ER folding sensor GT. *EMBO J.* 24:1730–38
21. Solda T, Galli C, Kaufman RJ, Molinari M. 2007. Substrate-specific requirements for UGT1-dependent release from calnexin. *Mol. Cell* 27:238–49
22. Gabathuler R, Reid G, Kolaitis G, Driscoll J, Jefferies WA. 1994. Comparison of cell lines deficient in antigen presentation reveals a functional role for TAP-1 alone in antigen processing. *J. Exp. Med.* 180:1415–25
23. Lampen MH, Verweij MC, Querido B, van der Burg SH, Wiertz EJ, van Hall T. 2010. CD8⁺ T cell responses against TAP-inhibited cells are readily detected in the human population. *J. Immunol.* 185:6508–17
24. Wei ML, Cresswell P. 1992. HLA-A2 molecules in an antigen-processing mutant cell contain signal sequence-derived peptides. *Nature* 356:443–46
25. Peh CA, Laham N, Burrows SR, Zhu Y, McCluskey J. 2000. Distinct functions of tapasin revealed by polymorphism in MHC class I peptide loading. *J. Immunol.* 164:292–99
26. Purcell AW, Gorman JJ, Garcia-Peydro M, Paradela A, Burrows SR, et al. 2001. Quantitative and qualitative influences of tapasin on the class I peptide repertoire. *J. Immunol.* 166:1016–27
27. Grandea AG III, Golovina TN, Hamilton SE, Sriram V, Spies T, et al. 2000. Impaired assembly yet normal trafficking of MHC class I molecules in *Tapasin* mutant mice. *Immunity* 13:213–22
28. Garbi N, Tan P, Diehl AD, Chambers BJ, Ljunggren HG, et al. 2000. Impaired immune responses and altered peptide repertoire in tapasin-deficient mice. *Nat. Immunol.* 1(3):234–38
29. Williams AP, Peh CA, Purcell AW, McCluskey J, Elliott T. 2002. Optimization of the MHC class I peptide cargo is dependent on tapasin. *Immunity* 16:509–20
30. Howarth M, Williams A, Tolstrup AB, Elliott T. 2004. Tapasin enhances MHC class I peptide presentation according to peptide half-life. *Proc. Natl. Acad. Sci. USA* 101:11737–42
31. Wearsch PA, Cresswell P. 2007. Selective loading of high-affinity peptides onto major histocompatibility complex class I molecules by the tapasin-ERp57 heterodimer. *Nat. Immunol.* 8:873–81
32. Wearsch PA, Peaper DR, Cresswell P. 2011. Essential glycan-dependent interactions optimize MHC class I peptide loading. *Proc. Natl. Acad. Sci. USA* 108:4950–55
33. Chen M, Bouvier M. 2007. Analysis of interactions in a tapasin/class I complex provides a mechanism for peptide selection. *EMBO J.* 26:1681–90

34. Gao B, Adhikari R, Howarth M, Nakamura K, Gold MC, et al. 2002. Assembly and antigen-presenting function of MHC class I molecules in cells lacking the ER chaperone calreticulin. *Immunity* 16:99–109
35. Garbi N, Tanaka S, Momburg F, Hammerling GJ. 2006. Impaired assembly of the major histocompatibility complex class I peptide-loading complex in mice deficient in the oxidoreductase ERp57. *Nat. Immunol.* 7:93–102
36. Peaper DR, Cresswell P. 2008. The redox activity of ERp57 is not essential for its functions in MHC class I peptide loading. *Proc. Natl. Acad. Sci. USA* 105:10477–82
37. Zhang W, Wearsch PA, Zhu Y, Leonhardt RM, Cresswell P. 2011. A role for UDP-glucose glycoprotein glucosyltransferase in expression and quality control of MHC class I molecules. *Proc. Natl. Acad. Sci. USA* 108:4956–61
38. Ruddock LW, Molinari M. 2006. N-glycan processing in ER quality control. *J. Cell Sci.* 119:4373–80
39. Serwold T, Gonzalez F, Kim J, Jacob R, Shastri N. 2002. ERAAP customizes peptides for MHC class I molecules in the endoplasmic reticulum. *Nature* 419:480–83
40. Saric T, Chang SC, Hattori A, York IA, Markant S, et al. 2002. An IFN- γ -induced aminopeptidase in the ER, ERAP1, trims precursors to MHC class I-presented peptides. *Nat. Immunol.* 3:1169–76
41. Saveanu L, Carroll O, Lindo V, Del Val M, Lopez D, et al. 2005. Concerted peptide trimming by human ERAP1 and ERAP2 aminopeptidase complexes in the endoplasmic reticulum. *Nat. Immunol.* 6:689–97
42. Koopmann JO, Post M, Neefjes JJ, Hammerling GJ, Momburg F. 1996. Translocation of long peptides by transporters associated with antigen processing (TAP). *Eur. J. Immunol.* 26:1720–28
43. Nguyen TT, Chang SC, Evnouchidou I, York IA, Zikos C, et al. 2011. Structural basis for antigenic peptide precursor processing by the endoplasmic reticulum aminopeptidase ERAP1. *Nat. Struct. Mol. Biol.* 18:604–13
44. Hammer GE, Gonzalez F, Champsaur M, Cado D, Shastri N. 2006. The aminopeptidase ERAAP shapes the peptide repertoire displayed by major histocompatibility complex class I molecules. *Nat. Immunol.* 7:103–12
45. Hammer GE, Gonzalez F, James E, Nolla H, Shastri N. 2007. In the absence of aminopeptidase ERAAP, MHC class I molecules present many unstable and highly immunogenic peptides. *Nat. Immunol.* 8:101–8
46. Blanchard N, Kanaseki T, Escobar H, Delebecque F, Nagarajan NA, et al. 2010. Endoplasmic reticulum aminopeptidase associated with antigen processing defines the composition and structure of MHC class I peptide repertoire in normal and virus-infected cells. *J. Immunol.* 184:3033–42
47. Landsverk OJ, Bakke O, Gregers TF. 2009. MHC II and the endocytic pathway: regulation by invariant chain. *Scand. J. Immunol.* 70:184–93
48. Fineschi B, Sakaguchi K, Appella E, Miller J. 1996. The proteolytic environment involved in MHC class II-restricted antigen presentation can be modulated by the p41 form of invariant chain. *J. Immunol.* 157:3211–15
49. Pond L, Kuhn LA, Teyton L, Schutze MP, Tainer JA, et al. 1995. A role for acidic residues in di-leucine motif-based targeting to the endocytic pathway. *J. Biol. Chem.* 270:19989–97
50. Zhong G, Romagnoli P, Germain RN. 1997. Related leucine-based cytoplasmic targeting signals in invariant chain and major histocompatibility complex class II molecules control endocytic presentation of distinct determinants in a single protein. *J. Exp. Med.* 185:429–38
51. Ceman S, Sant AJ. 1995. The function of invariant chain in class II-restricted antigen presentation. *Semin. Immunol.* 7:373–87
52. Naujokas MF, Morin M, Anderson MS, Peterson M, Miller J. 1993. The chondroitin sulfate form of invariant chain can enhance stimulation of T cell responses through interaction with CD44. *Cell* 74:257–68
53. Kang SJ, Cresswell P. 2002. Regulation of intracellular trafficking of human CD1d by association with MHC class II molecules. *EMBO J.* 21:1650–60
54. Sugita M, Brenner MB. 1995. Association of the invariant chain with major histocompatibility complex class I molecules directs trafficking to endocytic compartments. *J. Biol. Chem.* 270:1443–48
55. Ye L, Liu X, Rout SN, Li Z, Yan Y, et al. 2008. The MHC class II-associated invariant chain interacts with the neonatal Fc γ receptor and modulates its trafficking to endosomal/lysosomal compartments. *J. Immunol.* 181:2572–85

56. Jayawardena-Wolf J, Benlagha K, Chiu YH, Mehr R, Bendelac A. 2001. CD1d endosomal trafficking is independently regulated by an intrinsic CD1d-encoded tyrosine motif and by the invariant chain. *Immunity* 15:897–908
57. Basha G, Omilusik K, Chavez-Steenbock A, Reinicke AT, Lack N, et al. 2012. A CD74-dependent MHC class I endolysosomal cross-presentation pathway. *Nat. Immunol.* 13:237–45
58. Marks MS, Blum JS, Cresswell P. 1990. Invariant chain trimers are sequestered in the rough endoplasmic reticulum in the absence of association with HLA class II antigens. *J. Cell Biol.* 111:839–55
59. Roche PA, Marks MS, Cresswell P. 1991. Formation of a nine-subunit complex by HLA class II glycoproteins and the invariant chain. *Nature* 354:392–94
60. Anderson MS, Miller J. 1992. Invariant chain can function as a chaperone protein for class II major histocompatibility complex molecules. *Proc. Natl. Acad. Sci. USA* 89:2282–86
61. Bikoff EK, Huang LY, Episkopou V, van Meerwijk J, Germain RN, Robertson EJ. 1993. Defective major histocompatibility complex class II assembly, transport, peptide acquisition, and CD4⁺ T cell selection in mice lacking invariant chain expression. *J. Exp. Med.* 177:1699–712
62. van Lith M, McEwen-Smith RM, Benham AM. 2010. HLA-DP, HLA-DQ, and HLA-DR have different requirements for invariant chain and HLA-DM. *J. Biol. Chem.* 285:40800–8
63. Roche PA, Cresswell P. 1990. Invariant chain association with HLA-DR molecules inhibits immunogenic peptide binding. *Nature* 345:615–18
64. Teyton L, O'Sullivan D, Dickson PW, Lotteau V, Sette A, et al. 1990. Invariant chain distinguishes between the exogenous and endogenous antigen presentation pathways. *Nature* 348:39–44
65. Roche PA, Teletski CL, Stang E, Bakke O, Long EO. 1993. Cell surface HLA-DR-invariant chain complexes are targeted to endosomes by rapid internalization. *Proc. Natl. Acad. Sci. USA* 90:8581–85
66. Watts C. 2012. The endosome-lysosome pathway and information generation in the immune system. *Biochim. Biophys. Acta* 1824:14–21
67. Riberdy JM, Newcomb JR, Surman MJ, Barbosa JA, Cresswell P. 1992. HLA-DR molecules from an antigen-processing mutant cell line are associated with invariant chain peptides. *Nature* 360:474–77
68. Sette A, Ceman S, Kubo RT, Sakaguchi K, Appella E, et al. 1992. Invariant chain peptides in most HLA-DR molecules of an antigen-processing mutant. *Science* 258:1801–4
69. Ghosh P, Amaya M, Mellins E, Wiley DC. 1995. The structure of an intermediate in class II MHC maturation: CLIP bound to HLA-DR3. *Nature* 378:457–62
70. Busch R, Rinderknecht CH, Roh S, Lee AW, Harding JJ, et al. 2005. Achieving stability through editing and chaperoning: regulation of MHC class II peptide binding and expression. *Immunol. Rev.* 207:242–60
71. Miyazaki T, Wolf P, Tourne S, Waltzinger C, Dierich A, et al. 1996. Mice lacking H2-M complexes, enigmatic elements of the MHC class II peptide-loading pathway. *Cell* 84:531–41
72. Rohn TA, Boes M, Wolters D, Spindeldreher S, Muller B, et al. 2004. Upregulation of the CLIP self peptide on mature dendritic cells antagonizes T helper type 1 polarization. *Nat. Immunol.* 5:909–18
73. Mohan JF, Petzold SJ, Unanue ER. 2011. Register shifting of an insulin peptide-MHC complex allows diabetogenic T cells to escape thymic deletion. *J. Exp. Med.* 208:2375–83
74. Pu Z, Lovitch SB, Bikoff EK, Unanue ER. 2004. T cells distinguish MHC-peptide complexes formed in separate vesicles and edited by H2-DM. *Immunity* 20:467–76
75. Morris P, Shaman J, Attaya M, Amaya M, Goodman S, et al. 1994. An essential role for HLA-DM in antigen presentation by class II major histocompatibility molecules. *Nature* 368:551–54
76. Denzin LK, Cresswell P. 1995. HLA-DM induces CLIP dissociation from MHC class II $\alpha\beta$ dimers and facilitates peptide loading. *Cell* 82:155–65
77. Fremont DH, Crawford F, Marrack P, Hendrickson WA, Kappler J. 1998. Crystal structure of mouse H2-M. *Immunity* 9:385–93
78. Mosyak L, Zaller DM, Wiley DC. 1998. The structure of HLA-DM, the peptide exchange catalyst that loads antigen onto class II MHC molecules during antigen presentation. *Immunity* 9:377–83
79. Marks MS, Roche PA, van Donselaar E, Woodruff L, Peters PJ, Bonifacino JS. 1995. A lysosomal targeting signal in the cytoplasmic tail of the β chain directs HLA-DM to MHC class II compartments. *J. Cell Biol.* 131:351–69
80. Lindstedt R, Liljedahl M, Peleraux A, Peterson PA, Karlsson L. 1995. The MHC class II molecule H2-M is targeted to an endosomal compartment by a tyrosine-based targeting motif. *Immunity* 3:561–72

81. Pierre P, Shachar I, Matza D, Gatti E, Flavell RA, Mellman I. 2000. Invariant chain controls H2-M proteolysis in mouse splenocytes and dendritic cells. *J. Exp. Med.* 191:1057–62
82. Sloan VS, Cameron P, Porter G, Gammon M, Amaya M, et al. 1995. Mediation by HLA-DM of dissociation of peptides from HLA-DR. *Nature* 375:802–6
83. Sherman MA, Weber DA, Jensen PE. 1995. DM enhances peptide binding to class II MHC by release of invariant chain-derived peptide. *Immunity* 3:197–205
84. Fung-Leung WP, Surh CD, Liljedahl M, Pang J, Leturcq D, et al. 1996. Antigen presentation and T cell development in H2-M-deficient mice. *Science* 271:1278–81
85. Martin WD, Hicks GG, Mendiratta SK, Leva HI, Ruley HE, Van Kaer L. 1996. H2-M mutant mice are defective in the peptide loading of class II molecules, antigen presentation, and T cell repertoire selection. *Cell* 84:543–50
86. Kropshofer H, Vogt AB, Moldenhauer G, Hammer J, Blum JS, Hammerling GJ. 1996. Editing of the HLA-DR-peptide repertoire by HLA-DM. *EMBO J.* 15:6144–54
87. Kovats S, Whiteley PE, Concannon P, Rudensky AY, Blum JS. 1997. Presentation of abundant endogenous class II DR-restricted antigens by DM-negative B cell lines. *Eur. J. Immunol.* 27:1014–21
88. Kovats S, Grubin CE, Eastman S, deRoos P, Dongre A, et al. 1998. Invariant chain-independent function of H-2M in the formation of endogenous peptide-major histocompatibility complex class II complexes in vivo. *J. Exp. Med.* 187:245–51
89. Ma C, Blum JS. 1997. Receptor-mediated endocytosis of antigens overcomes the requirement for HLA-DM in class II-restricted antigen presentation. *J. Immunol.* 158:1–4
90. Denzin LK, Sant'Angelo DB, Hammond C, Surman MJ, Cresswell P. 1997. Negative regulation by HLA-DO of MHC class II-restricted antigen processing. *Science* 278:106–9
91. Liljedahl M, Winqvist O, Surh CD, Wong P, Ngo K, et al. 1998. Altered antigen presentation in mice lacking H2-O. *Immunity* 8:233–43
92. Chen X, Jensen PE. 2004. The expression of HLA-DO (H2-O) in B lymphocytes. *Immunol. Res.* 29:19–28
93. Hornell TM, Burster T, Jahnsen FL, Pashine A, Ochoa MT, et al. 2006. Human dendritic cell expression of HLA-DO is subset specific and regulated by maturation. *J. Immunol.* 176:3536–47
94. Fallas JL, Yi W, Draghi NA, O'Rourke HM, Denzin LK. 2007. Expression patterns of H2-O in mouse B cells and dendritic cells correlate with cell function. *J. Immunol.* 178:1488–97
95. Porter GW, Yi W, Denzin LK. 2011. TLR agonists downregulate H2-O in CD8 α - dendritic cells. *J. Immunol.* 187:4151–60
96. Liljedahl M, Kuwana T, Fung-Leung WP, Jackson MR, Peterson PA, Karlsson L. 1996. HLA-DO is a lysosomal resident which requires association with HLA-DM for efficient intracellular transport. *EMBO J.* 15:4817–24
97. Yoon T, Macmillan H, Mortimer SE, Jiang W, Rinderknecht CH, et al. 2012. Mapping the HLA-DO/HLA-DM complex by FRET and mutagenesis. *Proc. Natl. Acad. Sci. USA* 109:11276–81
98. Guce AI, Mortimer SE, Yoon T, Painter CA, Jiang W, et al. 2013. HLA-DO acts as a substrate mimic to inhibit HLA-DM by a competitive mechanism. *Nat. Struct. Mol. Biol.* 20:90–98
99. Perraudeau M, Taylor PR, Stauss HJ, Lindstedt R, Bygrave AE, et al. 2000. Altered major histocompatibility complex class II peptide loading in H2-O-deficient mice. *Eur. J. Immunol.* 30:2871–80
100. Fallas JL, Tobin HM, Lou O, Guo D, Sant'Angelo DB, Denzin LK. 2004. Ectopic expression of HLA-DO in mouse dendritic cells diminishes MHC class II antigen presentation. *J. Immunol.* 173:1549–60
101. Yi W, Seth NP, Martillotti T, Wucherpfennig KW, Sant'Angelo DB, Denzin LK. 2010. Targeted regulation of self-peptide presentation prevents type I diabetes in mice without disrupting general immunocompetence. *J. Clin. Investig.* 120:1324–36
102. Alix E, Mukherjee S, Roy CR. 2011. Subversion of membrane transport pathways by vacuolar pathogens. *J. Cell Biol.* 195:943–52
103. Ham H, Sreelatha A, Orth K. 2011. Manipulation of host membranes by bacterial effectors. *Nat. Rev. Microbiol.* 9:635–46
104. Kuballa P, Nolte WM, Castoreno AB, Xavier RJ. 2012. Autophagy and the immune system. *Annu. Rev. Immunol.* 30:611–46
105. Watts C. 1997. Capture and processing of exogenous antigens for presentation on MHC molecules. *Annu. Rev. Immunol.* 15:821–50

106. Lanzavecchia A. 1985. Antigen-specific interaction between T and B cells. *Nature* 314:537–9
107. Davidson HW, West MA, Watts C. 1990. Endocytosis, intracellular trafficking, and processing of membrane IgG and monovalent antigen/membrane IgG complexes in B lymphocytes. *J. Immunol.* 144:4101–9
108. Gil-Torregrosa BC, Lennon-Dumenil AM, Kessler B, Guermonprez P, Ploegh HL, et al. 2004. Control of cross-presentation during dendritic cell maturation. *Eur J. Immunol.* 34:398–407
109. Bonifaz LC, Bonnyay DP, Charalambous A, Darguste DI, Fujii S, et al. 2004. In vivo targeting of antigens to maturing dendritic cells via the DEC-205 receptor improves T cell vaccination. *J. Exp. Med.* 199:815–24
110. Lorenz RG, Blum JS, Allen PM. 1990. Constitutive competition by self proteins for antigen presentation can be overcome by receptor-enhanced uptake. *J. Immunol.* 144:1600–6
111. McCoy KL, Page MS, Merkel BJ, Inman JK, Stutzman R. 1993. Differences among various lineages of antigen-presenting cells in processing exogenous antigen internalized through transferrin receptors. *J. Immunol.* 151:6757–68
112. Burgdorf S, Kautz A, Bohnert V, Knolle PA, Kurts C. 2007. Distinct pathways of antigen uptake and intracellular routing in CD4 and CD8 T cell activation. *Science* 316:612–16
113. Castellino F, Boucher PE, Eichelberg K, Mayhew M, Rothman JE, et al. 2000. Receptor-mediated uptake of antigen/heat shock protein complexes results in major histocompatibility complex class I antigen presentation via two distinct processing pathways. *J. Exp. Med.* 191:1957–64
114. Tobian AA, Harding CV, Canaday DH. 2005. *Mycobacterium tuberculosis* heat shock fusion protein enhances class I MHC cross-processing and -presentation by B lymphocytes. *J. Immunol.* 174:5209–14
115. Houlihan JL, Metzler JJ, Blum JS. 2009. HSP90 α and HSP90 β isoforms selectively modulate MHC class II antigen presentation in B cells. *J. Immunol.* 182:7451–58
116. Matsutake T, Sawamura T, Srivastava PK. 2010. High efficiency CD91- and LOX-1-mediated representation of gp96-chaperoned peptides by MHC II molecules. *Cancer Immun.* 10:7
117. Ramachandra L, Simmons D, Harding CV. 2009. MHC molecules and microbial antigen processing in phagosomes. *Curr. Opin. Immunol.* 21:98–104
118. Schelhaas M. 2010. Come in and take your coat off—how host cells provide endocytosis for virus entry. *Cell. Microbiol.* 12:1378–88
119. Schulz O, Reis e Sousa C. 2002. Cross-presentation of cell-associated antigens by CD8 α^+ dendritic cells is attributable to their ability to internalize dead cells. *Immunology* 107:183–89
120. Vidard L, Kovacsics-Bankowski M, Kraeft SK, Chen LB, Benacerraf B, Rock KL. 1996. Analysis of MHC class II presentation of particulate antigens of B lymphocytes. *J. Immunol.* 156:2809–18
121. Gao J, Ma X, Gu W, Fu M, An J, et al. 2012. Novel functions of murine B1 cells: active phagocytic and microbicidal abilities. *Eur. J. Immunol.* 42:982–92
122. Parra D, Rieger AM, Li J, Zhang YA, Randall LM, et al. 2012. Pivotal advance: peritoneal cavity B-1 B cells have phagocytic and microbicidal capacities and present phagocytosed antigen to CD4 $^+$ T cells. *J. Leukoc. Biol.* 91:525–36
123. Kim SH, Visser A, Cruijsen C, van der Velden AW, Boes M. 2008. Recruitment of Rab27a to phagosomes controls microbial antigen cross-presentation by dendritic cells. *Infect. Immun.* 76:5373–80
124. Sancho D, Joffre OP, Keller AM, Rogers NC, Martinez D, et al. 2009. Identification of a dendritic cell receptor that couples sensing of necrosis to immunity. *Nature* 458:899–903
125. Joffre OP, Sancho D, Zelenay S, Keller AM, Reis e Sousa C. 2010. Efficient and versatile manipulation of the peripheral CD4 $^+$ T-cell compartment by antigen targeting to DNLR-1/CLEC9A. *Eur. J. Immunol.* 40:1255–65
126. Chicz RM, Urban RG, Gorga JC, Vignali DA, Lane WS, Strominger JL. 1993. Specificity and promiscuity among naturally processed peptides bound to HLA-DR alleles. *J. Exp. Med.* 178:27–47
127. Guagliardi LE, Koppelman B, Blum JS, Marks MS, Cresswell P, Brodsky FM. 1990. Co-localization of molecules involved in antigen processing and presentation in an early endocytic compartment. *Nature* 343:133–39
128. Harding CV, Unanue ER, Slot JW, Schwartz AL, Geuze HJ. 1990. Functional and ultrastructural evidence for intracellular formation of major histocompatibility complex class II-peptide complexes during antigen processing. *Proc. Natl. Acad. Sci. USA* 87:5553–57

129. Peters PJ, Neefjes JJ, Oorschot V, Ploegh HL, Geuze HJ. 1991. Segregation of MHC class II molecules from MHC class I molecules in the Golgi complex for transport to lysosomal compartments. *Nature* 349:669–76
130. Huang Y, Biswas C, Klos Dehring DA, Sriram U, Williamson EK, et al. 2011. The actin regulatory protein HS1 is required for antigen uptake and presentation by dendritic cells. *J. Immunol.* 187:5952–63
131. Ackerman AL, Kyritsis C, Tampe R, Cresswell P. 2005. Access of soluble antigens to the endoplasmic reticulum can explain cross-presentation by dendritic cells. *Nat. Immunol.* 6:107–13
132. Ackerman AL, Kyritsis C, Tampe R, Cresswell P. 2003. Early phagosomes in dendritic cells form a cellular compartment sufficient for cross presentation of exogenous antigens. *Proc. Natl. Acad. Sci. USA* 100:12889–94
133. Chiu I, Davis DM, Strominger JL. 1999. Trafficking of spontaneously endocytosed MHC proteins. *Proc. Natl. Acad. Sci. USA* 96:13944–49
134. Reid PA, Watts C. 1990. Cycling of cell-surface MHC glycoproteins through primaquine-sensitive intracellular compartments. *Nature* 346:655–57
135. Lizée G, Basha G, Tiong J, Julien JP, Tian M, et al. 2003. Control of dendritic cell cross-presentation by the major histocompatibility complex class I cytoplasmic domain. *Nat. Immunol.* 4:1065–73
136. Harding CV, Unanue ER. 1990. Low-temperature inhibition of antigen processing and iron uptake from transferrin: deficits in endosome functions at 18 degrees C. *Eur. J. Immunol.* 20:323–29
137. Griffin JP, Chu R, Harding CV. 1997. Early endosomes and a late endocytic compartment generate different peptide-class II MHC complexes via distinct processing mechanisms. *J. Immunol.* 158:1523–32
138. Pathak SS, Blum JS. 2000. Endocytic recycling is required for the presentation of an exogenous peptide via MHC class II molecules. *Traffic* 1:561–69
139. Saveanu L, Carroll O, Weimershaus M, Guermonprez P, Firat E, et al. 2009. IRAP identifies an endosomal compartment required for MHC class I cross-presentation. *Science* 325:213–17
140. Harding CV, Unanue ER. 1991. Modulation of antigen presentation and peptide-MHC-specific, LFA-1-dependent T cell-macrophage adhesion. *J. Immunol.* 147:767–73
141. Muller S, Dennemarker J, Reinheckel T. 2012. Specific functions of lysosomal proteases in endocytic and autophagic pathways. *Biochim. Biophys. Acta* 1824:34–43
142. Maric M, Arunachalam B, Phan UT, Dong C, Garrett WS, et al. 2001. Defective antigen processing in GILT-free mice. *Science* 294:1361–65
143. Haque MA, Li P, Jackson SK, Zarour HM, Hawes JW, et al. 2002. Absence of γ -interferon-inducible lysosomal thiol reductase in melanomas disrupts T cell recognition of select immunodominant epitopes. *J. Exp. Med.* 195:1267–77
144. Delamarre L, Pack M, Chang H, Mellman I, Trombetta ES. 2005. Differential lysosomal proteolysis in antigen-presenting cells determines antigen fate. *Science* 307:1630–34
145. Neefjes JJ, Stollorz V, Peters PJ, Geuze HJ, Ploegh HL. 1990. The biosynthetic pathway of MHC class II but not class I molecules intersects the endocytic route. *Cell* 61:171–83
146. Vascotto F, Lankar D, Faure-Andre G, Vargas P, Diaz J, et al. 2007. The actin-based motor protein myosin II regulates MHC class II trafficking and BCR-driven antigen presentation. *J. Cell Biol.* 176:1007–19
147. van Niel G, Wubbolts R, ten Broeke T, Buschow SI, Ossendorp FA, et al. 2006. Dendritic cells regulate exposure of MHC class II at their plasma membrane by oligoubiquitination. *Immunity* 25:885–94
148. De Gassart A, Camossetto V, Thibodeau J, Ceppi M, Catalan N, et al. 2008. MHC class II stabilization at the surface of human dendritic cells is the result of maturation-dependent MARCH I down-regulation. *Proc. Natl. Acad. Sci. USA* 105:3491–96
149. Ishido S, Goto E, Matsuki Y, Ohmura-Hoshino M. 2009. E3 ubiquitin ligases for MHC molecules. *Curr. Opin. Immunol.* 21:78–83
150. van Lith M, van Ham M, Griekspoor A, Tjin E, Verwoerd D, et al. 2001. Regulation of MHC class II antigen presentation by sorting of recycling HLA-DM/DO and class II within the multivesicular body. *J. Immunol.* 167:884–92
151. Xiu F, Cote MH, Bourgeois-Daigneault MC, Brunet A, Gauvreau ME, et al. 2011. Cutting edge: HLA-DO impairs the incorporation of HLA-DM into exosomes. *J. Immunol.* 187:1547–51

152. Anderson HA, Hiltbold EM, Roche PA. 2000. Concentration of MHC class II molecules in lipid rafts facilitates antigen presentation. *Nat. Immunol.* 1:156–62
153. Harding CV, Geuze HJ. 1992. Class II MHC molecules are present in macrophage lysosomes and phagolysosomes that function in the phagocytic processing of *Listeria monocytogenes* for presentation to T cells. *J. Cell Biol.* 119:531–42
154. Houde M, Bertholet S, Gagnon E, Brunet S, Goyette G, et al. 2003. Phagosomes are competent organelles for antigen cross-presentation. *Nature* 425:402–6
155. Muraille E, Gounon P, Cazareth J, Hoebeke J, Lippuner C, et al. 2010. Direct visualization of peptide/MHC complexes at the surface and in the intracellular compartments of cells infected in vivo by *Leishmania major*. *PLoS Pathog.* 6:e1001154
156. Mantegazza AR, Guttentag SH, El-Benna J, Sasai M, Iwasaki A, et al. 2012. Adaptor protein-3 in dendritic cells facilitates phagosomal toll-like receptor signaling and antigen presentation to CD4⁺ T cells. *Immunity* 36:782–94
157. Amigorena S, Savina A. 2010. Intracellular mechanisms of antigen cross presentation in dendritic cells. *Curr. Opin. Immunol.* 22:109–17
158. Singh CR, Moulton RA, Armitige LY, Bidani A, Snuggs M, et al. 2006. Processing and presentation of a mycobacterial antigen 85B epitope by murine macrophages is dependent on the phagosomal acquisition of vacuolar proton ATPase and *in situ* activation of cathepsin D. *J. Immunol.* 177:3250–59
159. Yates RM, Hermetter A, Taylor GA, Russell DG. 2007. Macrophage activation downregulates the degradative capacity of the phagosome. *Traffic* 8:241–50
160. Jutras I, Houde M, Currier N, Boulais J, Duclos S, et al. 2008. Modulation of the phagosome proteome by interferon- γ . *Mol. Cell. Proteomics*. 7:697–715
161. Sanjuan MA, Dillon CP, Tait SW, Moshiach S, Dorsey F, et al. 2007. Toll-like receptor signalling in macrophages links the autophagy pathway to phagocytosis. *Nature* 450:1253–57
162. Kim BH, Shenoy AR, Kumar P, Das R, Tiwari S, MacMicking JD. 2011. A family of IFN- γ -inducible 65-kD GTPases protects against bacterial infection. *Science* 332:717–21
163. Yates RM, Russell DG. 2005. Phagosome maturation proceeds independently of stimulation of toll-like receptors 2 and 4. *Immunity* 23:409–17
164. Blander JM. 2008. Phagocytosis and antigen presentation: a partnership initiated by Toll-like receptors. *Ann. Rheum. Dis.* 67(Suppl. 3):iii44–49
165. Savina A, Jancic C, Hugues S, Guermonprez P, Vargas P, et al. 2006. NOX2 controls phagosomal pH to regulate antigen processing during crosspresentation by dendritic cells. *Cell* 126:205–18
166. Lim JP, Gleeson PA. 2011. Macropinocytosis: an endocytic pathway for internalising large gulps. *Immunol. Cell Biol.* 89:836–43
167. Hewlett LJ, Prescott AR, Watts C. 1994. The coated pit and macropinocytic pathways serve distinct endosome populations. *J. Cell Biol.* 124:689–703
168. West MA, Wallin RP, Matthews SP, Svensson HG, Zaru R, et al. 2004. Enhanced dendritic cell antigen capture via toll-like receptor-induced actin remodeling. *Science* 305:1153–57
169. von Delwig A, Hilkens CM, Altmann DM, Holmdahl R, Isaacs JD, et al. 2006. Inhibition of macropinocytosis blocks antigen presentation of type II collagen in vitro and in vivo in HLA-DR1 transgenic mice. *Arthritis Res. Ther.* 8:R93
170. Tanaka Y, Taneichi M, Kasai M, Kakiuchi T, Uchida T. 2010. Liposome-coupled antigens are internalized by antigen-presenting cells via pinocytosis and cross-presented to CD8⁺ T cells. *PLoS ONE* 5:e15225
171. Liu X, Zhan Z, Li D, Xu L, Ma F, et al. 2011. Intracellular MHC class II molecules promote TLR-triggered innate immune responses by maintaining activation of the kinase Btk. *Nat. Immunol.* 12:416–24
172. Xu S, Liu X, Bao Y, Zhu X, Han C, et al. 2012. Constitutive MHC class I molecules negatively regulate TLR-triggered inflammatory responses via the Fps-SHP-2 pathway. *Nat. Immunol.* 13:551–59
173. Crotzer VL, Blum JS. 2010. Autophagy and adaptive immunity. *Immunology* 131:9–17
174. Sahu R, Kaushik S, Clement CC, Cannizzo ES, Scharf B, et al. 2011. Microautophagy of cytosolic proteins by late endosomes. *Dev. Cell* 20:131–39
175. Munz C. 2012. Antigen processing for MHC class II presentation via autophagy. *Front. Immunol.* 3:9

176. Nedjic J, Aichinger M, Emmerich J, Mizushima N, Klein L. 2008. Autophagy in thymic epithelium shapes the T-cell repertoire and is essential for tolerance. *Nature* 455:396–400
177. Jagannath C, Lindsey DR, Dhandayuthapani S, Xu Y, Hunter RL Jr, Eissa NT. 2009. Autophagy enhances the efficacy of BCG vaccine by increasing peptide presentation in mouse dendritic cells. *Nat. Med.* 15:267–76
178. Dragovic SM, Hill T, Christianson GJ, Kim S, Elliott T, et al. 2011. Proteasomes, TAP, and endoplasmic reticulum-associated aminopeptidase associated with antigen processing control CD4⁺ Th cell responses by regulating indirect presentation of MHC class II-restricted cytoplasmic antigens. *J. Immunol.* 186:6683–92
179. Li Y, Wang LX, Pang P, Cui Z, Aung S, et al. 2011. Tumor-derived autophagosome vaccine: mechanism of cross-presentation and therapeutic efficacy. *Clin. Cancer Res.* 17:7047–57
180. Tewari MK, Sinnathamby G, Rajagopal D, Eisenlohr LC. 2005. A cytosolic pathway for MHC class II-restricted antigen processing that is proteasome and TAP dependent. *Nat. Immunol.* 6:287–94
181. Lich JD, Elliott JF, Blum JS. 2000. Cytoplasmic processing is a prerequisite for presentation of an endogenous antigen by major histocompatibility complex class II proteins. *J. Exp. Med.* 191:1513–24
182. Mukherjee P, Dani A, Bhatia S, Singh N, Rudensky AY, et al. 2001. Efficient presentation of both cytosolic and endogenous transmembrane protein antigens on MHC class II is dependent on cytoplasmic proteolysis. *J. Immunol.* 167:2632–41
183. Dorfle D, Appel S, Grunebach F, Weck MM, Muller MR, et al. 2005. Processing and presentation of HLA class I and II epitopes by dendritic cells after transfection with in vitro-transcribed MUC1 RNA. *Blood* 105:3199–205
184. Akram A, Inman RD. 2012. Immunodominance: a pivotal principle in host response to viral infections. *Clin. Immunol.* 143:99–115
185. Moudgil KD, Sercarz EE. 2005. Crypticity of self antigenic determinants is the cornerstone of a theory of autoimmunity. *Discov. Med.* 5:378–82
186. Dai YD, Jensen KP, Marrero I, Li N, Quinn A, Sercarz EE. 2008. N-terminal flanking residues of a diabetes-associated GAD65 determinant are necessary for activation of antigen-specific T cells in diabetes-resistant mice. *Eur. J. Immunol.* 38:968–76
187. Mimura Y, Mimura-Kimura Y, Doores K, Golgher D, Davis BG, et al. 2007. Folding of an MHC class II-restricted tumor antigen controls its antigenicity via MHC-guided processing. *Proc. Natl. Acad. Sci. USA* 104:5983–88
188. Bergman CM, Marta CB, Maric M, Pfeiffer SE, Cresswell P, Ruddle NH. 2012. A switch in pathogenic mechanism in myelin oligodendrocyte glycoprotein-induced experimental autoimmune encephalomyelitis in IFN- γ -inducible lysosomal thiol reductase-free mice. *J. Immunol.* 188:6001–9
189. Rausch MP, Irvine KR, Antony PA, Restifo NP, Cresswell P, Hastings KT. 2010. GILT accelerates autoimmunity to the melanoma antigen tyrosinase-related protein 1. *J. Immunol.* 185:2828–35
190. Delamarre L, Couture R, Mellman I, Trombetta ES. 2006. Enhancing immunogenicity by limiting susceptibility to lysosomal proteolysis. *J. Exp. Med.* 203:2049–55
191. Davidson HW, Reid PA, Lanzavecchia A, Watts C. 1991. Processed antigen binds to newly synthesized MHC class II molecules in antigen-specific B lymphocytes. *Cell* 67:105–16
192. Sercarz EE, Maverakis E. 2003. MHC-guided processing: binding of large antigen fragments. *Nat. Rev. Immunol.* 3:621–29
193. Moss CX, Tree TI, Watts C. 2007. Reconstruction of a pathway of antigen processing and class II MHC peptide capture. *EMBO J.* 26:2137–47
194. Brooks K, Knight AM. 2004. Lowering the affinity between antigen and the B cell receptor can enhance antigen presentation. *Eur. J. Immunol.* 34:837–43
195. Hartman IZ, Kim A, Cotter RJ, Walter K, Dalai SK, et al. 2010. A reductionist cell-free major histocompatibility complex class II antigen processing system identifies immunodominant epitopes. *Nat. Med.* 16:1333–40
196. Nanda NK, Sant AJ. 2000. DM determines the cryptic and immunodominant fate of T cell epitopes. *J. Exp. Med.* 192:781–88

197. Mohan JF, Levisetti MG, Calderon B, Herzog JW, Petzold SJ, Unanue ER. 2010. Unique autoreactive T cells recognize insulin peptides generated within the islets of Langerhans in autoimmune diabetes. *Nat. Immunol.* 11:350–54
198. Singh R, Cresswell P. 2010. Defective cross-presentation of viral antigens in GILT-free mice. *Science* 328:1394–98
199. Siddiqui S, Basta S. 2011. CD8⁺ T cell immunodominance in lymphocytic choriomeningitis virus infection is modified in the presence of Toll-like receptor agonists. *J. Virol.* 85:13224–33
200. Boon T, Coulie PG, Van den Eynde BJ, van der Bruggen P. 2006. Human T cell responses against melanoma. *Annu. Rev. Immunol.* 24:175–208
201. Hahn YS, Braciale VL, Braciale TJ. 1991. Presentation of viral antigen to class I major histocompatibility complex-restricted cytotoxic T lymphocyte. Recognition of an immunodominant influenza hemagglutinin site by cytotoxic T lymphocyte is independent of the position of the site in the hemagglutinin translation product. *J. Exp. Med.* 174:733–36
202. Hanke T, Graham FL, Rosenthal KL, Johnson DC. 1991. Identification of an immunodominant cytotoxic T-lymphocyte recognition site in glycoprotein B of herpes simplex virus by using recombinant adenovirus vectors and synthetic peptides. *J. Virol.* 65:1177–86
203. Schubert U, Anton LC, Gibbs J, Norbury CC, Yewdell JW, Bennink JR. 2000. Rapid degradation of a large fraction of newly synthesized proteins by proteasomes. *Nature* 404:770–74
204. Yewdell JW. 2011. DRiPs solidify: progress in understanding endogenous MHC class I antigen processing. *Trends Immunol.* 32:548–58
205. Townsend AR, Gotch FM, Davey J. 1985. Cytotoxic T cells recognize fragments of the influenza nucleoprotein. *Cell* 42:457–67
206. Reits EA, Vos JC, Gromme M, Neefjes J. 2000. The major substrates for TAP in vivo are derived from newly synthesized proteins. *Nature* 404:774–78
207. Princiotta MF, Finzi D, Qian SB, Gibbs J, Schuchmann S, et al. 2003. Quantitating protein synthesis, degradation, and endogenous antigen processing. *Immunity* 18:343–54
208. Mackay LK, Long HM, Brooks JM, Taylor GS, Leung CS, et al. 2009. T cell detection of a B-cell tropic virus infection: newly-synthesized versus mature viral proteins as antigen sources for CD4 and CD8 epitope display. *PLoS Pathog.* 5:e1000699
209. Apcher S, Daskalogianni C, Lejeune F, Manoury B, Imhoos G, et al. 2011. Major source of antigenic peptides for the MHC class I pathway is produced during the pioneer round of mRNA translation. *Proc. Natl. Acad. Sci. USA* 108:11572–77
210. Apcher S, Manoury B, Fähraeus R. 2012. The role of mRNA translation in direct MHC class I antigen presentation. *Curr. Opin. Immunol.* 24:71–76
211. Granados DP, Yahyaoui W, Laumont CM, Daouda T, Muratore-Schroeder TL, et al. 2012. MHC I-associated peptides preferentially derive from transcripts bearing miRNA response elements. *Blood* 119:e181–91
212. Villanueva MS, Sijts AJ, Pamer EG. 1995. Listeriolysin is processed efficiently into an MHC class I-associated epitope in *Listeria monocytogenes*-infected cells. *J. Immunol.* 155:5227–33
213. Kunisawa J, Shastri N. 2006. Hsp90 α chaperones large C-terminally extended proteolytic intermediates in the MHC class I antigen processing pathway. *Immunity* 24:523–34
214. Cascio P, Hilton C, Kisselev AF, Rock KL, Goldberg AL. 2001. 26S proteasomes and immunoproteasomes produce mainly N-extended versions of an antigenic peptide. *EMBO J.* 20:2357–66
215. Kunisawa J, Shastri N. 2003. The group II chaperonin TRiC protects proteolytic intermediates from degradation in the MHC class I antigen processing pathway. *Mol. Cell* 12:565–76
216. Beninga J, Rock KL, Goldberg AL. 1998. Interferon- γ can stimulate post-proteasomal trimming of the N terminus of an antigenic peptide by inducing leucine aminopeptidase. *J. Biol. Chem.* 273:18734–42
217. Urban S, Textoris-Taube K, Reimann B, Janek K, Dannenberg T, et al. 2012. The efficiency of human cytomegalovirus pp65_{495–503} CD8⁺ T cell epitope generation is determined by the balanced activities of cytosolic and endoplasmic reticulum-resident peptidases. *J. Immunol.* 189:529–38
218. Sykulev Y, Joo M, Vturina I, Tsomides TJ, Eisen HN. 1996. Evidence that a single peptide-MHC complex on a target cell can elicit a cytolytic T cell response. *Immunity* 4:565–71

219. Vigneron N, Van den Eynde BJ. 2011. Insights into the processing of MHC class I ligands gained from the study of human tumor epitopes. *Cell. Mol. Life Sci.* 68:1503–20
220. Starck SR, Jiang V, Pavon-Eternod M, Prasad S, McCarthy B, et al. 2012. Leucine-tRNA initiates at CUG start codons for protein synthesis and presentation by MHC class I. *Science* 336:1719–23
221. Vigneron N, Stroobant V, Chapiro J, Ooms A, Degiovanni G, et al. 2004. An antigenic peptide produced by peptide splicing in the proteasome. *Science* 304:587–90
222. Warren EH, Vigneron NJ, Gavin MA, Coulie PG, Stroobant V, et al. 2006. An antigen produced by splicing of noncontiguous peptides in the reverse order. *Science* 313:1444–47
223. Skipper JC, Hendrickson RC, Gulden PH, Brichard V, Van Pel A, et al. 1996. An HLA-A2-restricted tyrosinase antigen on melanoma cells results from posttranslational modification and suggests a novel pathway for processing of membrane proteins. *J. Exp. Med.* 183:527–34
224. Smith MH, Ploegh HL, Weissman JS. 2011. Road to ruin: targeting proteins for degradation in the endoplasmic reticulum. *Science* 334:1086–90
225. Suzuki T, Seko A, Kitajima K, Inoue Y, Inoue S. 1994. Purification and enzymatic properties of peptide:N-glycanase from C3H mouse-derived L-929 fibroblast cells. Possible widespread occurrence of post-translational remodification of proteins by N-deglycosylation. *J. Biol. Chem.* 269:17611–18
226. Gagnon E, Duclos S, Rondeau C, Chevet E, Cameron PH, et al. 2002. Endoplasmic reticulum-mediated phagocytosis is a mechanism of entry into macrophages. *Cell* 110:119–31
227. Ackerman AL, Giudini A, Cresswell P. 2006. A role for the endoplasmic reticulum protein retrotranslocation machinery during crosspresentation by dendritic cells. *Immunity* 25:607–17
228. Lin ML, Zhan Y, Proietto AI, Prato S, Wu L, et al. 2008. Selective suicide of cross-presenting CD8⁺ dendritic cells by cytochrome *c* injection shows functional heterogeneity within this subset. *Proc. Natl. Acad. Sci. USA* 105:3029–34
229. Giudini A, Cresswell P. 2008. Hsp90-mediated cytosolic refolding of exogenous proteins internalized by dendritic cells. *EMBO J.* 27:201–11
230. Burgdorf S, Scholz C, Kautz A, Tampe R, Kurts C. 2008. Spatial and mechanistic separation of cross-presentation and endogenous antigen presentation. *Nat. Immunol.* 9:558–66
231. Cebrian I, Visentin G, Blanchard N, Jouve M, Bobard A, et al. 2011. Sec22b regulates phagosomal maturation and antigen crosspresentation by dendritic cells. *Cell* 147:1355–68
232. Madden DR, Garboczi DN, Wiley DC. 1993. The antigenic identity of peptide-MHC complexes: a comparison of the conformations of five viral peptides presented by HLA-A2. *Cell* 75:693–708
233. Stern LJ, Brown JH, Jardetzky TS, Gorga JC, Urban RG, et al. 1994. Crystal structure of the human class II MHC protein HLA-DR1 complexed with an influenza virus peptide. *Nature* 368:215–21

Contents

Years in Cologne

- Klaus Rajewsky* 1

The Biology of Recent Thymic Emigrants

- Pamela J. Fink* 31

Immunogenic Cell Death in Cancer Therapy

- Guido Kroemer, Lorenzo Galluzzi, Oliver Kepp, and Laurence Zitvogel* 51

Recognition of Bacteria by Inflammasomes

- Jakob von Moltke, Janelle S. Ayres, Eric M. Kofod, Joseph Chavarría-Smith, and Russell E. Vance* 73

The Immunology of Fibrosis

- Georg Wick, Cecilia Grundtman, Christina Mayerl, Thomas-Florian Wimpissinger, Johann Feichtinger, Bettina Zelger, Roswitha Sgong, and Dolores Wolfram* 107

Memory T Cell Subsets, Migration Patterns, and Tissue Residence

- Scott N. Mueller, Thomas Gebhardt, Francis R. Carbone, and William R. Heath* 137

Control of Human Viral Infections by Natural Killer Cells

- Stephanie Jost and Marcus Altfeld* 163

Functional T Cell Immunodeficiencies (with T Cells Present)

- Luigi D. Notarangelo* 195

Controlling Natural Killer Cell Responses: Integration of Signals for Activation and Inhibition

- Eric O. Long, Hun Sik Kim, Dongfang Liu, Mary E. Peterson, and Sumati Rajagopalan* 227

Metabolic Regulation of T Lymphocytes

- Nancie J. MacIver, Ryan D. Michalek, and Jeffrey C. Rathmell* 259

Mesenchymal Stem Cell: Keystone of the Hematopoietic Stem Cell Niche

and a Stepping-Stone for Regenerative Medicine

- Paul S. Frenette, Sandra Pinho, Daniel Lucas, and Christoph Scheiermann* 285

Interleukin-4- and Interleukin-13-Mediated Alternatively Activated

Macrophages: Roles in Homeostasis and Disease

- Steven J. Van Dyken and Richard M. Locksley* 317

Brain-Reactive Antibodies and Disease

- B. Diamond, G. Honig, S. Mader, L. Brimberg, and B.T. Volpe* 345

Immunology of the Maternal-Fetal Interface <i>Adrian Erlebacher</i>	387
Regulation of Ligands for the NKG2D Activating Receptor <i>David H. Raulet, Stephan Gasser, Benjamin G. Gowen, Weiwen Deng, and Heiyoun Jung</i>	413
Pathways of Antigen Processing <i>Janice S. Blum, Pamela A. Wearsch, and Peter Cresswell</i>	443
The Immune Response in Tuberculosis <i>Anne O'Garra, Paul S. Redford, Finlay W. McNab, and Chloe I. Bloom, Robert J. Wilkinson, and Matthew P.R. Berry</i>	475
The Adaptable Major Histocompatibility Complex (MHC) Fold: Structure and Function of Nonclassical and MHC Class I-Like Molecules <i>Erin J. Adams and Adrienne M. Luoma</i>	529
The Dendritic Cell Lineage: Ontogeny and Function of Dendritic Cells and Their Subsets in the Steady State and the Inflamed Setting <i>Miriam Merad, Priyanka Sathe, Julie Helft, Jennifer Miller, and Arthur Mortha</i> ...	563
T Cell-Mediated Host Immune Defenses in the Lung <i>Kong Chen and Jay K. Kolls</i>	605
Human Hemato-Lymphoid System Mice: Current Use and Future Potential for Medicine <i>Anthony Rongvaux, Hitoshi Takizawa, Till Striweg, Tim Willinger, Elizabeth E. Eynon, Richard A. Flavell, and Markus G. Manz</i>	635
Signaling by the Phosphoinositide 3-Kinase Family in Immune Cells <i>Klaus Okkenhaug</i>	675
Broadly Neutralizing Antiviral Antibodies <i>Davide Corti and Antonio Lanzavecchia</i>	705
Molecular Control of Steady-State Dendritic Cell Maturation and Immune Homeostasis <i>Gianna Elena Hammer and Averil Ma</i>	743

Indexes

Cumulative Index of Contributing Authors, Volumes 21–31	793
Cumulative Index of Articles Titles, Volumes 21–31	800

Errata

An online log of corrections to *Annual Review of Immunology* articles may be found at
<http://immunol.annualreviews.org/errata.shtml>



Tailor the adaptive immune response with
Vaccine Adjuvants



This information is current as of November 17, 2017.

Pillars Article: T-Cell Antigen CD28 Mediates Adhesion with B Cells by Interacting with Activation Antigen B7/BB-1. 1990. *Proc. Natl. Acad. Sci. USA* 87: 5031 – 5035

Peter S. Linsley, Edward A. Clark and Jeffrey A. Ledbetter

J Immunol 2009; 182:2559-2563; ;
<http://www.jimmunol.org/content/182/5/2559.citation>

Why *The JI*?

- **Rapid Reviews!** 30 days* from submission to initial decision
- **No Triage!** Every submission reviewed by practicing scientists
- **Speedy Publication!** 4 weeks from acceptance to publication

*average

Subscription Information about subscribing to *The Journal of Immunology* is online at: <http://jimmunol.org/subscription>

Permissions Submit copyright permission requests at: <http://www.aai.org/About/Publications/JI/copyright.html>

Email Alerts Receive free email-alerts when new articles cite this article. Sign up at: <http://jimmunol.org/alerts>

The Journal of Immunology is published twice each month by The American Association of Immunologists, Inc., 1451 Rockville Pike, Suite 650, Rockville, MD 20852 Copyright © 2009 by The American Association of Immunologists, Inc. All rights reserved. Print ISSN: 0022-1767 Online ISSN: 1550-6606.



Reprinted from *Proceedings of the National Academy of Sciences, U.S.A.* 87: 5031–5035. © 1990, by permission of the authors.

Proc. Natl. Acad. Sci. USA
Vol. 87, pp. 5031–5035, July 1990
Immunology

T-cell antigen CD28 mediates adhesion with B cells by interacting with activation antigen B7/BB-1

PETER S. LINSLEY*, EDWARD A. CLARK†, AND JEFFREY A. LEDBETTER*

*Oncogen, 3005 First Avenue, Seattle, WA 98121; and †Department of Microbiology, University of Washington, Seattle, WA 98195

Communicated by Seymour J. Klebanoff, March 30, 1990

ABSTRACT Studies using monoclonal antibodies (mAbs) have implicated the homodimeric glycoprotein CD28 as an important regulator of human T-cell activation, in part by posttranscriptional control of cytokine mRNA levels. Although the CD28 antigen has functional and structural characteristics of a receptor, a natural ligand for this molecule has not been identified. Here we show that the CD28 antigen, expressed in Chinese hamster ovary (CHO) cells, mediated specific intercellular adhesion with human lymphoblastoid and leukemic B-cell lines and with activated primary murine B cells. CD28-mediated adhesion was not dependant upon divalent cations. Several mAbs were identified that inhibited CD28-mediated adhesion, including mAb BB-1 against the B-cell activation antigen B7/BB-1 and some mAbs against major histocompatibility complex class I antigens. B7/BB-1 expression correlated closely with CD28-mediated adhesion, but class I expression did not. Transfected COS cells expressing the B7/BB-1 antigen adhered to CD28⁺ CHO cells; this adhesion was blocked by mAbs to CD28 and B7/BB-1. The specific recognition by CD28 of the B-cell activation antigen B7/BB-1 represents a heterophilic interaction between members of the immunoglobulin superfamily that may serve to regulate T-cell cytokine levels at sites of B-cell activation.

The generation of a T-lymphocyte immune response is a complex process involving cell–cell interactions (1) and production of soluble immune mediators (cytokines or lymphokines) (2). This response is regulated by several T-cell surface molecules, including the T-cell receptor complex (3) and other “accessory” surface molecules (1).

One such accessory molecule is the CD28 antigen, a homodimeric glycoprotein of the immunoglobulin superfamily (4) found on most mature human T cells (5). Current evidence suggests that this molecule functions in an alternative T-cell activation pathway distinct from that initiated by the T-cell receptor complex (for review, see ref. 6). Monoclonal antibodies (mAbs) to CD28 can augment T-cell responses initiated by various polyclonal stimuli (5–7). These stimulatory effects may result from mAb-induced cytokine production (8) as a consequence of increased mRNA stabilization (9). Anti-CD28 mAbs can also have inhibitory effects; i.e., they can block autologous mixed lymphocyte reactions (10) and activation of antigen-specific T-cell clones (11).

The *in vivo* function of CD28 is not known, although its structure (4) suggests that like other members of the immunoglobulin superfamily (12) it might function as a receptor. CD28 could conceivably function as a cytokine receptor, although this seems unlikely since it shares no homology with other lymphokine or cytokine receptors (4).

Alternatively, CD28 might be a receptor that mediates cell–cell contact. In this paper, we describe experiments designed to test this possibility. For this purpose, we have taken an approach based on experiments used to demonstrate

intercellular adhesion mediated by major histocompatibility complex (MHC) class I (13) and class II (14) molecules with the CD8 and CD4 accessory molecules, respectively. We have expressed the CD28 antigen to high levels in Chinese hamster ovary (CHO) cells and have used these transfected cells to develop a CD28-mediated cell adhesion assay. By using this assay as a screening method, we have demonstrated an interaction between CD28 and a natural ligand expressed on activated B lymphocytes, the B7/BB-1 antigen.

MATERIALS AND METHODS

mAbs. mAb 9.3 (anti-CD28, ref. 15) was purified from ascites fluid before use. A number of mAbs to B-cell associated antigens were tested for their abilities to inhibit CD28-mediated adhesion. mAbs 60.3 (CD18); 1F5 (CD20); G29-5 (CD21); G28-7, HD39, and HD6 (CD22); HD50 (CD23); KB61 (CD32); G28-1 (CD37); G28-10 (CD39); G28-5 (CD40); HERMES1 (CD44); 9.4 (CD45); LB-2 (CD54); and 72F3 (CD71) have been described and characterized (16–18). These mAbs were purified before use. 8TA4-1 (ref. 19, anti-IgD); 2C3 (ref. 20, anti-IgM); Namb1, H1DE, p10.1, and W6/32 (refs. 20 and 21, anti-human class I); and HB10a (ref. 20, anti-MHC class II) were also purified before use. mAbs B43 (CD19); BL-40 (CD72); AD2, 1E9.28.1, and 7G2.2.11 (CD73); EBU-141, LN1 (CDw75); CRIS-1 (CD76); 424/4A11 and 424/3D9 (CD77); Leu 21, Ba, 1588, LO-panB-1, FN1, and FN4 (CDw78); and M9, G28-10, HuLym10, 2-7, F2B2.6, 121, L26, HD77, NU-B1, BLAST-1, BB-1, anti-BL7, anti-HC2, and L23 were used as coded samples provided to participants in the Fourth International Conference on Human Leukocyte Differentiation Antigens (September 1989, Vienna) (22). Most of these were used in ascites fluid form. mAbs BB-1 and LB-1 (23) were also purified from ascites fluid before use. Anti-integrin receptor mAbs, P3E3, P4C2, and P4G9 (24), were used as hybridoma culture supernatants.

Plasmids and Transfections. cDNA clones encoding the T-cell antigens CD4, CD5, and CD28 (4) in the expression vector π H3M (4) were kindly provided by Sandro Aruffo and Brian Seed (Massachusetts General Hospital, Boston). An expressible cDNA clone encoding the B7/BB-1 antigen (25) was provided by Gordon Freeman (Dana-Farber Cancer Institute, Boston). Dihydrofolate reductase-deficient CHO cells were cotransfected as described (26) with a mixture of plasmids, π H3M-CD28 (4) and pSV2dhfr (27). COS cells were transfected with B7/BB-1, CD4, or CD5 cDNAs in the presence of DEAE-dextran using a protocol supplied by B. Seed and A. Aruffo.

CD28-Mediated Adhesion Assay. Cells to be tested for adhesion were labeled with ^{51}Cr , washed, and preincubated in complete RPMI medium [RPMI 1640 medium containing 10% (vol/vol) fetal bovine serum, penicillin (100 units/ml), and streptomycin (100 $\mu\text{g}/\text{ml}$)] containing 10 mM EDTA

Abbreviations: mAb, monoclonal antibody; MHC, major histocompatibility complex; FITC, fluorescein isothiocyanate; LPS, lipopolysaccharide.

The publication costs of this article were defrayed in part by page charge payment. This article must therefore be hereby marked “advertisement” in accordance with 18 U.S.C. §1734 solely to indicate this fact.

5032 Immunology: Linsley *et al.*

unless otherwise indicated. mAbs to be tested for adhesion inhibition were then added to 10 µg/ml, and cells were incubated for ≈1 hr at 23°C. In some experiments, a mouse mAb having irrelevant specificity was added to the labeling and preincubation reaction mixtures to saturate Fc receptors. Labeled cells (1–10 × 10⁶ cells per well in 0.2 ml of complete RPMI medium containing EDTA and mAbs, where indicated) were then added to the CHO monolayers. When adhesion inhibition by mAb 9.3 was measured, the mAb or its F(ab')₂ were added to the CHO cells 1 hr prior to addition of labeled cells. Adhesion was initiated by centrifugation in a plate carrier and continued at 37°C for 1 hr. Monolayers were then washed five times with ice-cold complete RPMI medium and solubilized by addition of 0.5 M NaOH, and radioactivity was measured in a γ counter. Numbers of bound cells were calculated by dividing total bound radioactivity (cpm) by the specific activity (cpm per cell) of labeled cells. When COS cells were used, results are expressed as cpm bound since their viability at the end of the experiment was generally <50%.

RESULTS

Isolation of CHO Cells Expressing the CD28 Antigen. If CD28 binds to a cell surface ligand, then cells expressing the ligand should adhere more readily to cells expressing CD28 than to cells that do not. To test this hypothesis, we first cotransfected an expressible cDNA clone encoding CD28 (4) plus a selectable marker (pSV2dhfr, ref. 27) into dihydrofolate-reductase-deficient CHO cells. Transfectants were isolated, and the dihydrofolate reductase marker was amplified by growth in increasing concentrations of methotrexate. Cell lines expressing high (CD28⁺) and low (CD28⁻) levels of the CD28 antigen were isolated from amplified populations by fluorescence-activated cell sorting after immunostaining with mAb 9.3. After two rounds of cell sorting selection, the CD28⁺ population stained uniformly and strongly with fluorescein isothiocyanate (FITC)-conjugated mAb 9.3 (mean channel, 116 linear fluorescence units), and the CD28⁻ population stained no brighter (mean channel, 3.9 linear fluorescence units) than unstained cells (mean channel, 3.7 linear fluorescence units). Staining by CD28⁺ CHO cells was ≈10-fold brighter than phytohemagglutinin-stimulated T cells (mean channel, 11.3 linear fluorescence units).

Cell Adhesion Assay for a CD28 Ligand. We next developed an adhesion assay to detect differential binding to CD28⁺ and CD28⁻ CHO cells by cells expressing a CD28 ligand. Cells were first labeled with ⁵¹Cr and then incubated with either CD28⁺ or CD28⁻ CHO cells. In pilot experiments, T51 lymphoblastoid cells were found to adhere more to CD28⁺ CHO than to CD28⁻ CHO. Furthermore, adhesion of T51 cells to CD28⁺ CHO cells was partially blocked by mAb 9.3, but adhesion to CD28⁻ CHO cells was not consistently affected.

These experiments suggested that T51 cells adhered specifically to CD28⁺ CHO cells. Since blocking of adhesion by mAb 9.3 was incomplete, we searched for ways to increase the specificity of the CD28 adhesion assay.

The effects of divalent cation depletion with EDTA on T51 cell adhesion to CD28⁺ and CD28⁻ CHO cells were examined in the experiment shown in Fig. 1. Preliminary experiments showed that EDTA treatment caused loss of CHO cells during washing, so the CHO monolayers were fixed with paraformaldehyde prior to EDTA treatment. Fixation did not significantly affect CD28-mediated adhesion by T51 cells either in the presence or absence of mAb 9.3 (data not shown). As shown in Fig. 1, the specificity of CD28-mediated adhesion was greatly increased in the presence of EDTA. CD28-mediated adhesion in the presence of EDTA could also be seen quite clearly by microscopic examination after im-

Proc. Natl. Acad. Sci. USA 87 (1990)

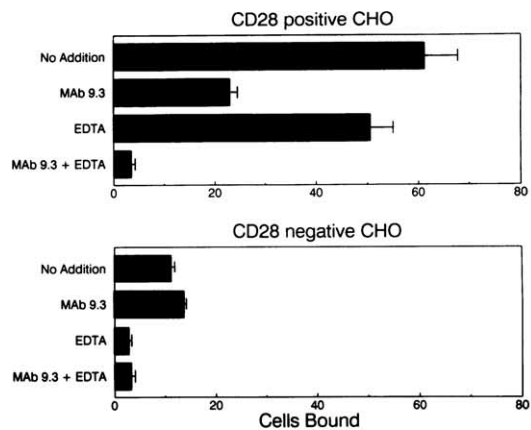


FIG. 1. T51 lymphoblastoid cells adhere specifically to CD28-transfected CHO cells. Monolayers of CD28⁺ and CD28⁻ CHO cells (1–1.2 × 10⁵ cells per cm² in 48-well plastic dishes) were fixed in 0.5% paraformaldehyde for 20 min at 23°C, washed, blocked in complete RPMI medium, and then preincubated alone or with mAb 9.3 or mAb 9.3 F(ab')₂ at 10 µg/ml in complete RPMI for 1 hr at 37°C. T51 cells were labeled with ⁵¹Cr, preincubated alone or with 10 mM EDTA, and added to CHO cells, and cellular adhesion was measured. Data are the number of cells bound ($\times 10^{-3}$; mean \pm SD; error bars) of three replicate determinations.

munohistological staining of T51 cells (Fig. 2). A similar, but slightly less significant increase in adhesion specificity was also measured in the presence of the calcium-specific chelator, EGTA (data not shown).

CD28 Ligand Is a B-Cell Activation Marker. The increased specificity of CD28-mediated adhesion in EDTA made it possible to more readily detect adhesion by cells other than T51. A number of additional cell lines were tested, including three lymphoblastoid lines (T51, 1A2, and 5E1), four Burkitt lymphoma lines (Daudi, Raji, Jijoye, and Namalwa), one acute lymphoblastic (B cell) leukemia (REH), three T-cell leukemias (CEM, Jurkat, and HSB2), and two monocytic

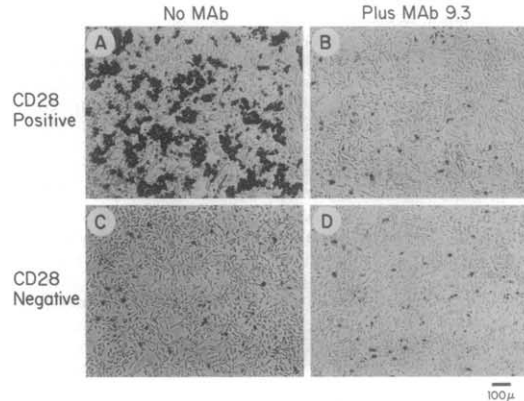


FIG. 2. Microscopic visualization of T51 cells adhering to CD28-transfected CHO cells. Cellular adhesion between unlabeled T51 cells and CD28⁺ (A and B) or CD28⁻ (C and D) CHO cells was determined in the presence of 10 mM EDTA as described in Fig. 1. (B and D) Adherent T51 cells were stained with biotinylated anti-human class II mAb HB10a, fixed with 0.2% glutaraldehyde, and visualized by sequential incubation with avidin-conjugated horse-radish peroxidase (Vector) and diaminobenzidine. (A and C) No additional mAb was added. (Bar = 100 µm.)

leukemias (THP-1 and HL60). As a source of primary B cells, murine splenic B cells, before and after activation with lipopolysaccharide (LPS), were tested. All cells were tested for adhesion to both CD28⁺ and CD28⁻ CHO cells, in the absence and presence of mAb 9.3. Three representative experiments showing adhesion to CD28⁺ CHO cells are shown in Fig. 3. Inhibition by mAb 9.3 is shown as an indicator of specificity; in most cases, adhesion measured in the presence of mAb 9.3 was approximately equal to adhesion to CD28⁻ cells.

CD28-specific adhesion (i.e., adhesion inhibited >70% by mAb 9.3) was clearly observed with T51, 5E1, Raji, and Jijoye cells. Daudi cells also showed specific adhesion, although to a lesser extent. Other cell lines did not show specific CD28-mediated adhesion, although some (e.g., Namalwa) showed relatively high nonspecific adhesion. Primary mouse splenic B cells did not show CD28-mediated adhesion but acquired the ability to adhere after activation with LPS. In other experiments, six additional lymphoblastoid lines showed CD28-mediated adhesion, but the U937 cell line, cryopreserved human tonsil B cells, and phytohemagglutinin-stimulated T cells did not show adhesion. These experiments indicate that a CD28 ligand is found on the cell surface of activated B cells of human or mouse origin.

CD28-Mediated Adhesion Is Specifically Blocked by BB-1, a mAb to a B-Cell Activation Antigen. In initial attempts to define B-cell molecules involved in CD28-mediated adhesion, we measured adhesion by lymphoblastoid cell lines with mutations in other known cellular adhesion molecules. The 616 cells (MHC class II deficient, ref. 28) bound to CD28⁺ CHO cells equally well or better than parental T51 cells. Likewise, a CD18-deficient cell line derived from a patient

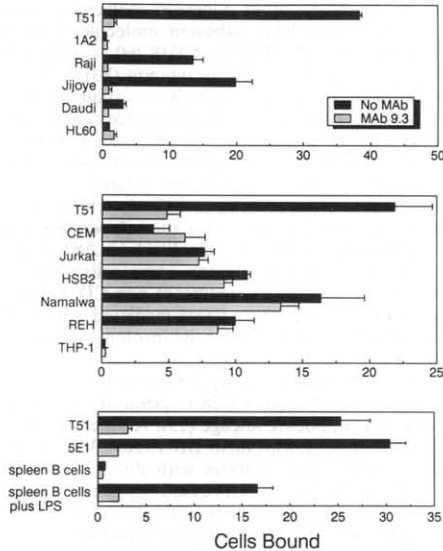


FIG. 3. Ligand mediating CD28-specific adhesion is found on certain B-cell lines and on activated primary B cells. The ability of various human cell lines and of normal and activated murine spleen B cells to adhere specifically to CD28⁺ CHO cells was examined in three experiments. The indicated cells were labeled with ⁵¹Cr and CD28-mediated adhesion was measured as described in Fig. 1. Data are number of cells bound ($\times 10^{-3}$). Spleen B cells were purified from BALB/c mice by treatment of total spleen cells with an anti-Thy-1.2 mAb (30H12) and baby rabbit complement. These cells were activated by treatment for 72 hr with *Escherichia coli* LPS (List Biological Laboratories, Campbell, CA) at 10 μ g/ml in complete RPMI medium.

with leukocyte-adhesion deficiency (Gambaro cells, ref. 29) also adhered specifically to CD28. Thus, MHC class II and CD18 molecules do not mediate adhesion to CD28.

We then tested a panel of mAbs to B-cell surface antigens for their ability to inhibit CD28-mediated adhesion of T51 cells. For these experiments, we tested a total of 57 mAbs reactive with T51 cells. Initial screening experiments were carried out in the absence of EDTA, and any mAbs that blocked adhesion were subsequently retested in the presence and absence of EDTA. Of these mAbs, only those directed against MHC class I molecules (Nam1, H1DE, P10.1, and W6/32) and one to an unclustered B-cell antigen [BB-1, originally described as a B-cell activation marker (23)] were consistently able to block CD28-mediated adhesion by >30%.

The dose dependence of adhesion inhibition by the anti-class I mAb H1DE, by BB-1, and by 9.3 were compared in the presence of EDTA in the experiment shown in Fig. 4. mAb 9.3 was most effective at blocking, but mAb BB-1 was able to block ~60% of adhesion at concentrations <1 μ g/ml. mAb H1DE also partially blocked adhesion at all concentrations tested. When EDTA was omitted from the adhesion assay, blocking by class I mAbs was consistently less and required higher mAb concentrations than mAbs 9.3 or BB-1 (data not shown).

Binding of mAb BB-1 by Various Cells Correlates with CD28-Specific Adhesion. To investigate the roles of molecules recognized by anti-class I and BB-1 mAbs in CD28-mediated adhesion, we compared levels of these antigens on cell lines tested for CD28-specific adhesion in Fig. 3. Cell lines 1A2, Namalwa, REH, and HL-60 (which did not adhere specifically to CD28) bound high levels of mAb H1DE by indirect immunofluorescence, whereas Daudi cells (which did adhere) did not show detectable binding. Therefore, a direct correlation between CD28-mediated adhesion and expression of class I antigens was not observed. On the other hand, we did observe a correlation between adhesion to CD28 and staining by FITC-conjugated mAb BB-1 (Table 1). All of the cell lines that adhered specifically to CD28 antigen (Fig. 3) bound higher levels in the FITC conjugate than those that did not adhere specifically. Antigen specificity was demonstrated in all cases by the ability of unlabeled mAb BB-1 to compete for binding of the FITC conjugate. In other experiments

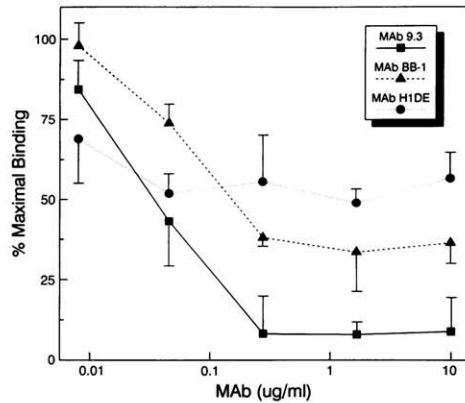


FIG. 4. CD28-mediated adhesion to human B-cell lines is blocked by mAbs to certain B-cell antigens. Jijoye cells were labeled with ⁵¹Cr and allowed to adhere to CD28⁺ CHO cells in the presence of 10 mM EDTA as described in Fig. 1. Adhesion measured in the presence of the indicated amounts of mAbs 9.3, H1DE (anti-human class I MHC), or BB-1 is expressed as a percentage of maximal adhesion measured in the absence of mAb (45,000 cells bound). ug, μ g.

Table 1. Cells that adhere to CD28 also bind mAb BB-1

Line	Cell type	No mAb	Mean fluorescence, linear units		Specific binding
			Alone	+ BB-1	
Positive for CD28 adhesion					
T51	B-LCL	2.3	16.4	3.0	13.4
SE1	B-LCL	2.1	13.0	2.4	10.6
Jijoye	BL	2.3	17.8	2.8	15.0
Raji	BL	2.1	7.1	2.8	4.3
Daudi	BL	2.1	6.4	2.8	3.6
Negative for CD28 adhesion					
1A2	B-LCL	2.1	4.5	4.3	<1
Namalwa	BL	2.2	3.8	2.2	1.6
REH	B-ALL	2.0	2.1	2.0	<1
CEM	T-ALL	2.3	2.0	1.9	<1
Jurkat	T-ALL	2.2	2.2	2.0	<1
HSB2	T-ALL	2.1	2.3	2.3	<1
HL60	AML	2.3	3.1	3.1	<1
THP-1	AML	2.3	3.1	3.0	<1

Cell lines tested for CD28-mediated adhesion in Fig. 3 were tested for B7/BB-1 antigen levels by direct immunofluorescence. mAb BB-1 was directly conjugated with FITC (FITC-BB-1). The conjugate was added to cells at saturating concentrations in complete RPMI medium for 1 hr at 4°C. Nonspecific binding of FITC-conjugated mAbs was measured by adding the FITC conjugate after antigen preblocking (20–30 min at 4°C) with unlabeled mAb BB-1. Cell types: B-LCL, B-lymphoblastoid cell line; BL, Burkitt lymphoma; B-ALL, B-cell-derived acute lymphoblastic leukemia; T-ALL, T-cell-derived acute lymphoblastic leukemia; AML, acute monocytic leukemia. Positive for CD28 adhesion, >70% inhibition of adhesion by mAb 9.3; negative for CD28 adhesion, <70% inhibition of adhesion by mAb 9.3. Specific binding = (FITC-BB-1 alone labeling) – (FITC-BB-1 + unlabeled BB-1 labeling).

iments, additional lymphoblastoid cell lines that showed CD28-mediated adhesion stained with FITC-conjugated BB-1, but cells that did not show CD28-mediated adhesion (U937 and cryopreserved human tonsil B cells) were not stained.

COS Cells Expressing Antigen B7/BB-1 Adhere Specifically to CD28. Freeman *et al.* (25) have isolated and sequenced a cDNA clone encoding a B-cell activation antigen recognized by mAb B7. COS cells transfected with this cDNA were stained by mAb B7 and mAb BB-1 (25). The cloning of this antigen, which we provisionally refer to as B7/BB-1 until it

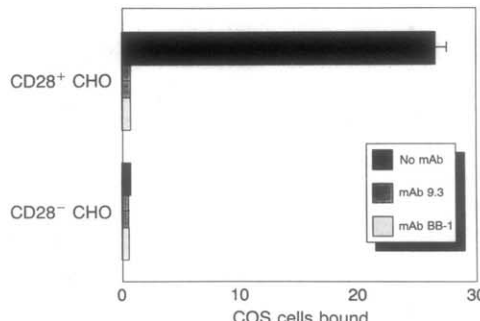


FIG. 5. Antigen B7/BB-1 mediates CD28-specific cellular adhesion. COS cells were transfected with an expressible cDNA clone for antigen B7/BB-1 (25). Forty-eight hours later, transfected COS cells were removed from their dishes by incubation in isotonic phosphate-buffered saline containing 10 mM EDTA and labeled with ⁵¹Cr. Adhesion between B7/BB-1-transfected COS cells and CD28⁺ or CD28⁻ CHO cells was then measured in the presence of 10 mM EDTA as described in Fig. 1 and expressed as cpm × 10⁻³. Where indicated, adhesion was measured in the presence of mAbs 9.3 or BB-1 (10 µg/ml).

is assigned a CD designation, enabled us to test directly its role in CD28-mediated adhesion. A cDNA clone encoding the B7/BB-1 antigen was transfected into COS cells. Transfectants were tested for expression of B7/BB-1 antigen by fluorescence-activated cell sorter analysis after indirect staining with mAb BB-1 (data not shown) and for adhesion to CD28. As shown in Fig. 5, B7/BB-1-transfected COS cells adhered readily to CD28⁺ CHO cells; adhesion was completely blocked by mAbs 9.3 and BB-1. No adhesion to CD28⁻ CHO cells was detected. This experiment was repeated five times with identical results. In other experiments, adhesion was not blocked by nonreactive isotype-matched controls or by mAb H1DE, which reacts with class I antigens on COS cells. When COS cells were transfected with expressible CD4 or CD5 cDNA clones, no CD28-mediated adhesion was detected. Thus, transfection of B7/BB-1 into COS cells confers the ability to adhere specifically to CD28.

DISCUSSION

We have demonstrated CD28-mediated adhesion by several lymphoblastoid and leukemic B-cell lines and by primary murine spleen cells after activation with LPS. These results indicate the presence of a natural ligand for the CD28 antigen on the cell surface of some activated B lymphocytes. Several lines of evidence show that the B-cell molecule that interacts with CD28 is activation antigen B7/BB-1. Since both CD28 (4) and B7/BB-1 (25) are members of the immunoglobulin superfamily, their interaction represents another example of heterophilic recognition between members of this gene family (12).

CD28-mediated adhesion differs in several respects from other cell adhesion systems. CD28-mediated adhesion was not blocked by mAbs to other adhesion molecules, including mAbs to the intercellular adhesion molecule 1 (ICAM-1) (LB-2), MHC class II (HB10a), CD18 (60.3), CD44 (HERMES-1 homing receptor), and an integrin (P3E3, P4C2, and P4G9). CD28-mediated adhesion is also resistant to EDTA and EGTA, indicating that this system does not require divalent cations, in contrast to integrins (30) and some homing receptors (31) that require divalent cations. In our system, in which CD28 was expressed to high levels relative to those on activated T cells, it was sometimes difficult to measure CD28-mediated adhesion because of cation-dependent "background" adhesion (i.e., that not blocked by mAb 9.3, see Fig. 1). Even under optimal conditions, some cells (such as Namalwa, see Fig. 3) showed significant non-CD28-dependent adhesion to CHO cells. Non-CD28-mediated adhesion systems may also be responsible for the incomplete blockage by mAb BB-1 of B-cell adhesion (Fig. 4).

Finally, CD28-mediated adhesion appears more restricted in its cellular distribution. CD28 is primarily expressed by cells of the T-lymphocyte lineage (15). Antigen B7/BB-1, as measured by staining with mAb BB-1 (20, 23) and mAb B7 (33) and Northern blot analysis with the B7/BB-1 cDNA clone (25), is primarily expressed by cells of the B-lymphocyte lineage. Consistent with this distribution, we have to date only detected a CD28 ligand on cells of B-lymphocyte lineage. Thus, available data suggest that CD28 mediates adhesion mainly between T and B cells. However, since CD28 expression has been detected on plasma cells (34) and B7/BB-1 has been detected on monocytes (25), it is possible that other cell types may also employ this system. In contrast, the CD2/lymphocyte function-associated antigen 3 (LFA-3), lymphocyte function-associated antigen 1 (LFA-1)/intercellular adhesion molecules 1 and 2 (ICAM 1 and ICAM 2), and very late antigen adhesion systems are more widely distributed (1, 32, 35).

Many adhesion molecules mediate T-cell–B-cell interactions during an immune response and levels of several,

including CD28 and B7/BB-1, increase after activation (1, 11, 25, 32, 33, 35, 36). Increased levels of these molecules may help explain why activated B cells are more effective at stimulating antigen-specific T-cell proliferation than are resting B cells (37–40). Since B7/BB-1 is not expressed on resting B cells (25, 33), CD28-mediated adhesion may play a role in maintaining or amplifying the immune response, rather than initiating it. Such a role is also consistent with the function of CD28 in regulating lymphokine and cytokine levels (8, 9).

Evidence supporting a role for CD28-mediated adhesion in antigen-specific T-cell responses comes from experiments showing inhibition of these responses by anti-CD28 mAbs (10, 11). CD28-mediated adhesion might also be important for T-helper-cell regulation of antigen-specific B-lymphocyte responses (41). Although homologues of CD28 and B7/BB-1 have not yet been identified in other mammalian species, our observation that activated murine B cells show CD28-mediated adhesion suggests that interactions between CD28 and its ligand have been conserved during evolution.

We thank Drs. Gordon Freeman and Lee Nadler for providing the B7/BB-1 cDNA clone; the many investigators who provided mAbs; Derek Hewgill for help with the cell sorter; Nancy Norris, Laura Grosmaire, Jeff Kallestad, and Bill Brady for expert technical assistance; and Dr. Karl Erik Hellstrom for continued support and comments on the manuscript.

1. Springer, T. A., Dustin, M. L., Kishimoto, T. K. & Marlin, S. D. (1987) *Annu. Rev. Immunol.* **5**, 223–252.
2. Dinarello, C. A. & Mier, J. W. (1987) *N. Engl. J. Med.* **317**, 940–945.
3. Weiss, A., Imboden, J., Hardy, K., Manger, B., Terhorst, C. & Stobo, J. (1986) *Annu. Rev. Immunol.* **4**, 593–619.
4. Aruffo, A. & Seed, B. (1987) *Proc. Natl. Acad. Sci. USA* **84**, 8573–8577.
5. Damle, N. K., Mohagheghpour, N., Hansen, J. A. & Engleman, E. G. (1983) *J. Immunol.* **131**, 2296–2300.
6. June, C. H., Ledbetter, J. A., Linsley, P. S. & Thompson, C. B. (1989) *Immunol. Today* **11**, 211–216.
7. June, C. H., Ledbetter, J. A., Gillespie, M. M., Lindsten, T. & Thompson, C. B. (1987) *Mol. Cell. Biol.* **7**, 4472–4481.
8. Thompson, C. B., Lindsten, T., Ledbetter, J. A., Kunkel, S. L., Young, H. A., Emerson, S. G., Leiden, J. M. & June, C. H. (1989) *Proc. Natl. Acad. Sci. USA* **86**, 1333–1337.
9. Lindsten, T., June, C. H., Ledbetter, J. A., Stella, G. & Thompson, C. B. (1989) *Science* **244**, 339–343.
10. Damle, N. K., Hansen, J. A., Good, R. A. & Gupta, S. (1981) *Proc. Natl. Acad. Sci. USA* **78**, 5096–6001.
11. Lesslauer, W., Konig, F., Ottenhoff, T., Giphart, M., Goulimy, E. & van Rood, J. J. (1986) *Eur. J. Immunol.* **16**, 1289–1296.
12. Williams, A. F. & Barclay, A. N. (1988) *Annu. Rev. Immunol.* **6**, 381–405.
13. Norment, A. M., Salter, R. D., Parham, P., Engelhard, V. H. & Littman, D. R. (1988) *Nature (London)* **336**, 79–81.
14. Doyle, C. & Strominger, J. L. (1987) *Nature (London)* **330**, 256–259.

15. Hansen, J. A., Martin, P. J. & Nowinski, R. C. (1980) *Immunogenetics* **10**, 247–260.
16. Bernard, A., Boumsell, L., Dausset, J., Milstein, C. & Schlossman, S. F., eds. (1984) *Leukocyte Typing* (Springer, New York).
17. Reinherz, E. L., Haynes, B. F., Nadler, L. M. & Bernstein, I. D., eds. (1986) *Leukocyte Typing II* (Springer, New York).
18. McMichael, A. J., Beverly, P. C. L., Cobbold, S., Crumpton, M. J., Gilks, W., Gotch, F. M., Hogg, N., Horton, M., Ling, N., MacLennan, I. C. M., Mason, D. Y., Milstein, C., Spiegelhalter, D. & Waldmann, H., eds. (1987) *Leukocyte Typing III* (Oxford Univ. Press, New York).
19. Kuritani, T. & Cooper, M. D. (1982) *J. Exp. Med.* **155**, 839–848.
20. Clark, E. A., Ledbetter, J. A., Holly, R. C., Dinndorf, P. A. & Shu, G. (1986) *Hum. Immunol.* **16**, 100–113.
21. Gilliland, L. K., Norris, N. A., Grosmaire, L. S., Ferrone, S., Gladstone, P. & Ledbetter, J. A. (1989) *Hum. Immunol.* **25**, 269–289.
22. W. Knapp, ed. (1990) *Leukocyte Typing IV* (Oxford Univ. Press, New York), in press.
23. Yokochi, T., Holly, R. D. & Clark, E. A. (1981) *J. Immunol.* **128**, 823–827.
24. Wayner, E. A., Garcia-Pardo, A., Humphries, M. J., McDonald, J. A. & Carter, W. G. (1989) *J. Cell. Biol.* **109**, 1321–1330.
25. Freeman, G. J., Freedman, A. S., Segil, J. M., Lee, G., Whitman, J. F. & Nadler, L. M. (1989) *J. Immunol.* **143**, 2714–2722.
26. Gentry, L. E., Webb, N. R., Lim, G. J., Brunner, A. M., Randalis, J. E., Twardzik, D. R., Lioubin, M. N., Marquardt, H. & Purchio, A. F. (1987) *Mol. Cell. Biol.* **7**, 3418–3427.
27. Subramani, S., Mulligan, R. & Berg, P. (1981) *Mol. Cell. Biol.* **1**, 854–864.
28. Gladstone, P. & Pious, D. (1978) *Nature (London)* **271**, 459–461.
29. Beatty, P. G., Harlan, J. M., Rosen, H., Hansen, J. A., Ochs, H. D., Price, T. D., Taylor, R. F. & Klebanoff, S. J. (1984) *Lancet* **i**, 535–537.
30. Kishimoto, T. K., Larson, R. S., Corbi, A. L., Dustin, M. L., Staunton, D. E. & Springer, T. A. (1989) *Adv. Immunol.* **46**, 149–182.
31. Stoolman, L. M. (1989) *Cell* **56**, 907–910.
32. Shaw, S. & Shimuzu, Y. (1988) *Curr. Opinion Immunol.* **1**, 92–97.
33. Freedman, A. S., Freeman, G., Horowitz, J. C., Daley, J. & Nadler, L. M. (1987) *J. Immunol.* **139**, 3260–3267.
34. Kozbor, D., Moretta, A., Messner, H. A., Moretta, L. & Croce, C. M. (1987) *J. Immunol.* **138**, 4128–4132.
35. Hemler, M. E. (1988) *Immunol. Today* **9**, 109–113.
36. Turka, L. A., Ledbetter, J. A., Lee, K., June, C. H. & Thompson, C. B. (1990) *J. Immunol.* **144**, 1646–1653.
37. Kakiuchi, T., Chestnut, R. & Grey, H. (1983) *J. Immunol.* **131**, 109–114.
38. Krieger, J. K., Grammer, S. F., Grey, H. & Chestnut, R. W. (1985) *J. Immunol.* **135**, 2937–2945.
39. McKenzie, D. (1988) *J. Immunol.* **141**, 2907–2911.
40. Hawrylowicz, C. M. & Unanue, E. R. (1988) *J. Immunol.* **141**, 4083–4088.
41. Moller, G., ed. (1987) *Immunology Review* (Munksgaard, Copenhagen), Vol. 99, pp. 1–299.

Distinct roles for CD28 and Cytotoxic T Lymphocyte-associated Molecule-4 Receptors during T Cell Activation?

By Peter S. Linsley

From the Bristol-Myers Squibb Pharmaceutical Research Institute, Seattle, Washington 98121

Cytotoxic T lymphocyte-associated molecule-4 (CTLA-4) is a lymphocyte cell surface receptor originally discovered in a search for molecules having a role in T cell cytotoxicity (1). This molecule is a member of the immunoglobulin superfamily and is homologous to another T cell surface receptor, CD28. Both CD28 and CTLA-4 bind the same counter-receptors, members of the B7 family on APCs. While the role of CD28 during T cell responses to antigen has been well studied, much less is known about the role of CTLA-4. Recent studies on the function of this molecule have been controversial and have yielded seemingly conflicting results. In this issue, a new study (2) provides further evidence on the function of this molecule and lends support to growing evidence that CTLA-4 is a receptor having unique function during an immune response. What follows in this article is an account of the development of this story, an analysis of the significance of the new data, and a discussion of potential fruitful areas of future research on CTLA-4.

Role of B7 Molecules in T Cell Costimulation. The interactions of T lymphocytes with APC are key to the generation of an immune response to foreign pathogens, transplanted organs, or to self tissue during autoimmune disease. The specificity of these T cell-APC interactions is provided by the recognition of antigenic peptide-MHC complexes by clonotypic TCR. However, TCR engagement alone generally does not lead to full T cell activation, but may instead lead to T cell clonal anergy. A successful immune response requires additional interactions between the T cell and the APC. These costimulatory interactions thus determine the outcome of TCR engagement, i.e., whether this engagement activates or inactivates subsequent immune responses (3). While the molecular nature of these costimulatory interactions is not fully understood, it is now clear that a key T cell costimulatory signal is provided by interaction of CD28 receptors on T cells with B7 counter-receptors on APC (4). Engagement of the CD28 receptor by B7 molecules triggers a signaling pathway that regulates T cell cytokine production, particularly IL-2 (4). Two B7 molecules are known, B7-1 (CD80) and B70/B7-2 (CD86), each of which binds CD28 with similar avidity and elicits similar functional effects (5).

CTLA-4. CTLA-4 is a second high avidity receptor for B7 molecules that was cloned from a subtracted cytolytic T cell cDNA library (1, 6). CTLA-4 transcripts were detected in activated lymphocytes and were coinduced with T cell cytotoxicity. Human and mouse genes encoding CTLA-4 map to the same chromosomal band as CD28 (7, 8), and human

CTLA-4 and CD28 have been linked at the molecular level on a yeast artificial chromosome clone (9). Recombinant soluble CTLA-4 binds CD80 and CD86 with higher avidity than recombinant soluble CD28 (5, 10).

Although originally identified as a cytolytic T cell-associated molecule, CTLA-4 transcripts have been detected in both CD4⁺ and CD8⁺ T cell clones (11). Cell surface expression of CTLA-4 on activated T cells has been detected using specific mAbs. In human T cells (12), CTLA-4 is expressed equally on CD4⁺ and CD8⁺ T subsets of activated T cells, whereas with murine cells, CTLA-4 expression is higher on the CD8⁺ subset (13). Expression of CTLA-4 is highly activation dependent; CTLA-4 is not detected on resting cells but is induced during T cell activation (1, 11-13). Expression is regulated in part by levels of mRNA (1, 11). With activated human T cells, maximal CTLA-4 protein expression was ~2-3% of CD28 (12). CTLA-4 is therefore a high avidity, low abundance receptor for B7 molecules.

Functions of CTLA-4 during T Cell Activation. Relatively little is known of the role of CTLA-4 during T cell activation, and the few experiments reported are largely contradictory. Complete conservation was noted in the amino acid sequences of the cytoplasmic tails of murine and human homologues of CTLA-4 (14). Since the cytoplasmic tail of CTLA-4 presumably mediates signal transduction, this sequence conservation suggested that CTLA-4 has an important conserved signaling function. The cytoplasmic tails of CTLA-4 and CD28 show more limited sequence homology (7), so it was therefore difficult to predict from sequence comparisons alone whether CTLA-4 would have similar or different functions than CD28.

Initial experiments (12) showed that combinations of CTLA-4 mAb and anti-CD28 mAb or Fab fragments were synergistic in blocking adhesion of activated CD4⁺ lymphocytes to CD80-transfected CHO cells, and in blocking T cell proliferation during a mixed lymphocyte reaction (MLR). Anti-CTLA-4 mAb had weak costimulatory activity together with anti-TCR mAb on previously primed CD4⁺ T cells, but the effects were less than those observed with anti-CD28 mAb plus anti-TCR mAb. Combinations of suboptimal amounts of anti-TCR mAb, anti-CD28 mAb plus anti-CTLA-4 mAb were synergistic in their costimulatory ability (12). Another study from this group (15) extended the original findings and showed that the cooperative costimulatory effects of anti-CTLA-4 and anti-CD28 mAbs were greatest at low concentrations of anti-CD28 mAb (and, hence, low occupancy

of CD28 receptors). Taken together, these observations led to the proposal that CD28 and CTLA-4 cooperatively regulate T cell activation and costimulation by B7 molecules.

A more recent study by Walunas et al. (13) suggested that CTLA-4 can also serve as a negative regulator of T cell activation. These investigators showed that in contrast to previous studies with human lymphocytes, anti-CTLA-4 mAb increased T cell proliferation in murine MLR. Similar results were obtained with Fab fragments of anti-CTLA-4 mAb. These results were interpreted to mean that anti-CTLA-4 mAb elicited its stimulatory effects by blocking interactions of CTLA-4 with its natural ligand, an interaction that was inhibitory for T cell proliferation in the MLR. Additional support for this proposal came from the observation that anti-CTLA-4 mAb inhibited proliferation of T cells costimulated with anti-CD3 and anti-CD28 mAbs. These studies led to the proposal that CTLA-4 interaction with its natural ligand downregulates an immune response.

Another recently published study (16) also suggested an antagonistic function for CTLA-4. These authors showed that anti-CTLA-4 mAbs triggered antigen-specific apoptosis in previously activated human T cells. With naive T cells, however, anti-CTLA-4 mAbs provided agonistic effects to combinations of anti-CD3 and anti-CD28 mAbs. Thus, the effects of anti-CTLA-4 mAbs were determined by the activation state of the cells studied.

Thus, these initial studies have led to two different and distinct models for the role of CTLA-4 in T cell activation (Fig. 1). In one model, CD28 and CTLA-4 function cooperatively to upregulate T cell activation; in the other model, CTLA-4 antagonizes CD28 and downregulates T cell activation.

The new study by Krummel and Allison (2) provides new data on the function of CTLA-4. These authors show that when used together with anti-CD3 mAb immobilized on

plastic wells, anti-CTLA-4 and anti-CD28 mAbs were synergistic in their ability to costimulate the proliferation of murine T cells. These data were interpreted to mean that anti-CTLA-4 mAb blocked an inhibitory effect on T cell proliferation caused by interaction between endogenous B7 molecules on T cells with CTLA-4. Other experiments showed that cross-linking of anti-CD3 plus anti-CD28 mAbs had a powerful costimulatory effect on T cell proliferation, cross-linking of anti-CTLA-4 mAb together with the other antibodies inhibited T cell proliferation. When the TCR, CD28, and CTLA-4 mAbs were immobilized on plastic beads, anti-CTLA-4 mAbs inhibited the proliferative effects of anti-CD28 plus anti-CD3 mAbs. Increasing amounts of anti-CTLA-4 mAbs progressively inhibited the costimulatory effects of anti-CD28 mAbs.

Thus, anti-CTLA-4 mAbs can either stimulate or inhibit T cell activation, depending on experimental conditions. The study by Krummel and Allison demonstrates several factors that are critical for determining the direction of the effects of anti-CTLA-4 mAbs. These include the endogenous expression of B7 by T cells. A mixture of mAbs to B7-1 and B7-2 showed similar stimulatory effects as anti-CTLA-4 mAb when the TCR signal was provided by mAb immobilized on plastic wells. Since B7-2 was expressed at low (nonstimulatory) levels on the T cells used in these experiments, T cell-T cell interactions mediated by interaction of B7-2 and CTLA-4 may have been inhibitory for T cell proliferation. It is unclear how endogenous expression of B7 affects the inhibitory effects of anti-CTLA-4 mAbs seen under other conditions. Also, the degree of co-cross-linking of CD3, with CD28, and/or CTLA-4 was important for determining the extent of proliferation. Taken together, the data suggest that the outcome of the T cell antigen receptor engagement is determined by integration of signals provided by CD28 and CTLA-4.

What do these findings tell us about the role of CTLA-4 in T cell activation? Perhaps most simply, they suggest that stimulation of CD28 and CTLA-4 TCRs may have different effects on T cell activation. Does this mean that CTLA-4 and CD28 have intrinsically opposite effects during T cell activation? Not necessarily. Experience in other signaling systems has taught us that it is quite common for receptor triggering to be context dependent, i.e., opposite effects are elicited under different experimental conditions. For example, it has long been known that cytokines and their receptors are multifunctional (17); many cytokines can stimulate proliferation under certain conditions and inhibit under others. The reasons for these different effects are not fully understood, but may involve differences in receptor occupancy, coupling to the signal transducing receptors, or the presence or absence of other cofactors. We should keep in mind that, generally speaking, a receptor that has only one effect is one that has not been fully studied. Perhaps the main message from the studies of Krummel and Allison is that CTLA-4 has come of age. Thus, we now realize that CTLA-4 is a receptor with its own unique properties and its own mechanisms of integrating with the lymphocyte signal transduction machinery.

Future Directions. As usual, coming of age means that life

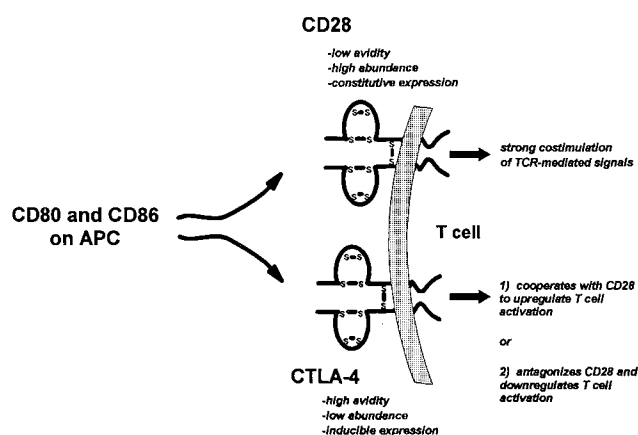


Figure 1. Summary of properties of T cell surface receptors CD28 and CTLA-4: expression, binding, and functional properties. The subunit structure of CD28 and CTLA-4 receptors is indicated schematically; each is homodimeric. The relative positions of inter- and intramolecular disulfide bonds of CD28 and CTLA-4 are depicted. Differences are emphasized in functional properties of CD28 and CTLA-4 as indicated by studies using specific mAbs.

becomes more complicated. The studies of Krummel and Allison also indicate that the process of T cell costimulation is more complicated than previously imagined, and more highly regulated. Since CTLA-4 and CD28 are coexpressed on the same cells and share common ligands, their engagement cannot be considered as independent events. The net result of engagement of CD28 and CTLA-4 receptors by B7 ligands will be determined by (a) the different affinities of CTLA-4 and CD28 for their B7 ligands; (b) the different expression levels of CTLA-4 and CD28; and (c) different effects of signaling through these two receptors (Fig. 1). How these factors are integrated by the lymphocyte signaling machinery is largely unknown at this juncture.

Future experiments will be necessary to more fully elucidate the roles of signals through the CTLA-4 and CD28 receptors. Perhaps all the reported experimental results are correct but their validity is limited to the particular experimental conditions that have been used. Further *in vitro* studies with human and murine T cells may help clarify the different effects of anti-CTLA-4 mAbs. One area that needs clarification is whether CTLA-4 has different functions in the different lymphocyte subsets used by different groups or in different species. Another area is whether mAbs to different epitopes on CTLA-4 have different effects. Undoubtedly, gene-targeted disruptions of CD28 and CTLA-4 genes will be valuable in future studies. CD28 knockout mice are defective in certain but not other immune responses (18). It will be important to determine the role of CTLA-4 in these mice. One study (19) suggested that CTLA-4 did not function *in vitro* when lymphocytes from these mice were studied, but more needs to be done, particularly during *in vivo* immune responses. A report on the properties of CTLA-4 knockout mice is eagerly awaited. Perhaps other transgenic studies will also be useful. If CTLA-4 triggering has a negative effect on T cell activation *in vivo*, then constitutive expression of CTLA-4 on transgenic T cells should have a negative effect on the immune responses of such animals.

Finally, a more complete understanding of the signal transduction pathways of CTLA-4 and CD28 receptors is needed.

While there is a tendency to attribute some of the effects of anti-CTLA-4 mAbs as evidence for a "negative signal" transmitted by this receptor (2, 13), it is unclear what this term means. Despite the importance of CD28 receptor triggering during T cell activation, relatively little is known of its signal transduction pathway(s) and even less is known of pathway(s) used by CTLA-4. It is perhaps typical of our state of knowledge about CTLA-4 that the two published studies (20, 21) on its signaling have given conflicting results. Both of these studies examined whether CTLA-4 triggering stimulated association of PI-3 kinase with a Y-X-X-M motif in its cytoplasmic tail, as has been demonstrated with a similar motif in the CD28 cytoplasmic tail (reviewed in reference 22). Stein et al. (20) found that CD8-CTLA-4 cytoplasmic tail chimeric constructs did not associate with the p85 subunit of PI-3 kinase after stimulation with mAb. The analogous CD8-D28 cytoplasmic tail constructs did associate with PI-3 kinase after triggering. In contrast, Schneider et al. (21) showed that triggering with mAbs of native CTLA-4 in a T cell line led to PI-3 kinase association with CTLA-4 and activation of PI-3 kinase activity, similar to what has been reported for the CD28 receptor (22). Clearly more must be done to elucidate the signal transduction pathway(s) of CTLA-4, and to determine how this pathway(s) compares with that of CD28.

Over the last several years, the CD28/CTLA-4/CD80/CD86 receptor system has emerged as a key control point in the pathway(s) leading to T cell activation during immune responses. Blockade of this pathway leads to immunosuppression, prolongs organ graft acceptance, and ameliorates autoimmune disease in rodent models (23, 24); stimulation of this pathway can facilitate immune rejection of tumors (25). Now that the importance of this system has been established, we are beginning to unravel its molecular details. We have begun to appreciate that each of the players in this system has evolved unique characteristics that contribute to the exquisite regulation of this powerful system. The flurry of recent studies on the CTLA-4 receptor signifies the beginning of our understanding of the role of this fascinating molecule in T cell immune responses.

I thank Jeff Ledbetter, Nitin Damle, Robert Peach, and Paul Gladstone for helpful discussions and critical reviews of the manuscript. I also thank Leslie Linsley for editorial assistance.

Address correspondence to Peter S. Linsley, Bristol-Myers Squibb Pharmaceutical Research Institute, 3005 First Avenue, Seattle, WA 98121.

Received for publication 21 March 1995.

References

1. Brunet, J.F., F. Denizot, M.F. Luciani, M. Roux-Dosseto, M. Suzan, M.G. Mattei, and P. Golstein. 1987. A new member of the immunoglobulin superfamily—CTLA-4. *Nature (Lond.)* 328:267–270.
2. Krummel, M.F., and J.P. Allison. 1995. CD28 and CTLA-4 deliver opposing signals which regulate the response of T cells to stimulation. *J. Exp. Med.* 182:.
3. Mueller, D.L., M.K. Jenkins, and R.H. Schwartz. 1989. Clonal expansion vs. functional clonal inactivation: a costimulatory pathway determines the outcome of T cell receptor occupancy.

- Annu. Rev. Immunol.* 7:445–480.
4. Schwartz, R.H. 1992. Costimulation of T lymphocytes: the role of CD28, CTLA-4, and B7/BB1 in interleukin-2 production and immunotherapy. *Cell*. 71:1065–1068.
 5. Lanier, L.L., S. O'Fallon, C. Somoza, J.H. Phillips, P.S. Linsley, K. Okumura, D. Ito, and M. Azuma. 1995. CD80 (B7) and CD86 (B70) provide similar costimulatory signals for T cell proliferation, cytokine production and generation of CTL. *J. Immunol.* 154:97–105.
 6. Brunet, J.F., F. Denizot, and P. Golstein. 1988. A differential molecular biology search for genes preferentially expressed in functional T lymphocytes: the CTLA genes. *Immunol. Rev.* 103:21–36.
 7. Harper, K., C. Balzano, E. Rouvier, M.-G. Mattei, M.-F. Luciani, and P. Golstein. 1991. CTLA-4 and CD28 activated lymphocyte molecules are closely related in both mouse and man as to sequence, message expression, gene structure and chromosomal location. *J. Immunol.* 147:1037–1044.
 8. Lafage-Pochitaloff, M., R. Costello, D. Couez, J. Simonetti, P. Mannoni, C. Mawas, and D. Olive. 1990. Human CD28 and CTLA-4 Ig superfamily genes are located on chromosome 2 at bands q33-q34. *Immunogenetics*. 31:198–201.
 9. Buonavista, N., C. Balzano, P. Pontarotti, D. Le Paslier, and P. Golstein. 1992. Molecular linkage of the human CTLA4 and CD28 Ig-superfamily genes in yeast artificial chromosomes. *Genomics*. 13:856–861.
 10. Linsley, P.S., W. Brady, L. Grosmaire, J.A. Ledbetter, and N. Damle. 1991. CTLA-4 is a second receptor for the B cell activation antigen B7. *J. Exp. Med.* 174:561–570.
 11. Freeman, G.J., D.B. Lombard, C.D. Gimmi, S.A. Brod, K. Lee, J.C. Laning, D.A. Hafler, M.E. Dorf, G.S. Gray, H. Reiser et al. 1992. CTLA-4 and CD28 mRNA are coexpressed in most T cells after activation. Expression of CTLA-4 and CD28 mRNA does not correlate with the pattern of lymphokine production. *J. Immunol.* 149:3795–3801.
 12. Linsley, P.S., J.L. Greene, P. Tan, J. Bradshaw, J.A. Ledbetter, C. Anasetti, and N. Damle. 1992. Coexpression and Functional Cooperativity of CTLA-4 and CD28 on activated T lymphocytes. *J. Exp. Med.* 176:1595–1604.
 13. Walunas, T.L., D.J. Lenschow, C.Y. Bakker, P.S. Linsley, G.J. Freeman, J.M. Green, C.B. Thompson, and J.A. Bluestone. 1994. CTLA-4 can function as a negative regulator of T cell activation. *Immunity*. 1:405–413.
 14. Dariavach P., M.G. Mattei, P. Golstein, and M.P. Lefranc. 1988. Human Ig superfamily CTLA-4 gene: chromosomal localization and identity of protein sequence between murine and human CTLA-4 cytoplasmic domains. *Eur. J. Immunol.* 18: 1901–1905.
 15. Damle, N.K., K. Klussman, G. Leytze, S. Myrdal, A. Aruffo, J.A. Ledbetter, and P.S. Linsley. 1994. Costimulation of T lymphocytes with integrin ligands intercellular adhesion molecule-1 or vascular cell adhesion molecule-1 induces functional expression of CTLA-4, a second receptor for B7. *J. Immunol.* 152: 2686–2697.
 16. Gribben, J.G., G.J. Freeman, V.A. Bousiotis, P. Rennert, C.L. Jellis, E. Greenfield, M. Barber, V.A. Restivo, Jr., X. Ke, G.S. Gray, and L.M. Nadler. 1995. CTLA4 mediates antigen-specific apoptosis of human T cells. *Proc. Natl. Acad. Sci. USA*. 92: 811–815.
 17. Sporn, M.B., and A.B. Roberts. 1988. Peptide growth factors are multifunctional. *Nature (Lond.)*. 332:217–219.
 18. Shahinian, A., K. Pfeffer, K.P. Lee, T.M. Kundig, K. Kishihara, A. Wakeham, K. Kawai, P.S. Ohashi, C.B. Thompson, and T.W. Mak. 1993. Differential T cell costimulatory requirements in CD28-deficient mice. *Science (Wash. DC)*. 261:609.
 19. Green, J.M., P.J. Noel, A.I. Sperling, T.L. Walunas, G.S. Gray, J.A. Bluestone, and C.B. Thompson. 1994. Absence of B7-dependent responses in CD28-deficient mice. *Immunity*. 1:501–508.
 20. Stein, P.H., J.D. Fraser, and A. Weiss. 1994. The cytoplasmic domain of CD28 is both necessary and sufficient for costimulation of interleukin-2 secretion and association with phosphatidylinositol 3'-kinase. *Mol. Cell. Biol.* 14:3392–3402.
 21. Schneider, H., V.S. Prasad, S.E. Shoelson, and C.E. Rudd. 1995. CTLA-4 binding to lipid kinase phosphatidyl 3-kinase in T cells. *J. Exp. Med.* 181:351–356.
 22. Rudd, C.E., O. Janssen, Y.C. Cai, A.J. da Silva, M. Raab, and K.V. Prasad. 1994. Two-step TCR zeta/CD3-CD4 and CD28 signaling in T cells: SH2/SH3 domains, protein-tyrosine and lipid kinases. *Immunol. Today*. 15:225–234.
 23. Lenschow, D.J., Y. Zeng, J.R. Thistlewaite, A. Montag, W. Brady, M.G. Gibson, P.S. Linsley, and J.A. Bluestone. 1992. Long-term survival of xenogeneic pancreatic islet grafts induced by CTLA4Ig. *Science (Wash. DC)*. 257:789–792.
 24. Finck, B.K., P.S. Linsley, and D. Wofsy. 1994. Treatment of murine lupus with CTLA4Ig. *Science (Wash. DC)*. 265:1225–1227.
 25. Chen, L., P.S. Linsley, and K.E. Hellström. 1993. Costimulation of T cells for tumor immunity. *Immunology Today*. 14: 483–486.

CD28 and CTLA-4 Have Opposing Effects on the Response of T cells to Stimulation

By Matthew F. Krummel and James P. Allison

From the Department of Molecular and Cell Biology and Cancer Research Laboratory, University of California, Berkeley, California 94720

Summary

The importance of the B7/CD28/CTLA-4 molecules has been established in studies of antigen-presenting cell-derived B7 and its interaction with the T cell costimulatory molecule CD28. CTLA-4, a T cell surface glycoprotein that is related to CD28, can also interact with B7-1 and B7-2. However, less is known about the function of CTLA-4, which is expressed at highest levels after activation. We have generated an antibody to CTLA-4 to investigate the consequences of engagement of this molecule in a carefully defined system using highly purified T cells. We show here that the presence of low levels of B7-2 on freshly explanted T cells can partially inhibit T cell proliferation, and this inhibition is mediated by interactions with CTLA-4. Cross-linking of CTLA-4 together with the TCR and CD28 strongly inhibits proliferation and IL-2 secretion by T cells. Finally, results show that CD28 and CTLA-4 deliver opposing signals that appear to be integrated by the T cell in determining the response to activation. These data strongly suggest that the outcome of T cell antigen receptor stimulation is regulated by CD28 costimulatory signals, as well as inhibitory signals derived from CTLA-4.

Recent work has demonstrated that CD28, a protein expressed on resting and activated cells, is the major costimulatory molecule for proliferation of T cells (1–3). CD28 engagement via antibodies augments the proliferation of T cells in response to immobilized anti-TCR antibodies (4). Additionally, antibody engagement can supply costimulation to T cells encountering APCs deficient in costimulation (4, 5) and prevents the resultant anergic state that otherwise occurs in long-term clones (4). Finally, Fab fragments of anti-CD28 can fully block proliferation by costimulation competent APCs (4).

Several lines of evidence indicate that B7-1 (CD80) and B7-2 (CD86) (6) are the major costimulatory ligands on the APC. First, a chimeric fusion protein of CD28 binds B7-1 and B7-2 (7, 8). Second, anti-B7 antibodies block T cell activation by a variety of APCs (9, 10). Finally, induction of expression of B7-1 or B7-2 by transfection with cDNAs confers costimulatory activity on cells that do not otherwise provide costimulation (11–14). Interestingly, APCs and especially dendritic cells, which are thought to be involved in the early phases of T cells activation, express moderate levels of functional B7-2 without activation (6, 15). These levels increase nearly 100-fold with overnight activation, enhancing their APC function.

B7-1 and B7-2 also bind CTLA-4, a close relative of CD28. Chimeric fusion proteins consisting of the ectodomain of CTLA-4 bind B7-1 and B7-2 (8, 16–18) and can block T cell activation by costimulation competent accessory cells (10,

12). Notably, studies with soluble fusion protein indicate that CTLA-4 binds both B7 family members with an affinity ~20-fold higher than that of CD28. This higher affinity probably accounts for the ability of the CTLA-4 Ig fusion protein to block costimulation *in vitro* (10, 12) and to suppress graft rejection and antibody production *in vivo* (19, 20).

While the ability of CTLA-4 fusion proteins to bind CD28 ligands and block T cell activation is clear, the function of the native molecule has been obscure. Originally identified as cDNA cloned from a subtracted CTL clone library (21), CTLA-4 is homologous to CD28, especially in the extracellular domain, and both contain a conserved sequence motif, MYPPY, thought to be involved in B7 binding (22). Recent work has shown that CTLA-4 mRNA is expressed within a few hours of activation (23). Studies with mAbs to both human and mouse CTLA-4 demonstrated surface expression within 48 h of activation. However, functional studies have led to different conclusions about its role in activation. Linsley et al. in a study of human T cells found that anti-CTLA-4 antibodies enhanced proliferation of T cells activated with anti-CD3 and anti-CD28, suggesting that the function of CTLA-4 was to augment or sustain costimulation (24, 25). Walunas et al. found that both intact and monovalent fragments of antibodies to mouse CTLA-4 enhanced T cell responses in allogeneic MLR, but that intact antibody inhibited proliferation under conditions where Fc receptor cross-linking was provided (26). These results suggest that CTLA-4 might play a role in negative regulation of T cell activation.

We describe here an analysis of CD28 and CTLA-4 signaling on highly purified T cells, noting the presence of B7 on the T cells themselves. The results indicate that the two molecules have opposing effects on lymphokine production and proliferation, and that the outcome of T cell activation is determined by integration of signals transduced by these two molecules.

Materials and Methods

Immunization and Hybridoma Production. 6-wk-old golden Syrian hamsters received five footpad injections of 50 μ l (packed volume) heat-killed *Staphylococcus* A bacteria coated with \sim 100 μ g CTLA-4 Ig (27) and suspended in 0.2 ml PBS. 3 d after the final injection, draining lymph nodes were removed, and lymphocytes were isolated and fused with the P3X3.6G8.653 myeloma line using a standard polyethylene glycol fusion technique (28). Hybridoma supernatants were tested for reactivity to CTLA-4 Ig and for a lack of reactivity to CD4 Ig by ELISA (29). Hybridomas from positive wells were repetitively cloned by limiting dilution in the presence of irradiated mouse thymocyte feeder layers. Antibody 9H10 was specific for CTLA-4 by three criteria: (a) Reactivity against CTLA-4 Ig but not CD4 Ig; (b) the ability to block CTLA-4 Ig binding to B7 transfecants; (c) the ability to stain activated T cells but not freshly isolated T cells; and (d) the ability to stain a CTLA-4 transfecant but not control transfecants.

Antibodies. Antibodies used include anti-CD3 clone 500A2 (30), anti-CD28 clone 37.51 (31), anti-B7-1 clone 1610A (9), anti-B7-2 (17), anti-V γ 3 clone 536 (32), anti-class II MHC clone 28-16-8s (33), and anti-IA^{d/b} clone BP107 (34). Conjugates of these antibodies were prepared in our laboratory. PE, biotin, and FITC conjugates of anti-CD4 and anti-CD8 were purchased from CALTAG Laboratories (South San Francisco, CA) and PharMingen (San Diego, CA).

T Cell Activation Cultures. Spleens from 4–6-wk-old BALB/c mice were harvested and minced, and suspensions were treated with Geys RBC lysis solution (35). Cells were cultured in RPMI containing 10% FCS and soluble anti-CD3 antibody at 10 μ g/ml.

Flow Cytometry. 2×10^5 cells were suspended in 10 μ l ice-cold PBS/1% calf serum/0.05% sodium azide. Antibodies were added for 30 min followed by two 4-ml washes in PBS/calf serum/sodium azide. Data were acquired on a FACScan® (Becton Dickinson and Co. (Mountain View, CA) and the LYSIS II program was used to electronically gate on relevant populations.

Proliferation Assays. LN cells were isolated from 6–8-wk-old BALB/c mice (Charles River Laboratories, Wilmington, MA). Isolated lymphocytes were obtained by mincing and filtration through nylon sieves. Cells were then treated with anti-class II antibodies 28.16.8s and BP107 and a mixture of rabbit and guinea pig complement (Accurate Chemical and Scientific Corp., Westbury, NY). Viable cells were isolated over lympholyte 1.119 (Sigma Chemical Co., St. Louis, MO) and residual Ig-positive cells were removed by repetitive panning on rabbit anti-mouse IgG coated tissue culture plates. Typical preparations analyzed by FACS® were typically found to be 99% Thy1.2+ with <0.5% B220-positive cells. Round-bottomed 96-well plates were used for all assays. Where indicated, wells were coated with anti-CD3 at 0.1 μ g/ml in 50- μ l vol for 2 h at 37°C, then washed extensively and blocked for 30 min at 37°C with complete RPMI 1640. T cells were added at 10 5 per well in 200 μ l complete RPMI 1640. For soluble assays, anti-CD28 was added at a 1:1,000 dilution of ascites, anti-CTLA-4 was added at 10 μ g/ml, and B7 antibodies were added at 2.5 μ g/ml

and 10 μ g/ml for anti-B7-1 and anti-B7-2, respectively. For cross-linking assays, anti-CD8 was added at 4 μ g/ml, anti-CD3 was added at 5 μ g/ml, anti-CTLA-4 was added at 20 μ g/ml, and anti-V γ 3 control antibody F536 was added to produce a constant total antibody concentration of 30 μ g/ml. Polyclonal goat anti-hamster antibody (Pierce Chemical Co., Rockford, IL) was added at a final concentration of 20 μ g/ml. All cultures were incubated at 37°C for 72 h, then pulsed with 1 μ Ci of [³H]thymidine for an additional 16 h before harvesting.

Antibody Incorporation onto Latex Microspheres. Sulfate polystyrene latex microspheres of 5 \pm 0.1 μ M mean diameter were obtained from Interfacial Dynamics Corporation (Portland, OR). Approximately 1 \times 10⁷ beads per ml were suspended in PBS and the indicated antibodies were incubated for 1.5 h at 37°C. Anti-CD3 was added at 1 μ g/ml to deliver the antigen-specific signal, and binding solutions were normalized with control antibody 536 to maintain a constant total antibody concentration of 5 μ g/ml during binding. Previous data have shown maximal binding is achieved when this concentration is added per 10⁷ particles (36). Beads were washed extensively with PBS and resuspended in 1 ml RPMI-10% FCS and allowed to block for at least 30 min at room temperature. 10⁵ cells were incubated in 96-well cultures with 10⁵ each of the indicated bead preparation.

Results

Activation Induces Expression of CTLA-4 on Both CD4⁺ and CD8⁺ T cells. Antibody 9H10 was used to assess CTLA-4 expression on freshly isolated and activated T cells. As shown in Fig. 1 A, CTLA-4 was undetectable on freshly isolated T cells. CTLA-4 was readily detected on T cells 48 h after stimulation by addition of anti-CD3 to splenocytes, and it was returned to resting levels by 72 h. CD28 expression was not greatly altered by stimulation. CTLA-4 was expressed by both CD4⁺ and CD8⁺ T cells, with significantly higher levels on the latter.

Blockade of CTLA-4 or B7-1/2 Enhances Anti-CD28 Costimulation. To determine the functional consequences of CTLA-4 engagement, soluble anti-CTLA-4 or anti-CD28 antibodies were added singly or together to cultures of purified T cells exposed to immobilized anti-CD3. As shown in Fig. 2, while anti-CD28 greatly enhances the minimal proliferation induced by CD3 stimulation, anti-CTLA-4 has no effect. This suggests that CTLA-4 does not function as an alternate costimulatory receptor. Despite its lack of costimulatory activity on its own, anti-CTLA-4 markedly increases T cell proliferation when given together with anti-CD28.

At least two mechanisms could account for the potentiating effects of anti-CTLA-4: enhancement of activation signals or removal of inhibitory signals. Given the observation that anti-CTLA-4 lacked costimulatory activity on its own, we favored the latter possibility—that blockade of CTLA-4 by the antibody might prevent interaction of CTLA-4 on the T cell surface with B7-1 and/or B7-2 and thus prevent delivery of an inhibitory signal. This is further suggested by the observation that anti-CTLA-4 Fab fragments have similar effects as anti-CTLA-4 mAbs in this assay system (data not shown). Since the cells used in our experiments were >99% Thy1⁺ and contained no detectable MHC class-II⁺ or B220⁺ cells,

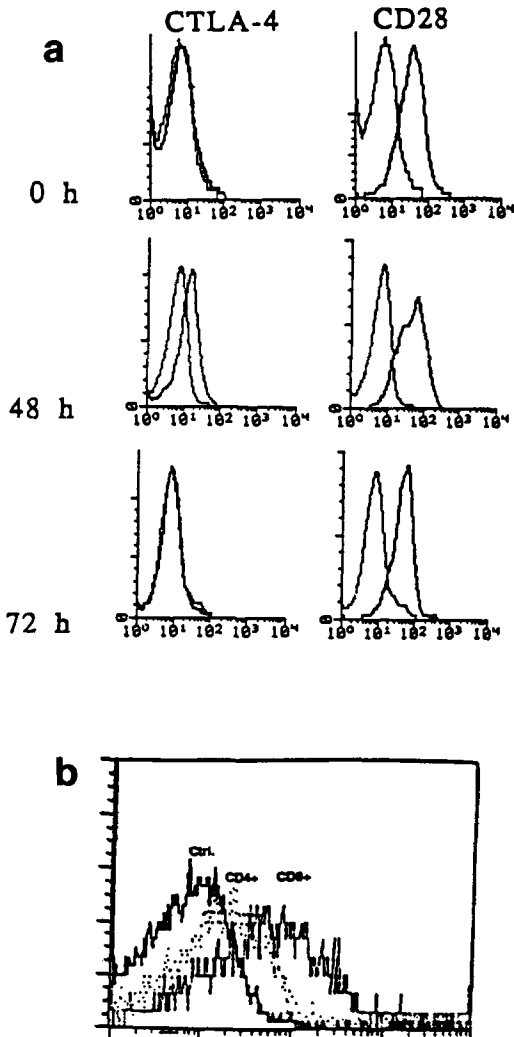


Figure 1. Expression of CTLA-4 and CD28 on resting and activated splenic T cells. BALB/c splenic cell suspensions (2×10^6 /ml) were stimulated in vitro with $10 \mu\text{g}/\text{ml}$ soluble anti-CD3. (a) Cells were double stained with Thy1.2PE and either hamster Ig-control FITC, anti-CTLA-4 FITC, or anti-CD28 FITC. Data were electronically gated for Thy1.2-positive cells; CTLA-4 and CD28 expressions are shown on freshly explanted cells and after 48- and 72-h incubations with anti-CD3. (b) 48-h cultures were stained for anti-CD4 biotin or anti-CD8 biotin followed by avidin tricolor and FITCylated irrelevant or CTLA-4 antibodies. Subpopulation-gated data show modestly higher CTLA-4 expression on CD8 populations.

this possibility would require that the T cells themselves provide a source of ligand. As shown in Fig. 3, flow cytometric analysis revealed that the freshly isolated T cells did indeed express significant levels of B7-2 and trace levels of B7-1.

To determine the functional consequence of B7 expression by T cells in our assay system, we determined the effects of anti-B7 antibodies on CD28-mediated costimulation. As shown in Fig. 2, anti-B7 antibodies by themselves had no significant effect on anti-CD3-induced T cell proliferation. The addition of anti-B7 antibodies to cultures containing anti-CD28 resulted in a threefold increase in proliferation over that obtained with anti-CD28 alone. A similar increase in

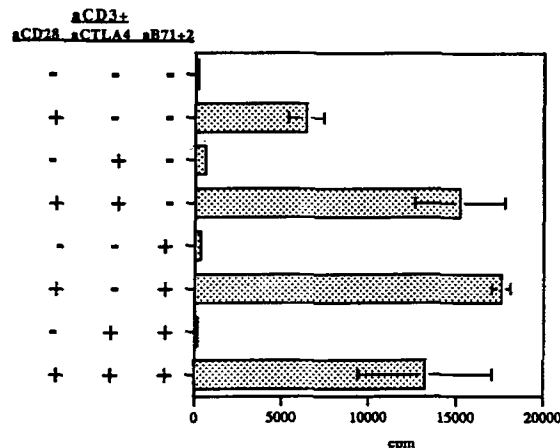


Figure 2. Influence of anti-CTLA-4 and anti-B7 antibodies on proliferative responses of purified lymph node T cells. 10^5 BALB/c LN T cells were cultured for 72 h in 96-well microwells coated with $0.1 \mu\text{g}/\text{ml}$ anti-CD3. Anti-CD28 was used at a 1:1,000 dilution of ascites and B7 antibodies were used at 2.5 and $10 \mu\text{g}/\text{ml}$ for anti-B7-1 and anti-B7-2, respectively. Anti-CTLA-4 antibody 9H10 was added at $10 \mu\text{g}/\text{ml}$.

proliferation was obtained when chimeric CTLA-4 Ig instead of anti-B7 antibodies was added to block B7 interactions (data not shown). The magnitude of the increase was similar to that obtained when anti-CTLA-4 is added to CD28-treated cells in the absence of B7 blockade. The addition of anti-CTLA-4 to cultures in which anti-B7 antibodies are present results in no further increase in CD28 costimulation; indeed, a slight but reproducible decrease is observed.

Together, these results suggest that T cells express B7 at levels that are insufficient to provide costimulation via CD28 engagement in the assay system used. However, perhaps because of the fact that CTLA-4 has a much higher affinity than CD28 for B7 binding, these levels are sufficient to generate a signal that at least partially inhibits activation. Blockade of the CTLA-4/B7 interaction with either anti-CTLA-4 or anti-B7 antibodies removes the inhibitory signal, resulting in an increase of the costimulatory effect of CD28 ligation.

Cross-linking of CTLA-4 with the TCR and CD28 Inhibits T Cell Proliferation and IL-2 Production. The results shown

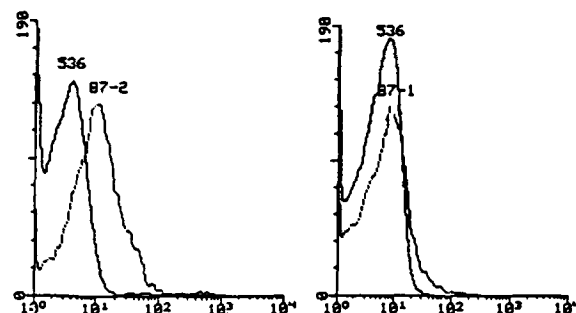


Figure 3. Expression of B7-2 and B7-1 on purified, freshly isolated lymph node T cells. Cells that were $>99\%$ Thy1.2 $^+$ were isolated and stained with GL1 (anti-B7-2), 1610A (anti-B7-1), or irrelevant antibodies.

in Fig. 2 suggested that soluble, bivalent anti-CTLA-4 antibody was effective in blocking B7-mediated signals, but was inefficient in providing signals. We next examined the effects of using anti-hamster Ig to cross-link CD3, CD28, and CTLA-4 singly or together. As shown in Fig. 4, no proliferation was obtained when CD3, CD28, or CTLA-4 were cross-linked individually. As expected, cross-linking of CD3 together with CD28 resulted in potent costimulation, while cross-linking of CD3 and CTLA-4 had no effect. Co-cross-linking of CTLA-4 together with CD3 and CD28 consistently resulted in a 5- to 10-fold reduction in proliferation. This inhibition was largely reversed by the addition of IL-2 to the cultures, suggesting that the effect is not caused by toxicity. Finally, cross-linking of CTLA-4 with CD3 and CD28 also resulted in a profound decrease in IL-2 production in the cultures (Fig. 4B). These results demonstrate that CTLA-4 can deliver signals that inhibit T cell responses to TCR ligation, and that the effects observed in the experi-

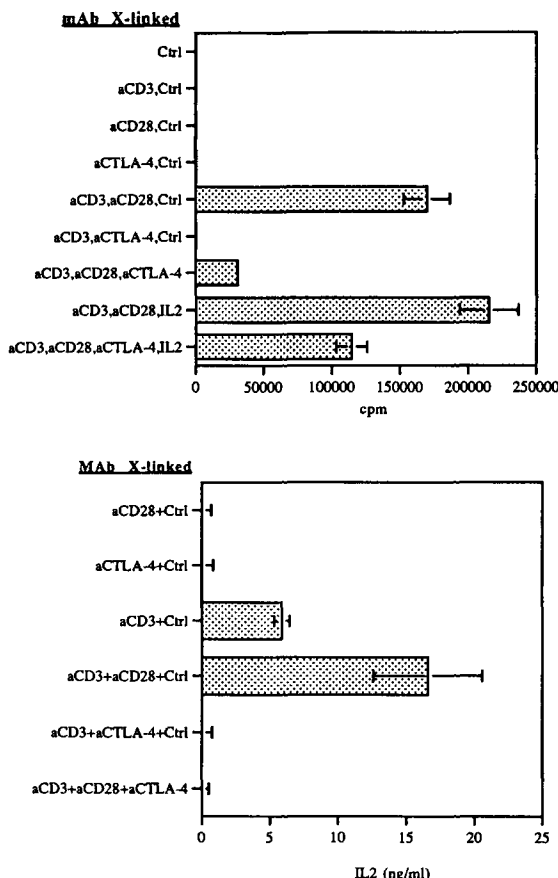


Figure 4. Cross-linked anti-CTLA-4 can diminish both proliferation and lymphokine production by purified LN T cells. 10^5 BALB/c LN T cells were cultured with the indicated hamster antibodies together with control hamster Ig added at 20 $\mu\text{g}/\text{ml}$ to cross-link. Where indicated, anti-CD3 was added at 5 $\mu\text{g}/\text{ml}$, anti-CD28 was added at 4 $\mu\text{g}/\text{ml}$, anti-CTLA-4 was added at 20 $\mu\text{g}/\text{ml}$, and control was added to normalize antibody concentration at 30 $\mu\text{g}/\text{ml}$. (a) Cells were cultured for 72 h, pulsed with 1 μCi [^3H]thymidine, and harvested after an additional 16 h. (b) Supernatants were removed and analyzed for IL-2 production at 48 h using an ELISA detection system.

ment presented in Fig. 2 most likely result from perturbation of B7/CTLA-4 interactions.

CD28 and CTLA-4 Deliver Quantitatively Opposing Signals. The preceding data indicate that CTLA-4 cross-linking in the presence of CD28 signaling can inhibit IL-2 secretion and proliferation. We next sought to determine whether signaling above the threshold for CTLA-4 inhibition is independent of the magnitude of CD28 costimulation, or whether the threshold increases as CD28 signaling increases. To address this issue, T cells were stimulated by incubation with polystyrene beads coated with a constant amount of anti-CD3 and varying amounts of anti-CD28 and anti-CTLA-4. As shown in Fig. 5, costimulation with increasing amounts of anti-CD28 in the absence of anti-CTLA-4 resulted in a gradual increase in proliferation, reaching at the highest dose a 1,500-fold increase over that obtained with anti-CD3 alone. The addition of increasing amounts of anti-CTLA-4 reduced that proliferation in a stepwise manner at all doses of anti-CD28. These results suggest that T cells integrate signals from CD28 with signals from CTLA-4, and the balance of these signals regulates the magnitude of the response to TCR ligation.

Discussion

The results presented here clearly demonstrate that CTLA-4 does not serve as a functional alternative to CD28 in providing costimulatory signals to T cells. This finding is in agreement with earlier studies showing that CTLA-4 did not replace CD28 function in CD28 mutant mice (37). The finding that anti-CTLA-4 increases proliferation of T cells activated by anti-CD3 and anti-CD28 is in agreement with the results of Linsley et al. (24). However, the fact that a similar result is obtained when blocking antibodies to B7 are included suggests that this apparent cooperativity of CTLA-4 is in fact a result of removal of preexisting inhibitory B7-CTLA-4 in-

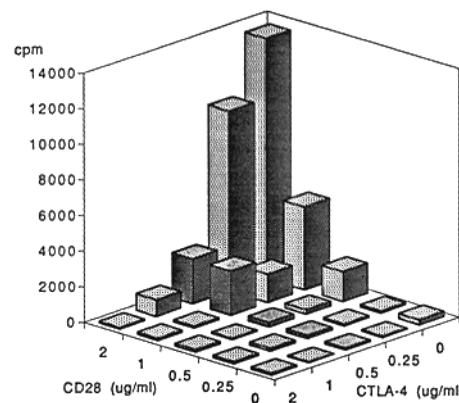


Figure 5. Proliferation in response to a constant CD3 signal is affected by the relative concentrations of CD28 and CTLA-4 signals. 10^7 $5 \mu\text{M}$ microspheres were coated with 1 $\mu\text{g}/\text{ml}$ of anti-CD3, the indicated concentrations of anti-CD28 and anti-CTLA-4, and control hamster Ig constituting a total antibody concentration of 5 $\mu\text{g}/\text{ml}$. 10^5 coated spheres were incubated in 96-well cultures with 10^5 purified LN T cells for 72 h, pulsed with 1 μCi [^3H]thymidine, and harvested after an additional 16 h.

teractions by the soluble CTLA-4 antibodies rather than a synergism between the two antibody-generated signals. The ability of CTLA-4 to directly signal is supported by the fact that cross-linking of anti-CTLA-4, either with second antibody or by presentation immobilized on beads, results in inhibition of both IL-2 production and proliferation. This direct demonstration of signaling by CTLA-4 supports the report of Walunas et al. (26) that CTLA-4 is a negative regulator of T cell activation.

Our demonstration of a dynamic competition between CD28 and CTLA-4 indicates that in addition to CD3 and CD28 signal integration, there exists an integration point for CTLA-4-derived signals. At present there is little knowledge of the biochemical events that follow CD28 or CTLA-4 ligation. There have been reports that CD28 stimulation results in induction of protein tyrosine kinase activity (38), and recent evidence suggest the Tec family kinase ITK represents one associated protein kinase (39). In addition, it has been demonstrated that phosphoinositides accumulate in T cells stimulated by ligation of CD28 with B7-1, suggesting an involvement of phosphatidylinositol 3'-kinase (PI3K)¹ with CD28 (40). In this regard, it is of interest that the cytoplasmic domains of both CD28 and CTLA-4 contain the sequence YM/VXM, a motif found in several growth factor receptors that associate with PI3K (41, 42). Several recent reports have documented a stimulation-induced association between CD28 and PI3K, and it has been reported that mutation of the PI3K-binding motif destroys the costimulatory activity of CD28 (43–47). These findings strongly suggest that binding of PI3K plays an important role in CD28 signaling. With respect to CTLA-4, however, there have been contradictory findings. Whereas a chimeric protein containing the cytoplasmic domain of CTLA-4 was unable to bind PI3K (46), another study

reported the coprecipitation of PI3K activity with CTLA-4 (48). In any event, these findings raise the possibility that CD28 and CTLA-4 might compete for PI3K and affect its role in subsequent signal transduction.

It is also possible that CD28 and CTLA-4 signals might intersect at later stages in the pathway. It has been demonstrated that the CD28 and CD3 pathways intersect at the level of the MAP kinase JNK (49). CTLA-4 might in somehow interfere with this coupling, thus preventing costimulation. Finally, it is possible that CTLA-4 signals might interfere with those of CD28 even further downstream by interfering with IL-2 transcriptions or mRNA stabilization (46, 50).

Our results further suggest that regulation of the outcome of T cell stimulation is a complex process with regard to events at the cell surface. It is clear that in the absence of costimulatory signals provided by the B7 family, T cells do not proliferate. It appears that even small amounts of B7, such as those present on T cells themselves, are ineffectual in supporting CD28-mediated costimulation of anti-CD3 responses. This appears to be less a consequence of the absence of CD28 signal being delivered, but rather a result of an inhibitory signal delivered through CTLA-4. This implies that either CTLA-4 is quickly expressed after activation and aborts the response, or that CTLA-4 is expressed at functionally significant levels on resting T cells. At higher levels of B7 expression, as might be encountered on activated dendritic cells and activated B cells, CTLA-4 expression on the T cells might become limiting, and the costimulation provided by CD28 becomes dominant. As expression of CTLA-4 rises after activation, the signals generated through CTLA-4 might become dominant and terminate the response. Decay of CTLA-4 expression with time would allow the T cell to return to a state where the CD28 costimulatory signal would predominate. In any event, accumulating evidence suggests that in addition to antigen receptor and CD28-mediated signals, a third signal, provided by CTLA-4, is important in determining the outcome of T cell activation.

¹ Abbreviation used in this paper: PI3K, phosphatidylinositol 3'-kinase.

We are grateful to Drs. P. Lane and K. Karljaleinen for providing CTLA-4Ig and CD4Ig fusion chimeras. We thank David Raulet for critical reading of the manuscript.

This work was supported by National Institutes of Health grants CA40041 and CA09179.

Address correspondence to James P. Allison, Dept. of Molecular and Cell Biology and Cancer Research Laboratory, University of California, Berkeley, CA 94720.

Received for publication 8 December 1994 and in revised form 6 March 1995.

References

- June, C.H., J.A. Bluestone, L.M. Nadler, and C.B. Thompson. 1994. The B7 and CD28 receptor families. *Immunol. Today*. 15:321–331.
- Jenkins, M.K. 1994. The ups and downs of costimulation. *Immunity*. 1:443–446.
- Linsley, P.S., and J.A. Ledbetter. 1993. The role of the CD28 receptor during T cell responses to antigen. *Annu. Rev. Immunol.* 11:191–212.
- Harding, F., J.G. McArthur, J.A. Gross, D.H. Raulet, and J.P. Allison. 1994. CD28 mediated signalling costimulates murine

- T cells and prevents the induction of anergy in T cell clones. *Nature (Lond.)*. 356:607–609.
5. Holsti, M.A., J. McArthur, J.P. Allison, and D.H. Raulet. 1994. Role of IL-6, IL-1, and CD28 signaling in responses of mouse CD4⁺ T cells to immobilized anti-TCR monoclonal antibody. *J. Immunol.* 152:1618–1624.
 6. Caux, C., B. Vanvervliet, C. Massacrier, M. Azuma, K. Okumura, L.L. Lanier, and J. Banchereau. 1994. B7/B7-2 is identical to CD86 and is the major functional ligand for CD28 expressed on human dendritic cells. *J. Exp. Med.* 180:1841–1847.
 7. Linsley, P.S., E.A. Clark, and J.A. Ledbetter. 1990. The T cell antigen, CD28, mediates adhesion with B cells by interacting with the activation antigen, B7/BB-1. *Proc. Natl. Acad. Sci. USA*. 87:5031–5035.
 8. Azuma, M., D. Ito, H. Yagita, K. Okumura, J.H. Phillips, L. Lanier, and C. Somoza. 1993. B70 antigen is a second ligand for CTLA-4 and CD28. *Nature (Lond.)*. 366:76–79.
 9. Razi-Wolf, Z., G.J. Freeman, F. Galvin, B. Benacerraf, L. Nadler, and H. Reiser. 1992. Expression and function of the murine B7 antigen, the major costimulatory molecule expressed by peritoneal exudate cells. *Proc. Natl. Acad. Sci. USA*. 89:4210–4214.
 10. Reiser, H., G.J. Freeman, Z. Razi-Wolf, C.D. Gimmi, B. Benacerraf, and N.M. Nadler. 1992. Murine B7 antigen provides a costimulatory signal for activation of murine T lymphocytes via the T cell receptor/CD3 complex. *Proc. Natl. Acad. Sci. USA*. 89:271–275.
 11. Linsley, P.S., W. Brady, L. Grosmaire, A. Aruffo, N.K. Damle, and J.A. Ledbetter. 1991. Binding of the B cell activation antigen B7 to CD28 costimulates T cell proliferation and interleukin 2 mRNA accumulation. *J. Exp. Med.* 173:721–730.
 12. Gimmi, C.D., G.J. Freeman, J.G. Gribben, K. Sugita, A.S. Freedman, C. Morimoto, and L.M. Nadler. 1991. B-cell surface antigen B7 provides a costimulatory signal that induces T cells to proliferate and secrete interleukin 2. *Proc. Natl. Acad. Sci. USA*. 88:6575–6579.
 13. Reiser, H., G.J. Freeman, Z. Razi-Wolf, C.D. Gimmi, B. Benacerraf, and L.M. Nadler. 1992. Murine B7 antigen provides an efficient costimulatory signal for activation of murine T lymphocytes via the T-cell receptor/CD3 complex. *Proc. Natl. Acad. Sci. USA*. 89:271–275.
 14. Murphy, E.E., G. Terres, S.E. Macatonia, C.S. Hsieh, J. Mattson, L.L. Lanier, M. Wysocka, G. Trinchieri, K. Murphy, and A. O'Garra. 1994. B7 and interleukin-12 cooperate for proliferation and IFN- γ production by mouse Th1 clones that are unresponsive to B7 costimulation. *J. Exp. Med.* In press.
 15. Inaba, K., M. Witmer-Pack, M. Inaba, K.S. Hathcock, H. Sakuta, M. Azuma, H. Yagita, K. Okumura, P.S. Linsley, S. Ikebara, et al. 1994. The tissue distribution of the B7-2 costimulator in mice: Abundant expression on dendritic cells in situ and during maturation in vitro. *J. Exp. Med.* 180:1849–1860.
 16. Linsley, P.S., W. Brady, M. Urnes, L.S. Grosmaire, N.K. Damle, and J.A. Ledbetter. 1991. CTLA-4 is a second receptor for the B cell activation antigen B7. *J. Exp. Med.* 174:561–569.
 17. Freeman, G.J., F. Borriello, R.J. Hodes, H. Reiser, K.S. Hathcock, G. Laszlo, A.J. McKnight, J. Kim, L. Ku, D.B. Lombard, et al. 1993. Uncovering of functional alternative CTLA-4 counter-receptor in B7-deficient mice. *Science (Wash. DC)*. 262:907–909.
 18. Lenschow, D.J., G.H.-T. Su, L.A. Zuckerman, N. Nabavi, C.L. Jellis, G.S. Gray, J. Miller, and J.A. Bluestone. 1993. Expression and functional significance of an additional ligand for CTLA-4. *Proc. Natl. Acad. Sci. USA*. 90:11054–11058.
 19. Linsley, P.S., P.M. Wallace, J. Johnson, M.G. Gibson, J.L. Greene, J.A. Ledbetter, C. Singh, and M.A. Tepper. 1992. Immunosuppression in vivo by a soluble form of the CTLA-4 T cell activation molecule. *Science (Wash. DC)*. 257:792–795.
 20. Lenschow, D.J., Y. Zeng, J.R. Thistlewaite, A. Montag, W. Brady, M.G. Gibson, P.S. Linsley, and J.A. Bluestone. 1992. Long-term survival of xenogeneic pancreatic islet grafts induced by CTLA4Ig. *Science (Wash. DC)*. 257:789–792.
 21. Brunet, J.F., F. Denizot, M.F. Luciani, M. Roux-Dosseto, M. Suzan, M.F. Mattei, and P. Golstein. 1987. A new member of the immunoglobulin superfamily CTLA-4. *Nature (Lond.)*. 328:267–270.
 22. Harper, K., C. Balzano, E. Rouvier, M.G. Mattei, M.F. Luciani, and P. Golstein. 1991. CTLA-4 and CD28 activated lymphocyte molecules are closely related in both mouse and human as to sequence, message expression, gene structure, and chromosomal location. *J. Immunol.* 147:1037–1044.
 23. Lindsten, T., K.P. Lee, E.S. Harris, B. Petryniak, N. Craighead, P.J. Reynolds, D.B. Lombard, G.J. Freeman, L.M. Nadler, G.S. Gray, et al. 1993. Characterization of CTLA-4 structure and expression on human T cells. *J. Immunol.* 151:3489–3499.
 24. Linsley, P.S., J.L. Greene, P. Tan, J. Bradshaw, J.A. Ledbetter, C. Anasetti, and N.K. Damle. 1992. Coexpression and functional cooperativity of CTLA-4 and CD28 on activated T lymphocytes. *J. Exp. Med.* 176:1595–1604.
 25. Damle, N.K., K. Klussman, G. Leytze, S. Myrdal, A. Aruffo, J.A. Ledbetter, and P.S. Linsley. 1994. Costimulation of T lymphocytes with integrin ligands intercellular adhesion molecule-1 or vascular cell adhesion molecule-1 induces functional expression of CTLA-4, a second receptor for B7. *J. Immunol.* 152:2686–2697.
 26. Walunas, T.L., D.J. Lenschow, C.Y. Bakker, P.S. Linsley, G.J. Freeman, J.M. Green, C.B. Thompson, and J.A. Bluestone. 1994. CTLA-4 can function as a negative regulator of T cell activation. *Immunity*. 1:405–413.
 27. Lane, P., W. Gerhard, S. Hubele, A. Lanzavecchia, and F. McConnell. 1993. Expression and functional properties of mouse BB1/B7 using a fusion protein between mouse CTLA-4 and human g1. *Immunology*. 80:56–61.
 28. McKearn, T.J., F.W. Fitch, D.E. Smilie, M. Sarmiento, and F.P. Stuart. 1979. Properties of rat anti-MHC antibodies produced by cloned rat-mouse hybridomas. *Immunol. Rev.* 47:91–98.
 29. Jitsukawa, T., S. Nakajima, I. Sugawara, and H. Watanabe. 1989. Increased coating efficiency of antigens and preservation of original antigenic structures after coating in ELISA. *J. Immunol. Methods*. 116:251–256.
 30. Allison, J.P., W.L. Havran, M. Poenie, J. Kimura, L. Degraffenreid, S. Ajami, G. Duwe, A. Weiss, and R. Tsien. 1987. Expression and function of CD3 on murine thymocytes. In *The T Cell Receptor, UCLA Symposia on Molecular and Cellular Biology, New Series*. J. Kappler, and M. Davis, editors. Alan R. Liss, Inc., New York. pp. 33–45.
 31. Gross, J.A., E. Callas, and J.P. Allison. 1992. Identification and distribution of the costimulatory receptor CD28 in the mouse. *J. Immunol.* 149:380–388.
 32. Havran, W.L., S.C. Grell, G. Duwe, J. Kimura, A. Wilson, A.M. Kruisbeek, R.L. O'Brien, W. Born, R.E. Tigelaar, and J.P. Allison. 1989. Limited diversity of TCR g chain expression of murine Thy-1⁺ dendritic epidermal cells revealed by Vg3-specific monoclonal antibody. *Proc. Natl. Acad. Sci. USA*. 86:4185–4189.

33. Ozato, K., and D.H. Sachs. 1981. Monoclonal antibodies to mouse MHC antigens. *J. Immunol.* 126:317-323.
34. Symington, F., and J. Sprent. 1981. A monoclonal antibody detecting an Ia specificity mapping in the I-A or I-E subregion. *Immunogenetics.* 14:53-61.
35. Mishell, B., and S. Shiigi. 1980. Selected Methods in Cellular Immunology. W.H. Freeman Co., San Francisco. pp. 23-24.
36. Mescher, M.F. 1992. Surface contact requirements for activation of cytotoxic T lymphocytes. *J. Immunol.* 149:2402-2405.
37. Green, J.M., P.J. Noel, A.I. Sperling, T.L. Walunas, G.S. Gray, J.A. Bluestone, and C.B. Thompson. 1994. Absence of B7-dependent responses in CD28-deficient mice. *Immunity.* 1:501-508.
38. Lu, Y., A. Granelli-Piperno, J.M. Bjorndahl, C.A. Phillips, and J.M. Trevillyan. 1992. CD28-induced T cell activation. Evidence for a protein-tyrosine kinase signal transduction pathway. *J. Immunol.* 149:24-29.
39. August, A., S. Gibson, Y. Kawakami, G.B. Mills, and B. Dupont. 1994. CD28 is associated with and induces the immediate tyrosine phosphorylation and activation of the Tec family kinase ITK/EMT in the human Jurkat leukemic T-cell line. *Proc. Natl. Acad. Sci. USA.* 91:9347-9351.
40. Ward, S.G., J. Westwick, N.D. Hall, and D.M. Sansom. 1993. Ligation of CD28 receptor by B7 induces formation of D-3 phosphotides in T lymphocytes independently of T cell receptor activation. *Eur. J. Immunol.* 23:2572-2577.
41. Songyang, Z., S.E. Shoelson, J. McGlade, P. Olivier, T. Pawson, X.R. Bustelo, M. Barbacid, H. Sabe, H. Hanafusa, T. Yi, et al. 1994. Specific motifs recognized by the SH2 domains of Csk, 3BP2, fps/fes, GRB-2, HCP, SHC, Syk, Vav. *Mol. Cell. Biol.* 14:2777-2785.
42. Songyang, Z., S.E. Shoelson, M. Chaudhuri, G. Gish, T. Pawson, W.G. Haser, F. King, T. Roberts, S. Ratnofsky, R.J. Lechleider, et al. 1993. SH2 domains recognize specific phosphopeptide sequences. *Cell.* 72:767-778.
43. August, A., and B. Dupont. 1993. CD28 of T lymphocytes associates with phosphatidylinositol 3-kinase. *Int. Immunol.* 6:769-774.
44. Prasad, K.V., Y.C. Cai, M. Raab, B. Duckworth, L. Cantley, S.E. Shoelson, and C.E. Rudd. 1994. T-cell antigen CD28 interacts with the lipid kinase phosphatidylinositol 3-kinase by a cytoplasmic Tyr(P)-Met-Xaa-Met motif. *Proc. Natl. Acad. Sci. USA.* 91:2834-2838.
45. Truitt, K.E., C.M. Hicks, and J.B. Imboden. 1994. Stimulation of CD28 triggers an association between CD28 and phosphatidylinositol 3'-kinase in Jurkat T cells. *J. Exp. Med.* 179:1071-1076.
46. Stein, P.H., J.D. Fraser, and A. Weiss. 1994. The cytoplasmic domain of CD28 is both necessary and sufficient for costimulation of interleukin-2 secretion and association with phosphatidylinositol 3'-kinase. *Mol. Cell. Biol.* 14:3392-3402.
47. Pages, F., M. Ragueneau, R. Rottapel, A. Truneh, J. Nunes, J. Imbert, and D. Olive. 1994. Binding of phosphatidyl-inositol-3-OH kinase to CD28 is required for T-cell signalling. *Nature (Lond.).* 369:327-329.
48. Schneider, H., V.S. Prasad, S.E. Shoelson, and C.E. Rudd. 1995. CTLA-4 binding to the lipid kinase phosphatidylinositol 3-kinase in T cells. *J. Exp. Med.* 181:351-355.
49. Su, B., E. Jacinto, M. Hibi, T. Kallunki, M. Karin, and Y. Ben-Neriah. 1994. JNK is involved in signal integration during costimulation of T lymphocytes. *Cell.* 77:727-736.
50. Lindsten, T., C.H. June, J.A. Ledbetter, G. Stella, and C.B. Thompson. 1989. Regulation of lymphokine messenger RNA stability by a surface-mediated T cell activation pathway. *Science (Wash. DC).* 244:339-343.

Immune Checkpoint Targeting in Cancer Therapy: Toward Combination Strategies with Curative Potential

Padmanee Sharma^{1,2,*} and James P. Allison^{1,*}

¹Department of Immunology

²Department of Genitourinary Medical Oncology

MD Anderson Cancer Center, Houston, TX 77030, USA

*Correspondence: padsharma@mdanderson.org (P.S.), jallison@mdanderson.org (J.P.A.)

<http://dx.doi.org/10.1016/j.cell.2015.03.030>

Research in two fronts has enabled the development of therapies that provide significant benefit to cancer patients. One area stems from a detailed knowledge of mutations that activate or inactivate signaling pathways that drive cancer development. This work triggered the development of targeted therapies that lead to clinical responses in the majority of patients bearing the targeted mutation, although responses are often of limited duration. In the second front are the advances in molecular immunology that unveiled the complexity of the mechanisms regulating cellular immune responses. These developments led to the successful targeting of immune checkpoints to unleash anti-tumor T cell responses, resulting in durable long-lasting responses but only in a fraction of patients. In this Review, we discuss the evolution of research in these two areas and propose that intercrossing them and increasing funding to guide research of combination of agents represent a path forward for the development of curative therapies for the majority of cancer patients.

Introduction

The scientific community united against a common enemy in 1971 when President Nixon signed a bill initiating the “War on Cancer,” which provided funding for scientific research focused on improving our understanding and treatment of cancer. Without doubt, the intervening years were followed by great advances in the elucidation of the molecular mechanisms that regulate growth and death of normal cells, including a deep understanding of how these pathways progressively go awry during the development of cancer. This understanding led to the era of genomically targeted therapies and “precision medicine” in the treatment of cancer. Genomically targeted therapies can result in remarkable clinical responses. The ability of cancer cells to adapt to these agents by virtue of their genomic instability and other resistance mechanisms eventually leads to disease progression in the majority of patients nonetheless. Unraveling the mechanisms by which cancer cells become resistant to drugs and developing new agents to target the relevant pathways have become logical next steps in this approach for cancer treatment. However, given the genetic and epigenetic instability of cancer cells, it is likely that each new drug or combination of drugs targeting the tumor cells will meet with more complex mechanisms of acquired resistance. Recent findings suggest that T cells, bearing antigen receptors that are generated by random rearrangement of gene segments, followed by selective processes that result in a vast repertoire of T cell clones, provide sufficient diversity and adaptability to match the complexity of tumors. Discoveries regarding regulation of T cell responses have provided key principles regarding immune

checkpoints that are being translated into clinical success, with durable responses and long-term survival greater than 10 years in a subset of patients with metastatic melanoma, as well as yielding promising results in several other tumor types. Now, with the perspective of combining genomically targeted agents and immune checkpoint therapies, we are finally poised to deliver curative therapies to cancer patients. To support this goal and accelerate these efforts, changes in directions of research support and funding may be required.

Precision Medicine: Targeting the Drivers

In the past three decades, enormous strides have been made in elucidating the molecular mechanisms involved in the development of cancer (Hanahan and Weinberg, 2011). It is now clear that the oncogenic process involves somatic mutations that result in activation of genes that are normally involved in regulation of cell division and programmed cell death, as well as inactivation of genes involved in protection against DNA damage or driving apoptosis (Bishop, 1991; Solomon et al., 1991; Weinberg, 1991; Knudson, 2001). These genetic links led to the decision early in the war on cancer to undertake sequencing of cancer genomes to provide a comprehensive view of somatic mutational landscapes in cancer and identify possible therapeutic targets. Infrastructure and funding were provided to coordinate the sequencing efforts. It has become apparent that the level of somatic mutations differs widely between and within different tumor types ranging from very low rates in childhood leukemias to very high rates in tumors associated with carcinogens (Alexandrov et al., 2013).

Mutations can be divided into two broad classes: those whose products “drive” tumorigenesis in a dominant fashion and “passengers” with no obvious role in the tumor causation. The Cancer Genome Atlas (TCGA) projects have enabled identification of many of these mutations (Chen et al., 2014; Cancer Genome Atlas Research Network, 2014). This has allowed for the rational design of drugs that target and selectively interfere with oncogenic signaling pathways. This approach has revolutionized cancer medicine by moving away from the “one size fits all” approach—for instance, traditional chemotherapy, which attacks all dividing cells, including both cancer-differentiating or regenerating normal cells—to a more personalized strategy of treating patients with a specific drug only if their cancer bears particular molecular mutations that are target of that drug.

As an example of genomically targeted therapies, an inhibitor against BRAF was developed when it was discovered that ~40%–60% of cutaneous melanomas carry mutations in BRAF, which induces constitutive activation of the MAPK pathway (Curtin et al., 2005; Davies et al., 2002). In a randomized phase III trial comparing a BRAF inhibitor (vemurafenib) versus dacarbazine, the vemurafenib treatment group had a response rate of ~48% versus 5% in the dacarbazine arm (Chapman et al., 2011). However, the median duration of response was short, only 6.7 months (Sosman et al., 2012). Another oncogenic pathway that has been targeted is the tyrosine kinase chromosomal rearrangement, which results in the fusion oncogene EML4-ALK that is found in ~5% of NSCLC patients (Soda et al., 2007). The EML4 fusion partner mediates ligand-independent oligomerization and/or dimerization of anaplastic lymphoma kinase (ALK), resulting in constitutive kinase activity. Standard chemotherapies in this subgroup of patients have been associated with response rates of up to 10% (Hanna et al., 2004). Crizotinib, a tyrosine kinase inhibitor targeting ALK (Kwak et al., 2010), was shown to elicit a response rate of ~65% with a median duration of response of less than 8 months in a phase III trial (Shaw et al., 2013). Although there was a significant increase in progression-free survival for patients treated with crizotinib, regrettably, there was no overall survival benefit in the interim analysis. Therefore, although the concept of targeting “driver mutations” has great merit and has demonstrated clinical responses, the reality remains that the majority of patients treated with these agents will derive short-term clinical responses with eventual development of resistance mechanisms that lead to disease progression and death.

Mechanisms operative in acquired resistance fall into three main categories: alterations in the targeted gene (as a result of mutation, amplification, or alternative splicing); other changes that do not affect the original target but re-activate the signaling pathway involved (i.e., NRAS and MEK mutations in BRAF mutant melanoma); and changes that activate alternate pathways (such as activation of growth factor receptors). Considerable effort has gone into finding ways to enhance efficacy of genomically targeted therapies. One effort involves multiple agents that target different molecules in the same pathway, such as the combination of a BRAF inhibitor and a MEK-inhibitor (Larkin et al., 2014; Robert et al., 2015a). This approach helps to reduce compensatory feedback loops, as well as to block the development of resistance due to mutations downstream that

pathway. A different strategy consists of blocking parallel pathways to prevent emerging resistance (Martz et al., 2014). Still, the chief challenge of these combinatorial approaches is the multiplicity of resistance mechanisms and the fact that different mechanisms may be in operation in different cells due to intratumor heterogeneity. Given these observations, it is difficult to envision realistic approaches to effectively overcome the myriad of resistance mechanisms that may arise in the course of cancer treatment. The continued evolvability of the tumor cells and their mechanisms of escape from targeted therapies raise the question as to whether combinations of genomically targeted agents will ever be curative.

Advantages of Mobilizing T Cells for Cancer Therapy

As the knowledge of the intricate biology of cancer has progressed, so has the understanding of the fundamental cellular and molecular mechanisms that orchestrate the interplay of the innate and adaptive arms of the immune system. In a simplistic way, the innate system is composed primarily of cytokines, the complement system, and phagocytes such as macrophages, neutrophils, dendritic cells, and natural killer (NK) cells. Cells of the innate immune system have hard-wired receptors to detect products of infectious microorganisms and dying cells. Macrophages and neutrophils provide an early defense against microorganisms, whereas dendritic cells provide a key interface to the adaptive immune system, composed of B and T cells with their somatically generated, clonally expressed repertoire of antigen receptors.

The understanding of the basic principles governing the controlling immunity provided the rational for the development of powerful strategies to actively engage the immune system for cancer therapy. Strategies to unleash T cells against tumors are particularly compelling, as the activity of these cells presents important features that are advantageous over other cancer therapies. The first is their specificity. T cells express antigen receptors that recognize cell-surface complexes of MHC molecules and peptides sampled from virtually all the proteins in the cell and are not limited to peptide antigens derived from cell-surface molecules. The second feature is memory. Primary T cell responses are generally followed by the production of long-lived memory T cells with accelerated kinetics of secondary response if the antigen recurs. Finally, the T cell response is adaptable and can accommodate not only tumor heterogeneity but also responses to novel antigens expressed by recurring tumors. It has been calculated that the somatic recombination process that generates the antigen receptors of T cells can generate as many as 10^{15} different receptors (Davis and Bjorkman, 1988). Of this theoretical number, each individual human has perhaps 10^9 different receptors. The immense size of the repertoire suggests that the immune system is indeed well equipped to deal with mutability and adaptability of cancer.

Harnessing T Cell Responses to Tumor Antigens

With the advent of genomic and cDNA expression cloning methods and sequencing of peptides eluted from tumor cell MHC molecules, an avalanche of tumor antigens defined by tumor-specific T cells has been identified in both mice and in humans. Most of these are shared between cancer cells of different

individuals and fall into four groups: products of oncogenic viruses (Epstein-Barr virus in certain leukemias and human papilloma virus in cervical and some head and neck cancers); antigens related to tissue-specific differentiation molecules (tyrosinase and related proteins in melanoma and prostate-specific antigen and prostatic acid phosphatase in prostate cancer); molecules normally expressed only during fetal development (carcino-embryonic antigen in colon cancer, α -fetoprotein in liver cancer); and cancer-testes (CT) antigens, which are normally expressed during gametogenesis but are found in many cancer cells as a result of changes in epigenetic regulation (MAGE and NY-ESO-1).

Additionally, somatic mutations also can result in the generation of tumor-specific peptides with the potential to bind major histocompatibility complex (MHC) molecules and therefore be recognized by the immune system as neoantigens (Sjöblom et al., 2006; Segal et al., 2008). The analysis of the epitope landscape of breast and colon carcinoma cells revealed that the products of seven to ten mutant genes in colorectal and breast cancer, respectively, have the potential for binding to HLA-A*0201 alone. Because each heterozygote individual carries as many as 6 different HLA class I genes, this means an average of 42–60 potential neoantigens that can be presented to T cells. In support of these estimates, recent studies have demonstrated that neoantigens generated by somatic mutation are recognized by T cells in both mouse and human cancers (Linemann et al., 2015; Gros et al., 2014; Tran et al., 2014; Gubin et al., 2014).

At first, as a result of earlier studies identifying shared antigens, the field of cancer immunotherapy became focused on developing therapeutic vaccines to expand T cells against these shared antigens expressed on tumors. Many studies focused on stimulating T cell responses with peptides, proteins, whole-tumor cells including those modified to express cytokines, DNA, recombinant viral-based vaccines, or antigen-pulsed dendritic cells given alone or in combination with various adjuvants or cytokines. Although these trials were conducted with the best available science at the time and provided promising anecdotal evidence that induction of immune responses could elicit clinical benefit, they remained largely negative and generally failed to show objective clinical responses (see Rosenberg et al., 2004 for review). Enthusiasm waned somewhat as the number of failed clinical trials mounted.

Many reasons might have contributed to the failure of these vaccination strategies, including choice of antigen, failure to provide adequate costimulation, or functional inactivation of tumor-reactive T cells (Melero et al., 2014). A number of T-cell-extrinsic suppressive mechanisms such as TGF β , FoxP3 $^{+}$ regulatory T cells (Treg), and tryptophan metabolites (IDO) that can hamper anti-tumor responses have also been identified, and there have been efforts to minimize the suppressive effects of these in pre-clinical and clinical studies.

Unraveling the Complexity of T Cell Activation

Another contributing factor to the failure of earlier cancer vaccine trials was perhaps the lack of understanding and appreciation of the full complexity of cell-intrinsic pathways that regulate T cell activation. By the late 1980s, it was known that simple engage-

ment of peptide/MHC complexes by the antigen receptor is insufficient for activation of T cells and may render them anergic (Jenkins and Schwartz, 1987; Mueller et al., 1989). In order to become fully activated, T cells must encounter antigen in the context of antigen-presenting cells (APCs) such as dendritic cells, which provide costimulatory signals mediated by B7 molecules (B7-1 and B7-2) that will engage their ligand, CD28, in the T cell (Greenwald et al., 2005). Thus, T cells specific for a tumor antigen will not be activated by an initial encounter with tumor cells or may even be rendered anergic because, with the exception of a few lymphomas, tumors do not express costimulatory B7 molecules (Townsend and Allison, 1993). Thus, tumors are essentially invisible to T cells until the T cells are activated as a result of cross-priming by dendritic cells that present tumor antigens acquired from dying tumor cells. Simultaneous recognition of antigen/MHC complexes and costimulatory ligands by T cells initiates a complex set of genetic programs that result in cytokine production, cell-cycle progression, and production of anti-apoptotic factors that result in proliferation and functional differentiation of T cells. Consistent with the importance of both antigen receptor and costimulatory signals in initiating anti-tumor responses, many therapeutic vaccines now incorporate both antigen and dendritic cells or agents that enhance costimulatory signaling.

By the mid-90s, it became clear that T cell priming elicits not only programs leading to induction of T cell responses but also a parallel program that will eventually stop the response. The critical inhibitory program is mediated by CTLA-4, a homolog of CD28 that also binds B7-1 and B7-2, although with much greater avidity than that CD28. Expression of the *ctla-4* gene is initiated upon T cell activation, and it traffics to and accumulates in the immunological synapse, eventually attenuating or preventing CD28 costimulation by competition for B7 binding and negative signaling (Walunas et al., 1994; Krummel and Allison, 1995). The fact that *ctla-4* knockout mice suffer from a rapid and lethal lymphadenopathy (Waterhouse et al., 1995; Tivol et al., 1995; Chambers et al., 1997) speaks for a negative role for CTLA-4 in limiting T cell responses to prevent damage to normal tissues.

Thus, activation of T cells as a result of antigen receptor signaling and CD28 costimulation is followed not only by induction of genetic programs leading to proliferation and functional differentiation but also by induction of an inhibitory program mediated by CTLA-4, which will ultimately stop proliferation. Extrapolating this paradigm to anti-tumor T cell responses, if eradication of the tumor has not been completed by the time that the inhibitory signal of CTLA-4 is triggered, the T cells will be turned off and will be unable to complete the task. Importantly, this also suggests that, after this program is initiated, vaccines used to stimulate antigen receptor signaling may actually serve to strengthen the “off” signal as a result of additional induction of *ctla-4* expression by antigen receptor signaling. In any event, this suggests the importance of shifting strategies for cancer immunotherapy from activating T cells to unleashing them.

Inactivating the Brakes to Increase Anti-tumor Immunity

Consistent with the observations that CD28 and CTLA-4 had opposing effects on T cell responses in vitro, in the late 90s, it

was found that, although blocking antibodies to CD28 impaired anti-tumor responses in mice, blocking antibodies to CTLA-4 enhanced anti-tumor responses in mouse tumor models (Leach et al., 1996). In fact, the treatment of mice with anti-CTLA-4 antibodies as monotherapy results in complete tumor rejection and long-lived immunity. Later on, mechanistic studies revealed that anti-tumor activity was associated with increased ratio of both CD4 and CD8 effector cells to FoxP3⁺ regulatory T cells (Quenzada et al., 2006). The success of CTLA-4 blockade in these initial studies raised two compelling points. First, because the target molecule was on the T cell and not the tumor cell, it was feasible to imagine that the same strategy would work on many different histologic tumors, as well as on tumors caused by different genetic lesions. Second, taking into consideration that CTLA-4 inhibited CD28-mediated costimulation by a cell-intrinsic mechanism (Peggs et al., 2009), its blockade could allow for enhanced T cell costimulation, which in turn would increase the efficacy of tumor vaccines, as well as agents that kill tumor cells under conditions that promote inflammatory responses. These possibilities were further supported by the results of a series of studies in different mouse models, including the demonstration that blockade of CTLA-4 was not limited to any particular tumor type but was rather broadly effective. CTLA-4 also was able to synergize with a vaccine consisting of tumor cells engineered to express the cytokine GM-CSF to eradicate tumors (Hurwitz et al., 1998; van Elsas et al., 1999). Finally, CTLA-4 could be combined with local delivery of irradiation, cryoablation, or an oncolytic virus to induce systemic tumor immunity and eradication of distant metastases (Zamarin et al., 2014; Waitz et al., 2012; Tang et al., 2014). These preclinical studies supported the development of clinical anti-CTLA-4 therapy.

Immune Checkpoint Therapy: The Clinical Success

CTLA-4 blockade was translated to the clinic with a fully human antibody to human CTLA-4 (ipilimumab, Medarex, Bristol-Myers Squibb). Tumor regression was observed in phase I/II trials in patients with a variety of tumor types, including melanoma, renal cell carcinoma, prostate cancer, urothelial carcinoma, and ovarian cancer (Yang et al., 2007; Hodi et al., 2008; Carthon et al., 2010; van den Eertwegh et al., 2012). Two phase III clinical trials with ipilimumab were recently completed in prostate cancer, the first in patients with castrate-resistant prostate cancer who had not received prior chemotherapy treatment and the second in a more advanced disease setting, in which patients with castrate-resistant prostate cancer presented disease that had progressed on chemotherapy treatment. The former trial is yet to be reported. The latter trial reports the lack of statistical significance (*p* value of 0.053) to indicate a survival benefit for patients who received ipilimumab treatment. However, subset analyses indicate that patients who have favorable clinical characteristics such as lack of liver metastases do benefit from ipilimumab therapy (Kwon et al., 2014). Two phase III clinical trials with anti-CTLA-4 (ipilimumab) were also conducted in patients with advanced melanoma and demonstrated improved overall survival for patients treated with ipilimumab (Hodi et al., 2010; Robert et al., 2011). Importantly, these trials indicate long-term durable responses with greater than 20% of treated patients

living for more than 4 years, including a recent analysis indicating survival of 10 years or more for a subset of patients (Schadendorf et al., 2015). The FDA approved ipilimumab as treatment for patients with melanoma in 2011.

The clinical success of anti-CTLA-4 opened a new field termed “immune checkpoint therapy” as additional T cell intrinsic pathways were identified and targeted for clinical development (Sharma et al., 2011; Pardoll, 2012). Another T-cell-intrinsic inhibitory pathway identified after CTLA-4 was that mediated by PD-1 (programmed death 1) and its ligand PD-L1. PD-1 was initially cloned in 1992 in a study of molecules involved in negative selection of T cells by programmed cell death in the thymus (Ishida et al., 1992). Its function as an immune checkpoint was not established until 2000 upon identification of its ligands (Freeman et al., 2000). PD-L1 was then shown to protect tumor cells by inducing T cell apoptosis (Dong et al., 2002). Later, preclinical studies in animal models evaluated anti-PD-1 and anti-PD-L1 antibodies as immune checkpoint therapies to treat tumors (Keir et al., 2008).

Much like CTLA-4, PD-1 is expressed only in activated T cells. However, unlike CTLA-4, PD-1 inhibits T cell responses by interfering with T cell receptor signaling as opposed to outcompeting CD28 for binding to B7. PD-1 also has two ligands, PD-L1 and PD-L2. PD-L2 is predominantly expressed on APCs, whereas PD-L1 can be expressed on many cell types, including cells comprising the immune system, epithelial cells, and endothelial cells. Antibodies targeting PD-L1 have shown clinical responses in multiple tumor types, including melanoma, renal cell carcinoma, non-small-cell lung cancer (Brahmer et al., 2012), and bladder cancer (Powles et al., 2014). Similarly, phase I clinical trials with a monoclonal antibody against PD-1 demonstrated clinical responses in multiple tumor types, including melanoma, renal cell carcinoma, non-small-cell carcinoma (Topalian et al., 2012), Hodgkin’s lymphoma (Ansell et al., 2015), and head and neck cancers (Seiwert et al., 2014, J. Clin. Oncol., abstract). Recently, a large phase I clinical trial with an anti-PD-1 antibody known as MK-3475 showed response rates of ~37%–38% in patients with advanced melanoma, including patients who had progressive disease after prior ipilimumab treatment (Hamid et al., 2013), triggering the approval of MK-3475 (pembrolizumab, Merck) by the FDA in September 2014. A phase III clinical trial that treated patients with metastatic melanoma with a different anti-PD-1 antibody (nivolumab, Bristol-Myers Squibb, BMS) also demonstrated improved responses and overall survival benefit as compared to chemotherapy treatment (Robert et al., 2015b). Nivolumab was FDA approved for patients with metastatic melanoma in December 2014. In addition, nivolumab was FDA approved in March 2015 for patients with previously treated advanced or metastatic non-small-cell lung cancer based on a phase III clinical trial, which reported an improvement in overall survival for patients treated with nivolumab as compared to patients treated with docetaxel chemotherapy.

Because CTLA-4 and PD-1 regulate different inhibitory pathways on T cells, combination therapy with antibodies targeting both molecules was tested and found to improve anti-tumor responses in a pre-clinical murine model (Curran et al., 2010). A recently reported phase I clinical trial with anti-CTLA-4 in combination with anti-PD-1 also demonstrated tumor regression

in ~50% of treated patients with advanced melanoma, in most cases with tumor regression of 80% or higher (Wolchok et al., 2013). There are ongoing clinical trials with anti-CTLA-4 (ipilimumab, BMS or tremelimumab, MedImmune/AstraZeneca) plus anti-PD-1 or anti-PD-L1 in other tumor types, with preliminary data indicating promising results (Hammers et al., 2014, J. Clin. Oncol., abstract; Callahan et al., 2014, J. Clin. Oncol., abstract) that highlight this combination as an effective immunotherapy strategy for cancer patients.

As with other cancer therapies, immune checkpoint therapies may lead to side effects and toxicities (see Postow et al., 2015; Gao et al., 2015 for recent reviews). Briefly, these side effects consist of immune-related adverse events that are defined by inflammatory conditions, including dermatitis, colitis, hepatitis, pancreatitis, pneumonitis, and hypophysitis. These side effects can be managed and usually involve administration of immuno-suppressive agents such as corticosteroids, which do not appear to interfere with clinical benefit that is derived from the immune checkpoint agents. The profile of side effects that occur with both anti-CTLA-4 and anti-PD-1/PD-L1 antibodies is similar; however, the side effects appear to occur more frequently in the setting of anti-CTLA-4 therapy as compared to anti-PD-1 and anti-PD-L1 therapies. The continued success of immune checkpoint therapies in the clinic will require education of the oncology community regarding recognition and treatment of the side effects elicited by these agents.

Novel Immunologic Targets for Cancer Immunotherapy

Although blockade of the CTLA-4 and PD-1/PD-L1 pathways is furthest along in clinical development, it only represents the tip of the iceberg in the realm of potential targets that can serve to improve anti-tumor responses. Ongoing studies on regulation of immune responses have led to the identification of multiple other immunologic pathways that may be targeted for the development of therapies, either as monotherapy or in combination strategies, for the successful treatment of cancer patients. These include immune checkpoints or inhibitory pathways, as well as co-stimulatory molecules, which act to enhance immune responses. A partial list of new immune checkpoints that are being evaluated in pre-clinical tumor models and/or in the clinic with cancer patients includes LAG-3 (Triebel et al., 1990), TIM-3 (Sakuishi et al., 2010), and VISTA (Wang et al., 2011), whereas co-stimulatory molecules include ICOS (Fan et al., 2014), OX40 (Curti et al., 2013), and 4-1BB (Melero et al., 1997).

Of these emerging immune checkpoints, LAG-3 is the furthest along in clinical development with a fusion protein (IMP321, Immunetep) and an antibody (BMS-986016, BMS) in clinical trials. The fusion protein was tested as monotherapy in patients with renal cell carcinoma, which was well tolerated and led to stabilization of disease in some patients (Brignone et al., 2009). IMP321 was also tested in combination with paclitaxel chemotherapy in patients with metastatic breast cancer, which led to an objective response rate of 50% (Brignone et al., 2010). Based on these promising results, a phase III clinical trial is expected to begin accrual in 2015. Other clinical trials are ongoing with an antibody against LAG-3 (BMS-986016), which is also being tested in combination with anti-PD-1 (nivolumab) (NCT01968109, <http://www.clinicaltrials.gov>). TIM-3 is another

immune checkpoint for which agents are being developed for clinical testing. Pre-clinical studies indicate that TIM-3 is co-expressed with PD-1 on tumor-infiltrating lymphocytes, and combination therapy targeting these two pathways improves anti-tumor immune responses (Sakuishi et al., 2010). Finally, an antibody targeting VISTA was recently shown to improve anti-tumor immune responses in mice (Le Mercier et al., 2014), with clinical development soon to follow. Again, these agents represent only a partial list of the immune checkpoint agents that are currently under development for clinical testing, with expectations that they will be tested in combination strategies based on in-depth analyses of human tumors to provide an understanding of co-expression of these, and other immunologic targets, to guide rational combinations.

Regarding the co-stimulatory molecules, OX40 and 41BB, which are members of the TNF-receptor superfamily, are furthest along in clinical development. A murine anti-OX40 antibody, given as a single dose, was tested in a phase I clinical trial and found to have an acceptable safety profile, as well as evidence of anti-tumor responses in a subset of patients (Curti et al., 2013). Humanized antibodies against OX40 are expected to enter clinical trial in 2015. Anti-41BB (BMS-663513) is a fully humanized monoclonal antibody that has been tested in a phase I/II study in patients with melanoma, renal cell carcinoma, and ovarian cancer, with promising clinical responses, as well as toxicities, especially at higher doses, which led to re-evaluation of the dose and schedule of treatment (Sznol et al., 2008, J. Clin. Oncol., abstract). Currently, there are five clinical trials with anti-41BB (urelumab, BMS-663513) that are recruiting patients with various tumor types (<http://www.clinicaltrials.gov>), including combination with anti-PD-1 (nivolumab), with data expected to be presented from these trials during the next 1 to 2 years. The third co-stimulatory molecule is inducible co-stimulator (ICOS), a member of the CD28/B7 family whose expression increases on T cells upon T cell activation. ICOS⁺ effector T cells (Teff), as opposed to ICOS⁺ regulatory T cells (Treg), increase after patients receive treatment with anti-CTLA-4 (Liakou et al., 2008), correlating with clinical benefit in a small retrospective study (Carthon et al., 2010). ICOS thus may serve as a pharmacodynamic biomarker to indicate that anti-CTLA-4 has "hit its target" enhancing T cell activation (Ng Tang et al., 2013). Also, the association of agonistic targeting of ICOS and blockade of CTLA-4 can lead to improved anti-tumor immune responses and tumor rejection in mice (Fan et al., 2014). Anti-ICOS antibodies are expected to enter into clinical trials in 2015. It is likely that combination therapy to simultaneously engage co-stimulatory pathways and limit inhibitory pathways will be a successful path forward to provide clinical benefit. Importantly, based on the profile of toxicities observed to date, it will be critical to closely monitor these combination strategies for potential adjustments of dosage and management of toxicities that may arise.

Reconciliation: Curative Therapeutic Combinations

The last few decades have witnessed the emergence of two effective but fundamentally different strategies for cancer therapy, each with its own strengths and weaknesses. Genomic-guided identification of mutations that drive cancer has led to

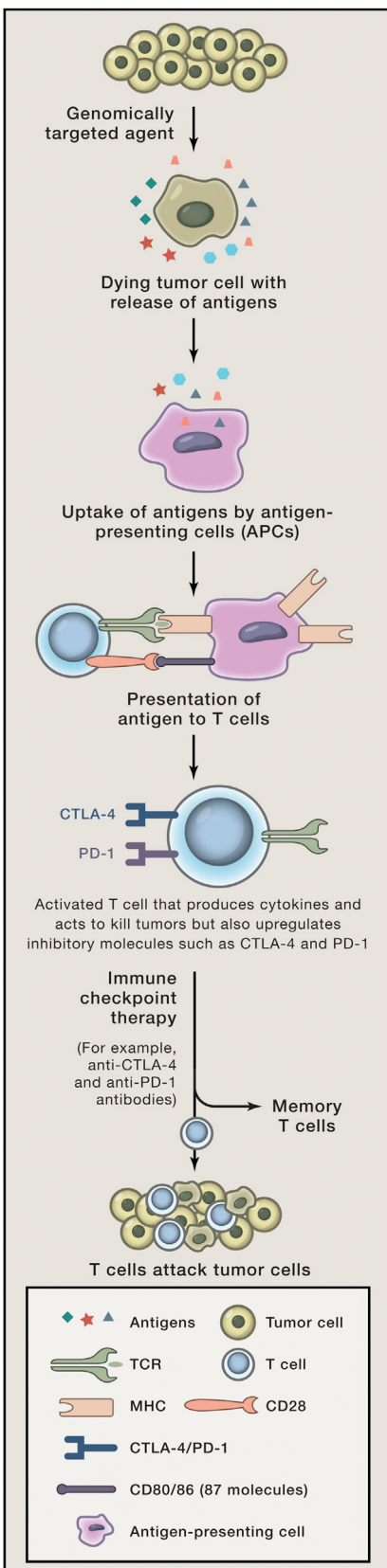


Figure 1. Combination Therapy May Improve Anti-tumor Responses

Depiction of tumor cells dying as a result of genomically targeted therapies with release of tumor antigens; tumor antigens are taken up by APCs and are presented in the context of B7 costimulatory molecules to T cells; T cells recognize antigens on APCs to become activated; activated T cells also upregulate inhibitory checkpoints such as CTLA-4 and PD-1; immune checkpoint therapy prevents attenuation of T cell responses, thereby allowing T cells to kill tumor cells; and T cells may differentiate into memory T cells that can reactivate in the presence of recurrent tumor.

the development of drugs that result in remarkable responses in the majority of patients whose tumors have the targeted lesion, but the responses are relatively short-lived. As was the case with chemotherapies, it is not unreasonable that combinations of genomically targeted agents will be more powerful against cancer than single agents. It is possible that the use of multiple agents may enhance their effectiveness in terms of increasing overall survival. However, the myriad of mechanisms of acquired resistance and the complexity of the target landscape due to inherent genomic instability may prove extremely difficult to overcome through the sole use of genomically targeted strategies, attaining to achieve cure. In contrast, immune checkpoint therapy is inherently multivalent because targeting a single checkpoint can potentially release T cells with specificity for peptides derived from many different antigens present in a tumor, including differentiation, cancer testis, and even neoantigens generated by mutational events inherent in the genomic instability that drives cancer (Snyder et al., 2014; Linnemann et al., 2015). As a result of the generation of improved anti-tumor T cell responses, immune checkpoint therapy results in durable responses but only in a fraction of patients. As discussed in the previous sections, it is certainly possible to target multiple immune checkpoints with different mechanisms for improved anti-tumor responses in greater numbers of patients. Will patients benefit from combination of these two strategies?

Efforts to combine molecularly targeted agents and immunotherapy have already begun. A phase I clinical trial with agents that inhibit receptor tyrosine kinases, sunitinib, or pazopanib, in combination with anti-PD-1, was recently reported and showed promising overall response rates of 40%–50% in patients with metastatic renal cell carcinoma (RCC) (Amin et al., 2014, *J. Clin. Oncol.*, abstract). These types of combinations will require further follow-up to evaluate for survival and durability of responses. An area that has not yet received enough attention is the immunological impact of genetically targeted agents. Vemurafenib, an FDA-approved BRAF inhibitor used for the treatment of melanoma, has been shown to increase expression of tumor antigens and MHC molecules (Frederick et al., 2013), increasing the sensitivity of the tumor cells to immune attack. Vemurafenib also has potent effects on T cells, enhancing the effects of antigen-mediated activation, perhaps as a result of enhanced activation of the MAP kinase pathway after T cell antigen receptor signaling (Atefi et al., 2014). These data suggest that certain agents may be well suited for combination with immunotherapy. However, a clinical trial testing a BRAF inhibitor (vemurafenib) in combination with anti-CTLA-4 (ipilimumab) was terminated due to hepatotoxicity (Ribas et al., 2013). A second clinical trial with a BRAF inhibitor (dabrafenib) in combination with anti-CTLA-4 (ipilimumab) is currently ongoing, and

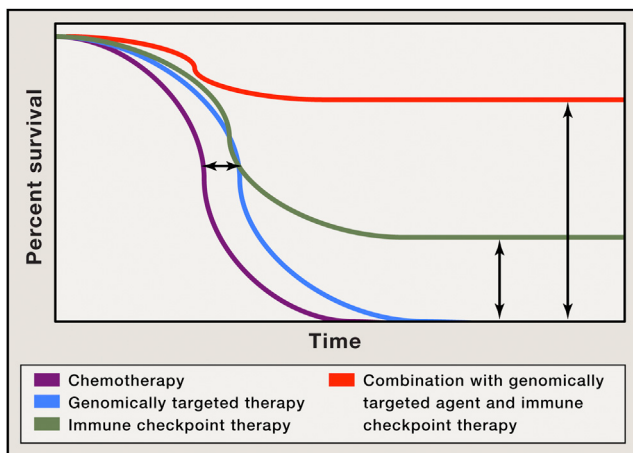


Figure 2. Improved Overall Survival as a Result of Combination Therapy

Depiction of Kaplan-Meier survival curve with genomically targeted agents (blue line) as compared to standard therapies (purple line), indicating an improvement in median overall survival but lack of durable responses; improved median overall survival and durable responses in a fraction of patients treated with immune checkpoint therapy (green line); possibility for improved median overall survival with durable responses for the majority of patients in the setting of combination treatment with genomically targeted agents and immune checkpoint therapy (red line).

preliminary data indicate that this combination appears to be well tolerated (Puzanov et al., 2014, *J. Clin. Oncol.*, abstract), which highlights the need to consider differences in drugs, dose, and/or schedule when evaluating agents for combination strategies. Understanding how different genetically targeted agents affect the responsiveness to immunotherapy may help guide choices of combinations of drugs.

From a mechanistic perspective, it is possible that combination strategies with immune checkpoint therapies and genomically targeted agents will result in induction of immune memory, leading to more durable control of tumor growth than what is achievable with either modality alone. Genomically targeted therapies with high objective response rates actually could serve as “cancer vaccines,” inducing the killing of tumor cells and resulting in the release of tumor antigens and neoantigens, which can then be presented by APCs to tumor-specific T cells (Figure 1). These T cells would become activated but also upregulate inhibitory checkpoints such as CTLA-4 and PD-1, which can be blocked with antibodies to permit enhanced anti-tumor T cell responses, including memory T cell responses, to enable long-term control of disease and possible cure. In addition, the use of targeted agents to directly kill tumor cells, with release of tumor antigens, may focus the activated immune response generated by immunotherapy agents on tumor antigens rather than self-antigens expressed on normal tissues, resulting in fewer adverse events. Furthermore, identification of neoantigens may result in the development of personalized vaccines composed of these neoantigens for novel vaccine strategies plus immune checkpoint agents (Gubin et al., 2014; Tran et al., 2014; Linnemann et al., 2015).

Although it is clear that clinical responses can be elicited with immune checkpoint therapies or genomically targeted agents, it

appears that genomically targeted agents alone tend to improve median survival without providing long-term durable responses (Figure 2, blue line). Targeting immune checkpoints improves median survival but remarkably also provides long-term durable responses, raising the tail of the survival curve (Figure 2, green line). When combined, these therapies are likely to have an additive or even synergistic therapeutic effect that not only would potentially further improve median survival but would also raise the tail of the survival curve, increasing the number of patients that appreciate long-term clinical benefit (Figure 2, red line).

A Future of Curative Cancer Therapies

Federal funding for research has been overwhelmingly directed toward genomically targeted therapies as compared to immune checkpoint therapies. The fundamental research that led to the identification of CTLA-4 as an immune checkpoint, as well as the pre-clinical studies showing the potential of its blockade in cancer therapy, were funded by the National Cancer Institute, but since then, there have been no major initiatives to accelerate progress in this area. Given the durability of the responses that have been obtained with immune checkpoint therapies, it seems reasonable also to allocate enough funds and resources to research focused on immune checkpoint therapies and combination therapy of genomically targeted agents and immunotherapy with promising curative potential. Efforts to determine the impact of genomically targeted therapies on the immune system should also be prioritized, as they will help to identify which agents can enhance anti-tumor T cell responses and guide the choice of combinations from the two classes of agents. At this stage, it does not seem a stretch to say that increasing funding to combination therapies will be key to development of new safe treatments that may prove to be curative for many patients with many types of cancer.

ACKNOWLEDGMENTS

P.S. and J.P.A. are founders and advisors for Jounce Therapeutics. P.S. also serves as a consultant for Bristol-Myers Squibb, Amgen, and Glaxo SmithKline. J.P.A. is an inventor of intellectual property owned by the University of California, Berkeley, and licensed to Bristol-Myers Squibb and has received royalties from Bristol-Myers Squibb. Our research is supported by a PCF Challenge Grant in Immunology (J.P.A. and P.S.), NCI/NIH 1-R01 CA1633793-01 (P.S.), Cancer Prevention Research in Texas grants (J.P.A. and P.S.), and a Stand Up To Cancer–Cancer Research Institute Cancer Immunology Dream Team Translational Cancer Research Grant (P.S. and J.P.A.). Stand Up To Cancer is a program of the Entertainment Industry Foundation administered by the American Association for Cancer Research.

REFERENCES

- Alexandrov, L.B., Nik-Zainal, S., Wedge, D.C., Aparicio, S.A., Behjati, S., Biankin, A.V., Bignell, G.R., Bolli, N., Borg, A., Børresen-Dale, A.L., et al.; Australian Pancreatic Cancer Genome Initiative; ICGC Breast Cancer Consortium; ICGC MMML-Seq Consortium; ICGC PedBrain (2013). Signatures of mutational processes in human cancer. *Nature* 500, 415–421.
- Ansell, S.M., Lesokhin, A.M., Borrello, I., Halwani, A., Scott, E.C., Gutierrez, M., Schuster, S.J., Millenson, M.M., Cattray, D., Freeman, G.J., et al. (2015). PD-1 blockade with nivolumab in relapsed or refractory Hodgkin’s lymphoma. *N. Engl. J. Med.* 372, 311–319.
- Atefi, M., Avramis, E., Lassen, A., Wong, D.J., Robert, L., Foulad, D., Cerniglia, M., Titz, B., Chodon, T., Graeber, T.G., et al. (2014). Effects of MAPK and PI3K

- pathways on PD-L1 expression in melanoma. *Clin. Cancer Res.* 20, 3446–3457.
- Bishop, J.M. (1991). Molecular themes in oncogenesis. *Cell* 64, 235–248.
- Brahmer, J.R., Tykodi, S.S., Chow, L.Q., Hwu, W.J., Topalian, S.L., Hwu, P., Drake, C.G., Camacho, L.H., Kauh, J., Odunsi, K., et al. (2012). Safety and activity of anti-PD-L1 antibody in patients with advanced cancer. *N. Engl. J. Med.* 366, 2455–2465.
- Brignone, C., Escudier, B., Grygar, C., Marcu, M., and Triebel, F. (2009). A phase I pharmacokinetic and biological correlative study of IMP321, a novel MHC class II agonist, in patients with advanced renal cell carcinoma. *Clin. Cancer Res.* 15, 6225–6231.
- Brignone, C., Gutierrez, M., Mefti, F., Brain, E., Jarcau, R., Cvitkovic, F., Bousetta, N., Medioni, J., Gligorov, J., Grygar, C., et al. (2010). First-line chemoimmunotherapy in metastatic breast carcinoma: combination of paclitaxel and IMP321 (LAG-3 Ig) enhances immune responses and antitumor activity. *J. Transl. Med.* 8, 71.
- Cancer Genome Atlas Research Network (2014). Comprehensive molecular characterization of gastric adenocarcinoma. *Nature* 513, 202–209.
- Carthon, B.C., Wolchok, J.D., Yuan, J., Kamat, A., Ng Tang, D.S., Sun, J., Ku, G., Troncoso, P., Logothetis, C.J., Allison, J.P., and Sharma, P. (2010). Preoperative CTLA-4 blockade: tolerability and immune monitoring in the setting of a presurgical clinical trial. *Clin. Cancer Res.* 16, 2861–2871.
- Chambers, C.A., Sullivan, T.J., and Allison, J.P. (1997). Lymphoproliferation in CTLA-4-deficient mice is mediated by costimulation-dependent activation of CD4+ T cells. *Immunity* 7, 885–895.
- Chapman, P.B., Hauschild, A., Robert, C., Haanen, J.B., Ascierto, P., Larkin, J., Dummer, R., Garbe, C., Testori, A., Maio, M., et al.; BRIM-3 Study Group (2011). Improved survival with vemurafenib in melanoma with BRAF V600E mutation. *N. Engl. J. Med.* 364, 2507–2516.
- Chen, Y., McGee, J., Chen, X., Doman, T.N., Gong, X., Zhang, Y., Hamm, N., Ma, X., Higgs, R.E., Bhagwat, S.V., et al. (2014). Identification of druggable cancer driver genes amplified across TCGA datasets. *PLoS ONE* 9, e98293.
- Curran, M.A., Montalvo, W., Yagita, H., and Allison, J.P. (2010). PD-1 and CTLA-4 combination blockade expands infiltrating T cells and reduces regulatory T and myeloid cells within B16 melanoma tumors. *Proc. Natl. Acad. Sci. USA* 107, 4275–4280.
- Curti, B.D., Kovacsics-Bankowski, M., Morris, N., Walker, E., Chisholm, L., Floyd, K., Walker, J., Gonzalez, I., Meeuwsen, T., Fox, B.A., et al. (2013). OX40 is a potent immune-stimulating target in late-stage cancer patients. *Cancer Res.* 73, 7189–7198.
- Curtin, J.A., Fridlyand, J., Kageshita, T., Patel, H.N., Busam, K.J., Kutzner, H., Cho, K.H., Aiba, S., Bröcker, E.B., LeBoit, P.E., et al. (2005). Distinct sets of genetic alterations in melanoma. *N. Engl. J. Med.* 353, 2135–2147.
- Davies, H., Bignell, G.R., Cox, C., Stephens, P., Edkins, S., Clegg, S., Teague, J., Woffendin, H., Garnett, M.J., Bottomley, W., et al. (2002). Mutations of the BRAF gene in human cancer. *Nature* 417, 949–954.
- Davis, M.M., and Bjorkman, P.J. (1988). T-cell antigen receptor genes and T-cell recognition. *Nature* 334, 395–402.
- Dong, H., Strome, S.E., Salomao, D.R., Tamura, H., Hirano, F., Flies, D.B., Roche, P.C., Lu, J., Zhu, G., Tamada, K., et al. (2002). Tumor-associated B7-H1 promotes T-cell apoptosis: a potential mechanism of immune evasion. *Nat. Med.* 8, 793–800.
- Fan, X., Quezada, S.A., Sepulveda, M.A., Sharma, P., and Allison, J.P. (2014). Engagement of the ICOS pathway markedly enhances efficacy of CTLA-4 blockade in cancer immunotherapy. *J. Exp. Med.* 211, 715–725.
- Frederick, D.T., Piris, A., Cogdill, A.P., Cooper, Z.A., Lezcano, C., Ferrone, C.R., Mitra, D., Boni, A., Newton, L.P., Liu, C., et al. (2013). BRAF inhibition is associated with enhanced melanoma antigen expression and a more favorable tumor microenvironment in patients with metastatic melanoma. *Clin. Cancer Res.* 19, 1225–1231.
- Freeman, G.J., Long, A.J., Iwai, Y., Bourque, K., Chernova, T., Nishimura, H., Fitz, L.J., Malenkovich, N., Okazaki, T., Byrne, M.C., et al. (2000). Engagement of the PD-1 immunoinhibitory receptor by a novel B7 family member leads to negative regulation of lymphocyte activation. *J. Exp. Med.* 192, 1027–1034.
- Gao, J., He, Q., Subudhi, S., Aparicio, A., Zurita-Saavedra, A., Lee, D.H., Jimenez, C., Suarez-Almazor, M., and Sharma, P. (2015). Review of immune-related adverse events in prostate cancer patients treated with ipilimumab: MD Anderson experience. *Oncogene*.
- Greenwald, R.J., Freeman, G.J., and Sharpe, A.H. (2005). The B7 family revisited. *Annu. Rev. Immunol.* 23, 515–548.
- Gros, A., Robbins, P.F., Yao, X., Li, Y.F., Turcotte, S., Tran, E., Wunderlich, J.R., Mixon, A., Farid, S., Dudley, M.E., et al. (2014). PD-1 identifies the patient-specific CD8⁺ tumor-reactive repertoire infiltrating human tumors. *J. Clin. Invest.* 124, 2246–2259.
- Gubin, M.M., Zhang, X., Schuster, H., Caron, E., Ward, J.P., Noguchi, T., Ivanova, Y., Hundal, J., Arthur, C.D., Krebber, W.J., et al. (2014). Checkpoint blockade cancer immunotherapy targets tumour-specific mutant antigens. *Nature* 515, 577–581.
- Hamid, O., Robert, C., Daud, A., Hodi, F.S., Hwu, W.J., Kefford, R., Wolchok, J.D., Hersey, P., Joseph, R.W., Weber, J.S., et al. (2013). Safety and tumor responses with lambrolizumab (anti-PD-1) in melanoma. *N. Engl. J. Med.* 369, 134–144.
- Hanahan, D., and Weinberg, R.A. (2011). Hallmarks of cancer: the next generation. *Cell* 144, 646–674.
- Hanna, N., Shepherd, F.A., Fossella, F.V., Pereira, J.R., De Marinis, F., von Pawel, J., Gatzemeier, U., Tsao, T.C., Pless, M., Muller, T., et al. (2004). Randomized phase III trial of pemetrexed versus docetaxel in patients with non-small-cell lung cancer previously treated with chemotherapy. *J. Clin. Oncol.* 22, 1589–1597.
- Hodi, F.S., Butler, M., Oble, D.A., Seiden, M.V., Haluska, F.G., Kruse, A., Macrae, S., Nelson, M., Canning, C., Lowy, I., et al. (2008). Immunologic and clinical effects of antibody blockade of cytotoxic T lymphocyte-associated antigen 4 in previously vaccinated cancer patients. *Proc. Natl. Acad. Sci. USA* 105, 3005–3010.
- Hodi, F.S., O'Day, S.J., McDermott, D.F., Weber, R.W., Sosman, J.A., Haanen, J.B., Gonzalez, R., Robert, C., Schadendorf, D., Hassel, J.C., et al. (2010). Improved survival with ipilimumab in patients with metastatic melanoma. *N. Engl. J. Med.* 363, 711–723.
- Hurwitz, A.A., Yu, T.F., Leach, D.R., and Allison, J.P. (1998). CTLA-4 blockade synergizes with tumor-derived granulocyte-macrophage colony-stimulating factor for treatment of an experimental mammary carcinoma. *Proc. Natl. Acad. Sci. USA* 95, 10067–10071.
- Ishida, Y., Agata, Y., Shibahara, K., and Honjo, T. (1992). Induced expression of PD-1, a novel member of the immunoglobulin gene superfamily, upon programmed cell death. *EMBO J.* 11, 3887–3895.
- Jenkins, M.K., and Schwartz, R.H. (1987). Antigen presentation by chemically modified splenocytes induces antigen-specific T cell unresponsiveness in vitro and in vivo. *J. Exp. Med.* 165, 302–319.
- Keir, M.E., Butte, M.J., Freeman, G.J., and Sharpe, A.H. (2008). PD-1 and its ligands in tolerance and immunity. *Annu. Rev. Immunol.* 26, 677–704.
- Knudson, A.G. (2001). Two genetic hits (more or less) to cancer. *Nat. Rev. Cancer* 1, 157–162.
- Krummel, M.F., and Allison, J.P. (1995). CD28 and CTLA-4 have opposing effects on the response of T cells to stimulation. *J. Exp. Med.* 182, 459–465.
- Kwak, E.L., Bang, Y.J., Camidge, D.R., Shaw, A.T., Solomon, B., Maki, R.G., Ou, S.H., Dezube, B.J., Jänne, P.A., Costa, D.B., et al. (2010). Anaplastic lymphoma kinase inhibition in non-small-cell lung cancer. *N. Engl. J. Med.* 363, 1693–1703.
- Kwon, E.D., Drake, C.G., Scher, H.I., Fizazi, K., Bossi, A., van den Eertwegh, A.J., Krainer, M., Houede, N., Santos, R., Mahammed, H., et al.; CA184-043 Investigators (2014). Ipilimumab versus placebo after radiotherapy in patients with metastatic castration-resistant prostate cancer that had progressed after docetaxel chemotherapy (CA184-043): a multicentre, randomised, double-blind, phase 3 trial. *Lancet Oncol.* 15, 700–712.

- Larkin, J., Ascierto, P.A., Dréno, B., Atkinson, V., Liszkay, G., Maio, M., Mandalà, M., Demidov, L., Stroyakovskiy, D., Thomas, L., et al. (2014). Combined vemurafenib and cobimetinib in BRAF-mutated melanoma. *N. Engl. J. Med.* **371**, 1867–1876.
- Le Mercier, I., Chen, W., Lines, J.L., Day, M., Li, J., Sergent, P., Noelle, R.J., and Wang, L. (2014). VISTA regulates the development of protective antitumor immunity. *Cancer Res.* **74**, 1933–1944.
- Leach, D.R., Krummel, M.F., and Allison, J.P. (1996). Enhancement of anti-tumor immunity by CTLA-4 blockade. *Science* **271**, 1734–1736.
- Liakou, C.I., Kamat, A., Tang, D.N., Chen, H., Sun, J., Troncoso, P., Logothetis, C., and Sharma, P. (2008). CTLA-4 blockade increases IFNgamma-producing CD4+ICOShi cells to shift the ratio of effector to regulatory T cells in cancer patients. *Proc. Natl. Acad. Sci. USA* **105**, 14987–14992.
- Linnemann, C., van Buuren, M.M., Bies, L., Verdegaal, E.M., Schotte, R., Calis, J.J., Behjati, S., Velds, A., Hilkemann, H., Atmoui, D.E., et al. (2015). High-throughput epitope discovery reveals frequent recognition of neo-antigens by CD4+ T cells in human melanoma. *Nat. Med.* **21**, 81–85.
- Martz, C.A., Ottina, K.A., Singleton, K.R., Jasper, J.S., Wardell, S.E., Peraza-Penton, A., Anderson, G.R., Winter, P.S., Wang, T., Alley, H.M., et al. (2014). Systematic identification of signaling pathways with potential to confer anti-cancer drug resistance. *Sci. Signal.* **7**, ra121.
- Melero, I., Shuford, W.W., Newby, S.A., Aruffo, A., Ledbetter, J.A., Hellström, K.E., Mittler, R.S., and Chen, L. (1997). Monoclonal antibodies against the 4-1BB T-cell activation molecule eradicate established tumors. *Nat. Med.* **3**, 682–685.
- Melero, I., Gaudernack, G., Gerritsen, W., Huber, C., Parmiani, G., Scholl, S., Thatcher, N., Wagstaff, J., Zielinski, C., Faulkner, I., and Mellstedt, H. (2014). Therapeutic vaccines for cancer: an overview of clinical trials. *Nat. Rev. Clin. Oncol.* **11**, 509–524.
- Mueller, D.L., Jenkins, M.K., and Schwartz, R.H. (1989). An accessory cell-derived costimulatory signal acts independently of protein kinase C activation to allow T cell proliferation and prevent the induction of unresponsiveness. *J. Immunol.* **142**, 2617–2628.
- Ng Tang, D., Shen, Y., Sun, J., Wen, S., Wolchok, J.D., Yuan, J., Allison, J.P., and Sharma, P. (2013). Increased frequency of ICOS+ CD4 T cells as a pharmacodynamic biomarker for anti-CTLA-4 therapy. *Cancer Immunol. Res.* **1**, 229–234.
- Pardoll, D.M. (2012). The blockade of immune checkpoints in cancer immunotherapy. *Nat. Rev. Cancer.* **12**, 252–264.
- Peggs, K.S., Quezada, S.A., Chambers, C.A., Korman, A.J., and Allison, J.P. (2009). Blockade of CTLA-4 on both effector and regulatory T cell compartments contributes to the antitumor activity of anti-CTLA-4 antibodies. *J. Exp. Med.* **206**, 1717–1725.
- Postow, M.A., Callahan, M.K., and Wolchok, J.D. (2015). Immune checkpoint blockade in cancer therapy. *J. Clin. Oncol.* Published online January 20, 2015. <http://dx.doi.org/10.1200/JCO.2014.59.4358>.
- Powles, T., Eder, J.P., Fine, G.D., Braiteh, F.S., Loriot, Y., Cruz, C., Bellmunt, J., Burris, H.A., Petrylak, D.P., Teng, S.L., et al. (2014). MPDL3280A (anti-PD-L1) treatment leads to clinical activity in metastatic bladder cancer. *Nature* **515**, 558–562.
- Quezada, S.A., Peggs, K.S., Curran, M.A., and Allison, J.P. (2006). CTLA4 blockade and GM-CSF combination immunotherapy alters the intratumor balance of effector and regulatory T cells. *J. Clin. Invest.* **116**, 1935–1945.
- Ribas, A., Hodi, F.S., Callahan, M., Konto, C., and Wolchok, J. (2013). Hepatotoxicity with combination of vemurafenib and ipilimumab. *N. Engl. J. Med.* **368**, 1365–1366.
- Robert, C., Thomas, L., Bondarenko, I., O'Day, S., Weber, J., Garbe, C., Lebbe, C., Baurain, J.F., Testori, A., Grob, J.J., et al. (2011). Ipilimumab plus dacarbazine for previously untreated metastatic melanoma. *N. Engl. J. Med.* **364**, 2517–2526.
- Robert, C., Karaszewska, B., Schachter, J., Rutkowski, P., Mackiewicz, A., Stroikovski, D., Lichinitser, M., Dummer, R., Grange, F., Mortier, L., et al. (2015a). Improved overall survival in melanoma with combined dabrafenib and trametinib. *N. Engl. J. Med.* **372**, 30–39.
- Robert, C., Long, G.V., Brady, B., Dutriaux, C., Maio, M., Mortier, L., Hassel, J.C., Rutkowski, P., McNeil, C., Kalinka-Warzocha, E., et al. (2015b). Nivolumab in previously untreated melanoma without BRAF mutation. *N. Engl. J. Med.* **372**, 320–330.
- Rosenberg, S.A., Yang, J.C., and Restifo, N.P. (2004). Cancer immunotherapy: moving beyond current vaccines. *Nat. Med.* **10**, 909–915.
- Sakuishi, K., Apetoh, L., Sullivan, J.M., Blazar, B.R., Kuchroo, V.K., and Anderson, A.C. (2010). Targeting Tim-3 and PD-1 pathways to reverse T cell exhaustion and restore anti-tumor immunity. *J. Exp. Med.* **207**, 2187–2194.
- Schadendorf, D., Hodi, F.S., Robert, C., Weber, J.S., Margolin, K., Hamid, O., Patt, D., Chen, T.T., Berman, D.M., and Wolchok, J.D. (2015). Pooled analysis of long-term survival data from phase II and phase III trials of ipilimumab in unresectable or metastatic melanoma. *J. Clin. Oncol.* Published online February 9, 2015. <http://dx.doi.org/10.1200/JCO.2014.56.2736>.
- Segal, N.H., Parsons, D.W., Peggs, K.S., Velculescu, V., Kinzler, K.W., Vogelstein, B., and Allison, J.P. (2008). Epitope landscape in breast and colorectal cancer. *Cancer Res.* **68**, 889–892.
- Sharma, P., Wagner, K., Wolchok, J.D., and Allison, J.P. (2011). Novel cancer immunotherapy agents with survival benefit: recent successes and next steps. *Nat. Rev. Cancer* **11**, 805–812.
- Shaw, A.T., Kim, D.W., Nakagawa, K., Seto, T., Crinó, L., Ahn, M.J., De Pas, T., Besse, B., Solomon, B.J., Blackhall, F., et al. (2013). Crizotinib versus chemotherapy in advanced ALK-positive lung cancer. *N. Engl. J. Med.* **368**, 2385–2394.
- Sjöblom, T., Jones, S., Wood, L.D., Parsons, D.W., Lin, J., Barber, T.D., Mandelker, D., Leary, R.J., Ptak, J., Silliman, N., et al. (2006). The consensus coding sequences of human breast and colorectal cancers. *Science* **314**, 268–274.
- Snyder, A., Makarov, V., Merghoub, T., Yuan, J., Zaretsky, J.M., Desrichard, A., Walsh, L.A., Postow, M.A., Wong, P., Ho, T.S., et al. (2014). Genetic basis for clinical response to CTLA-4 blockade in melanoma. *N. Engl. J. Med.* **371**, 2189–2199.
- Soda, M., Choi, Y.L., Enomoto, M., Takada, S., Yamashita, Y., Ishikawa, S., Fujiwara, S., Watanabe, H., Kurashina, K., Hatanaka, H., et al. (2007). Identification of the transforming EML4-ALK fusion gene in non-small-cell lung cancer. *Nature* **448**, 561–566.
- Solomon, E., Borrow, J., and Goddard, A.D. (1991). Chromosome aberrations and cancer. *Science* **254**, 1153–1160.
- Sosman, J.A., Kim, K.B., Schuchter, L., Gonzalez, R., Pavlick, A.C., Weber, J.S., McArthur, G.A., Hutson, T.E., Moschos, S.J., Flaherty, K.T., et al. (2012). Survival in BRAF V600-mutant advanced melanoma treated with vemurafenib. *N. Engl. J. Med.* **366**, 707–714.
- Tang, C., Wang, X., Soh, H., Seyedin, S., Cortez, M.A., Krishnan, S., Massarelli, E., Hong, D., Naing, A., Diab, A., et al. (2014). Combining radiation and immunotherapy: a new systemic therapy for solid tumors? *Cancer Immunol. Res.* **2**, 831–838.
- Tivol, E.A., Borriello, F., Schweitzer, A.N., Lynch, W.P., Bluestone, J.A., and Sharpe, A.H. (1995). Loss of CTLA-4 leads to massive lymphoproliferation and fatal multiorgan tissue destruction, revealing a critical negative regulatory role of CTLA-4. *Immunity* **3**, 541–547.
- Topalian, S.L., Hodi, F.S., Brahmer, J.R., Gettinger, S.N., Smith, D.C., McDermott, D.F., Powderly, J.D., Carvajal, R.D., Sosman, J.A., Atkins, M.B., et al. (2012). Safety, activity, and immune correlates of anti-PD-1 antibody in cancer. *N. Engl. J. Med.* **366**, 2443–2454.
- Townsend, S.E., and Allison, J.P. (1993). Tumor rejection after direct costimulation of CD8+ T cells by B7-transfected melanoma cells. *Science* **259**, 368–370.
- Tran, E., Turcotte, S., Gros, A., Robbins, P.F., Lu, Y.C., Dudley, M.E., Wunderlich, J.R., Somerville, R.P., Hogan, K., Hinrichs, C.S., et al. (2014). Cancer immunotherapy based on mutation-specific CD4+ T cells in a patient with epithelial cancer. *Science* **344**, 641–645.

- Triebel, F., Jitsukawa, S., Baixeras, E., Roman-Roman, S., Genevee, C., Viegas-Pequignot, E., and Hercend, T. (1990). LAG-3, a novel lymphocyte activation gene closely related to CD4. *J. Exp. Med.* 171, 1393–1405.
- van den Eertwegh, A.J., Versluis, J., van den Berg, H.P., Santegoets, S.J., van Moorselaar, R.J., van der Sluis, T.M., Gall, H.E., Harding, T.C., Jooss, K., Lowy, I., et al. (2012). Combined immunotherapy with granulocyte-macrophage colony-stimulating factor-transduced allogeneic prostate cancer cells and ipilimumab in patients with metastatic castration-resistant prostate cancer: a phase 1 dose-escalation trial. *Lancet Oncol.* 13, 509–517.
- van Elsas, A., Hurwitz, A.A., and Allison, J.P. (1999). Combination immunotherapy of B16 melanoma using anti-cytotoxic T lymphocyte-associated antigen 4 (CTLA-4) and granulocyte/macrophage colony-stimulating factor (GM-CSF)-producing vaccines induces rejection of subcutaneous and metastatic tumors accompanied by autoimmune depigmentation. *J. Exp. Med.* 190, 355–366.
- Waitz, R., Fassò, M., and Allison, J.P. (2012). CTLA-4 blockade synergizes with cryoablation to mediate tumor rejection. *Oncolimmunology* 1, 544–546.
- Walunas, T.L., Lenschow, D.J., Bakker, C.Y., Linsley, P.S., Freeman, G.J., Green, J.M., Thompson, C.B., and Bluestone, J.A. (1994). CTLA-4 can function as a negative regulator of T cell activation. *Immunity* 1, 405–413.
- Wang, L., Rubinstein, R., Lines, J.L., Wasiuk, A., Ahonen, C., Guo, Y., Lu, L.F., Gondek, D., Wang, Y., Fava, R.A., et al. (2011). VISTA, a novel mouse Ig superfamily ligand that negatively regulates T cell responses. *J. Exp. Med.* 208, 577–592.
- Waterhouse, P., Penninger, J.M., Timms, E., Wakeham, A., Shahinian, A., Lee, K.P., Thompson, C.B., Griesser, H., and Mak, T.W. (1995). Lymphoproliferative disorders with early lethality in mice deficient in Ctla-4. *Science* 270, 985–988.
- Weinberg, R.A. (1991). Tumor suppressor genes. *Science* 254, 1138–1146.
- Wolchok, J.D., Kluger, H., Callahan, M.K., Postow, M.A., Rizvi, N.A., Lesokhin, A.M., Segal, N.H., Ariyan, C.E., Gordon, R.A., Reed, K., et al. (2013). Nivolumab plus ipilimumab in advanced melanoma. *N. Engl. J. Med.* 369, 122–133.
- Yang, J.C., Hughes, M., Kammula, U., Royal, R., Sherry, R.M., Topalian, S.L., Suri, K.B., Levy, C., Allen, T., Mavroukakis, S., et al. (2007). Ipilimumab (anti-CTLA4 antibody) causes regression of metastatic renal cell cancer associated with enteritis and hypophysitis. *J. Immunother.* 30, 825–830.
- Zamarin, D., Holmgård, R.B., Subudhi, S.K., Park, J.S., Mansour, M., Palese, P., Merghoub, T., Wolchok, J.D., and Allison, J.P. (2014). Localized oncolytic virotherapy overcomes systemic tumor resistance to immune checkpoint blockade immunotherapy. *Sci. Transl. Med.* 6, 226ra32.



Enhancement of Antitumor Immunity by CTLA-4 Blockade

Author(s): Dana R. Leach, Matthew F. Krummel and James P. Allison

Source: *Science*, New Series, Vol. 271, No. 5256 (Mar. 22, 1996), pp. 1734-1736

Published by: [American Association for the Advancement of Science](#)

Stable URL: <http://www.jstor.org/stable/2890840>

Accessed: 17/07/2013 12:44

Your use of the JSTOR archive indicates your acceptance of the Terms & Conditions of Use, available at
<http://www.jstor.org/page/info/about/policies/terms.jsp>

JSTOR is a not-for-profit service that helps scholars, researchers, and students discover, use, and build upon a wide range of content in a trusted digital archive. We use information technology and tools to increase productivity and facilitate new forms of scholarship. For more information about JSTOR, please contact support@jstor.org.



American Association for the Advancement of Science is collaborating with JSTOR to digitize, preserve and extend access to *Science*.

<http://www.jstor.org>

- try and 10% of whom were of other ethnic backgrounds. The stop codon mutation was screened in 70 Finnish EPM1 carrier parents. All 70 of these individuals contained the common ancestral haplotype around the EPM1 locus on one of their chromosomes. To distinguish mutations from polymorphisms, we considered only the nonancestral haplotype chromosome of these 70 individuals. DNA from these individuals was amplified by PCR, and the products were directly sequenced with the AmpliCycle sequencing kit (Perkin-Elmer).
17. R. Jerala, M. Trstenjak, B. Lenarcic, V. Turk, *FEBS Lett.* **239**, 41 (1988).
 18. M. Abrahamson, M. Q. Islam, J. Szpirer, C. Szpirer, G. Levan, *Hum. Genet.* **82**, 223 (1989); J. Ghiso, O. Jensson, B. Frangione, *Proc. Natl. Acad. Sci. U.S.A.* **83**, 2974 (1986).
 19. R. Eldridge, M. Iivanainen, R. Stern, T. Koerber, B. J.

Wilder, *Lancet ii*, 838 (1983).
 20. We thank the families with EPM1 for contributing to this study; C. Iannicola, C. Prange, D. Vollrath, J. Kere, and members of the Myers and Cox laboratories and the Stanford Human Genome Center for discussions and support; A.-L. Träskelin and R. Tolvanen for technical assistance; and R. Eldridge and B. J. Wilder for providing patient samples from the American family. This work was supported by NIH grants HD-24610 and P50 HG-00206 (to R.M.M. and D.R.C.), postdoctoral grant NIH F32GM17502 (to J.A.W.), NIH grant NS31831 (to A.D.I.C.), the Academy of Finland and the Sigrid Juselius Foundation (to A.D.I.C. and A.-E.L.), and the Epilepsy Research Foundation of Finland (to A.-E.L.). Part of this study was done at the Folkhälsoinstitutet of Genetics (Helsinki).

26 January 1996; accepted 14 February 1996

Enhancement of Antitumor Immunity by CTLA-4 Blockade

Dana R. Leach, Matthew F. Krummel, James P. Allison*

One reason for the poor immunogenicity of many tumors may be that they cannot provide signals for CD28-mediated costimulation necessary to fully activate T cells. It has recently become apparent that CTLA-4, a second counterreceptor for the B7 family of costimulatory molecules, is a negative regulator of T cell activation. Here, in vivo administration of antibodies to CTLA-4 resulted in the rejection of tumors, including preestablished tumors. Furthermore, this rejection resulted in immunity to a secondary exposure to tumor cells. These results suggest that blockade of the inhibitory effects of CTLA-4 can allow for, and potentiate, effective immune responses against tumor cells.

Despite expressing antigens recognizable by a host's immune system, tumors are very poor in initiating effective immune responses. One reason for this poor immunogenicity may be that the presentation of antigen alone is insufficient to activate T cells. In addition to T cell receptor engagement of an antigenic peptide bound to major histocompatibility complex (MHC) molecules, additional costimulatory signals are necessary for T cell activation (1). The most important of these costimulatory signals appears to be provided by the interaction of CD28 on T cells with its primary ligands B7-1 (CD80) and B7-2 (CD86) on the surface of specialized antigen-presenting cells (APCs) (2–4). Expression of B7 costimulatory molecules is limited to specialized APCs. Therefore, even though most tissue-derived tumors may present antigen in the context of MHC molecules, they may fail to elicit effective immunity because of a lack of costimulatory ability. Several studies support this notion. In a variety of model systems, transfected tumor cells expressing costimulatory B7 molecules induced potent responses against both modified and unmodified tumor cells (5–8). It appears that

tumor cells transfected with B7 are able to behave as APCs, presumably allowing direct activation of tumor-specific T cells.

Recent evidence suggests that costimulation is more complex than originally thought and involves competing stimulatory and inhibitory signaling events (3, 9–12). CTLA-4, a homolog of CD28, binds both B7-1 and B7-2 with affinities much greater than does CD28 (13–16). In vitro, antibody cross-linking of CTLA-4 has been shown to inhibit T cell proliferation and interleukin-2 production induced by antibody to CD3 (anti-CD3), whereas blockade of CTLA-4 with soluble intact or Fab fragments of antibody enhances proliferative responses (17, 18). Similarly, soluble intact or Fab fragments of anti-CTLA-4 greatly augment T cell responses to nominal peptide antigen or the superantigen *Staphylococcus enterotoxin B* in vivo (19, 20). It has also been suggested that CTLA-4 engagement can induce apoptosis in activated T cells (21). Finally, mice deficient in CTLA-4 exhibit severe T cell proliferative disorders (22). These results demonstrate that CTLA-4 is a negative regulator of T cell responses and raise the possibility that blockade of inhibitory signals delivered by CTLA-4–B7 interactions might augment T cell responses to tumor cells and enhance antitumor immunity.

We first sought to determine whether

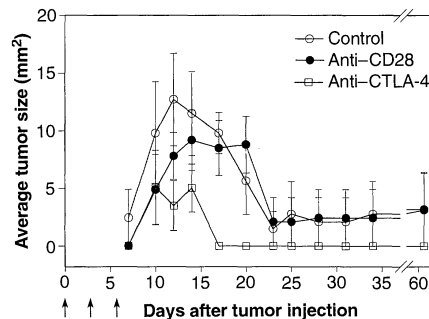


Fig. 1. Treatment with anti-CTLA-4 accelerates rejection of a B7-1-positive colon carcinoma (23). A volume of $100 \mu\text{l}$ of cell suspension (4×10^6 cells) was injected subcutaneously into the left flanks of groups of five female BALB/c mice. Two of the groups received three intraperitoneal injections of either anti-CTLA-4 or anti-CD28 (18). Injections of 100, 50, and 50 μg of antibody were given on days 0, 3, and 6, respectively, as indicated by the arrows. Control animals received no injections. Data points represent the average of the products of bisecting tumor diameters. Error bars represent standard error of the mean.

CTLA-4 blockade with nonstimulatory, bivalent antibody (18, 20) would accelerate rejection of B7-positive tumor cells. Previously, we showed that B7-1 expression was partially successful at inducing rejection of the transplantable murine colon carcinoma 51BLim10 (23). We reasoned that CTLA-4 blockade would remove inhibitory signals in the costimulatory pathway, resulting in enhanced rejection of the tumor cells. We injected groups of BALB/c mice with B7-1-transfected 51BLim10 tumor cells (B7-51BLim10) (23). Two groups were treated with a series of intraperitoneal injections of either anti-CTLA-4 or anti-CD28 (18, 24). Treatment with anti-CTLA-4 inhibited B7-51BLim10 tumor growth as compared with the anti-CD28-treated mice or the untreated controls (Fig. 1). All mice in the untreated and anti-CD28-treated groups developed small tumors that grew progressively for 5 to 10 days and then ultimately regressed in 8 of the 10 mice by about day 23 after injection. The two small tumors that did not regress remained static for more than 90 days. In contrast, three of five mice treated with anti-CTLA-4 developed very small tumors, all of which regressed completely by day 17. Although these results were encouraging and were consistent with our hypothesis, they were not very dramatic because B7-1 expression resulted in fairly rapid rejection of transfected 51BLim10 cells even in the absence of CTLA-4 blockade; however, these results confirmed that anti-CTLA-4 did not inhibit tumor rejection.

We next examined the effects of CTLA-4 blockade on the growth of V51BLim10, a vector control tumor cell line that does not express B7 (23). All mice either injected with 4×10^6 V51BLim10

Cancer Research Laboratory and Department of Molecular and Cell Biology, University of California, Berkeley, CA 94720, USA.

*To whom correspondence should be addressed.

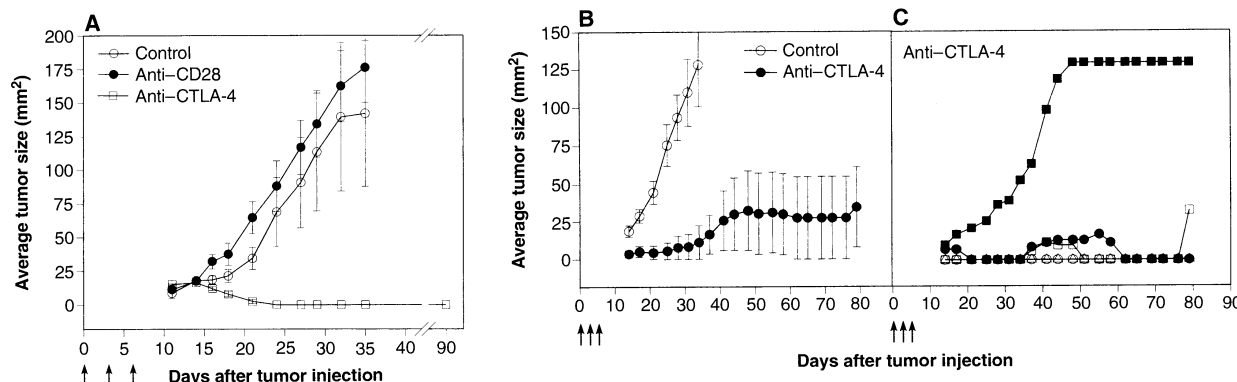


Fig. 2. Treatment with anti-CTLA-4 enhances rejection of B7-negative colon carcinoma cells and results in protection against subsequent challenge with wild-type colon carcinoma cells. Groups of BALB/c mice were injected with B7-negative V51BLim10 vector control cells (V51BLim10), left untreated, or treated with anti-CTLA-4 or control antibody. Mice were euthanized when tumors reached a size of 200 mm² or became ulcerated. If individual mice within a group were euthanized, the final measurement was carried over to subsequent time points. **(A)** Average tumor size in mice injected with 4×10^6 tumor cells. Groups of five mice were injected with 4×10^6 V51BLim10 tumor cells. Treated groups were injected three times with 100 µg of anti-CTLA-4 or irrelevant hamster antibody. **(B)** Average tumor size in mice injected with 2×10^6 V51BLim10 tumor cells. Two groups of five mice were injected with tumor cells and treated as above with anti-CTLA-4 or irrelevant hamster antibody. **(C)** Individual tumor growth in mice injected with 2×10^6 V51BLim10 cells and treated with anti-CTLA-4. Three of the mice remained tumor-free beyond 80 days. **(D)** Challenge tumor growth in anti-CTLA-4-treated mice. Five anti-CTLA-4-treated mice that had completely rejected V51BLim10 tumor cells were rechallenged 70 days later with 4×10^6 wild-type tumor cells injected subcutaneously in the opposite flank. Five naïve mice were also injected as controls. All control mice developed progressively growing tumors and were euthanized on day 35 after inoculation. Three of five previously immunized mice remained tumor-free 70 days after rechallenge.

tumor cells and left untreated, or treated with anti-CD28, developed progressively growing tumors and required euthanasia by 35 days after inoculation (Fig. 2A). In contrast, all mice treated with anti-CTLA-4 completely rejected their tumors after a short period of limited growth. Similarly, control mice injected with 2×10^6 tumor cells developed rapidly growing tumors and required euthanasia by day 35 (Fig. 2B). Anti-CTLA-4 treatment had a dramatic effect on tumor growth, but one mouse did develop a tumor quickly (accounting for a majority of the growth indicated in Fig. 2B) and another developed a tumor much later (Fig. 2C). Anti-CTLA-4 appeared to be less effective at a tumor dose of 1×10^6 cells, where treatment resulted in significantly reduced tumor growth rates, but four of five mice developed progressively growing tumors (25). Thus, although curative responses were not obtained in all cases, it is clear that CTLA-4 blockade significantly enhanced rejection of B7-negative tumor cells.

We next sought to determine whether tumor rejection as a consequence of CTLA-4 blockade was associated with enhanced immunity to a secondary challenge. Mice that had rejected V51BLim10 tumor cells as a result of treatment with anti-CTLA-4 were challenged with 4×10^6 wild-type V51BLim10 cells 70 days after their ini-

tial tumor injections. These mice showed significant protection against a secondary challenge as compared with naïve controls (Fig. 2D). All control animals had progressively growing tumors by 14 days after injection, developed massive tumor burdens, and required euthanasia by day 35. Only one of the previously immunized mice had a detectable tumor by day 14, and growth of this tumor was very slow. Ultimately, two more tumors developed in the immunized mice 42 days after challenge. Two mice remained tumor-free throughout the course of the experiment. These results demonstrate that tumor rejection mediated by CTLA-4 blockade results in immunologic memory.

To determine whether anti-CTLA-4 treatment could have an effect on the growth of established tumors, we injected groups of mice with 2×10^6 wild-type V51BLim10 tumor cells and treated them with anti-CTLA-4 beginning on day 0 as before, or beginning 7 days later at which time most mice had palpable tumors. Mice treated with anti-CTLA-4 at either time period had significantly reduced tumor growth compared with untreated controls (Fig. 3). In fact, delaying treatment appeared to be more effective, with two of five mice remaining tumor-free beyond 30 days after inoculation.

The effects of anti-CTLA-4 treatment

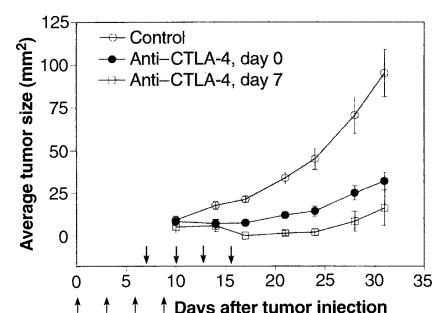
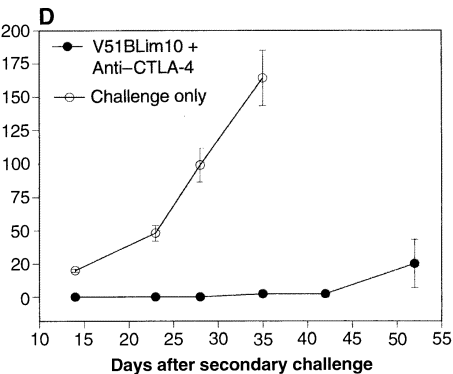


Fig. 3. Treatment with anti-CTLA-4 reduces the growth of established tumor. Groups of mice were injected subcutaneously with 2×10^6 V51BLim10 tumor cells. Control animals ($n = 10$) were injected intraperitoneally with 100 µg of irrelevant hamster antibody on days 0, 3, 6, and 9, as indicated by the upward-pointing arrows. One anti-CTLA-4 treatment group ($n = 10$) received intraperitoneal injections on the same days. The other treated mice ($n = 5$) were given intraperitoneal injections of anti-CTLA-4 beginning on day 7 and subsequently on days 10, 13, and 16 (downward-pointing arrows).

were not limited to variants of the murine colon carcinoma V51BLim10. Similar results were obtained with a rapidly growing fibrosarcoma of A/JCr mice, Sa1N (26) (Fig. 4). All control mice injected subcutaneously with 1×10^6 Sa1N cells developed measur-

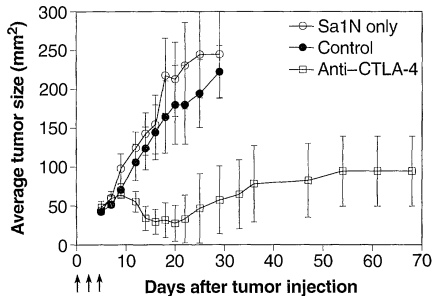


Fig. 4. Treatment with anti-CTLA-4 reduces the growth of the murine fibrosarcoma Sa1N. Groups of five mice were injected subcutaneously in the flank with a suspension of 1×10^6 Sa1N fibrosarcoma cells. Treated groups were injected intraperitoneally with 100 µg of anti-CTLA-4 or irrelevant hamster control antibody at days 0, 3, and 6 as indicated by the arrows. All control animals were killed by day 30. Two of five animals treated with anti-CTLA-4 remained tumor-free at day 55.

able, rapidly growing tumors within 7 days, whereas only two mice treated with anti-CTLA-4 had tumors by day 30, and one additional mouse developed a tumor around day 40 after injection. The remaining mice were still tumor-free 70 days after injection. In another experiment, control mice injected with 4×10^5 Sa1N tumor cells also developed rapidly growing tumors, whereas 7 of 10 mice treated with anti-CTLA-4 were tumor-free by day 25 after injection (25).

Our results indicate that removing inhibitory signals in the costimulatory pathway can enhance antitumor immunity. Although it has been shown that anti-CTLA-4 interferes with signals that normally down-regulate T cell responses in vivo (17, 18), the exact mechanisms of antitumor immunity elicited by CTLA-4 blockade are not clear. In the case of B7-negative tumors, antigens are most likely transferred to and presented by host APCs (27), where CTLA-4 blockade might effect T cell responses in two nonexclusive ways. First, removal of inhibitory signals may lower the overall threshold of T cell activation and allow normally unreactive T cells to become activated. Alternatively, CTLA-4 blockade might sustain proliferation of activated T cells by removing inhibitory signals that would normally terminate the response, thus allowing for greater expansion of tumor-specific T cells.

Regardless of the mechanism, it is clear that CTLA-4 blockade enhances antitumor responses. Most importantly, we have observed these effects against unmanipulated, wild-type tumors. Current methods of enhancing antitumor immunity generally require the engineering of tumor cells (8). Some of these methods, such as the induction of B7 expression, rely on enhancing the costimulatory activity of the tumor cells

themselves. Others, such as engineering tumor cells to express MHC class II molecules (26, 28, 29) or to produce granulocyte-macrophage colony-stimulating factor (27, 30, 31) or pulsing dendritic cells with tumor antigen ex vivo (32, 33), seek to enhance antigen presentation, antigen transfer, or both. Thus, CTLA-4 blockade, by removing potentially competing inhibitory signals, may be a particularly useful adjunct to other therapeutic approaches involving the costimulatory pathway.

REFERENCES AND NOTES

- D. L. Mueller, M. K. Jenkins, R. H. Schwartz, *Ann. Rev. Immunol.* **7**, 445 (1989).
- P. S. Linsley and J. A. Ledbetter, *ibid.* **11**, 191 (1993).
- C. H. June, J. A. Bluestone, L. M. Nadler, C. B. Thompson, *Immunol. Today* **15**, 321 (1994).
- J. P. Allison, *Curr. Opin. Immunol.* **6**, 414 (1994).
- L. Chen, S. Ashe, W. A. Brady, I. Hellstrom, K. E. Hellstrom et al., *Cell* **71**, 1093 (1992).
- S. E. Townsend and J. P. Allison, *Science* **259**, 368 (1993).
- S. Baskar et al., *Proc. Natl. Acad. Sci. U.S.A.* **90**, 5687 (1993).
- J. P. Allison, A. A. Hurwitz, D. R. Leach, *Curr. Opin. Immunol.* **7**, 682 (1995).
- M. K. Jenkins, *Immunity* **1**, 443 (1994).
- J. A. Bluestone, *ibid.* **2**, 555 (1995).
- P. S. Linsley, *J. Exp. Med.* **182**, 289 (1995).
- J. P. Allison and M. F. Krummel, *Science* **270**, 932 (1995).
- J. F. Brunet et al., *Nature* **328**, 267 (1987).
- K. Harper et al., *J. Immunol.* **147**, 1037 (1991).
- P. S. Linsley et al., *J. Exp. Med.* **174**, 561 (1991).
- P. S. Linsley et al., *Immunity* **1**, 793 (1994).
- T. L. Walunas et al., *ibid.*, p. 405.
- M. F. Krummel and J. P. Allison, *J. Exp. Med.* **182**, 459 (1995). Antibodies used in these studies were protein G-purified from hybridoma supernatants and quantified by ultraviolet spectrophotometry.
- E. R. Kearney et al., *J. Immunol.* **155**, 1033 (1995).
- M. F. Krummel, T. J. Sullivan, J. P. Allison, *Int. Immunol.*, in press.
- J. G. Gribben et al., *Proc. Natl. Acad. Sci. U.S.A.* **92**, 811 (1995).
- P. Waterhouse et al., *Science* **270**, 985 (1995).
- S. E. Townsend, F. W. Su, J. M. Atherton, J. P. Allison, *Cancer Res.* **54**, 6477 (1994). 51BLIM10 colon carcinoma cells were transfected with a plasmid construct containing the gene for murine B7-1 and cloned by limiting dilution. Fresh cultures of tumor cells were established from early passage frozen stocks and maintained in culture for no more than 30 days before use. Tumor cells were harvested by trypsinization from tissue culture plates, washed three times in serum-free medium, and suspended at 4×10^7 cells per milliliter. Expression of B7-1 molecules on transfected cells was verified by flow cytometry before injection. V51BLIM10 and wild-type 51BLIM10 tumor cells do not express detectable amounts of B7-1, B7-2, or CTIA-4 as determined by flow cytometric analyses.
- J. A. Gross, E. Callas, J. P. Allison, *J. Immunol.* **149**, 380 (1992).
- D. R. Leach, M. F. Krummel, J. P. Allison, data not shown.
- S. Baskar, L. Glimcher, N. Nabavi, R. T. Jones, S. Ostrand-Rosenberg, *J. Exp. Med.* **181**, 619 (1995).
- A. Y. C. Huang et al., *Science* **264**, 961 (1994).
- S. Ostrand-Rosenberg, A. Thakur, V. Clements, *J. Immunol.* **144**, 4068 (1990).
- D. R. Leach and G. N. Callahan, *ibid.* **154**, 738 (1995).
- G. Dranoff et al., *Proc. Natl. Acad. Sci. U.S.A.* **90**, 3539 (1993).
- H. I. Levitsky, A. Lazenby, R. J. Hayashi, D. M. Parikh, *J. Exp. Med.* **179**, 1215 (1994).
- V. Flamand et al., *Eur. J. Immunol.* **24**, 605 (1994).
- S. Grabebe, S. Beissert, T. Schwarz, R. D. Granstein, *Immunol. Today* **16**, 117 (1995).
- We thank S. Ostrand-Rosenberg and R. Warren for providing tumor lines. Supported by NIH grants CA57986, CA09179, and CA40041.

17 November 1995; accepted 16 January 1996

Light-Induced Degradation of TIMELESS and Entrainment of the *Drosophila* Circadian Clock

Michael P. Myers, Karen Wager-Smith,
Adrian Rothenfluh-Hilfiker, Michael W. Young*

Two genes, *period* (*per*) and *timeless* (*tim*), are required for production of circadian rhythms in *Drosophila*. The proteins encoded by these genes (PER and TIM) physically interact, and the timing of their association and nuclear localization is believed to promote cycles of *per* and *tim* transcription through an autoregulatory feedback loop. Here it is shown that TIM protein may also couple this molecular pacemaker to the environment, because TIM is rapidly degraded after exposure to light. TIM accumulated rhythmically in nuclei of eyes and in pacemaker cells of the brain. The phase of these rhythms was differentially advanced or delayed by light pulses delivered at different times of day, corresponding with phase shifts induced in the behavioral rhythms.

Circadian rhythms, found in most eukaryotes and some prokaryotes (1), are ~24-hour rhythms governed by an internal clock that functions autonomously but can

Howard Hughes Medical Institute, National Science Foundation Science and Technology Center for Biological Timing, and the Laboratory of Genetics, The Rockefeller University, 1230 York Avenue, New York, NY 10021, USA.

*To whom correspondence should be addressed.

be entrained by environmental cycles of light or temperature. Circadian rhythms produced in constant darkness can also be reset by pulses of light. Such light pulses will shift the phase of the clock in different directions (advance or delay) and to a varying extent in a manner that depends on the time of light exposure (2).

In the fruit fly *Drosophila melanogaster*, two genes, *period* (3) and *timeless* (4), are



NIH Public Access

Author Manuscript

N Engl J Med. Author manuscript; available in PMC 2013 January 19.

Published in final edited form as:

N Engl J Med. 2010 August 19; 363(8): 711–723. doi:10.1056/NEJMoa1003466.

Improved Survival with Ipilimumab in Patients with Metastatic Melanoma

F. Stephen Hodi, M.D., Steven J. O'Day, M.D., David F. McDermott, M.D., Robert W. Weber, M.D., Jeffrey A. Sosman, M.D., John B. Haanen, M.D., Rene Gonzalez, M.D., Caroline Robert, M.D., Ph.D., Dirk Schadendorf, M.D., Jessica C. Hassel, M.D., Wallace Akerley, M.D., Alfons J.M. van den Eertwegh, M.D., Ph.D., Jose Lutzky, M.D., Paul Lorigan, M.D., Julia M. Vaubel, M.D., Gerald P. Linette, M.D., Ph.D., David Hogg, M.D., Christian H. Ottensmeier, M.D., Ph.D., Celeste Lebbé, M.D., Christian Peschel, M.D., Ian Quirt, M.D., Joseph I. Clark, M.D., Jedd D. Wolchok, M.D., Ph.D., Jeffrey S. Weber, M.D., Ph.D., Jason Tian, Ph.D., Michael J. Yellin, M.D., Geoffrey M. Nichol, M.B., Ch.B., Axel Hoos, M.D., Ph.D., and Walter J. Urba, M.D., Ph.D.

The authors' affiliations and participating investigators are listed in the Appendix

Abstract

BACKGROUND—An improvement in overall survival among patients with metastatic melanoma has been an elusive goal. In this phase 3 study, ipilimumab — which blocks cytotoxic T-lymphocyte-associated antigen 4 to potentiate an antitumor T-cell response — administered with or without a glycoprotein 100 (gp100) peptide vaccine was compared with gp100 alone in patients with previously treated metastatic melanoma.

METHODS—A total of 676 HLA-A*0201-positive patients with unresectable stage III or IV melanoma, whose disease had progressed while they were receiving therapy for metastatic disease, were randomly assigned, in a 3:1:1 ratio, to receive ipilimumab plus gp100 (403 patients), ipilimumab alone (137), or gp100 alone (136). Ipilimumab, at a dose of 3 mg per kilogram of body weight, was administered with or without gp100 every 3 weeks for up to four treatments (induction). Eligible patients could receive reinduction therapy. The primary end point was overall survival.

RESULTS—The median overall survival was 10.0 months among patients receiving ipilimumab plus gp100, as compared with 6.4 months among patients receiving gp100 alone (hazard ratio for death, 0.68; $P<0.001$). The median overall survival with ipilimumab alone was 10.1 months (hazard ratio for death in the comparison with gp100 alone, 0.66; $P = 0.003$). No difference in overall survival was detected between the ipilimumab groups (hazard ratio with ipilimumab plus gp100, 1.04; $P = 0.76$). Grade 3 or 4 immune-related adverse events occurred in 10 to 15% of patients treated with ipilimumab and in 3% treated with gp100 alone. There were 14 deaths related to the study drugs (2.1%), and 7 were associated with immune-related adverse events.

CONCLUSIONS—Ipilimumab, with or without a gp100 peptide vaccine, as compared with gp100 alone, improved overall survival in patients with previously treated metastatic melanoma. Adverse events can be severe, long-lasting, or both, but most are reversible with appropriate treatment. (Funded by Medarex and Bristol-Myers Squibb; [ClinicalTrials.gov](#) number, NCT00094653.)

Copyright © 2010 Massachusetts Medical Society. All rights reserved.

Address reprint requests to Dr. Hodi at the Dana-Farber Cancer Institute, 44 Binney St., Boston, MA 02115, or at stephen_hodi@dfci.harvard.edu..

Drs. Hodi and O'Day contributed equally to this article.

THE INCIDENCE OF METASTATIC MELANOMA has increased over the past three decades,^{1,2} and the death rate continues to rise faster than the rate with most cancers.³ The World Health Organization (WHO) estimates that worldwide there are 66,000 deaths annually from skin cancer, with approximately 80% due to melanoma.⁴ In the United States alone, an estimated 8600 persons died from melanoma in 2009.¹ The median survival of patients with melanoma who have distant metastases (American Joint Committee on Cancer stage IV) is less than 1 year.^{5,6} No therapy is approved beyond the first-line therapy for metastatic melanoma, and enrollment in a clinical trial is the standard of care. No therapy has been shown in a phase 3, randomized, controlled trial to improve overall survival in patients with metastatic melanoma.⁶⁻⁹

Regulatory pathways that limit the immune response to cancer are becoming increasingly well characterized. Cytotoxic T-lymphocyte-associated antigen 4 (CTLA-4) is an immune checkpoint molecule that down-regulates pathways of T-cell activation.¹⁰ Ipilimumab, a fully human monoclonal antibody (IgG1) that blocks CTLA-4 to promote antitumor immunity,¹¹⁻¹⁴ has shown activity in patients with metastatic melanoma when it has been used as monotherapy in phase 2 studies.¹⁵⁻¹⁷ Ipilimumab has also shown activity when combined with other agents,^{18,19} including cancer vaccines.^{20,21} One well-studied cancer vaccine comprises HLA-A*0201-restricted peptides derived from the melanosomal protein, glycoprotein 100 (gp100). Monotherapy with this vaccine induces immune responses but has limited antitumor activity.²² However, the results of a recent study suggest that gp100 may improve the efficacy of high-dose interleukin-2 in patients with metastatic melanoma.²³ With no accepted standard of care, gp100 was used as an active control for our phase 3 study, which evaluated whether ipilimumab with or without gp100 improves overall survival, as compared with gp100 alone, among patients with metastatic melanoma who had undergone previous treatment.

METHODS

PATIENTS

Patients were eligible for inclusion in the study if they had a diagnosis of unresectable stage III or IV melanoma and had received a previous therapeutic regimen containing one or more of the following: dacarbazine, temozolomide, fotemustine, carboplatin, or interleukin-2. Other inclusion criteria were age of at least 18 years; life expectancy of at least 4 months; Eastern Cooperative Oncology Group (ECOG) performance status of 0 (fully active, able to carry on all predisease performance without restriction) or 1 (restricted in physically strenuous activity but ambulatory and able to carry out work of a light or sedentary nature, such as light housework or office work)²⁴; positive status for HLA-A*0201; normal hematologic, hepatic, and renal function; and no systemic treatment in the previous 28 days. Exclusion criteria were any other cancer from which the patient had been disease-free for less than 5 years (except treated and cured basal-cell or squamous-cell skin cancer, superficial bladder cancer, or treated carcinoma in situ of the cervix, breast, or bladder); primary ocular melanoma; previous receipt of anti-CTLA-4 antibody or cancer vaccine; autoimmune disease; active, untreated metastases in the central nervous system; pregnancy or lactation; concomitant treatment with any nonstudy anticancer therapy or immunosuppressive agent; or long-term use of systemic corticosteroids.

The protocol was approved by the institutional review board at each participating institution and was conducted in accordance with the ethical principles originating from the Declaration of Helsinki and with Good Clinical Practice as defined by the International Conference on Harmonization. All patients (or their legal representatives) gave written informed consent before enrollment.

STUDY DESIGN AND TREATMENT

In this randomized, double-blind, phase 3 study, we enrolled patients at 125 centers in 13 countries in North America, South America, Europe, and Africa. Between September 2004 and August 2008, patients were randomly assigned to one of three study groups, with stratification according to baseline metastasis stage (M0, M1a, or M1b vs. M1c, classified according to the tumor–node–metastasis [TNM] categorization for melanoma of the American Joint Committee on Cancer), and receipt or nonreceipt of previous interleukin-2 therapy. The full original protocol, a list of amendments, and the final protocol, as well as the statistical analysis plan, are available with the full text of this article at NEJM.org.

Patients were randomly assigned, in a 3:1:1 ratio, to treatment with an induction course of ipilimumab, at a dose of 3 mg per kilogram of body weight, plus a gp100 peptide vaccine; ipilimumab plus gp100 placebo; or gp100 plus ipilimumab placebo — all administered once every 3 weeks for four treatments. In the vaccine groups, patients received two modified HLA-A*0201-restricted peptides, injected subcutaneously as an emulsion with incomplete Freund's adjuvant (Montanide ISA-51): a gp100:209-217(210M) peptide, 1 mg injected in the right anterior thigh, and a gp100:280-288(288V) peptide, 1 mg injected in the left anterior thigh. Peptide injections were given immediately after a 90-minute intravenous infusion of ipilimumab or placebo. Treatment began on day 1 of week 1, and if there were no toxic effects that could not be tolerated, no rapidly progressive disease, and no significant decline in performance status, patients received an additional treatment during weeks 4, 7, and 10. Patients in whom new lesions developed or baseline lesions grew were allowed to receive additional treatments to complete induction. Patients with stable disease for 3 months' duration after week 12 or a confirmed partial or complete response were offered additional courses of therapy (reinduction) with their assigned treatment regimen if they had disease progression.

The original primary end point was the best overall response rate (i.e., the proportion of patients with a partial or complete response). The primary end point was amended to overall survival (with the amendment formally approved on January 15, 2009) in the ongoing blinded study, on the basis of phase 2 data and in alignment with another ongoing phase 3 trial of ipilimumab involving patients with metastatic melanoma.²⁵ The primary comparison in overall survival was between the ipilimumab-plus-gp100 group and the gp100-alone group. Prespecified secondary end points included a comparison of overall survival between the ipilimumab-alone and the gp100-alone groups and between the two ipilimumab groups, the best overall response rate, the duration of response, and progression-free survival. Subgroup comparisons of overall survival were performed across five prespecified categories: metastasis stage (M0, M1a, or M1b vs. M1c), receipt or nonreceipt of previous interleukin-2 therapy, baseline levels of serum lactate dehydrogenase (less than or equal to the upper limit of the normal range vs. higher than the upper limit of the normal range), age (<65 years vs. ≥65 years), and sex.

The trial was designed jointly by the senior academic authors and the sponsors, Medarex and Bristol-Myers Squibb. Data were collected by the sponsors and analyzed in collaboration with the senior academic authors, who vouch for the completeness and accuracy of the data and analyses and for the conformance of this report to the protocol, as amended. An initial draft of the manuscript was prepared by six of the academic authors in collaboration with the sponsor and a professional medical writer paid by the sponsor. All the authors contributed to subsequent drafts and made the decision to submit the manuscript for publication. All the authors signed a confidentiality disclosure agreement with the sponsor.

ASSESSMENTS

For the assessment of a patient's eligibility, each patient's HLA-A*0201 status was determined at a central laboratory. Patients who met the study criteria were assigned to receive treatment within 35 days after HLA typing and within 28 days after diagnostic imaging. Computed tomography with contrast material or magnetic resonance imaging of the brain, chest, abdomen, pelvis, and other anatomical regions, as clinically indicated, was performed. Cutaneous lesions were photographed. Tumor assessments were performed at baseline, and all patients who did not have documented early disease progression and who had stable disease or better at week 12 had confirmatory scans at weeks 16 and 24 and every 3 months thereafter. Tumor responses were determined by the investigators with the use of modified WHO criteria to evaluate bidimensionally measurable lesions.²⁶

Adverse events were graded according to the National Cancer Institute's Common Terminology Criteria for Adverse Events, version 3.0. An immune-related adverse event was defined as an adverse event that was associated with exposure to the study drug and that was consistent with an immune phenomenon. Protocol guidelines for the management of immune-related adverse events included the administration of corticosteroids (orally or intravenously), a delay in a scheduled dose, or discontinuation of therapy.¹⁵⁻¹⁷ Assigned doses were delayed in the case of nondermatologic immune-related adverse events of grade 2 or higher until the event improved to grade 1 or lower; if the event did not improve to grade 1 or lower, treatment was discontinued permanently. Monitoring of adverse events continued for at least 70 days after the last dose of study drugs had been administered or until any ongoing event resolved or stabilized. All patients, including those with low-grade changes in bowel frequency or stool consistency, were followed closely. A data and safety monitoring committee provided independent over-sight of safety and the risk–benefit ratio.

During the study enrollment, the following stopping rule was in place: if 10% or more of the patients in any study treatment group, evaluated cumulatively every 3 months, had a nondermatologic-related toxic adverse event of grade 3 or higher that was attributable to the investigational agents and that could not be alleviated or controlled by appropriate care or corticosteroid therapy within 14 days after the initiation of supportive care or corticosteroid therapy, assignment of patients to that study group would be suspended until the sponsor and the data and safety monitoring committee had reviewed the events and determined the appropriate course of action.

STATISTICAL ANALYSIS

The original study sample size of 750 patients was determined on the basis of the primary end point of best overall response rate but was revised with the new primary end point of overall survival. We estimated that with 385 events (deaths) among a total of 500 patients randomly assigned to the ipilimumab-plus-gp100 and the gp100-alone groups, the study would have at least 90% power to detect a difference in overall survival, at a two-sided alpha level of 0.05, with the use of a log-rank test. A total of 481 events were required in all three groups (assuming that the events were distributed in a 3:1:1 ratio in the ipilimumab-plus-gp100, ipilimumab-alone, and gp100-alone groups, respectively). Therefore, all patients who were randomly assigned in the study were to be followed until at least 481 events had occurred in the study. Enrollment was completed on July 25, 2008, when more than 650 patients had been enrolled. A post hoc power analysis showed that the 219 events observed among a total of 273 patients randomly assigned to the ipilimumab-alone and gp100-alone groups provided at least 80% power to detect a difference in overall survival between the two groups, at a two-sided alpha level of 0.05, with the assumption that ipilimumab alone has the same treatment effect as the combination regimen of ipilimumab plus gp100.

Survival was defined as the time from randomization to death from any cause, and progression-free survival as the time from randomization to documented disease progression or death. Event-time distributions were estimated with the use of the Kaplan–Meier method. Cox proportional-hazards models, stratified according to metastasis status and receipt or nonreceipt of previous interleukin therapy, were used to estimate hazard ratios and to test for significance of the timing of events. All reported P values are two-sided, and confidence intervals are at the 95% level. Survival rates were based on Kaplan–Meier estimation, and confidence intervals were calculated with the use of the bootstrap method. Descriptive statistics were used for adverse events.

RESULTS

PATIENTS AND TREATMENT

Among 676 patients enrolled in the study, 403 were randomly assigned to receive ipilimumab plus gp100, 137 to receive ipilimumab alone, and 136 to receive gp100 alone (control group) (Fig. 1 in the Supplementary Appendix, available at NEJM.org). Included among these patients were 82 patients who had metastases in the central nervous system at baseline, of whom 77 received the study drug. The baseline characteristics of the patients are shown in Table 1. Efficacy analyses were performed on the intention-to-treat population, which included all patients who had undergone randomization (676 patients). The safety population included all patients who had undergone randomization and who had received any amount of study drug (643 patients). A total of 242 of 403 patients in the ipilimumab-plus-gp100 group (60.0%), 88 of 137 in the ipilimumab-alone group (64.2%), and 78 of 136 in the gp100-alone group (57.4%) received all four ipilimumab doses or placebo infusions. The most frequent reason for discontinuation of therapy was disease progression.

EFFICACY

All the analyses of the efficacy end points reported here were prespecified as per protocol. Patients were followed for up to 55 months, with median follow-up times for survival of 21.0 months in the ipilimumab-plus-gp100 group, 27.8 months in the ipilimumab-alone group, and 17.2 months in the gp100-alone group. The median overall survival in the ipilimumab-plus-gp100 group was 10.0 months (95% confidence interval [CI], 8.5 to 11.5), as compared with 6.4 months (95% CI, 5.5 to 8.7) in the gp100-alone group (hazard ratio for death, 0.68; $P<0.001$). The median overall survival in the ipilimumab-alone group was 10.1 months (95% CI, 8.0 to 13.8) (hazard ratio for death with ipilimumab alone as compared with gp100 alone, 0.66; $P=0.003$). No difference in overall survival was detected between the two ipilimumab groups (hazard ratio for death with ipilimumab plus gp100, 1.04; $P=0.76$) (Fig. 1). Analyses of survival showed that the rates of overall survival in the ipilimumab-plus-gp100 group, the ipilimumab-alone group, and the gp100-alone group, respectively, were 43.6%, 45.6%, and 25.3% at 12 months, 30.0%, 33.2%, and 16.3% at 18 months, and 21.6%, 23.5%, and 13.7% at 24 months. The effect of ipilimumab on overall survival was independent of age, sex, baseline serum lactate dehydrogenase levels, metastasis stage of disease, and receipt or nonreceipt of previous interleukin-2 therapy (Fig. 2).

A 19% reduction in the risk of progression was noted with ipilimumab plus gp100, as compared with gp100 alone (hazard ratio, 0.81; $P<0.05$), and a 36% reduction in risk of progression was seen with ipilimumab alone as compared with gp100 alone (hazard ratio, 0.64; $P<0.001$). The reduction in risk with ipilimumab plus gp100 was less than that with ipilimumab alone (hazard ratio with ipilimumab plus gp100, 1.25; $P = 0.04$). The median values for progression-free survival were similar in all groups at the time of the first

assessment of progression (week 12), after which there was a separation between the curves (Fig. 1B).

The highest percentage of patients with an objective response or stable disease was in the ipilimumab-alone group (Table 2); this group had a best overall response rate of 10.9% and a disease control rate (the proportion of patients with a partial or complete response or stable disease) of 28.5%. In the ipilimumab-alone group, 9 of 15 patients (60.0%) maintained an objective response for at least 2 years (26.5 to 44.2 months [ongoing]), and in the ipilimumab-plus-gp100 group, 4 of 23 patients (17.4%) maintained the response for at least 2 years (27.9 to 44.4 months [ongoing]). Neither of the two patients in the gp100-alone group who had a partial response maintained the response for 2 years. Responses to ipilimumab continued to improve beyond week 24: in the ipilimumab-plus-gp100 group, 3 patients with disease progression improved to stable disease, 3 with stable disease improved to a partial response, and 1 with a partial response improved to a complete response; in the ipilimumab-alone group, 2 patients with stable disease improved to a partial response and 3 with a partial response improved to a complete response. Among 31 patients given reinduction therapy with ipilimumab, a partial or complete response or stable disease was achieved by 21 (Table 2).

ADVERSE EVENTS

The adverse events reported in the safety population are listed in Table 3. The most common adverse events related to the study drugs were immune-related events, which occurred in approximately 60% of the patients treated with ipilimumab and 32% of the patients treated with gp100. The frequency of grade 3 or 4 immune-related adverse events was 10 to 15% in the ipilimumab groups and 3.0% in the gp100-alone group. All immune-related events occurred during the induction and reinduction periods; the immune-related adverse events most often affected the skin and gastrointestinal tract. The median time to the resolution of immune-related adverse events of grade 2, 3, or 4 was 6.3 weeks (95% CI, 4.3 to 8.4) in the ipilimumab-plus-gp100 group, 4.9 weeks (95% CI, 3.1 to 6.4) in the ipilimumab-alone group, and 3.1 weeks (95% CI, 1.1 to not reached) in the gp100-alone group.

The most common immune-related adverse event was diarrhea, which occurred at any grade in 27 to 31% of the patients in the ipilimumab groups. After the administration of corticosteroids, the median time to the resolution of diarrhea of grade 2 or higher was 2.0 weeks for 40 of 44 patients in the ipilimumab-plus-gp100 group and 2.3 weeks for 14 of 15 patients in the ipilimumab-alone group. In addition to corticosteroids, 4 patients received infliximab (anti-tumor necrosis factor α antibody) for diarrhea of grade 3 or higher or colitis. Among the 94 persons who survived for 2 years, residual effects of adverse events included those related to injection-site reactions (16 patients), vitiligo (12), diarrhea or colitis (e.g., proctocolitis with rectal pain) (4), and endocrine immune-related adverse events (e.g., inflammation of the pituitary) that required hormone-replacement therapy (8). Ongoing events in the persons who survived for 2 years included rash, pruritus, diarrhea, anorexia, and fatigue, generally of grade 1 or 2 (in 5 to 15% of the patients) and grade 3 leukocytosis (in one patient). There were 14 deaths related to the study drugs (2.1%), of which 7 were associated with immune-related adverse events.

DISCUSSION

This phase 3 study showed that ipilimumab, either alone or with gp100, improved overall survival as compared with gp100 alone in patients with metastatic melanoma who had undergone previous treatment. More than 70% of the patients had M1c disease (presence of visceral metastases) and more than 36% had elevated lactate dehydrogenase levels, both of which are associated with very poor survival.^{27,28} The eligibility criteria for patients in this

study included HLA-A*0201-positive status, on the basis of the mechanism of action of gp100. However, CTLA-4 blockade by ipilimumab is independent of HLA status, as indicated by efficacy and safety outcomes in earlier clinical trials that were similar between HLA-A*0201-positive and HLA-A*0201-negative patients²¹ (and unpublished data).

In our study, the efficacy of ipilimumab was not improved by the addition of gp100. It is unlikely that this is due to a lack of gp100 expression in the tumors, because differentiation antigens have been shown to be strongly expressed in more than 90% of melanoma tumors, regardless of stage.²⁹ Some studies of adjuvant therapy for melanoma showed that patients who were administered non-gp100 vaccines had shorter survival than did patients in the control groups.^{30,31} In contrast, phase 3 trials showed that in subgroups of patients with melanoma, vaccines had clinical activity when used as either adjuvant therapy or therapy for metastatic disease.^{32,33} Cumulative data show that gp100-based vaccines have immunologic activity, although clinical activity is minimal when gp100 vaccines are administered as monotherapy.²² In a randomized, phase 3 study involving patients with metastatic melanoma, a significant improvement in progression-free survival and response rate, and a nonsignificant improvement in overall survival, were seen with gp100-plus-high-dose interleukin-2, as compared with interleukin-2 alone.²³ Although gp100 appeared to attenuate ipilimumab responses in our study, it is important to consider the fact that some radiographic responses of immunotherapeutic agents are not captured by standard response criteria.³⁴ Regardless, such effects of gp100 did not translate into a difference in overall survival between the two ipilimumab groups.

The data in this study are consistent with the results of phase 2 trials of ipilimumab monotherapy in the same patient population.¹⁵⁻¹⁷ The data from phase 2 studies suggest that there is a long-term survival effect of ipilimumab monotherapy; ipilimumab monotherapy at a dose of 3 mg per kilogram resulted in 1-year and 2-year survival rates of 39.3% and 24.2%, respectively.¹⁶ The long-term effect of ipilimumab in our study is shown by survival analyses at late time points, which showed 1-year and 2-year survival rates of 45.6% and 23.5%, respectively. In recent, randomized, phase 3 trials involving patients with unresectable stage III or IV melanoma who had received previous treatment, 1-year survival rates were reported to be 22% to 38% with various treatment regimens.^{35,36} The median overall survival in these studies ranged from 5.9 to 9.7 months. Neither these nor other randomized, controlled trials had shown a significant improvement in overall survival.

The adverse-event profile of ipilimumab in this study is consistent with that reported in phase 2 trials,¹⁵⁻¹⁷ with the majority of adverse events being immune-related and consistent with the proposed mechanism of action of ipilimumab.¹¹⁻¹⁴ As shown in phase 2 studies, prompt medical attention and early administration of corticosteroids are critical to the management of immune-related adverse events.¹⁵⁻¹⁷ Management guidelines (algorithms) for immune-related adverse events involve close patient follow-up and the administration of high-dose systemic corticosteroids — which were used as necessary in our study — for grade 3 or 4 events.^{37,38}

In conclusion, this randomized, controlled trial showed that there was a significant improvement in overall survival among patients with metastatic melanoma. In some patients, side effects can be life-threatening and may be treatment-limiting. Reinduction with ipilimumab at the time of disease progression can result in further clinical benefit. Overall, our findings suggest that the T-cell potentiator ipilimumab may be useful as a treatment for patients with metastatic melanoma whose disease progressed while they were receiving one or more previous therapies.

Supplementary Material

Refer to Web version on PubMed Central for supplementary material.

Acknowledgments

Supported by Medarex and Bristol-Myers Squibb.

All study sites and institutions received funding from Medarex or Bristol-Myers Squibb to cover the expenses of the investigators for undertaking this trial.

Dr. Hodi reports receiving consulting fees from Bristol-Myers Squibb–Medarex, Novartis, and Genentech; Dr. O’Day, receiving consulting fees, grants, honoraria, and fees for participation in speakers’ bureaus from Bristol-Myers Squibb; Dr. McDermott, receiving consulting fees from Bristol-Myers Squibb–Medarex; Dr. Gonzalez, receiving honoraria from Bristol-Myers Squibb; Dr. Schadendorf, serving on a board for and receiving consulting fees, fees for expert testimony, and fees for participation in speakers’ bureaus from Bristol-Myers Squibb; Dr. van den Eertwegh, receiving consulting fees from and serving on a board for Bristol-Myers Squibb; Dr. Lutzky, receiving consulting fees and honoraria from Bristol-Myers Squibb; Dr. Lorigan, receiving consulting fees from Bristol-Myers Squibb; Dr. Hogg, serving on a board for Bristol-Myers Squibb (pending); Dr. Ottensmeier, receiving honoraria and grant funding from Bristol-Myers Squibb; Dr. Lebbé, serving on a board for Bristol-Myers Squibb; Dr. Wolchok, serving on a board for Bristol-Myers Squibb; Dr. J.S. Weber, receiving consulting fees from Bristol-Myers Squibb; Drs. Tian, Yellin, and Nichol being former employees of Medarex; Dr. Hoos being currently employed by Bristol-Myers Squibb with stock or stock options; and Dr. Urba, receiving consulting fees from Bristol-Myers Squibb–Medarex. No other potential conflicts of interest relevant to this article were reported.

Disclosure forms provided by the authors are available with the full text of this article at NEJM.org

We thank the patients who volunteered to participate in this study and staff members at the study sites who cared for them; the members of the data and safety monitoring committee; and representatives of the sponsors who were involved in data collection and analyses (in particular, Tai-Tsang Chen, Xiaoping Zhu, Marianne Messina, and Helena Brett-Smith). Editorial and writing assistance was provided by Ward A. Pedersen of StemScientific, funded by Bristol-Myers Squibb.

APPENDIX

The authors’ affiliations are as follows: The Dana-Farber Cancer Institute (F.S.H.) and Beth Israel Deaconess Medical Center (D.F.M.) — both in Boston; the Angeles Clinic and Research Institute, Los Angeles (S.J.O.); St. Mary’s Medical Center, San Francisco (R.W.W.); Vanderbilt University Medical Center, Nashville (J.A.S.); Netherlands Cancer Institute (J.B.H.) and VU University Medical Center (A.J.M.E.) — both in Amsterdam; University of Colorado Cancer Center, Aurora (R.G.); Institut Gustave Roussy, Villejuif, France (C.R.); University Hospital Essen, Essen (D.S., J.M.V.), German Cancer Research Center, University of Mannheim, Mannheim (J.C.H.), and Technical University Munich, Munich (C.P.) — all in Germany; Huntsman Cancer Institute, Salt Lake City (W.A.); Mount Sinai Comprehensive Cancer Center, Miami (J.L.); Christie Hospital NHS Trust, Manchester (P.L.), and Southampton University Hospitals, Southampton (C.H.O.) — both in the United Kingdom; Washington University School of Medicine, St. Louis (G.P.L.); Princess Margaret Hospital, Toronto (D.H., I.Q.); Saint Louis Hospital, Paris (C.L.); Loyola University Medical Center, Maywood, IL (J.I.C.); Memorial Sloan-Kettering Cancer Center, New York (J.D.W.); H. Lee Moffitt Cancer Center, Tampa, FL (J.S.W.); Medarex, Bloomsbury, NJ (J.T., M.J.Y., G.M.N.); Bristol-Myers Squibb, Wallingford, CT (A.H.); and the Earle A. Chiles Research Institute, Portland, OR (W.J.U.).

In addition to the authors, the following investigators (listed by country in alphabetical order) participated in the study: Argentina: M. Chacón, L. Koliren, G.L. Lerzo, R.L. Santos — all in Buenos Aires; Belgium: A. Awada (Brussels), V. Cocquyt (Ghent), J. Kerger (Yvoir), J. Thomas (Leuven), T. Velu (Brussels); Brazil: C. Barrios (Porto Alegre), C. Dzik (São Paulo), M. Federico (São Paulo), J. Hohmann (Barretos), M. Liberrati (Londrina), A.

Lima (Santo André), G. Schwartsmann (Porto Alegre), J. Segalla (Jaú); Canada: T. Baetz (Kingston, ON), T. Cheng (Calgary, AB), W. Miller (Montreal), S. Rorke (St. John's, NL), S. Verma (Ottawa), R. Wong (Winnipeg, MB); Chile: H. Harbst (Santiago), P. Gonzalez-Mella (Viña del Mar), P. Salman (Santiago); France: F. Cambazard (Saint-Etienne), O. Dereure (Montpellier), B. Dreno (Nantes), L. Geoffrois (Vandoeuvre-lès-Nancy), J-J. Grob (Marseille), T. Lesimple (Dunkerque), S. Négrier (Lyon), N. Penel (Lille), A. Thyss (Nice); Germany: J.C. Becker (Würzburg), C. Garbe (Tübingen), S. Grabbe (Moln), U. Keilholz (Berlin), C. Loquai (Mainz), H. Naehler (Heidelberg), G. Shuler (Erlangen), U. Trefzer (Berlin), J. Welzel (Augsburg); Hungary: Z. Karolyi (Miskolc); Netherlands: R.L.H. Jansen (Maastricht); South Africa: G.L. Cohen (Pretoria), J.I. Raats (Panorama), D.A. Vorobiof (Morningside); Switzerland: R. Dummer (Zurich), O. Michielin (Lausanne); United Kingdom: J. Barber (Cardiff), S. Danson (Sheffield), M. Gore (London), S. Houston (Surrey), C.G. Kelly (Newcastle-upon-Tyne), M. Middleton (Oxford), P.M. Patel (Nottingham), E. Rankin (Dundee, Scotland); United States: M. Adler (Vista, CA), T. Amatruda (Robbinsdale, MN), A. Amin (Charlotte, NC), C. Anderson (Columbia, MO), L. Blakely (Memphis, TN), E. Borden (Cleveland), S. Burdette-Radoux (Burlington, VT), R. Chapman (Detroit), J. Chesney (Louisville, KY), A. Cohn (Denver), F.A. Collichio (Chapel Hill, NC), G. Daniels (La Jolla, CA), J. Drabick (Hershey, PA), J.A. Figueroa (Lubbock, TX), J. Fleagle (Boulder, CO), J. Goydos (New Brunswick, NJ), N. Haas (Philadelphia), E. Hersh (Tucson, AZ), H.L. Kaufman (New York), K.D. Khan (Indianapolis), A. Khurshid (Arlington, TX), J.M. Kirkwood (Pittsburgh), J.J. Kirshner (East Syracuse, NY), H. Kluger (New Haven, CT), D. Lawrence (Boston), D. Lawson (Atlanta), P.D. Leming (Cincinnati), K. Margolin (Seattle), M. Mastrangelo (Philadelphia), B. Mirtsching (Dallas), W. Paroly (San Diego, CA), A.L. Pecora (Hackensack, NJ), D. Pham (Jacksonville, FL), R. Rangineni (St. Joseph, MO), N. Rothschild (West Palm Beach, FL), W.E. Samlowski (Las Vegas), D. Schwartzenuber (Goshen, IN), M. Scola (Morristown, NJ), W.H. Sharfman (Lutherville, MD), J.J. Stephenson (Greenville, SC), N.S. Tchekmedyan (Long Beach, CA), J. Wade (Decatur, IL), M. Wax (Berkeley Heights, NJ), A. Weeks (Collierville, TN), J.L. Zapas (Baltimore).

REFERENCES

1. American Cancer Society. [Accessed June 4, 2010] Cancer facts & figures 2009. at <http://www.cancer.org/downloads/STT/500809web.pdf>
2. Gray-Schopfer V, Wellbrock C, Marais R. Melanoma biology and new targeted therapy. *Nature*. 2007; 445:851–7. [PubMed: 17314971]
3. Lens MB, Dawes M. Global perspectives of contemporary epidemiological trends of cutaneous malignant melanoma. *Br J Dermatol*. 2004; 150:179–85. [PubMed: 14996086]
4. World Health Organization. Skin cancers. at <http://www.who.int/uv/faq/skincancer/en/index1.html>.
5. Tsao H, Atkins MB, Sober AJ. Management of cutaneous melanoma. *N Engl J Med*. 2004; 351:998–1012. Erratum, *N Engl J Med* 2004;351:2461. [PubMed: 15342808]
6. Agarwala SS. Current systemic therapy for metastatic melanoma. *Expert Rev Anticancer Ther*. 2009; 9:587–95. [PubMed: 19445576]
7. Eggermont AM, Kirkwood JM. Reevaluating the role of dacarbazine in metastatic melanoma: what have we learned in 30 years? *Eur J Cancer*. 2004; 40:1825–36. [PubMed: 15288283]
8. Petrella T, Quirt I, Verma S, Haynes AE, Charette M, Bak K. Single-agent interleukin-2 in the treatment of metastatic melanoma: a systematic review. *Cancer Treat Rev*. 2007; 33:484–96. [PubMed: 17562357]
9. Trinh VA. Current management of metastatic melanoma. *Am J Health Syst Pharm*. 2008; 65(Suppl 9):S3–S8. [PubMed: 19052264]
10. Melero I, Hervas-Stubbs S, Glennie M, Pardoll DM, Chen L. Immunostimulatory monoclonal antibodies for cancer therapy. *Nat Rev Cancer*. 2007; 7:95–106. [PubMed: 17251916]

11. O'Day SJ, Hamid O, Urba WJ. Targeting cytotoxic T-lymphocyte antigen-4 (CTLA-4): a novel strategy for the treatment of melanoma and other malignancies. *Cancer*. 2007; 110:2614–27. [PubMed: 18000991]
12. Fong L, Small EJ. Anti-cytotoxic T-lymphocyte antigen-4 antibody: the first in an emerging class of immunomodulatory antibodies for cancer treatment. *J Clin Oncol*. 2008; 26:5275–83. [PubMed: 18838703]
13. Robert C, Ghiringhelli F. What is the role of cytotoxic T lymphocyte-associated antigen 4 blockade in patients with metastatic melanoma? *Oncologist*. 2009; 14:848–61. [PubMed: 19648604]
14. Weber J. Ipilimumab: controversies in its development, utility and autoimmune adverse events. *Cancer Immunol Immunother*. 2009; 58:823–30. [PubMed: 19198837]
15. Weber J, Thompson JA, Hamid O, et al. A randomized, double-blind, placebo-controlled, phase II study comparing the tolerability and efficacy of ipilimumab administered with or without prophylactic budesonide in patients with unresectable stage III or IV melanoma. *Clin Cancer Res*. 2009; 15:5591–8. [PubMed: 19671877]
16. Wolchok JD, Neyns B, Linette G, et al. Ipilimumab monotherapy in patients with pretreated advanced melanoma: a randomised, double-blind, multicentre, phase 2, dose-ranging study. *Lancet Oncol*. 2010; 11:155–64. [PubMed: 20004617]
17. O'Day SJ, Maio M, Chiarioti-Silene V, et al. Efficacy and safety of ipilimumab monotherapy in patients with previously treated, advanced melanoma: a multicenter, single-arm phase II study. *Ann Oncol*. Feb 10.2010 Epub ahead of print.
18. Maker AV, Phan GQ, Attia P, et al. Tumor regression and autoimmunity in patients treated with cytotoxic T lymphocyte-associated antigen 4 blockade and interleukin 2: a phase I/II study. *Ann Surg Oncol*. 2005; 12:1005–16. [PubMed: 16283570]
19. Agarwala SS. Novel immunotherapies as potential therapeutic partners for traditional or targeted agents: cytotoxic T-lymphocyte antigen-4 blockade in advanced melanoma. *Melanoma Res*. 2010; 20:1–10. [PubMed: 19952852]
20. Attia P, Phan GQ, Maker AV, et al. Autoimmunity correlates with tumor regression in patients with metastatic melanoma treated with anti-cytotoxic T-lymphocyte antigen-4. *J Clin Oncol*. 2005; 23:6043–53. [PubMed: 16087944]
21. Downey SG, Klapper JA, Smith FO, et al. Prognostic factors related to clinical response in patients with metastatic melanoma treated by CTL-associated antigen-4 blockade. *Clin Cancer Res*. 2007; 13:6681–8. [PubMed: 17982122]
22. Rosenberg SA, Yang JC, Restifo NP. Cancer immunotherapy: moving beyond current vaccines. *Nat Med*. 2004; 10:909–15. [PubMed: 15340416]
23. Schwartzentruber DJ, Lawson D, Richards J, et al. A phase III multi-institutional randomized study of immunization with the gp100:209–217(210M) peptide followed by high-dose IL-2 compared with high-dose IL-2 alone in patients with metastatic melanoma. *J Clin Oncol*. 2009; 27(Suppl): 463s. abstract.
24. Oken MM, Creech RH, Tormey DC, et al. Toxicity and response criteria of the Eastern Cooperative Oncology Group. *Am J Clin Oncol*. 1982; 5:649–55. [PubMed: 7165009]
25. [Accessed June 4, 2010] Dacarbazine and ipilimumab vs. dacarbazine with placebo in untreated unresectable stage III or IV melanoma. [ClinicalTrials.gov at <http://www.clinicaltrials.gov/ct/show/NCT00324155>](http://www.clinicaltrials.gov/ct/show/NCT00324155)
26. James K, Eisenhauer E, Christian M, et al. Measuring response in solid tumors: unidimensional versus bidimensional measurement. *J Natl Cancer Inst*. 1999; 91:523–8. [PubMed: 10088622]
27. Korn EL, Liu PY, Lee SJ, et al. Meta-analysis of phase II cooperative group trials in metastatic stage IV melanoma to determine progression-free and overall survival benchmarks for future phase II trials. *J Clin Oncol*. 2008; 26:527–34. [PubMed: 18235113]
28. Bedikian AY, Johnson MM, Warneke CL, et al. Prognostic factors that determine the long-term survival of patients with unresectable metastatic melanoma. *Cancer Invest*. 2008; 26:624–33. [PubMed: 18584354]
29. Barrow C, Browning J, MacGregor D, et al. Tumor antigen expression in melanoma varies according to antigen and stage. *Clin Cancer Res*. 2006; 12:764–71. [PubMed: 16467087]

30. Morton DL, Mozzillo N, Thompson JF, et al. An international, randomized, phase III trial of bacillus Calmette-Guerin (BCG) plus allogeneic melanoma vaccine (MCV) or placebo after complete resection of melanoma metastatic to regional or distant sites. *J Clin Oncol.* 2007; 25(Suppl):474s. abstract.
31. Eggermont AM, Suciu S, Ruka W, et al. EORTC 18961: post-operative adjuvant ganglioside GM2-KLH21 vaccination treatment vs observation in stage II (T3-T4N0M0) melanoma: 2nd interim analysis led to an early disclosure of the results. *J Clin Oncol.* 2008; 26(Suppl):484s. abstract.
32. Testori A, Richards J, Whitman E, et al. Phase III comparison of vitespen, an autologous tumor-derived heat shock protein gp96 peptide complex vaccine, with physician's choice of treatment for stage IV melanoma. *J Clin Oncol.* 2008; 26:955–62. [PubMed: 18281670]
33. Sosman JA, Unger JM, Liu PY, et al. Adjuvant immunotherapy of resected, intermediate-thickness, node-negative melanoma with an allogeneic tumor vaccine: impact of HLA class I antigen expression on outcome. *J Clin Oncol.* 2002; 20:2067–75. [PubMed: 11956267]
34. Wolchok JD, Hoos A, O'Day S, et al. Guidelines for the evaluation of immune therapy activity in solid tumors: immune-related response criteria. *Clin Cancer Res.* 2009; 15:7412–20. [PubMed: 19934295]
35. Eisen T, Trefzer U, Hamilton A, et al. Results of a multicenter, randomized, double-blind phase 2/3 study of lenalidomide in the treatment of pretreated relapsed or refractory metastatic malignant melanoma. *Cancer.* 2010; 116:146–54. [PubMed: 19862820]
36. Hauschild A, Agarwala SS, Trefzer U, et al. Results of a phase III, randomized, placebo-controlled study of sorafenib in combination with carboplatin and paclitaxel as second-line treatment in patients with unresectable stage III or stage IV melanoma. *J Clin Oncol.* 2009; 27:2823–30. [PubMed: 19349552]
37. Weber J. Anti-CTLA-4 antibody ipilimumab: case studies of clinical response and immune-related adverse events. *Oncologist.* 2007; 12:864–72. [PubMed: 17673617]
38. Lin R, Yellin MJ, Lowy I, Safferman A, Chin K, Ibrahim R. An analysis of the effectiveness of specific guidelines for the management of ipilimumab-mediated diarrhea/colitis: prevention of gastrointestinal perforation and/or colectomy. *J Clin Oncol.* 2008; 26(Suppl):497s. abstract.

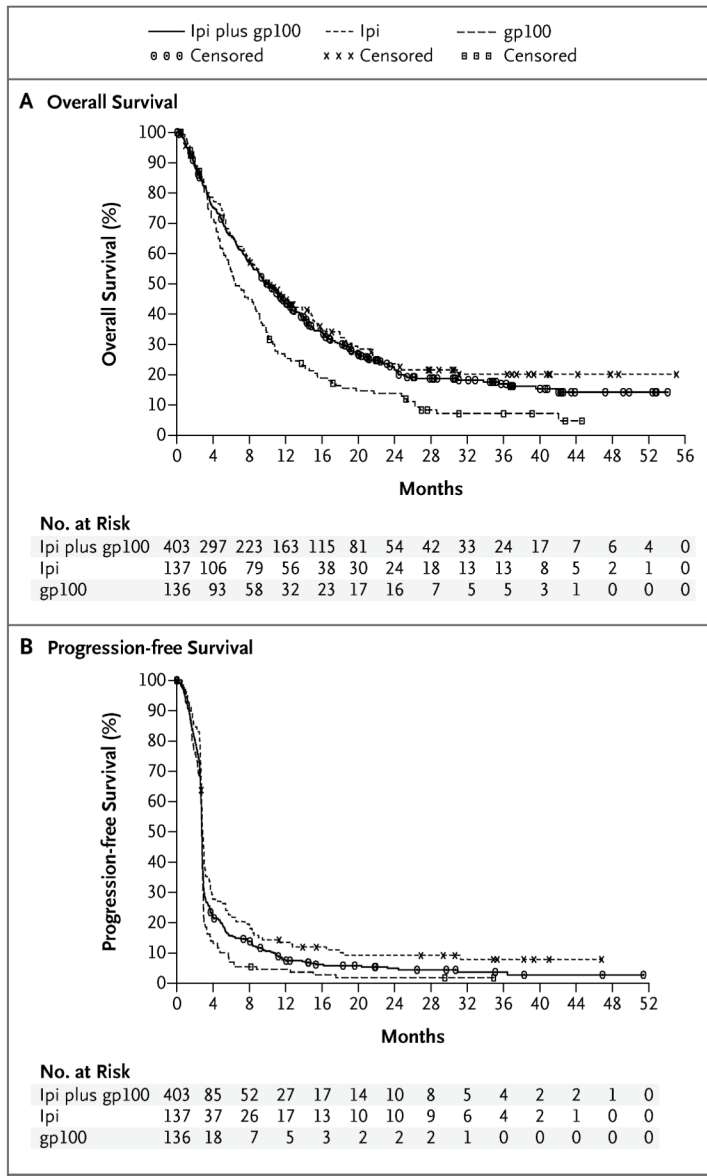
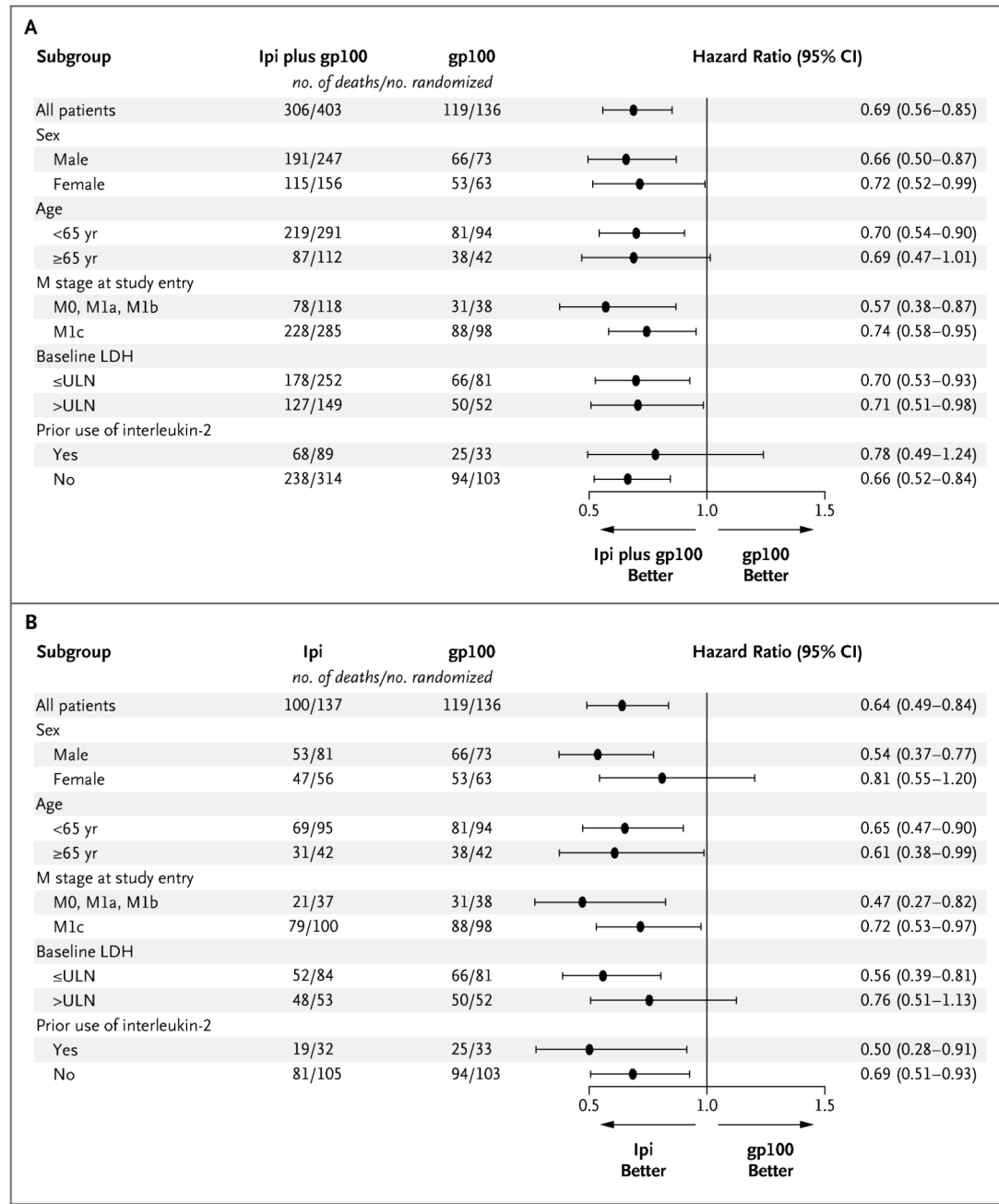


Figure 1. Kaplan-Meier Curves for Overall Survival and Progression-free Survival in the Intention-to-Treat Population

The median follow-up for overall survival (Panel A) in the ipilimumab (Ipi)-plus-glycoprotein 100 (gp100) group was 21.0 months, and the median overall survival was 10.0 months (95% CI, 8.5 to 11.5); in the ipilimumab-alone group, the median follow-up was 27.8 months, and the median overall survival, 10.1 months (95% CI, 8.0 to 13.8); and in the gp100-alone group, the median follow-up was 17.2 months, and the median overall survival, 6.4 months (95% CI, 5.5 to 8.7). The median progression-free survival (Panel B) was 2.76 months (95% CI, 2.73 to 2.79) in the ipilimumab-plus-gp100 group, 2.86 months (95% CI, 2.76 to 3.02) in the ipilimumab-alone group, and 2.76 months (95% CI, 2.73 to 2.83) in the gp100-alone group. The rates of progression-free survival at week 12 were 49.1% (95% CI, 44.1 to 53.9) in the ipilimumab-plus-gp100 group, 57.7% (95% CI, 48.9 to 65.5) in the ipilimumab-alone group, and 48.5% (95% CI, 39.6 to 56.7) in the gp100-alone group.

**Figure 2. Subgroup Analyses of Overall Survival**

The prespecified analyses of overall survival among subgroups of patients, as defined by baseline demographic characteristics and stratification factors (metastasis [M] stage, classified according to the tumor–node–metastasis [TNM] categorization for melanoma of the American Joint Committee on Cancer; and receipt or nonreceipt of interleukin-2 therapy), showed that hazard ratios were lower than 1 (indicating a lower risk of death) for each subgroup in the ipilimumab (Ipi)-plus-glycoprotein 100 (gp100) group as compared with the gp100-alone group (Panel A) and for each subgroup in the ipilimumab-alone group as compared with the gp100-alone group (Panel B). Hazard ratios were estimated with the use of unstratified Cox proportional-hazards models. Horizontal lines represent 95%

confidence intervals. LDH denotes lactate dehydrogenase, and ULN the upper limit of the normal range.

\$watermark-text

\$watermark-text

\$watermark-text

Table 1
Baseline Characteristics of the Patients[★]

Variable	Ipilimumab plus gp100 (N = 403)	Ipilimumab Alone (N = 137)	gp100 Alone (N = 136)	Total (N = 676)
Mean age — yr	55.6	56.8	57.4	56.2
Sex — no. (%)				
Male	247 (61.3)	81 (59.1)	73 (53.7)	401 (59.3)
Female	156 (38.7)	56 (40.9)	63 (46.3)	275 (40.7)
ECOG performance status — no. (%) [†]				
0	232 (57.6)	72 (52.6)	70 (51.5)	374 (55.3)
1	166 (41.2)	64 (46.7)	61 (44.9)	291 (43.0)
2	4 (1.0)	1 (0.7)	4 (2.9)	9 (1.3)
3	1 (0.2)	0	0	1 (0.1)
Unknown	0	0	1 (0.7)	1 (0.1)
M stage — no. (%) [‡]				
M0	5 (1.2)	1 (0.7)	4 (2.9)	10 (1.5)
M1a	37 (9.2)	14 (10.2)	11 (8.1)	62 (9.2)
M1b	76 (18.9)	22 (16.1)	23 (16.9)	121 (17.9)
M1c	285 (70.7)	100 (73.0)	98 (72.1)	483 (71.4)
Lactate dehydrogenase level — no. (%)				
≤Upper limit of the normal range	252 (62.5)	84 (61.3)	81 (59.6)	417 (61.7)
>Upper limit of the normal range	149 (37.0)	53 (38.7)	52 (38.2)	254 (37.6)
Unknown	2 (0.5)	0	3 (2.2)	5 (0.7)
CNS metastases at baseline — no. (%)	46 (11.4)	15 (10.9)	21 (15.4)	82 (12.1)
Received study drug	42 (10.4)	15 (10.9)	20 (14.7)	77 (11.4)
Had had previous treatment for CNS metastases	39 (9.7)	15 (10.9)	19 (14.0)	73 (10.8)
Previous systemic therapy for metastatic disease — no. (%)	403 (100.0)	137 (100.0)	136 (100.0)	676 (100.0)
Previous interleukin-2 therapy — no. (%)	89 (22.1)	32 (23.4)	33 (24.3)	154 (22.8)

[★]Percentages may not total 100 because of rounding. CNS denotes central nervous system.

[†]The Eastern Cooperative Oncology Group (ECOG) status ranges from 0 to 5, with higher scores indicating greater impairment (5 indicates death).

[‡]The metastasis (M) stage was classified according to the tumor–node–metastasis (TNM) categorization for melanoma of the American Joint Committee on Cancer.

Table 2
Best Response to Treatment and Time-to-Event Data[†]

Response and Time to Event	Ipilimumab plus gp100 (N = 403)	Ipilimumab Alone (N = 137)	gp100 Alone (N = 136)
Overall survival			
Total no. of deaths	306	100	119
Comparison with gp100 alone			
Hazard ratio (95% CI)	0.68 (0.55–0.85)	0.66 (0.51–0.87)	—
P value by log-rank test	<0.001	0.003	—
Comparison with ipilimumab alone			
Hazard ratio (95% CI)	1.04 (0.83–1.30)	—	—
P value by log-rank test	0.76	—	—
Evaluation of therapy			
Induction			
Best overall response — no. (%)			
Complete response	1 (0.2)	2 (1.5)	0
Partial response	22 (5.5)	13 (9.5)	2 (1.5)
Stable disease	58 (14.4)	24 (17.5)	13 (9.6)
Progressive disease	239 (59.3)	70 (51.1)	89 (65.4)
Not evaluated	83 (20.6)	28 (20.4)	32 (23.5)
Best overall response rate — % (95% CI)	5.7 (3.7–8.4)	10.9 (6.3–17.4)	1.5 (0.2–5.2)
P value for comparison with gp100 alone	0.04	0.001	—
P value for comparison with ipilimumab alone	0.04	—	—
Disease control rate — % (95% CI) [‡]	20.1 (16.3–24.3)	28.5 (21.1–36.8)	11.0 (6.3–17.5)
P value for comparison with gp100 alone	0.02	<0.001	—
P value for comparison with ipilimumab alone	0.04	—	—
Time to event — mo			
Time to progression — median (95% CI)	2.76 (2.73–2.79)	2.86 (2.76–3.02)	2.76 (2.73–2.83)
Time to response — mean (95% CI)	3.32 (2.91–3.74)	3.18 (2.75–3.60)	2.74 (2.12–3.37)
Duration of response — median (95% CI)	11.5 (5.4–NR)	NR (28.1–NR)	NR (2.0–NR)
Reinduction [‡]			
Best overall response — no./total no. (%)			
Complete response	0	1/8 (12.5)	0
Partial response	3/23 (13.0)	2/8 (25.0)	0
Stable disease	12/23 (52.2)	3/8 (37.5)	0
Progressive disease	8/23 (34.8)	2/8 (25.0)	1/1 (100.0)

[†]Of the 143 patients who could not be evaluated for a response, 33 patients did not receive any study drug and 110 patients did not have baseline or week-12 tumor assessments (or both). Percentages may not total 100 because of rounding. NR denotes not reached.

[‡]The disease control rate is the percentage of patients with a partial or complete response or stable disease.

[‡]A total of 40 patients (29 in the ipilimumab-plus-gp100 group; 9 in the ipilimumab-alone group, and 2 in the gp100-alone group) were given reinduction therapy, but 8 were not included in the efficacy analyses: 3 had major protocol violations and 5 were not eligible owing to the fact that they had had a best overall response of progressive disease during induction and were given reinduction therapy inadvertently.

Adverse Events in the Safety Population*

Table 3

Adverse Event	Ipilimumab plus gp100 (N = 380)			Ipilimumab Alone (N = 131)			gp100 Alone (N = 132)		
	Total	Grade 3	Grade 4	Total	Grade 3	Grade 4	Total	Grade 3	Grade 4
<i>number of patients (percent)</i>									
Any event	374 (98.4)	147 (38.7)	26 (6.8)	127 (96.9)	49 (37.4)	11 (8.4)	128 (97.0)	54 (40.9)	8 (6.1)
Any drug-related event	338 (88.9)	62 (16.3)	4 (1.1)	105 (80.2)	25 (19.1)	5 (3.8)	104 (78.8)	15 (11.4)	0
<i>n</i>									
Gastrointestinal disorders									
Diarrhea	146 (38.4)	16 (4.2)	1 (0.3)	43 (32.8)	7 (5.3)	0	26 (19.7)	1 (0.8)	0
Nausea	129 (33.9)	5 (1.3)	1 (0.3)	46 (35.1)	3 (2.3)	0	52 (39.4)	3 (2.3)	0
Constipation	81 (21.3)	3 (0.8)	0	27 (20.6)	3 (2.3)	0	34 (25.8)	1 (0.8)	0
Vomiting	75 (19.7)	6 (1.6)	1 (0.3)	31 (23.7)	3 (2.3)	0	29 (22.0)	3 (2.3)	0
Abdominal pain	67 (17.6)	6 (1.6)	0	20 (15.3)	2 (1.5)	0	22 (16.7)	6 (4.5)	1 (0.8)
Other									
Fatigue	137 (36.1)	19 (5.0)	0	55 (42.0)	9 (6.9)	0	41 (31.1)	4 (3.0)	0
Decreased appetite	88 (23.2)	5 (1.3)	1 (0.3)	35 (26.7)	2 (1.5)	0	29 (22.0)	3 (2.3)	1 (0.8)
Pyrexia	78 (20.5)	2 (0.5)	0	16 (12.2)	0	0	23 (17.4)	2 (1.5)	0
Headache	65 (17.1)	4 (1.1)	0	19 (14.5)	3 (2.3)	0	19 (14.4)	3 (2.3)	0
Cough	55 (14.5)	1 (0.3)	0	21 (16.0)	0	0	18 (13.6)	0	0
Dyspnea	46 (12.1)	12 (3.2)	2 (0.5)	19 (14.5)	4 (3.1)	1 (0.8)	25 (18.9)	6 (4.5)	0
Anemia	41 (10.8)	11 (2.9)	0	15 (11.5)	4 (3.1)	0	23 (17.4)	11 (8.3)	0
Any immune-related event									
221 (58.2)	37 (9.7)	2 (0.5)	80 (61.1)	16 (12.2)	3 (2.3)	42 (31.8)	4 (3.0)	0	
Dermatologic									
Pruritus	152 (40.0)	8 (2.1)	1 (0.3)	57 (43.5)	2 (1.5)	0	22 (16.7)	0	0
Rash	67 (17.6)	1 (0.3)	0	32 (24.4)	0	0	14 (10.6)	0	0
Vitiligo	67 (17.6)	5 (1.3)	0	25 (19.1)	1 (0.8)	0	6 (4.5)	0	0
Gastrointestinal									
Diarrhea	122 (32.1)	20 (5.3)	2 (0.5)	38 (29.0)	10 (7.6)	0	19 (14.4)	1 (0.8)	0
Colitis	115 (30.3)	14 (3.7)	0	36 (27.5)	6 (4.6)	0	18 (13.6)	1 (0.8)	0
Endocrine									
Hypothyroidism	20 (5.3)	11 (2.9)	1 (0.3)	10 (7.6)	7 (5.3)	0	1 (0.8)	0	0
Hypopituitarism	3 (0.8)	2 (0.5)	0	3 (2.3)	1 (0.8)	1 (0.8)	0	0	0

Adverse Event	Ipilimumab plus gp100 (N = 380)			Ipilimumab Alone (N = 131)			gp100 Alone (N = 132)		
	Total	Grade 3	Grade 4	Total	Grade 3	Grade 4	Total	Grade 3	Grade 4
Hypophysitis	2 (0.5)	2 (0.5)	0	2 (1.5)	2 (1.5)	0	0	0	0
Adrenal insufficiency	3 (0.8)	2 (0.5)	0	2 (1.5)	0	0	0	0	0
Increase in serum thyrotropin level	2 (0.5)	0	0	1 (0.8)	0	0	0	0	0
Decrease in serum corticotropin level	0	0	0	2 (1.5)	0	1 (0.8)	0	0	0
Hepatic	8 (2.1)	4 (1.1)	0	5 (3.8)	0	0	6 (4.5)	3 (2.3)	0
Increase in alanine aminotransferase	3 (0.8)	2 (0.5)	0	2 (1.5)	0	0	3 (2.3)	0	0
Increase in aspartate aminotransferase	4(1.1)	1 (0.3)	0	1 (0.8)	0	0	2 (1.5)	0	0
Hepatitis	2 (0.5)	1 (0.3)	0	1 (0.8)	0	0	0	0	0
Other	12 (3.2)	5 (1.3)	0	6 (4.6)	2 (1.5)	1 (0.8)	3 (2.3)	1 (0.8)	0

*The adverse events listed here were reported in at least 15% of patients. The most common immune-related adverse events and those of particular clinical relevance are also listed. Patients could have more than one adverse event. Included are all patients who received at least one dose of a study drug (643 patients). A total of 14 deaths (2.2%) were determined by the investigators to be related to the study drug (8 in the ipilimumab-plus-gp100 group, 4 in the ipilimumab-alone group, and 2 in the gp100-alone group). Seven of the 14 deaths related to the study drug were associated with immune-related adverse events: 5 in the ipilimumab-plus-gp100 group (1 patient had grade 3 colitis and septicemia; 3 patients had bowel perforation–inflammatory colitis, bowel perforation, or multorgan failure–peritonitis; and 1 patient had Guillain–Barré syndrome, which is considered to be consistent with a neurologic immune-related adverse event) and 2 in the ipilimumab-alone group (1 patient had colic bowel perforation and the other had liver failure). Deaths related to the study drug that were not associated with immune-related adverse events included deaths from sepsis, myelofibrosis, and acute respiratory distress syndrome (3 patients in the ipilimumab-plus-gp100 group); severe infection–renal failure–septic shock, and vascular leak syndrome (2 patients in the ipilimumab-alone group), and cachexia and septic shock (2 patients in the gp100-alone group).



Tailor the adaptive immune response with
Vaccine Adjuvants



This information is current as of January 17, 2018.

Hitting the Target: How T Cells Detect and Eliminate Tumors

Anthony E. Zamora, Jeremy Chase Crawford and Paul G. Thomas

J Immunol 2018; 200:392-399; ;
doi: 10.4049/jimmunol.1701413
<http://www.jimmunol.org/content/200/2/392>

Why *The JI*?

- **Rapid Reviews!** 30 days* from submission to initial decision
- **No Triage!** Every submission reviewed by practicing scientists
- **Speedy Publication!** 4 weeks from acceptance to publication

*average

References This article **cites 74 articles**, 37 of which you can access for free at:
<http://www.jimmunol.org/content/200/2/392.full#ref-list-1>

Subscription Information about subscribing to *The Journal of Immunology* is online at:
<http://jimmunol.org/subscription>

Permissions Submit copyright permission requests at:
<http://www.aai.org/About/Publications/JI/copyright.html>

Email Alerts Receive free email-alerts when new articles cite this article. Sign up at:
<http://jimmunol.org/alerts>



Hitting the Target: How T Cells Detect and Eliminate Tumors

Anthony E. Zamora, Jeremy Chase Crawford, and Paul G. Thomas

The successes of antitumor immuno-based therapies and the application of next-generation sequencing to mutation profiling have produced insights into the specific targets of antitumor T cells. Mutated proteins have tremendous potential as targets for interventions using autologous T cells or engineered cell therapies and may serve as important correlates of efficacy for immunoregulatory interventions including immune checkpoint blockade. As mutated self, tumors present an exceptional case for host immunity, which has primarily evolved in response to foreign pathogens. Tumor Ags' resemblance to self may limit immune recognition, but key features appear to be the same between antipathogen and antitumor responses. Determining which targets will make efficacious Ags and which responses might be elicited therapeutically are key questions for the field. Here we discuss current knowledge on antitumor specificity, the mutations that provide immunogenic targets, and how cross-reactivity and immunodominance may contribute to variation in immune responses among tumor types. *The Journal of Immunology*, 2018, 200: 392–399.

CD8 and CD4 $\alpha\beta$ T cells recognize peptides in the context of class I and class II MHC, respectively. Viral immunologists have defined peptide MHC (pMHC) epitopes from numerous pathogens, prompting the emergence of a set of central principles that span infectious models. First, self-epitopes are distinguished from pathogenic epitopes at least in part by the mechanism of central tolerance, where TCRs strongly reactive to self-epitopes are deleted in the thymus by the process of negative selection (although self-reactive T cells do emerge in the periphery). Second, despite a potentially vast number of peptides that could be recognized by the T cell repertoire of the host, only a small portion of the overall viral proteome is sampled to produce the targets of host immunity. Third, individuals that share the same MHC will reliably produce similar response magnitudes to the same epitopes from the same pathogens. These consistent, structured

profiles of immune response, termed immunodominance hierarchies, are regulated by numerous factors, including the extent of peptide presentation in the MHC, the kinetics of pMHC decay, and the nature of the corresponding TCR repertoire.

Because of central tolerance, only limited features of the tumor proteome should be accessible for immune recognition. When approaching the synapse between the human immune system and cancer, the importance of specificity can be viewed from both an immune- and tumor-centric perspective. Immunological specificity has been shaped evolutionarily by foreign pathogens resulting in a system normally capable of discerning self from nonself with a great deal of precision. In the context of cancer, however, the immune system is presented with an evolutionary conundrum: although safeguards such as immunological tolerance help prevent aberrant responses to self-antigens by T cells, they may also limit the diversity, repertoire, and function of tumor-reactive immune cells. This realization has resulted in an ongoing search for the holy grail of cancer: an antigenic target that is simultaneously abundant in cancerous cells and absent in normal tissues. The following sections and Table I describe the three broad categories of tumor Ags—tumor-associated Ags (TAAs), cancer-germline or cancer/testis Ags (CTAs), and tumor-specific Ags (TSAs)—and include a discussion on the specificity of these Ags and the extent to which each is shared among patients and/or specific cancer types.

Ags with low tumor specificity

Tumor-associated Ags. Of all the tumor Ags studied to date, among the best characterized and earliest targets for cancer vaccine approaches are the TAAs. TAAs are normal host proteins that demonstrate distinct expression profiles between host and tumor cells. In general, the dysregulation of gene pathways as a result of mutations within the tumor cells results in the atypical expression of unmutated proteins that would otherwise be expressed at relatively lower levels, or not at all, in normal cells of that tissue type in its current developmental state. Specifically, TAAs are composed of what have been termed differentiation Ags, which are proteins that are shared between the tumor and the normal tissue of origin but distinct from other tissues, and overexpressed Ags, which are

Department of Immunology, St. Jude Children's Research Hospital, Memphis, TN 38105

ORCIDs: 0000-0001-5712-5339 (A.E.Z.); 0000-0003-4096-6048 (J.C.C.); 0000-0001-7955-0256 (P.G.T.).

Received for publication October 10, 2017. Accepted for publication November 16, 2017.

This work was supported by Cancer Center Support Grants P30CA021765 and R01AI107625 and by the American Lebanese Syrian Associated Charities.

Address correspondence and reprint requests to Dr. Paul G. Thomas, St. Jude Children's Research Hospital, MS 351, 262 Danny Thomas Place, Memphis, TN 38105. E-mail address: Paul.Thomas@stjude.org

Abbreviations used in this article: CAR, chimeric Ag receptor; CTA, cancer/testis Ag; ICB, immune checkpoint blockade; pMHC, peptide MHC; TAA, tumor-associated Ag; TIL, tumor-infiltrating lymphocyte; TSA, tumor-specific Ag.

Copyright © 2018 by The American Association of Immunologists, Inc. 0022-1767/18/\$35.00

Table I. Types of tumor Ags and their advantages and disadvantages as therapeutic targets

Class of Tumor Ag	Description of Ag	Examples of Ag Type	Advantages of Targeting	Disadvantages of Targeting
Ags with low specificity	Differentiation Ag	Associated with proteins displaying a cell lineage-specific pattern of expression or present during specific developmental stages.	CD19, MART-1, gp100, TRP2, CEA	Antigenic targets shared between patients Development of off-the-shelf treatments
	Overexpressed Ag	Normal cellular proteins expressed in greater abundance in cancerous cells.	WT1, ERBB2, PRAME, RAGE-1, mesothelin	Antigenic targets shared between patients Development of off-the-shelf treatments
Ags with high specificity	Mutated Ag	Gene mutations resulting in the expression of new peptides (from point mutations, altering the phase of a gene's reading frame, or chromosomal translocations).	CDK4, KRAS, BRCA1/2, p53, TGF- β RII	Decreased likelihood of on-target, off-tumor toxicity Potential sharing of driver/fusion mutations between patients with the same cancer type
Oncogenic viral Ag	Abnormal proteins expressed by cells infected with oncoviruses that can be at the origin of several types of cancers.	HPV E6/E7, EBV EBNA1/LMP1/LMP2	Viral Ags shared between patients with cancers with viral etiology Development of off-the-shelf treatments	Relatively low frequency of cancer types with known viral etiology
Cancer/testis (germline) Ag	Expressed in testes, fetal ovaries, or trophoblasts, but absent in healthy somatic cells. Selectively expressed by specific types of cancer.	MAGE, BAGE, GAGE, NY-ESO-1	Antigenic targets shared between patients with the same cancer type Development of off-the-shelf treatments	Are not ubiquitously expressed across cancer types Potential for unanticipated on-target, off-tumor toxicity

The spectrum of tumor Ags, including those with low and high specificity for the tumor, is described, with specific examples of each type and the features that contribute to their therapeutic efficacy.

HPV, human papillomavirus.

aberrantly expressed normal proteins that provide a growth and/or survival advantage to the tumors.

Differentiation Ags. Much of the interest in differentiation Ags as potential targets of the immune system and therapeutic approaches stems from studies on melanoma, where researchers have documented spontaneous T cell responses against peptides derived from GP100 (1–4), Melan-A/MART-1 (5, 6), and tyrosinase (7, 8). Although these responses have been observed in patients with melanoma due to the Ag expression patterns on melanoma cells, the potential to treat a wide range of patients continues to drive new research focused on specifically targeting cancerous cells that aberrantly express differentiation Ags. CD19 is another such differentiation Ag, in this case found on normal and malignant B cells, that can be targeted in patients with acute lymphoblastic leukemia and other B cell tumors (reviewed in Ref. 9). Recently, adoptive transfer of anti-CD19 chimeric Ag receptor (CAR) T cells in patients with relapsed and refractory acute lymphoblastic leukemia has shown high rates (up to 90%) of complete remission in part due to the strength and antitumor activity of this immunotherapy (9). Despite the demonstrable sensitivity of anti-CD19 therapies in clearing B cell malignancies, the specificity of such approaches is expected to include noncancerous cells as well due to the near ubiquity of CD19 expression among B cells throughout their development. Many promising differentiation Ags may therefore exhibit off-target antigenicity, the consequences of which can range from temporary loss of inessential cells to the permanent destruction of vital tissues that may require secondary treatment or ongoing supplementation. Therefore, the most ideal differentiation Ags are those derived from proteins that would normally only be expressed during early ontogeny.

Overexpressed Ags. Overexpressed Ags are another class of TAAs that have been shown to play a role in driving the malignant phenotype of many tumors. In leukemic cells, Wilms tumor 1 is commonly overexpressed and helps drive the oncogenic process (10, 11). In several epithelial tumors, such as breast and ovarian cancer, overexpression of ERBB2 (HER2/NEU) is typically associated with poor prognoses, but this protein may also serve as a potential immunotherapy target because of its increased expression on the surface of cancerous cells that exhibit heightened proliferation (12, 13).

Much of the early interest in targeting TAAs is owed to the sharing of Ags among patients and across various types of cancer, which allows for broadly administrable, off-the-shelf treatments. However, a major limitation in targeting TAAs results from their similarity to self-peptides, which greatly limits endogenous T cell responses due to central tolerance or lower TCR-pMHC binding affinity compared with those associated with recognition of foreign Ags (14). Findings from several recent studies also caution against using adoptive transfer or receptor engineering approaches against TAAs, as previous efforts have resulted in unexpected on-target, off-tumor toxicities, as described in the unfortunate case of a patient with metastatic colon cancer who was treated with CAR T cells against ERBB2 and died as a result of off-tumor effects acting on lung epithelial cells that expressed low levels of ERBB2 (15).

Ags with high tumor specificity

Cancer/testis Ags. Van der Bruggen et al. (16) identified the first human tumor Ag, MAGE-1, a CTA recognized by endogenous T cells. CTAs are expressed in testes, fetal ovaries, or trophoblasts, but are otherwise absent in healthy somatic cells. Since this study

in the early 1990s (16), an increased focus on specificity, and by extension the realization that a more in-depth characterization of Ag localization would be useful, resulted in increased efforts to target CTAs. The attractiveness in targeting CTAs can, in part, be attributed to: 1) their disrupted gene regulation in various tumor types, 2) their limited expression in normal tissues, 3) their lack of presentation in germline and trophoblastic cells, which do not display MHC class I molecules on their surface, and 4) their immunogenic potential. Although vaccine and adoptive cell therapies targeting CTAs have shown promise in some clinical trials with NY-ESO-1 (17) and MAGE (18), a recent attempt to use adoptive cell therapies to target MAGE-A3 led to severe toxicities and even death as a result of unanticipated expression of this gene in the brain (18).

Tumor-specific Ags. TSAs generally arise from tumor-specific mutations, which result in the exclusive expression of neoantigens in tumors and, by definition, their absence in normal cells. However, another source of TSAs that have been shown to elicit tumor recognition by T cells are the viral proteins expressed by cells infected with oncoviruses such as human papillomavirus (19, 20) and EBV (21). In either case, the cancer-restricted expression intrinsic to TSAs theoretically plays into the immune system's strength of distinguishing self from nonself by bypassing the mechanisms that would otherwise eliminate the tumor-reactive T cells that bind self-pMHC with high affinity. Support for the notion that neoantigens are sufficiently dissimilar to self to be targetable by the immune system was shown in two seminal human studies in 2005 (22, 23). In a study by Robbins and colleagues (23), ex vivo-expanded tumor infiltrating lymphocytes (TILs) were adoptively transferred into a patient with melanoma. In addition to the complete regression of the tumor, the patient also exhibited persistent T cell populations that recognized mutated GAS7 and GAPDH. Wölfel and colleagues (22), on the other hand, used cDNA library screens to show that autologous T cells (using clonal T cells and mixed lymphocyte tumor cell cultures) had greater responses against neoantigens than TAAs in human melanoma. This early work, in addition to the recent advancements in next-generation sequencing applications and epitope prediction algorithms, has resulted in a major shift toward the utilization of personalized immunotherapies to selectively target TSAs.

The efforts to exploit TSAs as therapeutic targets and to characterize responses in patients undergoing immune checkpoint blockade (ICB) therapy has led to in-depth mapping of TSA-specific T cells in a number of studies. One finding that has consistently emerged, particularly from studies of melanoma, is that relatively few putative neoepitopes generate a detectable T cell response (24). "Hit rates" of finding a tetramer positive or peptide-reactive T cell population in patients have been as low as 0.5–2% of screened Ags. For example, in one study a patient had 249 non-synonymous mutations in a melanoma, of which 126 were predicted to bind to HLA-A*0201. Screening these neoantigens against the patient's own TILs resulted in a response to 2 of the 126 putative neoantigens. However, T cell responses were generated to a much larger proportion of these peptides in in vitro cultures of PBMCs from healthy donors (25). In another study on melanoma, researchers generated 75 tetramers corresponding to potential epitopes mapped to

the patient's tumor, yet only one T cell response was detected (26).

There are multiple potential explanations as to why so few of the potential neoepitopes in a tumor elicit a T cell response, including that the predicted neoepitopes may not actually be processed and presented on the tumor. Some studies have addressed this by experimentally validating that the predicted peptides can bind the predicted HLA molecule (27). In a study screening a patient with chronic lymphocytic leukemia with this method, where 18 candidate neoepitope peptides were experimentally confirmed to bind HLA, only one neoepitope elicited a detectable response. Beyond an "overestimate" of available neoepitopes, it is also possible that nonresponsiveness to particular neoepitopes may result from constraints on the available repertoire that arise due to similarity to self (although, as discussed below, this seems likely to have a modest effect on limiting responses). An implication of this low response rate, though, is the concern that low mutation burden tumors, including many pediatric tumors, may not generate enough TSA and TAA to be effectively targeted by endogenous T cell responses.

Mutational landscape

The generation of tumor neoantigens is a direct result of the genomic instability that gives rise to cancer cells, where the accumulation of mutations and genomic rearrangements within a cell can disrupt important gene pathways (e.g., those that prevent cell death, limit cellular division, or cause further genomic instability) by interfering with the normal expression or functionality of genes integral to such processes (28). Of particular relevance to tumor-specific antigenicity are the subset of these somatic mutations and rearrangements that ultimately result in the synthesis of mutated and/or chimeric amino acid chains, parts of which can subsequently be processed for presentation in the MHC. Importantly, the genomic changes underlying tumor neoantigens can be true drivers of the cancer phenotype or simply tumor-specific genetic hitchhikers of those drivers, with Ags in the latter category potentially more susceptible to immune escape.

The typical mutation load underlying cancer cells varies widely, from as few as 0.8 to over 47 coding mutations per megabase (estimated median), with some tumor mutation burdens projected at over 1200 per megabase (29). These variations in mutation load have been well studied in relation to patient age (e.g., (29)) and cancer/tissue type, with adult skin and lung cancers among those typically characterized by the most mutations and leukemias among those characterized by the fewest (29–31). The number of novel peptides resulting from tumor mutations likewise varies in proportion to total mutation burden, and the vast majority of studies aimed at identifying immune response to cancer-derived neoepitopes have as a result focused on those cancers that average among the highest of mutation burdens. From those studies, on average fewer than 2% of the mutations investigated in these highly mutated tumors have been shown to elicit endogenous T cell responses (25, 26, 32), such that cancer neoantigens are often thought to result from a probabilistic process in which a greater number of mutations result in a greater likelihood of generating an immunogenic neoantigen. The general acceptance of this hypothesis within the field of immuno-oncology has proven particularly discouraging for the prospects of using immunotherapies

broadly in cancer treatment, as many adult tumors and most pediatric cancers exhibit relatively few somatic mutations. A recent study provides further insight into the tumor mutational landscape by identifying HLA alleles predicted to be good presenters of particular tumor driver mutations. A subsequent statistical analysis indicated those tumor drivers were unlikely to occur within the context of those particular HLA haplotypes (33). This analysis and another report found that when such tumors did emerge in an individual carrying an HLA allele that could present the corresponding driver mutation, the tumors were often associated with allelic loss of the relevant HLA gene (34). Regardless, the discovery of endogenous T cell responses to tumor-specific neoepitopes provides both a targeted list of Ags for patient-specific vaccination and the opportunity to identify receptors that may prove integral to the success of T cell engineering therapeutics.

Whereas vaccination and TCR engineering approaches require the direct identification of the targeted TSAs, a separate class of anticancer immunotherapy, ICB, is not bound by these same constraints. Remarkable clinical activity against a variety of tumor types has been attributed to the ability of several ICB therapies (mostly targeting CTLA-4 and PD-1) to enhance T cell activity against cancer neoantigens (35–37). Although immunotherapeutic approaches using ICB have not deliberately focused on the antigenic targets recognized by a patient's T cells, data from clinical trials on patients with melanoma (38, 39) and non-small cell lung carcinoma (40–42) suggest that mutational load and neoantigen abundance is positively correlated with objective response rates in patients treated with ICB (43). Although these findings provide indisputable evidence that the immune system recognizes and targets neoantigens in cancers with high rates of somatic mutation, this does not preclude the possibility that similar (or perhaps even more favorable) responses could be obtained in tumors with lower mutational burdens. In a recent study, Munson et al. (44) found that the extent of CD8 T cell infiltration into tumors and TCR sharing across patients with breast cancer correlated with improved survival. Additionally, TCR sharing was readily detected between patients with breast cancer (in both TILs and blood), whereas the same TCRs were only found sparingly in control blood from cancer-free donors. These findings suggest that the shared TCRs in cancer-bearing patients are tumor-specific and may recognize shared Ags among patients with breast cancer. It is important to note that the authors did not conclusively rule out the possibility that the shared TCRs could also be recognizing viral or environmental Ags shared among patients; however, the idea that these shared TCRs were specific for tumor Ags was further supported by data showing that, in comparison with T cells from tumor-free lymph nodes, T cells from tumor-involved lymph nodes were 4-fold more likely to contain TCRs also present in the primary tumor TILs. Further studies using reconstructed TCRs would be required to demonstrate specificity of the TCRs for tumor Ags, but regardless, these important findings will likely reinvigorate efforts to identify and prioritize therapeutic treatments that can be used to exploit the immune system and selectively target tumor Ags across various types of cancer.

Immunodominance in cancer

As described previously, cancer arises due to an accumulation of genetic alterations, which leads to the production and

processing of mutant proteins (neoantigens) that are otherwise absent from host cells (28, 30). From a purely theoretical perspective, the upper limit of expressed neoantigens could be approximated from the number of somatic mutations and genome rearrangements present in a specific tumor type. However, it is well known from viral models that this number would grossly overestimate the actual number of expressed and presented Ags, as the processing pathways involved with MHC class I Ag presentation greatly diminishes the number of potential antigenic peptides (45). Although peptide processing contributes to the narrowing pool of presented peptides, the greatest factor affecting the abundance of pMHC complexes and influencing the immunogenicity of the resultant epitopes comes from insufficient peptide-MHC binding affinities, which results in unstable pMHC complexes and significantly limits the expression of the corresponding peptides on the cell surface. A recent paper by Abelin et al. (46) used a monoallelic cell expression system and mass spectrometry of eluted peptides in an attempt to more accurately profile the HLA peptidome while accounting for the role of expression and peptide-MHC binding in peptide presentation. Although this approach accurately reflects the peptides presented by single HLA allele-transduced B cells, future studies and analyses would be necessary to determine whether these findings are generalizable to primary tumor cells that express multiple HLA alleles. Furthermore, in order for these peptides to induce an immune response, T cells must contain a cognate TCR capable of binding the pMHC complex with sufficient avidity to induce an effective T cell response, which results in a polyclonal pool of CD8⁺ T cells recognizing immunodominant and subdominant Ags. This phenomenon is known as immunodominance (45), and is likely another mechanism limiting the breadth of targets that can be recognized by the immune system. Immunodominance is the structured response hierarchy among epitope-specific T cell populations targeting subsets of epitopes from an antigenic mix. This has been studied frequently in the context of pathogenic infections, where a small subset of potential epitopes generates cognate T cell responses and those responses have reliable magnitude hierarchies. Thus, infections with the same pathogen in animals sharing the same MHC haplotype will generally produce the same response profile.

The mechanisms of immunodominance are not yet fully elucidated. Several factors have been proposed to contribute, including the number of pMHC complexes presented on the cell surface, the precursor frequency of the responding T cell population, the binding affinity and off-rate of peptide for MHC, and the avidity of the pMHC-TCR interaction (47–49). However, some of these associations have not held up with additional data, such as the contribution of precursor frequency, which was found not to be correlated with response size in the influenza model system (50).

Immunodominance could function in the tumor environment by focusing the response on a small subset of presented neoepitopes or TAA-derived epitopes. A study of hepatocellular carcinoma TAA responses found clear evidence of immunodominance across multiple patients, with a small subset of expressed TAA being targeted by each patient, although there did not seem to be consistency in which Ags were preferentially targeted among patients (51). As noted, several factors could ultimately influence the presentation of a

particular epitope in a given patient, including protein expression variation, processing efficiency, and HLA polymorphisms. The breadth of the response was associated with improved progression-free survival and proved somewhat analogous to observations in hepatitis C virus where CD8 T cell response breadth has been correlated with improved viral control (52). A strong hierarchy has also been observed in at least one melanoma patient's responses to the NY-ESO-1 TAA (53). Although these findings show clear instances of immunodominance with regard to the antitumor response by CD8 T cells, the underlying mechanisms driving these Ag hierarchies are unclear. Further studies are needed to address whether specific factors associated with immunodominance disproportionately contribute to shaping the immune repertoire as it is currently unclear whether the relative level of expression between tumor Ags, the rapidity by which competing tumor Ags induce an immune response, or some other factor plays the greatest role in shaping the repertoire.

The potential for immunodominance to regulate antitumor responses has been appreciated for some time and raises important considerations for immune therapies and cancer vaccination (54, 55). Indeed, variation in immunodominance among individuals with distinct HLA haplotypes contributed to differential outcomes after NY-ESO-1 vaccination (56). As efforts continue to determine the key predictors of immunodominant responses, these parameters could be incorporated into the tumor Ag computational pipelines to improve

their accuracy and utility (Fig. 1). If the apparent low response rate to the TSA and TAA landscape in tumors is in part due to immunodominant focusing, one consequence of this might be that even tumors with low mutation burdens will elicit useful responses. That is, a larger proportion of the available neoepitopes will be targeted in these tumors, because the limitation on TSA- and TAA-driven responses is driven not by a lack of antigenicity but rather by the immune system's immunodominant focusing. Future studies exploring responses in low mutation burden tumors should address this hypothesis (57).

Specificity and cross-reactivity

As discussed earlier, TSAs may provide the most promising targets for tumor clearance while limiting undesirable effects on normal tissue. TSA-focused strategies involve the elicitation or *in vitro* generation of pools of T cells that have been tuned against these defined TSAs by vaccination or TCR transduction. Notably, these Ags are generally extremely similar to self, with a single mutation underlying the majority of characterized TSAs. The exceptions are the rarer mutations generated by insertion, deletion, or fusion, which have the potential to create epitopes that differ from the "parent" self-peptide(s) by multiple consecutive amino acids.

Due to the special nature of the relationship between TSA-derived epitopes and self, there are two concerns that arise when considering them as targets: repertoire limitations and

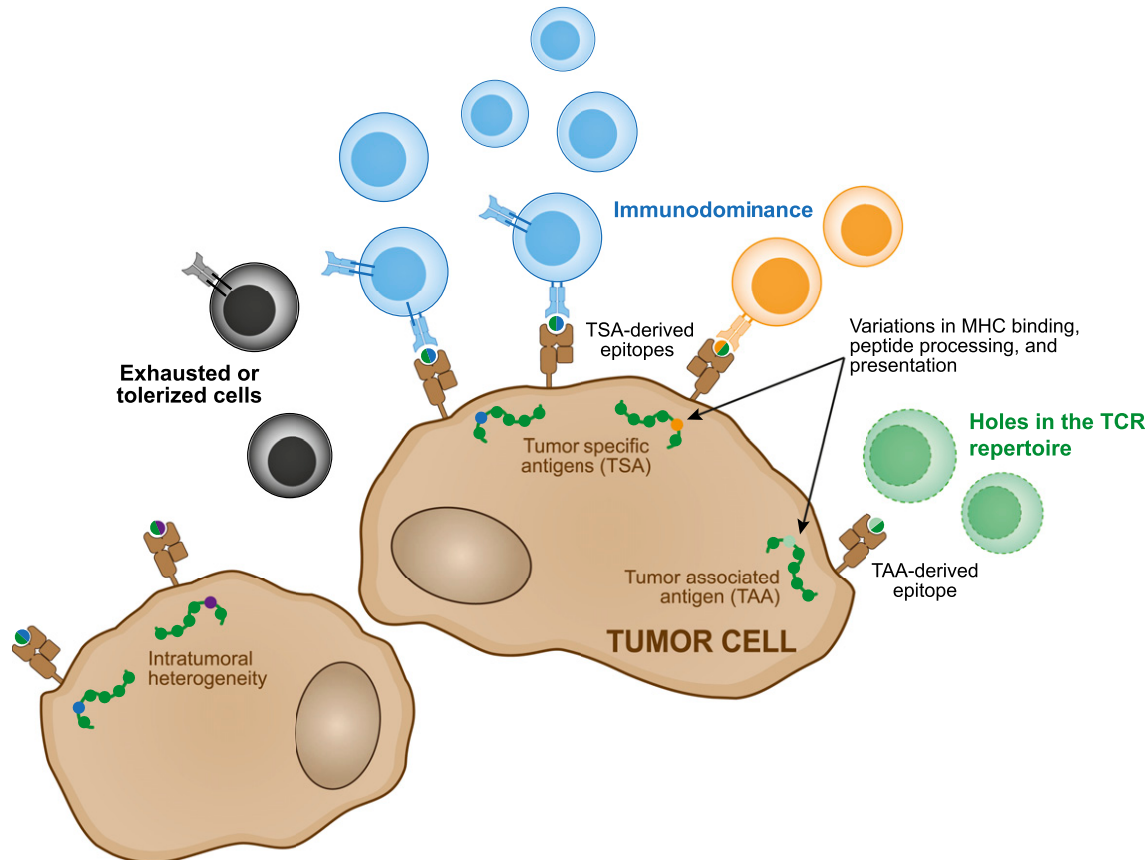


FIGURE 1. Features that determine antitumor T cell reactivity. Two major types of Ags, tumor-associated and tumor-specific, can be recognized by endogenous T cell responses. The ability for epitopes derived from these Ags to be detected by responding T cells is modulated by the host's HLA type and the epitope's processing and presentation efficiency. Intratumoral heterogeneity may also allow individual tumor cells to escape recognition. On the T cell side, immunodominance hierarchies can be generated leading to an individual Ag being the major target of the response. Additionally, holes in the TCR repertoire and T cell tolerization and exhaustion can limit response efficacy.

cross-reactivity. Because of negative selection, TCRs directly responsive to self should be underrepresented or entirely missing from the peripheral repertoire. Although TSAs are by definition not identical to self, their proximity may constrain the potential responding repertoire if most TSA-reactive TCRs would also have been reactive against the parent self-epitope. However, a series of recent studies have suggested that the restrictions on the repertoire by negative selection may be somewhat limited. One study focusing on human T cell responses found that T cells against known self-antigens, such as SMCY in males, could still be found in the periphery. Although these cells were present at lower levels than in females and in a tolerogenic state in males, they could be reactivated with higher doses of Ag (58). In the same study, a single epitope was mutated at each residue that would permit change without preventing peptide-MHC binding, and each mutation generated an epitope that reliably bound T cells. The interpretation of these results is that there were few absolute holes in the repertoire as conventionally understood and that clonal deletion only “pruned” self-reactive specificities. Thus, even if an epitope is proximal to self, there will likely still be T cells capable of recognizing it.

TSA-derived epitopes generated by single nucleotide variants are analogous to the situation that arises during an infection when an epitope is mutated at a single residue. This has been well studied in the context of viral infections, where natural selection can favor single nonsynonymous mutations in the viral genome that facilitate immune escape. Frequently, these mutations can significantly limit or even fully evade the immune repertoires generated against the original epitope, for instance allowing pathogen persistence in the case of HIV and hepatitis C virus (59). A TSA generated by such a variant may similarly not share significant overlap in reactive immune repertoires with T cells that would target the unmutated self-peptide. Yet, various neoepitope prediction pipelines have incorporated distance-to-self as a factor in predicting the potential immunogenicity of a TSA (60, 61). At least two factors can be considered for this assessment: 1) whether the mutation creates a variation that will generate a potential cleavage site for peptide processing, and 2) whether the potential epitope is sufficiently distinct biochemically that the responding TCRs are unlikely to cross-react with self. The latter factor is currently somewhat difficult to model, given our limited ability to predict peptide-MHC-TCR interactions at a structural level, but highly divergent amino acid residues are generally more likely to create distinct epitope surfaces.

Further demonstration of the repertoire's ability to mount anti-TSA responses comes from vaccination studies utilizing TSA targets in melanoma. In one study, healthy HLA-matched donors were used to elicit responses against tumor Ags from melanoma patients (25). Many of these were private mutations, and the healthy donors could elicit robust responses to these mutated epitopes, although it should be noted that the method used to elicit the healthy donor responses (long-term *in vitro* stimulation) was not applied to PBMCs from the patients. More recently, two groups have successfully immunized melanoma patients with targeted arrays of TSAs and adjuvant, demonstrating that even autologous responses can be boosted in patients that have presumably had significant exposure to these Ags (62, 63).

Although there is good evidence that repertoire limitations can be overcome, there is still the potential that the targeted approaches of TSAs may generate cross-reactive responses to the parent self-epitope, in effect breaking tolerance. This concern is particularly significant for adoptively transferred TCR approaches that do not rely on the elicitation of autologous responses. The goal of these therapies would be analogous to CAR TCR therapies, where TCRs specific for the TSA-associated epitope are engineered into autologous T cells that are then expanded and infused back into the patient. However, if the TCRs exhibit significant cross-reactivity to the self-epitope, a large infusion of cells bearing these receptors could target the unmutated parent self-epitope. Beyond off-target affinity for the parent epitope, unexpected reactivities could also occur against other endogenous peptides, as was reported for a trial of TCR-based therapy targeted at MAGE-A3, where the used TCR also targeted a self-epitope from the striated muscle protein titin (64). Notably, this TCR was derived from an endogenous response but was affinity-enhanced via phage display selection. The wild-type TCR did not respond to the titin-derived epitope except at very high concentrations, suggesting that it would not have mediated the same reactivity. This result serves as an important cautionary note for engineered TCR approaches and suggests that endogenous peripheral tolerance mechanisms are able to shape antitumor responses away from significant normal self-reactivity.

Several approaches have been suggested to limit self-reactivity by engineered TCRs. As noted, relying solely on endogenously generated TCRs may significantly limit potential self-reactivities due to editing by central and peripheral tolerance mechanisms. In contrast, TCRs selected *in vitro* or TCRs from humanized mouse models may have undetected reactivities and have the potential to be antigenic themselves (65). Additionally, some concerns have been raised about promiscuous pairing of introduced TCR chains with the endogenous chains present in a T cell, leading to hybrid receptors that may have markedly varied targets (66). To avoid this possibility, altering the TCR constant regions to pair preferentially with the cognate engineered chain has been achieved by the introduction of a second cysteine or by swapping human constant regions for murine homologs; both strategies resulted in higher expression of TCR on the cell surface (67, 68).

The potential for off-target or undetected specificity of an introduced TCR raises the issue of the cross-reactivity of the TCR repertoire, which has been estimated by various methods to be quite vast (exceeding 1 million peptides per TCR in one experimental report (69)). The argument for the inherent cross-reactivity of the TCR repertoire can be inferred directly from the basic principles of adaptive immunity: given the broad reactivity of the immune system to novel Ags, the potential landscape of MHC-binding peptides, and the size of the TCR repertoire in any individual, the size of the potential pMHC target pool is many orders of magnitude greater than the size of an individual's repertoire. Yet although it is clear that a TCR should be highly cross-reactive, it is less clear in which “neighborhood” that cross-reactivity will occur (70).

One landmark study addressing this question identified the targets of individual TCRs by screening yeast display libraries, where researchers demonstrated that an individual

TCR targeted relatively conserved features of a given peptide surface but was agnostic to even dramatic changes at other residues in the peptide (71). Although the potential peptide targets contained a strikingly high diversity of peptides, there were consistent commonalities among the peptide groups that even allowed prediction of reactive peptides not yet observed. Furthermore, even peptides that were reactive that bore no similarity could be “connected” by a series of intermediate reactive peptides that were a single mutation away from another reactive peptide.

The predictive aspects of this work suggest that it might be possible to determine if a TCR is likely to react with both a TSA-derived epitope and the parent peptide, although this capability is beyond current *in silico* approaches without sufficient training data sets.

Conclusions

T cell-mediated therapies for tumors can be broadly classified in three categories: 1) adoptive cell therapies, 2) vaccines, and 3) immune modulating therapies including ICB and cytokine therapy. Characterizing specificity is required for the first two types. Although ICB can be used without any knowledge of the TSA or TAA that T cells are targeting, several studies have found associations between tumor mutation burden (and in particular putative neoepitope burden) and improved outcomes (29, 40, 72). The reason for this association is not entirely clear; it may correlate with overall antitumor response magnitude, or certain high-quality responses may be more likely to be generated if a large number of TSAs are available for targeting.

For therapies in development, including vaccines and adoptive cell therapies, specific targets that might be shared across individuals are particularly attractive for generating off-the-shelf therapies that can be quickly applied. CD19 CAR T cells, NY-ESO-1 vaccines, and adoptive TCR therapies targeting common fusions and driver mutations are all broadly applicable across an entire tumor type or even multiple tumor types. One concern with these approaches is that they focus the response on a single target (though it may include multiple epitopes). Targeting multiple mutations is more likely to prevent tumor escape and account for the highly heterogeneous mutation landscapes characteristic of most tumors. However, finding multiple targets in a single tumor will likely require using private antigenic targets, (i.e., derived from mutations that are patient-specific). This introduces complexities in therapeutic development and delivery, but the tremendous promise of these approaches justifies the investment in developing workflows that will make these therapies widely tractable.

Isolating and cloning tumor-specific TCRs can now be done relatively rapidly. The actual determination of specificity remains as the final bottleneck, although determining specificity may not be required in every case. Further, recent advances include the development of algorithms to predict TCR specificity based on training data, and future progress in such endeavors likely stands to at least increase the efficiency of matching TCR sequences with epitopes (73, 74). Cloning and expressing TCRs offer the advantage that the cells in which they are transduced could be engineered to have increased functional activity, reduced likelihood of developing exhaustion phenotypes, and safety features such as kill switches or multiple Ag specificity requirements (75, 76). As they would generate

high levels of tumor specificity with reduced off-target effects, these features seem to offer the best hope for safe and efficacious therapies even if many technological challenges remain.

Disclosures

The authors have no financial conflicts of interest.

References

- Bakker, A. B., M. W. Schreurs, G. Tafazzul, A. J. de Boer, Y. Kawakami, G. J. Adema, and C. G. Figdor. 1995. Identification of a novel peptide derived from the melanocyte-specific gp100 antigen as the dominant epitope recognized by an HLA-A2.1-restricted anti-melanoma CTL line. *Int. J. Cancer* 62: 97–102.
- Cox, A. L., J. Skipper, Y. Chen, R. A. Henderson, T. L. Darrow, J. Shabanowitz, V. H. Engelhard, D. F. Hunt, and C. L. Slingluff, Jr. 1994. Identification of a peptide recognized by five melanoma-specific human cytotoxic T cell lines. *Science* 264: 716–719.
- Kawakami, Y., S. Eliyahu, C. H. Delgado, P. F. Robbins, K. Sakaguchi, E. Appella, J. R. Yannelli, G. J. Adema, T. Mikl, and S. A. Rosenberg. 1994. Identification of a human melanoma antigen recognized by tumor-infiltrating lymphocytes associated with *in vivo* tumor rejection. *Proc. Natl. Acad. Sci. USA* 91: 6458–6462.
- Kawakami, Y., S. Eliyahu, C. Jennings, K. Sakaguchi, X. Kang, S. Southwood, P. F. Robbins, A. Sette, E. Appella, and S. A. Rosenberg. 1995. Recognition of multiple epitopes in the human melanoma antigen gp100 by tumor-infiltrating T lymphocytes associated with *in vivo* tumor regression. *J. Immunol.* 154: 3961–3968.
- Coulie, P. G., V. Brichard, A. Van Pel, T. Wölfel, J. Schneider, C. Traversari, S. Mattei, E. De Plaein, C. Lurquin, J. P. Szikora, et al. 1994. A new gene coding for a differentiation antigen recognized by autologous cytolytic T lymphocytes on HLA-A2 melanomas. *J. Exp. Med.* 180: 35–42.
- Kawakami, Y., S. Eliyahu, K. Sakaguchi, P. F. Robbins, L. Rivoltini, J. R. Yannelli, E. Appella, and S. A. Rosenberg. 1994. Identification of the immunodominant peptides of the MART-1 human melanoma antigen recognized by the majority of HLA-A2-restricted tumor infiltrating lymphocytes. *J. Exp. Med.* 180: 347–352.
- Brichard, V., A. Van Pel, T. Wölfel, C. Wölfel, E. De Plaein, B. Lethé, P. Coulie, and T. Boon. 1993. The tyrosinase gene codes for an antigen recognized by autologous cytolytic T lymphocytes on HLA-A2 melanomas. *J. Exp. Med.* 178: 489–495.
- Wölfel, T., A. Van Pel, V. Brichard, J. Schneider, B. Seliger, K. H. Meyer zum Büschenfelde, and T. Boon. 1994. Two tyrosinase nonapeptides recognized on HLA-A2 melanomas by autologous cytolytic T lymphocytes. *Eur. J. Immunol.* 24: 759–764.
- Maude, S. L., D. T. Teachey, D. L. Porter, and S. A. Grupp. 2015. CD19-targeted chimeric antigen receptor T-cell therapy for acute lymphoblastic leukemia. *Blood* 125: 4017–4023.
- Rodrigues, P. C., S. N. Oliveira, M. B. Viana, E. I. Matsuda, A. E. Nowill, S. R. Brandalise, and J. A. Yunes. 2007. Prognostic significance of WT1 gene expression in pediatric acute myeloid leukemia. *Pediatr. Blood Cancer* 49: 133–138.
- Scharnhorst, V., A. J. van der Eb, and A. G. Jochemsen. 2001. WT1 proteins: functions in growth and differentiation. *Gene* 273: 141–161.
- Disis, M. L., D. R. Wallace, T. A. Gooley, Y. Dang, M. Slota, H. Lu, A. L. Coveler, J. S. Childs, D. M. Higgins, P. A. Fintak, et al. 2009. Concurrent trastuzumab and HER2/neu-specific vaccination in patients with metastatic breast cancer. *J. Clin. Oncol.* 27: 4685–4692.
- Iqbal, N., and N. Iqbal. 2014. Human epidermal growth factor receptor 2 (HER2) in cancers: overexpression and therapeutic implications. *Mol. Biol. Int.* 2014: 852748.
- Stone, J. D., D. T. Harris, and D. M. Kranz. 2015. TCR affinity for p/MHC formed by tumor antigens that are self-proteins: impact on efficacy and toxicity. *Curr. Opin. Immunol.* 33: 16–22.
- Morgan, R. A., J. C. Yang, M. Kitano, M. E. Dudley, C. M. Laurencot, and S. A. Rosenberg. 2010. Case report of a serious adverse event following the administration of T cells transduced with a chimeric antigen receptor recognizing ERBB2. *Mol. Ther.* 18: 843–851.
- van der Bruggen, P., C. Traversari, P. Chomez, C. Lurquin, E. De Plaein, B. Van den Eynde, A. Knuth, and T. Boon. 1991. A gene encoding an antigen recognized by cytolytic T lymphocytes on a human melanoma. *Science* 254: 1643–1647.
- Robbins, P. F., S. H. Kassim, T. L. Tran, J. S. Crystal, R. A. Morgan, S. A. Feldman, J. C. Yang, M. E. Dudley, J. R. Wunderlich, R. M. Sherry, et al. 2015. A pilot trial using lymphocytes genetically engineered with an NY-ESO-1-reactive T-cell receptor: long-term follow-up and correlates with response. *Clin. Cancer Res.* 21: 1019–1027.
- Morgan, R. A., N. Chinnasamy, D. Abate-Daga, A. Gros, P. F. Robbins, Z. Zheng, M. E. Dudley, S. A. Feldman, J. C. Yang, R. M. Sherry, et al. 2013. Cancer regression and neurological toxicity following anti-MAGE-A3 TCR gene therapy. *J. Immunother.* 36: 133–151.
- Stevanović, S., A. Pasetto, S. R. Helman, J. J. Gartner, T. D. Prickett, B. Howie, H. S. Robins, P. F. Robbins, C. A. Klebanoff, S. A. Rosenberg, and C. S. Hinrichs. 2017. Landscape of immunogenic tumor antigens in successful immunotherapy of virally induced epithelial cancer. *Science* 356: 200–205.
- Draper, L. M., M. L. Kwong, A. Gros, S. Stevanović, E. Tran, S. Kerkar, M. Raffeld, S. A. Rosenberg, and C. S. Hinrichs. 2015. Targeting of HPV-16+ epithelial cancer cells by TCR gene engineered T cells directed against E6. *Clin. Cancer Res.* 21: 4431–4439.
- Thompson, M. P., and R. Kurzrock. 2004. Epstein-Barr virus and cancer. *Clin. Cancer Res.* 10: 803–821.
- Lennertz, V., M. Fatho, C. Gentilini, R. A. Frye, A. Lifke, D. Ferel, C. Wölfel, C. Huber, and T. Wölfel. 2005. The response of autologous T cells to a human melanoma is dominated by mutated neoantigens. *Proc. Natl. Acad. Sci. USA* 102: 16013–16018.

23. Zhou, J., M. E. Dudley, S. A. Rosenberg, and P. F. Robbins. 2005. Persistence of multiple tumor-specific T-cell clones is associated with complete tumor regression in a melanoma patient receiving adoptive cell transfer therapy. *J. Immunother.* 28: 53–62.
24. Pritchard, A. L., J. G. Burel, M. A. Neller, N. K. Hayward, J. A. Lopez, M. Fatho, V. Lennerz, T. Wölfel, and C. W. Schmidt. 2015. Exome sequencing to predict neoantigens in melanoma. *Cancer Immunol. Res.* 3: 992–998.
25. Strønen, E., M. Toebe, S. Kelderman, M. M. van Buuren, W. Yang, N. van Rooij, M. Donia, M.-L. Bösch, F. Lund-Johansen, J. Olweus, and T. N. Schumacher. 2016. Targeting of cancer neoantigens with donor-derived T cell receptor repertoires. *Science* 352: 1337–1341.
26. Cohen, C. J., J. J. Gartner, M. Horowitz-Fried, K. Shamalov, K. Trebska-McGowan, V. V. Bliskovsky, M. R. Parkhurst, C. Ankri, T. D. Prickett, J. S. Crystal, et al. 2015. Isolation of neoantigen-specific T cells from tumor and peripheral lymphocytes. *J. Clin. Invest.* 125: 3981–3991.
27. Rajasagi, M., S. A. Shukla, E. F. Fritsch, D. B. Keskin, D. DeLuca, E. Carmona, W. Zhang, C. Sougnez, K. Cibulskis, J. Sidney, et al. 2014. Systematic identification of personal tumor-specific neoantigens in chronic lymphocytic leukemia. *Blood* 124: 453–462.
28. Hanahan, D., and R. A. Weinberg. 2000. The hallmarks of cancer. *Cell* 100: 57–70.
29. Chalmers, Z. R., C. F. Connolly, D. Fabrizio, L. Gay, S. M. Ali, R. Ennis, A. Schrock, B. Campbell, A. Shlien, J. Chmielecki, et al. 2017. Analysis of 100,000 human cancer genomes reveals the landscape of tumor mutational burden. *Genome Med.* 9: 34.
30. Vogelstein, B., N. Papadopoulos, V. E. Velculescu, S. Zhou, L. A. Diaz, Jr., and K. W. Kinzler. 2013. Cancer genome landscapes. *Science* 339: 1546–1558.
31. Lawrence, M. S., P. Stojanov, P. Polak, G. V. Kryukov, K. Cibulskis, A. Sivachenko, S. L. Carter, C. Stewart, C. H. Mermel, S. A. Roberts, et al. 2013. Mutational heterogeneity in cancer and the search for new cancer-associated genes. *Nature* 499: 214–218.
32. Gros, A., M. R. Parkhurst, E. Tran, A. Pasetto, P. F. Robbins, S. Ilyas, T. D. Prickett, J. J. Gartner, J. S. Crystal, I. M. Roberts, et al. 2016. Prospective identification of neoantigen-specific lymphocytes in the peripheral blood of melanoma patients. *Nat. Med.* 22: 433–438.
33. Marty, R., S. Kaabinejad, D. Rossell, M. J. Slifker, J. van de Haar, H. B. Engin, N. de Prisco, T. Ideker, W. H. Hildebrand, J. Font-Burgada, and H. Carter. 2017. MHC-I genotype restricts the oncogenic mutational landscape. *Cell*. DOI: 10.1016/j.cell.2017.09.050.
34. McGranahan, N., R. Rosenthal, C. T. Hiley, A. J. Rowan, T. B. K. Watkins, G. A. Wilson, N. J. Birkbak, S. Veeriah, P. Van Loo, J. Herrero, and C. Swanton, TRACERx Consortium. 2017. Allele-specific HLA loss and immune escape in lung cancer evolution. *Cell*. DOI: 10.1016/j.cell.2017.10.001.
35. Schumacher, T. N., and R. D. Schreiber. 2015. Neoantigens in cancer immunotherapy. *Science* 348: 69–74.
36. Gubin, M. M., M. N. Artyomov, E. R. Mardis, and R. D. Schreiber. 2015. Tumor neoantigens: building a framework for personalized cancer immunotherapy. *J. Clin. Invest.* 125: 3413–3421.
37. Sharma, P., and J. P. Allison. 2015. The future of immune checkpoint therapy. *Science* 348: 56–61.
38. Ribas, A., L. H. Camacho, G. Lopez-Berestein, D. Pavlov, C. A. Bulanagui, R. Millham, B. Comin-Anduix, J. M. Reuben, E. Seja, C. A. Parker, et al. 2005. Antitumor activity in melanoma and anti-self responses in a phase I trial with the anti-cytotoxic T lymphocyte-associated antigen 4 monoclonal antibody CP-675,206. *J. Clin. Oncol.* 23: 8968–8977.
39. Weber, J. S., S. O'Day, W. Urba, J. Powderly, G. Nichol, M. Yellin, J. Snively, and E. Hersh. 2008. Phase I/II study of ipilimumab for patients with metastatic melanoma. *J. Clin. Oncol.* 26: 5950–5956.
40. Rizvi, N. A., M. D. Hellmann, A. Snyder, P. Kvistborg, V. Makarov, J. J. Havel, W. Lee, J. Yuan, P. Wong, T. S. Ho, et al. 2015. Cancer immunology. Mutational landscape determines sensitivity to PD-1 blockade in non-small cell lung cancer. *Science* 348: 124–128.
41. Gettinger, S. N., L. Horn, L. Gandhi, D. R. Spigel, S. J. Antonia, N. A. Rizvi, J. D. Powderly, R. S. Heist, R. D. Carvajal, D. M. Jackman, et al. 2015. Overall survival and long-term safety of nivolumab (anti-programmed death 1 antibody, BMS-936558, ONO-4538) in patients with previously treated advanced non-small-cell lung cancer. *J. Clin. Oncol.* 33: 2004–2012.
42. Rizvi, N. A., J. Mazières, D. Planchard, T. E. Stinchcombe, G. K. Dy, S. J. Antonia, L. Horn, H. Lena, E. Minenza, B. Mennecier, et al. 2015. Activity and safety of nivolumab, an anti-PD-1 immune checkpoint inhibitor, for patients with advanced, refractory squamous non-small-cell lung cancer (CheckMate 063): a phase 2, single-arm trial. *Lancet Oncol.* 16: 257–265.
43. Yarchoan, M., B. A. Johnson, III, E. R. Lutz, D. A. Laheru, and E. M. Jaffee. 2017. Targeting neoantigens to augment antitumour immunity. *Nat. Rev. Cancer* 17: 209–222.
44. Munson, D. J., C. A. Egelston, K. E. Chiotti, Z. E. Parra, T. C. Bruno, B. L. Moore, T. A. Nakano, D. L. Simons, G. Jimenez, J. H. Yim, et al. 2016. Identification of shared TCR sequences from T cells in human breast cancer using emulsion RT-PCR. *Proc. Natl. Acad. Sci. USA* 113: 8272–8277.
45. Yewdell, J. W. 2006. Confronting complexity: real-world immunodominance in antiviral CD8+ T cell responses. *Immunity* 25: 533–543.
46. Abelin, J. G., D. B. Keskin, S. Sarkizova, C. R. Hartigan, W. Zhang, J. Sidney, J. Stevens, W. Lane, G. L. Zhang, T. M. Eisenhaure, et al. 2017. Mass spectrometry profiling of HLA-associated peptideomes in mono-allelic cells enables more accurate epitope prediction. *Immunity* 46: 315–326.
47. Moon, J. J., H. H. Chu, M. Pepper, S. J. McSorley, S. C. Jameson, R. M. Kedl, and M. K. Jenkins. 2007. Naive CD4(+) T cell frequency varies for different epitopes and predicts repertoire diversity and response magnitude. *Immunity* 27: 203–213.
48. Obar, J. J., K. M. Khanna, and L. Lefrançois. 2008. Endogenous naïve CD8+ T cell precursor frequency regulates primary and memory responses to infection. *Immunity* 28: 859–869.
49. Lazaraki, C. A., F. A. Chaves, S. A. Jenks, S. Wu, K. A. Richards, J. M. Weaver, and A. J. Sant. 2005. The kinetic stability of MHC class II:peptide complexes is a key parameter that dictates immunodominance. *Immunity* 23: 29–40.
50. Cuklac, T., J. Chadderton, W. Zeng, J. G. Cullen, W. T. Kan, P. C. Doherty, D. C. Jackson, S. J. Turner, and N. L. La Gruta. 2014. The influenza virus-specific CTL immunodominance hierarchy in mice is determined by the relative frequency of high-avidity T cells. *J. Immunol.* 192: 4061–4068.
51. Flecken, T., N. Schmidt, S. Hild, E. Gostick, O. Drogatz, R. Zeiser, P. Schemmer, H. Bruns, T. Eiermann, D. A. Price, et al. 2014. Immunodominance and functional alterations of tumor-associated antigen-specific CD8+ T-cell responses in hepatocellular carcinoma. *Hepatology* 59: 1415–1426.
52. Sung, P. S., V. Racanelli, and E.-C. Shin. 2014. CD8(+) T-cell responses in acute hepatitis C virus infection. *Front. Immunol.* 5: 266.
53. Jackson, H., N. Dimopoulos, N. A. Mifsud, T. Y. Tai, Q. Chen, S. Svobodova, J. Browning, I. Luescher, L. Stockert, L. J. Old, et al. 2006. Striking immunodominance hierarchy of naturally occurring CD8+ and CD4+ T cell responses to tumor antigen NY-ESO-1. *J. Immunol.* 176: 5908–5917.
54. Chen, W., and J. McCluskey. 2006. Immunodominance and immunodomination: critical factors in developing effective CD8+ T-cell-based cancer vaccines. *Adv. Cancer Res.* 95: 203–247.
55. Schreiber, H., T. H. Wu, J. Nachman, and W. M. Kast. 2002. Immunodominance and tumor escape. *Semin. Cancer Biol.* 12: 25–31.
56. Bioley, G., P. Guillaume, I. Luescher, A. Yeh, B. Dupont, N. Bhardwaj, G. Mears, L. J. Old, D. Valmori, and M. Ayyoub. 2009. HLA class I - associated immunodominance affects CTL responsiveness to an ESO recombinant protein tumor antigen vaccine. *Clin. Cancer Res.* 15: 299–306.
57. Chang, T.-C., R. A. Carter, Y. Li, Y. Li, H. Wang, M. N. Edmonson, X. Chen, P. Arnold, T. L. Geiger, G. Wu, et al. 2017. The neoepitope landscape in pediatric cancers. *Genome Med.* 9: 78.
58. Yu, W., N. Jiang, P. J. R. Ebert, B. A. Kidd, S. Müller, P. J. Lund, J. Juang, K. Adachi, T. Tse, M. E. Birnbaum, et al. 2015. Clonal deletion prunes but does not eliminate self-specific $\alpha\beta$ CD8(+) T lymphocytes. *Immunity* 42: 929–941.
59. Bowen, D. G., and C. M. Walker. 2005. Mutational escape from CD8+ T cell immunity: HCV evolution, from chimpanzees to man. *J. Exp. Med.* 201: 1709–1714.
60. van Buuren, M. M., J. J. Calis, and T. N. Schumacher. 2014. High sensitivity of cancer exome-based CD8 T cell neo-antigen identification. *OncolImmunology* 3: e28836.
61. Schubert, B., L. de la Garza, C. Mohr, M. Walzer, and O. Kohlbacher. 2017. ImmunoNodes - graphical development of complex immunoinformatics workflows. *BMC Bioinformatics* 18: 242.
62. Ott, P. A., Z. Hu, D. B. Keskin, S. A. Shukla, J. Sun, D. J. Bozym, W. Zhang, A. Luoma, A. Giobbie-Hurder, L. Peter, et al. 2017. An immunogenic personal neoantigen vaccine for patients with melanoma. *Nature* 547: 217–221.
63. Sahin, U., E. Derhovanessian, M. Miller, B.-P. Kloke, P. Simon, M. Löwer, V. Bukur, A. D. Tadmor, U. Luxemburger, B. Schrörs, et al. 2017. Personalized RNA mutanome vaccines mobilize poly-specific therapeutic immunity against cancer. *Nature* 547: 222–226.
64. Linette, G. P., E. A. Stadtmauer, M. V. Maus, A. P. Rapoport, B. L. Levine, L. Emery, L. Litzyk, A. Bagg, B. M. Carreno, P. J. Cimino, et al. 2013. Cardiovascular toxicity and titin cross-reactivity of affinity-enhanced T cells in myeloma and melanoma. *Blood* 122: 863–871.
65. Davis, J. L., M. R. Theoret, Z. Zheng, C. H. J. Lamers, S. A. Rosenberg, and R. A. Morgan. 2010. Development of human anti-murine T-cell receptor antibodies in both responding and nonresponding patients enrolled in TCR gene therapy trials. *Clin. Cancer Res.* 16: 5852–5861.
66. Kuball, J., M. L. Dossett, M. Wolf, W. Y. Ho, R.-H. Voss, C. Fowler, and P. D. Greenberg. 2007. Facilitating matched pairing and expression of TCR chains introduced into human T cells. *Blood* 109: 2331–2338.
67. Cohen, C. J., Y. F. Li, M. El-Gamil, P. F. Robbins, S. A. Rosenberg, and R. A. Morgan. 2007. Enhanced antitumor activity of T cells engineered to express T-cell receptors with a second disulfide bond. *Cancer Res.* 67: 3898–3903.
68. Cohen, C. J., Y. Zhao, Z. Zheng, S. A. Rosenberg, and R. A. Morgan. 2006. Enhanced antitumor activity of murine-human hybrid T-cell receptor (TCR) in human lymphocytes is associated with improved pairing and TCR/CD3 stability. *Cancer Res.* 66: 8878–8886.
69. Woodridge, L., J. Ekeruche-Makinde, H. A. van den Berg, A. Skowera, J. J. Miles, M. P. Tan, G. Dolton, M. Clement, S. Llewellyn-Lacey, D. A. Price, et al. 2012. A single autoimmune T cell receptor recognizes more than a million different peptides. *J. Biol. Chem.* 287: 1168–1177.
70. Singh, N. K., T. P. Riley, S. C. B. Baker, T. Borrman, Z. Weng, and B. M. Baker. 2017. Emerging concepts in TCR specificity: rationalizing and (Maybe) predicting outcomes. *J. Immunol.* 199: 2203–2213.
71. Birnbaum, M. E., J. L. Mendoza, D. K. Sethi, S. Dong, J. Glanville, J. Dobbins, E. Ozkan, M. M. Davis, K. Wucherpfennig, and K. C. Garcia. 2014. Deconstructing the peptide-MHC specificity of T cell recognition. *Cell* 157: 1073–1087.
72. Yuan, J., P. S. Hegde, R. Clynes, P. G. Foukas, A. Harari, T. O. Kleen, P. Kvistborg, C. Macall, H. T. Maecker, D. B. Page, et al. 2016. Novel technologies and emerging biomarkers for personalized cancer immunotherapy. *J. Immunother. Cancer* 4: 3.
73. Dash, P., A. J. Fiore-Gartland, T. Hertz, G. C. Wang, S. Sharma, A. Souquette, J. C. Crawford, E. B. Clemens, T. H. O. Nguyen, K. Kedzierska, et al. 2017. Quantifiable predictive features define epitope-specific T cell receptor repertoires. *Nature* 547: 89–93.
74. Glanville, J., H. Huang, A. Nau, O. Hatton, L. E. Wagar, F. Rubelt, X. Ji, A. Han, S. M. Kram, C. Petrus, et al. 2017. Identifying specificity groups in the T cell receptor repertoire. *Nature* 547: 94–98.
75. Sharpe, M., and N. Mount. 2015. Genetically modified T cells in cancer therapy: opportunities and challenges. *Dis. Model. Mech.* 8: 337–350.
76. Ghoneim, H. E., A. E. Zamora, P. G. Thomas, and B. A. Youngblood. 2016. Cell-intrinsic barriers of T cell-based immunotherapy. *Trends Mol. Med.* 22: 1000–1011.

ORIGINAL ARTICLE

Genetic Basis for Clinical Response to CTLA-4 Blockade in Melanoma

Alexandra Snyder, M.D., Vladimir Makarov, M.D., Taha Merghoub, Ph.D., Jianda Yuan, M.D., Ph.D., Jesse M. Zaretsky, B.S., Alexis Desrichard, Ph.D., Logan A. Walsh, Ph.D., Michael A. Postow, M.D., Phillip Wong, Ph.D., Teresa S. Ho, B.S., Travis J. Hollmann, M.D., Ph.D., Cameron Bruggeman, M.A., Kasthuri Kannan, Ph.D., Yanyun Li, M.D., Ph.D., Ceyhan Elipenahli, B.S., Cailian Liu, M.D., Christopher T. Harbison, Ph.D., Lisu Wang, M.D., Antoni Ribas, M.D., Ph.D., Jedd D. Wolchok, M.D., Ph.D., and Timothy A. Chan, M.D., Ph.D.

ABSTRACT

BACKGROUND

Immune checkpoint inhibitors are effective cancer treatments, but molecular determinants of clinical benefit are unknown. Ipilimumab and tremelimumab are antibodies against cytotoxic T-lymphocyte antigen 4 (CTLA-4). Anti-CTLA-4 treatment prolongs overall survival in patients with melanoma. CTLA-4 blockade activates T cells and enables them to destroy tumor cells.

METHODS

We obtained tumor tissue from patients with melanoma who were treated with ipilimumab or tremelimumab. Whole-exome sequencing was performed on tumors and matched blood samples. Somatic mutations and candidate neoantigens generated from these mutations were characterized. Neoantigen peptides were tested for the ability to activate lymphocytes from ipilimumab-treated patients.

RESULTS

Malignant melanoma exomes from 64 patients treated with CTLA-4 blockade were characterized with the use of massively parallel sequencing. A discovery set consisted of 11 patients who derived a long-term clinical benefit and 14 patients who derived a minimal benefit or no benefit. Mutational load was associated with the degree of clinical benefit ($P=0.01$) but alone was not sufficient to predict benefit. Using genomewide somatic neoepitope analysis and patient-specific HLA typing, we identified candidate tumor neoantigens for each patient. We elucidated a neoantigen landscape that is specifically present in tumors with a strong response to CTLA-4 blockade. We validated this signature in a second set of 39 patients with melanoma who were treated with anti-CTLA-4 antibodies. Predicted neoantigens activated T cells from the patients treated with ipilimumab.

CONCLUSIONS

These findings define a genetic basis for benefit from CTLA-4 blockade in melanoma and provide a rationale for examining exomes of patients for whom anti-CTLA-4 agents are being considered. (Funded by the Frederick Adler Fund and others.)

From the Department of Medicine (A.S., T.M., M.A.P., J.D.W.), Human Oncology and Pathogenesis Program (A.S., V.M., A.D., L.A.W., K.K., T.A.C.), Swim across America–Ludwig Collaborative Research Laboratory (T.M., Y.L., C.E., C.L., J.D.W.), Department of Radiation Oncology (T.A.C.), Department of Pathology (T.J.H.), and Immunology Program, Ludwig Center for Cancer Immunotherapy (J.Y., P.W., T.S.H., J.D.W.), Memorial Sloan Kettering Cancer Center; Weill Cornell Medical College (A.S., M.A.P., J.D.W., T.A.C.); and Department of Mathematics, Columbia University (C.B.) — all in New York; the Department of Molecular and Medical Pharmacology (J.M.Z., A.R.) and the Department of Medicine, Division of Hematology–Oncology, Jonsson Comprehensive Cancer Center (A.R.), University of California, Los Angeles, Los Angeles; and Bristol-Myers Squibb, Princeton, NJ (C.T.H., L.W.). Address reprint requests to Dr. Chan at the Human Oncology and Pathogenesis Program, Memorial Sloan Kettering Cancer Center, 1275 York Ave., Box 20, New York, NY 10065, or at chant@mskcc.org; or to Dr. Wolchok at the Ludwig Center for Cancer Immunotherapy, Memorial Sloan Kettering Cancer Center, 1275 York Ave., New York, NY 10065, or at wolchokj@mskcc.org.

Drs. Snyder, Makarov, Merghoub, and Yuan and Drs. Wolchok and Chan contributed equally to this article.

This article was published on November 19, 2014, and updated on November 21, 2014, at NEJM.org.

N Engl J Med 2014;371:2189-99.

DOI: 10.1056/NEJMoa1406498

Copyright © 2014 Massachusetts Medical Society.

IMMUNE CHECKPOINT BLOCKADE HAS LED to durable antitumor effects in patients with metastatic melanoma, non-small-cell lung cancer, and other tumor types, but the factors determining whether a patient will have a response remain elusive.^{1,2} The fully human monoclonal antibodies ipilimumab and tremelimumab block cytotoxic T-lymphocyte antigen 4 (CTLA-4), resulting in T-cell activation. Some studies have established correlations between outcomes with ipilimumab and peripheral-blood lymphocyte count, markers of T-cell activation,³ an “inflammatory” microenvironment,^{4,5} and maintenance of high-frequency T-cell receptor clonotypes.⁶

The relationship among the genomic landscape of the tumor, the mutational load, and the benefit from treatment remains obscure. The immunogenicity resulting from nonsynonymous melanoma mutations has been shown in a mouse model,⁷ and the antigenic diversity of human melanoma tumors has been modeled *in silico*⁸ and in melanoma-specific CD8 T-cell responses after treatment with ipilimumab.⁹ Effector and helper T-cell function and regulatory T-cell depletion are necessary for the efficacy of CTLA-4 blockade,¹⁰ but there is not an association between a specific HLA type and a clinical benefit.¹¹ Melanomas have very high mutational burdens (0.5 to >100 mutations per megabase) as compared with other solid tumors.¹² Elegant studies have shown that somatic mutations can give rise to neoepitopes¹³ and that these may serve as neoantigens.^{14–16} We conducted a study to determine whether the genetic landscape of a tumor affects the clinical benefit provided by CTLA-4 blocking agents.

METHODS

SAMPLE ACQUISITION AND DNA PREPARATION

For the discovery set, we conducted whole-exome sequencing of DNA from tumors and matched normal blood from 25 ipilimumab-treated patients. A validation set included an additional 39 patients, of whom 5 were treated with tremelimumab. Primary tumor samples and matched normal peripheral-blood specimens were obtained after the patients had provided written informed consent. DNA was extracted, and exon capture was performed with the use of the SureSelect Human All Exon 50-Mb kit (Agilent Technologies). Enriched

exome libraries were sequenced on the HiSeq 2000 platform (Illumina) to provide a mean exome coverage of more than 100× (Memorial Sloan Kettering Cancer Center Genomics Core and Broad Institute).

IMMUNOGENICITY ANALYSIS OF SOMATIC MUTATIONS

We created a bioinformatic tool to translate all mutations in exomes and then evaluate binding with major histocompatibility complex (MHC) class I molecules. The neoantigen signature was generated from the nonamers containing four amino acid strings of peptides that are common to tumors from patients with a long-term benefit from therapy. Details are provided in the Supplementary Appendix, available with the full text of this article at NEJM.org.

INTRACELLULAR CYTOKINE STAINING

Candidate neoantigen peptides were synthesized (GenScript), cultured with autologous peripheral-blood mononuclear cells (PBMCs), and then analyzed by means of intracellular cytokine staining for interleukin-2, CD107a, macrophage inflammatory protein 1 β , tumor necrosis factor α , and interferon- γ on restimulation of cells with the candidate peptides.

STATISTICAL ANALYSIS

The Mann-Whitney test was used to compare mutational loads, and the log-rank test was used to compare Kaplan-Meier curves. The statistical methods used in the study are more fully described in the Supplementary Appendix.

RESULTS

MUTATIONAL LANDSCAPE OF MELANOMAS FROM THE STUDY PATIENTS

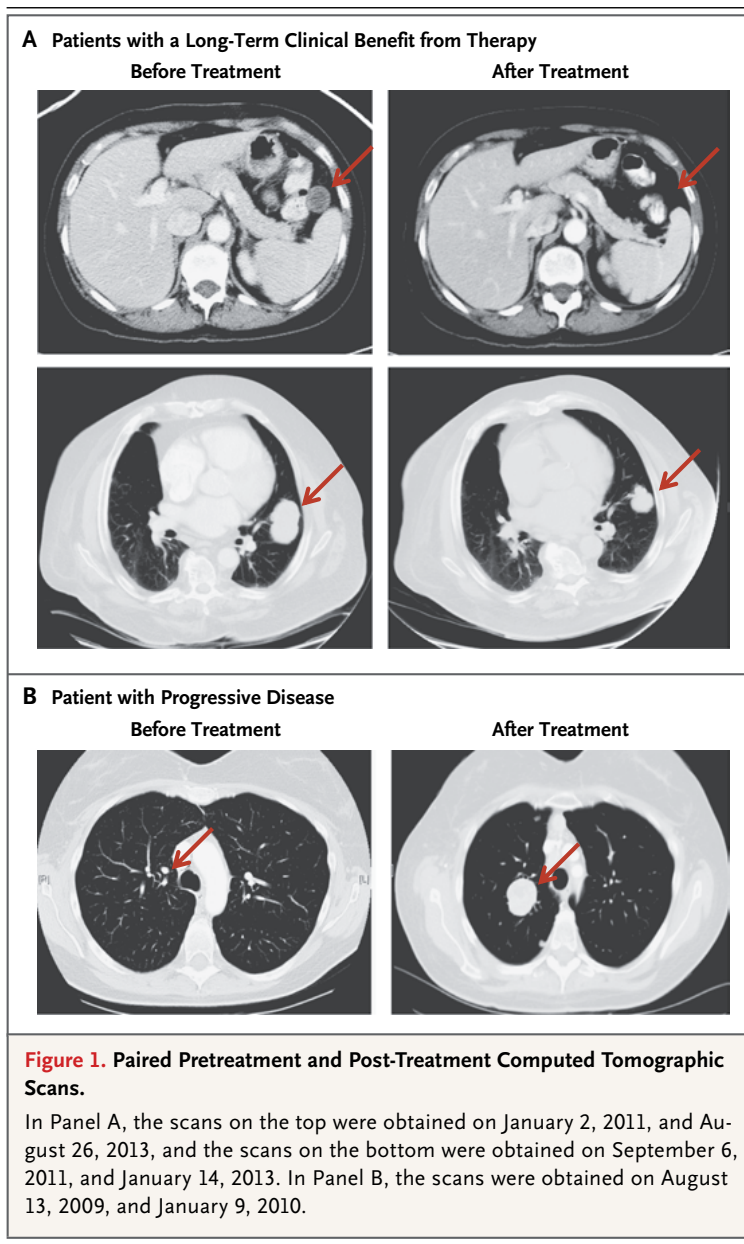
Baseline patient characteristics are shown in Table 1 (for more detailed information, see Tables S1 and S2 in the Supplementary Appendix). The study involved patients with and those without a long-term clinical benefit from therapy (CTLA-4 blockade alone or CTLA-4 blockade with resection of an isolated stable or nonresponding lesion). A long-term clinical benefit was defined by radiographic evidence of freedom from disease or evidence of a stable or decreased volume of disease for more than 6 months. Lack of a long-term ben-

Table 1. Clinical Characteristics of the Patients in the Discovery and Validation Sets, According to Clinical Benefit from Therapy.

Characteristic	Discovery Set		Validation Set	
	Long-Term Benefit (N=11)	Minimal or No Benefit (N=14)	Long-Term Benefit (N=25)	Minimal or No Benefit (N=14)
Age at start of treatment — yr				
Median	63	60	66	57
Range	39–70	48–79	33–90	18–74
Sex — no. of patients (%)				
Female	3 (27)	8 (57)	9 (36)	5 (36)
Male	8 (73)	6 (43)	16 (64)	9 (64)
Disease origin — no. of patients (%)				
Acral	0	3 (21)	1 (4)	1 (7)
Uveal	0	0	1 (4)	0
Cutaneous	10 (91)	8 (57)	15 (60)	11 (79)
Unknown primary	1 (9)	3 (21)	3 (12)	0
Not available	0	0	5 (20)	2 (14)
BRAF or NRAS mutation — no. of patients (%)				
No	1 (9)	6 (43)	17 (68)	11 (79)
Yes	10 (91)	8 (57)	8 (32)	3 (21)
Lactate dehydrogenase level at start of therapy — no. of patients (%)				
Normal	8 (73)	8 (57)	8 (32)	9 (64)
Above normal	2 (18)	5 (36)	3 (12)	3 (21)
Not available	1 (9)	1 (7)	14 (56)	2 (14)
Duration of response to therapy — wk				
Median	59	14	130	11
Range	42–361	11–23	64–376	3–29
Previous therapies — no.*				
Median	1	1	0	0
Range	0–3	0–2	0–2	0–3
Melanoma stage at time of diagnosis — no. of patients (%)				
IIIC	0	0	3 (12)	0
M1a	0	1 (7)	4 (16)	1 (7)
M1b	5 (45)	1 (7)	2 (8)	3 (21)
M1c	6 (55)	12 (86)	16 (64)	10 (71)
Overall survival — yr†				
Median	4.4	0.9	3.3	0.8
Range	2.0–6.9	0.4–2.7	1.6–7.2	0.2–2.1

* Previous therapies included interleukin-2 and cytotoxic chemotherapy.

† Overall survival was calculated from the date of the first dose of ipilimumab to the date of death or censoring of data.



efit was defined by tumor growth on every computed tomographic scan after the initiation of treatment (no benefit) or a clinical benefit lasting 6 months or less (minimal benefit). Representative scans are shown in Figure 1, and Figure S1 in the Supplementary Appendix.

To determine the genetic features associated with a sustained benefit from CTLA-4 blockade, we analyzed DNA in tumor and matched blood samples using whole-exome sequencing. In the discovery set, we generated 6.4 Gb of mapped sequence, with more than 99% of the target sequence covered to at least 10 \times depth and a mean exome coverage of 103 \times (Table S3 and Fig. S2 in

the Supplementary Appendix). The wide ranges of mutational burdens (Fig. 2A, and Table S3 in the Supplementary Appendix) and recurrent and driver mutations (Fig. S2C and S2D and Table S4 in the Supplementary Appendix) among samples were consistent with previously reported findings.^{17–19} The ratio of transitions to transversions (Fig. S2E in the Supplementary Appendix) and the frequency of nucleotide changes (Fig. S2F in the Supplementary Appendix) were similar in the discovery and validation sets.¹² No gene was universally mutated across patients with a sustained benefit.

ASSOCIATION BETWEEN MUTATIONAL BURDEN AND CLINICAL BENEFIT

We hypothesized that an increased mutational burden in metastatic melanoma samples would correlate with a benefit from CTLA-4 blockade. There was a significant difference in mutational load between patients with a long-term clinical benefit and those with a minimal benefit or no benefit, both in the discovery set ($P=0.01$ by the Mann-Whitney test) and in the validation set ($P=0.009$ by the Mann-Whitney test) (Fig. 2A, and Table S5 in the Supplementary Appendix). In the discovery set, a high mutational load was significantly correlated with improved overall survival ($P=0.04$ by the log-rank test) (Fig. 2B), and there was a trend toward improved survival in the validation set (Fig. S3A in the Supplementary Appendix). The latter set included eight patients with nonresponding tumors who otherwise had systemic disease control, which may confound the relationship between mutational load and survival. Further subdivision into four clinical categories was suggestive of a dose-response relationship in the discovery set (Fig. S3B in the Supplementary Appendix). These data indicate that a high mutational load correlates with a sustained clinical benefit from CTLA-4 blockade but that a high load alone is not sufficient to impart a clinical benefit, because there were tumors with a high mutational burden that did not respond to therapy.

SOMATIC NEOEPITOPES IN RESPONDING TUMORS AND EFFICACY OF CTLA-4 BLOCKADE

MHC class I presentation and cytotoxic T-cell recognition are required for ipilimumab activity.¹⁰ Because mutational load alone did not explain a clinical benefit from CTLA-4 blockade, we hypothe-

esized that the presence of specific tumor neoantigens might explain the varied therapeutic benefit. To identify these neoepitopes, we developed a bioinformatic pipeline incorporating prediction of MHC class I binding, modeling of T-cell receptor binding, patient-specific HLA type, and epitope-homology analysis (see the Methods section and Fig. S4 in the Supplementary Appendix).

We created a computational algorithm, called NAseek, to translate all nonsynonymous missense mutations into mutant and nonmutant peptides (see the Methods section and Fig. S4 in the Supplementary Appendix). We examined whether a subgroup of somatic neoepitopes would alter the strength of peptide–MHC binding, using patient-specific HLA types (Table S3 in the Supplementary Appendix). We first compared the overall antigenicity trend of all mutant versus nonmutant peptides. In aggregate, the mutant peptides were predicted to bind MHC class I molecules with higher affinity than the corresponding nonmutant peptides (Fig. S5 in the Supplementary Appendix).

Using only peptides predicted to bind to MHC class I molecules (binding affinity, ≤ 500 nM), we searched for conserved stretches of amino acids shared by multiple tumors. We used standard methods of machine learning, hierarchical clustering, and signature derivation to identify consensus sequences (see the Methods section in the Supplementary Appendix).²⁰ We identified a number of tetrapeptide sequences that were shared by patients with a long-term clinical benefit but completely absent in patients with a minimal benefit or no benefit (Fig. 3A and 3B, and Table S6 in the Supplementary Appendix). It has been shown that short amino acid substrings comprise conserved regions across antigens recognized by a T-cell receptor.²¹ In these experiments, recognition of epitopes was driven by consensus tetrapeptides within the immunogenic peptides, and tetrapeptides within cross-reacting T-cell receptor epitopes were necessary and sufficient to drive T-cell proliferation, findings that are consistent with evidence that this polypeptide length can drive recognition by T-cell receptors.²² Tetrapeptides are used to model genome phylogeny because they occur relatively infrequently in proteins and typically reflect function.²³

We used the discovery set to generate a predictive signature from the candidate neoepitopes

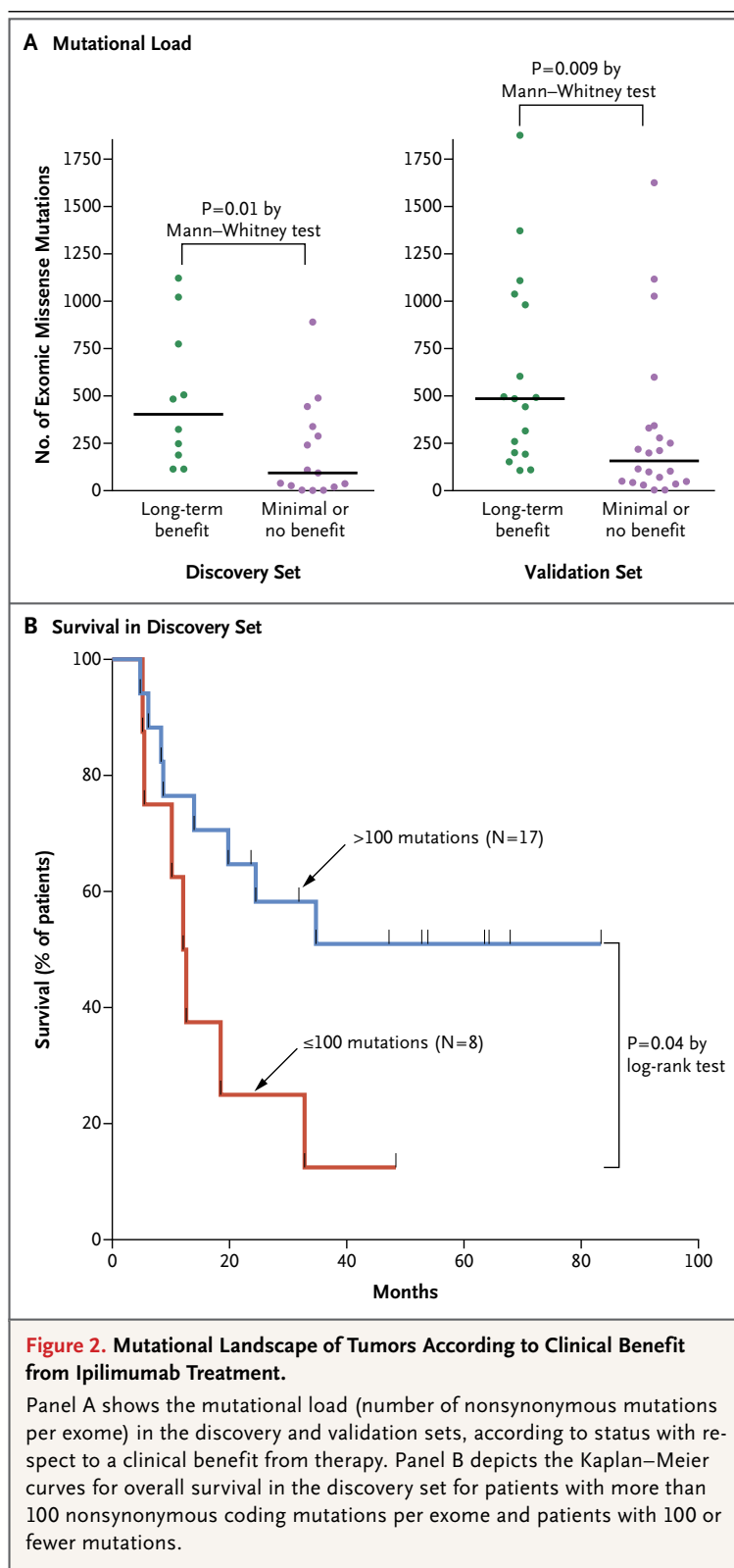


Figure 2. Mutational Landscape of Tumors According to Clinical Benefit from Ipilimumab Treatment.

Panel A shows the mutational load (number of nonsynonymous mutations per exome) in the discovery and validation sets, according to status with respect to a clinical benefit from therapy. Panel B depicts the Kaplan–Meier curves for overall survival in the discovery set for patients with more than 100 nonsynonymous coding mutations per exome and patients with 100 or fewer mutations.

(see the Methods section in the Supplementary Appendix). We found that the tetrapeptides common to each group (candidate neoepitopes) in-

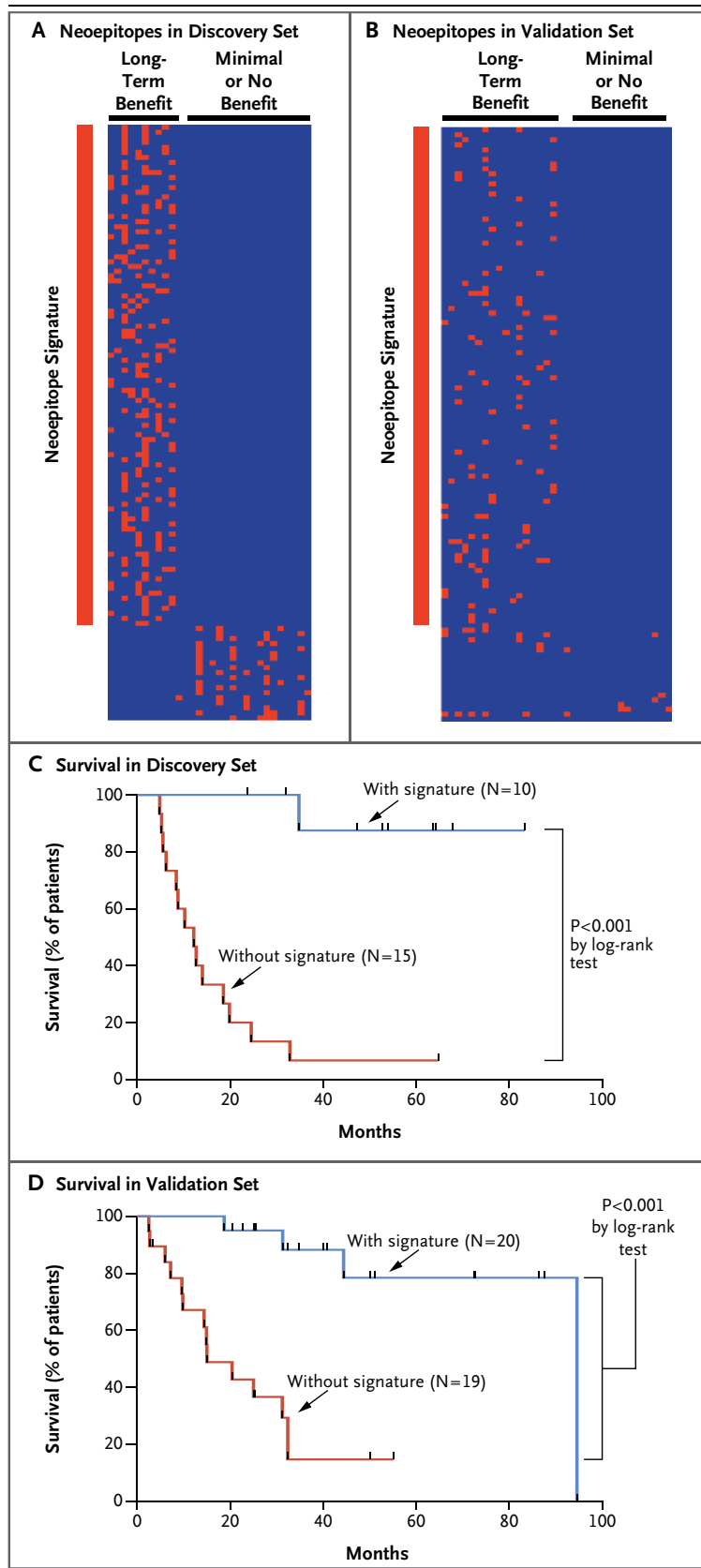


Figure 3. Association of a Neoepitope Signature with a Clinical Benefit from CTLA-4 Blockade.

Candidate neoepitopes were identified by means of mutational analysis, as described in the Methods section in the Supplementary Appendix. Panel A shows a heatmap of candidate tetrapeptide neoantigens that were present in patients with a long-term clinical benefit but absent in patients with a minimal benefit or no benefit in the discovery set (comprising 25 patients). Each row represents a neoepitope; each column represents a patient. The vertical red line indicates the tetrapeptide signature associated with a response to blockade of cytotoxic T-lymphocyte antigen 4 (CTLA-4). The exact tetrapeptides, chromosomal loci, and non-mutant and mutant nonamers in which they occur are listed in Table S6 in the Supplementary Appendix. Panel B shows the same information for the validation set (comprising 39 patients). Panel C shows the Kaplan-Meier curves for overall survival in the discovery set for patients with the signature and those without the signature. Panel D shows the same data for the validation set.

cluded 101 shared exclusively among patients in the discovery set who had a long-term clinical benefit; this was also independently observed in the validation set (Fig. 3A and 3B, and Tables S6 and S7 in the Supplementary Appendix). This set of neoepitopes defines a signature linked to a benefit from CTLA-4 blockade. Because of the size of our discovery set, we cannot exclude the possibility that additional biologically relevant epitopes exist and conversely that there are biologically relevant epitopes that were predicted bioinformatically but were not expressed or presented in patients with a minimal benefit or no benefit (Tables S7A and S7B in the Supplementary Appendix).

Shared tetrapeptide neoepitopes did not simply result from a high mutational load. For example, in the discovery set, the patient with a minimal benefit or no benefit who had the greatest number of mutations (Patient SD7357, who had 1028 mutations) did not share any of the tetrapeptide signatures. This concept was illustrated again in the validation set, in which even tumors from patients with more than 1000 mutations (Patients NR9521 and NR4631) did not respond (Table S3 in the Supplementary Appendix). Simulation testing with five different models showed that the association between the neoepitope signature and a long-term clinical

benefit was highly significant and was unlikely to have resulted from chance alone ($P<0.001$ for four methods and $P=0.002$ for a fifth method) (Fig. S6 in the Supplementary Appendix). A high mutational load appeared to increase the probability, but not guarantee formation, of a neoepitope signature associated with a benefit. Consensus analysis revealed that the neoepitopes were not random. The frequencies of amino acids that made up the tetrapeptides in the group of patients with a long-term clinical benefit were different from those observed in the group with a minimal benefit or no benefit (Fig. S7A in the Supplementary Appendix).

The neoepitope signature derived from the discovery set correlated strongly with survival in both the discovery and validation sets ($P<0.001$ for both comparisons by the log-rank test) (Fig. 3C and 3D). The correlation between mutational load and survival was not as strong (Fig. 2B, and Fig. S3A in the Supplementary Appendix).

The shared tetrapeptides were encoded by mutations in diverse genes across the genome (Fig. S7B and Table S6 in the Supplementary Appendix). Using RNA-sequencing data from the Cancer Genome Atlas, we confirmed that the genes harboring our somatic neoepitopes were widely expressed in melanoma (Table S8 in the Supplementary Appendix). In some cases, the amino acid change resulting from the somatic mutation led to a change in the tetrapeptide itself. In others, the mutant amino acid was separate from the tetrapeptide and altered MHC binding, as has been described previously.²⁴⁻²⁶

In addition, candidate neoepitopes common to both clinical groups were analyzed with the use of the Immune Epitope Database (www.iedb.org). This is the most comprehensive database of experimentally validated, published, and curated antigens, and it has been used to develop algorithms to identify antigens with high accuracy.¹⁴ The candidate neoepitopes common to patients with a long-term clinical benefit were homologous to many more viral and bacterial antigens in the database than were the neoepitopes common to patients with a minimal benefit or no benefit (Table S9 in the Supplementary Appendix). For example, the tetrapeptide substring ESSA was shared by patients with a long-term clinical benefit (Fig. 4A) and corresponds to the

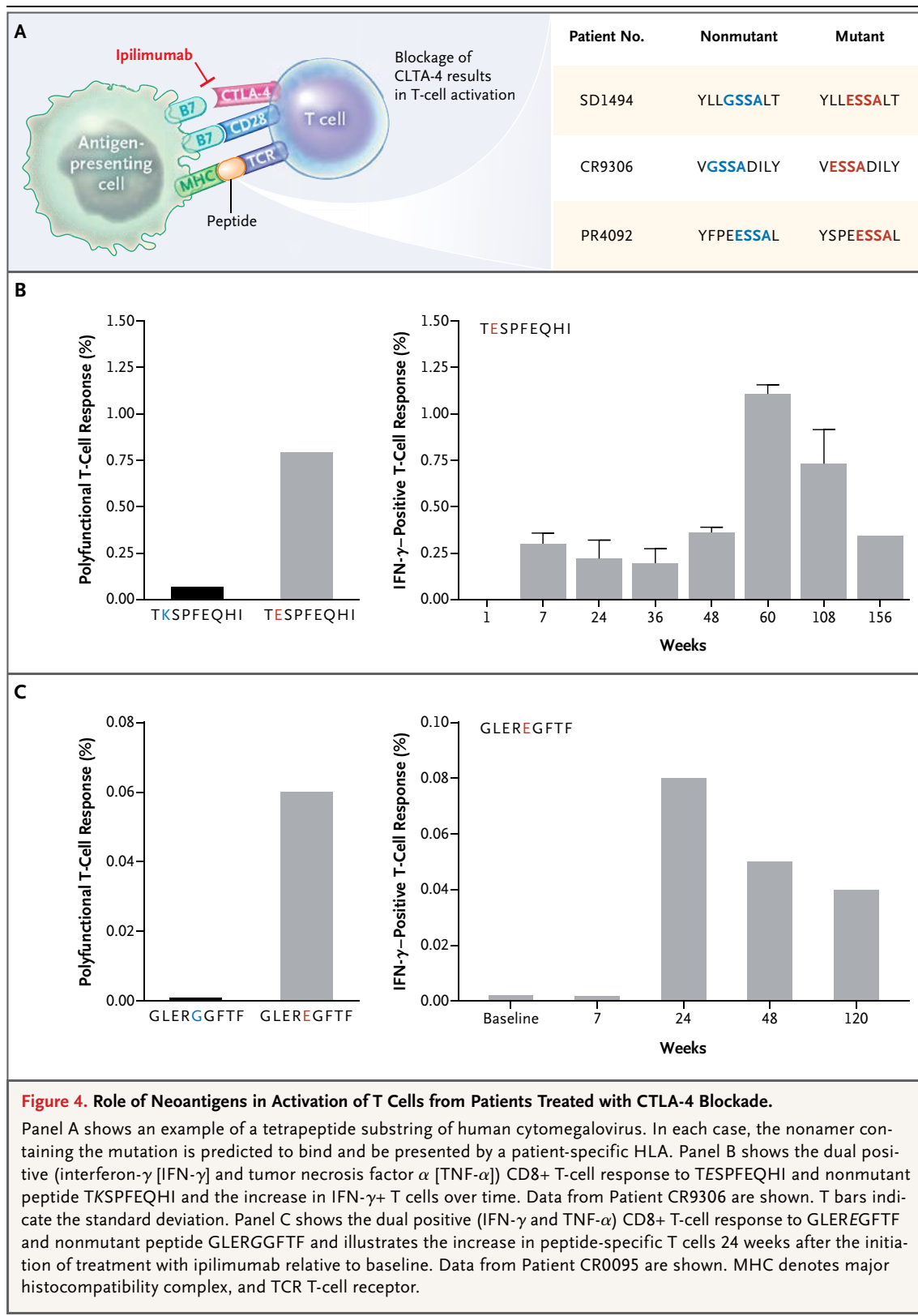
precise antigenic portion of human cytomegalovirus immediate early epitope (MESSAKRKMDP-DNP_D).²⁷ These data suggest that the neoepitopes in patients with strong clinical benefit from CTLA-4 blockade may resemble epitopes from pathogens that T cells are likely to recognize. The cross-reactive peptides defined by short peptide consensus sequences that were discovered by Birnbaum et al. with the use of an unbiased screen also had substantial homology to antigens in microbes.²¹ Although tantalizing, these observations will require further study to confirm.

Using a whole-exome sequencing approach, we characterized the predicted antigenic peptide space (see the Methods section in the Supplementary Appendix). As further validation of our study, we reidentified melanoma antigen recognized by T cells (MART-1, also known as MelanA), an experimentally validated melanocytic antigen (Fig. S8).²⁸ EKLS, which comprises the core amino acids of the MART-1 MHC class II epitope, was shared by patients with a long-term clinical benefit, and the phosphoserine moiety is critical for T-cell receptor recognition.²⁹ The frequency of leukocyte common antigen-positive cells and ratio of CD8-positive cells to FOXP3-positive cells were substantially different between patients with a long-term clinical benefit from ipilimumab and those with a minimal benefit or no benefit (Fig. S9 in the Supplementary Appendix).

IN VITRO VALIDATION OF PREDICTED IMMUNOGENIC PEPTIDES

Translation of next-generation sequencing into in vitro validation of peptide predictions has proven challenging, even in expert hands, with very low published validation rates.¹⁵ In vitro assays are hampered by the paucity of clinical samples, the sensitivity of preserved cells to the freeze-thaw process, the low frequency of anti-neoantigen T cells in clinical samples, and the very low sensitivity of T cells in vitro in the absence of the complex in vivo immunogenic microenvironment.

We attempted to optimize prediction by integrating multiple high-throughput approaches (Fig. S4 in the Supplementary Appendix). On the basis of our prediction algorithm, we generated pools of peptides and performed assays of T-cell activation for patients for whom we had suffi-



cient lymphocytes (see the Methods section in the Supplementary Appendix). Positive pools were observed for three of five patients (Fig. S10A, S10B, and S10C in the Supplementary Appendix). We identified the exact peptides for patients with adequate PBMCs. We found a polyfunctional T-cell response to the peptide TESPFEQHI in Patient CR9306 (Fig. S10D in the Supplementary Appendix) but not to its nonmutant counterpart, TKSPFEQHI. This response peaked at 60 weeks after the initiation of treatment (Fig. 4B). T-cell responses were absent in healthy donors (Fig. S10E in the Supplementary Appendix). TESPFEQHI had a predicted MHC class I affinity for B4402 of 472 nM, as compared with 18323 nM for TKSPFEQHI. ESPF is a common tetrapeptide found in the response signature and is a substring (positions 176 through 179) of the hepatitis D virus large delta epitope p27 (PESPF and ESPFAR).³⁰ TESPFEQHI results from a mutation in FAM3C (c.A577G;p.K193E), a gene highly expressed in melanoma (Table S8 in the Supplementary Appendix).

We also found that peptide GLEREGFTF elicited a polyfunctional T-cell response in Patient CR0095 (Fig. 4C, and Fig. S10F in the Supplementary Appendix), whereas nonmutant GLERGGFTF did not. This response peaked at 24 weeks after the initiation of treatment (Fig. 4C). GLEREGFTF arises from a mutation in CSMD1 (c.G10337A;p.G3446E), which is also highly expressed in melanoma (Table S8 in the Supplementary Appendix), and the peptide has 80% homology to a known *Burkholderia pseudomallei* antigen (Immune Epitope Database Reference ID: 1027043). The lack of T-cell activation may not rule out a given neoantigen because in vitro assays are limited in sensitivity, as described above.

DISCUSSION

Anti-CTLA-4 and anti-programmed cell death 1 antibodies have resulted in long-term disease control in a subgroup of patients with melanoma.^{1,2} Here, we have illustrated the importance of tumor genetics in defining the basis of the clinical benefit from CTLA-4 blockade.

Our observations suggest a number of principles relevant to immunotherapy for cancer.

Although a high mutational load is associated with a benefit from immune checkpoint abrogation, this factor alone is not sufficient to impart a clinical benefit. Rather, there are somatic neoepitopes that are shared by patients with a prolonged benefit and are absent in those without a prolonged benefit. Owing to somatic mutations, a subset of proteins present in the tumor becomes recognized by the immune system as nonself, given their novelty in the tumor context.^{8,14,31,32} These concepts were formulated in the discovery set and confirmed in the validation set.

It is well known in the field of infectious diseases that an individual amino acid within a peptide can affect immunogenicity by altering peptide–MHC or peptide–T-cell receptor interactions.^{33,34} In cancers, the altered amino acid residue resulting from a single missense mutation can create a T-cell epitope from a previously self peptide.^{31,32,35} In the patients described here, altered amino acids resulting from tumor mutations caused the tumors to display somatic neoepitopes that elicited an antitumor response augmented by CTLA-4 blockade.

Our study has limitations. Although large for a genomic study (128 exomes), our sample size was limited, patients had received a variety of previous treatments, and tumor samples were obtained at various time points. Furthermore, although the panel of somatic neoepitopes (Fig. 3A and 3B, and Table S6 in the Supplementary Appendix) may constitute the most important ones, the *in vivo* relative immunologic contribution of each peptide is unclear. However, data showing that functionally important immunogenic epitopes persisted after treatment with expanded tumor-infiltrating lymphocytes suggest that the response to mutations may persist over time.¹⁶ Although the recapitulation of the neoantigen signature in the validation set suggests that this may provide a generally applicable tool for prediction of a benefit from immunotherapy, further studies will be needed to investigate the role of MHC class II molecules and the relative effects and characteristics of neoantigens in different cancers.

Our use of whole-exome sequencing to identify a genetic basis associated with a benefit from

CTLA-4 blockade provides proof of principle that tumor genomics can inform responses to immunotherapy. For the field of cancer genetics, these data suggest a need for an expanded definition of the previous categories of driver and passenger mutations. Our data show that exonic missense mutations in general confer increased MHC class I binding (Fig. S5A and S5B in the Supplementary Appendix) and confirm the hypothesis³⁶ that some mutations formerly categorized as passengers may in fact represent “immune determinants.”

Supported by grants from the Frederick Adler Fund, the National Institutes of Health, Swim across America, the Ludwig Trust, the Melanoma Research Alliance, the Stand Up to Cancer–Cancer Research Institute Immunotherapy Dream Team, the Hazen Polsky Foundation, and the STARR Cancer Consortium and by a Ruth L. Kirschstein National Research Service Award (T32CA009512, to Dr. Snyder). Bristol-Myers Squibb, the employer of two authors, did not provide funding for this study.

Disclosure forms provided by the authors are available with the full text of this article at NEJM.org.

We thank Martin Miller at Memorial Sloan Kettering Cancer Center (MSKCC) for his assistance with the NetMHC server, Agnes Viale and Kety Huberman at the MSKCC Genomics Core, Annamalai Selvakumar and Alice Yeh at the MSKCC HLA typing laboratory for their technical assistance, and John Khoury for assistance in chart review.

REFERENCES

- Hodi FS, O'Day SJ, McDermott DF, et al. Improved survival with ipilimumab in patients with metastatic melanoma. *N Engl J Med* 2010;363:711-23. [Erratum, *N Engl J Med* 2010;363:1290.]
- Wolchok JD, Kluger H, Callahan MK, et al. Nivolumab plus ipilimumab in advanced melanoma. *N Engl J Med* 2013;369:122-33.
- Ku GY, Yuan J, Page DB, et al. Single-institution experience with ipilimumab in advanced melanoma patients in the compassionate use setting: lymphocyte count after 2 doses correlates with survival. *Cancer* 2010;116:1767-75.
- Ji RR, Chasalow SD, Wang L, et al. An immune-active tumor microenvironment favors clinical response to ipilimumab. *Cancer Immunol Immunother* 2012;61:1019-31.
- Gajewski TF, Louahed J, Brichard VG. Gene signature in melanoma associated with clinical activity: a potential clue to unlock cancer immunotherapy. *Cancer* 2010;16:399-403.
- Cha E, Klinger M, Hou Y, et al. Improved survival with T cell clonotype stability after anti-CTLA-4 treatment in cancer patients. *Sci Transl Med* 2014;6:238ra70.
- Castle JC, Kreiter S, Diekmann J, et al. Exploiting the mutanome for tumor vaccination. *Cancer Res* 2012;72:1081-91.
- Srivastava N, Srivastava PK. Modeling the repertoire of true tumor-specific MHC I epitopes in a human tumor. *PLoS One* 2009;4(7):e6094.
- Kvistborg P, Philips D, Kelderman S, et al. Anti-CTLA-4 therapy broadens the melanoma-reactive CD8+ T cell response. *Sci Transl Med* 2014;6:254ra128.
- Peggs KS, Quezada SA, Chambers CA, Korman AJ, Allison JP. Blockade of CTLA-4 on both effector and regulatory T cell compartments contributes to the antitumor activity of anti-CTLA-4 antibodies. *J Exp Med* 2009;206:1717-25.
- Wolchok JD, Weber JS, Hamid O, et al. Ipilimumab efficacy and safety in patients with advanced melanoma: a retrospective analysis of HLA subtype from four trials. *Cancer Immun* 2010;10:9.
- Alexandrov LB, Nik-Zainal S, Wedge DC, et al. Signatures of mutational processes in human cancer. *Nature* 2013;500:415-21.
- Segal NH, Parsons DW, Peggs KS, et al. Epitope landscape in breast and colorectal cancer. *Cancer Res* 2008;68:889-92.
- Matsushita H, Vesely MD, Koboldt DC, et al. Cancer exome analysis reveals a T-cell-dependent mechanism of cancer immunoediting. *Nature* 2012;482:400-4.
- van Rooij N, van Buuren MM, Philips D, et al. Tumor exome analysis reveals neoantigen-specific T-cell reactivity in an ipilimumab-responsive melanoma. *J Clin Oncol* 2013;31(32):e439-e442.
- Tran E, Turcotte S, Gros A, et al. Cancer immunotherapy based on mutation-specific CD4+ T cells in a patient with epithelial cancer. *Science* 2014;344:641-5.
- Wei X, Walia V, Lin JC, et al. Exome sequencing identifies GRIN2A as frequently mutated in melanoma. *Nat Genet* 2011;43:442-6.
- Berger MF, Hodis E, Heffernan TP, et al. Melanoma genome sequencing reveals frequent PREX2 mutations. *Nature* 2012;485:502-6.
- Hodis E, Watson IR, Kryukov GV, et al. A landscape of driver mutations in melanoma. *Cell* 2012;150:251-63.
- Park YY, Park ES, Kim SB, et al. Development and validation of a prognostic gene-expression signature for lung adenocarcinoma. *PLoS One* 2012;7(9):e44225.
- Birnbaum ME, Mendoza JL, Sethi DK, et al. Deconstructing the peptide-MHC specificity of T cell recognition. *Cell* 2014;157:1073-87.
- Morita D, Yamamoto Y, Suzuki J, Mori N, Igarashi T, Sugita M. Molecular requirements for T cell recognition of N-myristoylated peptides derived from the simian immunodeficiency virus Nef protein. *J Virol* 2013;87:482-8.
- Stuart GW, Moffett K, Leader JJ. A comprehensive vertebrate phylogeny using vector representations of protein sequences from whole genomes. *Mol Biol Evol* 2002;19:554-62.
- Aleksic M, Dushek O, Zhang H, et al. Dependence of T cell antigen recognition on T cell receptor-peptide MHC confinement time. *Immunity* 2010;32:163-74.
- Insaidoo FK, Borbulevych OY, Hosain M, Santhanagopalan SM, Baxter TK, Baker BM. Loss of T cell antigen recognition arising from changes in peptide and major histocompatibility complex protein flexibility: implications for vaccine design. *J Biol Chem* 2011;286:40163-73.
- Sliz P, Michelin O, Cerottini JC, et al. Crystal structures of two closely related but antigenically distinct HLA-A2/melanocyte-melanoma tumor-antigen peptide complexes. *J Immunol* 2001;167:3276-84.
- Lim JB, Kim HO, Jeong SH, et al. Identification of HLA-A*2402-restricted HCMV immediate early-1 (IE-1) epitopes as targets for CD8+ HCMV-specific cytotoxic T lymphocytes. *J Transl Med* 2009;7:72.
- Wong R, Lau R, Chang J, et al. Immune responses to a class II helper peptide epitope in patients with stage III/IV resected melanoma. *Clin Cancer Res* 2004;10:5004-13.
- Li Y, Depontieu FR, Sidney J, et al. Structural basis for the presentation of tumor-associated MHC class II-restricted phosphopeptides to CD4+ T cells. *J Mol Biol* 2010;399:596-603.
- Poisson F, Baillou F, Dubois F, Janvier B, Roingeard P, Goudeau A. Immune response to synthetic peptides of hepatitis delta antigen. *J Clin Microbiol* 1993;31:2343-9.
- Monach PA, Meredith SC, Siegel CT, Schreiber H. A unique tumor antigen produced by a single amino acid substitution. *Immunity* 1995;2:45-59.
- Dubey P, Hendrickson RC, Meredith SC, et al. The immunodominant antigen of an ultraviolet-induced regressive tumor is generated by a somatic point mutation

- in the DEAD box helicase p68. *J Exp Med* 1997;185:695-705.
- 33.** Allen PM, Matsueda GR, Evans RJ, Dunbar JB Jr, Marshall GR, Unanue ER. Identification of the T-cell and Ia contact residues of a T-cell antigenic epitope. *Nature* 1987;327:713-5.
- 34.** Anderson MW, Gorski J, Cutting edge: TCR contacts as anchors: effects on affinity and HLA-DM stability. *J Immunol* 2003;171:5683-7.
- 35.** Noguchi Y, Chen YT, Old LJ. A mouse mutant p53 product recognized by CD4+ and CD8+ T cells. *Proc Natl Acad Sci U S A* 1994;91:3171-5.
- 36.** Srivastava PK, Duan F. Harnessing the antigenic fingerprint of each individual cancer for immunotherapy of human cancer: genomics shows a new way and its challenges. *Cancer Immunol Immunother* 2013;62:967-74.

Copyright © 2014 Massachusetts Medical Society.

This copy is for your personal, non-commercial use only.

If you wish to distribute this article to others, you can order high-quality copies for your colleagues, clients, or customers by [clicking here](#).

Permission to republish or repurpose articles or portions of articles can be obtained by following the guidelines [here](#).

The following resources related to this article are available online at www.sciencemag.org (this information is current as of May 12, 2014):

Updated information and services, including high-resolution figures, can be found in the online version of this article at:

<http://www.sciencemag.org/content/344/6184/641.full.html>

Supporting Online Material can be found at:

<http://www.sciencemag.org/content/suppl/2014/05/07/344.6184.641.DC1.html>

A list of selected additional articles on the Science Web sites related to this article can be found at:

<http://www.sciencemag.org/content/344/6184/641.full.html#related>

This article cites 26 articles, 19 of which can be accessed free:

<http://www.sciencemag.org/content/344/6184/641.full.html#ref-list-1>

This article appears in the following subject collections:

Immunology

<http://www.sciencemag.org/cgi/collection/immunology>

Medicine, Diseases

<http://www.sciencemag.org/cgi/collection/medicine>

co-regulators, the DELLA proteins (12), which potentiate the ability of SPL9 (directly) and LFY (indirectly) to induce *API* and to trigger the onset of flower formation (fig. S9). LFY initiates the reduction in gibberellin levels—which results in increased DELLA accumulation—at least in part by inducing expression of the gibberellin catabolism enzyme ELA1.

Our findings may help explain the previously paradoxical observation that gibberellin acts positively in the switch to reproductive development in most plants but negatively in some woody plant species, such as grapevine (29). In addition, our data make gibberellin a prime candidate for a “branching” factor predicted by mathematical modeling of inflorescence architectures (30). Finally, our results suggest that the degree of inflorescence branching, which determines seed yield and, thus, reproductive success, could be adjusted by altering gibberellin accumulation before the inflorescence forms or the rate of gibberellin catabolism thereafter.

References and Notes

- T. A. Steeves, I. Sussex, *Pattern in Plant Development* (Cambridge Univ. Press, Cambridge, 1989).
- R. S. Poethig, *Science* **250**, 923–930 (1990).
- O. J. Ratcliffe, D. J. Bradley, E. S. Coen, *Development* **126**, 1109–1120 (1999).
- F. D. Hempel *et al.*, *Development* **124**, 3845–3853 (1997).
- C. M. Winter *et al.*, *Dev. Cell* **20**, 430–443 (2011).
- M. Schmid *et al.*, *Nat. Genet.* **37**, 501–506 (2005).
- M. Schmid *et al.*, *Development* **130**, 6001–6012 (2003).
- D. Weigel, J. Alvarez, D. R. Smyth, M. F. Yanofsky, E. M. Meyerowitz, *Cell* **69**, 843–859 (1992).
- D. Weigel, O. Nilsson, *Nature* **377**, 495–500 (1995).
- Y. Zhang *et al.*, *Plant J.* **67**, 342–353 (2011).
- T. Nomura *et al.*, *Plant Cell Physiol.* **54**, 1837–1851 (2013).
- A. Dill, H. S. Jung, T. P. Sun, *Proc. Natl. Acad. Sci. U.S.A.* **98**, 14162–14167 (2001).
- R. Zentella *et al.*, *Plant Cell* **19**, 3037–3057 (2007).
- M. Koornneef, J. H. van der Veen, *Theor. Appl. Genet.* **58**, 257–263 (1980).
- J. Langridge, *Nature* **180**, 36–37 (1957).
- V. C. Galvão, D. Horrer, F. Küttner, M. Schmid, *Development* **139**, 4072–4082 (2012).
- A. Porri, S. Torti, M. Romera-Branchat, G. Coupland, *Development* **139**, 2198–2209 (2012).
- S. Yu *et al.*, *Plant Cell* **24**, 3320–3332 (2012).
- R. N. Wilson, J. W. Heckman, C. R. Somerville, *Plant Physiol.* **100**, 403–408 (1992).
- M. Koornneef, C. J. Hanhart, J. H. van der Veen, *Mol. Gen. Genet.* **229**, 57–66 (1991).
- W. Rademacher, *Annu. Rev. Plant Physiol. Plant Mol. Biol.* **51**, 501–531 (2000).
- J. M. Davière, P. Achard, *Development* **140**, 1147–1151 (2013).
- X. Hou, L. Y. Lee, K. Xia, Y. Yan, H. Yu, *Dev. Cell* **19**, 884–894 (2010).
- K. Hirano *et al.*, *Plant J.* **71**, 443–453 (2012).
- J. W. Wang, B. Czech, D. Weigel, *Cell* **138**, 738–749 (2009).
- N. Yu *et al.*, *Plant Cell* **22**, 2322–2335 (2010).
- M. A. Blázquez, D. Weigel, *Nature* **404**, 889–892 (2000).
- S. Eriksson, H. Böhnenius, T. Moritz, O. Nilsson, *Plant Cell* **18**, 2172–2181 (2006).
- P. K. Boss, M. R. Thomas, *Nature* **416**, 847–850 (2002).
- P. Prusinkiewicz, Y. Erasmus, B. Lane, L. D. Harder, E. Coen, *Science* **316**, 1452–1456 (2007).

Acknowledgments: We are grateful to Wagner laboratory members and K. Gallagher, R. S. Poethig, and J. D. Wagner for critical comments. We thank R. Austin for the LFY binding motif functional depth analyses, T. Sun for pRGA:RGA-GFP and GA pathway mutant seeds, X. Chen for 35S:AlcR pAlcA:MIR156f and pRGA:RGA-HA seeds, M. Schmid for RGL1 and rgl1delta17 constructs, S. Poethig for pSPL9:FLAG and 35S:SPL9-GR seeds, H. Yu for ga1-3 rgl2-1 rga-2 35S:RGA-GR seeds, G. Angenent for pAP1:AP1-GFP seeds, and the *Arabidopsis* Biological Resource Center for insertion mutant seeds and the F6A4 bacterial artificial chromosome clone. This work was supported by NSF grants IOS 0849298 and 1257111 to D.W. and training grant T32-HD007516 (Developmental Biology) support to C.M.W.

Supplementary Materials

www.sciencemag.org/content/344/6184/638/suppl/DC1

Materials and Methods

Figs. S1 to S9

Tables S1 and S2

References (31–65)

7 January 2014; accepted 2 April 2014

10.1126/science.1250498

Cancer Immunotherapy Based on Mutation-Specific CD4+ T Cells in a Patient with Epithelial Cancer

Eric Tran,¹ Simon Turcotte,^{1*} Alena Gros,¹ Paul F. Robbins,¹ Yong-Chen Lu,¹ Mark E. Dudley,^{1†} John R. Wunderlich,¹ Robert P. Somerville,¹ Katherine Hogan,¹ Christian S. Hinrichs,¹ Maria R. Parkhurst,¹ James C. Yang,¹ Steven A. Rosenberg^{1‡}

Limited evidence exists that humans mount a mutation-specific T cell response to epithelial cancers. We used a whole-exomic-sequencing-based approach to demonstrate that tumor-infiltrating lymphocytes (TIL) from a patient with metastatic cholangiocarcinoma contained CD4+ T helper 1 (T_H1) cells recognizing a mutation in erbB2 interacting protein (ERBB2IP) expressed by the cancer. After adoptive transfer of TIL containing about 25% mutation-specific polyfunctional T_H1 cells, the patient achieved a decrease in target lesions with prolonged stabilization of disease. Upon disease progression, the patient was retreated with a >95% pure population of mutation-reactive T_H1 cells and again experienced tumor regression. These results provide evidence that a CD4+ T cell response against a mutated antigen can be harnessed to mediate regression of a metastatic epithelial cancer.

The human immune system has evolved to recognize and eliminate cells expressing foreign, nonself antigens. All malignant tumors harbor nonsynonymous mutations or other genetic alterations (1), some of which may generate neo-“nonself” epitopes that could potentially trigger an antitumor T cell response. Indeed, mutation-reactive T cells can frequently be found infiltrating human melanomas (2) and likely play a critical role in the clinical efficacy of adoptive cell therapy (ACT) and other immunotherapies in melanoma (3–7).

However, limited evidence exists demonstrating that the human immune system can mount an endogenous, mutation-specific T cell response against epithelial cancers that comprise over 80% of all human malignancies (8–11), and it is unclear whether this response can be harnessed to develop effective personalized cancer immunotherapies (12). Moreover, epithelial cancers often contain fewer mutations than melanoma (1), which may decrease the probability of eliciting a mutation-specific T cell response. We thus first set out to determine

whether tumor-infiltrating lymphocytes (TIL) recognizing patient-specific mutations can be identified in patients with metastatic gastrointestinal (GI) cancers.

To this end, a 43-year-old woman with widely metastatic cholangiocarcinoma (patient 3737, table S1) who progressed through multiple chemotherapy regimens was enrolled in a TIL-based ACT protocol for patients with GI cancers (NCT01174121) (13). Lung metastases were resected and used as a source for whole-exomic sequencing and generation of T cells for treatment. Whole-exomic sequencing revealed 26 nonsynonymous mutations (table S2). To test whether the patient’s TIL recognized any of these mutations, we used a minigene approach. Briefly, for each mutation we designed a minigene construct that encoded for the mutated amino acid flanked on each side by 12 amino acids from the endogenous protein (fig. S1). Multiple minigenes were synthesized in tandem to generate tandem minigene (TMG) constructs (fig. S1 and table S3), which were then used as templates for the generation of in vitro transcribed (IVT) RNA (13). Each of these IVT TMG RNAs was then

¹Surgery Branch, National Cancer Institute (NCI), National Institutes of Health, Bethesda, MD 20892, USA.

*Present address: Department of Surgery, Université de Montréal, and Institut du Cancer de Montréal, Centre de Recherche du Centre Hospitalier de l’Université de Montréal, Montréal, QC H2X0A9, Canada.

†Present address: Cell and Gene Therapies, Novartis Institutes for BioMedical Research Incorporated, Cambridge, MA 02139, USA.

‡Corresponding author. E-mail: sar@nih.gov

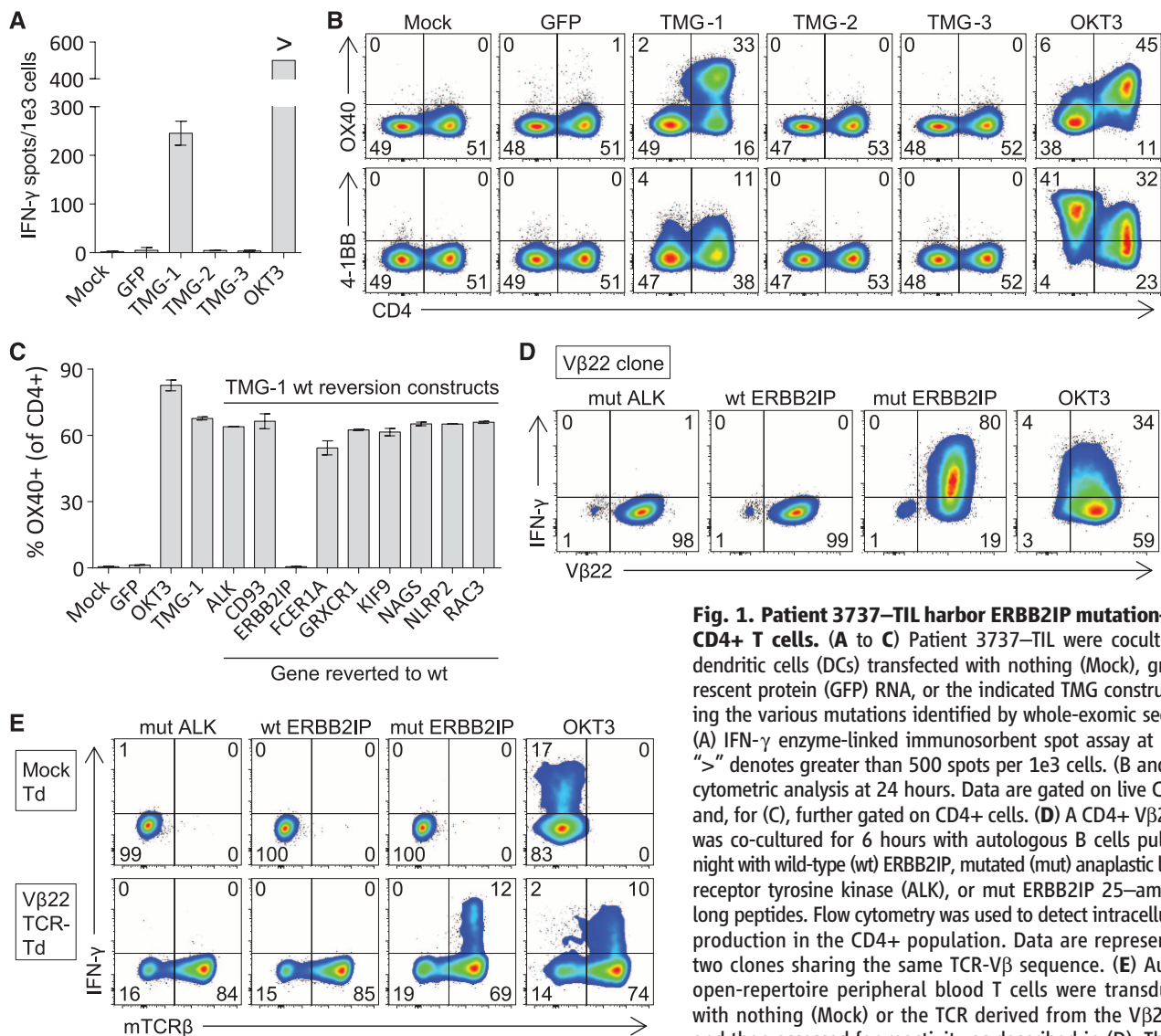


Fig. 1. Patient 3737-TIL harbor ERBB2IP mutation-specific CD4+ T cells. (A to C) Patient 3737-TIL were cocultured with dendritic cells (DCs) transfected with nothing (Mock), green fluorescent protein (GFP) RNA, or the indicated TMG construct encoding the various mutations identified by whole-exomic sequencing. (A) IFN- γ enzyme-linked immunosorbent spot assay at 20 hours. “>” denotes greater than 500 spots per 1e3 cells. (B and C) Flow-cytometric analysis at 24 hours. Data are gated on live CD3+ cells and, for (C), further gated on CD4+ cells. (D) A CD4+ V β 22+ clone was co-cultured for 6 hours with autologous B cells pulsed overnight with wild-type (wt) ERBB2IP, mutated (mut) anaplastic lymphoma receptor tyrosine kinase (ALK), or mut ERBB2IP 25-amino acid-long peptides. Flow cytometry was used to detect intracellular IFN- γ production in the CD4+ population. Data are representative of two clones sharing the same TCR-V β sequence. (E) Autologous open-reertoire peripheral blood T cells were transduced (Td) with nothing (Mock) or the TCR derived from the V β 22+ clone and then assessed for reactivity as described in (D). The endogenous V β 22+ TCR constant regions were swapped with mouse constant regions, allowing for the detection of the introduced TCR using antibodies against the mouse TCR β constant region (mTCR β). Plate-bound OKT3 was used as a control in all assays. All data are representative of at least two independent experiments. Error bars are SD.

individually transfected into autologous antigen-presenting cells, followed by a coculture with TIL to determine whether any of the processed and presented mutated antigens were recognized by TIL. We observed reactivity of 3737-TIL to a mutated antigen present in TMG-1 but not TMG-2 or TMG-3 (Fig. 1A). Moreover, the reactivity predominated in the CD4+ T cell population, as demonstrated by up-regulation of the activation markers OX40 and 4-1BB (Fig. 1B). Although some 4-1BB up-regulation was observed in the CD4-negative (CD8+) T cell population, we sorted these cells and found no reactivity against the TMG. To determine which of the nine mutations in TMG-1 was being recognized by 3737-TIL, we synthesized nine additional TMG-1 constructs, each one containing a reversion of one of the mutations back to the wild-type sequence. Reactivity of 3737-TIL to TMG-1 was abrogated only when the erb2 interacting protein (*ERBB2IP*) muta-

tion was reverted back to the wild-type sequence, indicating that the TIL specifically recognized the ERBB2IP^{E805G} mutation (Fig. 1C). The response was restricted by HLA-DQB1*0601, and the minimal epitope was located within the 13-amino acid sequence NSKEETGHLENGN (where E is Glu; G, Gly; H, His; K, Lys; L, Leu; N, Asn; S, Ser; and T, Thr) (fig. S2).

We next characterized the clonality of the mutated ERBB2IP-specific CD4+ T cells by sorting them after antigen-specific activation, using OX40 as a marker of activation (fig. S3A). These cells were then bulk-expanded and cloned by limiting dilution. A flow cytometry-based survey of the T cell receptor-V β (TCR-V β) repertoire demonstrated that the bulk-expanded population was >95% V β 22+ and that 10/11 clones assessed were purely V β 22+ (fig. S3, B and C). TCR sequence analysis revealed the same TCR β variable, diversity, joining (V-D-J) sequence in

6/6 V β 22+ clones tested (table S4), suggesting that the majority of the ERBB2IP mutation-reactive T cells was composed of a dominant V β 22+ T cell clone. T cell clones expressing this V β 22 TCR specifically produced the cytokine interferon (IFN)- γ upon stimulation with the mutated ERBB2IP peptide (Fig. 1D). Moreover, autologous open-reertoire peripheral blood T cells genetically modified with this TCR-V β 22 chain matched with its alpha chain (table S5) conferred specific reactivity to the mutated ERBB2IP peptide (Fig. 1E), demonstrating that this TCR specifically recognized the ERBB2IP^{E805G} mutation.

The patient underwent adoptive transfer of 42.4 billion TIL containing CD4+ ERBB2IP mutation-reactive T cells followed by four doses of interleukin (IL)-2 to enhance T cell proliferation and function (fig. S4). Flow cytometry analysis demonstrated that about 25% of the entire 3737-TIL product administered was composed of the

Fig. 2. Adoptive transfer of TIL containing ERBB2IP mutation-reactive T cells. (A) Flow-cytometric analysis of the TCR-V β repertoire of 3737-TIL, gated on live CD4+ or CD8+ T cells. (B) Patient 3737-TIL were cocultured with DCs transfected with TMG-1 or TMG-1

encoding the wt ERBB2IP reversion, and flow cytometry was used to assess OX40 and V β 22 expression on CD4+ T cells at 24 hours post-stimulation. Plate-bound OKT3 stimulation was used as a positive control. (A) and (B) are representative of at least two independent experiments. (C) IFN- γ enzyme-linked immunosorbent assay on patient 3737 serum samples pre- and post-adoptive cell transfer of 3737-TIL. Error bars are SEM. (D) Tumor growth curves [Response Evaluation Criteria in Solid Tumors (RECIST), sum of maximum diameters] before and after infusion of 3737-TIL. Data are expressed as a change in percent from pretreatment baseline and stratified on lung, liver, and total tumors.

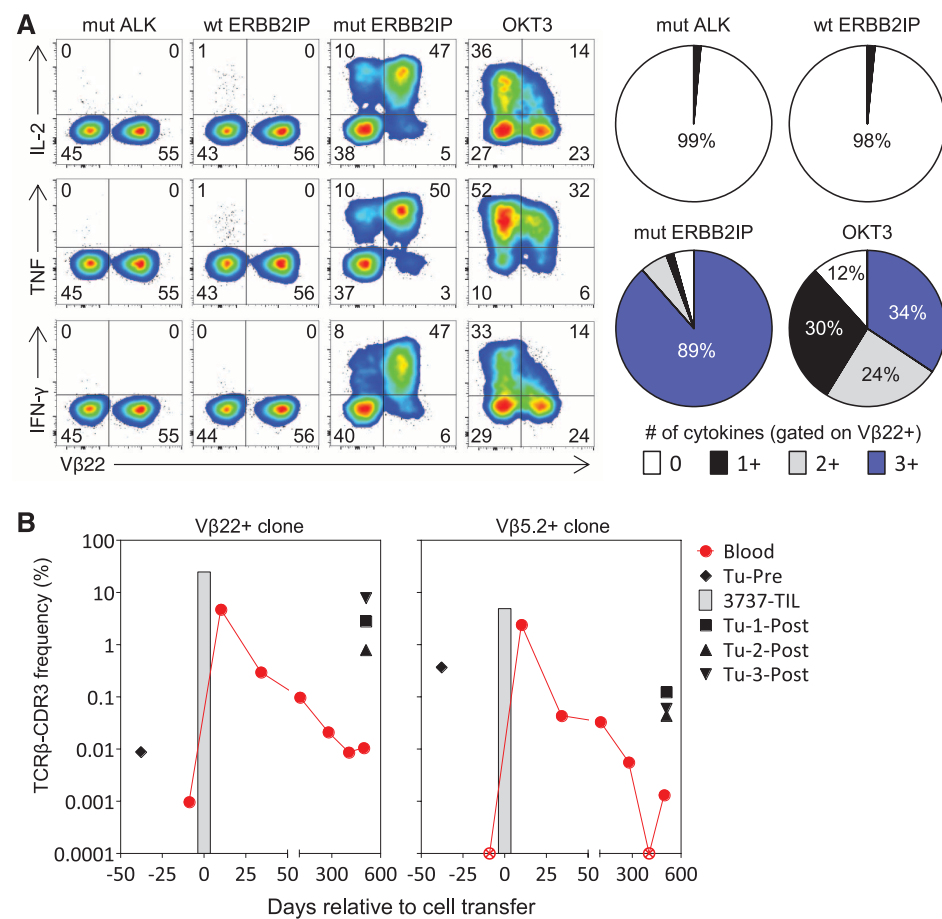
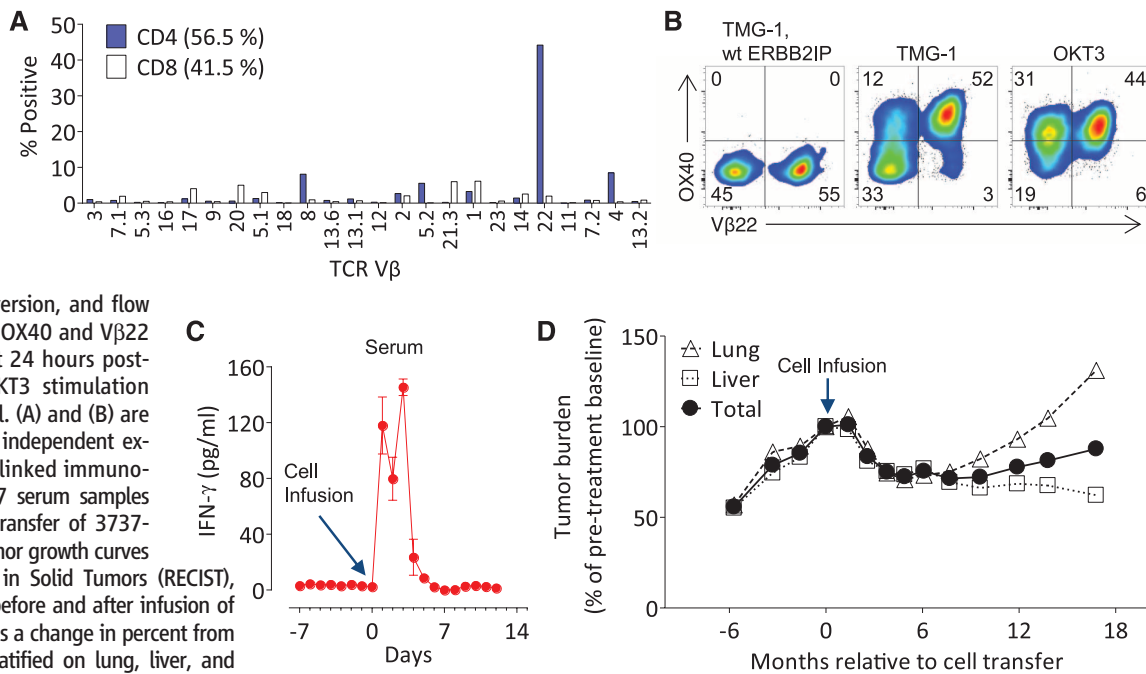


Fig. 3. Functional phenotype and persistence of ERBB2IP mutation-specific CD4+ T cells. (A) Patient 3737-TIL were cocultured for 6 hours with autologous B cells pulsed overnight with wt ERBB2IP, mut ALK, or mut ERBB2IP 25-amino acid-long peptides. Flow cytometry was used to assess expression of V β 22 and to detect intracellular production of IL-2, TNF, and IFN- γ in the CD4+ population. Pie charts display the percentage of V β 22+ cells that expressed the indicated number of cytokines. Data are representative of at least three independent experiments. (B) TCR-V β deep sequencing of 3737-TIL and blood and tumors of patient 3737 at various times pre- and post-adoptive cell transfer with 3737-TIL. Data show the frequency of the two ERBB2IP mutation-specific TCR β -CDR3 clonotypes. \otimes , not detected.

V β 22+, mutation-reactive T cells (Fig. 2, A and B), equating to the infusion of over 10 billion ERBB2IP mutation-specific CD4+ T cells. Elevated levels of IFN- γ were detected in the patient's serum for the first 5 days after cell infusion (Fig. 2C). Although the patient had clear evidence of progressive disease before the cell infusion, tumor regression was observed by the 2-month follow-up, and all target lung and liver lesions continued to regress, reaching a maximum reduction of 30% at 7 months post-treatment (Fig. 2D). The patient experienced disease stabilization for about 13 months after cell infusion, after which disease progression was observed only in the lungs but not liver.

To determine whether there was evidence that the CD4+ ERBB2IP mutation-reactive T cells played a role in the disease stabilization, we evaluated the in vitro phenotype and function and in vivo persistence of these cells. A number of pre-clinical studies (14–20) and one case report in melanoma (21) have demonstrated that T helper 1 ($T_{H}1$) cells, through a variety of mechanisms including the secretion of the pleiotropic cytokines IFN- γ and tumor necrosis factor (TNF) (22, 23), can mediate tumor regression. Moreover, CD4+ T cells that can simultaneously produce multiple effector cytokines (polyfunctional T cells) have been correlated with effective antitumor T cell responses (19, 24). We found that the V β 22+ ERBB2IP mutation-reactive CD4+ T cells were polyfunctional $T_{H}1$ cells, because stimulation with the mutated ERBB2IP peptide induced the robust coexpression of IFN- γ , TNF, and IL-2 (Fig. 3A) but little to no IL-4 or IL-17. Further phenotypic characterization revealed that these cells were predominantly effector memory CD4+ T cells with cytolytic potential (fig. S5, A and B).

There also appeared to be a minor population of polyfunctional V β 22-negative, ERBB2IP mutation-reactive CD4+ T cells present in 3737-TIL (Figs. 2B and 3A). Sorting of the V β 22-negative cells followed by activation of these cells revealed that one or more additional clonotypes reactive to this epitope were present in 3737-TIL (fig. S6, A and B), the most dominant clonotype of which was V β 5.2 (fig. S6, C and D). The majority of the V β 5.2+ cells produced multiple cytokines in an antigen-specific manner (fig. S6E and table S6). There also appeared to be a minor population of V β 5.2-negative (and V β 22-negative) CD4+ T cells that recognized mutated ERBB2IP (fig. S6E). Thus, the TIL used to treat patient 3737 contained at least three different polyfunctional CD4+ T cell clones that recognized the same mutation in ERBB2IP, suggesting that this mutation was highly immunogenic.

The in vivo persistence of adoptively transferred T cells in the blood at 1 month post-cell transfer is correlated with improved outcomes in melanoma patients treated with ACT (25). We thus evaluated the in vivo persistence of the ERBB2IP mutation-reactive CD4+ T cell clones in patient 3737. TCR-V β deep sequencing revealed that these clonotypes were rare or not detectable in the peripheral blood before ACT (Fig. 3B). Ten days after ACT, both clones were present at greater than 2% of the total T cells in the peripheral blood, but declined to less than 0.3% by day 34 post-cell infusion (Fig. 3B). Three lung metastases, which were resected nearly a year and a half after ACT, were infiltrated by the ERBB2IP mutation-reactive T cells (Fig. 3B), suggesting

that these cells contributed to the cancer regression and disease stabilization. The V β 22+ ERBB2IP mutation-reactive clone was the most frequent clone detected in tumor nodule-3 (Tu-3-Post) and represented nearly 8% of total T cells in the tumor (Fig. 3B), whereas this clone was the second and twelfth most frequent in tumor nodules-1 and -2, respectively. The V β 5.2+ ERBB2IP mutation-reactive clone was also enriched compared with its frequency in blood in all three tumor nodules (Fig. 3B). Thus, patient 3737 experienced tumor regression with stabilization of disease for more than 1 year after receiving over 10 billion ERBB2IP mutation-specific polyfunctional T_H1 cells that infiltrated and persisted in the metastatic lesions.

We observed relatively high levels of *ERBB2IP* expression in both the original and the recurrent lung lesions as determined by quantitative reverse transcription polymerase chain reaction (fig. S7A), and Sanger sequencing validated the presence of the ERBB2IP mutation in all tumor lesions (fig. S7B). The T cell infiltrate and major histocompatibility complex expression of the tumors *in situ* are summarized in tables S7 and S8, respectively. The presence of T cells reactive to the ERBB2IP mutation in progressing tumors that expressed this mutation suggests the presence of immunosuppressive influences at the tumor site that may need to be overcome to increase the anti-cancer effects of the transferred cells.

To specifically evaluate the contribution of mutation-reactive T_H1 cells to the antitumor response *in vivo*, we generated and adoptively transferred a TIL product that was comprised of >95% of the V β 22+ ERBB2IP mutation-reactive

T_H1 cells (Fig. 4, A and B) (13). Again, the patient experienced a decrease in target lesions, but, unlike the first treatment, tumor regression was observed even at the first-month follow-up and continues as of the last follow-up at 6 months (Fig. 4C).

Mapping of the mutational landscape of human cancers is occurring at a rapid pace, but strategies to exploit this information for clinical benefit remain to be fully realized. Here, we used a whole-exome sequencing approach to demonstrate that the human immune system can mount an endogenous T_H1 response against a mutation expressed by an epithelial cancer, and we provide evidence that this response can be harnessed for therapeutic benefit. Given that a major hurdle for the success of immunotherapies for GI and other cancers is the apparent low frequency of tumor-reactive T cells (26), the strategies reported here could be used to generate a T cell product that is highly enriched in mutation-reactive T cells for use in ACT. The ability to immunologically target unique mutations in cancers can potentially extend highly personalized immunotherapies to patients with epithelial cancers, which account for about 90% of cancer deaths in the United States.

References and Notes

- B. Vogelstein *et al.*, *Science* **339**, 1546–1558 (2013).
- P. van der Bruggen, V. Stroobant, N. Vigneron, B. Van den Eynde, “Tumor antigens resulting from mutations,” *Cancer Immunity* (2013), <http://cancerimmunity.org/peptide/mutations/>.
- P. F. Robbins *et al.*, *Nat. Med.* **19**, 747–752 (2013).
- N. van Rooij *et al.*, *J. Clin. Oncol.* **31**, e439–e442 (2013).
- Y. C. Lu *et al.*, *J. Immunol.* **190**, 6034–6042 (2013).
- V. Corbière *et al.*, *Cancer Res.* **71**, 1253–1262 (2011).
- J. Huang *et al.*, *J. Immunol.* **172**, 6057–6064 (2004).
- H. Echchakir *et al.*, *Cancer Res.* **61**, 4078–4083 (2001).
- S. Mandruzzato, F. Brasseur, G. Andry, T. Boon, P. van der Bruggen, *J. Exp. Med.* **186**, 785–793 (1997).
- K. T. Hogan *et al.*, *Cancer Res.* **58**, 5144–5150 (1998).
- V. Karanikas *et al.*, *Cancer Res.* **61**, 3718–3724 (2001).
- S. Wedén *et al.*, *Int. J. Cancer* **128**, 1120–1128 (2011).
- Materials and methods are available as supplementary materials on *Science Online*.
- D. Mumberg *et al.*, *Proc. Natl. Acad. Sci. U.S.A.* **96**, 8633–8638 (1999).
- A. Corthay *et al.*, *Immunity* **22**, 371–383 (2005).
- S. A. Quezada *et al.*, *J. Exp. Med.* **207**, 637–650 (2010).
- Y. Xie *et al.*, *J. Exp. Med.* **207**, 651–667 (2010).
- P. D. Greenberg, D. E. Kern, M. A. Cheever, *J. Exp. Med.* **161**, 1122–1134 (1985).
- Z. C. Ding *et al.*, *Blood* **120**, 2229–2239 (2012).
- K. A. Shafer-Weaver *et al.*, *Cancer Res.* **69**, 6256–6264 (2009).
- N. N. Hunder *et al.*, *N. Engl. J. Med.* **358**, 2698–2703 (2008).
- H. Braumüller *et al.*, *Nature* **494**, 361–365 (2013).
- Z. Qin, T. Blankenstein, *Immunity* **12**, 677–686 (2000).
- J. Yuan *et al.*, *Proc. Natl. Acad. Sci. U.S.A.* **105**, 20410–20415 (2008).
- S. A. Rosenberg *et al.*, *Clin. Cancer Res.* **17**, 4550–4557 (2011).
- S. Turcotte *et al.*, *J. Immunol.* **191**, 2217–2225 (2013).

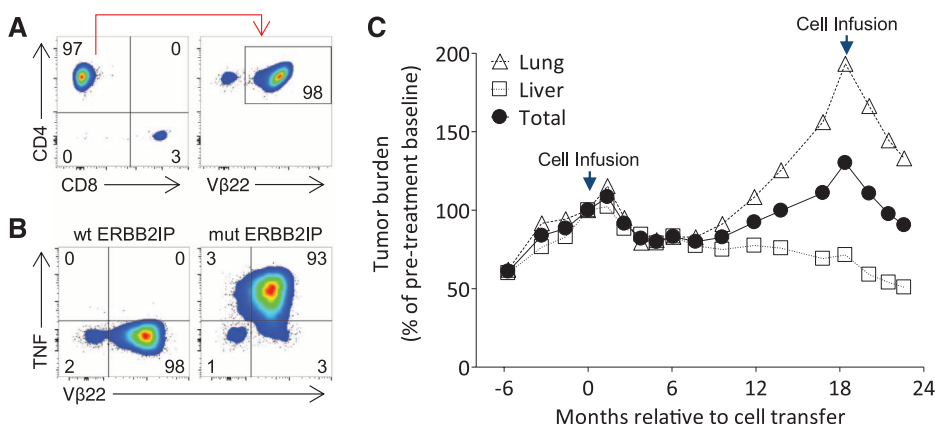


Fig. 4. Evidence of tumor regression after treatment with a highly pure population of V β 22+ ERBB2IP mutation-reactive CD4+ T cells. (A) Flow-cytometric analysis of the TIL product used for retreatment. Data are gated on live CD3+ T cells (left) and further gated on CD4+ cells (right). (B) Retreatment TIL were cocultured for 6 hours with autologous B cells pulsed overnight with wt or mut ERBB2IP 25-amino acid-long peptides. Flow cytometry was used to detect intracellular TNF production in the CD4+ population. (A) and (B) are representative of at least two independent experiments. (C) Tumor growth curves (sum of maximum diameters) of patient 3737 before and after first and second adoptive cell transfers. The first infusion product consisted of 42.4 billion T cells containing about 25% (10 billion) V β 22+ ERBB2IP mutation-reactive T_H1 cells. The second infusion product consisted of 126 billion T cells containing over 95% (120 billion) V β 22+ ERBB2IP mutation-reactive T_H1 cells. Data are expressed as a change from baseline and stratified on lung, liver, and total tumors. Some target lesions selected in (C) differ from Fig. 2D because only lesions that were present throughout both treatments were selected for measurement.

Acknowledgments: We thank the Milstein Family Foundation for their generous support; C.-C. R. Lee, Y. F. Li, A. Mixon, S. Farid, and J. Gartner for helpful technical support and reagents; and the Surgery Branch clinical team for outstanding patient care. The data presented in this manuscript are tabulated in the main paper and the supplementary materials. The raw whole-exome sequence data are available on the

Sequence Read Archive database: Bioproject PRJNA243084. This research was supported by the Intramural Research Program of the NIH and NCI.

Figs. S1 to S7
Tables S1 to S8
References (27, 28)

Supplementary Materials
www.sciencemag.org/content/344/6184/641/suppl/DC1
Materials and Methods

21 January 2014; accepted 9 April 2014
10.1126/science.1251102

The Transcription Factor Gata6 Links Tissue Macrophage Phenotype and Proliferative Renewal

Marcela Rosas,^{1*} Luke C. Davies,^{1*} Peter J. Giles,² Chia-Te Liao,¹ Bashar Kharfan,¹ Timothy C. Stone,² Valerie B. O'Donnell,¹ Donald J. Fraser,³ Simon A. Jones,¹ Philip R. Taylor^{1†}

Tissue-resident macrophages are heterogeneous as a consequence of anatomical niche-specific functions. Many populations self-renew independently of bone marrow in the adult, but the molecular mechanisms of this are poorly understood. We determined a transcriptional profile for the major self-renewing population of peritoneal macrophages in mice. These cells specifically expressed the transcription factor Gata6. Selective deficiency of Gata6 in myeloid cells caused substantial alterations in the transcriptome of peritoneal macrophages. Gata6 deficiency also resulted in dysregulated peritoneal macrophage proliferative renewal during homeostasis and in response to inflammation, which was associated with delays in the resolution of inflammation. Our investigations reveal that the tissue macrophage phenotype is under discrete tissue-selective transcriptional control and that this is fundamentally linked to the regulation of their proliferation/renewal.

Tissue-resident macrophages play fundamental roles specific to their microanatomical niche, ranging from dedicated homeostatic functions to immune surveillance (1). Such het-

erogeneity predicts that discrete transcriptional controls probably exist in specific macrophage populations that determine both their particular phenotypes and tissue-specific functions.

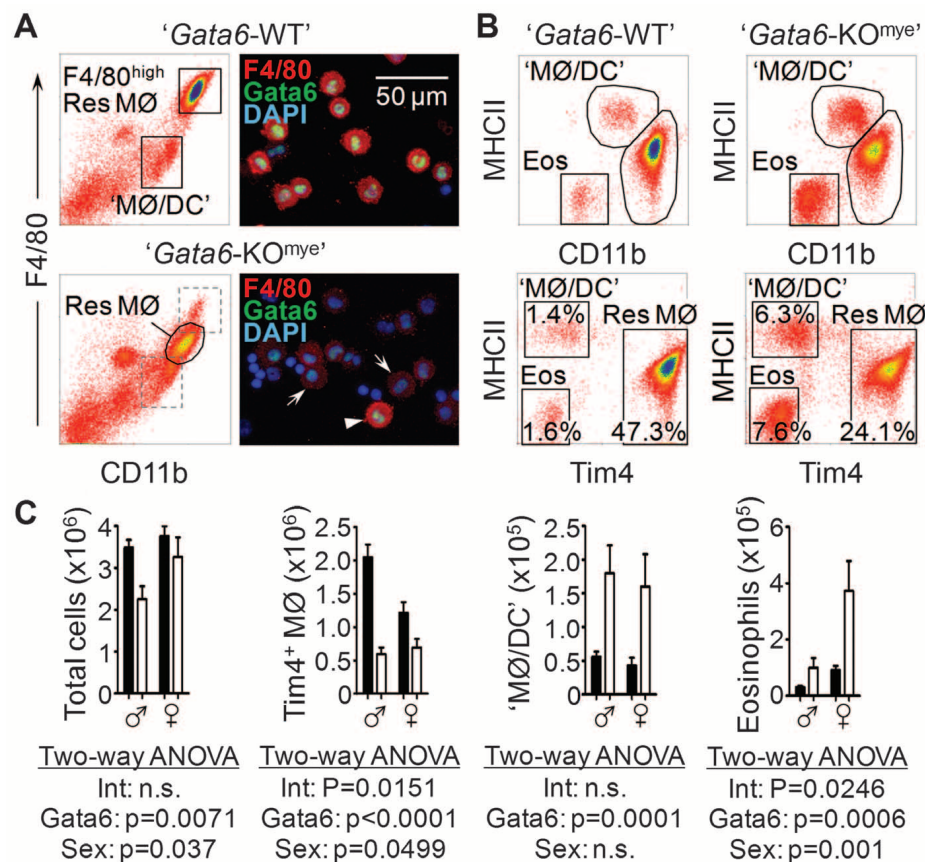
Many resident macrophages self-renew by local proliferation [(1) and references therein]. This is initiated after seeding of macrophages into tissues during development and their expansion during the neonatal period (1). Under specific conditions, these tissue-resident macrophages may also be derived from blood monocytes (1). Classic F4/80^{high}CD11b^{high} peritoneal-resident macrophages fit this model (2–7), and they proliferate above homeostatic levels in response to inflammation (6). Proliferation of human macrophages has also been observed in several contexts [reviewed in (1)]. However, the factors controlling these processes remain ill-defined. We hypothesized that discrete transcriptional controls would govern both the specific phenotype of tissue

¹Cardiff Institute of Infection and Immunity, Cardiff University School of Medicine, Heath Park, Cardiff CF14 4XN, UK. ²Central Biotechnology Services, Cardiff University School of Medicine, Heath Park, Cardiff CF14 4XN, UK. ³Institute of Molecular Medicine, Cardiff University School of Medicine, Heath Park, Cardiff CF14 4XN, UK.

*These authors contributed equally to this work.

†Corresponding author. E-mail: taylorpr@cf.ac.uk

Fig. 1. Selective myeloid cell alterations in the peritoneum of mice with myeloid Gata6 deficiency. (A) Representative flow cytometric and immunofluorescent assessment of peritoneal-resident macrophages from WT and Gata6-KO^{mye} mice. F4/80^{high} (arrowhead) and F4/80^{low} (arrows) macrophages are indicated. Fluorescent images were captured with a $\times 40$ objective lens, the scale bar is indicated, and the images are representative of four mice per group (fig. S9). (B) Representative flow cytometric analysis of the peritoneal myeloid cell (CD11b⁺CD19⁻) composition of the Gata6-WT and Gata6-KO^{mye} mice. Percentages indicate typical proportions of the cell types of all peritoneal cells. (C) Quantification of peritoneal myeloid cells in the Gata6-WT (black bars, $n = 9\text{♂}/7\text{♀}$) and Gata6-KO^{mye} mice (white bars, $n = 5\text{♂}/5\text{♀}$) analyzed by flow cytometry in (A) and (B) above. Data represent the mean \pm SEM of mice pooled from two independent experiments and were analyzed by two-way analysis of variance (ANOVA). MØ, macrophage; Res, tissue-resident; Eos, eosinophil; DC, dendritic cell; Int, interaction statistic; Gata6, Gata6 effects; Sex, sex effects.





ARE YOU A
**SCIENTIFIC
REBEL?**



Unleash your true potential
with the new **CytoFLEX LX**
Flow Cytometer

DARE TO EXPLORE



**BECKMAN
COULTER**
Life Sciences



This information is current as
of January 17, 2018.

Inhibitors of the PD-1 Pathway in Tumor Therapy

Martin W. LaFleur, Yuki Muroyama, Charles G. Drake and
Arlene H. Sharpe

J Immunol 2018; 200:375-383; ;
doi: 10.4049/jimmunol.1701044
<http://www.jimmunol.org/content/200/2/375>

Why *The JI*?

- **Rapid Reviews!** 30 days* from submission to initial decision
- **No Triage!** Every submission reviewed by practicing scientists
- **Speedy Publication!** 4 weeks from acceptance to publication

*average

References This article **cites 122 articles**, 38 of which you can access for free at:
<http://www.jimmunol.org/content/200/2/375.full#ref-list-1>

Subscription Information about subscribing to *The Journal of Immunology* is online at:
<http://jimmunol.org/subscription>

Permissions Submit copyright permission requests at:
<http://www.aai.org/About/Publications/JI/copyright.html>

Email Alerts Receive free email-alerts when new articles cite this article. Sign up at:
<http://jimmunol.org/alerts>

Inhibitors of the PD-1 Pathway in Tumor Therapy

Martin W. LaFleur,^{*,†,1} Yuki Muroyama,^{‡,§,¶,1} Charles G. Drake,^{§,¶,2} and Arlene H. Sharpe^{*,||,2}

The programmed death 1 (PD-1) pathway delivers inhibitory signals that function as a brake for immune responses. This pathway limits the initiation and duration of immune responses, thereby protecting tissues from immune-mediated damage and autoimmune diseases. However, the PD-1 pathway also inhibits immune responses to tumors. The critical role of PD-1 in preventing antitumor immunity is demonstrated by the transformative effects of PD-1 pathway blockade in a broad range of cancers with the hallmark of durability of response. Despite this success, most patients do not respond to PD-1 monotherapy, and some patients experience adverse events. In this review, we discuss the functions of the PD-1 pathway and its translation to cancer immunotherapy. We also consider current challenges and opportunities for PD-1 cancer immunotherapy, including mechanisms of response and resistance, identification of biomarkers of response to PD-1 therapy, characterization and treatment of PD-1 therapy-related adverse events, and development of safe and effective combination therapies. *The Journal of Immunology*, 2018, 200: 375–383.

The immune system can recognize and destroy tumors, but tumors evolve to escape immune attack. The tumor microenvironment (TME) is immunosuppressive and exploits inhibitory checkpoints, which normally promote T cell tolerance and control resolution of immune responses, to limit antitumor immunity. The remarkable success of immune checkpoint blockade, in which Abs are used to block checkpoints that inhibit T cell responses to tumors, illustrates the critical roles of these inhibitory checkpoints in obstructing antitumor immunity. The programmed death 1 (PD-1) pathway is a key target of checkpoint blockade.

The PD-1 inhibitory receptor regulates T cell activation, effector T cell responses, T cell tolerance, and T cell exhaustion (1, 2). PD-1 is rapidly induced on naive T cells following TCR engagement, countering T cell activation, and PD-1 expression decreases when Ag is cleared. When T cells are repetitively stimulated (as in cancer and chronic infection), PD-1 expression is sustained at high levels and T cells enter a dysfunctional state, termed exhaustion (2). Thus, PD-1 is expressed on both activated and exhausted T cells, and PD-1 expression alone does not signify T cell exhaustion. PD-1 is not only expressed on conventional CD4⁺ and CD8⁺ T cells, but also on regulatory T cells, B cells, NK cells, and NKT cells (3).

PD-1 has two ligands, programmed death-ligand (PD-L)1 (also called B7-H1; CD274) (4, 5) and PD-L2 (also called B7-DC; CD273) (6, 7). PD-L2 has higher affinity for PD-1, but more restricted expression than PD-L1. PD-L1 is widely expressed on many types of hematopoietic (T, B, macrophages, dendritic cells [DCs]) and nonhematopoietic cells (epithelial, stromal, and endothelial). PD-L2 is expressed mainly on hematopoietic cells (DCs, macrophages, B cells, and Th2 cells), but also on some epithelial cells, especially in the lung. Type 1 and type II IFNs, common γ -chain family cytokines (IL-2, IL-7, IL-15, and IL-21), IL-10, TNF, and VEGF can stimulate PD-L1 expression. IL-4 and GM-CSF are the most common stimuli for PD-L2 expression, but IFNs and common γ -chain family cytokines also can stimulate PD-L2. Upregulation of PD-1 ligands by proinflammatory stimuli may serve as a negative feedback mechanism to attenuate effector T cell responses, protecting tissues from immune-mediated injury or tumors from immune attack; this phenomenon has been termed “adaptive immune resistance” (8).

In addition to binding to PD-1, PD-L1 and PD-L2 each have a second unique binding partner. PD-L1 engagement of B7-1 (CD80) on T cells inhibits T cell responses (9). PD-L2 engagement of repulsive guidance molecule b (RGMb) (10)

Downloaded from <http://www.jimmunol.org/> by Laurel Eckhardt on January 17, 2018

^{*}Department of Microbiology and Immunobiology, Harvard Medical School, Boston, MA 02115; [†]Department of Pediatric Oncology, Dana Farber Cancer Institute, Boston, MA 02115; [‡]Department of Oncology, Sidney Kimmel Comprehensive Cancer Center, Johns Hopkins University School of Medicine, Baltimore, MD 21231; [§]Columbia Center for Translational Immunology, Columbia University Medical Center, New York, NY 10032; [¶]Herbert Irving Comprehensive Cancer Center, Columbia University Medical Center, New York, NY 10032; and ^{||}Evergrande Center for Immunologic Diseases, Harvard Medical School and Brigham and Women’s Hospital, Boston, MA 02115

¹M.W.L. and Y.M. contributed equally to this work.

²C.G.D. and A.H.S. contributed equally to this work.

ORCIDs: [0000-0002-5017-774X](#) (M.W.L.); [0000-0001-9839-6370](#) (Y.M.).

Received for publication July 19, 2017. Accepted for publication September 5, 2017.

This work was supported by National Institutes of Health Grants P01 AI56299, AI 40614 (both to A.H.S.) R01CA127153, and P30CA006973 (both to C.G.D.) and

grants from the Evergrande Center for Immunological Diseases (to A.H.S.) and the Prostate Cancer Foundation (to C.G.D.).

Address correspondence and reprint requests to Dr. Arlene H. Sharpe or Dr. Charles G. Drake, Department of Microbiology and Immunobiology, Harvard Medical School, 77 Avenue Louis Pasteur, NRB-837, Boston, MA 02115 (A.H.S.) or Columbia Center for Translational Immunology, Columbia University Medical Center, New York, NY 10032 (C.G.D.). E-mail addresses: arlene_sharpe@hms.harvard.edu (A.H.S.) or cgd2139@columbia.edu (C.G.D.).

Abbreviations used in this article: DC, dendritic cell; FDA, U.S. Food and Drug Administration; IC, immune cell; IRAE, immune-related adverse event; LCMV, lymphocytic choriomeningitis; MSI, microsatellite instability; NSCLC, non-small cell lung cancer; PD-1, programmed death 1; PD-1^{hi}, T cell with high PD-1 expression; PD-1^{int}, T cell with intermediate levels of PD-1; PD-L, programmed death-ligand; RCC, renal cell carcinoma.

Copyright © 2018 by The American Association of Immunologists, Inc. 0022-1767/18/\$25.00

promotes respiratory tolerance. Further work is needed to understand the functional effects of these interactions and how they are affected by PD-1 pathway blockade.

PD-1 signaling and molecular mechanisms

Most of our knowledge of PD-1 signaling in T cells comes from studies of PD-1 engagement following activation of naïve T cells. Upon PD-L1 or PD-L2 engagement, PD-1 becomes phosphorylated on its two tyrosine motifs: an ITIM and an immunoreceptor tyrosine-based switch motif in its cytoplasmic domain (11). This results in recruitment of protein tyrosine phosphatases (particularly SHP2), which dephosphorylate signaling molecules (including Lck and ZAP-70), and oppose positive signals downstream of the TCR and CD28 (11–13), leading to reduced T cell activation and effector functions. This leads to diminished signaling through the PI3K-AKT and Ras-MEK-ERK pathways (13), decreased expression of transcription factors important for effector T cell function (Tbet, Gata3, and Eomes), and diminished expression of the prosurvival factor Bcl-xL (14). Inhibition of the PI3K-AKT and Ras-MEK-ERK pathways also blocks cell cycle progression by reducing transcription of SKP2 (a ubiquitin ligase that regulates degradation of the cyclin-dependent kinase inhibitor p27^{kip1}), resulting in p27^{kip1} accumulation and cell cycle inhibition at the G₁ phase (15). PD-1 signaling also reduces production of cytotoxic molecules, thereby decreasing T cell killing capacity (16). PD-1 signaling has further suppressive roles; it can increase expression of the proapoptotic molecule Bim (17) and the transcription factor BATF, which inhibits T cell proliferation and cytokine production (18). Inhibition of T cell function depends on the level of PD-1 expression, with IL-2, TNF, and proliferation being most readily inhibited, followed by both cytotoxicity and IFN-γ and then by MIP-1β (16). In addition, PD-1 alters T cell motility and length of contact between T cells and DCs or target cells (19). PD-1 appears to prevent formation of stable contacts between T cells and DCs during T cell activation, thereby impairing development of effector functions.

PD-1 signaling also modulates T cell metabolism. Upon activation, naïve T cells undergo metabolic reprogramming to enable proliferation and differentiation, and glycolysis becomes the dominant energy source. PD-1 signals lead to a metabolic shift in T cells, suppressing glycolysis and enhancing fatty acid oxidation (20). By impairing metabolic reprogramming, PD-1 may affect T cell differentiation and function. Given the central role of AKT in metabolism, PD-1 inhibition of AKT activation likely contributes to this altered metabolic state. The molecular mechanisms by which PD-1 regulates T cells other than during their initial activation are less clear. Further work is needed to understand the effects of PD-1 signals in memory T cells, tolerant T cells, exhausted T cells, and regulatory T cells, as well as in other immune cell (IC) types. T cell differentiation state, Ag, inflammation, metabolic state, and other factors may influence the consequences of PD-1 signaling.

The PD-1 ligands also may regulate immune responses by sending a signal into ligand-expressing cells (21). There is evidence for cell-intrinsic functions of PD-L1 in tumor cells, myeloid cells, and T cells. Culture of tumor cell lines in vitro with anti-PD-L1 directly affected tumor cell metabolism in the absence of PD-1-expressing T cells (21). Expression of

glycolytic enzymes, AKT phosphorylation, and glucose uptake were reduced after anti-PD-L1 treatment in vitro (21). Consistent with this, the PD-L1 intracellular domain does not possess canonical conserved signaling motifs, but is highly conserved, suggesting functional significance.

Inhibitory functions of PD-1 signaling

Regulating tolerance and autoimmunity. The PD-1 pathway regulates both central and peripheral tolerance. PD-1 signaling influences positive selection in the thymus, because lack of PD-1 or PD-L1 at this stage increases the number of double positive thymocytes by reducing the TCR signaling threshold during positive selection (22). How PD-1 pathway modulation affects the T cell repertoire remains to be determined.

The PD-1 pathway controls both the induction and the maintenance of peripheral T cell tolerance. PD-1 limits the initial activation, proliferation, and differentiation of self-reactive CD4⁺ and CD8⁺ T cells, and constrains potentially pathogenic self-reactive CD4⁺ and CD8⁺ effector T cells. PD-1 deficiency or blockade accelerates autoimmunity in several mouse models of autoimmunity including lupus-prone mice (23), experimental autoimmune encephalomyelitis (24), type 1 diabetes in NOD (25), and the rat insulin promoter-membrane-bound OVA model of diabetes (26). The PD-1 pathway restrains priming and differentiation of naïve self-reactive T cells in secondary lymphoid organs. PD-L1 is expressed on tolerogenic DCs and helps to control the T cell fate decision between activation and tolerance (27). PD-1/PD-L1 interactions have crucial functions in target organs, controlling self-reactive T cells locally, maintaining tolerance in tissues, and protecting them from autoimmune-mediated damage. For example, in experimental autoimmune encephalomyelitis and diabetes models, PD-1 is highly expressed in the target organ on self-reactive T cells, and inflammation stimulates PD-L1 expression in the target organ, so PD-1/PD-L1 interactions have the potential to counteract stimulatory signals in the target tissues. PD-L1 expression on epithelial cells of organs such as the lungs, liver, and pancreas likely serves as a final barrier to immune destruction when tolerance is lost (1). The functional consequences of PD-L1 expression on other types of non-hematopoietic cells (e.g., endothelial and stromal cells) in tolerance is less clear. In NOD mice, PD-L1 on non-hematopoietic cells, including islet cells, plays an important role in inhibiting effector T cell responses and diabetes onset (25). Thus, the PD-1 pathway can regulate self-reactive T cells at multiple levels: thymic repertoire development, activation and differentiation in secondary lymphoid organs, and effector responses in target organs. Intriguingly, single nucleotide polymorphisms in the PDCD1 gene have been associated with human autoimmune diseases (28), but it is unclear whether any of these SNPs are causative or predictive of immune-related adverse events (IRAEs) in cancer patients treated with PD-1 pathway inhibitors.

Exploiting PD-1 inhibitory signals during chronic viral infection. The importance of the PD-1 pathway in regulating chronic viral infection was first described using the chronic lymphocytic choriomeningitis (LCMV) infection model in mice (2), and it rapidly extended to human chronic viral infections (HIV, hepatitis C virus, hepatitis B virus)

(18, 29). During chronic viral infections, cytotoxic T cells progressively lose the ability to produce IL-2, TNF- α , and IFN- γ and enter a dysfunctional state termed exhaustion (30). Persistent Ag encounter and TCR signaling stimulate high and sustained PD-1 expression (2), whereas inflammatory stimuli upregulate and sustain PD-L1 expression. The PD-1 pathway plays a major role in regulating T cell exhaustion, because its blockade during chronic viral infection can enhance CD8 $^{+}$ T cell responses and reduce viral burden (2).

PD-1 is not absolutely required for induction of the T cell exhaustion program; PD-1 prevents early overstimulation of T cells and excessive T cell death during chronic LCMV infection. In contrast, PD-1 plays a crucial role in the maintenance stage of the exhaustion program; the absence of PD-1 signaling results in accumulation of terminally exhausted T cells (31). Thus, PD-1 preserves exhausted T cells from terminal exhaustion and instead maintains partially exhausted T cells in a dysfunctional state from which they can be reinvigorated.

PD-1 blockade after the onset of LCMV-induced exhaustion enhances CD8 $^{+}$ T cell effector functions, due to response of a subset of cells to PD-1 blockade (32–34). High PD-1 expression on HIV-specific CD8 $^{+}$ T cells isolated from PBMCs of viremic individuals was associated with impaired cytokine production, proliferation, and survival. Further work is needed to understand relationships between populations of HIV-specific CD8 $^{+}$ T cells that express different PD-1 levels and their responses to PD-1 blockade during chronic human viral infections (35). During chronic LCMV infection, two distinct populations of Ag-specific dysfunctional T cells can be distinguished based on their PD-1 expression levels and responses to PD-1 blockade (36): T cells with intermediate levels of PD-1 (PD-1 $^{\text{int}}$) are dysfunctional but can be reinvigorated, whereas T cells with high PD-1 expression (PD-1 $^{\text{hi}}$) are terminally exhausted and cannot be reinvigorated (36). PD-1 $^{\text{int}}$ are found primarily in secondary lymphoid organs, whereas the PD-1 $^{\text{hi}}$ predominate in nonlymphoid tissues. PD-1 $^{\text{int}}$ have a better ability to proliferate and produce effector cytokines compared with PD-1 $^{\text{hi}}$, and they can convert into PD-1 $^{\text{hi}}$, which have higher cytotoxic function. Exhausted CD8 $^{+}$ T cells from mice and humans have a distinct epigenetic landscape compared with naive, effector, and memory cells (37), and PD-1 pathway blockade does not durably reprogram exhausted T cells epigenetically (38). Combination therapy with epigenetic-modifying agents may provide a means to reverse epigenetic changes in exhausted T cells.

Inhibiting antitumor immunity in preclinical models and translation to cancer

The PD-1/PD-L1 axis is of vital importance for restraining the antitumor T cell response (8). In preclinical models, PD-1/PD-L1 blockade results in enhanced antitumor T cell cytotoxicity, proinflammatory cytokine production, and proliferation. In addition, PD-1 blockade increased concentrations of glucose in the TME and rates of glycolysis (21). Thus, PD-1 pathway blockade may also function by altering metabolism in the TME (39).

Tumor cells can express PD-L1 and/or PD-L2, which can be induced by multiple pathways, including upregulation by cytokines, chromosomal copy gain, disruptions of the *PDL1* 3' untranslated region, mutations of the genes encoding PI3K

AKT, EGFR, and CDK5, MYC overexpression, and viral proteins (EBV LMP1) (40). PD-1 may restrain T cells that have been activated by tumor Ag-bearing APCs in lymph nodes, T cells trafficking to the tumor, and effector T cells within the tumor. In the TME, PD-L1 can be expressed on tumor cells, as well as endothelial cells, stromal cells, APC/myeloid subsets, and T cells. All can contribute to the immunosuppressive environment. Further studies are needed to address their specific contributions during antitumor immunity and the response to PD-1 checkpoint blockade.

In animal models, the effects of PD-1 pathway blockade vary with tumor type; some tumors are resistant to PD-1 blockade or clearance in PD-1 $^{-/-}$ mice, whereas others are very susceptible to loss of PD-1 signaling (41, 42). The cellular PD-1/PD-L1 interaction may also vary; tumor-derived PD-L1 was required for blocking CTL-mediated killing in the highly immunogenic MC38 colorectal carcinoma, yet host-derived PD-L1 was more important for the less immunogenic B16 and D4m melanoma lines (41). Differences in tumor immunogenicity may impact the relative contributions of tumor versus host-derived PD-L1. Moreover, studies of methylcholanthrene-induced sarcomas showed that the level of tumor-derived PD-L1 needed for immune escape was inversely proportional to the antigenicity of the tumor cell (42). More work is needed to understand differential sensitivity of PD-1 blockade in different tumor models (MC38, B16), as well as different TMEs, which have been broadly classified into: 1) inflamed or “hot” tumors with robust immune infiltration; 2) immune-excluded in which inflammatory cells are present at the tumor margin but do not enter the tumor parenchyma; and 3) “cold” tumors, which are devoid of inflammatory cells, that is, an “immune desert.”

The effects of PD-1 blockade depend on the presence of T cells, BATF3 $^{+}$ cross-presenting DCs, and the Sec22b cross-presentation pathway (39, 43). Priming of the antitumor T cell response also depends on activation of the STING pathway in these DCs, which produce IFN- β to initiate this response (44, 45). Furthermore, the microbiome plays a role because *Bifidobacterium* is important for promoting initial T cell priming during PD-1 blockade by enhancing the priming potential of DCs via a yet unknown mechanism (46). Given its broad expression, understanding differential roles of PD-1 signaling in CD4 $^{+}$ and CD8 $^{+}$ effector cells and regulatory T cells will be important for optimally targeting this pathway for cancer therapy. Fc Ab design will be important as well, given that Fc receptors on macrophages can affect the potency of PD-1 blockade (47, 48).

Most tumors require combination therapies for optimal clinical efficacy, and PD-1 has become a foundational building block for combination therapies primarily at the priming and effector steps (8, 49, 50). In animal models, enhancing T cell priming using combinations with TLR ligands such as CpG, vaccines such as GVAX, or oncolytic viruses have shown additive or synergistic effects with PD-1 blockade. At the tumor site, dysfunctional T cells express multiple coinhibitory receptors such as TIM-3, LAG-3, TIGIT, and VISTA, and their coblockade with PD-1 is generally at least additive. Dysfunctional T cells can also express costimulatory receptors, and stimulation of these pathways (OX-40, CD137, ICOS, and GITR) using agonist Abs also provides an additive effect with PD-1 blockade.

Lastly, current cancer therapies such as BRAF inhibitors, angiogenesis blockade, radiation, chemotherapies that induce immunogenic cell death (doxorubicin, oxaliplatin, and cyclophosphamide), and HDAC inhibitors also are additive with PD-1 blockade. Given the wide range of potential combinations, a mechanistic understanding of synergies is needed to rationally develop effective combination therapies.

PD-1/PD-L1 blockade in the clinic

A number of anti-PD-1 and anti-PD-L1 Abs have been approved by the U.S. Food and Drug Administration (FDA) for cancer treatment (Fig. 1, Table I) (51–76). The first approval was for the anti-PD-1 Ab pembrolizumab for melanoma in 2014, followed closely by a second anti-PD-1 Ab (nivolumab) (51–53). In 2015, a number of additional approvals followed, notably in non-small cell lung cancer (NSCLC) and in renal cell carcinoma (RCC) (56–58). The year 2015 also marked the first approval of combined immune checkpoint blockade; the combination of anti-PD-1 (nivolumab) and anti-CTLA-4 (ipilimumab) was approved for the treatment of melanoma (54). Subsequent approvals demonstrated the truly broad-spectrum activity of these agents in cancer, with approvals in urothelial cancer (67–72), head and neck cancer (73, 74), and Hodgkin's lymphoma, where the objective response rate approaches 55–75% (64–66). In a recent landmark trial, the anti-PD-1 agent pembrolizumab was granted cross-cancer approval for tumors with microsatellite instability (MSI) (76). In colorectal carcinoma, MSI is relatively common (~15% of cases) (77), but there are significant numbers of MSI⁺ cases among nearly all cancer types, including tumor types considered refractory to immunotherapy, such as prostate cancer. This approval marked

the first time an agent has been approved across multiple tumor types, based on a predictive genetic biomarker.

Mechanism of action of PD-1/PD-L1 blockade in humans

As described earlier, studies in animal models show that PD-1 blockade augments a CD8⁺ T cell antitumor response. Similar data have been generated in patients; for example, the presence of proliferating (Ki67⁺) T cells at the invasive tumor margin correlated with response in melanoma patients treated with anti-PD-1 (78). Similarly, a recent study showed that CD8⁺ T cell expansion mediated by PD-1 blockade can also be detected in the peripheral blood, where the ratio of reinvigorated circulating (Ki67⁺) exhausted CD8⁺ T cells to tumor burden appears to correlate with response (79). In addition, this reinvigoration was indicative of a clonal response because several of the T cell clones that were Ki67⁺ were also found in the tumor. As is the case in animal models, one open question is whether PD-1 immunotherapy blocks PD-1 interaction with PD-L1 on tumor cells or PD-L1 on APCs in the tumor or in the tumor-draining lymph node. Two recent studies showed CD28/B7 interactions are required for PD-1/PD-L1 blockade to function, implying that the primary interaction involves APCs (80, 81). Even though elegant knockout and blocking studies like this are impossible in patients, the observation that PD-L1 staining on tumor-infiltrating ICs correlates with response to PD-L1 blockade (with atezolizumab) (82) provides some support for this hypothesis. However, in other studies, responses to PD-1/PD-L1 blockade seem to correlate more strongly with PD-L1 expression on tumor cells (83); one factor that may explain these opposing findings is the use of different metrics/reagents for scoring PD-L1 positivity in the tumor. Similar to animal models, the role of PD-L1 on tumor cells, hematopoietic cells,

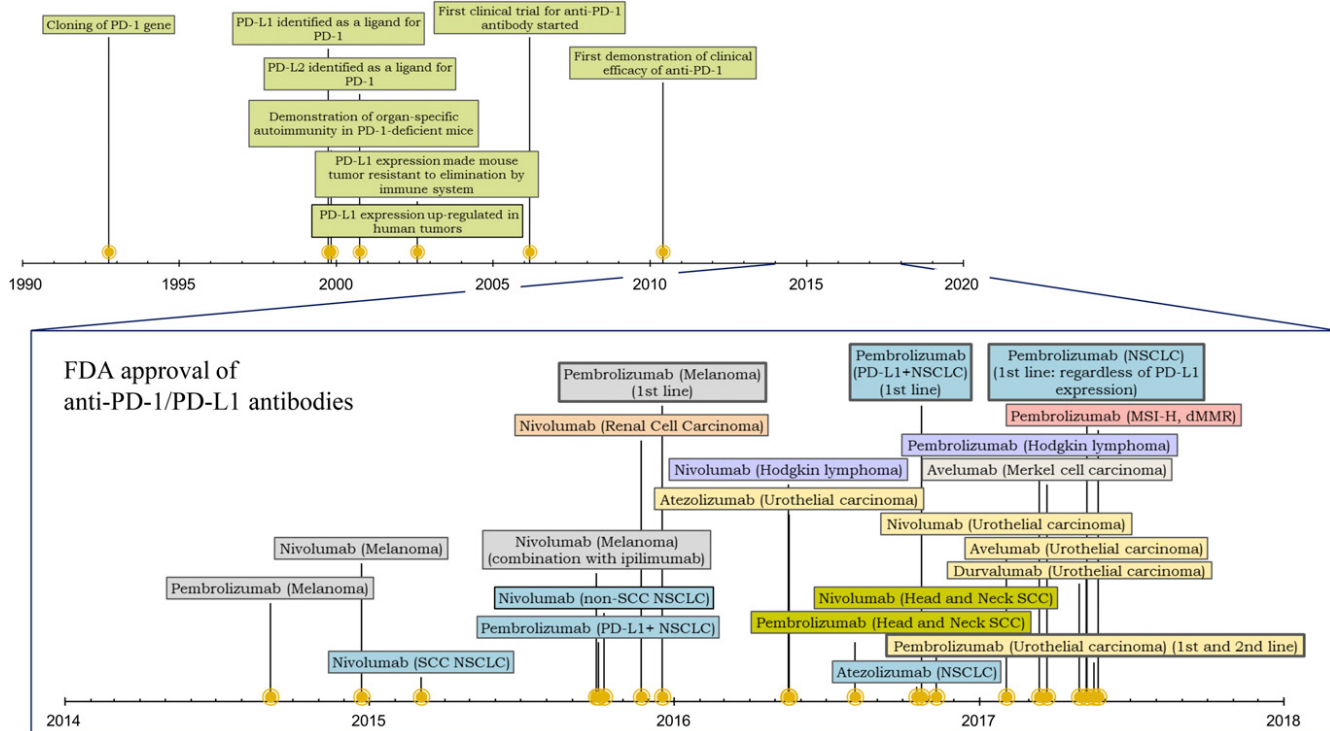


FIGURE 1. Timeline for basic and clinical development of PD-1/PD-L1 targeted cancer immunotherapy. Upper timeline, Preclinical studies. Lower/magnified timeline, FDA approvals.

Table I. FDA-approved anti-PD-1/PD-L1 agents

Target	Generic Name	Isotype	Tumor Types
PD-1	Pembrolizumab	Humanized IgG4 (hinge region modified)	Melanoma, NSCLC, Hodgkin's lymphoma, urothelial carcinoma, HNSCC, MSI-H, dMMR
	Nivolumab	Fully human IgG4/κ (hinge region modified)	Melanoma, NSCLC, Hodgkin's lymphoma, RCC, urothelial carcinoma, HNSCC
PD-L1	Atezolizumab	Humanized IgG1 (FcR-binding deficient)	NSCLC, urothelial carcinoma
	Durvalumab	Humanized IgG1 (FcR-binding deficient)	Urothelial carcinoma
	Avelumab	Fully human IgG1 λ	Urothelial carcinoma, Merkel cell carcinoma

dMMR, mismatch repair deficient; HNSCC, head and neck squamous cell carcinoma; MSI-H, MSI-high.

and nonhematopoietic cells may differ with different types of tumors.

Adverse events: mechanism, timing, and treatment

As discussed earlier, the PD-1/PD-L1 axis protects normal tissues from immune attack during episodes of local inflammation by promoting T cell tolerance. These PD-1 immunoregulatory functions likely explain why PD-1/PD-L1 blockade is associated with IRAEs. IRAEs can affect most major organs and include fever, rash, diarrhea, colitis, pneumonitis, myocarditis, hepatitis, elevated AST/ALT, endocrinopathies (hypothyroidism/hypophysitis), and pancreatitis/diabetes. Across multiple trials with multiple agents in multiple cancer types, the rate of grade III/IV adverse events (ones that must be treated) is remarkably consistent in the 15–20% range (84). The organ most commonly affected by IRAEs is the skin, with toxicity ranging from mild rash to more severe skin involvement requiring treatment with either topical or systemic corticosteroids. The two other most common IRAEs are fatigue and diarrhea, whereas pneumonitis, colitis, pancreatitis, myocarditis, hepatitis, and endocrinopathies are rarer. Whereas IRAEs are often mild, the involvement of certain organ systems is more worrisome and requires aggressive treatment. In the phase Ib trial of the anti-PD-1 Ab nivolumab, several cases of severe lung inflammation (pneumonitis) occurred, some of which were fatal (85). More recently, prompt intervention with immunosuppressive corticosteroids and TNF-α blockade has improved treatment safety (86). Another worrisome IRAE is inflammation of the cardiac muscle (myocarditis), which can also prove deadly (87). As described earlier, colitis may occur but is less common than that seen with CTLA-4 blockade. Interestingly, IRAEs involving various organ systems occur at different points in the treatment course, with skin-related events occurring early (generally 2–6 wk) and other IRAEs appearing later in the treatment course (within 12 wk) (84). There appear to be very few new events that occur after the first 6–9 mo of treatment (88–90). When tissue is available, pathological examination generally reveals a T cell infiltrate, consistent with the mechanism of action of PD-1/PD-L1 blocking agents. Immunologically, a deeper understanding of the immunological mechanisms involved in IRAEs is likely to provide additional insights regarding the pathogenesis of autoimmunity.

Biomarkers to predict anti-PD-1/anti-PD-L1 activity

Despite its remarkable success in some patients, objective tumor responses occur only in a minority of patients treated. This, coupled with the possibility of IRAEs, has led to the search for tissue or serum biomarkers that might predict which patients respond to anti-PD-1/PD-L1 therapy. Based on the notion that PD-1 pathway blockade inhibits interactions

between tumor cell PD-L1 and PD-1 on T cells, much work has focused on investigating PD-L1 expression as a biomarker to predict response using immunohistochemical quantification of PD-L1 in pretreatment and/or archival tumor tissue samples. These studies indicate that PD-L1 expression on either tumor or tumor-infiltrating ICs is at best an imperfect tool by which to enrich patients for treatment (83, 85, 91). One key challenge has been that clinical agents have each been paired with a different companion diagnostic (92). A second related challenge is that the various assays chose disparate cut points for PD-L1 positivity. In some instances, such as RCC and first-line bladder cancer (63, 67), there appears to be no correlation between PD-L1 expression and the likelihood of clinical response. Even when PD-L1 expression is predictive, there are always PD-L1–“negative” patients who respond, although this perhaps reflects sampling error (93), it makes it challenging for clinicians to withhold a potentially beneficial drug from patients with few or no other treatment options. The use of multiple biomarkers is likely to be more effective for predicting responders than PD-L1 expression alone. Nevertheless, in certain clinical scenarios, that is, first-line treatment of patients with lung cancer where chemotherapy is effective, PD-1 blockade with pembrolizumab is FDA-approved only for patients whose tumors are positive for PD-L1 expression (61).

Based on the notion that nonsynonymous mutations in cancer may give rise to novel class I-restricted epitopes (neoantigens), another potential biomarker under study is tumor mutational burden. Indeed, in melanoma (94), NSCLC (95, 96), and urothelial bladder cancer (97), tumor mutational burden correlates with the likelihood of response, although an optimal cut point for patient selection has yet to be defined prospectively for any of these cancer types. In addition, transcriptional signatures, including metabolic and immunological signatures, are actively being investigated (98, 99). A molecular signature of IFN signaling (100) is under development, which will quantify a set of 16 target gene expression levels, and is being prospectively analyzed in three ongoing randomized phase III trials. The use of PD-1 signaling and expression of downstream signaling molecules as potential biomarkers are also being investigated for identifying potential responders to PD-1 blockade (101).

Mechanisms of resistance to PD-1/PD-L1 blockade

Despite impressive clinical activity, most patients treated with PD-1/PD-L1 blocking agents either fail to respond or eventually develop resistance. Three interesting studies highlighted mechanisms of resistance to immune checkpoint blockade (102). Defects in class I Ag presentation (β_2 -microglobulin mutations) were associated with nonresponse; these data are

consistent with the notion that PD-1/PD-L1 blockade requires tumor Ag presentation to specific CD8⁺ T cells to be successful (103). A second study indicated the potential importance of the Wnt/β-catenin pathway, which had previously been shown to be immunosuppressive (104). Tumors in which this pathway was active were relatively noninflamed, that is, cold, and hence far less likely to respond to PD-1/PD-L1 blockade (105). A third study, in which patients were treated with anti-CTLA-4, identified defects in IFN (IFNGR1, IFNGR2, and JAK2) signaling in resistance (106). Additional work is needed to identify additional resistance mechanisms, determine the extent to which individual mechanisms are involved, and stratify which mechanisms are applicable to specific tumor types. Clinically, combination treatment regimens also highlight potential mechanisms of resistance; for example, the activity of combined PD-1/CTLA-4 blockade in melanoma (54) and in RCC (107) strongly implicate CTLA-4 activity as a factor limiting the efficacy of PD-1 blockade in patients. Other clinically apparent mechanisms of resistance include LAG-3 expression (108), IDO expression (109–111), as well as many others (112).

Combination therapies with PD-1

Mirroring animal studies (113, 114), combined checkpoint blockade has already enjoyed clinical success, with PD-1/CTLA-4 blockade FDA-approved in melanoma and the results of pivotal phase III trials eagerly awaited in multiple other tumor types including RCC (NCT02231749), NSCLC (NCT01454102, NCT02453282), and others. Building further upon preclinical studies, clinical trials that coordinately block other inhibitory checkpoints, including LAG-3 (115), TIM-3 (50), TIGIT (50, 116), and VISTA (117), are under way. Additional clinical trials combine PD-1 blockade with agents that address other aspects of the immunosuppressive tumor microenvironment, that is, inhibitors of the IDO pathway (118), adenosine signaling (119), and agents that affect CSF-1R signaling (120). There are also multiple “vaccine” approaches under study; these seek to turn cold tumors hot, hence enabling PD-1/PD-L1 blockade efficacy. Perhaps most exciting among the various vaccine approaches are personalized cancer vaccines, which seek to target a patient’s individual mutated peptides (121). Two very recent publications highlight the feasibility and potential activity of this approach (122, 123), yet the complexity and time frame involved in generating patient-specific vaccines still presents a clinical challenge. It is further worth noting that conventional cancer treatments such as radiation therapy, chemotherapy, and targeted agents can induce immunogenic cell death and might thus also serve in a way as cancer vaccines to prime an antitumor response (124).

Future directions

The impressive clinical success of PD-1/PD-L1 blockade is a great example of translation of basic immunology to patient care. To build on this success and develop effective combination therapies, a better mechanistic understanding of the efficacy of PD-1 pathway blockade is needed. More work is needed to understand mechanisms of response and resistance, and to develop biomarkers to predict response and IAEs. In addition, further investigations are needed to rationally develop effective combinations with PD-1 pathway inhibitors. For example,

understanding the unique and overlapping functions and signaling pathways of PD-1 with other inhibitory receptors is needed to optimally combine them. In addition to increasing the number of patients who do respond, there is a need to develop predictive biomarkers and understand the immunological mechanisms underlying durability. Tying into this, increased understanding of the role that PD-1 blockade plays in the formation and maintenance of memory T cells will be important. Lastly, by utilizing the newest genome-editing approaches, it may be possible to target coinhibitory molecules more specifically by modulating context-specific enhancers as opposed to the genes themselves. In summary, a deep understanding of the antitumor immune response generated by basic science studies will continue to drive the field forward, with favorable results for patients.

Disclosures

A.H.S. has served as a paid consultant for Novartis, Surface Oncology, SQZ Biotechnologies, and Adapimmune and has patents on the PD-1 pathway licensed by Roche and Novartis. C.G.D. has served as a paid consultant to Bristol-Myers Squibb, Compugen, Roche/Genentech, Regeneron, AstraZeneca/MedImmune, and Merck and is a coinventor on patents licensed from Johns Hopkins to AstraZeneca/MedImmune and to Bristol-Myers Squibb. The other authors have no financial conflicts of interest.

References

- Francisco, L. M., P. T. Sage, and A. H. Sharpe. 2010. The PD-1 pathway in tolerance and autoimmunity. *Immunol. Rev.* 236: 219–242.
- Barber, D. L., E. J. Wherry, D. Masopust, B. Zhu, J. P. Allison, A. H. Sharpe, G. J. Freeman, and R. Ahmed. 2006. Restoring function in exhausted CD8 T cells during chronic viral infection. *Nature* 439: 682–687.
- Schildberg, F. A., S. R. Klein, G. J. Freeman, and A. H. Sharpe. 2016. Coinhibitory pathways in the B7-CD28 ligand-receptor family. *Immunity* 44: 955–972.
- Freeman, G. J., A. J. Long, Y. Iwai, K. Bourque, T. Chernova, H. Nishimura, L. J. Fitz, N. Malenkovich, T. Okazaki, M. C. Byrne, et al. 2000. Engagement of the PD-1 immunoinhibitory receptor by a novel B7 family member leads to negative regulation of lymphocyte activation. *J. Exp. Med.* 192: 1027–1034.
- Dong, H., G. Zhu, K. Tamada, and L. Chen. 1999. B7-H1, a third member of the B7 family, co-stimulates T-cell proliferation and interleukin-10 secretion. *Nat. Med.* 5: 1365–1369.
- Latchman, Y., C. R. Wood, T. Chernova, D. Chaudhary, M. Borde, I. Chernova, Y. Iwai, A. J. Long, J. A. Brown, R. Nunes, et al. 2001. PD-L2 is a second ligand for PD-1 and inhibits T cell activation. *Nat. Immunol.* 2: 261–268.
- Tseng, S. Y., M. Otsuji, K. Gorski, X. Huang, J. E. Slansky, S. I. Pai, A. Shalabi, T. Shin, D. M. Pardoll, and H. Tsuchiya. 2001. B7-DC, a new dendritic cell molecule with potent costimulatory properties for T cells. *J. Exp. Med.* 193: 839–846.
- Pardoll, D., and C. Drake. 2012. Immunotherapy earns its spot in the ranks of cancer therapy. *J. Exp. Med.* 209: 201–209.
- Butte, M. J., M. E. Keir, T. B. Phamduy, A. H. Sharpe, and G. J. Freeman. 2007. Programmed death-1 ligand 1 interacts specifically with the B7-1 costimulatory molecule to inhibit T cell responses. *Immunity* 27: 111–122.
- Xiao, Y., S. Yu, B. Zhu, D. Bedoret, X. Bu, L. M. Francisco, P. Hua, J. S. Duke-Cohan, D. T. Umetsu, A. H. Sharpe, et al. 2014. RGMB is a novel binding partner for PD-L2 and its engagement with PD-L2 promotes respiratory tolerance. *J. Exp. Med.* 211: 943–959.
- Chemnitz, J. M., R. V. Parry, K. E. Nichols, C. H. June, and J. L. Riley. 2004. SHP-1 and SHP-2 associate with immunoreceptor tyrosine-based switch motif of programmed death 1 upon primary human T cell stimulation, but only receptor ligation prevents T cell activation. *J. Immunol.* 173: 945–954.
- Hui, E., J. Cheung, J. Zhu, X. Su, M. J. Taylor, H. A. Wallweber, D. K. Sasmal, J. Huang, J. M. Kim, I. Mellman, and R. D. Vale. 2017. T cell costimulatory receptor CD28 is a primary target for PD-1-mediated inhibition. *Science* 355: 1428–1433.
- Patsoukis, N., L. Li, D. Sari, V. Petkova, and V. A. Boussiotis. 2013. PD-1 increases PTEN phosphatase activity while decreasing PTEN protein stability by inhibiting casein kinase 2. *Mol. Cell. Biol.* 33: 3091–3098.
- Parry, R. V., J. M. Chemnitz, K. A. Frauwrirth, A. R. Lanfranco, I. Braunstein, S. V. Kobayashi, P. S. Linsley, C. B. Thompson, and J. L. Riley. 2005. CTLA-4 and PD-1 receptors inhibit T-cell activation by distinct mechanisms. *Mol. Cell. Biol.* 25: 9543–9553.
- Patsoukis, N., J. Brown, V. Petkova, F. Liu, L. Li, and V. A. Boussiotis. 2012. Selective effects of PD-1 on Akt and Ras pathways regulate molecular components of the cell cycle and inhibit T cell proliferation. *Sci. Signal.* 5: ra46.
- Wei, F., S. Zhong, Z. Ma, H. Kong, A. Medvec, R. Ahmed, G. J. Freeman, M. Krosgaard, and J. L. Riley. 2013. Strength of PD-1 signaling differentially

- affects T-cell effector functions. *Proc. Natl. Acad. Sci. USA* 110: E2480–E2489.
17. Gibbons, R. M., X. Liu, V. Pulko, S. M. Harrington, C. J. Krcio, E. D. Kwon, and H. Dong. 2012. B7-H1 limits the entry of effector CD8(+) T cells to the memory pool by upregulating Bim. *Oncolmunity* 1: 1061–1073.
 18. Quigley, M., F. Pereyra, B. Nilsson, F. Porichis, C. Fonseca, Q. Eichbaum, B. Julg, J. L. Jesneck, K. Brosnahan, S. Imam, et al. 2010. Transcriptional analysis of HIV-specific CD8+ T cells shows that PD-1 inhibits T cell function by up-regulating BATF. *Nat. Med.* 16: 1147–1151.
 19. Fife, B. T., K. E. Pauken, T. N. Eagar, T. Obu, J. Wu, Q. Tang, M. Azuma, M. F. Krummel, and J. A. Bluestone. 2009. Interactions between PD-1 and PD-L1 promote tolerance by blocking the TCR-induced stop signal. *Nat. Immunol.* 10: 1185–1192.
 20. Patsoukis, N., K. Bardhan, P. Chatterjee, D. Sari, B. Liu, L. N. Bell, E. D. Karoly, G. J. Freeman, V. Petkova, P. Seth, et al. 2015. PD-1 alters T-cell metabolic reprogramming by inhibiting glycolysis and promoting lipolysis and fatty acid oxidation. *Nat. Commun.* 6: 6692.
 21. Chang, C. H., J. Qiu, D. O'Sullivan, M. D. Buck, T. Noguchi, J. D. Curtis, Q. Chen, M. Gindin, M. M. Gubin, G. J. van der Windt, et al. 2015. Metabolic competition in the tumor microenvironment is a driver of cancer progression. *Cell* 162: 1229–1241.
 22. Keir, M. E., Y. E. Latchman, G. J. Freeman, and A. H. Sharpe. 2005. Programmed death-1 (PD-1):PD-ligand 1 interactions inhibit TCR-mediated positive selection of thymocytes. *J. Immunol.* 175: 7372–7379.
 23. Nishimura, H., M. Nose, H. Hiai, N. Minato, and T. Honjo. 1999. Development of lupus-like autoimmune diseases by disruption of the PD-1 gene encoding an ITIM motif-carrying immunoreceptor. *Immunity* 11: 141–151.
 24. Salama, A. D., T. Chitnis, J. Imitola, M. J. Ansari, H. Akiba, F. Tushima, M. Azuma, H. Yagita, M. H. Sayegh, and S. J. Khoury. 2003. Critical role of the programmed death-1 (PD-1) pathway in regulation of experimental autoimmune encephalomyelitis. [Published erratum appears in 2003 *J. Exp. Med.* 198: 677.] *J. Exp. Med.* 198: 71–78.
 25. Keir, M. E., S. C. Liang, I. Guleria, Y. E. Latchman, A. Qipo, L. A. Albacker, M. Koulmand, G. J. Freeman, M. H. Sayegh, and A. H. Sharpe. 2006. Tissue expression of PD-L1 mediates peripheral T cell tolerance. *J. Exp. Med.* 203: 883–895.
 26. Keir, M. E., G. J. Freeman, and A. H. Sharpe. 2007. PD-1 regulates self-reactive CD8+ T cell responses to antigen in lymph nodes and tissues. *J. Immunol.* 179: 5064–5070.
 27. Goldberg, M. V., C. H. Maris, E. L. Hipkiss, A. S. Flies, L. Zhen, R. M. Tudor, J. F. Gross, T. J. Harris, D. Getnet, K. A. Whartenby, et al. 2007. Role of PD-1 and its ligand, B7-H1, in early fate decisions of CD8 T cells. *Blood* 110: 186–192.
 28. Gianclecchi, E., D. V. Delfino, and A. Fierabracci. 2013. Recent insights into the role of the PD-1/PD-L1 pathway in immunological tolerance and autoimmunity. *Autoimmun. Rev.* 12: 1091–1100.
 29. Kurtschies, P. D., B. Raziorrouh, W. Schraut, M. Backmund, M. Wächtler, C. M. Wendtner, B. Bengsch, R. Thimme, G. Denk, R. Zachoval, et al. 2014. Dysfunctional CD8+ T cells in hepatitis B and C are characterized by a lack of antigen-specific T-bet induction. *J. Exp. Med.* 211: 2047–2059.
 30. Wherry, E. J., J. N. Blattman, K. Murali-Krishna, R. van der Most, and R. Ahmed. 2003. Viral persistence alters CD8 T-cell immunodominance and tissue distribution and results in distinct stages of functional impairment. *J. Virol.* 77: 4911–4927.
 31. Odorizzi, P. M., K. E. Pauken, M. A. Paley, A. Sharpe, and E. J. Wherry. 2015. Genetic absence of PD-1 promotes accumulation of terminally differentiated exhausted CD8+ T cells. *J. Exp. Med.* 212: 1125–1137.
 32. Blackburn, S. D., H. Shin, G. J. Freeman, and E. J. Wherry. 2008. Selective expansion of a subset of exhausted CD8 T cells by αPD-L1 blockade. *Proc. Natl. Acad. Sci. USA* 105: 15016–15021.
 33. Im, S. J., M. Hashimoto, M. Y. Gerner, J. Lee, H. T. Kissick, M. C. Burger, Q. Shan, J. S. Hale, J. Lee, T. H. Nasti, et al. 2016. Defining CD8+ T cells that provide the proliferative burst after PD-1 therapy. *Nature* 537: 417–421.
 34. He, R., S. Hou, C. Liu, A. Zhang, Q. Bai, M. Han, Y. Yang, G. Wei, T. Shen, X. Yang, et al. 2016. Follicular CXCR5-expressing CD8(+) T cells curtail chronic viral infection. *Nature* 537: 412–428.
 35. Petrovas, C., J. P. Casazza, J. M. Brenchley, D. A. Price, E. Gostick, W. C. Adams, M. L. Precopio, T. Schacker, M. Roederer, D. C. Douek, and R. A. Koup. 2006. PD-1 is a regulator of virus-specific CD8+ T cell survival in HIV infection. *J. Exp. Med.* 203: 2281–2292.
 36. Paley, M. A., D. C. Kroy, P. M. Odorizzi, J. B. Johnnidis, D. V. Dolfi, B. E. Barnett, E. K. Bikoff, E. J. Robertson, G. M. Lauer, S. L. Reiner, and E. J. Wherry. 2012. Progenitor and terminal subsets of CD8+ T cells cooperate to contain chronic viral infection. *Science* 338: 1220–1225.
 37. Sen, D. R., J. Kaminski, R. A. Barnitz, M. Kurachi, U. Gerdemann, K. B. Yates, H. W. Tsao, J. Godde, M. W. LaFleur, F. D. Brown, et al. 2016. The epigenetic landscape of T cell exhaustion. *Science* 354: 1165–1169.
 38. Pauken, K. E., M. A. Sammons, P. M. Odorizzi, S. Manne, J. Godec, O. Khan, A. M. Drake, Z. Chen, D. R. Sen, M. Kurachi, et al. 2016. Epigenetic stability of exhausted T cells limits durability of reinvigoration by PD-1 blockade. *Science* 354: 1160–1165.
 39. Gubin, M. M., X. Zhang, H. Schuster, E. Caron, J. P. Ward, T. Noguchi, Y. Ivanova, J. Hundal, C. D. Arthur, W. J. Krebber, et al. 2014. Checkpoint blockade cancer immunotherapy targets tumour-specific mutant antigens. *Nature* 515: 577–581.
 40. Salmanejad, A., V. Khoramshahi, A. Azani, E. Soltaninejad, S. Aslani, M. R. Zamani, M. Zal, A. Nesaei, and S. M. Hosseini. 2017. PD-1 and cancer: molecular mechanisms and polymorphisms. *Immunogenetics*. DOI: 10.1007/s00251-017-1015-5.
 41. Juneja, V. R., K. A. McGuire, R. T. Manguso, M. W. LaFleur, N. Collins, W. N. Haining, G. J. Freeman, and A. H. Sharpe. 2017. PD-L1 on tumor cells is sufficient for immune evasion in immunogenic tumors and inhibits CD8 T cell cytotoxicity. *J. Exp. Med.* 214: 895–904.
 42. Noguchi, T., J. P. Ward, M. M. Gubin, C. D. Arthur, S. H. Lee, J. Hundal, M. J. Selby, R. F. Graziano, E. R. Mardis, A. J. Korman, and R. D. Schreiber. 2017. Temporally distinct PD-L1 expression by tumor and host cells contributes to immune escape. *Cancer Immunol. Res.* 5: 106–117.
 43. Alloatti, A., D. C. Rookhuizen, L. Joannas, J. M. Carpier, S. Iborra, J. G. Magalhaes, N. Yatim, P. Koziak, D. Sancho, M. L. Albert, and S. Amigorena. 2017. Critical role for Sec22b-dependent antigen cross-presentation in antitumor immunity. *J. Exp. Med.* 214: 2231–2241.
 44. Spranger, S., D. Dai, B. Horton, and T. F. Gajewski. 2017. Tumor-residing Batf3 dendritic cells are required for effector T cell trafficking and adoptive T cell therapy. *Cancer Cell* 31: 711–723.e4.
 45. Deng, L., H. Liang, M. Xu, X. Yang, B. Burnette, A. Arina, X. D. Li, H. Mauceri, M. Beckett, T. Darga, et al. 2014. STING-dependent cytosolic DNA sensing promotes radiation-induced type I interferon-dependent antitumor immunity in immunogenic tumors. *Immunity* 41: 843–852.
 46. Sivan, A., L. Corrales, N. Hubert, J. B. Williams, K. Aquino-Michaels, Z. M. Earley, F. W. Benyamin, Y. M. Lei, B. Jabri, M. L. Alegre, et al. 2015. Commensal Bifidobacterium promotes antitumor immunity and facilitates anti-PD-L1 efficacy. *Science* 350: 1084–1089.
 47. Dahan, R., E. Segal, J. Engelhardt, M. Selby, A. J. Korman, and J. V. Ravetch. 2015. FcγRs modulate the anti-tumor activity of antibodies targeting the PD-1/PD-L1 axis. *Cancer Cell* 28: 285–295.
 48. Ornstein, M. C., and B. I. Rini. 2016. The safety and efficacy of nivolumab for the treatment of advanced renal cell carcinoma. *Expert Rev. Anticancer Ther.* 16: 577–584.
 49. Swart, M., I. Verbrugge, and J. B. Beltman. 2016. Combination approaches with immune-checkpoint blockade in cancer therapy. *Front. Oncol.* 6: 233.
 50. Anderson, A. C., N. Joller, and V. K. Kuchroo. 2016. Lag-3, Tim-3, and TIGIT: co-inhibitory receptors with specialized functions in immune regulation. *Immunity* 44: 989–1004.
 51. Robert, C., A. Ribas, J. D. Wolchok, F. S. Hodi, O. Hamid, R. Kefford, J. S. Weber, A. M. Joshua, W.-J. Hwu, T. C. Gangadhar, et al. 2014. Anti-programmed-death-receptor-1 treatment with pembrolizumab in ipilimumab-refractory advanced melanoma: a randomised dose-comparison cohort of a phase 1 trial. *Lancet* 384: 1109–1117.
 52. Ribas, A., I. Puzanov, R. Dummer, D. Schadendorf, O. Hamid, C. Robert, F. S. Hodi, J. Schachter, A. C. Pavlick, K. D. Lewis, et al. 2015. Pembrolizumab versus investigator-choice chemotherapy for ipilimumab-refractory melanoma (KEYNOTE-002): a randomised, controlled, phase 2 trial. *Lancet Oncol.* 16: 908–918.
 53. Weber, J. S., S. P. D'Angelo, D. Minor, F. S. Hodi, R. Gutzmer, B. Neys, C. Hoeller, N. I. Khushalani, W. H. Miller, Jr., C. D. Lao, et al. 2015. Nivolumab versus chemotherapy in patients with advanced melanoma who progressed after anti-CTLA-4 treatment (CheckMate 037): a randomised, controlled, open-label, phase 3 trial. *Lancet Oncol.* 16: 375–384.
 54. Postow, M. A., J. Chesney, A. C. Pavlick, C. Robert, K. Grossmann, D. McDermott, G. P. Linette, N. Meyer, J. K. Giguere, S. S. Agarwala, et al. 2015. Nivolumab and ipilimumab versus ipilimumab in untreated melanoma. *N. Engl. J. Med.* 372: 2006–2017.
 55. Robert, C., J. Schachter, G. V. Long, A. Arance, J. J. Grob, L. Mortier, A. Daud, M. S. Carlini, C. McNeil, M. Lotem, et al; KEYNOTE-006 investigators. 2015. Pembrolizumab versus ipilimumab in advanced melanoma. *N. Engl. J. Med.* 372: 2521–2532.
 56. Brahmer, J., K. L. Reckamp, P. Baas, L. Crinò, W. E. Eberhardt, E. Poddubskaya, S. Antonia, A. Pluzanski, E. E. Vokes, E. Holgado, et al. 2015. Nivolumab versus docetaxel in advanced squamous-cell non-small-cell lung cancer. *N. Engl. J. Med.* 373: 123–135.
 57. Herbst, R. S., P. Baas, D.-W. Kim, E. Felip, J. L. Pérez-Gracia, J.-Y. Han, J. Molina, J.-H. Kim, C. D. Arvis, M.-J. Ahn, et al. 2016. Pembrolizumab versus docetaxel for previously treated, PD-L1-positive, advanced non-small-cell lung cancer (KEYNOTE-010): a randomised controlled trial. *Lancet* 387: 1540–1550.
 58. Borghaei, H., L. Paz-Ares, L. Horn, D. R. Spigel, M. Steins, N. E. Ready, L. Q. Chow, E. E. Vokes, E. Felip, E. Holgado, et al. 2015. Nivolumab versus docetaxel in advanced nonsquamous non-small-cell lung cancer. *N. Engl. J. Med.* 373: 1627–1639.
 59. Rittmeyer, A., F. Barlesi, D. Waterkamp, K. Park, F. Ciardiello, J. von Pawel, S. M. Gadgil, T. Hida, D. M. Kowalski, M. C. Dols, et al; OAK Study Group. 2017. Atezolizumab versus docetaxel in patients with previously treated non-small-cell lung cancer (OAK): a phase 3, open-label, multicentre randomised controlled trial. *Lancet* 389: 255–265.
 60. Fehrenbacher, L., A. Spira, M. Ballinger, M. Kowanetz, J. Vansteenkiste, J. Mazieres, K. Park, D. Smith, A. Artal-Cortes, C. Lewanski, et al; POPLAR Study Group. 2016. Atezolizumab versus docetaxel for patients with previously treated non-small-cell lung cancer (POPLAR): a multicentre, open-label, phase 2 randomised controlled trial. *Lancet* 387: 1837–1846.
 61. Reck, M., D. Rodriguez-Abreu, A. G. Robinson, R. Hui, T. Csószai, A. Fülop, M. Gottfried, N. Peled, A. Tafreshi, S. Cuffe, et al; KEYNOTE-024 Investigators. 2016. Pembrolizumab versus chemotherapy for PD-L1-positive non-small-cell lung cancer. *N. Engl. J. Med.* 375: 1823–1833.
 62. Langer, C. J., S. M. Gadgil, H. Borghaei, V. A. Papadimitrakopoulou, A. Patnaik, S. F. Powell, R. D. Gentzler, R. G. Martins, J. P. Stevenson, S. I. Jalal, et al; KEYNOTE-021 Investigators. 2016. Carboplatin and pemetrexed with or

- without pembrolizumab for advanced, non-squamous non-small-cell lung cancer: a randomised, phase 2 cohort of the open-label KEYNOTE-021 study. *Lancet Oncol.* 17: 1497–1508.
63. Motzer, R. J., B. Escudier, D. F. McDermott, S. George, H. J. Hammers, S. Srinivas, S. S. Tykodi, J. A. Sosman, G. Procopio, E. R. Plimack, et al; CheckMate 025 Investigators. 2015. Nivolumab versus everolimus in advanced renal-cell carcinoma. *N. Engl. J. Med.* 373: 1803–1813.
 64. Younes, A., A. Santoro, M. Shipp, P. L. Zinzani, J. M. Timmerman, S. Ansell, P. Armand, M. Fanale, V. Ratanatharathorn, J. Kuruvilla, et al. 2016. Nivolumab for classical Hodgkin's lymphoma after failure of both autologous stem-cell transplantation and brentuximab vedotin: a multicentre, multicohort, single-arm phase 2 trial. *Lancet Oncol.* 17: 1283–1294.
 65. Ansell, S. M., A. M. Lesokhin, I. Borrello, A. Halwani, E. C. Scott, M. Gutierrez, S. J. Schuster, M. M. Millenson, D. Cattray, G. J. Freeman, et al. 2015. PD-1 blockade with nivolumab in relapsed or refractory Hodgkin's lymphoma. *N. Engl. J. Med.* 372: 311–319.
 66. Moskowitz, C. H., P. L. Zinzani, M. A. Fanale, P. Armand, N. A. Johnson, J. A. Radford, V. Ribrag, D. Molin, T. P. Vassilakopoulos, A. Tomita, et al. 2016. Pembrolizumab in relapsed/refractory classical Hodgkin lymphoma: primary end point analysis of the phase 2 keynote-087 study. *Blood* 128: 1107.
 67. Balar, A. V., M. D. Galsky, J. E. Rosenberg, T. Powles, D. P. Petrylak, J. Bellmunt, Y. Loriot, A. Necchi, J. Hoffman-Censits, J. L. Perez-Gracia, et al; IMvigor210 Study Group. 2017. Atezolizumab as first-line treatment in cisplatin-ineligible patients with locally advanced and metastatic urothelial carcinoma: a single-arm, multicentre, phase 2 trial. *Lancet* 389: 67–76.
 68. Sharma, P., M. Retz, A. Sieffker-Radtke, A. Baron, A. Necchi, J. Bedke, E. R. Plimack, D. Vaena, M.-O. Grimm, S. Bracarda, et al. 2017. Nivolumab in metastatic urothelial carcinoma after platinum therapy (CheckMate 275): a multicentre, single-arm, phase 2 trial. *Lancet Oncol.* 18: 312–322.
 69. Massard, C., M. S. Gordon, S. Sharma, S. Rafii, Z. A. Wainberg, J. Luke, T. J. Curiel, G. Colon-Otero, O. Hamid, R. E. Sanborn, et al. 2016. Safety and efficacy of durvalumab (MEDI4736), an anti-programmed cell death ligand-1 immune checkpoint inhibitor, in patients with advanced urothelial bladder cancer. *J. Clin. Oncol.* 34: 3119–3125.
 70. Apolo, A. B., J. R. Infante, O. Hamid, M. R. Patel, D. Wang, K. Kelly, A. E. Mega, C. D. Britten, A. C. Mita, A. Ravaud, et al. 2016. Safety, clinical activity, and PD-L1 expression of avelumab (MSB0010718C), an anti-PD-L1 antibody, in patients with metastatic urothelial carcinoma from the JAVELIN Solid Tumor phase Ib trial. *J. Clin. Oncol.* 34(Suppl. 2): 367.
 71. Balar, A., J. Bellmunt, P. H. O'Donnell, D. Castellano, P. Grivas, J. Vuky, T. Powles, E. R. Plimack, N. M. Hahn, R. de Wit, et al. 2016. Pembrolizumab (pembro) as first-line therapy for advanced/unresectable or metastatic urothelial cancer: preliminary results from the phase 2 KEYNOTE-052 study. *Ann. Oncol.* 27(suppl_6). Available at: <https://doi.org/10.1093/annonc/mdw435.25>.
 72. Bellmunt, J., R. de Wit, D. J. Vaughn, Y. Fradet, J.-L. Lee, L. Fong, N. J. Vogelzang, M. A. Climent, D. P. Petrylak, T. K. Choueiri, et al; KEYNOTE-045 Investigators. 2017. Pembrolizumab as second-line therapy for advanced urothelial carcinoma. *N. Engl. J. Med.* 376: 1015–1026.
 73. Muro, K., H. C. Chung, V. Shankaran, R. Geva, D. Catenacci, S. Gupta, J. P. Eder, T. Golan, D. T. Le, B. Burtness, et al. 2016. Pembrolizumab for patients with PD-L1-positive advanced gastric cancer (KEYNOTE-012): a multicentre, open-label, phase 1b trial. *Lancet Oncol.* 17: 717–726.
 74. Ferris, R. L., G. Blumenschein, Jr., J. Fayette, J. Guigay, A. D. Colevas, L. Licitra, K. Harrington, S. Kasper, E. E. Vokes, C. Even, et al. 2016. Nivolumab for recurrent squamous-cell carcinoma of the head and neck. *N. Engl. J. Med.* 375: 1856–1867.
 75. Kaufman, H. L., J. Russell, O. Hamid, S. Bhatia, P. Terheyden, S. P. D'Angelo, K. C. Shih, C. Lebbé, G. P. Linette, M. Milella, et al. 2016. Avelumab in patients with chemotherapy-refractory metastatic Merkel cell carcinoma: a multicentre, single-group, open-label, phase 2 trial. *Lancet Oncol.* 17: 1374–1385.
 76. Le, D. T., J. N. Uram, H. Wang, B. R. Bartlett, H. Kemberling, A. D. Eyring, A. D. Skora, B. S. Luber, N. S. Azad, D. Laheru, et al. 2015. PD-1 blockade in tumors with mismatch-repair deficiency. *N. Engl. J. Med.* 372: 2509–2520.
 77. Vilar, E., and S. B. Gruber. 2010. Microsatellite instability in colorectal cancer—the stable evidence. *Nat. Rev. Clin. Oncol.* 7: 153–162.
 78. Tumeh, P. C., C. L. Harview, J. H. Yearley, I. P. Shintaku, E. J. M. Taylor, L. Robert, B. Chmielowski, M. Spasic, G. Henry, V. Ciobanu, et al. 2014. PD-1 blockade induces responses by inhibiting adaptive immune resistance. *Nature* 515: 568–571.
 79. Huang, A. C., M. A. Postow, R. J. Orlowski, R. Mick, B. Bengsch, S. Manne, W. Xu, S. Harmon, J. R. Giles, B. Wenz, et al. 2017. T-cell invigoration to tumour burden ratio associated with anti-PD-1 response. *Nature* 545: 60–65.
 80. Kamphorst, A. O., A. Wieland, T. Nasti, S. Yang, R. Zhang, D. L. Barber, B. T. Konieczny, C. Z. Daugherty, L. Koenig, K. Yu, et al. 2017. Rescue of exhausted CD8 T cells by PD-1-targeted therapies is CD28-dependent. *Science* 355: 1423–1427.
 81. Hui, E., J. Cheung, J. Zhu, X. Su, M. J. Taylor, H. A. Wallweber, D. K. Sasman, J. Huang, J. M. Kim, I. Mellman, and R. D. Vale. 2017. T cell costimulatory receptor CD28 is a primary target for PD-1-mediated inhibition. *Science* 355: 1428–1433.
 82. Powles, T., J. P. Eder, G. D. Fine, F. S. Braiteh, Y. Loriot, C. Cruz, J. Bellmunt, H. A. Burris, D. P. Petrylak, S. L. Teng, et al. 2014. MPDL3280A (anti-PD-L1) treatment leads to clinical activity in metastatic bladder cancer. *Nature* 515: 558–562.
 83. Patel, S. P., and R. Kurzrock. 2015. PD-L1 expression as a predictive biomarker in cancer immunotherapy. *Mol. Cancer Ther.* 14: 847–856.
 84. Weber, J. S., M. Postow, C. D. Lao, and D. Schadendorf. 2016. Management of adverse events following treatment with anti-programmed death-1 agents. *Oncologist* 21: 1230–1240.
 85. Topalian, S. L., F. S. Hodi, J. R. Brahmer, S. N. Gettinger, D. C. Smith, D. F. McDermott, J. D. Powderly, R. D. Carvajal, J. A. Sosman, M. B. Atkins, et al. 2012. Safety, activity, and immune correlates of anti-PD-1 antibody in cancer. *N. Engl. J. Med.* 366: 2443–2454.
 86. Naidoo, J., X. Wang, K. M. Woo, T. Iyriboz, D. Halpenny, J. Cunningham, J. E. Chaft, N. H. Segal, M. K. Callahan, A. M. Lesokhin, et al. 2017. Pneumonitis in patients treated with anti-programmed death-1/programmed death ligand 1 therapy. *J. Clin. Oncol.* 35: 709–717.
 87. Läubli, H., C. Balmelli, M. Bossard, O. Pfister, K. Glatz, and A. Zippelius. 2015. Acute heart failure due to autoimmune myocarditis under pembrolizumab treatment for metastatic melanoma. *J. Immunother. Cancer* 3: 11.
 88. McDermott, D. F., C. G. Drake, M. Sznol, T. K. Choueiri, J. D. Powderly, D. C. Smith, J. R. Brahmer, R. D. Carvajal, H. J. Hammers, I. Puzanov, et al. 2015. Survival, durable response, and long-term safety in patients with previously treated advanced renal cell carcinoma receiving nivolumab. *J. Clin. Oncol.* 33: 2013–2020.
 89. Topalian, S. L., M. Sznol, D. F. McDermott, H. M. Kluger, R. D. Carvajal, W. H. Sharfman, J. R. Brahmer, D. P. Lawrence, M. B. Atkins, J. D. Powderly, et al. 2014. Survival, durable tumor remission, and long-term safety in patients with advanced melanoma receiving nivolumab. *J. Clin. Oncol.* 32: 1020–1030.
 90. Gettinger, S. N., L. Horn, L. Gandhi, D. R. Spigel, S. J. Antonia, N. A. Rizvi, J. D. Powderly, R. S. Heiss, R. D. Carvajal, D. M. Jackman, et al. 2015. Overall survival and long-term safety of nivolumab (anti-programmed death 1 antibody, BMS-936558, ONO-4538) in patients with previously treated advanced non-small-cell lung cancer. *J. Clin. Oncol.* 33: 2004–2012.
 91. Gibney, G. T., L. M. Weiner, and M. B. Atkins. 2016. Predictive biomarkers for checkpoint inhibitor-based immunotherapy. *Lancet Oncol.* 17: e542–e551.
 92. Hirsch, F. R., A. McElhinny, D. Stanforth, J. Ranger-Moore, M. Jansson, K. Kulangara, W. Richardson, P. Towne, D. Hanks, B. Vennapusa, et al. 2017. PD-L1 immunohistochemistry assays for lung cancer: results from phase 1 of the blueprint PD-L1 IHC assay comparison project. *J. Thorac. Oncol.* 12: 208–222.
 93. Rimm, D. L. G., G. Han, J. M. Taube, E. S. Yi, J. A. Bridge, D. B. Flieder, R. Homer, W. W. West, H. Wu, A. C. Roden, et al. 2017. A prospective, multi-institutional pathologist-based assessment of 4 immunohistochemistry assays for pd-l1 expression in non-small cell lung cancer. *JAMA Oncol.* 3: 1051–1058.
 94. Snyder, A., V. Makarov, T. Merghoub, J. Yuan, J. M. Zaretsky, A. Desrichard, L. A. Walsh, M. A. Postow, P. Wong, T. S. Ho, et al. 2014. Genetic basis for clinical response to CTLA-4 blockade in melanoma. *N. Engl. J. Med.* 371: 2189–2199.
 95. Rizvi, N. A., M. D. Hellmann, A. Snyder, P. Kvistborg, V. Makarov, J. J. Havel, W. Lee, J. Yuan, P. Wong, T. S. Ho, et al. 2015. Cancer immunology: Mutational landscape determines sensitivity to PD-1 blockade in non-small cell lung cancer. *Science* 348: 124–128.
 96. Carbone, D. P., M. Reck, L. Paz-Ares, B. Creelan, L. Horn, M. Steins, E. Felip, M. M. van den Heuvel, T.-E. Ciuleanu, F. Badin, et al; CheckMate 026 Investigators. 2017. First-line nivolumab in stage IV or recurrent non-small-cell lung cancer. *N. Engl. J. Med.* 376: 2415–2426.
 97. Rosenberg, J. E., J. Hoffman-Censits, T. Powles, M. S. van der Heijden, A. V. Balar, A. Necchi, N. Dawson, P. H. O'Donnell, A. Balmanoukian, Y. Loriot, et al. 2016. Atezolizumab in patients with locally advanced and metastatic urothelial carcinoma who have progressed following treatment with platinum-based chemotherapy: a single-arm, multicentre, phase 2 trial. *Lancet* 387: 1909–1920.
 98. Ascierto, M. L., T. L. McMiller, A. E. Berger, L. Danilova, R. A. Anders, G. J. Netto, H. Xu, T. S. Pritchard, J. Fan, C. Cheadle, et al. 2016. The intratumoral balance between metabolic and immunologic gene expression is associated with anti-PD-1 response in patients with renal cell carcinoma. *Cancer Immunol. Res.* 4: 726–733.
 99. Hugo, W., J. M. Zaretsky, L. Sun, C. Song, B. H. Moreno, S. Hu-Lieskovian, B. Berent-Maoz, J. Pang, B. Chmielowski, G. Cherry, et al. 2016. Genomic and transcriptomic features of response to anti-PD-1 therapy in metastatic melanoma. [Published erratum appears in 2017 Cell 168: 542.] *Cell* 165: 35–44.
 100. Ayers, M., J. Lunceford, M. Nebozhyn, E. Murphy, A. Loboda, D. R. Kaufman, A. Albright, J. D. Cheng, S. P. Kang, V. Shankaran, et al. 2017. IFN-γ-related mRNA profile predicts clinical response to PD-1 blockade. *J. Clin. Invest.* 127: 2930–2940.
 101. Dronca, R. S., X. Liu, S. M. Harrington, L. Chen, S. Cao, L. A. Kotschade, R. R. McWilliams, M. S. Block, W. K. Nevala, M. A. Thompson, et al. 2016. T cell Bim levels reflect responses to anti-PD-1 cancer therapy. *JCI Insight* 1: e86014.
 102. Sharma, P., S. Hu-Lieskovian, J. A. Wargo, and A. Ribas. 2017. Primary, adaptive, and acquired resistance to cancer immunotherapy. *Cell* 168: 707–723.
 103. Zaretsky, J. M., A. Garcia-Diaz, D. S. Shin, H. Escuin-Ordinatas, W. Hugo, S. Hu-Lieskovian, D. Y. Torrejon, G. Abril-Rodriguez, S. Sandoval, L. Barthly, et al. 2016. Mutations associated with acquired resistance to PD-1 blockade in Melanoma. *N. Engl. J. Med.* 375: 819–829.
 104. Zhan, T., N. Rindtorff, and M. Boutros. 2017. Wnt signaling in cancer. *Oncogene* 36: 1461–1473.
 105. Spranger, S., R. Bao, and T. F. Gajewski. 2015. Melanoma-intrinsic β-catenin signalling prevents anti-tumour immunity. *Nature* 523: 231–235.
 106. Gao, J., L. Z. Shi, H. Zhao, J. Chen, L. Xiong, Q. He, T. Chen, J. Roszik, C. Bernatchez, S. E. Woodman, et al. 2016. Loss of IFN-γ pathway genes in tumor cells as a mechanism of resistance to anti-CTLA-4 therapy. *Cell* 167: 397–404.e9.

107. Hammers, H. J., E. R. Plimack, J. R. Infante, B. I. Rini, D. F. McDermott, L. D. Lewis, M. H. Voss, P. Sharma, S. K. Pal, A. R. A. Razak, et al. 2017. Safety and efficacy of nivolumab in combination with ipilimumab in metastatic renal cell carcinoma: The CheckMate 016 Study. *J. Clin. Oncol.* 35: 3851–3858.
108. Ascierto, P. A., I. Melero, S. Bhatia, P. Bono, R. E. Sanborn, E. J. Lipson, M. K. Callahan, T. Gajewski, C. A. Gomez-Roca, F. Stephen Hodin, et al. 2017. Initial efficacy of anti-lymphocyte activation gene-3 (anti-LAG-3; BMS-986016) in combination with nivolumab (nivo) in pts with melanoma (MEL) previously treated with anti-PD-1/PD-L1 therapy. *J. Clin. Oncol.* 35(Suppl. 15): 9520.
109. Zakharia, Y., R. McWilliams, M. Shaheen, K. Grossman, J. Drabick, M. Milhem, O. Rixie, S. Khleif, R. Lott, E. Kennedy, et al. 2017. Abstract CT117: interim analysis of the phase 2 clinical trial of the IDO pathway inhibitor indoximod in combination with pembrolizumab for patients with advanced melanoma. *Cancer Res.* 2017(Suppl. 13): CT117.
110. Gangadhar, T. C., B. J. Schneider, T. M. Bauer, J. S. Wasser, A. I. Spira, S. P. Patel, A. S. Balmanoukian, J. Bauml, E. V. Schmidt, Y. Zhao, et al. 2017. Efficacy and safety of epacadostat plus pembrolizumab treatment of NSCLC: preliminary phase I/II results of ECHO-202/KEYNOTE-037. *J. Clin. Oncol.* 35 (Suppl. 15): 9014.
111. Siu, L. L., K. Gelmon, Q. Chu, R. Pachynski, O. Alese, P. Basciano, J. Walker, P. Mitra, L. Zhu, P. Phillips, et al. 2017. Abstract CT116: BMS-986205, an optimized indoleamine 2,3-dioxygenase 1 (IDO1) inhibitor, is well tolerated with potent pharmacodynamic (PD) activity, alone and in combination with nivolumab (nivo) in advanced cancers in a phase 1/2a trial. *Cancer Res.* 77(Suppl. 13): CT116.
112. Drake, C. G., E. Jaffee, and D. M. Pardoll. 2006. Mechanisms of immune evasion by tumors. *Adv. Immunol.* 90: 51–81.
113. Selby, M. J., J. J. Engelhardt, R. J. Johnston, L. S. Lu, M. Han, K. Thudium, D. Yao, M. Quigley, J. Valle, C. Wang, et al. 2016. Preclinical development of ipilimumab and nivolumab combination immunotherapy: mouse tumor models, in vitro functional studies, and Cynomolgus macaque toxicology. [Published erratum appears in 2016 PLoS One 11: e0167251.] *PLoS One* 11: e0161779.
114. Curran, M. A., W. Montalvo, H. Yagita, and J. P. Allison. 2010. PD-1 and CTLA-4 combination blockade expands infiltrating T cells and reduces regulatory T and myeloid cells within B16 melanoma tumors. *Proc. Natl. Acad. Sci. USA* 107: 4275–4280.
115. Andrews, L. P., A. E. Marciscano, C. G. Drake, and D. A. A. Vignali. 2017. LAG3 (CD223) as a cancer immunotherapy target. *Immunol. Rev.* 276: 80–96.
116. Manieri, N. A., E. Y. Chiang, and J. L. Grogan. 2017. TIGIT: a key inhibitor of the cancer immunity cycle. *Trends Immunol.* 38: 20–28.
117. Deng, J., I. Le Mercier, A. Kuta, and R. J. Noelle. 2016. A new VISTA on combination therapy for negative checkpoint regulator blockade. *J. Immunother. Cancer* 4: 86.
118. Munn, D. H., and A. L. Mellor. 2016. IDO in the tumor microenvironment: inflammation, counter-regulation, and tolerance. *Trends Immunol.* 37: 193–207.
119. Antonioli, L., C. Blandizzi, P. Pacher, and G. Haskó. 2013. Immunity, inflammation and cancer: a leading role for adenosine. *Nat. Rev. Cancer* 13: 842–857.
120. Mantovani, A., F. Marchesi, A. Malesci, L. Laghi, and P. Allavena. 2017. Tumour-associated macrophages as treatment targets in oncology. *Nat. Rev. Clin. Oncol.* 14: 399–416.
121. Gubin, M. M., M. N. Artyomov, E. R. Mardis, and R. D. Schreiber. 2015. Tumor neoantigens: building a framework for personalized cancer immunotherapy. *J. Clin. Invest.* 125: 3413–3421.
122. Ott, P. A., Z. Hu, D. B. Keskin, S. A. Shukla, J. Sun, D. J. Bozym, W. Zhang, A. Luoma, A. Giobbie-Hurder, L. Peter, et al. 2017. An immunogenic personal neoantigen vaccine for patients with melanoma. *Nature* 547: 217–221.
123. Sahin, U., E. Derhovanessian, M. Miller, B.-P. Kloke, P. Simon, M. Löwer, V. Bukur, A. D. Tadmor, U. Luxemburger, B. Schrörs, et al. 2017. Personalized RNA mutanome vaccines mobilize poly-specific therapeutic immunity against cancer. *Nature* 547: 222–226.
124. Galluzzi, L., A. Buqué, O. Kepp, L. Zitvogel, and G. Kroemer. 2015. Immunological effects of conventional chemotherapy and targeted anticancer agents. *Cancer Cell* 28: 690–714.

Involvement of PD-L1 on tumor cells in the escape from host immune system and tumor immunotherapy by PD-L1 blockade

Yoshiko Iwai^{*†}, Masayoshi Ishida^{†‡§}, Yoshimasa Tanaka^{†§}, Taku Okazaki^{*}, Tasuku Honjo^{*}, and Nagahiro Minato^{*¶}

^{*}Department of Medical Chemistry, Graduate School of Medicine, [§]Precursory Research for Embryonic Science and Technology (PRESTO), Japan Science and Technology Corporation, and [†]Department of Immunology and Cell Biology, Graduate School of Biostudies, Kyoto University, Kyoto 606-8501, Japan

Contributed by Tasuku Honjo, August 1, 2002

PD-1 is a receptor of the Ig superfamily that negatively regulates T cell antigen receptor signaling by interacting with the specific ligands (PD-L) and is suggested to play a role in the maintenance of self-tolerance. In the present study, we examined possible roles of the PD-1/PD-L system in tumor immunity. Transgenic expression of PD-L1, one of the PD-L, in P815 tumor cells rendered them less susceptible to the specific T cell antigen receptor-mediated lysis by cytotoxic T cells *in vitro*, and markedly enhanced their tumorigenesis and invasiveness *in vivo* in the syngeneic hosts as compared with the parental tumor cells that lacked endogenous PD-L. Both effects could be reversed by anti-PD-L1 Ab. Survey of murine tumor lines revealed that all of the myeloma cell lines examined naturally expressed PD-L1. Growth of the myeloma cells in normal syngeneic mice was inhibited significantly albeit transiently by the administration of anti-PD-L1 Ab *in vivo* and was suppressed completely in the syngeneic PD-1-deficient mice. These results suggest that the expression of PD-L1 can serve as a potent mechanism for potentially immunogenic tumors to escape from host immune responses and that blockade of interaction between PD-1 and PD-L may provide a promising strategy for specific tumor immunotherapy.

Antigen-induced activation and proliferation of T cells are regulated by both positive and negative costimulatory receptors belonging to the Ig superfamily. CD28 and ICOS are positive costimulatory receptors interacting with the ligands of B7 family on professional antigen-presenting cells and are essential for activation and proliferation of antigen-specific T cells (1, 2). By contrast, two distinct receptors on T cells, cytotoxic T lymphocyte (CTL)-A-4 and -PD-1, play opposite roles. CTL-A-4 shares the B7 ligands with CD28 (3), and CLTA-4 gene targeted mice develop fatal polyclonal proliferation of T cells early in life (4), indicating a pivotal role in restricting T cell expansion during normal immune response. PD-1, on the other hand, interacts with distinct ligands, PD-L1 and PD-L2, which are expressed not only on antigen-presenting cells but also other cell types in nonlymphoid tissues (5, 6). Although PD-1 gene-targeted mice show only marginal lymphoproliferation (7), they develop various autoimmune diseases later in life, suggesting the involvement of PD-1 in suppressing activation and/or proliferation of autoreactive T cells (8, 9). These results suggest that the two types of negative receptors may in part control different aspects or stages of immune responses.

Accumulating evidence indicates that specific T cell immune response can be raised against many tumors in human and mouse based on recent sensitive assay systems (10, 11). It is also shown that unaltered self-antigens expressed either aberrantly or in a tissue-specific manner on tumor cells can serve as major tumor rejection antigens, suggesting that antitumor immunity may be in part autoreactive response (12). Nonetheless, tumor-specific immune responses are normally very weak, if present at all, and not sufficient enough to eradicate the tumors. Identification of negative immunoreceptors on T cells, however, has provided a novel prospect that their manipulation may lead to the enhanced tumor-specific T cell immunity *in vivo*. Indeed, blockade of

CTLA-4 was indicated to augment the specific tumor immunity and to induce significant inhibition of tumors *in vivo* in a number of experimental murine models (13).

Unlike B7 molecules, PD-1 ligands (PD-Ls) are expressed on various nonlymphoid tissues in mouse such as heart, lung, liver, and kidney (5, 6). It is speculated that PD-Ls expressed on these vital tissues may function in part as “veto” molecules against the potentially autoreactive effector T cells (14). In this report, we explored the possibility for involvement of PD-1/PD-L1 system in tumor immunity by using experimental tumor models. We indicate that PD-L1 on inherently immunogenic tumor cells confers a potent escaping mechanism from the host T cell immunity and raise a possibility that blockade of PD-1-PD-L interaction may provide an effective approach for specific tumor immunotherapy.

Materials and Methods

Mice. BALB/c, BALB/c nu/nu, DBA/2, and C57BL/6 (B6) mice were purchased from Japan Clea, Hamamatsu, Japan. PD-1-deficient mice that had been backcrossed with B6 or BALB/c mice for over 15 generations were maintained in our animal facility in a specific pathogen-free condition.

Cells and Cultures. Mouse tumor cell lines, P815 (mastocytoma), B16 (melanoma), SP2/0, P3U1, X63, J558L, and PAI (myeloma/plasmacytomas), were maintained in the complete RPMI 1640 medium supplemented with 10% FCS, 10⁻⁵ M 2-mercaptoethanol and antibiotics. An allo (H-2L^d)-reactive cytotoxic T cell clone 2C derived from 2C-transgenic B6 mice was kindly provided by K. Ueda, Graduate School of Science, Kyoto University, and maintained in the complete RPMI 1640 medium supplemented with 5% rat ConA-conditioned medium by stimulating every 10–12 days with 100 Gy-irradiated P815 cells. To generate the syngeneic tumor-specific CTL, DBA/2 mice were injected i.p. with 100 Gy-irradiated P815 cells (5×10^6) at 2 wk apart, and the spleen cells were restimulated *in vitro* with irradiated P815 cells for 6 d followed by a limiting dilution in the presence of irradiated P815 cells, syngeneic splenocytes, and 25 units/ml human IL-2.

Abs and Flow-Cytometric Analysis. Rat anti-mouse PD-1 and PD-L1 mAb were established as described (15, 16), and anti-H-2L^d was purchased from e-Bioscience (San Diego, CA). Flow cytometric analysis was done with a FACScan (Becton Dickinson) as described (7).

Gene Transfection. A PD-L1 cDNA kindly provided by G. J. Freeman (Harvard Medical School, Boston) was digested with

IMMUNOLOGY

Abbreviations: PD-L, ligands for PD-1 receptor; PD-1 $-/-$, PD-1 gene knock-out mice; CTL, cytotoxic T lymphocyte.

[†]Y.I. and M.I. contributed equally to this work.

[¶]To whom reprint requests should be addressed. E-mail: minato@imm.med.kyoto-u.ac.jp.

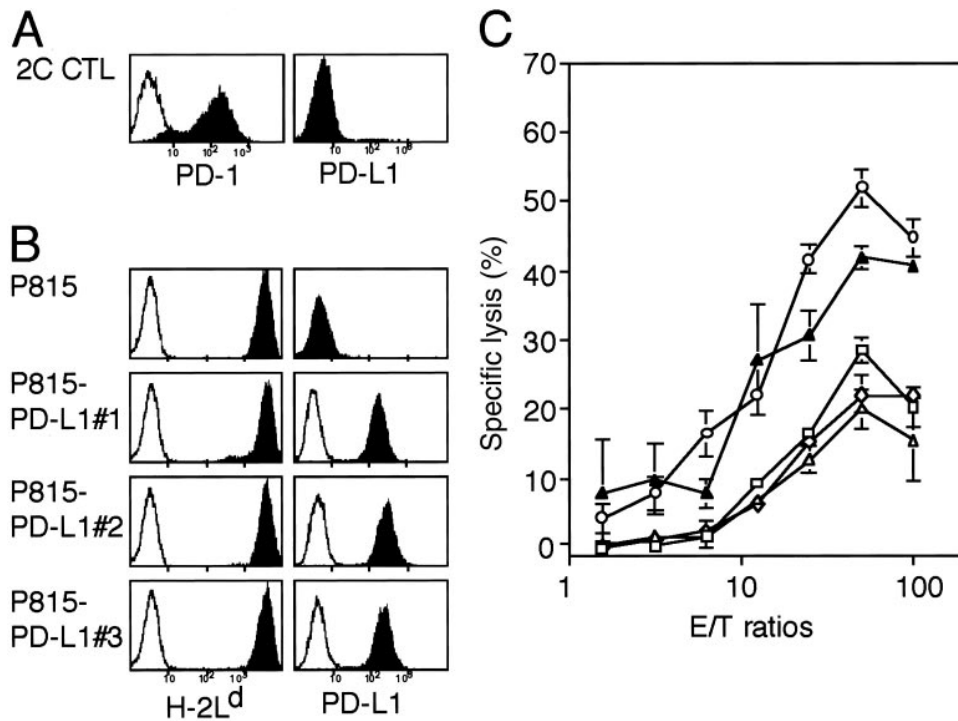


Fig. 1. Inhibition of the cytotoxic activity of CTL clone by engagement of the PD-1 receptor with PD-L1 on the specific target cells. (*A* and *B*) Expression of PD-1, H-2L^d, and PD-L1 on 2C CTL clone and P815 tumor cells as well as their stable transflectant clones of PD-L1(P815/PD-L1 nos. 1–3) were analyzed by using a flow cytometry. Although not shown, none of the cells expressed PD-L2. (*C*) Cells were incubated with ⁵¹Cr-labeled P815 (○) or three independent P815/PD-L1 clones (□, △) in the absence or presence (▲) of 10 µg/ml rat anti-PD-L1 mAb F(ab')₂ at varying effector-to-target (E/T) ratios for 4 h, and the specific ⁵¹Cr release was determined. The means and SE of triplicate cultures are indicated.

*Eco*RI and constructed into a pApuroXS expression vector. P815 cells were transfected with the pApuroXS-PD-L1 by electroporation at 360 V, 500 µF, followed by the selection with puromycin (3 µg/ml), and independent clones stably expressing PD-L1 were established.

Cytotoxicity and IFN Assay. Cytotoxicity assay was done with a ⁵¹Cr-release assay as described (17), and IFN-γ was assayed by using an enzyme-linked immunosorbent assay kit (e-Bioscience) according to the manufacturer's protocol.

Assay of Tumor Growth and Ab Treatment. To assess the tumor growth, tumor diameters were measured with calipers, and tumor volumes were approximated by the calculation as reported (18). For the treatment with Ab, anti-mouse PD-L1 mAb or normal rat IgG as a control was injected i.p. at 0.1 mg per mouse each time on days 1, 3, 5, and 7 after the tumor inoculation.

Histological Analysis. DBA/2 mice inoculated with P815/PD-L1 tumor cells were killed at day 20, and the tissues were fixed in 10% formaldehyde, mounted in paraffin, and stained with hematoxylin and eosin.

Results and Discussion

In an attempt to explore the possible roles of PD-1 receptor in the effector function of T cells, we first examined whether the engagement of PD-1 receptor affects the cytotoxic activity of a B6-derived H-2L^d-specific CTL clone, 2C (19). 2C CTL clone expressed significant PD-1 on stimulation with the specific target, P815 tumor cells (Fig. 1*A*). Because P815 cells expressed neither PD-L1 (Fig. 1*B*) nor PD-L2 (data not shown), we established three independent P815 transfectants stably expressing PD-L1. All of the P815/PD-L1 clones expressed the same

level of H-2L^d antigen (Fig. 1*B*) and proliferated at the same rate in the culture as the parental cells. However, as shown in Fig. 1*C*, the P815/PD-L1 clones were less susceptible to the cytotoxic activity of 2C CTL than the parental P815 cells. The reduced susceptibility of P815/PD-L1 clone to 2C CTL was reversed almost completely by the inclusion of anti-PD-L1 mAb F(ab')₂ in the assay culture (10 µg/ml), indicating that it was not due to an inherent property of the clone. The results suggested strongly that the engagement of PD-1 of CTL with PD-L1 on the specific target cells resulted in the inhibition of T cell receptor-mediated cytotoxic activity.

Because P815 tumor cells exhibit significant T cell immunogenicity, yet forms potentially lethal tumors in the syngeneic DBA/2 mice depending on the loading doses, it has been used as a model of tumor immunity for years. Several distinct rejection antigens recognized by the specific cytotoxic T cells in the syngeneic mice have been identified in P815 cells, including P1A antigen shared with various other tumor cells (20–22). We then compared the tumorigenesis of P815 and P815/PD-L1 cells in the syngeneic DBA/2 mice. P815 cells inoculated s.c. at 1 × 10⁶ cells per mouse formed only transient local tumors (Fig. 2*A Left*), although 70% of the mice eventually died in 6–7 wk because of latent i.p. dissemination of the tumor cells (Fig. 2*B*). The rest 30% of mice were apparently cured of tumors. On the other hand, P815/PD-L1 cells at the same dose formed progressive local tumors (Fig. 2*A Left*) and killed 100% of mice in as early as 2–4 wk (Fig. 2*B*). Autopsy examination revealed early invasion of the s.c. P815/PD-L1 cells into the peritoneal cavity across the abdominal wall and widespread dissemination into the abdominal cavity as well as the probable bloodborne metastasis in the livers and spleens (Fig. 2*C*). In the H-2-identical BALB/c nu/nu mice, however, both P815 and P815/PD-L1 tumor cells formed rapidly growing tumors with only marginal, if any, difference

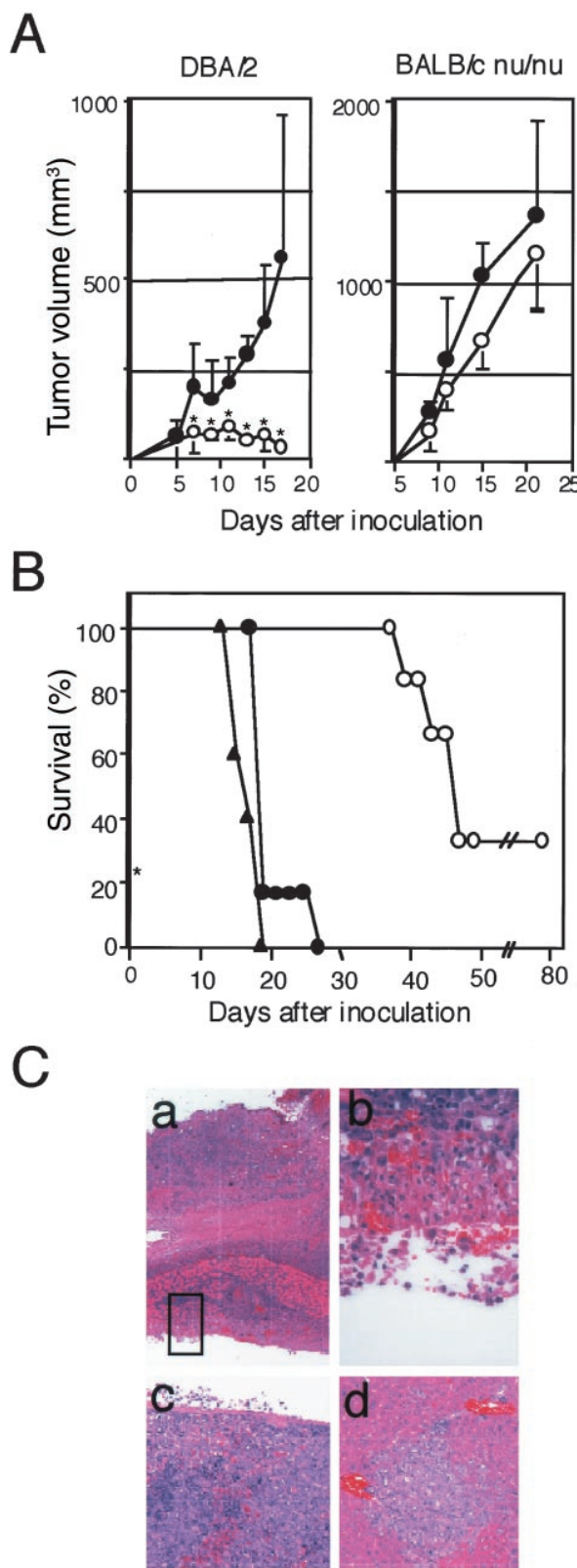


Fig. 2. Enhanced tumorigenicity and invasiveness of P815/PD-L1 cells in the syngeneic DBA/2 mice. (A) P815 (○) or P815/PD-L1 (●) cells were inoculated s.c. at 1×10^6 cells per mouse into DBA/2 (Left) or H-2-shared BALB/c nu/nu (Right) mice, and local tumor growth was monitored. The mean tumor volumes and SE of six mice in each group are indicated. *, $P < 0.01$ by Student's *t* test. (B) DBA/2 mice (six mice per group) were inoculated with P815 (○) or

(Fig. 2*A Right*) and killed them within 4 wk. The results indicated that the enhanced tumorigenicity of P815/PD-L1 cells in the normal syngeneic mice depended on the T cells.

Conforming to the inherent T cell immunogenicity of P815 cells, tumor-specific CD8⁺ CTL could be induced from the spleen cells of DBA/2 mice immunized with P815 cells, and they expressed significant PD-1 (Fig. 3*A*). The syngeneic CTL again exhibited less efficient cytotoxicity as well as IFN-γ production against P815/PD-L1 than P815 cells, and the reduced IFN-γ production in response to P815/PD-L1 cells was restored by the inclusion of anti-PD-L1 mAb F(ab')₂ (Fig. 3*A*). The results confirmed that PD-L1 on the tumor cells significantly inhibited the activation of specific T cells in the syngeneic mice by the tumor antigens. To prove a direct role of PD-L1 in the enhanced tumorigenicity of P815/PD-L1 cells *in vivo*, we injected rat anti-PD-L1 mAb or normal rat IgG as a control at 0.1 mg per mouse on days 1, 3, 5, and 7 after the inoculation of P815/PD-L1 cells (3×10^6 cells per mouse). Injection with the anti-PD-L1 mAb significantly inhibited the local tumor growth, with 40% of the recipients being completely cured of the tumor. On the other hand, 100% of the mice that received control IgG showed progressive tumor growth and were killed within 6 wk (Fig. 3*B*).

Survey of various tumor cell lines indicated that a significant proportion of murine tumor lines, most notably all of the independent myeloma lines so far examined, expressed PD-L1 (Fig. 4*A*). Therefore, we examined whether the PD-L1 naturally expressed on tumor cells indeed contributed to their tumorigenicity *in vivo*. As shown in Fig. 4*B*, J558L myeloma cells inoculated s.c. at 2.5×10^6 cells per mouse formed very rapidly growing tumors in the syngeneic BALB/c mice and killed them within 3 wk. Injection with the anti-PD-L1 Ab after tumor inoculation resulted in the significant suppression of the myeloma cell growth, although the tumors started to expand with delay of 1 wk or so in the most of mice (Fig. 4*B*). A few reasons may be considered for the only transient therapeutic effect of the anti-PD-L1 mAb on the myeloma cells as compared to that on P815/PD-L1 tumor cells, such as less T cell immunogenicity, more aggressive proliferative capacity, and possible selection for variant clones with reduced PD-L1 expression *in vivo* in the myeloma cells. It also should be noted that the presently available anti-PD-L1 Ab is rat origin.

To evaluate the potential effects of complete blockade of PD-1-PD-L1 interaction *in vivo*, we then examined the growth of J558L in PD-1^{-/-} mice of BALB/c background. As indicated in Fig. 4*C Left*, the growth of J558L myeloma was completely suppressed in PD-1^{-/-} BALB/c mice, whereas the tumors grew rapidly in the PD-1^{+/+} littermates. To exclude the possibility that PD-1^{-/-} mice were generally resistant to any immunogenic tumors because of the lack of inhibitory signals in the cross-priming reactions, we compared the growth of B16 tumor cells, which did not express PD-L1 at all (Fig. 4*A*), in the PD-1^{+/+} and ^{-/-} mice of B6 background. As shown in Fig. 4*C Right*, B16 cells formed largely comparable tumors in the PD-1^{+/+} and ^{-/-} mice. The results suggested that a sharp distinction in the tumorigenesis of J558L cells in the syngeneic PD-1^{+/+} and ^{-/-} mice could be attributed primarily to the expression of PD-L1 in the tumor cells. Thus, it was suggested strongly that more persistent and efficient procedures to block PD-1 or PD-L1 *in vivo*, soluble PD-L1 for instance, might

P815/PD-L1 (no. 1 ● and no. 2 ▲) cells as above and the survival rates were monitored. (C) DBA/2 mice inoculated s.c. with P815/PD-L1 cells were autopsied on day 18. Local s.c. tumors showing invasion across the abdominal wall into the peritoneal cavity (a and b) (x40 and x400), spleen showing massive invasion of tumor cells (c), and liver with focal metastatic region (d).

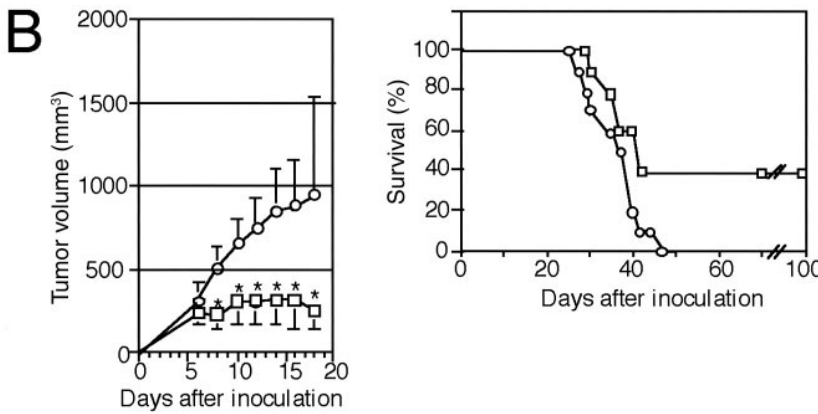
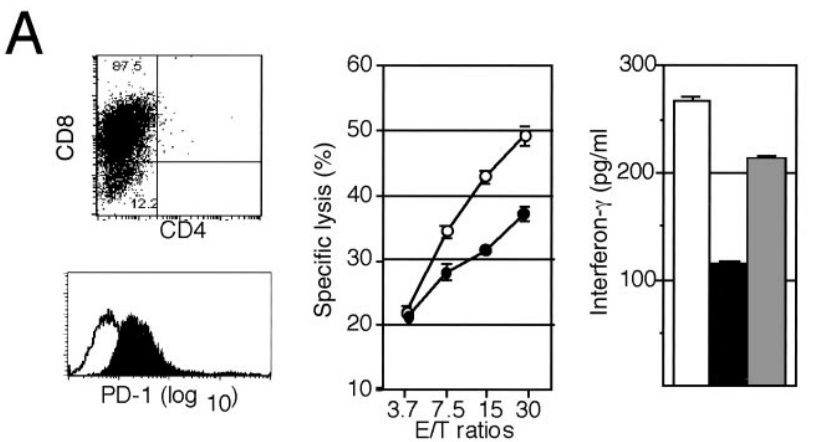


Fig. 3. Inhibition of the tumorigenesis of P815/PD-L1 cells by the injection with anti-PD-L1 mAb *in vivo*. (*A Left*) Syngeneic P815 tumor-specific T cells were generated in DBA/2 mice as described in *Materials and Methods* and analyzed for the expression of CD4, CD8, and PD-1. (*Center*) The CD8+ T cells were incubated with ⁵¹Cr-labeled P815 (○) or P815/PD-L1 (●) cells at varying effector-to-target ratios for 4 h, and the specific cytotoxicity was determined. The means and SE of triplicated cultures are indicated. (*Right*) The CD8+ T cells (2×10^6) were cocultured with 5×10^6 P815 (open bar) or P815/PD-L1 cells in the absence (solid bar) or presence (shaded bar) of anti-PD-L1 mAb F(ab')₂ (10 μ g/ml) for 24 h, and IFN- γ in the culture supernatants was determined by enzyme-linked immunosorbent assay. The means and SE of triplicated cultures are indicated. (*B*) DBA/2 mice (10 mice per group) were inoculated s.c. with 3×10^6 P815/PD-L1 cells, and normal rat IgG (○) or anti-PD-L1 mAb (□) was injected on days 1, 3, 5, and 7 at 0.1 mg per mouse each time. The mean tumor volumes and SE of 10 mice (*Left*) as well as their survival rates (*Right*) are indicated. *, $P < 0.01$ by Student's *t* test.

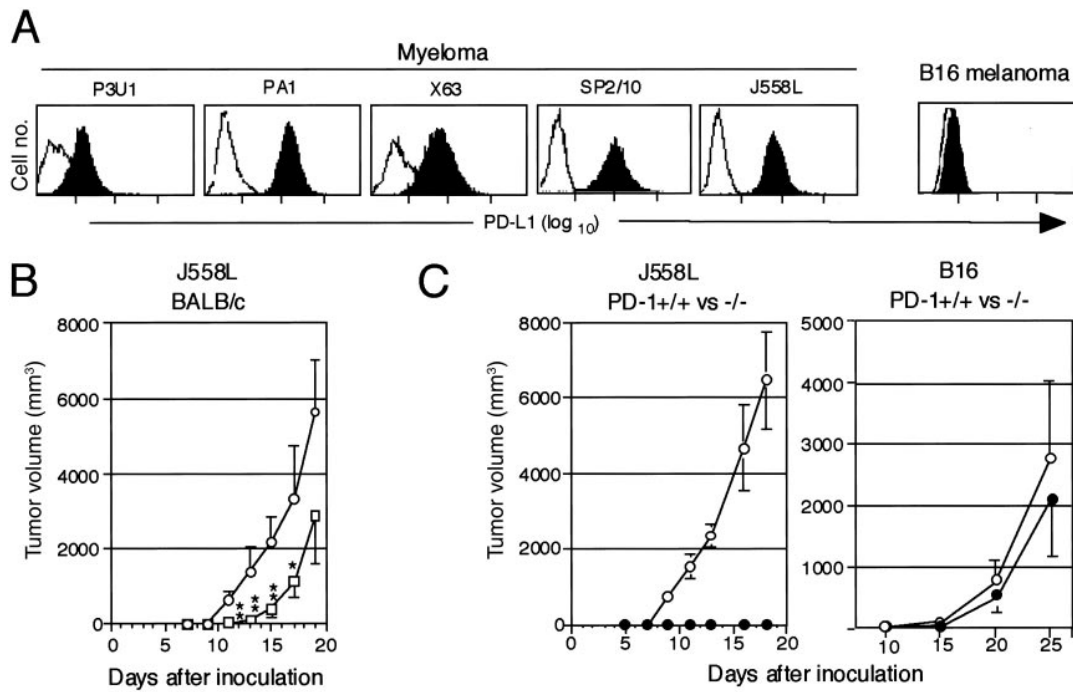


Fig. 4. Inhibition of the tumorigenesis of myeloma cells endogenously expressing PD-L1 in the normal syngeneic mice treated with anti-PD-L1 Ab or in the PD-1-deficient mice. (*A*) Expression of endogenous PD-L1 in myeloma and B16 melanoma cells was examined with flow cytometry. (*B*) J558L myeloma cells (2.5×10^5) were inoculated s.c. into the syngeneic BALB/c mice (nine mice per group) followed by the injection with normal rat IgG (○) or anti-PD-L1 mAb (□) (0.1 mg per mouse) on days 1, 3, 5, and 7. The mean tumor volumes and SE of nine mice are indicated. **, $P < 0.01$; *, $P < 0.1$ (by Student's *t* test). (*C*) J558L (Left, 2.5×10^5) or B16 (Right, 1×10^6) cells were inoculated s.c. into PD-1+/+ (○) and -/- (●) mice of BALB/c or B6 background, respectively. The mean tumor volumes and SE of four (the former) and 10 (the latter) mice are indicated.

provide much improved therapeutic effect, and the trials are currently ongoing.

It was reported that CTLA-4 blockade *in vivo* led to suppression or even rejection of a number of potentially lethal transplanted tumors, in which the effectiveness apparently correlated with the inherent immunogenicity of the tumors (23). These results indicate that weak immune responses against the tumors can be converted into more potent ones effective for tumor suppression and rejection by inhibiting the effects of negative immunoreceptors. Because tumor cells *per se* rarely express the ligands for CTLA-4, CTLA-4 is suggested to restrict the activation and expansion of the potential effector cells by cross-presentation of the tumor antigens via host B7⁺ antigen-presenting cells (24). Present results, on the other hand, indicate that PD-L1 expressed on tumor cells protects them from direct immune attack by the specific CTL at the effector level at least

in vitro, and enhances the tumorigenicity *in vivo*. Although the results imply the tumor-protective effect of PD-L1 at the level of immune effector cells such as CTL *in vivo*, an additional possibility remains open that the PD-L1 inhibits the T cell priming by cross-presentation of tumor antigens as well, because PD-L1 also is expressed on antigen-presenting cells (5). In any event, present results suggest strongly that effective blockade of PD-1-PD-L interaction *in vivo* should provide a promising strategy of immunotherapy for selected tumors expressing PD-L1. It would also be interesting to examine whether there are any synergistic therapeutic effects between blockade of PD-1 and CTLA-4 on the tumors *in vivo*.

We thank Dr. H. Hiai for histological examination and Drs. K. Ueda and G. Freeman for providing cells and plasmids. This work was supported by grants-in-aid for scientific research from the Ministry of Education, Science, Culture, Sports, and Technology (Japan).

1. Sperling, A. I. & Bluestone, J. A. (1996) *Immunol. Rev.* **153**, 155–182.
2. Tafuri, A., Shahinian, A., Bladt, F., Yoshinaga, S. K., Jordana, M., Wakeham, A., Boucher, L. M., Bouchard, D., Chan, V. S., Duncan, G., et al. (1996) *Nature (London)* **409**, 105–109.
3. Thompson, C. B. & Allison, J. P. (1997) *Immunity* **7**, 445–450.
4. Waterhouse, P., Penninger, J. M., Timms, E., Wakeham, A., Shahinian, A., Lee, K. P., Thompson, C. B., Griesser, H. & Mak, T. W. (1995) *Science* **270**, 985–988.
5. Freeman, G. J., Long, A. J., Iwai, Y., Bourque, K., Chernova, T., Nishimura, H., Fitz, L. J., Malenkovich, N., Okazaki, T., Byrne, M. C., et al. (2000) *J. Exp. Med.* **192**, 1027–1034.
6. Latchman, Y., Wood, C. R., Chernova, T., Chaudhary, D., Borde, M., Chernova, I., Iwai, Y., Long, A. J., Brown, J. A., Nunes, R., et al. (2001) *Nat. Immunol.* **2**, 261–268.
7. Nishimura, H., Minato, N., Nakano, T. & Honjo, T. (1998) *Int. Immunol.* **10**, 1563–1572.
8. Nishimura, H., Nose, M., Hiai, H., Minato, N. & Honjo, T. (1999) *Immunity* **11**, 141–151.
9. Nishimura, H., Okazaki, T., Tanaka, Y., Nakatani, K., Hara, M., Matsumori, A., Sasayama, S., Mizoguchi, A., Hiai, H., Minato, N. & Honjo, T. (2001) *Science* **291**, 319–322.
10. Boon, T., Cerottini, J. C., Van den Eynde, B., van der Bruggen, P. & Van Pel, A. (1994) *Annu. Rev. Immunol.* **12**, 337–365.
11. Tureci, O., Sahin, U. & Pfreundschuh, M. (1997) *Mol. Med. Today* **3**, 342–349.
12. Rosenberg, S. A. (1997) *Immunol. Today* **18**, 175–182.
13. Leach, D. R., Krummel, M. F. & Allison, J. P. (1996) *Science* **271**, 1734–1736.
14. Nishimura, H. & Honjo, T. (2001) *Trends Immunol.* **22**, 265–268.
15. Agata, Y., Kawasaki, A., Nishimura, H., Ishida, Y., Tsubata, T., Yagita, H. & Honjo, T. (1996) *Int. Immunol.* **8**, 765–772.
16. Ishida, M., Iwai, Y., Tanaka, Y., Okazaki, T., Freeman, G. J., Minato, N. & Honjo, T. (2002) *Immunol. Lett.* **84**, 57–62.
17. Kato, Y., Tanaka, Y., Miyagawa, F., Yamashita, S. & Minato, N. (2001) *J. Immunol.* **167**, 5092–5098.
18. Kimura, K., Nishimura, H., Matsuzaki, T., Yokokura, T., Nimura, Y. & Yoshikai, Y. (2000) *Cancer Immunol. Immunother.* **49**, 71–77.
19. Ueda, K., Wiesmuller, K. H., Kienle, S., Jung, G. & Walden, P. (1996) *J. Immunol.* **157**, 670–678.
20. Brandle, D., Bilsborough, J., Rulicke, T., Uyttenhove, C., Boon, T. & Van den Eynde, B. J. (1998) *Eur. J. Immunol.* **28**, 4010–4019.
21. Van den Eynde, B., Lethe, B., Van Pel, A., De Plaen, E. & Boon, T. (1991) *J. Exp. Med.* **173**, 1373–1384.
22. Ramarathinam, L., Sarma, S., Maric, M., Zhao, M., Yang, G., Chen, L. & Liu, Y. (1995) *J. Immunol.* **155**, 5323–5329.
23. Chambers, C. A., Kuhns, M. S., Egen, J. G. & Allison, J. P. (2001) *Annu. Rev. Immunol.* **19**, 565–594.
24. Huang, A. Y., Golumbek, P., Ahmadzadeh, M., Jaffee, E., Pardoll, D. & Levitsky, H. (1994) *Science* **264**, 961–965.

The NEW ENGLAND JOURNAL of MEDICINE

ESTABLISHED IN 1812

JUNE 28, 2012

VOL. 366 NO. 26

Safety, Activity, and Immune Correlates of Anti-PD-1 Antibody in Cancer

Suzanne L. Topalian, M.D., F. Stephen Hodi, M.D., Julie R. Brahmer, M.D., Scott N. Gettinger, M.D., David C. Smith, M.D., David F. McDermott, M.D., John D. Powderly, M.D., Richard D. Carvajal, M.D., Jeffrey A. Sosman, M.D., Michael B. Atkins, M.D., Philip D. Leming, M.D., David R. Spigel, M.D., Scott J. Antonia, M.D., Ph.D., Leora Horn, M.D., Charles G. Drake, M.D., Ph.D., Drew M. Pardoll, M.D., Ph.D., Lieping Chen, M.D., Ph.D., William H. Sharfman, M.D., Robert A. Anders, M.D., Ph.D., Janis M. Taube, M.D., Tracee L. McMiller, M.S., Haiying Xu, B.A., Alan J. Korman, Ph.D., Maria Jure-Kunkel, Ph.D., Shruti Agrawal, Ph.D., Daniel McDonald, M.B.A., Georgia D. Kollia, Ph.D., Ashok Gupta, M.D., Ph.D., Jon M. Wigginton, M.D., and Mario Sznol, M.D.

ABSTRACT

BACKGROUND

Blockade of programmed death 1 (PD-1), an inhibitory receptor expressed by T cells, can overcome immune resistance. We assessed the antitumor activity and safety of BMS-936558, an antibody that specifically blocks PD-1.

METHODS

We enrolled patients with advanced melanoma, non–small-cell lung cancer, castration-resistant prostate cancer, or renal-cell or colorectal cancer to receive anti-PD-1 antibody at a dose of 0.1 to 10.0 mg per kilogram of body weight every 2 weeks. Response was assessed after each 8-week treatment cycle. Patients received up to 12 cycles until disease progression or a complete response occurred.

RESULTS

A total of 296 patients received treatment through February 24, 2012. Grade 3 or 4 drug-related adverse events occurred in 14% of patients; there were three deaths from pulmonary toxicity. No maximum tolerated dose was defined. Adverse events consistent with immune-related causes were observed. Among 236 patients in whom response could be evaluated, objective responses (complete or partial responses) were observed in those with non–small-cell lung cancer, melanoma, or renal-cell cancer. Cumulative response rates (all doses) were 18% among patients with non–small-cell lung cancer (14 of 76 patients), 28% among patients with melanoma (26 of 94 patients), and 27% among patients with renal-cell cancer (9 of 33 patients). Responses were durable; 20 of 31 responses lasted 1 year or more in patients with 1 year or more of follow-up. To assess the role of intratumoral PD-1 ligand (PD-L1) expression in the modulation of the PD-1–PD-L1 pathway, immunohistochemical analysis was performed on pretreatment tumor specimens obtained from 42 patients. Of 17 patients with PD-L1-negative tumors, none had an objective response; 9 of 25 patients (36%) with PD-L1-positive tumors had an objective response ($P=0.006$).

CONCLUSIONS

Anti-PD-1 antibody produced objective responses in approximately one in four to one in five patients with non–small-cell lung cancer, melanoma, or renal-cell cancer; the adverse-event profile does not appear to preclude its use. Preliminary data suggest a relationship between PD-L1 expression on tumor cells and objective response. (Funded by Bristol-Myers Squibb and others; ClinicalTrials.gov number, NCT00730639.)

From the Johns Hopkins University School of Medicine and the Sidney Kimmel Comprehensive Cancer Center, Baltimore (S.L.T., J.R.B., C.G.D., D.M.P., W.H.S., R.A.A., J.M.T., T.L.M., H.X.); Dana-Farber Cancer Institute (F.S.H.) and Beth Israel Deaconess Medical Center (D.F.M., M.B.A.) — both in Boston; Yale University School of Medicine and Yale Cancer Center, New Haven, CT (S.N.G., L.C., M.S.); University of Michigan, Ann Arbor (D.C.S.); Carolina BioOncology Institute, Huntersville, NC (J.D.P.); Memorial Sloan-Kettering Cancer Center, New York (R.D.C.); Vanderbilt University Medical Center (J.A.S., L.H.) and Sarah Cannon Research Institute/Tennessee Oncology (D.R.S.) — both in Nashville; Cincinnati Hematology-Oncology, Cincinnati (P.D.L.); H. Lee Moffitt Cancer Center and Research Institute, Tampa, FL (S.J.A.); Bristol-Myers Squibb, Milpitas, CA (A.J.K.); and Bristol-Myers Squibb, Princeton, NJ (M.J.-K., S.A., D.M., G.D.K., A.G., J.M.W.). Address reprint requests to Dr. Topalian at the Department of Surgery, Johns Hopkins University School of Medicine, 1550 Orleans St., CRB 2, Rm. 508, Baltimore, MD 21287, or at stopali1@jhmi.edu.

This article (10.1056/NEJMoa1200690) was published on June 2, 2012, and updated on June 28, 2012, at NEJM.org.

N Engl J Med 2012;366:2443-54.

Copyright © 2012 Massachusetts Medical Society.

HUMAN CANCERS HARBOR NUMEROUS genetic and epigenetic alterations, generating neoantigens that are potentially recognizable by the immune system.¹ Although an endogenous immune response to cancer is observed in preclinical models and patients, this response is ineffective, because tumors develop multiple resistance mechanisms, including local immune suppression, induction of tolerance, and systemic dysfunction in T-cell signaling.²⁻⁵ Moreover, tumors may exploit several distinct pathways to actively evade immune destruction, including endogenous “immune checkpoints” that normally terminate immune responses after antigen activation. These observations have resulted in intensive efforts to develop immunotherapeutic approaches for cancer, including immune-checkpoint-pathway inhibitors such as anti-CTLA-4 antibody (ipilimumab) for the treatment of patients with advanced melanoma.⁶⁻⁸

Programmed death 1 (PD-1) is a key immune-checkpoint receptor expressed by activated T cells, and it mediates immunosuppression. PD-1 functions primarily in peripheral tissues, where T cells may encounter the immunosuppressive PD-1 ligands PD-L1 (B7-H1) and PD-L2 (B7-DC), which are expressed by tumor cells, stromal cells, or both.⁹⁻¹² Inhibition of the interaction between PD-1 and PD-L1 can enhance T-cell responses in vitro and mediate preclinical antitumor activity.^{11,13} In a dose-escalation study, the anti-PD-1 monoclonal antibody BMS-936558 (also known as MDX-1106 and ONO-4538) was administered as a single dose in 39 patients with advanced solid tumors.¹⁴ A favorable safety profile and preliminary evidence of clinical activity were shown in this pilot study, establishing the basis for the current multiple-dose trial involving patients with diverse cancers. We report clinical results for 296 patients in this trial.

METHODS

STUDY DESIGN

This study was sponsored by Bristol-Myers Squibb, which provided the study drug and worked jointly with the senior academic authors to design, collect, analyze, and interpret the study results. All the authors signed a confidentiality agreement with the sponsor. The protocol, including a detailed statistical analysis plan, is available with the full text of this article at NEJM.org. All drafts

of the manuscript were prepared by the authors with editorial assistance from a professional medical writer paid by the sponsor. All the authors vouch for the accuracy and completeness of the reported data and for the fidelity of this report to the trial protocol, and all the authors made the decision to submit the manuscript for publication.

This phase 1 study assessed the safety, anti-tumor activity, and pharmacokinetics of BMS-936558, a fully human IgG4-blocking monoclonal antibody directed against PD-1, in patients with selected advanced solid tumors. All patients (or their legal representatives) gave written informed consent before enrollment. The antibody was administered as an intravenous infusion every 2 weeks of each 8-week treatment cycle. Response was assessed after each treatment cycle. Patients received treatment for up to 2 years (12 cycles), unless they had a complete response, unacceptable adverse effects, or progressive disease or they withdrew consent. In clinically stable patients, study treatment could be continued beyond apparent initial disease progression until progression was confirmed, as outlined by proposed immune-response criteria.¹⁵ Patients with stable disease or an ongoing objective response (complete or partial response) at the end of treatment were followed for up to 1 year and were offered retreatment for 1 additional year in the event of disease progression.

Safety evaluations (clinical examination and laboratory assessments) were conducted for all treated patients at baseline and regular intervals. The severity of adverse events was graded according to the National Cancer Institute Common Terminology Criteria for Adverse Events, version 3.0.¹⁶

DOSE ESCALATION

Patients with advanced melanoma, non-small-cell lung cancer, renal-cell cancer, castration-resistant prostate cancer, or colorectal cancer were enrolled. Cohorts of three to six patients per dose level were enrolled sequentially at doses of 1.0, 3.0, or 10.0 mg per kilogram of body weight. Dose escalation proceeded when a minimum of three patients had completed the safety-evaluation period (56 days) at a given dose level, with dose-limiting toxicity in less than one third of patients. Intrapatient dose escalation was not permitted.

COHORT EXPANSION

A maximum tolerated dose was not reached. Initially, five expansion cohorts of approximately 16 patients each were enrolled at doses of 10.0 mg per kilogram for melanoma, non–small-cell lung cancer, renal-cell cancer, castration-resistant prostate cancer, and colorectal cancer. On the basis of initial signals of activity, additional expansion cohorts of approximately 16 patients each were enrolled for melanoma (at a dose of 1.0 or 3.0 mg per kilogram, followed by cohorts randomly assigned to 0.1, 0.3, or 1.0 mg per kilogram), lung cancer (patients with the squamous or nonsquamous subtype, randomly assigned to a dose of 1.0, 3.0, or 10.0 mg per kilogram), and renal-cell cancer (at a dose of 1.0 mg per kilogram).

PATIENTS

Eligible patients had documented advanced solid tumors; an age of 18 years or older; a life expectancy of 12 weeks or more; an Eastern Cooperative Oncology Group performance status of 0, 1, or 2 (on a scale from 0 to 5, with 0 indicating that the patient is asymptomatic, 1 that the patient is restricted in strenuous activity, and 2 that the patient is ambulatory but unable to work)¹⁷; measurable disease according to Response Evaluation Criteria in Solid Tumors (RECIST), version 1.0,¹⁸ with modification (see Methods S1 in the Supplementary Appendix, available at NEJM.org; and the protocol); adequate hematologic, hepatic, and renal function; and a history of one to five systemic treatment regimens. Patients with radiographically stable treated brain metastases were enrolled. Patients with a history of chronic autoimmune disease, prior therapy with antibodies that modulate T-cell function (e.g., anti-CTLA-4, anti-PD-1, and anti-PD-L1), conditions requiring immunosuppressive medications, or chronic infection (e.g., human immunodeficiency virus infection and hepatitis B or C) were excluded.

IMMUNOHISTOCHEMICAL ANALYSIS FOR PD-L1

Immunohistochemical analysis for PD-L1 was performed on archival or newly obtained pretreatment formalin-fixed, paraffin-embedded tumor specimens with the use of the murine antihuman PD-L1 monoclonal antibody 5H1.^{11,19} The percentage of tumor cells exhibiting cell-surface staining for PD-L1 was scored by two independent pathologists who were unaware of outcomes. PD-L1 positivity was defined per specimen by a

5% expression threshold^{19,20}; patients with multiple specimens were considered PD-L1-positive if any specimen met this criterion.

PHARMACOKINETICS AND PHARMACODYNAMICS

For pharmacokinetic analysis, serum concentrations of anti-PD-1 antibody were quantified with the use of an enzyme-linked immunosorbent assay. For pharmacodynamic analysis, peripheral-blood mononuclear cells (PBMCs) were isolated from patients at baseline and after the first treatment cycle to estimate PD-1–receptor occupancy by the antibody on circulating CD3+ T cells by means of flow cytometry.¹⁴

STATISTICAL ANALYSIS

Data on all 296 patients treated as of the date of analysis for this report (February 24, 2012) were used for summaries of baseline characteristics and adverse events. Pharmacokinetic and molecular-marker analyses included treated patients with available data as of February 24, 2012. The efficacy analysis included the 236 patients who could be evaluated for a response and who began treatment by July 1, 2011. Adverse events were coded with the use of the Medical Dictionary for Regulatory Activities (MedDRA), version 14.1. Adverse events of special interest, with a potential immune-related cause, were identified with the use of a predefined list of MedDRA terms. The best responses in individual patients were derived from investigator-reported data per modified RECIST, version 1.0. Objective responses were confirmed by at least one sequential tumor assessment, and objective response rates were calculated as [(complete responses + partial responses) ÷ number of patients] × 100. Fisher’s exact test was used to assess the association between PD-L1 expression and objective response.

R E S U L T S**BASELINE PATIENT CHARACTERISTICS**

A total of 296 patients with advanced solid tumors, including melanoma (104 patients), non–small-cell lung cancer (122), renal-cell cancer (34), castration-resistant prostate cancer (17), and colorectal cancer (19), began treatment with anti-PD-1 antibody between October 2008 and February 24, 2012. The majority of patients were heavily pretreated; 47% had received at least three prior regimens (Table S1-A in the Supplementary

Appendix). Notable prior therapies included immunotherapy and BRAF inhibitors in patients with melanoma (64% and 8% of patients, respectively); platinum-based chemotherapy and tyrosine kinase inhibitors in patients with lung cancer (94% and 34%, respectively); and nephrectomy, immunotherapy, and antiangiogenic therapy in patients with renal-cell cancer (94%, 59%, and 74%, respectively) (Tables S1-B, S1-C, and S1-D in the Supplementary Appendix). Baseline characteristics of the total treated population (296 patients) were similar to those of the efficacy population (236 patients).

SAFETY

A maximum tolerated dose was not defined at the doses tested in this study. A relative dose intensity (the proportion of administered doses relative to planned doses) of 90% or more was achieved in 86% of patients (Table S2-A in the Supplementary Appendix). Fifteen of 296 patients (5%) discontinued treatment owing to treatment-related adverse events (Tables S2-B and S3-A in the Supplementary Appendix). As of the date of analysis, 62 patients (21%) had died; disease progression was the most common cause of death (Table S2-C in the Supplementary Appendix).

The most common adverse events, regardless of causality, were fatigue, decreased appetite, diarrhea, nausea, cough, dyspnea, constipation, vomiting, rash, pyrexia, and headache (Table S3-A in the Supplementary Appendix). Common treatment-related adverse events included fatigue, rash, diarrhea, pruritus, decreased appetite, and nausea (Tables S3-A and S3-B in the Supplementary Appendix). Grade 3 or 4 treatment-related adverse events were observed in 41 of 296 patients (14%). Drug-related serious adverse events (as defined in Table S4 in the Supplementary Appendix) occurred in 32 of 296 patients (11%). The spectrum, frequency, and severity of treatment-related adverse events were generally similar across the dose levels tested. Drug-related adverse events of special interest (e.g., those with potential immune-related causes) included pneumonitis, vitiligo, colitis, hepatitis, hypophysitis, and thyroiditis (Table 1 and Fig. 1C).

Hepatic or gastrointestinal adverse events were managed with treatment interruption and, as necessary, with the administration of glucocorticoids. These events (e.g., diarrhea in 33 patients, including three grade 3 or 4 events and elevated alanine aminotransferase levels in 11 patients, including

two grade 3 or 4 events) were reversible in all cases. Endocrine disorders were managed with replacement therapy. At the discretion of the treating physician, treatment with anti-PD-1 antibody was reinitiated once the adverse event had been successfully managed. Drug-related pneumonitis occurred in 9 of the 296 patients (3%). Grade 3 or 4 pneumonitis developed in 3 patients (1%). No clear relationship between the occurrence of pneumonitis and tumor type, dose level, or the number of doses received was noted. Early-grade pneumonitis in 6 patients was reversible with treatment discontinuation, glucocorticoid administration, or both. In 3 patients with pneumonitis, infliximab, mycophenolate, or both were used for additional immunosuppression; however, given the small number of patients and variable outcomes, the effectiveness of such treatment was unclear. There were three drug-related deaths (1%) due to pneumonitis (two in patients with non–small-cell lung cancer and one in a patient with colorectal cancer).

CLINICAL ACTIVITY

Antitumor activity was observed at all doses tested. Objective responses were observed in a substantial proportion of patients with non–small-cell lung cancer, melanoma, or renal-cell cancer (Table 2 and Fig. 1) and in various sites of metastasis, including the liver, lung, lymph nodes, and bone. At the time of data analysis, two patients with lung cancer who received 10 mg per kilogram had unconfirmed responses, and eight additional patients (with melanoma, lung cancer, or renal-cell cancer) had a persistent reduction in baseline target lesions in the presence of new lesions (a finding consistent with an immune-related response pattern¹⁵). None of these patients were categorized as having had a response for the purpose of calculating objective-response rates. Objective responses, prolonged disease stabilization, or both were observed in patients who had received a variety of prior therapies. No objective responses were observed in patients with colorectal or prostate cancer.

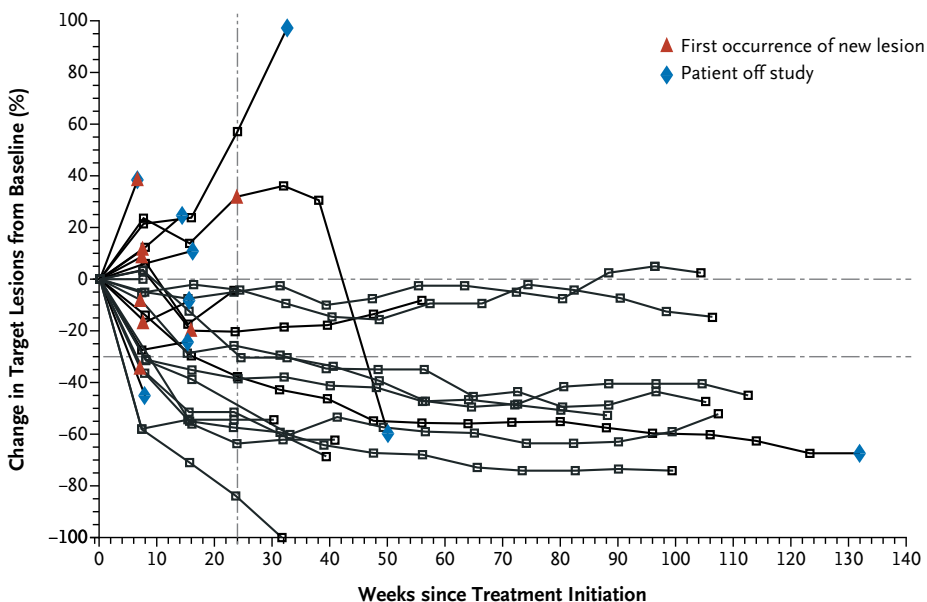
In patients with lung cancer, 14 objective responses were observed at doses of 1.0, 3.0, or 10.0 mg per kilogram, with response rates of 6%, 32%, and 18%, respectively. Objective responses were observed across non–small-cell histologic types: in 6 of 18 patients (33%) with squamous tumors, 7 of 56 (12%) with nonsquamous tumors, and 1 of 2 with tumors of unknown type.

Table 1. Treatment-Related Adverse Events of Special Interest That Occurred in at Least 1% of All Treated Patients.

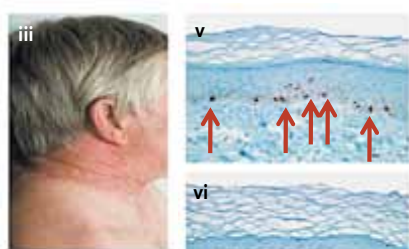
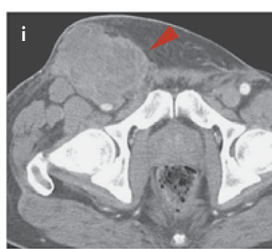
Event	Anti-PD-1 Antibody, 0.1 mg/kg (N=18)		Anti-PD-1 Antibody, 0.3 mg/kg (N=19)		Anti-PD-1 Antibody, 1.0 mg/kg (N=79)		Anti-PD-1 Antibody, 3.0 mg/kg (N=50)		Anti-PD-1 Antibody, 10.0 mg/kg (N=130)		Anti-PD-1 Antibody, Total (N=296)	
	All Events	Grade 3 or 4 Events	All Events	Grade 3 or 4 Events	All Events	Grade 3 or 4 Events						
number of patients (percent)												
Any adverse event of special interest*	8 (44)	0	6 (32)	0	39 (49)	5 (6)	19 (38)	2 (4)	50 (38)	11 (8)	122 (41)	18 (6)
Pulmonary disorders												
Pneumonitis	0	0	0	0	3 (4)	2 (3)	1 (2)	0	5 (4)	1 (1)	9 (3)	3 (1)
Allergic rhinitis	1 (6)	0	0	0	2 (3)	0	0	0	1 (1)	0	4 (1)	0
Diarrhea	1 (6)	0	2 (11)	0	15 (19)	0	3 (6)	0	12 (9)	3 (2)	33 (11)	3 (1)
Skin events												
Rash	3 (17)	0	2 (11)	0	16 (20)	0	4 (8)	0	11 (8)	0	36 (12)	0
Pruritus	0	0	2 (11)	0	13 (16)	0	4 (8)	0	9 (7)	1 (1)	28 (9)	1 (<1)
Vitiligo	3 (17)	0	0	0	3 (4)	0	2 (4)	0	0	0	8 (3)	0
Pruritic rash	0	0	0	0	1 (1)	0	1 (2)	0	4 (3)	0	6 (2)	0
Urticaria	0	0	0	0	0	0	3 (6)	0	2 (2)	0	5 (2)	0
Macular rash	0	0	0	0	0	0	1 (2)	0	3 (2)	1 (1)	4 (1)	1 (<1)
Alopecia	0	0	0	0	2 (3)	0	0	0	1 (1)	0	3 (1)	0
Hypopigmentation	0	0	0	0	2 (3)	0	0	0	1 (1)	0	3 (1)	0
Laboratory investigations†												
Alanine aminotransferase increased	0	0	1 (5)	0	4 (5)	0	2 (4)	0	4 (3)	2 (2)	11 (4)	2 (1)
Thyroid-stimulating hormone increased	2 (11)	0	0	0	2 (3)	0	2 (4)	0	3 (2)	1 (1)	9 (3)	1 (<1)
Aspartate aminotransferase increased	0	0	1 (5)	0	2 (3)	0	2 (4)	1 (2)	3 (2)	1 (1)	8 (3)	2 (1)
Endocrine disorders												
Hypothyroidism	0	0	1 (5)	0	2 (3)	0	1 (2)	0	3 (2)	1 (1)	7 (2)	1 (<1)
Hyperthyroidism	1 (6)	0	0	0	0	0	1 (2)	0	1 (1)	1 (1)	3 (1)	1 (<1)
Infusion-related reaction or hypersensitivity	0	0	0	0	2 (3)	0	3 (6)	0	4 (3)	1 (1)	9 (3)	1 (<1)

* The numbers reported within a column may not add up to the total number reported for “any adverse event of special interest” because patients who had more than one adverse event were counted for each event but were counted only once for “any adverse event of special interest” and because data for only those events that were reported in at least 1% of all treated patients are shown. Colitis, hepatitis, hypophysitis, and thyroiditis were among the adverse events of special interest that were reported in less than 1% of patients. PD-1 denotes programmed death 1.

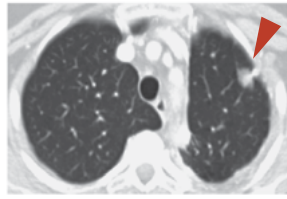
† Levels of alanine aminotransferase, thyroid-stimulating hormone, and aspartate aminotransferase were considered to be increased if they exceeded the upper limit of the normal range for the local laboratory.

A Patients with Melanoma**B Patient with Renal-Cell Cancer
Before Treatment**

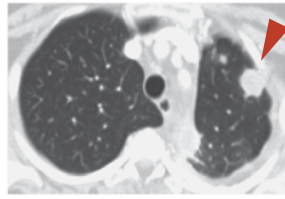
6 Months

**C Patient with Melanoma****D Patient with Non-Small-Cell Lung Cancer**

Before Treatment



2 Months



4 Months

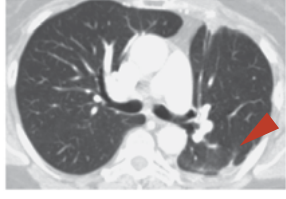
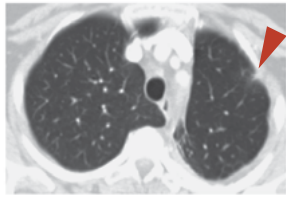


Figure 1 (facing page). Activity of Anti-Programmed Death 1 (PD-1) Antibody in Patients with Treatment-Refractory Melanoma, Non-Small-Cell Lung Cancer, or Renal-Cell Cancer.

In Panel A, a representative plot shows changes from baseline in the tumor burden, measured as the sum of the longest diameters of target lesions, in 27 patients with melanoma who received anti-PD-1 antibody at a dose of 1.0 mg per kilogram of body weight every 2 weeks. In the majority of patients who had an objective response, responses were durable and evident by the end of cycle 2 (16 weeks) of treatment. The vertical dashed line marks the 24-week time point at which the progression-free survival rate was calculated, and the horizontal dashed line marks the threshold for objective response (partial tumor regression) according to modified Response Evaluation Criteria in Solid Tumors. Tumor regression followed conventional as well as immune-related patterns of response, such as prolonged reduction in tumor burden in the presence of new lesions.^{15,21} Panel B shows partial regression of metastatic renal-cell cancer in a 57-year-old patient who received anti-PD-1 antibody at a dose of 1.0 mg per kilogram. This patient had previously undergone radical surgery, and progressive disease had developed after treatment with sunitinib, temsirolimus, sorafenib, and pazopanib. The arrowheads show regression of recurrent tumor in the operative field. Panel C shows a complete response in a 62-year-old patient with metastatic melanoma who received anti-PD-1 antibody at a dose of 3.0 mg per kilogram. Pretreatment computed tomographic scanning (i) revealed inguinal-lymph-node metastasis (arrowhead), which regressed completely after 13 months of treatment (ii). Numerous metastases in the subcutaneous tissue and retroperitoneum also regressed completely (not shown). Vitiligo, which developed after 6 months of treatment, is evident in photographs taken at 9 months under visible light (iii) and ultraviolet light (iv). Skin biopsy specimens with immunohistochemical staining for micro-ophthalmia-associated transcription factor show that melanocytes (arrows) are abundant at the epidermal-dermal junction in normal skin (v), scarce in skin partially affected by vitiligo (vi), and absent in skin fully affected by vitiligo (vii). Panel D shows a partial response in a patient with metastatic non-small-cell lung cancer (nonsquamous histologic type) who received anti-PD-1 antibody at a dose of 10.0 mg per kilogram. The arrowheads show initial progression in pulmonary lesions, followed by regression (an immune-related pattern of response).

All 14 patients with objective responses started treatment 24 weeks or more before data analysis, and of these, 8 had a response that lasted 24 weeks or more (Table 2). Five of 14 patients with objective responses started treatment 1 year or more before data analysis, and of these, 2 had a response that lasted 1 year or more. Stable disease lasting 24 weeks or more was observed in 5 patients (7%) with lung cancer, all of whom had nonsquamous tumors.

In patients with melanoma, 26 objective responses were observed at doses ranging from 0.1 to 10.0 mg per kilogram, with response rates ranging from 19 to 41% per dose level. At a dose of 3.0 mg per kilogram, objective responses were noted in 7 of 17 patients (41%). Of 26 patients with melanoma who had an objective response, 18 started treatment 1 year or more before February 24, 2012, and of these, 13 had a response that lasted 1 year or more. The remaining 8 patients with objective responses received study medication for less than 1 year, and 6 had responses ranging from 1.9 to 5.6 months. Stable disease lasting 24 weeks or more was observed in 6 patients (6%).

Among patients with renal-cell cancer, objective responses occurred in 4 of 17 patients (24%) treated with a dose of 1.0 mg per kilogram and 5 of 16 (31%) treated with 10.0 mg per kilogram. Of 8 patients with objective responses who started treatment 1 year or more before data analysis, 5 had a response that lasted 1 year or more. Stable disease lasting 24 weeks or more was observed in an additional 9 patients (27%).

PHARMACOKINETICS AND PHARMACODYNAMICS

The median time to the peak concentration of anti-PD-1 antibody was 1 to 4 hours after the start of infusion. The pharmacokinetics of the antibody were linear, with a dose-proportional increase in the peak concentration and area under the curve calculated from day 1 to day 14 in the dose range of 0.1 to 10.0 mg per kilogram (35 patients). The pharmacodynamics of anti-PD-1 antibody were assessed according to PD-1-receptor occupancy on circulating CD3+ T cells. In PBMCs from 65 patients with melanoma who were treated with one cycle of anti-PD-1 antibody at a dose of 0.1 to 10.0 mg per kilogram every 2 weeks, the median PD-1-receptor occupancy by anti-PD-1 antibody was 64 to 70% according to dose level (Fig. 2A).

PD-L1 EXPRESSION IN TUMORS

Sixty-one pretreatment tumor specimens from 42 patients (18 with melanoma, 10 with non-small-cell lung cancer, 7 with colorectal cancer, 5 with renal-cell cancer, and 2 with prostate cancer) (Table S5 in the Supplementary Appendix) were analyzed for PD-L1 expression on the surface of tumor cells (Fig. 2B). Biopsy specimens from 25 of the 42 patients were positive for PD-L1 expression by immunohistochemical analysis. Of these 25 patients, 9 (36%) had an objective

response. None of the 17 patients with PD-L1-negative tumors had an objective response. This analysis is based on optional biopsies in a non-random subset of the population, and testing of a statistical hypothesis was not prespecified. These preliminary results must therefore be interpreted with caution.

DISCUSSION

Our data show that approximately one in four to one in five patients treated with anti-PD-1 antibody had objective responses with durability; these occurred in heavily pretreated patients with diverse

tumor types. PD-1 blockade extends the spectrum of clinical activity by immunotherapy beyond immunogenic tumor types, such as melanoma and renal-cell cancer, to treatment-refractory, metastatic non-small-cell lung cancer, a tumor type that is generally not considered to be responsive to immunotherapy. The level of activity seen with anti-PD-1 antibody in patients with lung cancer who had received substantial amounts of prior therapy (55% with at least three lines of previous therapy) (Table S1-B in the Supplementary Appendix) and across histologic types is of interest, particularly in the patients with squamous tumors.^{22,23} These unexpected findings underscore

Table 2. Clinical Activity of Anti-PD-1 Antibody in the Efficacy Population.*

Dose of Anti-PD-1 Antibody	Objective Response†	Objective-Response Rate‡	Duration of Response§	Stable Disease ≥24 wk		Progression-free Survival Rate at 24 wk¶
				no. of patients/total no. of patients	% (95% CI)	
Melanoma						
0.1 mg/kg	4/14	29 (8–58)	7.5+, 5.6+, 5.6, 5.6	1/14	7 (0.2–34)	40 (13–66)
0.3 mg/kg	3/16	19 (4–46)	3.8+, 2.1+, 1.9+	1/16	6 (0.2–30)	31 (9–54)
1.0 mg/kg	8/27	30 (14–50)	24.9+, 22.9, 20.3+, 19.3+, 18.4+, 7.6+, 5.6+, 5.3+	3/27	11 (2–29)	45 (26–65)
3.0 mg/kg	7/17	41 (18–67)¶	22.4+, 18.3+, 15.2+, 12.9, 11.1, 9.3, 9.2+	1/17	6 (0.1–29)	55 (30–80)
10.0 mg/kg	4/20	20 (6–44)	24.6+, 23.9+, 18.0+, 17.0	0/20	0	30 (9–51)
All doses	26/94	28 (19–38)		6/94	6 (2–13)	41 (30–51)
Non-small-cell lung cancer						
Squamous						
1.0 mg/kg	0/5	0		0/5	0	0
3.0 mg/kg	3/6	50 (12–88)	ND	0/6	0	50 (10–90)
10.0 mg/kg	3/7	43 (10–82)	ND	0/7	0	43 (6–80)
All doses	6/18	33 (13–59)	ND	0/18	0	33 (12–55)
Nonsquamous						
1.0 mg/kg	0/12	0		1/12	8 (0.2–39)	14 (0–37)
3.0 mg/kg	3/13	23 (5–54)	ND	2/13	15 (2–45)	37 (10–64)
10.0 mg/kg	4/31	13 (4–30)	ND	2/31	6 (0.8–21)	21 (6–36)
All doses	7/56	12 (5–24)	ND	5/56	9 (3–20)	22 (11–34)
Unknown type						
1.0 mg/kg	1/1	NA	ND	0/1	0	NA
10.0 mg/kg	0/1	0		0/1	0	0
All types						
1.0 mg/kg	1/18	6 (0.1–27)	9.2+	1/18	6 (0.1–27)	16 (0–34)
3.0 mg/kg	6/19	32 (13–57)	30.8+, 7.6+, 5.5+, 3.7+, 1.9+, NA**	2/19	11 (1–33)	41 (18–64)
10.0 mg/kg	7/39	18 (8–34)	14.8+, 7.6+, 7.3+, 6.7, 4.2, 3.7+, 3.7	2/39	5 (0.6–17)	24 (11–38)
All doses	14/76	18 (11–29)		5/76	7 (2–15)	26 (16–36)

Table 2. (Continued.)

Dose of Anti-PD-1 Antibody	Objective Response [†]	Objective-Response Rate [‡]	Duration of Response [§]	Stable Disease ≥24 wk	Progression-free Survival Rate at 24 wk [¶]
	no. of patients/total no. of patients	% (95% CI)	mo	no. of patients/total no. of patients	% (95% CI)
Renal-cell cancer					
1.0 mg/kg	4/17	24 (7–50)	17.5+, 9.2+, 9.2, 5.6+	4/17	24 (7–50)
10.0 mg/kg	5/16	31 (11–59)	22.3+, 21.7+, 12.9, 12.0, 8.4	5/16	31 (11–59)
All doses	9/33	27 (13–46)		9/33	27 (13–46)

* The efficacy population consisted of patients in whom the response could be evaluated, whose treatment was initiated by July 1, 2011, and who had measurable disease at baseline with one of the following: at least one scan obtained during treatment, clinical evidence of disease progression, or death. NA denotes not applicable, and ND not determined.

† Responses were adjudicated according to the Response Evaluation Criteria in Solid Tumors (RECIST), version 1.0, with modification (see Methods S1 in the Supplementary Appendix and the protocol).

‡ Objective response rate = [(complete responses + partial responses) ÷ total no. of patients] × 100. Rates were calculated on the basis of confirmed responses, with confidence intervals calculated with the use of the Clopper–Pearson method.

§ Duration of response was defined as the time from the first response to the time of documented progression, death, or, for censored data (denoted by a plus sign), the most recent tumor assessment.

¶ The progression-free survival rate is the proportion of patients without disease progression who were alive at 24 weeks; the rate was calculated according to the Kaplan–Meier method, with confidence intervals calculated with the use of the Greenwood method.

|| Two patients (one with melanoma who received 3.0 mg of anti-PD-1 antibody per kilogram and one with renal-cell cancer who received 10.0 mg per kilogram) had a complete response.

** One patient continued to receive treatment after an initial detection of progressive disease in preexisting lesions and subsequently had a partial response; this patient was classified as having had a response for the purpose of calculating response rates according to RECIST, version 1.0, but was not included in the calculation of duration of response.

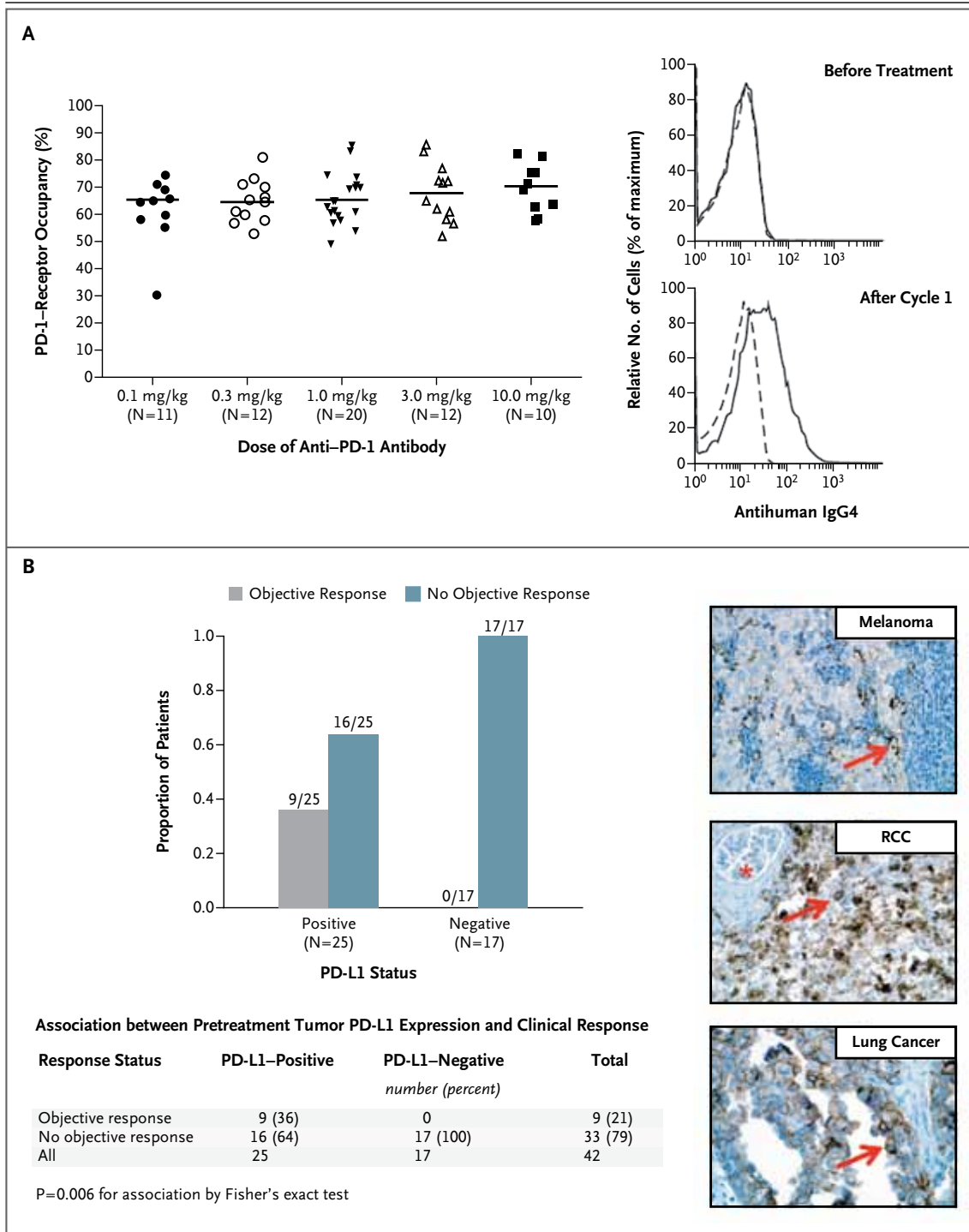
the possibility that any neoplasm could be immunogenic with proper immune activation; however, the reason why only a minority of patients had a response (i.e., tumor or patient [host] factors or both) is not known. The full therapeutic potential of PD-1 blockade across other tumor types remains to be defined.

The durability of objective responses across multiple cancer types in patients treated with anti-PD-1 antibody was also notable. Although anti-PD-1 antibody was not compared with other therapies in this study, this durability contrasts with the relatively modest durability of objective responses observed in many patients with non-small-cell lung cancer, melanoma, or renal-cell cancer who are treated with conventional chemotherapy, tyrosine kinase inhibitors, or both. The response durability in heavily pretreated patients with lung cancer who received anti-PD-1 antibody is particularly interesting, because standard salvage therapies historically have shown modest benefit in these patients.²⁴ As measured by standard RECIST criteria in this study, objective responses were long-lasting, with response durations of 1 year or more in 20 of 31 patients who had a response with 1 year or more of follow-up. In ad-

dition, patterns of tumor regression consistent with immune-related patterns of response^{15,21,25} were observed. That is, index lesions often responded as previously undetected lesions became detectable, a finding that is possibly related to lymphocyte infiltration of previously unknown small nests of tumor cells. Although the full effect of these unconventional response patterns remains to be defined in randomized trials with survival end points, these observations are reminiscent of findings with ipilimumab in which a significant extension of overall survival was observed in treated patients.^{7,8}

Drug-related grade 3 or 4 toxic effects occurred in 14% of patients who received anti-PD-1 antibody, suggesting that therapy can be delivered in an outpatient setting with minimal supportive care. Among adverse events of special interest, pneumonitis was observed, with findings ranging from isolated radiographic abnormalities to progressive, diffuse infiltrates associated with clinical symptoms in a small number of patients. Although three deaths occurred, mild-to-moderate pneumonitis was managed successfully with either observation or glucocorticoids.

A particular challenge in cancer immuno-



therapy has been the identification of mechanism-based predictive biomarkers that could be used to identify candidates for such treatment and guide disease-management decisions. Our findings suggest that PD-L1 expression in tumors is a candidate molecular marker that warrants further exploration for use in selecting patients for immunotherapy with anti-PD-1 antibody. Our observation of an objective response in 36% of the

patients with PD-L1-positive tumors and in none of those with PD-L1-negative tumors suggests that PD-L1 expression on the surface of tumor cells in pretreatment tumor specimens may be associated with an objective response. Although tumor-cell expression of PD-L1 may be driven by constitutive oncogenic pathways, recent research suggests that it may also reflect adaptive immune resistance in response to an endogenous

Figure 2 (facing page). Pharmacodynamic and Molecular-Marker Assessments.

Panel A shows PD-1–receptor occupancy by anti–PD-1 antibody. The graph at the left shows PD-1–receptor occupancy on circulating T cells in 65 patients with melanoma after one cycle (8 weeks) of treatment at a dose of 0.1 to 10.0 mg per kilogram every 2 weeks. Bars indicate median values. The graphs at the right show PD-1–receptor occupancy on CD3-gated peripheral-blood mononuclear cells from a patient with melanoma who received 0.1 mg per kilogram, before treatment (top) and after one treatment cycle (bottom). Cells were stained with biotinylated antihuman IgG4 to detect infused anti–PD-1 antibody bound to PD-1 molecules on the cell surface. Detection was accomplished with the use of streptavidin–phycoerythrin, followed by flow-cytometric analysis. Dashed lines indicate isotype staining controls, and solid lines antihuman IgG4. Panel B shows the correlation of pretreatment tumor cell-surface expression of PD-1 ligand (PD-L1), as determined with immunohistochemical analysis of formalin-fixed, paraffin-embedded specimens, with an objective response to PD-1 blockade in 42 patients with advanced cancers: 18 with melanoma, 10 with non–small-cell lung cancer, 7 with colorectal cancer, 5 with renal-cell cancer, and 2 with castration-resistant prostate cancer. Tumor cell-surface expression of PD-L1 was significantly correlated with an objective clinical response (graph at the left). No patients with PD-L1–negative tumors had an objective response. Of the 25 patients with PD-L1–positive tumors, 2 who were categorized as not having had a response at the time of data analysis are still under evaluation. Shown at the right are immunohistochemical analysis with the anti–PD-L1 monoclonal antibody 5H1 in a specimen of a lymph-node metastasis from a patient with melanoma (top), a nephrectomy specimen from a patient with renal-cell cancer (RCC) (middle), and a specimen of a brain metastasis from a patient with lung adenocarcinoma (bottom). The arrow in each specimen indicates one of many tumor cells with surface-membrane staining for PD-L1. The asterisk indicates a normal glomerulus in the nephrectomy specimen, which was negative for PD-L1 staining.

antitumor immune response, which may remain in check unless it is unleashed through blockade of the PD-1–PD-L1 pathway.¹⁹ Although our data on PD-L1 expression are consistent with current knowledge of the role of PD-L1 in tumor immune resistance, additional studies will be needed to define the role of PD-L1 as a potential predictive marker of response to anti–PD-1 antibody therapy.

This study and a companion study of anti–PD-L1 antibody, now reported in the *Journal*,²⁶ describe clinical activity with these agents that validates the importance of the PD-1–PD-L1 pathway for the treatment of some cancers. The signals of clinical activity in patients with non–small-cell lung cancer, melanoma, and renal-cell can-

cer treated with anti–PD-1 antibody and the possibility of basing patient selection for such treatment on PD-L1 expression in tumors need to be prospectively assessed. Phase 2 trials involving immunologic and molecular-marker correlates (ClinicalTrials.gov numbers, NCT01354431 and NCT01358721) are under way, and phase 3 studies of anti–PD-1 antibody for the treatment of non–small-cell lung cancer, melanoma, and renal-cell cancer are being planned. An assessment of such treatment for other tumor types is also of interest.

Supported by Bristol-Myers Squibb, Ono Pharmaceutical, and grants from the National Institutes of Health (5R01 CA142779, to Drs. Topalian and Pardoll) and the Melanoma Research Alliance (to Drs. Topalian and Pardoll).

Dr. Topalian reports receiving grant support and reimbursement for travel expenses from Bristol-Myers Squibb. Dr. Hodi reports receiving reimbursement for travel expenses from Bristol-Myers Squibb and funding for clinical trials from Bristol-Myers Squibb, Genentech, Pfizer, Novartis, and Synta Pharmaceuticals on behalf of his institution. Dr. Brahmer reports receiving grant support from MedImmune, Regeneron, Merck, and Synta Pharmaceuticals, consulting fees and reimbursement for travel expenses from Genentech, consulting fees from Eli Lilly, reimbursement for travel expenses from Bristol-Myers Squibb, and payment for the development of educational presentations from Quintiles and the Network for Continuing Medical Education. Dr. Smith reports receiving grant support from Bristol-Myers Squibb. Dr. McDermott reports receiving grant support and consulting fees from Prometheus Laboratories and consulting fees from Bristol-Myers Squibb and Roche/Genentech. Dr. Powderly reports receiving grant support (including for the development of educational presentations) and lecture fees from Bristol-Myers Squibb; receiving grant support, consulting fees, and lecture fees from Genentech; receiving grant support and consulting fees from Celldex; receiving grant support and consulting fees from Amplimmune; receiving grant support from Imclone; receiving consulting fees and lecture fees from Genoptix; receiving consulting fees from Veridex; receiving lecture fees from Dendreon; and being the founder of and holding stock in BioCytics, which has received contract work from Genentech and Millennium. Dr. Carvajal reports receiving consulting fees from Morphotek and Novartis and lecture fees from the Florida Society of Dermatology and Dermatologic Surgery and Imedex. Dr. Atkins reports receiving consulting fees from Bristol-Myers Squibb, Genentech, CureTech, Merck, Prometheus Laboratories, Nektar, and AstraZeneca. Dr. Spigel reports receiving consulting fees from Bristol-Myers Squibb on behalf of his institution. Dr. Drake reports receiving consulting fees and payment for the development of educational presentations from Bristol-Myers Squibb, receiving consulting fees from Dendreon and Pfizer, holding stock or stock options in Amplimmune, holding patents regarding the blockade of lymphocyte checkpoint molecules, and receiving patent royalties from Bristol-Myers Squibb and Amplimmune on behalf of his institution. Dr. Pardoll reports receiving consulting fees from Aduro Biotech, Immune Design, Nexitimmune, ImmuneXcite, Amplimmune, GlaxoSmithKline, Abbott, Jennerex, Pfizer, and Anza Therapeutics; receiving reimbursement for travel expenses from Bristol-Myers Squibb; holding patents regarding immunotherapy with the B7-DC gene and its products, combinatorial therapy of cancer with vaccines plus anti–B7-H1 antibodies, vaccine strategies, and the blockade of lymphocyte checkpoint molecules; and receiving patent royalties from Bristol-Myers Squibb, Amplimmune, GlaxoSmithKline, Aduro Biotech, and Biosante on behalf of his institution. Dr.

Chen reports serving as a board observer of, receiving consulting fees from, and holding stock options in Amplimmune; receiving patent licensing payment and research funding from Amplimmune on behalf of Johns Hopkins University and Yale University; receiving patent licensing payment regarding B7-H1-related technologies from Bristol-Myers Squibb on behalf of the Mayo Clinic; receiving funding for research on B7-H1 immunohistochemistry from Bristol-Myers Squibb; and receiving patent licensing payment from ImmunoNext on behalf of the Mayo Clinic. Dr. Sharfman reports receiving consulting fees from Genentech and Merck and lecture fees from Prometheus Laboratories. Dr. Anders reports receiving grant support and reimbursement for travel expenses from Bristol-Myers Squibb. Dr. Taube reports receiving grant support from Bristol-Myers Squibb on behalf of her institution. Ms. McMiller reports receiving compensation for sponsored laboratory research from Bristol-Myers Squibb on behalf of her institution. Dr. Korman reports being an employee of, holding stock or stock options in, and receiving reimbursement for travel expenses from Bristol-Myers Squibb. Drs. Jure-Kunkel, Agrawal, Kollia, Gupta, and Wigginton report being employees of and holding stock or stock options in Bristol-Myers Squibb. Mr. McDonald reports being an employee of, holding stock or stock options in, and receiving reimbursement for travel expenses from Bristol-Myers Squibb. Dr. Sznol reports receiving consulting fees from and owning stock options in Genesis Biopharma; receiving consulting fees from Bristol-Myers Squibb, Anaeropharma Science, Prometheus Laboratories, Nektar, and Abbott; and receiving lecture fees from the Center for Bio-

medical Continuing Education and Institute for Medical Education and Research, both of which are sponsored in part by Bristol-Myers Squibb. No other potential conflict of interest relevant to this article was reported.

Disclosure forms provided by the authors are available with the full text of this article at NEJM.org.

We thank the patients who participated in this study; clinical faculty and personnel, including Ashley Bagheri, Cheryll Carr, Tianna Dause, Robert Gray, Hans Hammers, Marina Laiko, Dung Le, Evan Lipson, Christian Meyer, Alice Pons, Pritish John, Joanne Riemer, and Theresa M. Salay, of the Johns Hopkins University School of Medicine and the Sidney Kimmel Comprehensive Cancer Center; Donald Lawrence of Massachusetts General Hospital; Toni Choueiri, Leena Gandhi, and David Jackman of Dana-Farber Cancer Institute; Daniel Cho, Natasha Coleman, Rose Marujo, and James Mier of Beth Israel Deaconess Medical Center; Miriam Akita, Marianne Davies, Emily Duffield, Christina Lakomski, Daniel Morgensztern, Isabel Oliva, Von Potter, Elin Rowen, Rebecca Sippes, and Danielle Wanik of Yale Cancer Center; Suzanne Burke, Kim Feldhaus, Elaine Granch, Nabeela Iqbal, and Prathima Koppolu of the University of Michigan; Jahleen Byers, Bryan Greene, Jill Hinson, Eric Keller, Lori Lipocky, and Vanica Pharoah of Carolina BioOncology Institute; and David Carbone, Ken Hande, William Pao, Igor Puzanov, and Serena Rucker of Vanderbilt University Medical Center; Qiankun Sun, statistician, and Mubing Li, lead statistical programmer, of Bristol-Myers Squibb; and Susan Leinbach, medical writer, of Clinical Solutions Group.

REFERENCES

1. Sjöblom T, Jones S, Wood LD, et al. The consensus coding sequences of human breast and colorectal cancers. *Science* 2006;314:268-74.
2. Topalian SL, Weiner GJ, Pardoll DM. Cancer immunotherapy comes of age. *J Clin Oncol* 2011;29:4828-36.
3. Mellman I, Coukos G, Dranoff G. Cancer immunotherapy comes of age. *Nature* 2011;480:480-9.
4. Drake CG, Jaffee E, Pardoll DM. Mechanisms of immune evasion by tumors. *Adv Immunol* 2006;90:51-81.
5. Mizoguchi H, O'Shea JJ, Longo DL, Loeffler CM, McVicar DW, Ochoa AC. Alterations in signal transduction molecules in T lymphocytes from tumor-bearing mice. *Science* 1992;258:1795-8.
6. Leach DR, Krummel MF, Allison JP. Enhancement of antitumor immunity by CTLA-4 blockade. *Science* 1996;271:1734-6.
7. Hodi FS, O'Day SJ, McDermott DF, et al. Improved survival with ipilimumab in patients with metastatic melanoma. *N Engl J Med* 2010;363:711-23.
8. Robert C, Thomas L, Bondarenko I, et al. Ipilimumab plus dacarbazine for previously untreated metastatic melanoma. *N Engl J Med* 2011;364:2517-26.
9. Dong H, Zhu G, Tamada K, Chen L. B7-H1, a third member of the B7 family, co-stimulates T-cell proliferation and interleukin-10 secretion. *Nat Med* 1999;5:1365-9.
10. Freeman GJ, Long AJ, Iwai Y, et al. Engagement of the PD-1 immunoinhibitory receptor by a novel B7 family member leads to negative regulation of lymphocyte activation. *J Exp Med* 2000;192:1027-34.
11. Dong H, Strome SE, Salomao DR, et al. Tumor-associated B7-H1 promotes T-cell apoptosis: a potential mechanism of immune evasion. *Nat Med* 2002;8:793-800. [Erratum, *Nat Med* 2002;8:1039.]
12. Topalian SL, Drake CG, Pardoll DM. Targeting the PD-1/B7-H1(PD-L1) pathway to activate anti-tumor immunity. *Curr Opin Immunol* 2012;24:207-12.
13. Iwai Y, Ishida M, Tanaka Y, Okazaki T, Honjo T, Minato N. Involvement of PD-L1 on tumor cells in the escape from host immune system and tumor immunotherapy by PD-L1 blockade. *Proc Natl Acad Sci U S A* 2002;99:12293-7.
14. Brahmer JR, Drake CG, Wollner I, et al. Phase I study of single-agent anti-programmed death-1 (MDX-1106) in refractory solid tumors: safety, clinical activity, pharmacodynamics, and immunologic correlates. *J Clin Oncol* 2010;28:3167-75.
15. Wolchok JD, Hoos A, O'Day S, et al. Guidelines for the evaluation of immune therapy activity in solid tumors: immune-related response criteria. *Clin Cancer Res* 2009;15:7412-20.
16. Cancer Therapy Evaluation Program (CTEP) Common Terminology Criteria for Adverse Events (CTCAE), Version 3.0. Bethesda, MD: National Cancer Institute, April 2003 (http://ctep.cancer.gov/protocolDevelopment/electronic_applications/docs/ctcae3.pdf).
17. Oken MM, Creech RH, Tormey DC, et al. Toxicity and response criteria of the Eastern Cooperative Oncology Group. *Am J Clin Oncol* 1982;5:649-55.
18. Therasse P, Arbuck SG, Eisenhauer EA, et al. New guidelines to evaluate the response to treatment in solid tumors: European Organization for Research and Treatment of Cancer, National Cancer Institute of the United States, National Cancer Institute of Canada. *J Natl Cancer Inst* 2000;92:205-16.
19. Taube JM, Anders RA, Young GD, et al. Colocalization of inflammatory response with B7-H1 expression in human melanocytic lesions supports an adaptive resistance mechanism of immune escape. *Science Transl Med* 2012;4:127ra37.
20. Thompson RH, Kuntz SM, Leibovich BC, et al. Tumor B7-H1 is associated with poor prognosis in renal cell carcinoma patients with long-term follow-up. *Cancer Res* 2006;66:3381-5.
21. Ribas A, Chmielowski B, Glaspy JA. Do we need a different set of response assessment criteria for tumor immunotherapy? *Clin Cancer Res* 2009;15:7116-8.
22. Gridelli C, Ardizzone A, Ciardiello F, et al. Second-line treatment of advanced non-small cell lung cancer. *J Thorac Oncol* 2008;3:430-40.
23. Miller VA. Optimizing therapy in previously treated non-small cell lung cancer. *Semin Oncol* 2006;33:Suppl 1:S25-S31.
24. Sagliotti G, Brodowicz T, Shepherd FA, et al. Treatment-by-histology interaction analyses in three phase III trials show superiority of pemetrexed in non-squamous non-small cell lung cancer. *J Thorac Oncol* 2011;6:64-70.
25. Sharma P, Wagner K, Wolchok JD, Allison JP. Novel cancer immunotherapy agents with survival benefit: recent successes and next steps. *Nat Rev Cancer* 2011;11:805-12.
26. Brahmer JR, Tykodi SS, Chow LQM, et al. Safety and activity of anti-PD-L1 antibody in patients with advanced cancer. *N Engl J Med* 2012;366:2455-65.

Copyright © 2012 Massachusetts Medical Society.

Metabolic shift induced by systemic activation of T cells in PD-1-deficient mice perturbs brain monoamines and emotional behavior

Michio Miyajima^{1,9}, Baihao Zhang^{1,2,9}, Yuki Sugiura^{3,9}, Kazuhiro Sonomura^{4,9}, Matteo M Guerrini¹, Yumi Tsutsui¹, Mikako Maruya¹, Alexis Vogelzang¹, Kenji Chamoto², Kurara Honda³, Takatoshi Hikida⁵, Satomi Ito¹, Hongyan Qin⁶, Rikako Sanuki⁷, Keiichiro Suzuki¹, Takahisa Furukawa⁷, Yasushi Ishihama⁸, Fumihiko Matsuda⁴, Makoto Suematsu³, Tasuku Honjo² & Sidonia Fagarasan¹

T cells reorganize their metabolic profiles after being activated, but the systemic metabolic effect of sustained activation of the immune system has remained unexplored. Here we report that augmented T cell responses in *Pdcd1*^{-/-} mice, which lack the inhibitory receptor PD-1, induced a metabolic serum signature characterized by depletion of amino acids. We found that the depletion of amino acids in serum was due to the accumulation of amino acids in activated *Pdcd1*^{-/-} T cells in the lymph nodes. A systemic decrease in tryptophan and tyrosine led to substantial deficiency in the neurotransmitters serotonin and dopamine in the brain, which resulted in behavioral changes dominated by anxiety-like behavior and exacerbated fear responses. Together these data indicate that excessive activation of T cells causes a systemic metabolomic shift with consequences that extend beyond the immune system.

Activated T cells adapt their cellular metabolism to sustain proliferation and effector functions and to maintain immunological memory¹. Quiescent T cells generate energy (ATP) through oxidative phosphorylation, which is fueled by the breakdown of glucose, fatty acids and amino acids. T cell activation is accompanied by a metabolic shift, including substantial induction of aerobic glycolysis. Although glycolysis is less efficient than oxidative phosphorylation in terms of ATP production, it supplies T cells with the metabolic intermediates essential for the synthesis of the proteins, nucleic acids and lipids needed for effector functions².

Engagement of the antigen-specific T cell antigen receptor (TCR) on T cells is essential for the acquisition of effector function, but the duration and strength of a response is the result of the integration of co-receptor signals. PD-1 (encoded by *Pdcd1*) is an inhibitory co-receptor induced after the activation of T cells. Engagement of PD-1 by its ligands (PD-L1 and PD-L2) causes phosphorylation of the cytoplasmic tail of PD-1 and dephosphorylation of signaling molecules induced by activation of the TCR, which ultimately suppresses the proliferation and cytokine production of T cells. Genetic deletion of PD-1 or antibody-mediated blockade of PD-1 leads to the expansion of T cell populations with an activated phenotype and enhanced immunity to infections and

tumors³. However, the accumulation of activated T cells provides an excess of germinal-center-promoting factors and facilitates the selection of antibodies with self-reactive properties^{4,5}. Indeed, PD-1 deficiency in mice and PD-1-blockade immunotherapy in patients has revealed strain- or patient-specific susceptibility to the development of autoimmune diseases such as gastritis, dilated cardiomyopathy, rheumatoid arthritis, systemic lupus erythematosus and Grave's disease³.

Here we investigated whether the metabolic readjustments within activated T cells following activation of the immune system affected systemic metabolism. Using *Pdcd1*^{-/-} mice as a model of systemic activation of T cells, we found that concentrations of free amino acids in the serum of *Pdcd1*^{-/-} mice decreased as a consequence of the accumulation of amino acids in activated T cells in the lymph nodes (LNs). This systemic drop in amino-acid availability downstream of strong activation of the immune system affected biochemical pathways that depend on free amino acids as precursor metabolites. Specifically, reduced availability of tryptophan and tyrosine in the brain of *Pdcd1*^{-/-} mice affected the synthesis of monoamine neurotransmitters, which resulted in increased anxiety-like behavior and fear responses. Thus, sustained activation of T cells can affect emotional behavior through systemic metabolic alteration.

¹Laboratory for Mucosal Immunity, Center for Integrative Medical Sciences, RIKEN Yokohama Institute, Yokohama, Japan. ²Department of Immunology and Genomic Medicine, Kyoto University Graduate School of Medicine, Kyoto, Japan. ³Department of Biochemistry and Integrative Biology, Keio University, Tokyo, Japan.

⁴Center for Genomic Medicine, Kyoto University Graduate School of Medicine, Kyoto University, Kyoto, Japan. ⁵Medical Innovation Center, Kyoto University Graduate School of Medicine, Kyoto, Japan. ⁶Department of Medical Genetics and Developmental Biology, 4th Military Medical University, Xi'an, China. ⁷Laboratory for Molecular and Developmental Biology, Institute for Protein Research, Osaka University, Osaka, Japan. ⁸Department of Molecular and Cellular Bioanalyses, Graduate School of Pharmaceutical Sciences, Kyoto University, Kyoto, Japan. ⁹These authors contributed equally to this work. Correspondence should be addressed to S.F. (sidonia.fagarasan@riken.jp).

Received 23 August; accepted 3 October; published online 23 October 2017; doi:10.1038/ni.3867

RESULTS

Diminished amino acids in serum of *Pdcd1*^{-/-} mice

We performed metabolomic profiling of serum from *Pdcd1*^{-/-} mice, focusing particularly on small, water-soluble molecules that can bridge diverse tissues via the circulation. Partial least-squares discriminant analysis (PLS-DA) of metabolites indicated that *Pdcd1*^{-/-} mice had a systemic metabolome profile different from that of wild-type mice (Fig. 1a), with the most significantly decreased abundance in compounds involved in energy production, such as components of the tricarboxylic acid (TCA) cycle and amino-acid metabolism (Fig. 1b and Supplementary Table 1). Most proteinogenic amino acids, including the essential amino acids (methionine (Met), threonine (Thr), histidine (His), lysine (Lys), tryptophan (Trp), phenylalanine (Phe), leucine (Leu), isoleucine (Ile) and valine (Val)) were 10–30% less abundant in *Pdcd1*^{-/-} mice than in wild-type non-littermate mice (Fig. 1c) or wild-type littermates (Fig. 1d). The reduction in abundance of the aromatic amino acids Trp, tyrosine (Tyr) and Phe in *Pdcd1*^{-/-} mice relative to that in wild-type mice was already significant by 2 months of age (Fig. 1e), and it further decreased by 4–6 months of age and persisted throughout a 1-year monitoring period, unlike results obtained for branched-chain amino acids (Leu, Ile and Val), which were similar in abundance in *Pdcd1*^{-/-} mice to their baseline amounts in wild-type mice at 2 months of age (Fig. 1e). These data indicated alterations in the metabolome of serum from PD-1 deficient mice, relative to that of wild-type mice; in particular, an accelerated decrease in aromatic amino acids.

T cells affect serum biochemistry in *Pdcd1*^{-/-} mice

PD-1 is expressed on activated T cells, although has also been reported to be expressed on some B cells and innate cell subsets^{6,7}. To investigate the contribution of T cells to the systemic metabolomic profile of *Pdcd1*^{-/-} mice, we measured amino acids in serum from 3-month-old *Cd3e*^{-/-} mice, which are deficient in the gene encoding the invariant signaling protein CD3ε and lack T cells, and age-matched *Pdcd1*^{-/-}/*Cd3e*^{-/-} mice. Except for minor changes, such as a 10% increase in Leu and 30% decrease in Thr in *Pdcd1*^{-/-}/*Cd3e*^{-/-} mice relative to their abundance in *Cd3e*^{-/-} mice, all other proteinogenic amino acids were similar in mice of these two genotypes (Fig. 2a). Thus, the reduction in the abundance of serum amino acids observed in the *Pdcd1*^{-/-} mice was largely T cell dependent.

As for the distribution of T cells among lymphoid tissues, by 4–6 months of age, *Pdcd1*^{-/-} mice had accumulated more T cells in the LNs and spleen than wild-type mice had, while the number of T cells in the colon and lamina propria of the small intestine was similar in both groups of mice (Fig. 2b). The absolute number of CD4⁺ T cells, CD8⁺ T cells and activated CD44^{hi} T cells was higher in *Pdcd1*^{-/-} LNs than in the LNs of age-matched wild-type mice at 2, 3 and 4–6 months of age (Fig. 2c); this corresponded to the age-dependent decrease in aromatic amino acids in the serum of *Pdcd1*^{-/-} mice (Fig. 1e). We next investigated whether activated T cells had a greater intracellular abundance of amino acids than that of naive T cells. CD44^{hi} T cells sorted from the LNs of wild-type mice had a greater intracellular abundance (1.5-fold) of Trp and Tyr, on a per-cell basis, than that of naive CD44^{lo} T cells (Fig. 2d). Large neutral amino acid such as Trp or Tyr are transported across the cell membrane by the system L transporter, a heterodimer composed of the heavy chain CD98 (encoded by *Slc3a2*) and the light chain LAT1 (encoded by *Slc7a5*)⁸. Indeed, *ex vivo* flow cytometry of LN cells identified higher surface expression of CD98 on activated CD44^{hi}CD4⁺ and CD44^{hi}CD8⁺ T cells than on naive CD44^{lo} T cells (Fig. 2e).

To further investigate whether the activation of T cells increased their uptake and accumulation of free amino acids intracellularly

despite extensive proliferation, we measured total protein, Trp and Tyr within cells after stimulation. We sorted T cells from the LNs of wild-type and *Pdcd1*^{-/-} mice and stimulated the TCR *in vitro* with antibody to the TCR invariant chain CD3 (anti-CD3) and antibody to the co-receptor CD28 (anti-CD28). We found that this stimulation induced the accumulation of intracellular Trp and Tyr at 48 h (1.5-fold) and at 96 h (2-fold) in activated T cells, relative to their abundance in non-activated T cells (Fig. 2f). The expression of *Slc3a2* and *Slc7a5* transcripts was increased at 24 h after stimulation in both wild-type T cells and *Pdcd1*^{-/-} T cells (Fig. 2g). These results were in line with published findings that stimulation of the TCR upregulates system L amino-acid transporters to sustain clonal expansion and differentiation⁹. As expected, the number of cells and, hence, total protein per well, increased substantially following stimulation with anti-CD3 and anti-CD28, which resulted in twofold more protein, on a per-cell basis, in activated T cells than in unstimulated T cells (Fig. 2h). The uptake of isotope-labeled Trp ([¹³C]Trp), as measured by liquid chromatography and mass spectrometry (LC-MS), was also greater in cells stimulated for 96 h with anti-CD3 and anti-CD28 than in unstimulated cells, and this coincided with less [¹³C]Trp in the culture medium (Fig. 2i). These results indicated that activated LN T cells upregulated their expression of amino-acid transporters and accumulated free intracellular amino acids *in vivo* and *in vitro*.

Effect of IFN-γ and microbiota on *Pdcd1*^{-/-} mice

Activated *Pdcd1*^{-/-} T cells produce the inflammatory cytokine interferon-γ (IFN-γ)¹⁰, which is known to mediate the induction of IDO (indoleamine 2,3-dioxygenase), a rate-limiting enzyme for the degradation of Trp in the kynurenine pathway^{11,12}. To assess whether the IFN-γ-mediated induction of IDO contributed to the decreased abundance of Trp in *Pdcd1*^{-/-} serum, we performed targeted LC-MS analysis of kynurenine, kynurenic acid and 3-hydroxy kynurenine, all of which are derived from the catabolism of Trp via the kynurenine pathway (Supplementary Fig. 1a). Despite a twofold increase in IFN-γ⁺ CD4⁺ T cells and IFN-γ⁺CD8⁺ T cells in *Pdcd1*^{-/-} mice relative to their abundance in age-matched wild-type mice (Fig. 3a), serum kynurenine, as well as the kynurenine metabolites, were decreased more than 50% in *Pdcd1*^{-/-} mice, relative to their abundance in age-matched wild-type mice (Fig. 3b). In line with the previously described role of IFN-γ in kynurenine production, the amount of kynurenine in the serum was 20% lower in *Pdcd1*^{-/-}/*Ifng*^{-/-} mice than in *Pdcd1*^{-/-} mice (Fig. 3c). However, the amount of Trp in serum from *Pdcd1*^{-/-}/*Ifng*^{-/-} mice did not differ from that of *Pdcd1*^{-/-} mice (Fig. 3c), and the serum metabolome profile and the abundance of amino acids in *Pdcd1*^{-/-}/*Ifng*^{-/-} mice and *Pdcd1*^{-/-} mice were comparable (Supplementary Fig. 1b,c). These results indicated that the reduction in the abundance of Trp in the serum of *Pdcd1*^{-/-} mice was not due to the increased production of IFN-γ by *Pdcd1*^{-/-} T cells.

PD-1 deficiency is also marked by microbial dysbiosis due to an impairment in the T cell selection of affinity-matured B cells that produce immunoglobulin A (IgA) in the gut⁵. Furthermore, some gut bacteria, particularly certain species of *Clostridia*, can influence Trp catabolism^{13,14}. Thus, we assessed the contribution of the microbiota to the systemic depletion of amino acids in *Pdcd1*^{-/-} mice. PLS-DA of gas chromatography–mass spectrometry (GC-MS) measurements of serum revealed non-overlapping metabolome profiles for germ-free (GF) *Pdcd1*^{-/-} mice and their respective age-matched, GF wild-type mice (Fig. 3d). GF *Pdcd1*^{-/-} mice had significantly less Trp and Tyr in the serum (Fig. 3e), as well as more CD44^{hi} CD4⁺ T cells and CD8⁺ T cells that produced large amounts of IFN-γ (Fig. 3a,f,g), than did GF

wild-type mice. These observations suggested that the microbiota was not the dominant cause of the amino-acid depletion in *Pcd1^{-/-}* mice.

We further assessed the contribution of genetic factors versus environmental factors to the systemic metabolome through the use of

gnotobiotic transfer of wild-type or *Pcd1^{-/-}* specific-pathogen-free fecal microbiota into GF hosts of each genotype. *Pcd1^{-/-}* hosts had less Trp and Tyr in their serum than did wild-type hosts, whether they had received microbiota from wild-type mice or *Pcd1^{-/-}* mice

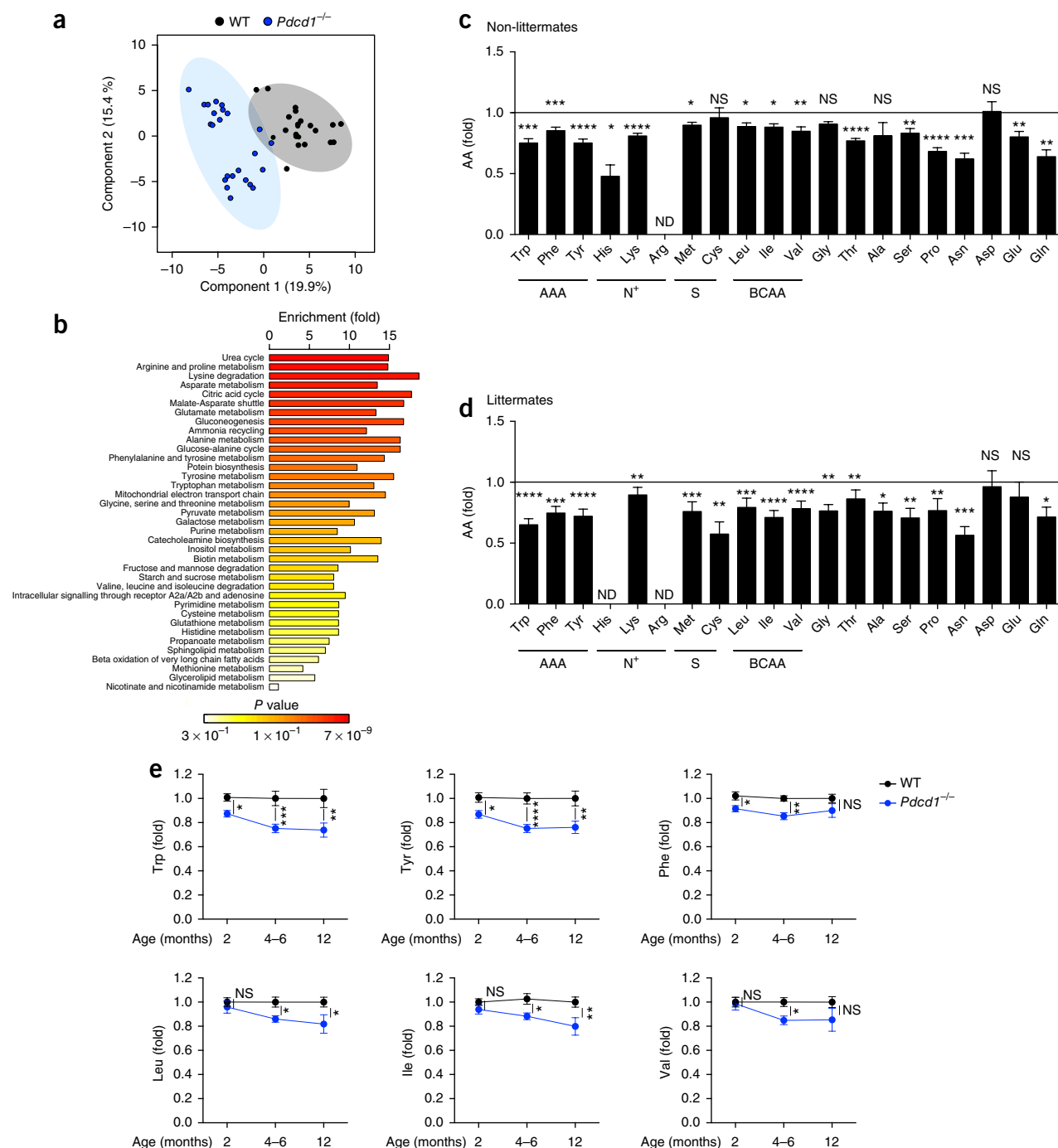


Figure 1 Depletion of amino acids in the serum of *Pcd1^{-/-}* mice. (a) PLS-DA of the serum metabolome of *Pcd1^{-/-}* mice ($n = 24$) and wild-type (WT) mice ($n = 22$). Each symbol represents the result for an individual mouse. (b) Metabolite-set-enrichment analysis of the compounds in each pathway in the data set in a that differ significantly (in abundance) in wild-type mice versus *Pcd1^{-/-}* mice. (c,d) GC-MS of amino acids (horizontal axis), grouped as aromatic amino acids (AAA), basic amino acids (N⁺), sulfur-containing amino acids (S) or branched-chain amino acids (BCAA), in the serum of 4- to 6-month-old *Pcd1^{-/-}* mice ($n = 24$) and wild-type mice ($n = 22$) that were not littermates (c) or were littermates ($n = 7$ –10 mice per group) (d), presented as the ratio of the abundance of each amino acid (AA) in *Pcd1^{-/-}* mice to that in wild-type mice. (e) Abundance of amino acids in the serum of *Pcd1^{-/-}* mice at various ages (horizontal axis: $n = 26$ (2 months), $n = 24$ (4–6 months) and $n = 7$ (12 months)). ND, not detected. NS, not significant ($P > 0.05$); * $P < 0.05$, ** $P < 0.005$, *** $P < 0.0005$ and **** $P < 0.0001$ (two-tailed unpaired Student's *t*-test (c,d) or analysis of variance (ANOVA) (e)). Data are pooled from two or more experiments (mean \pm s.e.m. in c,d, or mean \pm s.e.m. in e).

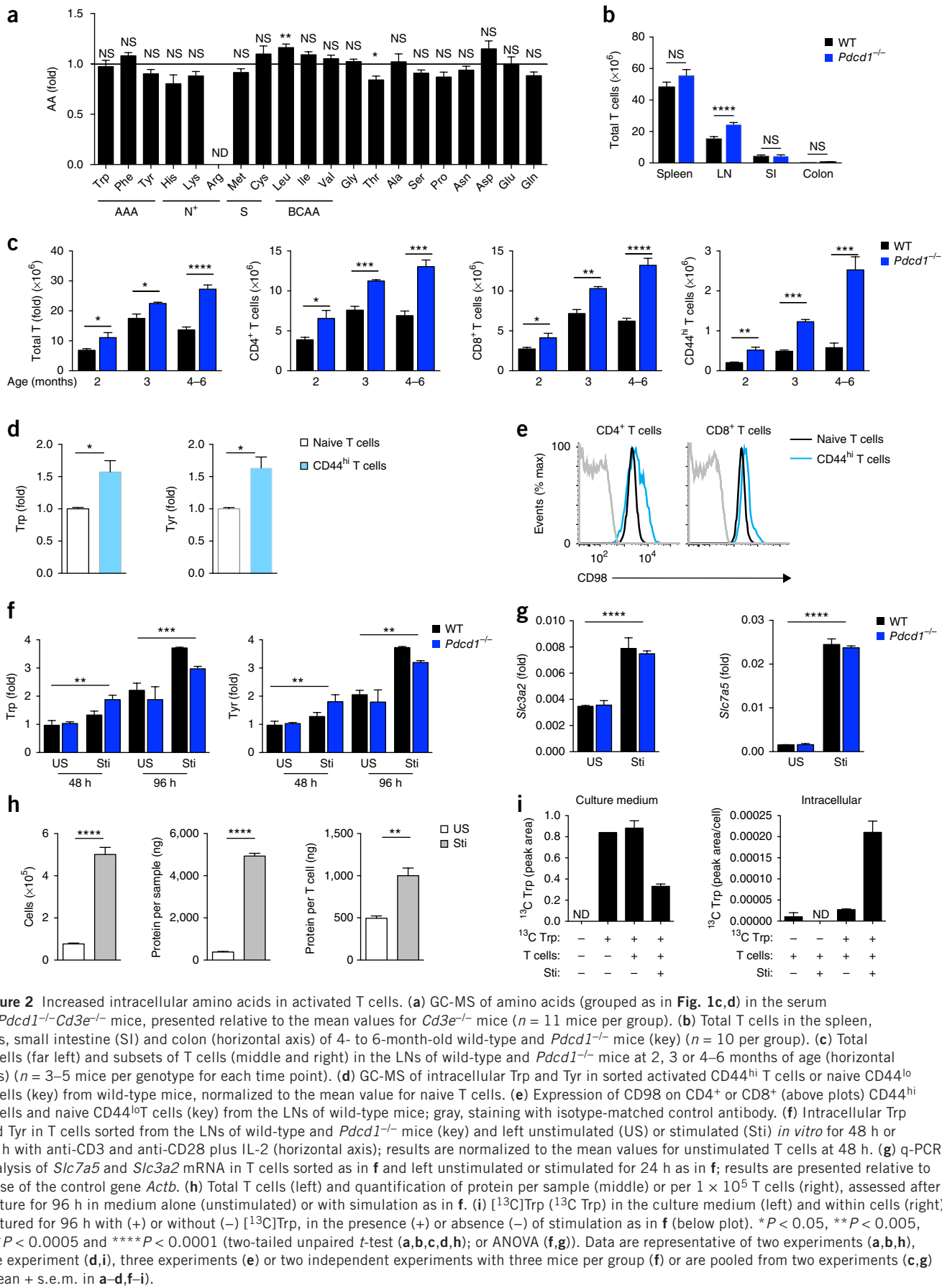


Figure 2 Increased intracellular amino acids in activated T cells. (a) GC-MS of amino acids (grouped as in Fig. 1c,d) in the serum of *Pdcd1^{-/-}Cd3e^{-/-}* mice, presented relative to the mean values for *Cd3e^{-/-}* mice ($n = 11$ mice per group). (b) Total T cells in the spleen, LNs, small intestine (SI) and colon (horizontal axis) of 4- to 6-month-old wild-type and *Pdcd1^{-/-}* mice (key) ($n = 10$ per group). (c) Total T cells (far left) and subsets of T cells (middle and right) in the LNs of wild-type and *Pdcd1^{-/-}* mice at 2, 3 or 4–6 months of age (horizontal axis) ($n = 3$ –5 mice per genotype for each time point). (d) GC-MS of intracellular Trp and Tyr in sorted activated CD44^{hi} T cells or naive CD44^{lo} T cells (key) from wild-type mice, normalized to the mean value for naive T cells. (e) Expression of CD98 on CD4⁺ or CD8⁺ (above plots) CD44^{hi} T cells and naive CD44^{lo} T cells (key) from the LNs of wild-type mice; gray, staining with isotype-matched control antibody. (f) Intracellular Trp and Tyr in T cells sorted from the LNs of wild-type and *Pdcd1^{-/-}* mice (key) and left unstimulated (US) or stimulated (Sti) *in vitro* for 48 h or 96 h with anti-CD3 and anti-CD28 plus IL-2 (horizontal axis); results are normalized to the mean values for unstimulated T cells at 48 h. (g) q-PCR analysis of *Slc7a5* and *Slc3a2* mRNA in T cells sorted as in f and left unstimulated or stimulated for 24 h as in f; results are presented relative to those of the control gene *Actb*. (h) Total T cells (left) and quantification of protein per sample (middle) or per 1×10^5 T cells (right), assessed after culture for 96 h in medium alone (unstimulated) or with simulation as in f. (i) [¹³C]Trp (¹³C Trp) in the culture medium (left) and within cells (right) cultured for 96 h with (+) or without (-) [¹³C]Trp, in the presence (+) or absence (-) of stimulation as in f (below plot). * $P < 0.05$, ** $P < 0.005$, *** $P < 0.0005$ and **** $P < 0.0001$ (two-tailed unpaired t-test (a,b,c,d,h); or ANOVA (f,g)). Data are representative of two experiments (a,b,h), one experiment (d,i), three experiments (e) or two independent experiments with three mice per group (f) or are pooled from two experiments (c,g) (mean + s.e.m. in a-d,f-i).

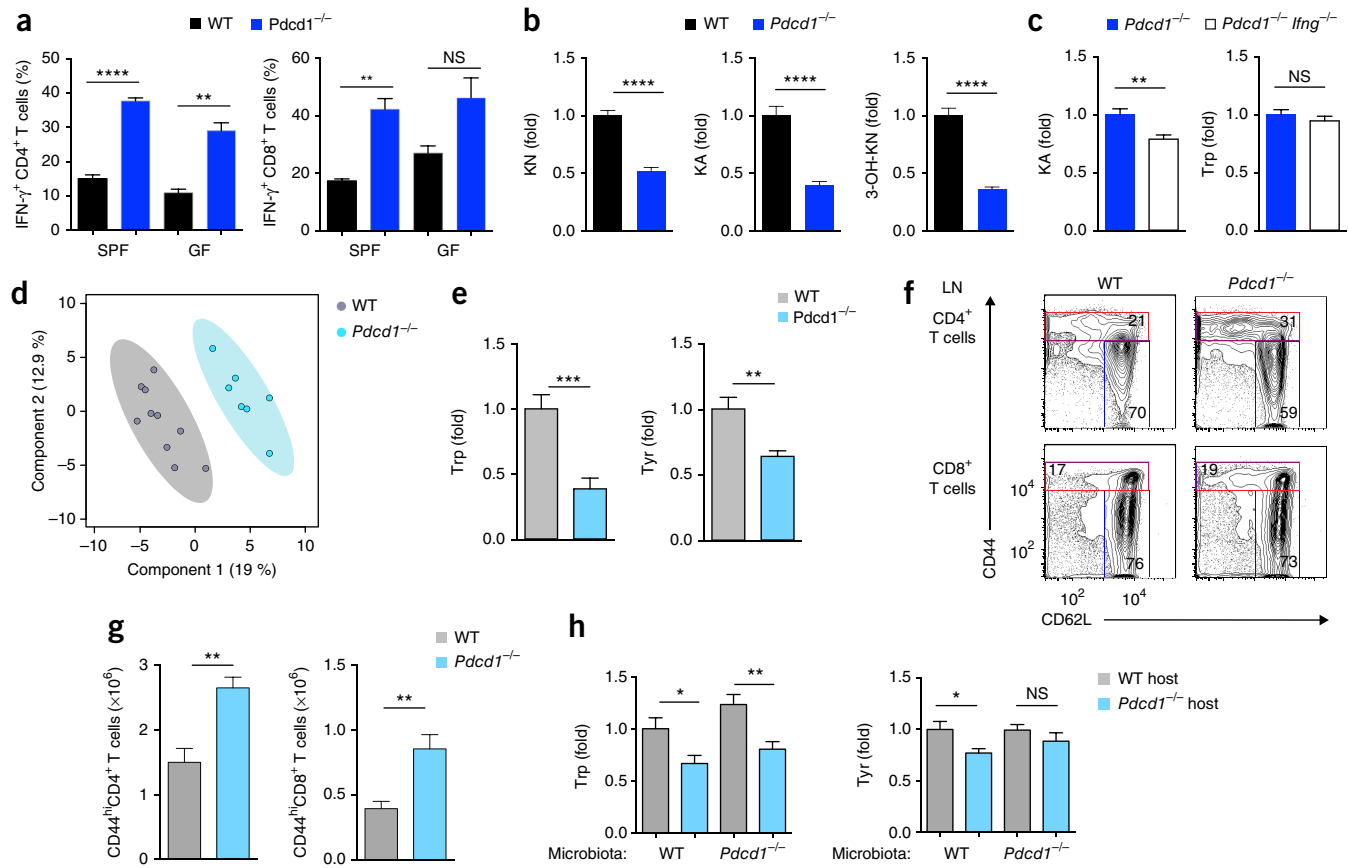


Figure 3 IFN- γ - and microbiota-independent depletion of amino acids in the serum of *Pdcd1^{-/-}* mice. **(a)** Frequency of IFN- γ ⁺ CD4⁺ or CD8⁺ T cells among cells obtained from specific-pathogen-free (SPF) or GF (horizontal axis) wild-type and *Pdcd1^{-/-}* mice (key) ($n = 3$ per group) and stimulated *in vitro* with PMA and ionomycin. **(b)** LC-MS of kynurenine (KN), kynurenic acid (KA) and 3-hydroxy kynurenine (3-OH-KN) in the serum of specific-pathogen-free *Pdcd1^{-/-}* mice ($n = 16$), presented relative to the mean value for wild-type mice ($n = 10$). **(c)** LC-MS of kynurenic acid and Trp in the serum of *Pdcd1^{-/-} Ifng^{-/-}* ($n = 14$), presented relative to the mean value for *Pdcd1^{-/-}* mice ($n = 12$). **(d)** PLS-DA of serum from GF wild-type mice ($n = 10$) and *Pdcd1^{-/-}* mice ($n = 7$). **(e)** Quantification of Trp and Tyr in serum from the mice in **d**. **(f)** Flow cytometry analyzing expression of the activation marker CD44 and memory marker CD62L by total CD4⁺ or CD8⁺ T cells (left margin) from the LNs of GF wild-type and *Pdcd1^{-/-}* mice (above plots). Numbers in outlined areas indicate percent CD44^{hi} (activated) cells (top, red outline) or CD44^{lo}CD62L⁺ (naive) cells (right, blue outline). **(g)** Total CD44^{hi} CD4⁺ or CD8⁺ T cells analyzed as in **g** for $n = 10$ mice per group. **(h)** GC-MS analysis of Trp and Tyr in the serum of gnotobiotic wild-type or *Pdcd1^{-/-}* (key) ($n = 7$ –12 per group) at 8 weeks after gavage of wild-type or *Pdcd1^{-/-}* fecal microbiota (horizontal axis); results are presented relative to those of GF wild-type mice given transplantation of wild-type fecal microbiota. NS, $P < 0.0578$ **(a)**; * $P < 0.05$, ** $P < 0.005$, *** $P < 0.0005$ and **** $P < 0.0001$ (two-tailed unpaired *t*-test). Data are from one of two experiments with similar results **(a)**, are pooled from two experiments **(b,c,g,h)** or are representative of two experiments **(d)** or two independent experiments **(e,f)** (mean \pm s.e.m. in **a–c,e,g,h**).

(Fig. 3h). Thus, the reduction in the abundance of amino acids in the serum of *Pdcd1^{-/-}* mice was due to genetic effects other than excessive IFN- γ production or gut dysbiosis.

Acute T cell activation causes serum amino-acid depletion

We next investigated whether strong stimulation of adaptive immunity had a systemic effect on amino-acid dynamics. For this, we immunized wild-type mice in the footpad with ovalbumin (OVA) in complete Freund's adjuvant or with saline (sham condition), then performed metabolome profiling of serum by LC-MS. At 7 d after immunization, Trp and Tyr were decreased 25% in the serum of OVA-immunized mice relative to their abundance in that of sham-immunized mice (Fig. 4a). In a second experimental system, we induced systemic activation of T cells by intravenous administration of adjuvant-free OVA to OT-I mice or OT-II mice, which have transgenic expression of OVA-specific TCRs on CD8⁺ T cells or CD4⁺ T cells, respectively. Both OT-I mice and OT-II mice underwent rapid depletion of serum Trp by day 5 after immunization (Fig. 4b), which indicated that activation of either the CD8⁺ T cell subset or the CD4⁺ T cell subset

influenced the levels of systemic amino acids, although no change in the amount of Tyr was observed in this model (Fig. 4b).

We also evaluated if serum amounts of amino acids were reduced by acute inhibition of PD-1, a technique used for cancer immunotherapy. We injected MC38 adenocarcinoma cells subcutaneously into 2-month-old wild-type mice, treated the tumor-bearing mice with anti-PD-1 or isotype-matched control antibody and then compared the abundance of amino acids in serum at day 13 after cell injection. Administration of 100 μ g of anti-PD-1 at days 5, 8 and 11 of tumor growth induced a significant reduction in the amount of amino acids in serum (Fig. 4c), to the extent observed in *Pdcd1^{-/-}* mice (Fig. 1c), but the administration of isotype-matched control antibody did not (Fig. 4c). This showed activation of T cells specific for tumor-derived antigens had a substantial effect on the amount of amino acids in serum.

Accumulation of amino acids in activated LNs of *Pdcd1^{-/-}* mice

We next investigated whether the depletion of serum amino acids in *Pdcd1^{-/-}* mice was due to peripheral activation of the immune system, defects in intestinal absorption or a reduction in hepatic biosynthesis.

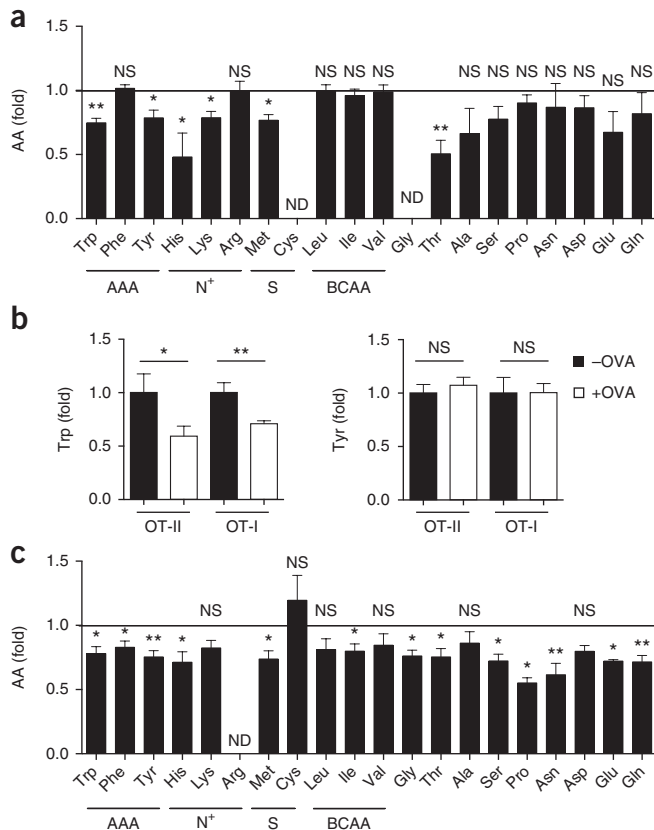


Figure 4 T cell activation depletes serum of amino acids in several models. (a) LC-MS of amino acids (grouped as in Fig. 1c,d) in serum from wild-type mice at 7 d after immunization (in the footpad) with OVA in complete Freund's adjuvant ($n = 7$); results are presented relative to the mean values for sham-immunized mice ($n = 5$). (b) Abundance of Trp and Tyr in serum from OT-II mice ($n = 10$) or OT-I mice ($n = 5$) (horizontal axis) on day 5 after injection of OVA (on days 0 and 3) (+ OVA (key)); results are presented relative to the mean values for OT-II mice ($n = 8$) or OT-I mice ($n = 4$) given injection of PBS (-OVA). (c) GC-MS of amino acids (as in a) in serum of wild-type mice ($n = 5$ per group) inoculated with MC38 tumor cells, then given injection of anti-PD-1 on day 5, 8 and 11 after inoculation and analyzed at day 13; results presented as relative to mean values for MC38-inoculated mice given injection of isotype-matched control antibody. * $P < 0.05$ and ** $P < 0.005$ (two-tailed unpaired t -test). Data are representative of two experiments (a, and b (OT-II)) or one experiment (b (OT-I) and c) (mean + s.e.m. throughout).

Thus, we measured local metabolites in the LNs, spleen, segments of the small and large intestine and liver by non-targeted metabolome analysis (Supplementary Fig. 2) and targeted metabolome analysis (Fig. 5). Principal-component analysis detected a change in metabolite profiles in the LNs of 5-month-old *Pdcd1*^{-/-} mice relative to those in the LNs of age-matched wild-type mice, but not in the gut or liver (Fig. 5a), consistent with the substantial activation of the immune system observed in these mice. The most significant differences between the LN metabolome of *Pdcd1*^{-/-} mice and that of wild-type mice involved amino-acid metabolism, intracellular signaling, transcription and protein synthesis (Fig. 5b). The abundance of aromatic amino acids, including Trp, was twofold greater in the LNs and, to a lesser extent, the spleen of *Pdcd1*^{-/-} mice than in those of wild-type, while the amount of amino acids in gut and liver was comparable in these mice (Fig. 5c and Supplementary Fig. 3). As with the amino acids, the abundance of nucleosides, glycolysis and

TCA-cycle metabolites was significantly greater in the LNs of *Pdcd1*^{-/-} mice than in those of wild-type mice (Fig. 5d-f), indicative of enhanced biochemical processes consistent with considerable, localized activation of the immune system. These results suggested that the depletion of amino acids from the serum was due to their accumulation in LNs to support the metabolic requirements necessitated by the enhanced activation of immune cells in *Pdcd1*^{-/-} mice.

Diminished brain monoamines in *Pdcd1*^{-/-} mice

In addition to being required for protein synthesis and energy generation in lymphocytes, free amino acids are precursors of monoamine neurotransmitters. Tyr and Trp are essential for synthesis of the neurotransmitters dopamine and 5-hydroxytryptamine (5-HT (serotonin)) (Supplementary Fig. 4a,b). Dopamine is critical for processes that drive executive functions, including motor control, motivation, learning and fear responses^{15,16}. 5-HT is thought to regulate many behavioral aspects, including mood, anxiety, aggression and fear-conditioning processes^{17,18}. By measuring whole-brain homogenates by LC-MS after focused microwave fixation, we observed that the amount of Tyr and Trp in the brain was significantly lower in 5-month-old *Pdcd1*^{-/-} mice than in age-matched wild-type mice (Fig. 6a), as were the levels of dopamine and 5-HT, as measured by high-performance liquid chromatography coupled to an electrochemical detector (HPLC-ECD) (Fig. 6a and Supplementary Fig. 4c). Additionally, *in situ* immunostaining showed less 5-HT in tryptophan hydroxylase-positive serotonergic neurons in midbrain raphe nuclei in *Pdcd1*^{-/-} mice than in those of wild-type mice (Fig. 6b). Imaging mass spectrometry also showed a 1.8-fold less dopamine in the striatum and 2.2-fold less 5-HT in the midbrain of *Pdcd1*^{-/-} mice than in that of wild-type mice (Fig. 6c). Similar biochemical changes were also detected in whole-brain homogenates of GF *Pdcd1*^{-/-} mice versus GF wild-type mice (Supplementary Fig. 4d). We observed no difference between *Pdcd1*^{-/-} brain and wild-type brain in the excitatory neurotransmitter glutamate and inhibitory neurotransmitter GABA (4-aminobutyric acid) (Fig. 6a and Supplementary Fig. 4d), which indicated that neurotransmitter-synthesis pathways varied in their sensitivity to diminished precursor availability. To assess extracellular brain metabolites, we performed *in vivo* microdialysis. We found significantly less Tyr and Trp at steady state in freely moving *Pdcd1*^{-/-} mice than in their wild-type counterparts, and less release of 5-HT in response to potassium challenge in the prefrontal cortex of *Pdcd1*^{-/-} mice than in that of wild-type mice (Supplementary Fig. 4e). These data suggested that among the tissues assessed, mainly the brain was affected by the depletion of Trp and Tyr from the serum of *Pdcd1*^{-/-} mice, and this resulted in reduced synthesis of the monoamine neurotransmitters dopamine and 5-HT.

To rule out the possibility that insufficiency in biosynthetic enzymes and/or cofactors contributed to the reduction in the abundance of dopamine and 5-HT in *Pdcd1*^{-/-} mice, we used q-PCR to measure mRNA encoding individual components of monoamine-synthesis pathways (Supplementary Fig. 4a,b). We observed no major difference between *Pdcd1*^{-/-} mice and wild-type mice in the expression of mRNA encoding tyrosine hydroxylase (encoded by *Th*), which is the rate-limiting enzyme for dopamine synthesis, or aromatic L-amino acid decarboxylase (encoded by *Aadc*). Expression of *Tph2*, which encodes the rate-limiting enzyme for 5-HT synthesis, was higher in the raphe nuclei of *Pdcd1*^{-/-} mice than in those of wild-type mice (Fig. 6d). The amount of tetrahydrobiopterin, a cofactor required for the activity of both tyrosine hydroxylase and tryptophan hydroxylase 2, was similar in *Pdcd1*^{-/-} mice and wild-type mice, as measured in whole-brain extracts by LC-MS (Fig. 6e). Thus, the *Pdcd1*^{-/-} brain

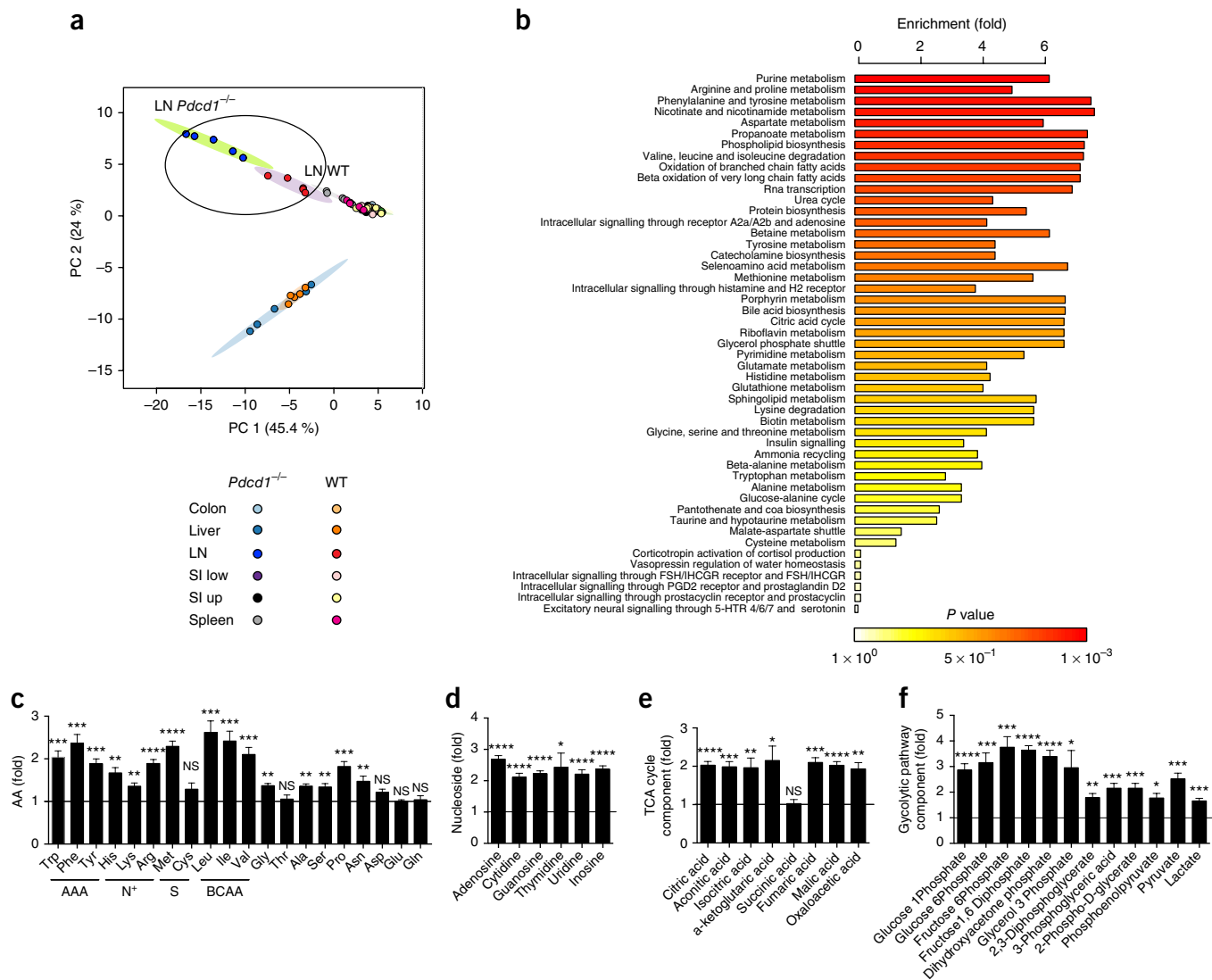


Figure 5 Accumulation of amino acids in the LNs of *Pdcd1*^{-/-} mice. (a) Principal-component analysis of the metabolome profile of the colon, liver, LNs, upper and lower segments of the small intestine (SI up and SI low, respectively) and spleen of *Pdcd1*^{-/-} mice and wild-type mice (key); difference between LN-derived *Pdcd1*^{-/-} samples and LN-derived wild-type samples is outlined. Each symbol represents the result for an individual mouse. (b) Metabolite-set-enrichment analysis (as in Fig. 1a) of the compounds in each pathway in the data set that differ significantly (in abundance) in LNs of *Pdcd1*^{-/-} mice versus those of wild-type mice. (c–e) LC-MS analysis of amino acids (grouped as in Fig. 1c,d) (c), nucleosides (d) and components of the TCA cycle (e) in the LNs of *Pdcd1*^{-/-} mice; results are presented relative to the mean values of wild-type mice ($n = 5$ per group). (f) Ion chromatography-tandem mass spectrometry analysis of components of the glycolytic pathway in *Pdcd1*^{-/-} mice; results are presented relative to the mean values of wild-type mice ($n = 5$ per group). * $P < 0.05$, ** $P < 0.005$, *** $P < 0.0005$ and **** $P < 0.0001$ (two-tailed unpaired *t*-test). Data are pooled from two experiments (mean + s.e.m. in c–f).

was not deficient in the critical enzymes and cofactors required for monoamine synthesis.

In addition to being caused by limited availability of precursor amino acids, the decrease in brain monoamines could have also been caused by their accelerated degradation. Thus, we measured the catabolites of dopamine and 5-HT in whole-brain extracts by LC-MS. The amount of norepinephrine, of which dopamine is a precursor, was significantly lower in *Pdcd1*^{-/-} mice than in wild-type mice (Fig. 6f). However, the abundance of other catabolites of dopamine (DOPAC (3,4-dihydroxyphenylacetic acid), 3-MT (3-methoxytyramine) and HVA (homovanillic acid)) and the 5-HT catabolite 5-HIAA (5-hydroxyindole aminoacetic acid) was similar in *Pdcd1*^{-/-} mice and wild-type mice (Fig. 6f), which might indicate accelerated degradation of dopamine and 5-HT in *Pdcd1*^{-/-} mice. Thus, decreased

availability of amino-acid precursors and possibly altered catabolism of dopamine and 5-HT in *Pdcd1*^{-/-} mice resulted in reduced amounts of brain monoamine in these mice.

Behavioral changes in *Pdcd1*^{-/-} mice

We next assessed whether the reduced levels of monoamines in the brains of *Pdcd1*^{-/-} mice had an effect on their behavior. When monitored in metabolic chambers, the daily energy expenditure and oxygen consumption of *Pdcd1*^{-/-} mice were significantly lower than those of wild-type mice (Supplementary Fig. 5a), indicative of a hypoactive phenotype. *Pdcd1*^{-/-} mice displayed less motility than that of wild-type mice during the first 2 d after transfer into the metabolic chamber (Supplementary Fig. 5a), suggestive of reduced exploratory behavior in a novel environment. We performed a larger

battery of neurological, sensorial and behavioral tests to measure locomotor activity, fear responses, anxiety and social interactions. In the elevated-plus maze test, a behavioral test that measures

anxiety in response to open spaces, *Pcd1*^{-/-} mice spent less time in the open arms or center of the platform and moved less overall than did wild-type mice (Fig. 7a). In the dark-light transition

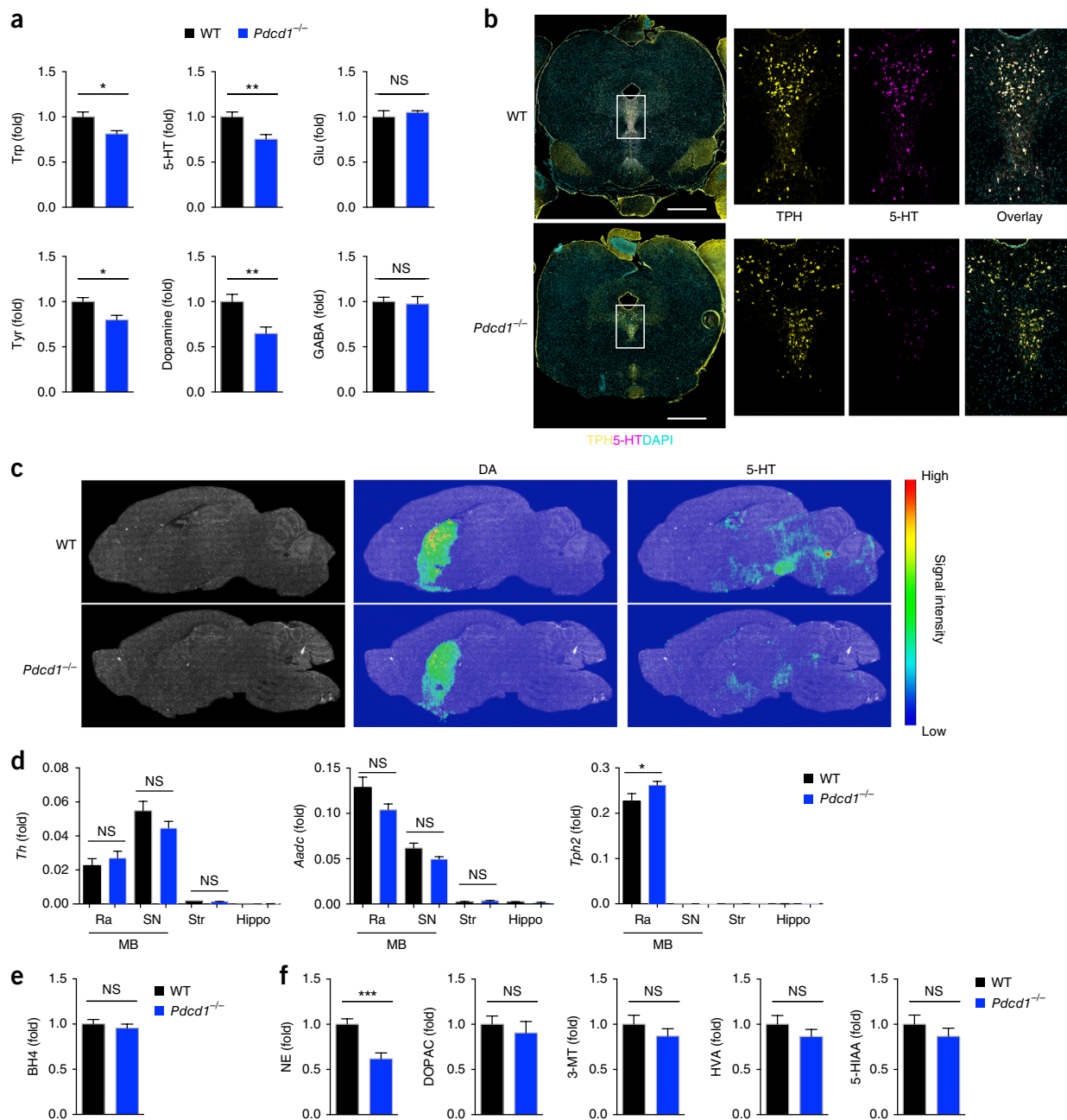


Figure 6 Reduced levels of monoamine neurotransmitters and their amino-acid precursors in the brain of *Pcd1*^{-/-} mice. **(a)** LC-MS analysis of the amino acids Trp, Glu and Tyr in the brain of wild-type mice ($n = 4$) and *Pcd1*^{-/-} mice ($n = 6$), and HPLC-ECD analysis of the neurotransmitters 5-HT, dopamine (DA) and GABA in the brain of wild-type mice ($n = 10$) and *Pcd1*^{-/-} mice ($n = 11$). **(b)** Microscopy of coronal brain sections of wild-type and *Pcd1*^{-/-} mice (left margin), stained for tryptophan hydroxylase (TPH), 5-HT and the DNA-binding dye DAPI (left); raphe nuclei (white rectangles at left) are enlarged 10x at right (single-color and overlay images). Scale bars, 1 mm. **(c)** Imaging mass spectrometry of the distribution and abundance of dopamine and 5-HT (above images) in sagittal sections of brain from wild-type and *Pcd1*^{-/-} mice (left margin): dopamine signal, 207,804,304 pixels (wild-type) and 112,989,802 pixels (*Pcd1*^{-/-}); 5-HT signal, 152,529,424 pixels (wild-type) and 66,408,795 pixels (*Pcd1*^{-/-}). **(d)** q-PCR analysis of *Th*, *Aadc* and *Tph2* mRNA in the raphe nuclei (Ra) and substantia nigra (SN) of the mid-brain (MB) and the striatum (Str) and hippocampus (Hippo) of wild-type and *Pcd1*^{-/-} mice (key) ($n = 5$ –6 per group (raphe nuclei and substantia nigra) or $n = 2$ per group (striatum and hippocampus)); results presented relative to those of the control gene *Gapdh*. **(e,f)** Abundance of tetrahydrobiopterin (BH4) (a cofactor of tyrosine hydroxylase and tryptophan hydroxylase 2) (e) and of norepinephrine (NE), DOPAC, 3-MT and HVA (catecholamines of dopamine) and 5-HIAA (5-HT catabolite) (f) in brain extracts from *Pcd1*^{-/-} mice, presented relative to results for wild-type mice ($n = 5$ –6 mice per group). * $P < 0.05$, ** $P < 0.005$ and *** $P < 0.0005$ (two-tailed unpaired *t*-test). Data are pooled from two experiments (a,d), four independent experiments (b) or two experiments with $n = 2$ –3 mice each (c,e,f) (mean + s.e.m. in a,d–f).

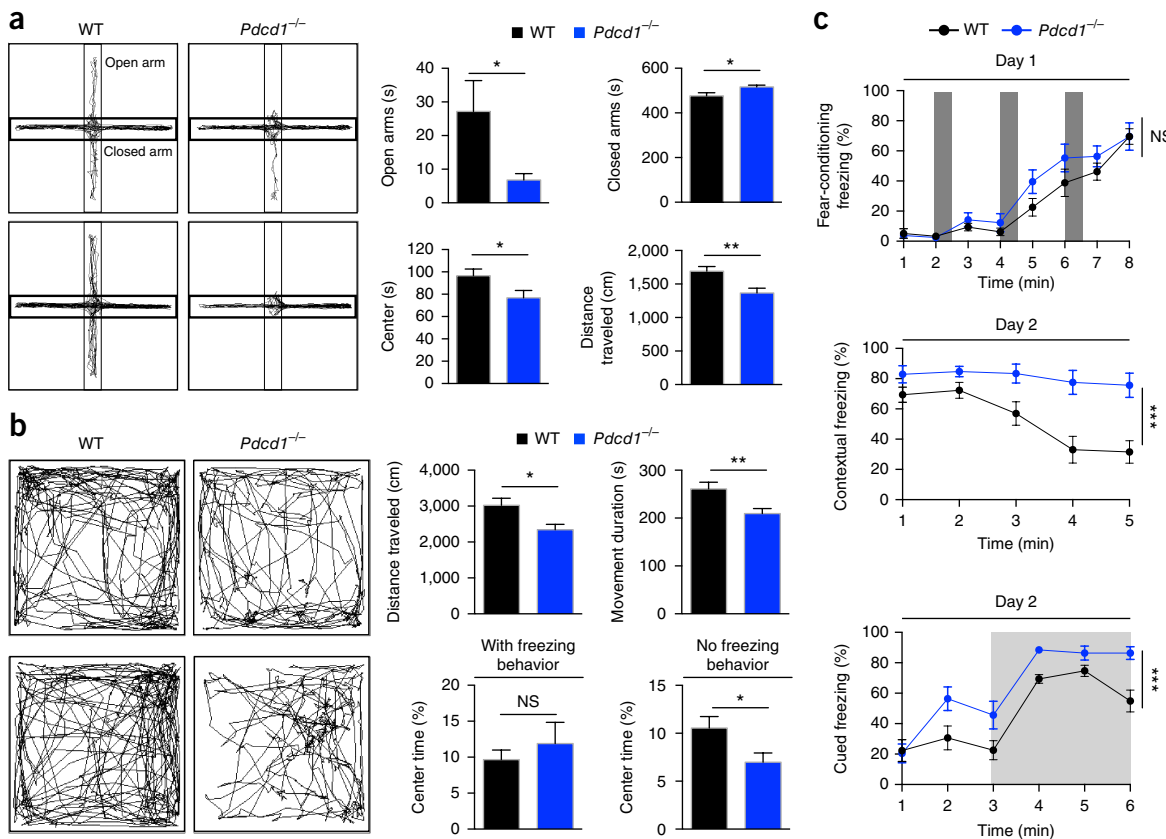


Figure 7 Increased anxiety-like behavior and enhanced fear responses in *Pdcd1*^{-/-} mice. **(a)** Elevated-plus maze results for wild-type mice ($n = 13$) and *Pdcd1*^{-/-} mice ($n = 13$) (left), as well as total time spent in open arms, center or closed arms of the maze (top right) and total distance traveled (bottom right). **(b)** Open-field test results for wild-type mice ($n = 11$) and *Pdcd1*^{-/-} mice ($n = 13$) (left half), as well as total distance traveled (top right), total movement duration (top far right) and percent time spent in center with (bottom far right) or without (bottom right) exclusion of *Pdcd1*^{-/-} mice ($n = 2$) showing a freezing-behavior movement pattern (as in bottom right plot at left). **(c)** Fear responses of wild-type and *Pdcd1*^{-/-} mice ($n = 11$ per group) during a fear-conditioning session on day 1 (top; dark gray areas, duration of the presentation of a pairing of a conditioned stimulus and an unconditioned stimulus), a contextual fear session (middle) and a cued fear session (bottom; light gray area, duration of the conditioned stimulus), both on day 2; results presented as percent time spent in freezing behavior. * $P < 0.05$, ** $P < 0.005$ and *** $P < 0.0005$ (two-tailed unpaired *t*-test (a,b) or ANOVA (c)). Data are representative of at least two experiments with similar results (mean + s.e.m. in a,b and mean \pm s.e.m. in c).

test, which measures the response to mild stressors such as a novel environment and light, *Pdcd1*^{-/-} mice were slower to enter the light zone than were wild-type mice, and they transitioned less between the dark zone and light zone and spent significantly less time in the light zone than did wild-type mice (Supplementary Fig. 5b). In an open-field test, which measures locomotion and anxiety, *Pdcd1*^{-/-} mice showed decreased locomotor activity (reduced distance of travel or movement duration) relative to that of wild-type mice (Fig. 7b). While *Pdcd1*^{-/-} mice generally spent less time in the center of the field than did wild-type mice, some froze there for extended periods (Fig. 7b). There were no significant differences between the groups of mice in the forced-swim test, which measures depression, although there was a trend toward less swimming and greater immobility in *Pdcd1*^{-/-} mice than in wild-type mice (Supplementary Fig. 5c). *Pdcd1*^{-/-} mice did not differ from wild-type mice in social interaction or pain sensitivity (Supplementary Fig. 5d,e). Elevated-plus maze and open-field tests performed on pairs of *Pdcd1*^{-/-} mice and their wild-type littermates produced similar results (Supplementary Fig. 6a,b), which suggested a limited effect of maternal influences or microbiota on the altered behavioral phenotype of *Pdcd1*^{-/-} mice.

To determine whether the long periods of immobility observed during elevated-plus maze and open-field testing in the *Pdcd1*^{-/-} mice

were associated with abnormal fear responses, we used a Pavlovian fear-conditioning test, a behavioral paradigm that explores the learning and reactions to aversive environmental stimuli. Although no major differences between *Pdcd1*^{-/-} mice and wild-type mice were observed during fear acquisition on day 1, both contextual fear responses and cued fear responses, which were tested on day 2, were significantly heightened in *Pdcd1*^{-/-} (Fig. 7c and Supplementary Fig. 6c). In addition, *Pdcd1*^{-/-} mice exhibited impaired extinction of fear memory (Supplementary Fig. 5f). No difference between *Pdcd1*^{-/-} mice and wild-type mice was observed for spatial memory, as evaluated by the alternation rate in a Y-maze test (Supplementary Fig. 5g). Overall, these results showed that *Pdcd1*^{-/-} mice exhibited hypo-locomotion, anxiety-like behavior and enhanced fear responses, relative to the phenotype of wild-type mice.

Pharmacological and dietary intervention ‘rescues’ behavior

We next investigated whether pharmacological supplementation with monoamines could ameliorate the conditioned fear responses of *Pdcd1*^{-/-} mice. Phenelzine and fluoxetine are known to modulate the expression of conditioned fear^{19,20} by altering the amounts of monoamine neurotransmitters in the brain. Selective serotonin-reuptake inhibitors such as fluoxetine act by delaying the reuptake of 5-HT, which leads to longer persistence of 5-HT in the synaptic

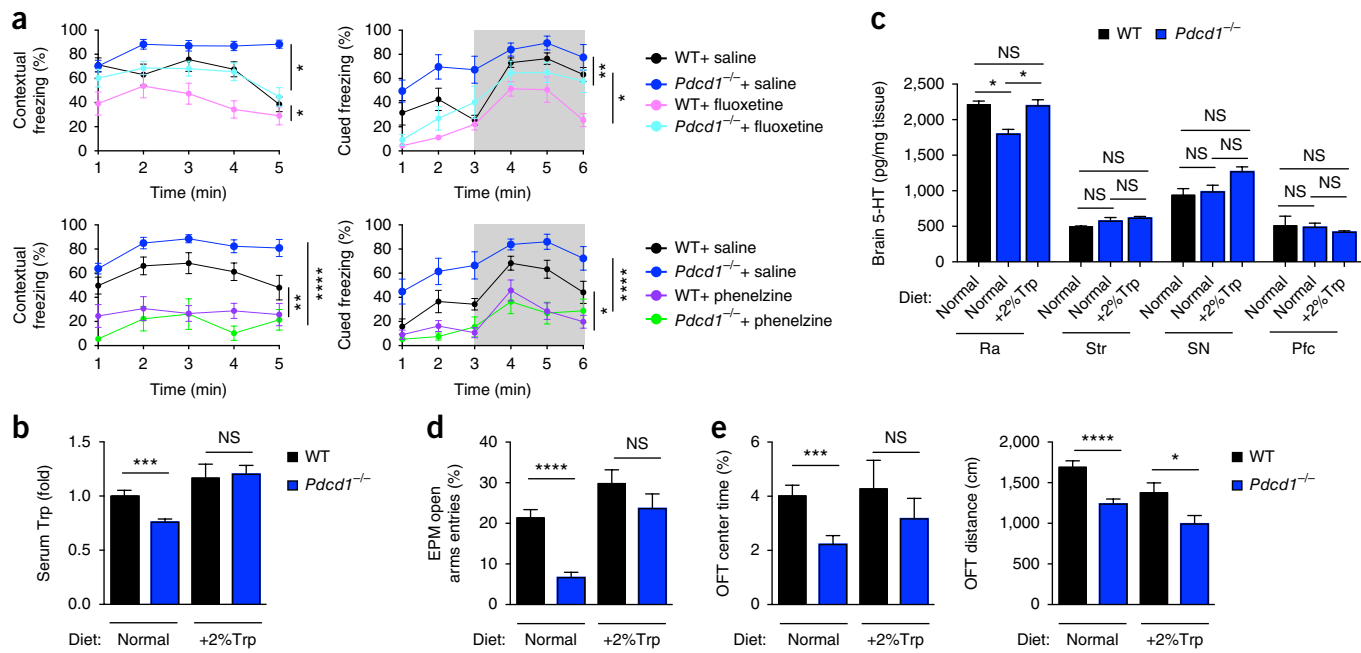


Figure 8 Pharmacological and dietary supplementation ameliorates the behavior of *Pdcd1*^{-/-} mice. **(a)** Fear responses (in contextual and cued tests as in Fig. 7c) of wild-type and *Pdcd1*^{-/-} mice ($n = 6\text{--}9$ per group) given saline (as a control) or fluoxetine (top row) or phenelzine (bottom row) (key) 1 d after a fear-conditioning session (presented as in Fig. 7c). **(b,c)** LC-MS of Trp in the serum (**b**) and of 5-HT in the raphe nuclei, striatum, substantia nigra and prefrontal cortex (Pfc) (**c**) of wild-type and *Pdcd1*^{-/-} mice (key) fed standard chow (Normal) or a diet supplemented with a high percentage of Trp (+2% Trp), for 1 month (below plot). **(d,e)** Anxiety-like behavior phenotype of wild-type and *Pdcd1*^{-/-} mice fed standard chow ($n = 28\text{--}29$ mice per group) or a 2% Trp diet ($n = 14$ mice per group), assessed as percent entries into the open arms in the elevated-plus maze (EPM) (**d**), percent time spent in the center of the open-field test (OFT) (**e**, left), and locomotor activity of those mice, assessed as total distance traveled in the open-field test (**e**, right). * $P < 0.05$, ** $P < 0.005$, *** $P < 0.0005$ and **** $P < 0.0001$ ((ANOVA **a**) or two-tailed unpaired *t*-test (**b–e**)). Data are pooled from two experiments (**a**; mean \pm s.e.m.) or are representative of two independent experiments with similar results (**b–e**; mean \pm s.e.m.).

space, while monoamine-oxidase inhibitors such as phenelzine inhibit monoamine-oxidase enzymes and thereby block the degradation of both 5-HT and dopamine²¹.

The administration of fluoxetine before the contextual conditioning normalized the fear responses in *Pdcd1*^{-/-} mice to the levels observed in untreated wild-type mice (Fig. 8a). Phenelzine had a more profound effect and decreased fear responses in both wild-type mice and *Pdcd1*^{-/-} mice, relative to the fear responses of untreated wild-type mice and *Pdcd1*^{-/-} mice (Fig. 8a). However, the possibility of collateral effects of the drugs on the peripheral nervous system could not be entirely excluded, because phenelzine slightly increased the locomotion of both wild-type mice and *Pdcd1*^{-/-} mice in an open-field test (Supplementary Fig. 6d).

We finally evaluated whether restoring the serum concentration of Trp by a diet supplemented with Trp was able to diminish the anxiety-like behavior of *Pdcd1*^{-/-} mice. In specific-pathogen-free mice, consumption of a diet supplemented with 2% (weight/weight) Trp for 1 month increased the amount of Trp in the serum of *Pdcd1*^{-/-} mice to that in the serum of wild-type mice fed standard chow (Fig. 8b) and normalized the expression of 5-HT in the brain, particularly in the raphe nuclei (Fig. 8c). In addition, supplementation with Trp ‘rescued’ the anxiety phenotype of *Pdcd1*^{-/-} mice to that of wild-type mice fed standard chow, as evaluated by the frequency of entry into the open arms in the elevated maze test and time spent in the center in the open field test, but it did not ameliorate the hypoactivity of *Pdcd1*^{-/-} mice (Fig. 8d,e). The results indicated that monoamine deficiency due to limited availability of precursor amino acids was responsible for certain behavioral changes in *Pdcd1*^{-/-} mice.

DISCUSSION

Here we have shown that T cell activation in PD-1-deficient mice induced metabolic changes that could be measured in the blood. The expanded population of CD44^{hi} T cells in the LNs of *Pdcd1*^{-/-} mice underwent intracellular accumulation of amino acids, which caused systemic depletion of those amino acids. Such systemic changes to the ‘aminome’ (the abundance and distribution of amino acids in an organism) were not observed in *Pdcd1*^{-/-} mice that lacked T cells, but this effect was replicated in acute models of T cell activation, at early time points probably preceding B cell activation and germinal-center induction.

Published *in vitro* studies have indicated that intracellular metabolic changes associated with T cell activation, such as increased metabolism of glutamine and glucose, are required for proliferation, survival and cytokine production^{22,23}. Simultaneous stimulation of human T cells via the TCR and PD-1 *in vitro* has been shown to inhibit glycolysis and the metabolism of some amino acids such as glutamine and the branched-chain amino acids²⁴. Our results revealed a strong and unexpected effect of T cell activation on the systemic metabolic profile, reflective of the powerful influence of the immune system on the biochemical networks of the body. Since PD-1 is expressed on all activated T cells, our experiments did not allow us to distinguish the effects of different functional subsets (effector versus central memory; CD4⁺ T cells versus CD8⁺ T cells) on the systemic ‘aminome’. Further studies are needed to delineate the functions of intracellular free-amino-acid stores in activated T cells in immune responses to different kinds of antigens, as well as their relative incorporation rates into downstream metabolism pathways for energy production or protein synthesis.

We further demonstrated that T cell activation diminished the pool of aromatic amino acids in serum, affected the production of neurotransmitters in the brain and induced specific behavioral changes. T cells are essential ‘arbiters’ of protective immune responses to infection and thus they monopolize the systemic amino acids available in the serum to support their effector functions; this reflects a physiological prioritization of immune-system enhancement at the cost of optimal brain function. Indeed, monoamine-neurotransmitter-biosynthesis rates in the brain were sensitive to depletion of Trp and Tyr from the serum in *Pdcd1*^{-/-} mice; this resulted in abnormal behavior that was ameliorated by dietary supplementation with Trp or pharmacological enhancement of the concentration of 5-HT or dopamine in the brain.

We found that activation of T cells driven by tumor-derived antigens and enhanced by blockade of PD-1 had a substantial effect on the amount of amino acids in serum. This raised the possibility that emotional responses might be altered in patients undergoing T cell-boosting immunotherapy or in patients with autoimmune T cell activation or infection. As anti-PD-1 is widely used for cancer treatment, future studies should address the development of affective and behavioral disorders that might be predicted to arise from long-term therapy, in addition to autoimmune manifestations. Further study is needed to confirm whether the distinct serum metabolome pattern of PD-1 inhibition is recapitulated in humans, in which case it might have beneficial application as a method of monitoring the efficacy of immunotherapy.

METHODS

Methods, including statements of data availability and any associated accession codes and references, are available in the [online version of the paper](#).

Note: Any Supplementary Information and Source Data files are available in the [online version of the paper](#).

ACKNOWLEDGMENTS

We thank S. Yamamoto, S. Oonawa and Y. Doi for technical help; S. Kawamoto, T. Chaya, and T. Kozuka for the help with metabolome and brain dissection and preparations; S. Narumiya, T. Sato and K. Tanaka for discussions and suggestion; Y. Iwakura (Tokyo University of Science) and M. Kubo (IMS RIKEN) for *Ifng*^{-/-} mice; B. Malissen (Centre d’Immunologie de Marseille-Luminy) for *Cd3e*^{-/-} mice; and N. Lonberg (Bristol-Myers Squibb) for anti-PD-1. Supported by Japan Agency for Medical Research and Development—Core Research for Evolutional Science and Technology (14532135 to S.F.), Japan Agency for Medical Research and Development (145208 and 16770835 to T.H.) and the Cell Science Foundation (K.C.).

AUTHOR CONTRIBUTIONS

M.Mi. performed most of the *in vivo* experiments; B.Z. performed all *in vitro* experiments and behavioral studies at Kyoto University facility; Y.S., K.So. and K.H. performed all metabolome analyses; M.M.G. performed quantitative PCR and 5-HT staining and collaborated in writing the manuscript; Y.T. and S.I. performed behavioral studies at the RIKEN IMS facility; M.Mi and M.Ma. performed all germ-free and gnotobiotic experiments; A.V. collaborated in the writing and revision of the manuscript; K.C. contributed to tumour and anti-PD-1 blockade experiments; T.Hi. contributed expertise in behavioral studies; H.Q. contributed initial observations of mouse behavior; R.S. performed brain-region dissection; K.Su. contributed to OT-I and OT-II *in vivo* experiments; T.F. Y.I., F.M., M.S. and T.Ho. contributed expertise in metabolome

and behavioral studies and conceptual design; and S.F. conceived of the conceptual design, analyzed the results and wrote the manuscript.

COMPETING FINANCIAL INTERESTS

The authors declare no competing financial interests.

Reprints and permissions information is available online at <http://www.nature.com/reprints/index.html>. Publisher’s note: Springer Nature remains neutral with regard to jurisdictional claims in published maps and institutional affiliations.

- O'Neill, L.A., Kishton, R.J. & Rathmell, J. A guide to immunometabolism for immunologists. *Nat. Rev. Immunol.* **16**, 553–565 (2016).
- Loftus, R.M. & Finlay, D.K. Immunometabolism: cellular metabolism turns immune regulator. *J. Biol. Chem.* **291**, 1–10 (2016).
- Okazaki, T., Chikuma, S., Iwai, Y., Fagarasan, S. & Honjo, T. A rheostat for immune responses: the unique properties of PD-1 and their advantages for clinical application. *Nat. Immunol.* **14**, 1212–1218 (2013).
- Good-Jacobson, K.L. *et al.* PD-1 regulates germinal center B cell survival and the formation and affinity of long-lived plasma cells. *Nat. Immunol.* **11**, 535–542 (2010).
- Kawamoto, S. *et al.* The inhibitory receptor PD-1 regulates IgA selection and bacterial composition in the gut. *Science* **336**, 485–489 (2012).
- Agata, Y. *et al.* Expression of the PD-1 antigen on the surface of stimulated mouse T and B lymphocytes. *Int. Immunol.* **8**, 765–772 (1996).
- Taylor, S. *et al.* PD-1 regulates KLRL1⁺ group 2 innate lymphoid cells. *J. Exp. Med.* **214**, 1663–1678 (2017).
- Hyde, R., Taylor, P.M. & Hundal, H.S. Amino acid transporters: roles in amino acid sensing and signalling in animal cells. *Biochem. J.* **373**, 1–18 (2003).
- Sinclair, L.V. *et al.* Control of amino-acid transport by antigen receptors coordinates the metabolic reprogramming essential for T cell differentiation. *Nat. Immunol.* **14**, 500–508 (2013).
- Iwai, Y., Terawaki, S. & Honjo, T. PD-1 blockade inhibits hematogenous spread of poorly immunogenic tumor cells by enhanced recruitment of effector T cells. *Int. Immunol.* **17**, 133–144 (2005).
- Hayaishi, O., Rothberg, S., Mehler, A.H. & Saito, Y. Studies on oxygenases: enzymatic formation of kynurenone from tryptophan. *J. Biol. Chem.* **229**, 889–896 (1957).
- Takikawa, O., Habara-Ohkubo, A. & Yoshida, R. Induction of indoleamine 2,3-dioxygenase in tumor cells transplanted into allogeneic mouse: interferon-γ is the inducer. *Adv. Exp. Med. Biol.* **294**, 437–444 (1991).
- Wikoff, W.R. *et al.* Metabolomics analysis reveals large effects of gut microflora on mammalian blood metabolites. *Proc. Natl. Acad. Sci. USA* **106**, 3698–3703 (2009).
- Yano, J.M. *et al.* Indigenous bacteria from the gut microbiota regulate host serotonin biosynthesis. *Cell* **161**, 264–276 (2015).
- Palmiter, R.D. Dopamine signaling in the dorsal striatum is essential for motivated behaviors: lessons from dopamine-deficient mice. *Ann. NY Acad. Sci.* **1129**, 35–46 (2008).
- Darvas, M., Wunsch, A.M., Gibbs, J.T. & Palmiter, R.D. Dopamine dependency for acquisition and performance of Pavlovian conditioned response. *Proc. Natl. Acad. Sci. USA* **111**, 2764–2769 (2014).
- Mosienko, V. *et al.* Exaggerated aggression and decreased anxiety in mice deficient in brain serotonin. *Transl. Psychiatry* **2**, e122 (2012).
- Bauer, E.P. Serotonin in fear conditioning processes. *Behav. Brain Res.* **277**, 68–77 (2015).
- Santos, J.M., Martinez, R.C. & Brandão, M.L. Effects of acute and subchronic treatments with fluoxetine and desipramine on the memory of fear in moderate and high-intensity contextual conditioning. *Eur. J. Pharmacol.* **542**, 121–128 (2006).
- Maki, Y. *et al.* Monoamine oxidase inhibitors reduce conditioned fear stress-induced freezing behavior in rats. *Eur. J. Pharmacol.* **406**, 411–418 (2000).
- Anthony, J. & Trevor, B.G.K. Marieke Kruizinga-Hall. Antidepressants. in *Katzung & Trevor's Pharmacology: Examination & Board Review*, 11e. Ch 30 (McGraw-Hill Education, 2015).
- Carr, E.L. *et al.* Glutamine uptake and metabolism are coordinately regulated by ERK/MAPK during T lymphocyte activation. *J. Immunol.* **185**, 1037–1044 (2010).
- Chang, C.H. *et al.* Posttranscriptional control of T cell effector function by aerobic glycolysis. *Cell* **153**, 1239–1251 (2013).
- Patoukis, N. *et al.* PD-1 alters T-cell metabolic reprogramming by inhibiting glycolysis and promoting lipolysis and fatty acid oxidation. *Nat. Commun.* **6**, 6692 (2015).

ONLINE METHODS

Mice. *Pcd1*^{-/-} mice (C57BL/6N), described previously²⁵, were provided by RIKEN Bioresource Center through the National Bio-Resource Project of the MEXT Japan. Heterozygous breeding generated matched wild-type for experiments as needed. *Cd3e*^{-/-} mice and *Ifng*^{-/-} mice (C57BL/6J), described previously^{26,27}, were crossed with *Pcd1*^{-/-} mice. Mice were bred and maintained under specific-pathogen-free (SPF) conditions at IMS RIKEN and in an SPF facility at Kyoto University Graduate School of Medicine. C57BL/6N wild-type mice were purchased from CLEA Japan. *Pcd1*^{-/-} mice and wild-type mice in germ-free (GF) and gnotobiotic conditions were generated and maintained in vinyl isolators at IMS RIKEN. For gnotobiotic experiments, 4-week-old GF wild-type or *Pcd1*^{-/-} mice received a suspension of feces pooled from three wild-type or *Pcd1*^{-/-} mice, administrated orally. Littermates or appropriate age- and sex-matched mice were randomly grouped and used for analyses. For behavioral testing, only male mice were used. All animal experiments were performed in accordance with approved protocols from the Institutional Animal Care at RIKEN and Kyoto University Graduate School of Medicine.

Measurement of metabolic parameters. Energy expenditure and oxygen consumption were measured with a metabolic chamber system, consisting of acrylic metabolic chambers, mass spectrometer (ARCO2000, ARCO SYSTEM) and gas sampler (ARCO2000-GS, ARCO SYSTEM). Animal movements were monitored by an animal movement analyzing system (ACTIMO-100M, SHINFACTORY). Energy expenditure was calculated according to the Lusk formula: $3.815 \times VO_2 + 1.232 \times VCO_2$. VO_2 is the oxygen consumption and VCO_2 is the carbon dioxide exhaustion. Mice were monitored under a normal 12h–12h light–dark cycle for 6 d. Mice were not subjected to acclimation before experiments.

Sample preparation for Serum metabolome. 50 µl of serum was mixed with 250 µl of solvent (methanol: water:chloroform = 2.5:1:1) containing 6 µl of 0.1 mg/ml 2-isopropylmalic acid (Sigma-Aldrich), which was used as an internal standard. The mixture was shaken at 1,200 r.p.m. for 30 min at 37 °C (Maximizer MBR-022UP, Taitec). After centrifugation at 16,000g for 5 min at 25 °C, 150 µl of supernatant was collected and mixed with 140 µl of purified water by a vortex mixer for 5 s. After centrifugation at 16,000g for 5 min at 25 °C, 180 µl and 50 µl of supernatant were collected for GC-MS and LC-MS analysis, respectively, and were then lyophilized. For GC-MS analysis, the lyophilized sample was dissolved in 80 µl of methoxyamine solution (20 mg/ml in pyridine, Sigma-Aldrich) and was shaken at 1,200 r.p.m. for 30 min at 37 °C. 40 µl of N-methyl-N-trimethylsilyl trifluoroacetamide solution (GL Science) were added for trimethylsilyl derivatization, followed by agitation at 1,200 r.p.m. for 30 min at 37 °C. After centrifugation, 50 µl of supernatant was transferred to a glass vial and subjected to GC-MS measurement. For LC-MS analysis, lyophilized sample was dissolved in 30 µl of 0.1% formic acid in water and 5 µl aliquot was injected into the LCMS-8060 (Shimadzu).

GC-MS analysis for serum metabolome. GC-MS analysis was conducted with a GCMS-QP2010 Ultra (Shimadzu). The derivatized metabolites were separated on a DB-5 column (30 m × 0.25 mm id; film thickness ,1.0 mm; Agilent Technologies). The helium carrier gas was set at the flow rate of 39 cm/s. The inlet temperature was 280 °C and the column temperature was first held at 80 °C for 2 min, then raised at a rate of 15 °C/min to 330 °C, and held for 6 min. 1 µl of the sample was injected into the GC-MS in the split mode (split ratio, 1:3). The mass spectra were obtained under following conditions: electron ionization (ionization voltage, 70 eV); ion source temperature, 200 °C; interface temperature, 250 °C; full scan mode in the range of m/z 85–500; scan rate, 0.3 s/scan. Metabolite peaks were manually identified based on retention time and mass spectrum matching with a GC/MS Metabolite Mass Spectral Database (Shimadzu). For semiquantitative analysis, the area of each metabolite peak was calculated and divided by the area of the internal standard peak. Principal component analysis, PLS-DA and metabolite set enrichment analysis were performed using MetaboAnalyst3.0 (available online at: <http://www.metaboanalyst.ca>)²⁸.

LC-MS analysis for serum metabolome. LC separation was conducted on a Shodex RSpak DE-213 column (150 mm × 2.0 mm id, Showa Denko) with a Nexera UHPLC system (Shimadzu). The mobile phase consisted of 0.1% formic acid in water (A) and 0.1% formic acid in acetonitrile (B). The gradient

program was as follows: 0–3 min, 0% B; 3–15 min, linear gradient to 60% B; 15–20 min, 95% B; 20–22.5 min, linear gradient to 0% B; hold for 7.5 min; flow rate, 0.2 ml/min. The column oven temperature was maintained at 40 °C. The LC system was coupled with a triple-quadrupole mass spectrometer LCMS-8060 (Shimadzu). LCMS-8060 was operated with the ESI in positive ion and multiple reaction monitoring (MRM) mode with the following ion transitions: kynurenine, *m/z* 208.90>192.05; kynurenic acid, *m/z* 190.10>144.00; 3-hydroxy-kynurene, *m/z* 225.10>208.20.

Brain metabolome. Brain tissue is sensitive to post-mortem changes in labile metabolites such as adenylates. To minimize autolytic changes, we employed focused microwave irradiation, which suspends metabolic processes by rapidly raising the tissue temperature to inactivate the enzymes within seconds. We used a laboratory microwave instrument (MMW-05 Muromachi-Kikai) designed for euthanasia of laboratory rodents. Mice were placed into a transparent water-jacket holder (MH28- HZ, Muromachi-Kikai). Microwave irradiation at 5 kW for 0.96 s elevates the temperature of the brain up to 80 °C, which is sufficient to inactivate metabolic enzymes, such as acetylcholine esterase²⁹. After microwave irradiation, brains were dissected with a surgical knife at room temperature, and cut into right and left hemisphere blocks for imaging MS and metabolome analyses, respectively. Brain blocks for imaging MS were embedded into a super cryo-embedding medium (SCEM, Section Lab Co.), and both tissue blocks were rapidly frozen in liquid nitrogen and stored at –80 °C.

Sample preparation for brain metabolome analysis. Extraction of metabolites from brain for metabolomics was performed as described previously³⁰. In brief, the frozen tissue block, together with internal control compounds (described below), was homogenized in ice-cold methanol (500 µl) using a manual homogenizer (Finger Masher (AM79330), Sarstedt), followed by the addition of an equal volume of chloroform and 0.4 times the volume of ultrapure water (LC/MS grade, Wako). The suspension was then centrifuged at 15,000g for 15 min at 4 °C. After centrifugation, the aqueous phase was filtered using an ultrafiltration tube (Ultrafree-MC, UFC3 LCC NB, Human Metabolome Technologies). The filtrate was concentrated with a vacuum concentrator (SpeedVac, Thermo). The concentrated filtrate was dissolved in 50 µl of ultrapure water and was analyzed by LC-MS/MS and HPLC-ECD.

Quantification of metabolites by internal and external standards. We used both internal standard compounds (added to the tissue before extraction) and external standard compounds (used to produce calibration curves for each compound) for concentration calculation. The details of the methods are provided below.

Internal standard compounds. We used 2-morpholino ethanesulfonic acid (MES) and 1,3,5-benzenetricarboxylic acid (trimesate) as internal standards for anionic metabolites, as these compounds have no endogenous equivalent in tissues. Loss of endogenous metabolites during sample preparation was corrected for by calculation of the recovery rate (%) for each sample measurement.

External standard compounds. An external calibration curve was used to calculate the absolute abundance of metabolites. Before sample measurement, we measured the mixture of authentic compounds of target metabolites at three different concentrations in ultrapure water to generate calibration curves. Quantification (amount of metabolites, nmol/mg tissue) was performed by comparison of the internal-standard-normalized peak areas against the calibration curves.

Liquid chromatography-tandem mass spectrometry for amino acid measurement. The amount of amino acids in the brain was quantified using liquid chromatography-tandem mass spectrometry. In brief, a triple-quadrupole mass spectrometer equipped with an electrospray ionization (ESI) ion source (LCMS-8040, Shimadzu) was used in the positive- and negative-ESI and multiple-reaction-monitoring (MRM) modes. The samples were resolved on the Discovery HS F5-3 column (2.1 mmI.D. x 150 mmL, 3µm particle, Sigma-Aldrich), using a step gradient with mobile phase A (0.1% formate) and mobile phase B (0.1% acetonitrile) at ratios of 100:0 (0–5 min), 75:25 (5–11 min), 65:35 (11–15 min), 5:95 (15–20 min) and 100:0 (20–25 min), at a flow rate of 0.25 ml/min and a column temperature of 40 °C. The LCMS-8040

was operated with the ESI in MRM mode with the previously reported conditions for amino-acid detection³¹.

Ion chromatography-tandem mass spectrometry for anionic metabolites.

For metabolome analysis focused on glucose metabolic central pathways (glycolysis and the TCA cycle), the anionic metabolites were measured using an orbitrap-type MS (Q-Exactive Focus, Thermo Fisher Scientific) connected to a high-performance ion-chromatography (IC) system (ICS-5000+, Thermo Fisher Scientific) that enables highly selective and sensitive metabolite quantification owing to the IC-separation and Fourier Transfer MS principle³². The IC was equipped with an anion electrolytic suppressor (Thermo Scientific Dionex AERS 500) to convert the potassium hydroxide gradient into pure water before the sample entered the mass spectrometer. The separation was performed using a Thermo Scientific Dionex IonPac AS11-HC, 4-μm-particle-size column. The IC flow rate was 0.25 ml/min supplemented post-column with 0.18 ml/min makeup flow of MeOH. The potassium hydroxide gradient conditions for IC separation were as follows: from 1 mM to 100 mM (0–40 min), 100 mM (40–50 min), and 1 mM (50.1–60 min), at a column temperature of 30 °C. The Q-Exactive Focus mass spectrometer was operated under an ESI negative mode for all detections. Full mass scan (*m/z* 70–900) was used at a resolution of 70,000. The automatic gain control target was set at 3×10^6 ions, and maximum ion injection time was 100 ms. Source ionization parameters were optimized with the spray voltage at 3 kV, and other parameters were as follows: transfer temperature at 320 °C, S-Lens level at 50, heater temperature at 300 °C, sheath gas at 36, and auxiliary gas at 10.

Measurement of dopamine, 5-HT and related metabolites by HPLC with an electrochemical detector (ECD). Metabolites extracted by the protocol described above were injected with an autosampler (M-510, Eicom) into an HPLC unit (Eicom) coupled to an ECD (ECD-300, Eicom). The samples were resolved on the Eicompak SC-5ODS column (φ3.0 × 150 mm, Eicom), using an isocratic mobile phase (5 mg/l EDTA-2Na, 220 mg/l sodium 1-octanesulfonate in acetate/citrate buffer (0.1 M, pH 3.5)/MeOH (83:17, v/v)), at a flow rate of 0.5 ml/min and a column temperature of 25 °C. At the ECD, analytes were subjected to oxidation reactions within the ECD unit with WE-3G graphite electrode (applied potential, +750 mV against an Ag/AgCl reference electrode). The resulting chromatograms were analyzed using the software EPC-300 (Eicom).

Non-targeted metabolome analysis of the liver, lymph nodes, small intestine and colon. For non-targeted analysis, metabolome data obtained by orbitrap-type MS (Q-Exactive focus, Thermo Fisher Scientific, San Jose, CA) connected to a HPLC (Ultimate3000 system, Thermo Fisher Scientific) with the discovery HS F5-3 column or an IC (ICS-5000+, Thermo Fisher Scientific) with the IonPac AS11-HC, 4-μm particle size column were analyzed. A Compound Discoverer 2.0 (Thermo Fisher Scientific) was used for the non-targeted metabolomics workflow as described³³. In brief, this software first aligned the total ion chromatograms of different samples along the retention time. Then, the detected features with an intensity of no less than 100,000 and an S/N larger than 5 in each set of data were extracted and merged into components. The resulting compounds were identified by both (i) formula prediction based on accurate *m/z* value and isotope peak patterns and (ii) MS/MS structural validation. Moreover, formula predicted signals were assigned into candidate compounds by database search (Chempider database; <http://www.chemspider.com/>). The PCA analysis as well as volcano-plotting based on a T-test were performed and are presented.

Preparation of tissue sections for MALDI-imaging analysis. Thin sections were cut with a cryomicrotome (CM3050, Leica Microsystems) and were thaw-mounted on an indium thin oxide-coated glass slide (Bruker Daltonics) at -16 °C. Brain tissues subjected to focused microwave tended to be more fragile than those treated by other methods; however, embedding the tissue with SCEM medium, which did not interfere with the ionization efficiency of metabolites, aided in successful sectioning^{30,34}.

Matrix coating and MALDI-MS Imaging acquisition. We employed on-tissue derivatization of brain neurotransmitters³⁵. Tissue sections were spray-coated manually with 2,4-diphenyl-pyranylum (1.5 mg/ml in 75% MeOH and 0.1% TFA) using an artistic airbrush (Procon Boy FWA Platinum 0.2-mm caliber

airbrush, Mr. Hobby), followed by DHB as a matrix (50 mg/ml, dissolved in 80% ethanol containing saturated ammonium sulfate (AS)). The addition of AS diminished the ion suppression effect of analytes caused by excess derivatization reagent³⁶. MALDI-IMS was performed using a 7T FT-ICR-MS (Solarix Bruker Daltonik) equipped with an Nd:YAG laser. The laser power was optimized to minimize in-source decay of metabolites. Data were acquired in the positive mode with raster scanning using a pitch distance of 80 μm. Each mass spectrum was the result of 300 laser shots at each data point. Signals with an *m/z* between 300 and 500 were collected by use of continuous accumulation of selected ions mode. Image reconstruction was performed using FlexImaging 4.0 software (Bruker Daltonics). Peaks of specific metabolite molecules were assigned by accurate MS analyses. The high mass accuracy provided by FT-ICR-MS allowed selective ion signals for derivatized-monoamine species to be obtained within a mass window of 5 ppm, which enabled identification of the specific elemental composition of compounds by querying of the highly accurate masses against databases³⁷.

In vivo microdialysis. *In vivo* microdialysis for freely moving mice was performed as described elsewhere³⁸. In brief, mice were anesthetized with isoflurane and were implanted stereotactically with a guide cannula (one site per mouse) in the prefrontal cortex (for dialysis probe, A+2 mm, L-0.5 mm, V-0.5 mm, from the bregma and skull) immobilized with dental acrylic. A 2-mm active probe membrane (A-1-4-02, Eicom, Kyoto, Japan) was used. After surgery, the mice were housed individually for at least 1 week before experiments. Approximately 3 h after the start of perfusion, the dialysates were collected using a fraction collector (EFC-82, Eicom). Ringer solution (147 mM Na⁺, 4 mM K⁺, 2.3 mM Ca²⁺ and 155.6 mM Cl⁻) was perfused by use of a micro-infusion pump ESP-32 (Eicom) with gas-tight syringes at rates of 1 μl/min. For the high-potassium challenge, high-potassium Ringer solution (51 mM Na⁺, 100 mM K⁺, 2.3 mM Ca²⁺ and 155.6 mM Cl⁻) was perfused at the same rate. The collected dialysates were injected into the HPLC system for 5-HT quantification as described above.

Antibodies and flow cytometry. The following antibodies were purchased from BD Bioscience: anti-CD8α (1: 100 dilution; clone 53-6.7, #557654), anti-IFN-α (1: 100 dilution; clone XMG1.2, #554412), anti-TCRβ (1: 50 dilution; clone H57-597, #553174) and anti-TCRβ (1: 50 dilution; clone H57-597, #560706). The following antibodies were purchased from eBioscience: anti-CD4 (1: 100 dilution; clone RM4-5, #47-0042-82), anti-CD44 (1: 100 dilution; clone IM7, #12-0441-82), anti-CD62L (1: 3200 dilution; clone MEL-14, #13-0621-82), anti-CD98 (1: 50 dilution; clone RL388, #12-0981-81), anti-B220 (1: 100 dilution; clone RA3-6B2, #11-0452-82) and rat IgG2a-κ isotype control (1: 100 dilution; clone eBR2a, #12-4321-42). The following antibodies were purchased from Biolegend: anti-CD11c (1: 100 dilution; clone N418, #117311), anti-CD11b (1: 100 dilution; clone M1/70, #101219) anti-CD3 (1: 100 dilution; clone 145-2C11, #100321), anti-CD4 (1: 100 dilution; clone RM4-5, #25-0042), anti-CD62L (1: 100 dilution; clone MEL-14, #104426) and CD44 (IM7, #103026). Streptavidin Pacific Blue (1: 200 dilution; #S11222) was purchased from Invitrogen. To measure cytokine production by T cells, spleens were dissected and then single-cell suspensions were maintained in DMEM(H) (KOHJIN BIO) plus 10% FCS and stimulated with PMA plus ionomycin (Sigma) and GolgiStop (BD Bioscience) at 37 °C for 3.5 h before surface and intracellular staining using cytofix/cytoperm (BD Bioscience). Flow cytometry was performed using a BD FACSAria II (BD Bioscience).

Immunofluorescence. For brain immunofluorescence, mice were intracardially perfused with 5 mM EDTA solution in phosphate-buffered saline (PBS) and then with 2% PFA solution in PBS (PBS 2% PFA). The brain was immediately isolated and cut into six regions using an Alto brain matrix (CellPoint Scientific). The sections were post-fixed for 6 h in PBS 2% PFA at 4 °C and were soaked in 30% sucrose in PBS overnight at 4 °C. The sections were then embedded in Tissue-Tek OCT blocks (Sakura). 10-μm coronal sections were cut by cryostat (Leica CM3050S). The appropriate sections were selected on a morphological basis and were stained with the following antibodies: polyclonal goat anti-mouse 5-hydroxytryptamine (1:100 dilution; Immunostar, #20079) and monoclonal anti-mouse Tryptophan Hydroxylase (1:100 dilution clone WH3, which recognizes tryptophan hydroxylase 1 and tryptophan hydroxylase 2, Sigma-Aldrich,

#T0678). The sections were counterstained with DAPI (Sigma-Aldrich, #T0678) and mounted with the Fluoromount-G antifade reagent (Southern Biotech). Images were acquired with BZ-X700 fluorescence microscope (Keyence).

Real-time PCR. Total RNA was isolated from cells using the TRIzol Reagent (Invitrogen). After DNase I treatment (Invitrogen), random hexamers were used for first-strand cDNA synthesis. All procedures were performed according to the manufacturer's instructions (Invitrogen). Quantitative PCR was performed on a LightCycler 480 thermal cycler (Roche Life Science) using the Thunderbird SYBR Green qPCR mix (Toyobo) and analyzed by dedicated software (Roche Life Science). The primers were designed using BEACON DESIGNER software (Premier Biosoft International). All reactions were performed in duplicate. The relative expression of mRNA was normalized on the expression of *Gapdh* or *Actb*. Primers were as follows: *Tph2* forward, TTGACCCAAAGACGACCTGCTT, and reverse, CGAGAAGGGACGGTAATTGACT; *Th* forward, ACCTA TGCACTCACCGAGC, and reverse, AACTGGCAAATGTGCGGTC; *Gapdh* forward, TGTGTCGCTGCTGGATCTGA, and reverse, CCTGCTTCAC CACCTCTTGAT; *Slc7a5* (ref. 9) forward, CTGGATCGAGCTGCTCATC, and reverse, GTTCACAGCTGTGAGGAGC; *Slc3a2* forward, GTTTTTGAATGC CACTGGCA, and reverse, AAAGTCTGCGAGGAGTCCTG; and *Actb* forward, CACCCTGTGCTGCTCACCGA, and reverse, AGTGTGGGT GACCCCGTCTCC.

Behavioral tests. All behavioral testing procedures were approved by the Institutional Animal Care at RIKEN and Kyoto University Graduate School of Medicine and were performed according to manual of Medical Research Support Center, Graduate School of Medicine, Kyoto University.

Elevated-plus maze test. The elevated-plus maze test was conducted as previously described³⁷. The maze (O'Hara&Co.) consists of two open arms (25 cm × 5 cm) and two closed arms of the same size, with transparent walls (15 cm). The arms and center square (5 cm × 5 cm) are made of white plastic plates elevated to a height of 55 cm above the floor. 3-mm-high plastic ledges decrease open arm falls. Individual mice were placed in the center square facing a closed arm, and data were recorded for 10 min.

Open field test. Individual mice were placed in the corner of an enclosed platform (40 cm × 40 cm × 30 cm; Accuscan Instruments). The total distance traveled, movement duration and time spent in the center area (20 cm × 20 cm) were recorded for 10 min. Results obtained from replicate experiments performed in different mouse facilities were the same.

Dark-light transition test. The dark–light transition test was conducted as previously described⁴⁰ using a cage with two sections (of equal size) divided by a partition containing a door (O'Hara&Co.). One 'light chamber' section was brightly illuminated at 390 lux, while the 'dark chamber' emitted 2 lux. Individual mice were placed into the 'dark chamber', and data were recorded as each mouse was allowed to move freely between the two chambers with the door open for 10 min.

Forced-swim test. Individual mice were placed in a Plexiglas cylinders 20 cm high and 10 cm wide filled with water (23 °C), and sessions were recorded for 10 min. Total distance traveled and percentage immobility (time spent without swimming) were measured from the third minute to the sixth minute.

Social-interaction test. The social interaction test was conducted as previously described⁴¹. Two mice of the same genotype but different home cages were placed into a box together. Data were recorded as mice interacted freely for 10 min.

Hot-plate test. The hot-plate test was used to evaluate pain sensitivity. Individual mice were placed on a hot plate at 55.0 ± 0.3 °C (Columbus Instruments), and latency to the first hind-paw response (foot shake or paw lick) was measured.

Y-maze test. The Y-maze consisted of three arms (A, B and C) made of matte gray plastic joined in the middle to form a Y shape (O'Hara&Co,

30 mm × 400 mm × 120 mm). Individual mice were placed into one of the arm of the maze (start arm, A) and were allowed to explore freely in the three arms of the maze for 5 min. Spontaneous alternation rate was calculated using following formula: (number of successive three times for entry into different arm) / (total entry number – 1) × 100.

Contextual and cued fear conditioning test. The contextual and cued fear-conditioning test was conducted as previously described⁴². Individual mice were placed in a test chamber (26 cm × 34 cm × 29 cm) inside a sound-attenuated square chamber (O'Hara&Co.) and received three pairings of conditioned stimulus (CS) and unconditioned stimulus (US) for fear conditioning. 30 s of white noise at 55 dB served as the CS. CS terminated together with a foot shock (2 s and 0.35 mA), which served as the US (interstimulus interval, 1.5 min). For the contextual test, at 24 h after conditioning, each mouse was again placed in the same chamber without CS and US for 5 min. 1–2 h later, the cued test was performed using a triangular chamber (35 cm × 35 cm × 40 cm), which was located in a different room. In cued testing, each mouse was habituated to the chamber over a period of 180 s before presentation with continued CS (180 s).

Fear-extinction test. The fear-extinction test procedure was as previously described⁴³ with slight modifications. On conditioning day 1, each mouse was placed in a square conditioning chamber as in contextual and cued fear-conditioning test above. After 2 min of acclimation, fear conditioning was delivered by three pairings of CS (white noise at 55 dB) and US (foot shock for 2 s at 0.35 mA). CS was presented for 30 s and was terminated together with a foot shock with an interstimulus interval of 30 s. On days 2–5 of extinction sessions, mice were trained to fear extinction in the triangular chamber used for cued test by presentation, five times, of CS with an interstimulus interval of 30 s. After the final CS-US, behavior was recorded for 1 min. Fear-extinction indices were calculated with the following formula: freezing percentage = (CS1 + CS2 at day 2) – (CS4 + CS5 at day 5).

Behavioral-image analysis. The acquisition and analysis of behavioral data were performed automatically using Image software developed by T. Miyakawa (O'Hara&Co.) based on the NIH Image program (NIH, Bethesda, MD, available at <http://rsb.info.nih.gov/nih-image/>) and ImageJ (Imagejdev.Org, available at <http://imagejdev.org/>).

Drugs and diet. Fluoxetine and phenelzine (Sigma-Aldrich) were dissolved in 0.9% saline (Otsuka) and were administered at doses of 20 mg/kg (fluoxetine) or 40 mg/kg (phenelzine). Mice were given intraperitoneal injection of either saline or drugs in a volume of 10 ml/kg at 1 h (fluoxetine) or 4 h (phenelzine) before the contextual test or open-field test. High-tryptophan diet supplementation contained 2% L-tryptophan (w/w) (Funabashi Farm) provided *ad libitum* for 4 weeks before behavior testing.

In vivo T cell activation by tumor or exogenous antigen. Mouse MC38 colon cancer cells (5×10^5) were injected intradermally into the right flank (day 0). Mice were treated intraperitoneally with 100 µg of monoclonal antibody to PD-1 (clone 4H2, Bristol-Myers Squibb) on days 5, 8 and 11. Serum was harvested on day 13 for metabolite measurement by GC-MS. The experiments were performed in accordance with approved protocols from the Institute of Laboratory Animals, Graduate School of Medicine, Kyoto University. OT-I mice⁴⁴ and OT-II mice⁴⁵ were bred in SPF facility at Graduate School of Medicine, Kyoto University. Mice were treated intravenously with 200 µg OVA (Sigma) on day 0 and day 3, and serum was harvested on day 5 for metabolite measurement by GS-MS. For footpad immunization, wild-type mice were immunized with complete Freund's adjuvant and OVA (1:1) in the left footpad (20 µg/mouse), and serum from 7 d after immunization underwent metabolite measurement as above.

T cell purification and *in vitro* activation. For *ex vivo*-sorting of T cells, LNs (axillary, brachial and inguinal) were pooled and disrupted to form a single-cell suspension. CD44^{hi} T cells (CD11c[−], CD11b[−], B220[−], CD4⁺ or CD8⁺, and CD44^{hi}) or naive T cells (CD11c[−], CD11b[−], B220[−], CD4⁺ or CD8⁺, CD44^{lo}, CD62L⁺) T cells were sorted using a FACSaria II cell sorter (BD Bioscience),

with replacement of FACSFlow (BD Bioscience) with PBS to avoid metabolite contamination. 1×10^6 sorted cells were washed with PBS and were rapidly frozen in liquid nitrogen for metabolite analysis.

LN T cells purified using a MagniSort mouse T cell enrichment kit (Invitrogen) were cultured for 48 or 96 h at a density of 1×10^6 cells per ml in 96-well plates bound to anti-CD3e (2.5 µg/ml; 145-2C11; BD Pharmingen) in the presence of anti-CD28 (2 µg/ml; 37.51; BD Pharmingen) and IL-2 (20 ng/ml; R&D system)). RPMI-1640 medium (Wako) supplemented with 10% (v/v) FBS, 1× MEM non-essential amino acids, 10 mM HEPES, 50 µM 2-mercaptoethanol, 1 mM sodium pyruvate, 100 U/ml penicillin and 100 U/ml streptomycin was used for culture. For [^{13}C]Trp-uptake assays, the medium was supplemented with 12 µM L-tryptophan- ^{13}C (TAIYO NIPPON SANSO) or L-tryptophan- ^{12}C (Sigma).

Statistical analysis. PRISM (Graphpad) was used for statistical analysis. Analyses were conducted using the two-tailed unpaired Student's *t*-test or analysis of variance (ANOVA). No statistical methods were used to predetermine sample size.

A Life Science Reporting Summary for this paper is available.

Data availability. The data that support the findings of this study are available from the corresponding author upon reasonable request. Methods are available in the online version of the paper. All supplementary information and source data files are available in the online version of the paper.

25. Nishimura, H., Minato, N., Nakano, T. & Honjo, T. Immunological studies on PD-1 deficient mice: implication of PD-1 as a negative regulator for B cell responses. *Int. Immunol.* **10**, 1563–1572 (1998).
26. Malissen, M. *et al.* Altered T cell development in mice with a targeted mutation of the CD3-epsilon gene. *EMBO J.* **14**, 4641–4653 (1995).
27. Tagawa, Y., Sekikawa, K. & Iwakura, Y. Suppression of concanavalin A-induced hepatitis in IFN- $\gamma^{-/-}$ mice, but not in TNF- $\alpha^{-/-}$ mice: role for IFN- γ in activating apoptosis of hepatocytes. *J. Immunol.* **159**, 1418–1428 (1997).
28. Xia, J., Sinelnikov, I.V., Han, B. & Wishart, D.S. MetaboAnalyst 3.0—making metabolomics more meaningful. *Nucleic Acids Res.* **43**, W1, W251–W257 (2015).
29. Moroji, T., Takahashi, K., Ogura, K., Toishi, T. & Arai, S. Rapid microwave fixation of rat brain. *J. Microwave Power.* **12**, 273–286 (1977).
30. Sugiura, Y., Honda, K., Kajimura, M. & Suematsu, M. Visualization and quantification of cerebral metabolic fluxes of glucose in awake mice. *Proteomics* **14**, 829–838 (2014).
31. Oka, M. *et al.* Arl8b is required for lysosomal degradation of maternal proteins in the visceral yolk sac endoderm of mouse embryos. *J. Cell. Sci.* <http://dx.doi.org/10.1242/jcs.200519> (2017).
32. Hu, S. *et al.* Targeted metabolomic analysis of head and neck cancer cells using high performance ion chromatography coupled with a Q exactive HF mass spectrometer. *Anal. Chem.* **87**, 6371–6379 (2015).
33. Zhou, Z. Non-target impurity profiling of marketplace Cetirizine using high-resolution mass spectrometry and multivariate data analysis. *Rapid Commun. Mass Spectrom.* **30**, 1941–1950 (2016).
34. Morikawa, T. *et al.* Hypoxic regulation of the cerebral microcirculation is mediated by a carbon monoxide-sensitive hydrogen sulfide pathway. *Proc. Natl. Acad. Sci. USA* **109**, 1293–1298 (2012).
35. Sharifiatgorji, M. *et al.* Direct targeted quantitative molecular imaging of neurotransmitters in brain tissue sections. *Neuron* **84**, 697–707 (2014).
36. Sugiyama, E., Masaki, N., Matsushita, S. & Setou, M. Ammonium Sulfate Improves Detection of Hydrophilic Quaternary Ammonium Compounds through Decreased Ion Suppression in Matrix-Assisted Laser Desorption/Ionization Imaging Mass Spectrometry. *Anal. Chem.* **87**, 11176–11181 (2015).
37. Marshall, A.G., Hendrickson, C.L. & Jackson, G.S. Fourier transform ion cyclotron resonance mass spectrometry: a primer. *Mass Spectrom. Rev.* **17**, 1–35 (1998).
38. Benveniste, H. & Hansen, A.J. Practical aspects of using microdialysis for determination of brain interstitial concentrations. In: Robinson, T.E., Jr., J.B.J. & Huston, J.P. (eds). *Microdialysis in the neurosciences*. Elsevier: New York, USA, 1991, pp 81–97.
39. Komada, M., Takao, K. & Miyakawa, T. Elevated plus maze for mice. *J. Vis. Exp.* **22**, e1088 (2008).
40. Takao, K. & Miyakawa, T. Light/dark transition test for mice. *J. Vis. Exp.* **1**, e104 (2006).
41. Miyakawa, T. *et al.* Conditional calcineurin knockout mice exhibit multiple abnormal behaviors related to schizophrenia. *Proc. Natl. Acad. Sci. USA* **100**, 8987–8992 (2003).
42. Koshimizu, H. *et al.* Adenomatous polyposis coli heterozygous knockout mice display hypoactivity and age-dependent working memory deficits. *Front. Behav. Neurosci.* **5**, 85 (2011).
43. Pattwell, S.S. *et al.* Altered fear learning across development in both mouse and human. *Proc. Natl. Acad. Sci. USA* **109**, 16318–16323 (2012).
44. Hogquist, K.A. *et al.* T cell receptor antagonist peptides induce positive selection. *Cell* **76**, 17–27 (1994).
45. Barnden, M.J., Allison, J., Heath, W.R. & Carbone, F.R. Defective TCR expression in transgenic mice constructed using cDNA-based alpha- and beta-chain genes under the control of heterologous regulatory elements. *Immunol. Cell Biol.* **76**, 34–40 (1998).

Life Sciences Reporting Summary

Corresponding author(s): Sidonia Fagarasan

 Initial submission Revised version Final submission

Nature Research wishes to improve the reproducibility of the work that we publish. This form is intended for publication with all accepted life science papers and provides structure for consistency and transparency in reporting. Every life science submission will use this form; some list items might not apply to an individual manuscript, but all fields must be completed for clarity.

For further information on the points included in this form, see [Reporting Life Sciences Research](#). For further information on Nature Research policies, including our [data availability policy](#), see [Authors & Referees](#) and the [Editorial Policy Checklist](#).

► Experimental design

1. Sample size

Describe how sample size was determined.

No sample size calculation was performed. For statistic analyses more than 3 samples were used and the number of samples were indicated in the figure legends.

2. Data exclusions

Describe any data exclusions.

Infrequently, mice showed signs of inflammation even in normal SPF condition. Therefore, when sacrificed, mice were routinely checked for the inflammation status and samples from mice showing severe inflammation status (splenomegaly and colitis) were excluded. And, Pdcd1^{-/-} mice generally spent less time in the center of the field than wild-type mice, but some froze there for extended periods. When animals displaying this confounding behaviour were excluded (Fig. 7b and Supplementary Fig. 6a).

3. Replication

Describe whether the experimental findings were reliably reproduced.

For each experiment, all attempts at replication were successful.

4. Randomization

Describe how samples/organisms/participants were allocated into experimental groups.

Samples were randomly allocated into experimental groups.

5. Blinding

Describe whether the investigators were blinded to group allocation during data collection and/or analysis.

We were not blinded to group allocation during data collection and analysis.

Note: all studies involving animals and/or human research participants must disclose whether blinding and randomization were used.

6. Statistical parameters

For all figures and tables that use statistical methods, confirm that the following items are present in relevant figure legends (or in the Methods section if additional space is needed).

n/a Confirmed

- The exact sample size (n) for each experimental group/condition, given as a discrete number and unit of measurement (animals, litters, cultures, etc.)
- A description of how samples were collected, noting whether measurements were taken from distinct samples or whether the same sample was measured repeatedly
- A statement indicating how many times each experiment was replicated
- The statistical test(s) used and whether they are one- or two-sided (note: only common tests should be described solely by name; more complex techniques should be described in the Methods section)
- A description of any assumptions or corrections, such as an adjustment for multiple comparisons
- The test results (e.g. P values) given as exact values whenever possible and with confidence intervals noted
- A clear description of statistics including central tendency (e.g. median, mean) and variation (e.g. standard deviation, interquartile range)
- Clearly defined error bars

See the web collection on [statistics for biologists](#) for further resources and guidance.

Software

Policy information about [availability of computer code](#)

7. Software

Describe the software used to analyze the data in this study.

Flowjo software were used for FACS analysis. BZ-X analyzer software was used for analysis of photomicrograph. Compound Discoverer 2.0 software was used for non-target analysis of mass spectrometry data. FlexImaging 4.0 software was used for Imaging mass spectrometry. MetaboAnalyst was used for analysis of metabolome data. PRISM software was used for statistical analysis.

For manuscripts utilizing custom algorithms or software that are central to the paper but not yet described in the published literature, software must be made available to editors and reviewers upon request. We strongly encourage code deposition in a community repository (e.g. GitHub). [Nature Methods guidance for providing algorithms and software for publication](#) provides further information on this topic.

Materials and reagents

Policy information about [availability of materials](#)

8. Materials availability

Indicate whether there are restrictions on availability of unique materials or if these materials are only available for distribution by a for-profit company.

No unique materials were used.

9. Antibodies

Describe the antibodies used and how they were validated for use in the system under study (i.e. assay and species).

Data was provided in the manuscript.

10. Eukaryotic cell lines

a. State the source of each eukaryotic cell line used.

No eukaryotic cell lines were used.

b. Describe the method of cell line authentication used.

No eukaryotic cell lines were used.

c. Report whether the cell lines were tested for mycoplasma contamination.

No eukaryotic cell lines were used.

d. If any of the cell lines used are listed in the database of commonly misidentified cell lines maintained by [ICLAC](#), provide a scientific rationale for their use.

No commonly misidentified cell lines were used.

► Animals and human research participants

Policy information about [studies involving animals](#); when reporting animal research, follow the [ARRIVE guidelines](#)

11. Description of research animals

Provide details on animals and/or animal-derived materials used in the study.

WT (C57BL/6N), PD-1-/- (C57BL/6N), PD-1-/- IFNg-/- (C57BL/6), PD-1-/- CD3-/- (C57BL/6), CD3-/- (C57BL/6), OT-I (C57BL/6J) and OT-II (C57BL/6J) mice were used in this study. Both male and female mice were used. 2 Mo-12 Mo old mice were used in this study.

Policy information about [studies involving human research participants](#)

12. Description of human research participants

Describe the covariate-relevant population characteristics of the human research participants.

This study did not involve human research participants.

Flow Cytometry Reporting Summary

Form fields will expand as needed. Please do not leave fields blank.

► Data presentation

For all flow cytometry data, confirm that:

1. The axis labels state the marker and fluorochrome used (e.g. CD4-FITC).
2. The axis scales are clearly visible. Include numbers along axes only for bottom left plot of group (a 'group' is an analysis of identical markers).
3. All plots are contour plots with outliers or pseudocolor plots.
4. A numerical value for number of cells or percentage (with statistics) is provided.

Methodological details

5. Describe the sample preparation.

The cells were collected from spleen, lymph nodes, small intestine or colon. Spleen and lymph nodes were mechanically smashed and filtered with strainer and used for flow cytometry. Small intestine and colon were prepared by classical EDTA-treatment followed by collagenase digestion, filtration of cells, staining and flow cytometry.

6. Identify the instrument used for data collection.

FACSAria II cell sorter (BD Bioscience) was used for data collection.

7. Describe the software used to collect and analyze the flow cytometry data.

FlowJo software was used for analysis.

8. Describe the abundance of the relevant cell populations within post-sort fractions.

The purity of the samples was not determined.

9. Describe the gating strategy used.

Gating strategies are provided in the manuscript.

Tick this box to confirm that a figure exemplifying the gating strategy is provided in the Supplementary Information.



True-Stain Monocyte Blocker™

Block Monocyte Non-Specific Antibody Binding



This information is current as of January 17, 2018.

Chimeric Antigen Receptor T Cell Therapy: Challenges to Bench-to-Bedside Efficacy

Shivani Srivastava and Stanley R. Riddell

J Immunol 2018; 200:459-468; ;
doi: 10.4049/jimmunol.1701155
<http://www.jimmunol.org/content/200/2/459>

Why *The JI*?

- **Rapid Reviews!** 30 days* from submission to initial decision
- **No Triage!** Every submission reviewed by practicing scientists
- **Speedy Publication!** 4 weeks from acceptance to publication

*average

References This article **cites 139 articles**, 58 of which you can access for free at:
<http://www.jimmunol.org/content/200/2/459.full#ref-list-1>

Subscription Information about subscribing to *The Journal of Immunology* is online at:
<http://jimmunol.org/subscription>

Permissions Submit copyright permission requests at:
<http://www.aai.org/About/Publications/JI/copyright.html>

Email Alerts Receive free email-alerts when new articles cite this article. Sign up at:
<http://jimmunol.org/alerts>



Chimeric Antigen Receptor T Cell Therapy: Challenges to Bench-to-Bedside Efficacy

Shivani Srivastava and Stanley R. Riddell

Immunotherapy with T cells genetically modified to express chimeric Ag receptors (CARs) that target tumor-associated molecules have impressive efficacy in hematological malignancies. The field has now embraced the challenge of applying this approach to treat common epithelial malignancies, which make up the majority of cancer cases but evade immunologic attack by a variety of subversive mechanisms. In this study, we review the principles that have guided CAR T cell design and the extraordinary clinical results being achieved in B cell malignancies targeting CD19 with a single infusion of engineered T cells. This success has raised expectations that CAR T cells can be applied to solid tumors, but numerous obstacles must be overcome to achieve the success observed in hematologic cancers. Potential solutions driven by advances in genetic engineering, synthetic biology, T cell biology, and improved tumor models that recapitulate the obstacles in human tumors are discussed. *The Journal of Immunology*, 2018, 200: 459–468.

Innovations in gene transfer and adoptive T cell transfer (ACT) have converged in a novel approach to cancer therapy in which a patient's T cells are genetically modified to express synthetic chimeric Ag receptors (CARs) that redirect T cell specificity toward tumor-associated Ags. CAR T cells have shown remarkable success in some hematologic malignancies and serve as an example of how advances in immunology can inform a new class of cancer therapeutics (1). In this study, we review the principles underlying CAR T cell therapy, discuss obstacles to further improve results in hematologic cancers, and extend this approach to common cancers that are the major cause of cancer mortality.

Principles of CAR design and T cell engineering

A CAR is a synthetic construct that, when expressed in T cells, mimics TCR activation and redirects specificity and effector function toward a specified Ag. For cancer therapy, this is accomplished by linking an extracellular ligand-binding do-

main specific for a tumor cell-surface Ag to an intracellular signaling module that activates T cells upon Ag binding. The earliest first-generation CARs contained only a CD3 ζ or Fc receptor γ signaling domain (2), and the addition of one (second generation) or more (third generation) costimulatory domains such as CD28, 4-1BB, or OX40 induced more cytokine production and T cell proliferation (3–5). The constellation of signaling modules in a CAR is usually selected based on analysis of tumor recognition in vitro and in preclinical in vivo models (6–8), and advances in synthetic biology are likely to improve upon constructs currently in clinical trials. For example, strategies for small molecule-mediated regulatory control of CAR expression (9), combinatorial Ag sensing (10), targeted integration of the CAR transgene into defined loci (11), logic gating of CAR recognition to improve tumor selectivity (12, 13), and suicide mechanisms for targeted elimination of transferred T cells (14, 15) have been described and could provide more potent and safe CARs.

The immune cell chassis used to express a CAR is most commonly a T cell derived from the peripheral blood. Peripheral T cells can be broadly divided by surface phenotype into naive T cell (T_N), memory T cell, and effector T cell (T_E) subsets. Memory T cells are further subdivided into stem cell memory cells, central memory cells (T_{CM}), effector memory T cells (T_{EM}), and tissue-resident memory cells, each of which has a distinct role in protective immunity (16–18). Current data support a progressive differentiation model such that activation of T_N by Ag gives rise to long-lived stem cell memory cells and T_{CM} that can self-renew and provide proliferating populations of shorter-lived T_{EM} and T_E (19–21). This understanding has led several groups to focus on defining the starting population of T cells that are genetically modified with CARs and used for ACT, initially in preclinical models and subsequently in clinical trials (22–27). Accumulating data suggest that engineering less differentiated T_N and/or T_{CM} , or culturing T cells in conditions that preserve these phenotypes, provides CAR T cell products with superior persistence in vivo (22–28). Thus, as with CAR design, cell product composition can be manipulated to improve potency and potentially reduce

Program in Immunology, Fred Hutchinson Cancer Research Center, Seattle, WA 98109

Received for publication August 11, 2017. Accepted for publication September 29, 2017.

This work was supported by National Institutes of Health Grants CA136551 and CA114536 (to S.R.R.) and by the Cancer Research Institute Irvington Postdoctoral Fellowship (to S.S.).

Address correspondence and reprint requests to Dr. Stanley R. Riddell, Fred Hutchinson Cancer Research Center, 1100 Fairview Avenue N, D3-100, Seattle, WA 98109. E-mail address: sriddell@fredhutch.org

Abbreviations used in this article: ACT, adoptive T cell transfer; ALL, acute lymphocytic leukemia; CAF, cancer-associated fibroblast; CAR, chimeric Ag receptor; CLL, chronic lymphocytic leukemia; CR, complete remission; CRS, cytokine release syndrome; GEM, genetically engineered mouse; ICD, immunogenic cell death; NHL, non-Hodgkin lymphoma; NSG, NOD/SCID/ $\gamma c^{-/-}$; ROS, reactive oxygen species; scFv, single chain variable fragment; T_{CM} , central memory T cell; T_E , effector T cell; T_{EM} , effector memory T cell; TME, tumor microenvironment; T_N , naive T cell; Treg, regulatory T cell.

Copyright © 2018 by The American Association of Immunologists, Inc. 0022-1767/18/\$35.00

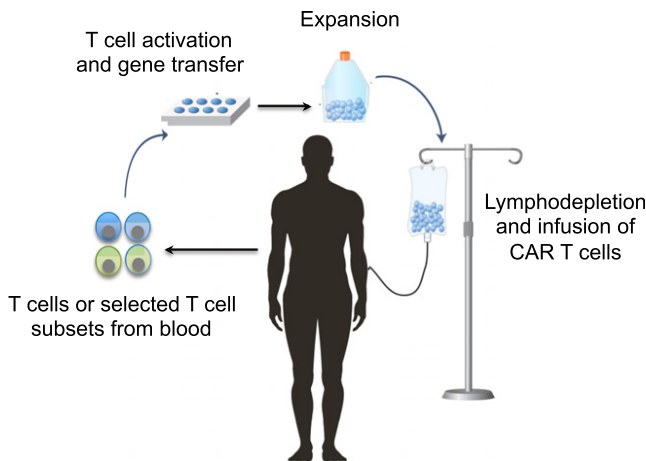


FIGURE 1. Adoptive cell therapy with CAR-modified T cells.

toxicity by providing consistent proliferation and persistence after ACT.

Clinical efficacy: B cell malignancies and beyond

Clinical trials of CAR T cells have proceeded rapidly in B cell malignancies. B cell malignancies are an attractive target for CAR T cells because they express B cell lineage-specific molecules such as CD19, CD20, and CD22, which are not expressed on other tissues, and preclinical data demonstrated that human B cell tumors could be eradicated in immune-compromised mice treated with CAR T cells (29–32). To prepare CAR T cell products for the treatment of patients, T cells are obtained from the blood, activated *in vitro* to facilitate gene insertion, and modified to express the CAR by viral or nonviral gene delivery. CAR T cells are then reinfused into the patient, often after the administration of lymphodepleting chemotherapy to promote engraftment and proliferation of transferred cells (Fig. 1). Initial reports in patients with relapsed and/or refractory chronic lymphocytic leukemia (CLL), acute lymphocytic leukemia (ALL), and non-Hodgkin lymphoma (NHL) showed remarkable antitumor effects of CD19-specific CAR T cells (33–36). Subsequent larger phase 1/2 trials at a number of centers confirmed the high level of efficacy of CAR T cells, particularly in ALL where complete remission (CR) rates of 70–93% are achieved (26–28, 37–40). CAR T cells administered in these studies varied in T cell subset composition, method of gene delivery, cell manufacturing platform, and used either CD28/CD3 ζ or 4-1BB/CD3 ζ costimulatory domains. Further studies are necessary to determine optimal product characteristics and CAR design.

A majority of patients with CLL and NHL demonstrate tumor regression after treatment with CD19 CAR T cells; however, the CR rates for these lymph node-based malignancies are lower than for ALL (27, 28, 34, 41–43). Defining the reasons for incomplete response in CLL and NHL is important to improve outcomes and is the subject of ongoing research. Combination therapy with checkpoint inhibitors, cytokines, modulators of the tumor microenvironment (TME), improved CAR design, and/or further genetic modifications of the T cells are being studied to improve efficacy. The initial response rates in patients with refractory leukemia and lymphoma are impressive, but the durability of responses will only be established with longer follow up. CRs have been

reported for up to 56 mo after CD19 CAR T cell therapy; and CR continues even after the disappearance of functional CD19 CAR T cells and recovery of normal B cells (44). Understanding the factors that correlate with long-term CR or with relapse will be critical to enhancing the efficacy of CAR T cell therapy.

The eradication of large tumor burdens by CAR T cells is not accomplished without toxicity. Cytokine release syndrome (CRS) is a common complication initiated by release of IFN- γ , TNF- α , and IL-2 by activated CD19 CAR T cells and is associated with fever, hemodynamic compromise, and macrophage activation with production of IL-6 and additional cytokines (45). The severity of CRS correlates with tumor burden, and interventions to block IL-6 signaling, or to suppress cytokine production by immune cells with dexamethasone, are the mainstays of therapy. Algorithms for timing interventions based on clinical and laboratory parameters are rapidly evolving. Neurologic adverse events are observed concurrent with or following CRS in a subset of patients treated with CD19 CAR T cells, and rare fatal cases have occurred. The pathogenesis of neurotoxicity remains to be elucidated: current data suggest that cytokines released by activated T cells play a role by affecting endothelial integrity (46). Finally, an anticipated side effect of targeting CD19 is that normal CD19 $^+$ B cells are eliminated. Transient and even prolonged loss of normal B cells can be managed clinically. However, vector designs that permit elimination of CAR T cells and restoration of B cell numbers are effective in animal models and could be applied in patients that achieve durable remission of their malignancy and have persisting CAR T cells (14).

The success of CAR T cells in ALL, CLL, and NHL has encouraged translation of this approach to other malignancies. CARs have been designed to target molecules such as CD123 and Lewis Y on acute myeloid leukemia (47, 48). However, none of the targets are as attractive as CD19 due to their expression on other critical hematopoietic cells and/or lack of uniform expression on the tumor. Multiple myeloma expresses several candidate molecules to target with CAR T cells including BCMA and CS1 (49, 50), and early clinical data targeting BCMA are promising (51). The application of CAR T cells to common solid tumors has proceeded cautiously following a fatal toxicity in a patient treated with a high dose of ErbB2-specific CAR T cells due to recognition of normal epithelial cells (52). Subsequent studies in patients with glioblastoma and sarcoma suggested it may be possible to target ErbB2 safely, although antitumor efficacy was limited in these studies (53, 54). In glioblastoma, a dramatic response was observed after local intracranial administration of CAR T cells specific for IL-13R α 2, and activity of systemically administered CAR T cells specific for EGFRvIII has been reported (55, 56). CAR T cells targeting gD2 have shown activity in patients with Ewing's sarcoma and neuroblastoma (57, 58). Trials using CAR T cells to target mesothelin, Muc16, Muc1, and ROR1 are in progress (59–63) but, as discussed below, may need to overcome unique obstacles compared with hematologic malignancies.

Barriers to CAR T cell efficacy and potential solutions

Tumor Ag loss. A challenge for CAR T cell therapy in solid tumors is identifying target Ags expressed homogeneously

throughout the tumor and not on normal vital tissues. The success of CAR T cells in B cell malignancies targeting CD19 is tempered by outgrowth of CD19⁻ tumor cells in some ALL patients (26, 64, 65). Few targets with homogeneous expression on epithelial cancers have been identified, and outgrowth of Ag-null tumor cells after CAR T cell therapy is an anticipated resistance mechanism. A strategy to circumvent tumor escape is to target multiple Ags simultaneously, such that only tumor cells that lack expression of all target molecules would escape an antitumor immune response (66). One way to target multiple Ags is to use promiscuous receptors as the Ag-binding portion of the CAR. NKG2D CARs, for example, target multiple ligands expressed on both tumor cells and immunosuppressive cells, whereas CARs using the promiscuous ErbB ligand T1E as the extracellular domain can bind multiple ErbB1-based homo- and heterodimers that are often overexpressed in tumors (67, 68). Another strategy is to link multiple single chain variable fragments (scFvs) in tandem. Several groups have demonstrated that cotargeting CD20 or CD123 in addition to CD19 with bispecific CAR T cells eliminates CD19 loss variants and is superior to targeting CD19 alone in xenograft models (69, 70). Bispecific CAR T cells were also superior to monospecific CAR T cells when targeting Ags with nonuniform expression on solid tumors, such as Muc1 and PSCA for pancreatic tumors, or Her2 and IL-13R α 2 for glioblastoma (71, 72). Of interest, bispecific T cells showed superior activity *in vivo* compared with 1:1 mixtures of monospecific CAR T cells targeting the same Ags, although the mechanism behind functional superiority remains unclear. Bispecific CARs showed enhanced ZAP70 phosphorylation and downstream signaling when both target Ags were engaged, suggesting that dual-positive tumor cells activate bispecific CAR T cells more efficiently (72). CD19, CD20, and CD22 are attractive for multivalent targeting because they are often coexpressed on B cell malignancies, but identifying other pairs of tumor-associated Ags that are coexpressed on common epithelial tumors but not normal tissues remains a challenge.

Minimizing the escape of Ag-null tumors may also depend on the ability of CAR T cells to induce epitope spreading and engage an endogenous immune response against other tumor-associated Ags. It is possible that CAR T cell-mediated lysis of tumor cells will result in release and cross-presentation of other tumor Ags to endogenous T cells, resulting in a more effective polyclonal antitumor response. Some preclinical studies using CAR T cells have demonstrated epitope spreading and even resistance to rechallenge with Ag-null tumors, suggesting the development of immunological memory to other tumor-associated Ags, although this has yet to be demonstrated in patients (73, 74). Mesothelin-targeting CAR T cells were reported to induce humoral epitope spreading in some patients, although not to Ags overexpressed by the tumor or involved in tumorigenesis (60). Cotreatment of CAR T cells with modulators that enhance cross-presentation or activation of the endogenous immune system may enhance the probability of epitope spreading. For example, CAR T cells secreting IL-12 were able to activate macrophages that mediated elimination of Ag-negative tumor cells in preclinical models (75). Likewise, T cells engineered to express CD40L may better activate cross-presenting CD8 α ⁺ dendritic cells, whereas those expressing 4-1BBL can provide

direct costimulation to bystander tumor-specific T cells (76, 77). Future studies will be needed to determine whether CAR T cells can be engineered to better engage an endogenous antitumor response and whether this can help combat tumor heterogeneity more effectively.

Toxicity to normal tissues. Because few truly tumor-specific targets have been identified, applying principles in synthetic biology that might enable CAR T cells to discriminate between tumor and normal cells expressing the same Ag could improve both the efficacy and safety of therapy. Tuning the affinity of the CAR scFv can allow T cells to distinguish between Ags that are overexpressed on tumor cells but expressed at lower levels on normal cells (78). Tumor Ags thought to be unsafe to target due to wide normal tissue expression, thus, may be targetable if expression levels are sufficiently higher on tumor versus normal cells. CARs designed from scFvs targeting either CD38 or EGFR with ~1000-fold reduced affinity conferred effective lysis of tumor cells but spared Ag-positive normal cells (79, 80). Whether this could truly achieve discrimination of tumor and normal cells based on level of Ag expression in clinical settings without the outgrowth of Ag low tumor cells remains to be determined.

Another strategy to increase tumor-specificity is to use AND logic gates that require recognition of two different Ags on the same target cell to elicit full CAR T cell activation (13). The success of this strategy requires identifying Ag pairs that are selectively coexpressed on tumor cells but not normal tissues. One implementation of this strategy is to split the CD3 ζ signaling and CD28 costimulatory domains across separate receptors, with each signaling domain linked to an scFv specific for a different Ag (81). However, several studies employing such split-receptor systems have found that CD3 ζ signaling alone is sufficient to induce some T cell effector functions, including lysis of single-positive cells (66, 81), suggesting toxicity to single-positive normal tissues may not be avoided. This problem could be solved by using a low-affinity scFv that is incapable of inducing T cell activation when linked only to the CD3 ζ signaling domain (13). Development of such dual-signaling CAR T cells is likely to require further optimization of each individual scFv. Other aspects of Ag pairs, such as size and ability to colocalize in the synapse, might also affect their ability to properly activate T cells.

Several groups have built constructs in which CAR expression is regulated by a drug-inducible promoter or in which the recognition and signaling domains are only associated in the presence of a small molecule dimerizer (9, 82, 83). CAR T cells can be transiently activated *in vivo* by drug administration, and their activity can theoretically be halted if toxicity occurs by withdrawal of the drug. Alternately, timing and location of drug delivery can be adjusted to minimize toxicity. For example, Her2-specific CAR T cells induced rapid pulmonary toxicity as a consequence of recognition of Her2 $^{+}$ cells in the lung (52). If a CAR-inducing drug was delivered several days after infusion, when the majority of intravenously infused T cells have migrated out of the lung, toxicity to normal cells in the lung might be diminished or averted. Likewise, by delivering the drug locally rather than systemically, CAR T cell activity could be restricted to particular tissue compartments.

Engineering T cells in which CAR expression is regulated by input signals found primarily in the TME is another potential

strategy. Tumors are often hypoxic, and oxygen-sensitive CAR T cells have been designed by fusing the CAR to a subdomain of the hypoxia transcription factor HIF-1 α , which is sensitive to protein degradation under normoxic conditions (84). Likewise, Roybal et al. (10) engineered a synthetic Notch receptor that upon recognition of one tumor-associated Ag releases a transcription factor that induces expression of a CAR specific for a second tumor-associated Ag. The advantage of these approaches is that CAR expression is restricted to the local tumor environment, minimizing the potential for off-tumor toxicity. However, as with AND gate CAR T cells, clinical application of the synthetic Notch strategy requires the identification of two tumor-associated Ags that are coexpressed in the tumor but do not overlap in their normal tissue expression. It is also uncertain whether the kinetics of CAR degradation after signal 1 is disengaged will be sufficiently rapid to minimize off-tumor toxicity. Despite these limitations, both approaches can theoretically improve tumor selectivity, and may prove advantageous in settings where Ag-positive tumor cells and normal tissues are spatially segregated, such that CAR expression is fully degraded before T cells that leave the tumor site encounter Ag-positive normal cells.

Trafficking to solid tumors. Analysis of the TME has identified a variety of obstacles such as trafficking, immunosuppressive molecules and cells, and immune checkpoints that CAR T cells will need to overcome to be effective in solid tumors (Fig. 2). The efficacy of CAR T cells in hematological malignancies in part may reflect efficient access to tumor cells in the bone marrow and lymph nodes where T cells normally traffic. Recognition of solid tumors requires egress from the blood into the tumor site, and many malignancies evolve such that T cell infiltration is actively impeded (85–87). In situations where the tumor is localized, regional rather than systemic administration of CAR T cells might be effective. Intracranial delivery has been shown to be safe and to have antitumor activity in glioblastoma (56), and intrapleural delivery of CAR T cells was superior to systemic administration in preclinical studies of human pleural malignancy (88).

Improved understanding of mechanisms that promote or exclude T cell infiltration into tumors is likely to create opportunities to improve CAR T cell trafficking, either by additional genetic modification of T cells (89) or by combining CAR T cells with oncolytic viruses or other strategies that promote inflammation at the tumor site (90, 91). CAR T cells can be engineered to express receptors like CCR2 and CCR4 that are specific for chemokines naturally overexpressed by tumors, enabling them to traffic more efficiently to tumors (92–94). Rather than custom engineering T cells to the chemokine profile of individual tumors, a more generalizable strategy is to induce tumors to secrete chemokines to which CAR T cells are already responsive. An oncolytic virus has been used to deliver the chemokine CCL5 (RANTES) to the tumor. CAR T cells already express receptors (CCR1, CCR3, and CCR5) for CCL5, and combination therapy with CCL5-expressing oncolytic virus and CAR T cells synergistically improved survival and tumor clearance in preclinical models (90).

CAR T cell access to tumors might also be improved by combining adoptive therapy with drugs that induce immunogenic cell death (ICD) of tumor cells. Unlike physiological

cell death, in which dying cells are cleared without an inflammatory response, ICD induces release of damage-associated molecular patterns, which directly activate dendritic cells to secrete T cell-attracting chemokines and cross-present tumor Ags (95). Local radiotherapy and certain chemotherapeutic agents induce ICD and activate endogenous T cell responses to tumor Ags (96, 97). These modalities also inhibit or eliminate immunosuppressive cell subsets in the TME, resulting in an overall shift to a proinflammatory state and improved immune responses (96–99). A similar regimen may improve CAR T cell infiltration by inducing production of chemokines and creating a favorable environment for CAR T cell function. Unlike genetic engineering-based approaches, such combination therapy has the advantage of modulating multiple immune pathways at once.

The differentiation state of the T cells selected for CAR modification can also influence CAR T cell function and migratory properties in vivo. T_{CM} have superior antitumor function relative to T_{EM} in xenograft models of hematological malignancies due to superior persistence and proliferation (22, 24, 25). However, T_{EM} express higher levels of chemokine receptors and adhesion molecules required for homing to inflamed peripheral tissues and may be better poised to enter solid tumor sites. Despite these attributes, a recent study demonstrated that in vitro-generated T_{EM} expressing a gp100-specific TCR were less effective on a per-cell basis than T_{CM} of the same Ag-specificity against B16 tumors (23). Superior activity was dependent on the ability of T_{CM} to traffic first to secondary lymphoid organs rather than peripheral tissues, which may be necessary to engage APCs in tumor-draining lymph nodes. CAR T cells, however, do not depend on interactions with APCs for activation, and one study demonstrated that CAR T cells engineered from CCR7[−] T cells accumulated better within solid tumors than those derived from CCR7⁺ T cells (100). These CAR T cells were more prone to activation-induced cell death, but when CD28 and OX40 costimulation were incorporated into the CAR construct, activation-induced cell death was reduced such that CCR7[−] CAR T cells were more effective at clearing tumors than CCR7⁺ CAR T cells. Thus, the best T cell subset for CAR T cell therapy for solid tumors may differ from the subset suited for hematological malignancies, or from the subset used for TCR-based T cell therapy. Further research is needed to define the genetic manipulations of specific T cell subsets that endow the cells with homing and functional properties needed to infiltrate and effectively target solid tumors.

Overcoming the immunosuppressive TME. Migration of CAR T cells into tumor sites is not sufficient to ensure tumor destruction because of the immunosuppressive TME (Fig. 2). Low pH, hypoxia, an absence of vital nutrients, and stromal and immune cells that release suppressive factors are characteristic of the TME and inhibit T cells. Additionally, tumor and infiltrating cells may express inhibitory receptor ligands like PD-L1 that can directly suppress tumor-specific T cells.

Several groups have attempted to enhance CAR T cell activity by combining ACT with modulators of the TME. A promising avenue is the use of checkpoint inhibitors that target the PD-1/PD-L1 or CTLA-4 pathways, which alone have shown efficacy in some cancers (101). Responsiveness to

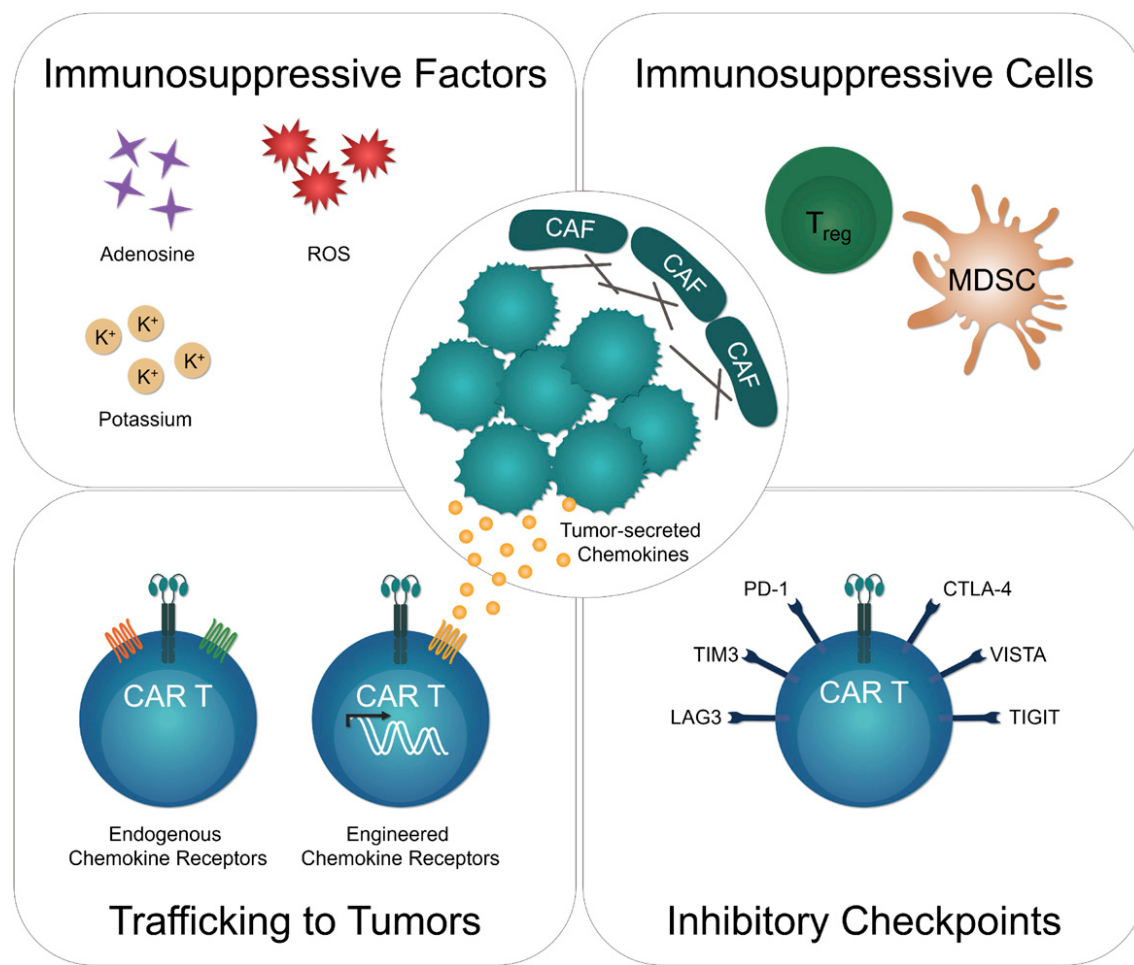


FIGURE 2. Barriers to CAR T cell therapy for solid tumors. Bottom left, CAR T cell trafficking depends on expression of receptors for chemokines secreted by the tumor. CAR T cells endogenously express chemokine receptors like CXCR3 and CCR5, but their cognate ligands are often not highly expressed by solid tumors. CAR T cells can be engineered to express receptors (e.g., CCR2, CCR4) for chemokines naturally secreted by the tumor to improve trafficking to tumors. Bottom right, Ag-activated CAR T cells in the TME upregulate expression of inhibitory receptors, which can lead to T cell dysfunction. Upper left, TME are rich in factors like adenosine, extracellular potassium, and ROS, which can inhibit T cells directly or indirectly. Upper right, Immunosuppressive cells like Tregs and myeloid-derived suppressor cells (MDSCs) can promote tumor growth and inhibit T cell activity both directly and indirectly. CAFs deposit extracellular matrix to limit T cell penetration and can recruit other immunosuppressive cells.

checkpoint blockade was improved by enhancing priming of tumor-specific T cells and might logically be combined with adoptive transfer of CAR T cells, although the risk of toxicity to normal tissues may be increased (99, 102, 103). Other groups have engineered CAR T cells to secrete anti-PD-L1 Abs (104), knocked out PD-1 and LAG-3 using CRISPR (105–107), or coexpressed switch receptors linking the PD-1 ectodomain to the CD28 endodomain such that engagement of PD-L1 delivers an activating rather than inhibitory signal to the T cell (108, 109). Anti-CTLA-4 Abs can also boost endogenous T cell responses to tumors, but the context in which they might improve CAR T cell responses is unclear. CTLA-4 inhibits T cell responses in part by competing with CD28 for binding to CD80/CD86 on dendritic cells and by physically excluding CD28 from the synapse (110). Thus, CAR T cells with a CD28-signaling endodomain may not be intrinsically affected by CTLA-4 regulation. This is supported by a study demonstrating that short hairpin RNA-mediated knockdown of CTLA-4 improved the function of first-generation CAR T cells *in vivo* but not second-generation CAR T cells with CD28 signaling domains (111). However, anti-CTLA-4 Abs also promote immune responses in a cell-extrinsic fashion by depleting CTLA-4⁺ regulatory T cells (Treg) (112, 113), which may benefit

CAR T cells. In addition to inhibitory receptor expression, T cell dysfunction may be acquired in the TME by dysregulation of signaling pathways through upregulation of SHP-1 or diacylglycerol kinase, and pharmacologic inhibition of these enzymes can improve the antitumor function of CAR T cells (114, 115).

Overcoming immunosuppressive cells in the TME is likely to be necessary for CAR T cell efficacy. Depletion of Tregs and myeloid-derived suppressor cells with blocking Abs or genetic manipulation has improved the efficacy of T cell therapy in animal models (116–118). Cancer-associated fibroblasts (CAFs), which comprise a majority of tumor stromal cells and express high levels of fibroblast activation protein (FAP), play a central role in establishing the immunosuppressive microenvironment and depositing extracellular matrix proteins to limit T cell penetration. Targeting CAFs with FAP-specific CAR T cells or engineering CAR T cells to secrete extracellular matrix-degrading enzymes improves their ability to infiltrate and lyse tumors (73, 119). Alternatively, engineering CAR T cells to express the proinflammatory cytokine IL-12 can modulate the TME and promote recruitment and activation of macrophages (73, 75, 120, 121).

A number of studies have focused on improving CAR T cell activity by altering their metabolic profiles to enhance cell function in hostile environments. Tumors are often characterized by high levels of adenosine and reactive oxygen species (ROS), both of which directly impair T cell responses (122, 123). Knocking down the adenosine 2A receptor with short hairpin RNA or cotransducing T cells with catalase to enable breakdown of ROS significantly improved CAR T cell persistence and function *in vivo* (124, 125). Likewise, tumors display elevated levels of extracellular potassium that directly impair TCR-driven Akt-mTOR phosphorylation and effector function. Engineering T cells to overexpress a potassium channel to enable greater potassium efflux effectively undoes this mode of suppression and improves T cell function within the tumor (126).

Overall, CAR T cells face a number of hurdles in combating solid tumors, but some obstacles may be easier to overcome than others. Advances in genetic engineering are proceeding rapidly, and our ability to engineer CARs that, for example, target multiple Ags to overcome tumor heterogeneity and Ag-loss or that coexpress modulators of the TME are now undergoing clinical evaluation. In contrast, one of the highest barriers to success may be the ability of CAR T cells to infiltrate solid tumors. A number of studies have shown that the success of checkpoint inhibitors depends on the presence of tumor-infiltrating T cells, and strategies aimed at enhancing T cell infiltration can overcome tumor resistance to checkpoint inhibition (99, 127). Increasing CAR T cell migration to tumors could potentially increase the response of tumors to other combination therapies as well, such as those aimed at targeting immunosuppressive cells, enhancing CAR survival, and activating the endogenous immune response. Thus, efficient

infiltration of tumors is likely to be a rate-limiting step for CAR T cell therapy.

Moving beyond empirical testing

Given the myriad ways in which tumors can suppress T cells, the number of genetic manipulations and combination therapies that could be tested in the clinic are seemingly limitless. A challenge for the field is the need for faithful preclinical models to screen therapeutic combinations before clinical translation. Better tools to analyze posttreatment biopsies will also help maximize our understanding of what resistance mechanisms may evolve and inform the design of future combination therapies.

Models for CAR T cell therapy. A challenge for preclinical studies evaluating the efficacy of CAR T cells is having clinically relevant models that recapitulate the obstacles in human solid tumors (Fig. 3). Most studies have relied on transplanted human tumor xenografts in immune-compromised NOD/SCID/ $\gamma c^{-/-}$ (NSG) mice that lack T cells, NK cells, and B cells. The NSG model allows rapid analysis of human T cell recognition of tumor cells *in vivo* and is useful to evaluate T cell persistence and effector function. However, NSG models fail to develop a clinically relevant TME and do not inform the safety of targets that lack epitope homology and/or normal tissue expression. ACT is also studied in immune-competent syngeneic mouse models, but a majority of these models implant tumor cells into foreign anatomical sites where the tumors grow rapidly and do not coevolve with the host immune system in the same way as human tumors (128). Moreover, endogenous antitumor immune responses are higher in transplanted than autochthonous tumors for the

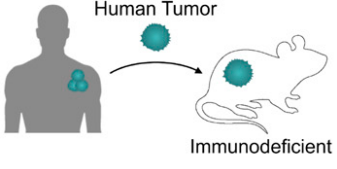
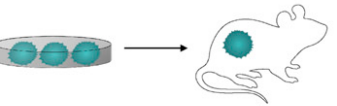
	Pros	Cons
Xenogeneic Transplantable	 <ul style="list-style-type: none"> Predicts persistence and lytic ability of human CAR T cells Predicts drug response of human tumors Technically easy to use 	<ul style="list-style-type: none"> No host immune system No tumor microenvironment Cannot answer questions about T cell trafficking, function within the tumor microenvironment, or interaction with host immune cells
Syngeneic Transplantable	 <ul style="list-style-type: none"> Intact host immune system Some TME develops Cell lines can be engineered to express neoantigens or tumor targets Technically easy to use 	<ul style="list-style-type: none"> Tumors are fully mature at implantation and do not co-evolve with host immune system Transplantation process can be artificially immunogenic TME is present but artificial
GEM Spontaneous	 <ul style="list-style-type: none"> Tumors develop from clinically relevant mutations and evolve naturally with host immune system Realistic TME develops 	<ul style="list-style-type: none"> Oncogenic mutations are present from birth; central tolerance may develop to mutations or neoantigens Model is slow and variable Time to tumor development is variable Introducing neoantigens or tumor targets requires complex breeding
GEM Inducible	 <ul style="list-style-type: none"> Tumors develop from clinically relevant mutations and evolve naturally with host immune system Realistic TME develops Tumor initiation can be synchronized by inducible event Neoantigens/tumor targets can be introduced easily 	<ul style="list-style-type: none"> Model is slow and variable Technically complex

FIGURE 3. Comparison of mouse models for human solid tumors.

same disease, suggesting the implantation process artificially increases immunogenicity (129, 130).

An alternative to transplantable models is to induce malignant transformation in normal cells *in situ* with defined oncogenic events. Such genetically engineered mouse (GEM) models recapitulate tumor initiation, progression, and the genetic and histopathological characteristics of human cancers (128). Oncogenic mutations in Kras and p53 can be introduced at birth through a Cre/lox system, such as in the KPC (Kras^{LSL-G12D/+}; p53^{fl/fl}; Pdx1-Cre) model of pancreatic adenocarcinoma, where a Pdx1-driven Cre restricts the mutations to the pancreas (131). A disadvantage of tissue-restricted Cre expression is that cancer is induced throughout the entire tissue, and the presence of mutations from birth may affect central tolerance and influence the evolution of immune responses differently than if mutations were acquired postnatally. To address this, Tyler Jacks's group developed an inducible KP GEM model of lung adenocarcinoma in which intratracheal infection with Cre-expressing lentivirus initiates p53 deletion and Kras^{G12D} activation in individual lung epithelial cells (132). Importantly, this model mimics both the development and therapeutic response of human lung adenocarcinomas (99). A drawback of GEM models, however, is their relative lack of CAR targets and neoantigens relative to carcinogen-induced models and human cancer (133). However, model Ags can easily be introduced in the KP model by engineering the lentivirus, and exposing Kras-mutant GEM mice to tobacco smoke can induce a more realistic mutational landscape.

GEM models that reflect the TME of human tumors may give more accurate estimates of treatment efficacy and offer insight into resistance mechanisms that evolve and pathways to target with combination therapy (134). For example, recent studies have used GEM models to study Tregs in tumor development and test strategies for Treg inhibition. One approach to Treg inhibition may be to block IL-35, an immunosuppressive cytokine secreted by tumor-resident Tregs that promotes T_E exhaustion in part by promoting expression of inhibitory receptors like PD-1, TIM-3, and LAG-3 (135). Interestingly, this model accurately predicted that IL-35 and PD-1 blockade would not synergize because IL-35 overexpression and PD-1 upregulation are part of the same suppressive pathway. Thus, it is anticipated that GEM models will be useful for studying impediments to CAR T cell therapy of solid tumors and for identifying rational combination therapies for clinical translation.

Advances in immune monitoring of clinical trials. Identifying methods to enhance CAR T cell therapy will be assisted by discovery-driven approaches to clinical trials. Collecting tumor biopsies and blood pre- and posttreatment, enables thorough analysis of tumors by flow cytometry, immunohistochemistry, and unbiased genome-wide RNA sequencing, and can identify correlates of clinical success or failure. Response to anti-CTLA-4 therapy of localized bladder cancer, for example, was associated with upregulation of ICOS on T cells (136, 137); subsequent studies in mice demonstrated that ICOS expression was required for the efficacy of anti-CTLA-4 *in vivo* and that activation of the ICOS/ICOSL pathway synergistically enhanced response to anti-CTLA-4 (138, 139). Similar analysis of pre- and posttreatment biopsies and transcriptomic and epigenetic analysis of CD19 CAR T cells are being

performed to identify mechanisms of resistance in the ~50% of NHL patients that do not achieve a CR, and where CD19 loss is not the mechanism of escape (27, 28, 42, 140).

New technologies with improved sensitivity and systems analysis will facilitate the identification of pathways associated with therapy response or resistance. Single-cell RNA sequencing can provide unbiased insight into tumor responses, revealing differences in gene transcription that may be obscured by heterogeneity at the cell-population level. At the protein level, methods such as cytometry by time of flight allow analysis of 40 (and up to 100 theoretically) proteins simultaneously, providing high resolution of cell phenotype, and can be coupled to immunohistochemical methods to obtain spatial information of proteins and protein modifications at subcellular resolution (141). Additionally, the development of multiplex immunohistochemistry allows detection of multiple biomarkers simultaneously on tumor biopsies and visualization of cell subsets with tissue architecture preserved. Integrating longitudinal data from gene expression, epigenetics, flow and mass cytometry, and immunohistochemistry will provide a comprehensive understanding of patient responses to therapy and should guide the development of rational, rather than empirical, combinations.

Conclusions

Progress in immune-based therapies is improving outcomes for many patients with advanced malignancies. The development of CAR T cells represents a convergence of insights from multiple scientific fields, but success has thus far been limited to B cell malignancies. Extending this approach to other cancers will require the development of strategies based on understanding the obstacles posed by tumor heterogeneity and the TME that is emerging from sophisticated analytical tools and superior models. These strategies will take advantage of our unprecedented ability to genetically manipulate T cells to confer novel functions, enabling them to target tumor cells and persist and function in hostile circumstances.

Disclosures

S.R.R. is a founder and consultant for Juno Therapeutics and receives research support from Juno Therapeutics. The other author has no financial conflicts of interest.

References

1. Sadelain, M., I. Rivière, and S. Riddell. 2017. Therapeutic T cell engineering. *Nature* 545: 423–431.
2. Eshhar, Z., T. Waks, G. Gross, and D. G. Schindler. 1993. Specific activation and targeting of cytotoxic lymphocytes through chimeric single chains consisting of antibody-binding domains and the gamma or zeta subunits of the immunoglobulin and T-cell receptors. *Proc. Natl. Acad. Sci. USA* 90: 720–724.
3. Maher, J., R. J. Brentjens, G. Gunset, I. Rivière, and M. Sadelain. 2002. Human T-lymphocyte cytotoxicity and proliferation directed by a single chimeric TCRzeta/CD28 receptor. *Nat. Biotechnol.* 20: 70–75.
4. Kershaw, M. H., M. W. Teng, M. J. Smyth, and P. K. Darcy. 2005. Supernatural T cells: genetic modification of T cells for cancer therapy. *Nat. Rev. Immunol.* 5: 928–940.
5. Imai, C., K. Miura, M. Andreansky, I. C. Nicholson, C. H. Pui, T. L. Geiger, and D. Campana. 2004. Chimeric receptors with 4-1BB signaling capacity provoke potent cytotoxicity against acute lymphoblastic leukemia. *Leukemia* 18: 676–684.
6. Srivastava, S., and S. R. Riddell. 2015. Engineering CAR-T cells: design concepts. *Trends Immunol.* 36: 494–502.
7. Kawalekar, O. U., R. S. O'Connor, J. A. Fraietta, L. Guo, S. E. McGettigan, A. D. Posey, Jr., P. R. Patel, S. Guedan, J. Scholler, B. Keith, et al. 2016. Distinct signaling of coreceptors regulates specific metabolism pathways and impacts memory development in CAR T cells. [Published erratum appears in 2016 *Immunity* 44: 712.] *Immunity* 44: 380–390.
8. Zhao, Z., M. Condomines, S. J. C. van der Stegen, F. Perna, C. C. Kloss, G. Gunset, J. Plotkin, and M. Sadelain. 2015. Structural design of engineered

- costimulation determines tumor rejection kinetics and persistence of CAR T cells. *Cancer Cell* 28: 415–428.
9. Wu, C. Y., K. T. Roybal, E. M. Puchner, J. Onuffer, and W. A. Lim. 2015. Remote control of therapeutic T cells through a small molecule-gated chimeric receptor. *Science* 350: aab4077.
 10. Roybal, K. T., L. J. Rupp, L. Morsut, W. J. Walker, K. A. McNally, J. S. Park, and W. A. Lim. 2016. Precision tumor recognition by T cells with combinatorial antigen-sensing circuits. *Cell* 164: 770–779.
 11. Eyquem, J., J. Mansilla-Soto, T. Giavridis, S. J. van der Stegen, M. Hamieh, K. M. Cunanan, A. Odak, M. Gönen, and M. Sadelain. 2017. Targeting a CAR to the TRAC locus with CRISPR/Cas9 enhances tumour rejection. *Nature* 543: 113–117.
 12. Fedorov, V. D., M. Themeli, and M. Sadelain. 2013. PD-1- and CTLA-4-based inhibitory chimeric antigen receptors (iCARs) divert off-target immunotherapy responses. *Sci. Transl. Med.* 5: 215ra172.
 13. Kloss, C. C., M. Condomines, M. Cartellieri, M. Bachmann, and M. Sadelain. 2013. Combinatorial antigen recognition with balanced signaling promotes selective tumor eradication by engineered T cells. *Nat. Biotechnol.* 31: 71–75.
 14. Paszkiewicz, P. J., S. P. Fräße, S. Srivastava, D. Sommermeyer, M. Hudecek, I. Drexler, M. Sadelain, L. Liu, M. C. Jensen, S. R. Riddell, and D. H. Busch. 2016. Targeted antibody-mediated depletion of murine CD19 CAR T cells permanently reverses B cell aplasia. *J. Clin. Invest.* 126: 4262–4272.
 15. Diaconu, I., B. Ballard, M. Zhang, Y. Chen, J. West, G. Dotti, and B. Savoldo. 2017. Inducible caspase-9 selectively modulates the toxicities of CD19-specific chimeric antigen receptor-modified T cells. *Mol. Ther.* 25: 580–592.
 16. Gattinoni, L., C. A. Klebanoff, and N. P. Restifo. 2012. Paths to stemness: building the ultimate antitumour T cell. *Nat. Rev. Cancer* 12: 671–684.
 17. Gattinoni, L., E. Lugli, Y. Ji, Z. Pos, C. M. Paulos, M. F. Quigley, J. R. Almeida, E. Gostick, Z. Yu, C. Carpenito, et al. 2011. A human memory T cell subset with stem cell-like properties. *Nat. Med.* 17: 1290–1297.
 18. Sathaliyawala, T., M. Kubota, N. Yudanin, D. Turner, P. Camp, J. J. Thome, K. L. Bickham, H. Lerner, M. Goldstein, M. Sykes, et al. 2013. Distribution and compartmentalization of human circulating and tissue-resident memory T cell subsets. *Immunity* 38: 187–197.
 19. Gerlach, C., J. C. Rohr, L. Perié, N. van Rooij, J. W. van Heijst, A. Velds, J. Urbanus, S. H. Naik, H. Jacobs, J. B. Beltman, et al. 2013. Heterogeneous differentiation patterns of individual CD8+ T cells. *Science* 340: 635–639.
 20. Buchholz, V. R., M. Flossdorf, I. Hensel, L. Kretschmer, B. Weissbrich, P. Gräf, A. Verschoor, M. Schiemann, T. Höfer, and D. H. Busch. 2013. Disparate individual fates compose robust CD8+ T cell immunity. *Science* 340: 630–635.
 21. Graef, P., V. R. Buchholz, C. Stemberger, M. Flossdorf, L. Henkel, M. Schiemann, I. Drexler, T. Höfer, S. R. Riddell, and D. H. Busch. 2014. Serial transfer of single-cell-derived immunocompetence reveals stemness of CD8(+) central memory T cells. *Immunity* 41: 116–126.
 22. Berger, C., M. C. Jensen, P. M. Lansdorp, M. Gough, C. Elliott, and S. R. Riddell. 2008. Adoptive transfer of effector CD8+ T cells derived from central memory cells establishes persistent T cell memory in primates. *J. Clin. Invest.* 118: 294–305.
 23. Klebanoff, C. A., L. Gattinoni, P. Torabi-Parizi, K. Kerstann, A. R. Cardones, S. E. Finkelstein, D. C. Palmer, P. A. Antony, S. T. Hwang, S. A. Rosenberg, et al. 2005. Central memory self/tumor-reactive CD8+ T cells confer superior antitumor immunity compared with effector memory T cells. *Proc. Natl. Acad. Sci. USA* 102: 9571–9576.
 24. Sommermeyer, D., M. Hudecek, P. L. Kosasih, T. Gogishvili, D. G. Maloney, C. J. Turtle, and S. R. Riddell. 2016. Chimeric antigen receptor-modified T cells derived from defined CD8+ and CD4+ subsets confer superior antitumor reactivity in vivo. *Leukemia* 30: 492–500.
 25. Wang, X., C. W. Wong, R. Urak, E. Taus, B. Aguirar, W. C. Chang, A. Mardiros, L. E. Budde, C. E. Brown, C. Berger, et al. 2015. Comparison of naïve and central memory derived CD8+ effector cell engraftment fitness and function following adoptive transfer. *Oncotarget* 5: e1072671.
 26. Turtle, C. J., L. A. Hanafi, C. Berger, T. A. Gooley, S. Cherian, M. Hudecek, D. Sommermeyer, K. Melville, B. Pender, T. M. Budiarto, et al. 2016. CD19 CAR-T cells of defined CD4+:CD8+ composition in adult B cell ALL patients. *J. Clin. Invest.* 126: 2123–2138.
 27. Turtle, C. J., K. A. Hay, L. A. Hanafi, D. Li, S. Cherian, X. Chen, B. Wood, A. Lozanski, J. C. Byrd, S. Heimfeld, et al. 2017. Durable molecular remissions in chronic lymphocytic leukemia treated with CD19-specific chimeric antigen receptor-modified T cells after failure of ibrutinib. *J. Clin. Oncol.* 35: 3010–3020.
 28. Turtle, C. J., L. A. Hanafi, C. Berger, M. Hudecek, B. Pender, E. Robinson, R. Hawkins, C. Chaney, S. Cherian, X. Chen, et al. 2016. Immunotherapy of non-Hodgkin's lymphoma with a defined ratio of CD8+ and CD4+ CD19-specific chimeric antigen receptor-modified T cells. *Sci. Transl. Med.* 8: 355ra116.
 29. Kowollik, C. M., M. S. Topp, S. Gonzalez, T. Pfeiffer, S. Olivares, N. Gonzalez, D. D. Smith, S. J. Forman, M. C. Jensen, and L. J. Cooper. 2006. CD28 costimulation provided through a CD19-specific chimeric antigen receptor enhances in vivo persistence and antitumor efficacy of adoptively transferred T cells. *Cancer Res.* 66: 10995–11004.
 30. Brentjens, R. J., E. Santos, Y. Nikhamin, R. Yeh, M. Matsushita, K. La Perle, A. Quintás-Cardama, S. M. Larson, and M. Sadelain. 2007. Genetically targeted T cells eradicate systemic acute lymphoblastic leukemia xenografts. *Clin. Cancer Res.* 13: 5426–5435.
 31. Milone, M. C., J. D. Fish, C. Carpenito, R. G. Carroll, G. K. Binder, D. Teachey, M. Samanta, M. Lakhal, B. Gloss, G. Danet-Desnoyers, et al. 2009. Chimeric receptors containing CD137 signal transduction domains mediate enhanced survival of T cells and increased antileukemic efficacy in vivo. *Mol. Ther.* 17: 1453–1464.
 32. Hudecek, M., D. Sommermeyer, P. L. Kosasih, A. Silva-Benedict, L. Liu, C. Rader, M. C. Jensen, and S. R. Riddell. 2015. The nonsignaling extracellular spacer domain of chimeric antigen receptors is decisive for in vivo antitumor activity. *Cancer Immunol. Res.* 3: 125–135.
 33. Brentjens, R. J., M. L. Davila, I. Riviere, J. Park, X. Wang, L. G. Cowell, S. Bartido, J. Stefanski, C. Taylor, M. Olszewska, et al. 2013. CD19-targeted T cells rapidly induce molecular remissions in adults with chemotherapy-refractory acute lymphoblastic leukemia. *Sci. Transl. Med.* 5: 177ra38.
 34. Kalos, M., B. L. Levine, D. L. Porter, S. Katz, S. A. Grupp, A. Bagg, and C. H. June. 2011. T cells with chimeric antigen receptors have potent antitumor effects and can establish memory in patients with advanced leukemia. *Sci. Transl. Med.* 3: 95ra73.
 35. Kochenderfer, J. N., M. E. Dudley, S. A. Feldman, W. H. Wilson, D. E. Spaner, I. Maric, M. Stetler-Stevenson, G. Q. Phan, M. S. Hughes, R. M. Sherry, et al. 2012. B-cell depletion and remissions of malignancy along with cytokine-associated toxicity in a clinical trial of anti-CD19 chimeric-antigen-receptor-transduced T cells. *Blood* 119: 2709–2720.
 36. Kochenderfer, J. N., W. H. Wilson, J. E. Janik, M. E. Dudley, M. Stetler-Stevenson, S. A. Feldman, I. Maric, M. Raffeld, D. A. Nathan, B. J. Lanier, et al. 2010. Eradication of B-lineage cells and regression of lymphoma in a patient treated with autologous T cells genetically engineered to recognize CD19. *Blood* 116: 4099–4102.
 37. Davila, M. L., I. Riviere, X. Wang, S. Bartido, J. Park, K. Curran, S. S. Chung, J. Stefanski, O. Borquez-Ojeda, M. Olszewska, et al. 2014. Efficacy and toxicity management of 19-28z CAR T cell therapy in B cell acute lymphoblastic leukemia. *Sci. Transl. Med.* 6: 224ra25.
 38. Gardner, R. A., O. Finney, C. Annesley, H. Brakke, C. Summers, K. Leger, M. Bleakley, C. Brown, S. McGeeroff, K. S. Kelly-Spratt, et al. 2017. Intent-to-treat leukemia remission by CD19 CAR T cells of defined formulation and dose in children and young adults. *Blood* 129: 3322–3331.
 39. Lee, D. W., J. N. Kochenderfer, M. Stetler-Stevenson, Y. K. Cui, C. Delbrook, S. A. Feldman, T. J. Fry, R. Orentas, M. Sabatino, N. N. Shah, et al. 2015. T cells expressing CD19 chimeric antigen receptors for acute lymphoblastic leukaemia in children and young adults: a phase I dose-escalation trial. *Lancet* 385: 517–528.
 40. Maude, S. L., N. Frey, P. A. Shaw, R. Aplenc, D. M. Barrett, N. J. Bunin, A. Chew, V. E. Gonzalez, Z. Zheng, S. F. Lacey, et al. 2014. Chimeric antigen receptor T cells for sustained remissions in leukemia. *N. Engl. J. Med.* 371: 1507–1517.
 41. Kochenderfer, J. N., M. E. Dudley, S. H. Kassim, R. P. Somerville, R. O. Carpenter, M. Stetler-Stevenson, J. C. Yang, G. Q. Phan, M. S. Hughes, R. M. Sherry, et al. 2015. Chemotherapy-refractory diffuse large B-cell lymphoma and indolent B-cell malignancies can be effectively treated with autologous T cells expressing an anti-CD19 chimeric antigen receptor. *J. Clin. Oncol.* 33: 540–549.
 42. Locke, F. L., S. S. Neelapu, N. L. Bartlett, T. Siddiqi, J. C. Chavez, C. M. Hosing, A. Ghobadi, L. E. Budde, A. Bot, J. M. Rossi, et al. 2017. Phase 1 results of ZUMA-1: a multicenter study of KTE-C19 anti-CD19 CAR T cell therapy in refractory aggressive lymphoma. *Mol. Ther.* 25: 285–295.
 43. Kochenderfer, J. N., R. P. T. Somerville, T. Lu, V. Shi, A. Bot, J. Rossi, A. Xue, S. L. Goff, J. C. Yang, R. M. Sherry, et al. 2017. Lymphoma remissions caused by anti-CD19 chimeric antigen receptor T cells are associated with high serum interleukin-15 levels. *J. Clin. Oncol.* 35: 1803–1813.
 44. Kochenderfer, J. N., R. P. T. Somerville, T. Lu, J. C. Yang, R. M. Sherry, S. A. Feldman, L. McIntyre, A. Bot, J. Rossi, N. Lam, and S. A. Rosenberg. 2017. Long-duration complete remissions of diffuse large B cell lymphoma after anti-CD19 chimeric antigen receptor T cell therapy. *Mol. Ther.* 25: 2245–2253.
 45. Lee, D. W., R. Gardner, D. L. Porter, C. U. Louis, N. Ahmed, M. Jensen, S. A. Grupp, and C. L. Mackall. 2014. Current concepts in the diagnosis and management of cytokine release syndrome. [Published erratum appears in 2015 Blood 126: 1048.] *Blood* 124: 188–195.
 46. Gust, J. K. A. Hay, L.-A. Hanafi, D. Li, D. Myerson, L. F. Gonzalez-Cuyar, C. Yeung, W. C. Liles, M. Wurfel, J. A. Lopez, et al. 2017. Endothelial activation and blood-brain barrier disruption in neurotoxicity after adoptive immunotherapy with CD19 CAR-T cells. *Cancer Discov.* DOI: 10.1158/2159-8290.CD-17-0698. 10.1158/2159-8290.CD-17-0698
 47. Ritchie, D. S., P. J. Neeson, A. Khot, S. Peinert, T. Tai, K. Tainton, K. Chen, M. Shin, D. M. Wall, D. Höinemann, et al. 2013. Persistence and efficacy of second generation CAR T cell against the LeY antigen in acute myeloid leukemia. *Mol. Ther.* 21: 2122–2129.
 48. Tettamanti, S., V. Marin, I. Pizzitola, C. F. Magnani, G. M. Giordano Attianese, E. Cribioli, F. Maltese, S. Galimberti, A. F. Lopez, A. Biondi, et al. 2013. Targeting of acute myeloid leukaemia by cytokine-induced killer cells redirected with a novel CD123-specific chimeric antigen receptor. *Br. J. Haematol.* 161: 389–401.
 49. Carpenter, R. O., M. O. Ebvwuwan, S. Pittaluga, J. J. Rose, M. Raffeld, S. Yang, R. E. Gress, F. T. Hakim, and J. N. Kochenderfer. 2013. B-cell maturation antigen is a promising target for adoptive T-cell therapy of multiple myeloma. *Clin. Cancer Res.* 19: 2048–2060.
 50. Chu, J., S. He, Y. Deng, J. Zhang, Y. Peng, T. Hughes, L. Yi, C. H. Kwon, Q. E. Wang, S. M. Devine, et al. 2014. Genetic modification of T cells redirected toward CS1 enhances eradication of myeloma cells. *Clin. Cancer Res.* 20: 3989–4000.
 51. Ali, S. A., V. Shi, I. Maric, M. Wang, D. F. Stroncek, J. J. Rose, J. N. Brudno, M. Stetler-Stevenson, S. A. Feldman, B. G. Hansen, et al. 2016. T cells expressing an anti-B-cell maturation antigen chimeric antigen receptor cause remissions of multiple myeloma. *Blood* 128: 1688–1700.
 52. Morgan, R. A., J. C. Yang, M. Kitano, M. E. Dudley, C. M. Laurencot, and S. A. Rosenberg. 2010. Case report of serious adverse event following the administration of T cells transduced with a chimeric antigen receptor recognizing ERBB2. *Mol. Ther.* 18: 843–851.
 53. Ahmed, N., V. Brawley, M. Hegde, K. Bielamowicz, M. Kalra, D. Landi, C. Robertson, T. L. Gray, O. Diouf, A. Wakefield, et al. 2017. HER2-specific

- chimeric antigen receptor-modified virus-specific T cells for progressive glioblastoma: a phase 1 dose-escalation trial. *JAMA Oncol.* 3: 1094–1101.
54. Ahmed, N., V. S. Brawley, M. Hegde, C. Robertson, A. Ghazi, C. Gerken, E. Liu, O. Dakhova, A. Ashoori, A. Corder, et al. 2015. Human epidermal growth factor receptor 2 (HER2)-specific chimeric antigen receptor-modified T cells for the immunotherapy of HER2-positive sarcoma. *J. Clin. Oncol.* 33: 1688–1696.
 55. O'Rourke, D. M., M. P. Nasrallah, A. Desai, J. J. Melenhorst, K. Mansfield, J. J. D. Morissette, M. Martinez-Lage, S. Brem, E. Maloney, A. Shen, et al. 2017. A single dose of peripherally infused EGFRvIII-directed CAR T cells mediates antigen loss and induces adaptive resistance in patients with recurrent glioblastoma. *Sci. Transl. Med.* 9: eaaa0984.
 56. Brown, C. E., D. Alizadeh, R. Starr, L. Weng, J. R. Wagner, A. Naranjo, J. R. Ostberg, M. S. Blanchard, J. Kilpatrick, J. Simpson, et al. 2016. Regression of glioblastoma after chimeric antigen receptor T-cell therapy. *N. Engl. J. Med.* 375: 2561–2569.
 57. Heczey, A., C. U. Louis, B. Savoldo, O. Dakhova, A. Durett, B. Grilley, H. Liu, M. F. Wu, Z. Mei, A. Gee, et al. 2017. CAR T cells administered in combination with lymphodepletion and PD-1 inhibition to patients with neuroblastoma. *Mol. Ther.* 25: 2214–2224.
 58. Pule, M. A., B. Savoldo, G. D. Myers, C. Rossig, H. V. Russell, G. Dotti, M. H. Huls, E. Liu, A. P. Gee, Z. Mei, et al. 2008. Virus-specific T cells engineered to coexpress tumor-specific receptors: persistence and antitumor activity in individuals with neuroblastoma. *Nat. Med.* 14: 1264–1270.
 59. Balakrishnan, A., T. Goodpaster, J. Randolph-Habecker, B. G. Hoffstrom, F. G. Jalikis, L. K. Koch, C. Berger, P. L. Kosasih, A. Rajan, D. Sommermeyer, et al. 2017. Analysis of ROR1 protein expression in human cancer and normal tissues. *Clin. Cancer Res.* 23: 3061–3071.
 60. Beatty, G. L., A. R. Haas, M. V. Maus, D. A. Torigian, M. C. Soulard, G. Plesa, A. Chew, Y. Zhao, B. L. Levine, S. M. Albelda, et al. 2014. Mesothelin-specific chimeric antigen receptor mRNA-engineered T cells induce anti-tumor activity in solid malignancies. *Cancer Immunol. Res.* 2: 112–120.
 61. Berger, C., D. Sommermeyer, M. Hudecek, M. Berger, A. Balakrishnan, P. J. Paszkiewicz, P. L. Kosasih, C. Rader, and S. R. Riddell. 2015. Safety of targeting ROR1 in primates with chimeric antigen receptor-modified T cells. *Cancer Immunol. Res.* 3: 206–216.
 62. Koneru, M., R. O'Cearbhail, S. Pendharkar, D. R. Spriggs, and R. J. Brentjens. 2015. A phase I clinical trial of adoptive T cell therapy using IL-12 secreting MUC-16(ecto) directed chimeric antigen receptors for recurrent ovarian cancer. *J. Transl. Med.* 13: 102.
 63. Wei, X., Y. Lai, J. Li, L. Qin, Y. Xu, R. Zhao, B. Li, S. Lin, S. Wang, Q. Wu, et al. 2017. PSCA and MUC1 in non-small-cell lung cancer as targets of chimeric antigen receptor T cells. *Oncimmunology* 6: e1284722.
 64. Gardner, R., D. Wu, S. Cherian, M. Fang, L. A. Hanafi, O. Finney, H. Smithers, M. C. Jensen, S. R. Riddell, D. G. Maloney, and C. J. Turtle. 2016. Acquisition of a CD19-negative myeloid phenotype allows immune escape of MLL-rearranged B-ALL from CD19 CAR-T-cell therapy. *Blood* 127: 2406–2410.
 65. Sotillo, E., D. M. Barrett, K. L. Black, A. Bagashev, D. Oldridge, G. Wu, R. Sussman, C. Lanauze, M. Ruella, M. R. Gazzara, et al. 2015. Convergence of acquired mutations and alternative splicing of CD19 enables resistance to CART-19 immunotherapy. *Cancer Discov.* 5: 1282–1295.
 66. Grada, Z., M. Hegde, T. Byrd, D. R. Shaffer, A. Ghazi, V. S. Brawley, A. Corder, K. Schönfeld, J. Koch, G. Dotti, et al. 2013. TanCAR: a novel bispecific chimeric antigen receptor for cancer immunotherapy. *Mol. Ther. Nucleic Acids* 2: e105.
 67. Davies, D. M., J. Foster, S. J. Van Der Stegen, A. C. Parente-Pereira, L. Chiapero-Stanke, G. J. Delinassios, S. E. Burbridge, V. Kao, Z. Liu, L. Bosshard-Carter, et al. 2012. Flexible targeting of ErbB dimers that drive tumorigenesis by using genetically engineered T cells. *Mol. Med.* 18: 565–576.
 68. Sentman, C. L., and K. R. Meehan. 2014. NKG2D CARs as cell therapy for cancer. *Cancer J.* 20: 156–159.
 69. Ruella, M., D. M. Barrett, S. S. Kenderian, O. Shestova, T. J. Hofmann, J. Perazzelli, M. Klischinsky, V. Aikawa, F. Nazimuddin, M. Kozlowski, et al. 2016. Dual CD19 and CD123 targeting prevents antigen-loss relapses after CD19-directed immunotherapies. *J. Clin. Invest.* 126: 3814–3826.
 70. Schneider, D., Y. Xiong, D. Wu, V. Nölle, S. Schmitz, W. Haso, A. Kaiser, B. Dropulic, and R. J. Orentas. 2017. A tandem CD19/CD20 CAR lentiviral vector drives on-target and off-target antigen modulation in leukemia cell lines. *J. Immunother.* Cancer 5: 42.
 71. Anuradhan, U., R. C. Chan, H. F. Hindi, R. Muchtarla, P. Bajgain, B. C. Hayes, W. E. Fisher, H. E. Heslop, C. M. Rooney, M. K. Brenner, et al. 2014. Kinetics of tumor destruction by chimeric antigen receptor-modified T cells. *Mol. Ther.* 22: 623–633.
 72. Hegde, M., A. Corder, K. K. Chow, M. Mukherjee, A. Ashoori, Y. Kew, Y. J. Zhang, D. S. Baskin, F. A. Merchant, V. S. Brawley, et al. 2013. Combinational targeting offsets antigen escape and enhances effector functions of adoptively transferred T cells in glioblastoma. [Published erratum appears in 2014 Mol. Ther. 22: 1063.] *Mol. Ther.* 21: 2087–2101.
 73. Wang, L. C., A. Lo, J. Scholler, J. Sun, R. S. Majumdar, V. Kapoor, M. Antzis, C. E. Cotter, L. A. Johnson, A. C. Durham, et al. 2014. Targeting fibroblast activation protein in tumor stroma with chimeric antigen receptor T cells can inhibit tumor growth and augment host immunity without severe toxicity. *Cancer Immunol. Res.* 2: 154–166.
 74. Zhang, T., M. R. Wu, and C. L. Sentman. 2012. An NKP30-based chimeric antigen receptor promotes T cell effector functions and antitumor efficacy in vivo. *J. Immunol.* 189: 2290–2299.
 75. Chmielewski, M., C. Kopecky, A. A. Hombach, and H. Abken. 2011. IL-12 release by engineered T cells expressing chimeric antigen receptors can effectively muster an antigen-independent macrophage response on tumor cells that have shut down tumor antigen expression. *Cancer Res.* 71: 5697–5706.
 76. Curran, K. J., B. A. Seinstra, Y. Nikhamin, R. Yeh, Y. Usachenko, D. G. van Leeuwen, T. Purdon, H. J. Pegram, and R. J. Brentjens. 2015. Enhancing anti-tumor efficacy of chimeric antigen receptor T cells through constitutive CD40L expression. *Mol. Ther.* 23: 769–778.
 77. Stephan, M. T., V. Ponomarev, R. J. Brentjens, A. H. Chang, K. V. Dobrenkov, G. Heller, and M. Sadelain. 2007. T cell-encoded CD80 and 4-1BBL induce auto- and transcostimulation, resulting in potent tumor rejection. *Nat. Med.* 13: 1440–1449.
 78. Cao, Y., J. D. Marks, Q. Huang, S. I. Rudnick, C. Xiong, W. N. Hittelman, X. Wen, J. W. Marks, L. H. Cheung, K. Boland, et al. 2012. Single-chain antibody-based immunotoxins targeting Her2/neu: design optimization and impact of affinity on antitumor efficacy and off-target toxicity. *Mol. Cancer Ther.* 11: 143–153.
 79. Drent, E., M. Themeli, R. Poels, R. de Jong-Korlaar, H. Yuan, J. de Bruijn, A. C. M. Martens, S. Zweegman, N. W. C. J. van de Donk, R. W. J. Groen, et al. 2017. A rational strategy for reducing on-target off-tumor effects of CD38-chimeric antigen receptors by affinity optimization. *Mol. Ther.* 25: 1946–1958.
 80. Liu, X., S. Jiang, C. Fang, S. Yang, D. Olalere, E. C. Pequinot, A. P. Cogdill, N. Li, M. Ramones, B. Granda, et al. 2015. Affinity-tuned ErbB2 or EGFR chimeric antigen receptor T cells exhibit an increased therapeutic index against tumors in mice. *Cancer Res.* 75: 3596–3607.
 81. Wilkie, S., M. C. van Schalkwyk, S. Hobbs, D. M. Davies, S. J. van der Stegen, A. C. Pereira, S. E. Burbridge, C. Box, S. A. Eccles, and J. Maher. 2012. Dual targeting of ErbB2 and MUC1 in breast cancer using chimeric antigen receptors engineered to provide complementary signaling. *J. Clin. Immunol.* 32: 1059–1070.
 82. Juillerat, A., A. Marchal, J. M. Filhol, J. Valton, A. Duclert, L. Poirot, and P. Duchateau. 2016. Design of chimeric antigen receptors with integrated controllable transient functions. *Sci. Rep.* 6: 18950.
 83. Sakemura, R., S. Terakura, K. Watanabe, J. Julamane, E. Takagi, K. Miyao, D. Koyama, T. Goto, R. Hanajiri, T. Nishida, et al. 2016. A tet-on inducible system for controlling CD19-chimeric antigen receptor expression upon drug administration. *Cancer Immunol. Res.* 4: 658–668.
 84. Juillerat, A., A. Marchal, J. M. Filhol, Y. Valogne, J. Valton, A. Duclert, P. Duchateau, and L. Poirot. 2017. An oxygen sensitive self-decision making engineered CAR T-cell. *Sci. Rep.* 7: 39833.
 85. Spranger, S., R. Bao, and T. F. Gajewski. 2015. Melanoma-intrinsic β -catenin signaling prevents anti-tumour immunity. *Nature* 523: 231–235.
 86. Spranger, S., D. Dai, B. Horton, and T. F. Gajewski. 2017. Tumor-residing Batf3 dendritic cells are required for effector T cell trafficking and adoptive T cell therapy. *Cancer Cell* 31: 711–723.e714.
 87. Kohanbash, G., D. A. Carrera, S. Shrivastav, B. J. Ahn, N. Jahan, T. Mazor, Z. S. Chheda, K. M. Downey, P. B. Watchmaker, C. Beppler, et al. 2017. Isocitrate dehydrogenase mutations suppress STAT1 and CD8+ T cell accumulation in gliomas. *J. Clin. Invest.* 127: 1425–1437.
 88. Adusumilli, P. S., L. Cherkassky, J. Villena-Vargas, C. Colovos, E. Servais, J. Plotkin, D. R. Jones, and M. Sadelain. 2014. Regional delivery of mesothelin-targeted CAR T cell therapy generates potent and long-lasting CD4-dependent tumor immunity. *Sci. Transl. Med.* 6: 261ra151.
 89. Newick, K., S. O'Brien, J. Sun, V. Kapoor, S. Maceyko, A. Lo, E. Puré, E. Moon, and S. M. Albelda. 2016. Augmentation of CAR T-cell trafficking and antitumor efficacy by blocking protein kinase a localization. *Cancer Immunol. Res.* 4: 541–551.
 90. Nishio, N., I. Diaconu, H. Liu, V. Cerullo, I. Caruana, V. Hoyos, L. Bouchier-Hayes, B. Savoldo, and G. Dotti. 2014. Armed oncolytic virus enhances immune functions of chimeric antigen receptor-modified T cells in solid tumors. *Cancer Res.* 74: 5195–5205.
 91. Wu, X., A. Giobbie-Hurder, X. Liao, D. Lawrence, D. McDermott, J. Zhou, S. Rodig, and F. S. Hodis. 2016. VEGF neutralization plus CTLA-4 blockade alters soluble and cellular factors associated with enhancing lymphocyte infiltration and humoral recognition in melanoma. *Cancer Immunol. Res.* 4: 858–868.
 92. Asai, H., H. Fujiwara, J. An, T. Ochi, Y. Miyazaki, K. Nagai, S. Okamoto, J. Mineno, K. Kuzushima, H. Shiku, et al. 2013. Co-introduced functional CCR2 potentiates in vivo anti-lung cancer functionality mediated by T cells double gene-modified to express WT1-specific T-cell receptor. *PLoS One* 8: e56820.
 93. Craddock, J. A., A. Lu, A. Bear, M. Pule, M. K. Brenner, C. M. Rooney, and A. E. Foster. 2010. Enhanced tumor trafficking of GD2 chimeric antigen receptor T cells by expression of the chemokine receptor CCR2b. *J. Immunother.* 33: 780–788.
 94. Di Stasi, A., B. De Angelis, C. M. Rooney, L. Zhang, A. Mahendravada, A. E. Foster, H. E. Heslop, M. K. Brenner, G. Dotti, and B. Savoldo. 2009. T lymphocytes coexpressing CCR4 and a chimeric antigen receptor targeting CD30 have improved homing and antitumor activity in a Hodgkin tumor model. *Blood* 113: 6392–6402.
 95. Galluzzi, L., A. Buqué, O. Kepp, L. Zitvogel, and G. Kroemer. 2017. Immunogenic cell death in cancer and infectious disease. *Nat. Rev. Immunol.* 17: 97–111.
 96. Derer, A., L. Deloch, Y. Rubner, R. Fietkau, B. Frey, and U. S. Gaip. 2015. Radio-immunotherapy-induced immunogenic cancer cells as basis for induction of systemic anti-tumor immune responses - pre-clinical evidence and ongoing clinical applications. *Front. Immunol.* 6: 505.
 97. Zitvogel, L., A. Apetoh, F. Ghiringhelli, and G. Kroemer. 2008. Immunological aspects of cancer chemotherapy. *Nat. Rev. Immunol.* 8: 59–73.
 98. North, R. J. 1982. Cyclophosphamide-facilitated adoptive immunotherapy of an established tumor depends on elimination of tumor-induced suppressor T cells. *J. Exp. Med.* 155: 1063–1074.

99. Pfirsche, C., C. Engblom, S. Rickelt, V. Cortez-Retamozo, C. Garris, F. Pucci, T. Yamazaki, V. Poirier-Colame, A. Newton, Y. Redouane, et al. 2016. Immuno-therapeutic chemotherapy sensitizes tumors to checkpoint blockade therapy. *Immunity* 44: 343–354.
100. Hombach, A. A., M. Chmielewski, G. Rappel, and H. Abken. 2013. Adoptive immunotherapy with redirected T cells produces CCR7⁺ cells that are trapped in the periphery and benefit from combined CD28-OX40 costimulation. *Hum. Gene Ther.* 24: 259–269.
101. Korman, A. J., K. S. Peggs, and J. P. Allison. 2006. Checkpoint blockade in cancer immunotherapy. *Adv. Immunol.* 90: 297–339.
102. John, L. B., C. Devaud, C. P. Duong, C. S. Yong, P. A. Beavis, N. M. Haynes, M. T. Chow, M. J. Smyth, M. H. Kershaw, and P. K. Darcy. 2013. Anti-PD-1 antibody therapy potently enhances the eradication of established tumors by gene-modified T cells. *Clin. Cancer Res.* 19: 5636–5646.
103. John, L. B., M. H. Kershaw, and P. K. Darcy. 2013. Blockade of PD-1 immunosuppression boosts CAR T-cell therapy. *Oncoinmunology* 2: e26286.
104. Suarez, E. R., K. de Chang, J. Sun, J. Sui, G. J. Freeman, S. Signoretta, Q. Zhu, and W. A. Marasco. 2016. Chimeric antigen receptor T cells secreting anti-PD-L1 antibodies more effectively regress renal cell carcinoma in a humanized mouse model. *Oncotarget* 7: 34341–34355.
105. Zhang, Y., X. Zhang, C. Cheng, W. Mu, X. Liu, N. Li, X. Wei, X. Liu, C. Xia, and H. Wang. 2017. CRISPR-Cas9 mediated LAG-3 disruption in CAR-T cells. *Front. Med. DOI:* 10.1007/s11684-017-0543-6.
106. Ren, J., X. Liu, C. Fang, S. Jiang, C. H. June, and Y. Zhao. 2017. Multiplex genome editing to generate universal CAR T cells resistant to PD1 inhibition. *Clin. Cancer Res.* 23: 2255–2266.
107. Rupp, L. J., K. Schumann, K. T. Roybal, R. E. Gate, C. J. Ye, W. A. Lim, and A. Marson. 2017. CRISPR/Cas9-mediated PD-1 disruption enhances anti-tumor efficacy of human chimeric antigen receptor T cells. *Sci. Rep.* 7: 737.
108. Liu, X., R. Ranganathan, S. Jiang, C. Fang, J. Sun, S. Kim, K. Newick, A. Lo, C. H. June, Y. Zhao, and E. K. Moon. 2016. A chimeric switch-receptor targeting PD1 augments the efficacy of second-generation CAR T cells in advanced solid tumors. *Cancer Res.* 76: 1578–1590.
109. Prosser, M. E., C. E. Brown, A. F. Shami, S. J. Forman, and M. C. Jensen. 2012. Tumor PD-L1 co-stimulates primary human CD8(+) cytotoxic T cells modified to express a PD1:CD28 chimera receptor. *Mol. Immunol.* 51: 263–272.
110. Yokosuka, T., W. Kobayashi, M. Takamatsu, K. Sakata-Sogawa, H. Zeng, A. Hashimoto-Tane, H. Yagita, M. Tokunaga, and T. Saito. 2010. Spatiotemporal basis of CTLA-4 costimulatory molecule-mediated negative regulation of T cell activation. *Immunity* 33: 326–339.
111. Condomines, M., J. Arnason, R. Benjamin, G. Gunset, J. Plotkin, and M. Sadelain. 2015. Tumor-targeted human T cells expressing CD28-based chimeric antigen receptors circumvent CTLA-4 inhibition. *PLoS One* 10: e0130518.
112. Romano, E., M. Kusio-Kobialka, P. G. Foukas, P. Baumgaertner, C. Meyer, P. Ballabeni, O. Michielin, B. Weide, P. Romero, and D. E. Speiser. 2015. Ipilimumab-dependent cell-mediated cytotoxicity of regulatory T cells ex vivo by nonclassical monocytes in melanoma patients. *Proc. Natl. Acad. Sci. USA* 112: 6140–6145.
113. Simpson, T. R., F. Li, W. Montalvo-Ortiz, M. A. Sepulveda, K. Bergerhoff, F. Arce, C. Roddie, J. Y. Henry, H. Yagita, J. D. Wolchok, et al. 2013. Fc-dependent depletion of tumor-infiltrating regulatory T cells co-defines the efficacy of anti-CTLA-4 therapy against melanoma. *J. Exp. Med.* 210: 1695–1710.
114. Moon, E. K., L. C. Wang, D. V. Dolfi, C. B. Wilson, R. Ranganathan, J. Sun, V. Kapoor, J. Scholler, E. Puré, M. C. Milone, et al. 2014. Multifactorial T-cell hypofunction that is reversible can limit the efficacy of chimeric antigen receptor-transduced human T cells in solid tumors. *Clin. Cancer Res.* 20: 4262–4273.
115. Riese, M. J., L. C. Wang, E. K. Moon, R. P. Joshi, A. Ranganathan, C. H. June, G. A. Koretzky, and S. M. Albelda. 2013. Enhanced effector responses in activated CD8⁺ T cells deficient in diacylglycerol kinases. *Cancer Res.* 73: 3566–3577.
116. Burga, R. A., M. Thorn, G. R. Point, P. Guha, C. T. Nguyen, L. A. Licata, R. P. DeMatteo, A. Ayala, N. Joseph Espan, R. P. Junghans, and S. C. Katz. 2015. Liver myeloid-derived suppressor cells expand in response to liver metastases in mice and inhibit the anti-tumor efficacy of anti-CEA CAR-T. *Cancer Immunol. Immunother.* 64: 817–829.
117. Long, A. H., S. L. Highfill, Y. Cui, J. P. Smith, A. J. Walker, S. Ramakrishna, R. El-Etrby, S. Galli, M. G. Tsokos, R. J. Orentas, and C. L. Mackall. 2016. Reduction of MDSCs with all-trans retinoic acid improves CAR therapy efficacy for sarcomas. *Cancer Immunol. Res.* 4: 869–880.
118. Zhou, Q., M. E. Munger, S. L. Highfill, J. Tolar, B. J. Weigel, M. Riddle, A. H. Sharpe, D. A. Valleria, M. Azuma, B. L. Levine, et al. 2010. Program death-1 signaling and regulatory T cells collaborate to resist the function of adoptively transferred cytotoxic T lymphocytes in advanced acute myeloid leukemia. *Blood* 116: 2484–2493.
119. Caruana, I., B. Savoldo, V. Hoyos, G. Weber, H. Liu, E. S. Kim, M. M. Ittmann, D. Marchetti, and G. Dotti. 2015. Heparanase promotes tumor infiltration and antitumor activity of CAR-directed T lymphocytes. *Nat. Med.* 21: 524–529.
120. Kerkar, S. P., P. Muranski, A. Kaiser, A. Boni, L. Sanchez-Perez, Z. Yu, D. C. Palmer, R. N. Reger, Z. A. Borman, L. Zhang, et al. 2010. Tumor-specific CD8⁺ T cells expressing interleukin-12 eradicate established cancers in lympho-depleted hosts. *Cancer Res.* 70: 6725–6734.
121. Pegram, H. J., J. C. Lee, E. G. Hayman, G. H. Imperato, T. F. Tedder, M. Sadelain, and R. J. Brentjens. 2012. Tumor-targeted T cells modified to secrete IL-12 eradicate systemic tumors without need for prior conditioning. *Blood* 119: 4133–4141.
122. Hoskin, D. W., J. S. Mader, S. J. Furlong, D. M. Conrad, and J. Blay. 2008. Inhibition of T cell and natural killer cell function by adenosine and its contribution to immune evasion by tumor cells (Review). *Int. J. Oncol.* 32: 527–535.
123. Hildeman, D. A., T. Mitchell, J. Kappler, and P. Marrack. 2003. T cell apoptosis and reactive oxygen species. *J. Clin. Invest.* 111: 575–581.
124. Beavis, P. A., M. A. Henderson, L. Giuffrida, J. K. Mills, K. Sek, R. S. Cross, A. J. Davenport, L. B. John, S. Mardiana, C. Y. Slaney, et al. 2017. Targeting the adenosine 2A receptor enhances chimeric antigen receptor T cell efficacy. *J. Clin. Invest.* 127: 929–941.
125. Ligtenberg, M. A., D. Mougiakakos, M. Mukhopadhyay, K. Witt, A. Lladser, M. Chmielewski, T. Riet, H. Abken, and R. Kiessling. 2016. Coexpressed catalase protects chimeric antigen receptor redirected T cells as well as bystander cells from oxidative stress-induced loss of antitumor activity. *J. Immunol.* 196: 759–766.
126. Eil, R., S. K. Vodnal, D. Clever, C. A. Klebanoff, M. Sukumar, J. H. Pan, D. C. Palmer, A. Gros, T. N. Yamamoto, S. J. Patel, et al. 2016. Ionic immune suppression within the tumour microenvironment limits T cell effector function. *Nature* 537: 539–543.
127. Tang, H., Y. Wang, L. K. Chlewicki, Y. Zhang, J. Guo, W. Liang, J. Wang, X. Wang, and Y. X. Fu. 2016. Facilitating T cell infiltration in tumor microenvironment overcomes resistance to PD-L1 blockade. [Published erratum appears in 2016 *Cancer Cell* 30: 500.] *Cancer Cell* 29: 285–296.
128. DuPage, M., and T. Jacks. 2013. Genetically engineered mouse models of cancer reveal new insights about the antitumor immune response. *Curr. Opin. Immunol.* 25: 192–199.
129. DuPage, M., A. F. Cheung, C. Mazumdar, M. M. Winslow, R. Bronson, L. M. Schmidt, D. Crowley, J. Chen, and T. Jacks. 2011. Endogenous T cell responses to antigens expressed in lung adenocarcinomas delay malignant tumor progression. *Cancer Cell* 19: 72–85.
130. Garbe, A. I., B. Vermeer, J. Gamrekeliashvili, R. von Wasielewski, F. R. Greten, A. M. Westendorf, J. Buer, R. M. Schmid, M. P. Manns, F. Korangy, and T. F. Greten. 2006. Genetically induced pancreatic adenocarcinoma is highly immunogenic and causes spontaneous tumor-specific immune responses. *Cancer Res.* 66: 508–516.
131. Hingorani, S. R., L. Wang, A. S. Multani, C. Combs, T. B. Deramaudt, R. H. Hruban, A. K. Rustgi, S. Chang, and D. A. Tuveson. 2005. Trp53R172H and KrasG12D cooperate to promote chromosomal instability and widely metastatic pancreatic ductal adenocarcinoma in mice. *Cancer Cell* 7: 469–483.
132. DuPage, M., A. L. Dooley, and T. Jacks. 2009. Conditional mouse lung cancer models using adenoviral or lentiviral delivery of Cre recombinase. *Nat. Protoc.* 4: 1064–1072.
133. McFadden, D. G., K. Politi, A. Bhutkar, F. K. Chen, X. Song, M. Pirun, P. M. Santiago, C. Kim-Kiselak, J. T. Platt, E. Lee, et al. 2016. Mutational landscape of EGFR-, MYC-, and Kras-driven genetically engineered mouse models of lung adenocarcinoma. *Proc. Natl. Acad. Sci. USA* 113: E6409–E6417.
134. Nakasone, E. S., H. A. Askatrud, T. Kees, J. H. Park, V. Plaks, A. J. Ewald, M. Fein, M. G. Rasch, Y. X. Tan, J. Qiu, et al. 2012. Imaging tumor-stroma interactions during chemotherapy reveals contributions of the microenvironment to resistance. *Cancer Cell* 21: 488–503.
135. Turnis, M. E., D. V. Sawant, A. L. Szmyczak-Workman, L. P. Andrews, G. M. Delgoffe, H. Yano, A. J. Beres, P. Vogel, C. J. Workman, and D. A. Vignali. 2016. Interleukin-35 limits anti-tumor immunity. *Immunity* 44: 316–329.
136. Liakou, C. I., A. Kamat, D. N. Tang, H. Chen, J. Sun, P. Troncoso, C. Logothetis, and P. Sharma. 2008. CTLA-4 blockade increases IFN-gamma-producing CD4+ICOShi cells to shift the ratio of effector to regulatory T cells in cancer patients. *Proc. Natl. Acad. Sci. USA* 105: 14987–14992.
137. Chen, H., C. I. Liakou, A. Kamat, C. Pettaway, J. F. Ward, D. N. Tang, J. Sun, A. A. Jungbluth, P. Troncoso, C. Logothetis, and P. Sharma. 2009. Anti-CTLA-4 therapy results in higher CD4+ICOShi T cell frequency and IFN-gamma levels in both nonmalignant and malignant prostate tissues. *Proc. Natl. Acad. Sci. USA* 106: 2729–2734.
138. Fu, T., Q. He, and P. Sharma. 2011. The ICOS/ICOSL pathway is required for optimal antitumor responses mediated by anti-CTLA-4 therapy. *Cancer Res.* 71: 5445–5454.
139. Zamarripa, D., R. B. Holmgård, J. Ricca, T. Plitt, P. Palese, P. Sharma, T. Mergouh, J. D. Wolchok, and J. P. Allison. 2017. Intratumoral modulation of the inducible co-stimulator ICOS by recombinant oncolytic virus promotes systemic anti-tumour immunity. *Nat. Commun.* 8: 14340.
140. Porter, D. L., W. T. Hwang, N. V. Frey, S. F. Lacey, P. A. Shaw, A. W. Loren, A. Bagg, K. T. Marcucci, A. Shen, V. Gonzalez, et al. 2015. Chimeric antigen receptor T cells persist and induce sustained remissions in relapsed refractory chronic lymphocytic leukemia. *Sci. Transl. Med.* 7: 303ra139.
141. Giesen, C., H. A. Wang, D. Schapiro, N. Zivanovic, A. Jacobs, B. Hattendorf, P. J. Schüffler, D. Grolimund, J. M. Buhmann, S. Brandt, et al. 2014. Highly multiplexed imaging of tumor tissues with subcellular resolution by mass cytometry. *Nat. Methods* 11: 417–422.

Specific activation and targeting of cytotoxic lymphocytes through chimeric single chains consisting of antibody-binding domains and the γ or ζ subunits of the immunoglobulin and T-cell receptors

(single-chain Fv domain/chimeric receptors/immunotargeting/T cell)

ZELIG ESHHAR*, TOVA WAKS, GIDEON GROSS†, AND DANIEL G. SCHINDLER

Department of Chemical Immunology, The Weizmann Institute of Science, Rehovot 76100, Israel

Communicated by Michael Sela, September 9, 1992 (received for review July 8, 1992)

ABSTRACT The generation of tumor-specific lymphocytes and their use in adoptive immunotherapy is limited to a few malignancies because most spontaneous tumors are very weak or not at all immunogenic. On the other hand, many anti-tumor antibodies have been described which bind tumor-associated antigens shared among tumors of the same histology. Combining the variable regions (Fv) of an antibody with the constant regions of the T-cell receptor (TCR) chains results in chimeric genes endowing T lymphocytes with antibody-type specificity, potentially allowing cellular adoptive immunotherapy against types of tumors not previously possible. To generalize and extend this approach to additional lymphocyte-activating molecules, we designed and constructed chimeric genes composed of a single-chain Fv domain (scFv) of an antibody linked with γ or ζ chains, the common signal-transducing subunits of the immunoglobulin receptor and the TCR. Such chimeric genes containing the Fv region of an anti-trinitrophenyl antibody could be expressed as functional surface receptors in a cytolytic T-cell hybridoma. They triggered interleukin 2 secretion upon encountering antigen and mediated non-major-histocompatibility-complex-restricted hapten-specific target cell lysis. Such chimeric receptors can be exploited to provide T cells and other effector lymphocytes, such as natural killer cells, with antibody-type recognition directly coupled to cellular activation.

Many clinical attempts to recruit the humoral or cellular arms of the immune system for passive anti-tumor immunotherapy have not fulfilled expectations. While it has been possible to obtain anti-tumor antibodies, their therapeutic potential has been limited so far to blood-borne tumors (1, 2), primarily because solid tumors are inaccessible to sufficient amounts of antibodies (3). On the other hand, the use of effector lymphocytes in adoptive immunotherapy, although effective in selected solid tumors, suffers from a lack of specificity [such as in the case of lymphokine-activated killer cells (LAK cells) (4)] or from the difficulty in recruiting tumor-infiltrating lymphocytes (TILs) and expanding such specific T cells for most malignancies (5). Yet, the observations that TILs can be obtained in melanoma and renal cell carcinoma tumors, that they can be effective in selected patients, and that foreign genes can function in these cells (6) demonstrate the therapeutic potential embodied in these cells.

A strategy which we and others have recently developed (7–11) allows us to combine the advantage of the antibody's specificity with the homing, tissue penetration, and target-cell destruction of T lymphocytes and to extend, by *ex-vivo* genetic manipulations, the spectrum of anti-tumor specificity of T cells. In this approach a chimeric T-cell receptor (cTCR) gene composed of the variable region domain (Fv) of an

antibody molecule and the constant region domain of the TCR were expressed in T cells. Upon encountering antigen, such cTCR could transmit signals for T-cell activation, secretion of lymphokines, and specific target cell lysis in a major histocompatibility complex (MHC) nonrestricted manner. Moreover, the cTCR-bearing cells undergo stimulation by immobilized antigen, proving that receptor-mediated T-cell activation is not only nonrestricted but also independent of MHC expression on target cells.

Broad application of the cTCR approach is dependent on efficient expression of the cTCR genes in primary T cells. Although retroviral vectors have been demonstrated to be effective for transgene expression in human T cells due to the fact that two genes have to be introduced to express functional cTCR and the very low efficiency of transduction of a single cell with two separate retroviral vectors, new vectors have to be tried which will allow the transduction of two genes in tandem.

To overcome these problems and to extend the applicability of the "T-body" approach to other cells and receptor molecules, we developed a single-chain approach to the cTCR. It is based on the demonstrated ability to express in bacteria an antibody single-chain Fv (scFv) (15, 16). Such scFv domains, which join the antibody's heavy and light variable (V_H and V_L) gene segments with a flexible linker, have proven to exhibit the same specificity and affinity as the natural Fab' fragment. In the present study we constructed chimeric molecules composed of the scFv linked to receptor subunits that might serve to transduce the signal from the scFv and confer antibody specificity to T cells as well as other lymphocytes. Among the polypeptides of the TCR/CD3 (the principal triggering receptor complex of T cells), especially promising are the ζ and its η isoform, which appear as either homo- or hetero-S—S-linked dimers and are responsible for mediating at least a fraction of the cellular activation programs triggered by the TCR recognition of ligand (17, 18). These polypeptides have very short extracellular domains, which can serve for the attachment of the scFv. A most attractive candidate in the group of natural killer (NK)-stimulatory receptors is the low-affinity receptor for IgG, Fc γ RIII (CD16). Occupancy or cross-linking of Fc γ RIII activates NK cells for cytokine production, expression of surface molecules, and cytolytic activity (19, 20). In

Abbreviations: TCR, T-cell receptor; cTCR, chimeric TCR; Fv, variable region domain of antibody; scFv, single-chain Fv; NK, natural killer; Fc γ R and Fc ϵ R, immunoglobulin γ - and ϵ -chain constant region receptors; scFvR, chimeric molecule between a scFv and a receptor chain; V, variable; V_H and V_L , heavy and light variable; C, constant; TNP, 2,4,6-trinitrophenyl; IL-2, interleukin 2; MHC, major histocompatibility complex; CTL, cytolytic T lymphocytes; mAb, monoclonal antibody; F γ G, fowl gamma globulin.

*To whom reprint requests should be addressed.

†Present address: Protein and Nucleic Acid Chemistry Division, Medical Research Council Laboratory of Molecular Biology, Hills Road, Cambridge CB2 2QH, United Kingdom.

NK cells, macrophages, and B and T cells, the Fc γ RIIIA appears as a heterooligomeric complex consisting of a ligand-binding α chain associated with a disulfide-linked γ or ζ chain. The Fc γ RIIIA signaling γ chain (21) serves also as part of the Fc ϵ RI complex, where it appears as a homodimer, is very similar to the CD3 ζ chain, and in fact can form heterodimers with it in some cytolytic T lymphocytes (CTL) and NK cells (22, 24). Remarkably, most recently prepared chimeras between these polypeptides and the extracellular domains of CD4 (25), CD8 (26), the interleukin 2 (IL-2) receptor α chain (27), or CD16 (28) proved to be active in signaling T-cell stimulation even in the absence of other TCR/CD3 components.

To endow T cells and NK cells with antibody-type recognition, we constructed chimeric genes composed of a scFv of an anti-2,4,6-trinitrophenyl (TNP) antibody and either the FcR γ chain or the CD3 complex ζ chain. Cytotoxic lymphocyte hybridomas expressing such chimeric scFvR γ or scFvR ζ genes interacted specifically with TNP-modified target cells, underwent activation as monitored by IL-2 secretion, and subsequently killed specifically TNP-modified target cells. These data suggest a functional expression in a continuous polypeptide of antigen-binding and signal-transducing properties which can be utilized as a targeting receptor on lymphocytes.

MATERIALS AND METHODS

Cell Lines and Antibodies. MD.45 is a CTL hybridoma of BALB/c mice allospecific to H-2^b (29). MD.27J is a TCR α -mutant of MD.45. A.20 is a B lymphoma of BALB/c origin (ATCC T1B 208). Cells were cultured in Dulbecco's modified Eagle's medium (DMEM) supplemented with 10% fetal calf serum. Sp6, an anti-TNP monoclonal antibody (mAb), and 20.5, an anti-Sp6 idiotype mAb, were provided by G. Köhler (Max-Planck-Institut für Immunobiologie, Freiburg, Germany) (30). Polyclonal antibodies to human Fc ϵ RI γ chain were provided by J.-P. Kinet (National Institutes of Health), and mAbs to the same protein (4D8) (31) were provided by J. Kochan (Hoffmann-La Roche). Rabbit antibodies to murine ζ chain were from M. Baniyash (Hebrew University Medical School, Jerusalem).

Construction of Chimeric Genes. The specific genes encoding the V_H and V_L domains of the Sp6 anti-TNP antibody were derived from the genomic constructs described previously for the preparation of the cTCR (32, 33) by PCR amplifications using oligodeoxynucleotide primers designed according to the 5' and 3' consensus amino acid sequences of immunoglobulin V regions (34) introducing the Xba I and BstEII restriction sites at the ends of the scFv. In constructing the scFv we used the V_L-linker-V_H design containing a linker sequence similar to linker 212 described by Colcher *et al.* (12). Accordingly, the V_L-3' and the V_H-5' primers include sequences comprising the 5' and 3' parts of the linker, introducing Sal I sites in their 3' and 5' ends, respectively. Following digestion of the purified PCR products with Xba I and Sal I (V_L) and Sal I and BstEII (V_H), the fragments were ligated into the Xba I and BstEII sites of a pRSV2neo-based expression vector containing the leader of SC15 κ light chain (kindly provided by S. Levy, Stanford University Medical School) and TCR constant region β chain (C β), prepared for the expression of anti-38C.13 cDNA cTCR genes (unpublished work and ref. 33). The C β of this plasmid was then replaced with either the γ chain amplified from a human cDNA clone (13) or the ζ chain amplified from Jurkat cDNA by using primers introducing BstEII and Xho I at the 5' and 3' ends. A diagram of the final scFvR γ expression vector is shown in Fig. 1. The sequences of the oligodeoxynucleotide primers used for the construction of the chimeric scFvR γ and scFvR ζ are delineated in the legend to Fig. 1.

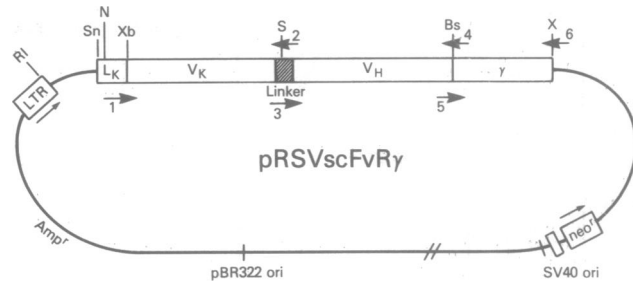


FIG. 1. Scheme of the chimeric scFvR expression vector. For other vectors, R can represent any receptor chain, such as the ζ subunit of CD3 described in this study. The boxes from left to right represent DNA segments corresponding to the Rous sarcoma virus long terminal repeat promoter (LTR), κ light chain leader (L κ), and variable region (V κ), the linker (hatched box), heavy chain variable region (V_H), the human γ chain, the G418-resistance gene (neo^r), and the simian virus 40 origin of replication. Restriction sites indicated are EcoRI (RI), SnaBI (Sn), Nco I (N), Xba I (Xb), Sal I (S), BstEII (Bs), and Xho I (X). The arrowheads represent the flanking regions amplified by using the following oligonucleotide primers: 1, V κ -5'-CCCGTCTAGAGGAGAYATYGTWATGACCCAGTCTCCA; 2, V κ -3'-CCCGTCGACCCTTTWATTCAGCTTWGTSSC; 3, V_H-5'-CGGGTCGACTTCCGGTAGCGGCAAATCCTCTGAAG-GCAAAGGTSAGGTSCAGCTGSAGSAGTCTGG; 4, V_H-3'-TGMRGAGACGGTGACCGTRGYCCTTGGCCCCAG; 5, γ -5'-CCGGTCACCGTCTCTTCAGCGGATCCTCAGCTCTGCTATA-TCTGGATG; 6, γ -3'-GGCAGCTGCTCGAGTCTAAAGCTACT-GTGGTGG; 7, ζ -5'-GCTGGATCCAAACTCTGCTTAC; and 8, ζ -3'-CGCCTCGAGCTGTTAGCGAGGGGGC. These primers were designed to match the consensus sequences of V_H and V κ . The relevant restriction sites are in bold letters.

Expression of the Chimeric scFvR γ / ζ Genes. Transfection of 20 μ g of pRSVscFvR γ / ζ DNA into 20 \times 10⁶ MD.45 or MD.27J hybridoma cells was performed by electroporation using an ISCO power supply at 1.9 kV (32). Transfectants were selected in G418 at 2 mg/ml. Expression of scFvR γ / ζ on the surface of transfected cells was evaluated by immunofluorescence staining using the 20.5 anti-Sp6 idiotype and fluorescein isothiocyanate (FITC)-labeled anti-mouse Fab' antibody. Functional assays included an IL-2 production assay and a cytotoxicity assay in which the ability of transfectants to respond specifically to TNP-modified A.20 target cells was evaluated as detailed in ref. 9. The amount of IL-2 was determined by using an IL-2-dependent CTL line and methyl tetrazolium acid staining (14). Cytotoxicity was assayed by ⁵¹Cr release (29). All determinations were performed in triplicate.

Immunoprecipitation and Immunoblotting. Washed pellets containing 10⁸ cells were lysed in 1 ml of 1% digitonin as described (32). Aliquots of nuclei-free supernatants were incubated with antibodies and then precipitated with second antibodies and protein G-Sepharose (Pharmacia). Alternatively, cell lysates were mixed with sample buffer to a final concentration of 1% NaDODSO₄ and either 10 mM iodoacetamide (for nonreducing gels) or 15 mM dithiothreitol (for reducing gels). The washed immunoprecipitates were dissociated in sample buffer under the same conditions. To avoid destruction of the Sp6 idiotope, the samples were incubated at 20°C for 30 min before NaDODSO₄/PAGE through a 5–20% gel gradient. Separated proteins were blotted onto nitrocellulose paper and allowed to react with anti-Sp6, anti- γ , or anti- ζ antibodies followed by peroxidase-labeled anti-immunoglobulin antibodies. Washed blots were developed by using a chemiluminescence kit (ECL, Amsterdam).

RESULTS

Construction and Expression of the Chimeric scFvR γ / ζ Chain Genes. To produce a chimeric receptor with an antigen

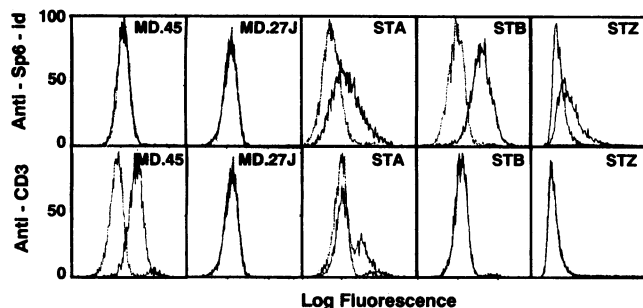


FIG. 2. Fluorescence-activated cell sorter (FACS) analysis of immunofluorescence staining of MD.45 hybridoma and its TCR α^- MD.27J mutant, their corresponding scFvR γ -transfected STA and STB clones, or STZ cells, which result from transfection of the scFvR γ chimeric gene into MD.27J. Solid line, staining with anti-Sp6 idiotype antibody 20.5 or anti-CD3 mAb 145.2C11. Broken line, control irrelevant antibody.

binding site of a given antibody and the signaling γ or ζ chains, we have adopted the scFv design (15, 16), which allows combining both entities into one continuous molecule. In engineering the pRSVscFvR γ/ζ expression vector (Fig. 1), harboring the V_L and V_H of the Sp6 anti-TNP mAb (23), we introduced elements that enable its usage as a modular expression cassette to accommodate scFvs from different antibodies in combination with γ , ζ , or other chains. This was achieved by using oligonucleotide primers composed of sequences common to the majority of the 5' and 3' sequences of either V_L or V_H regions, flanked by relatively unique restriction sites, which allow both in-frame ligation of the different units and removal to other vectors. We have chosen to use the 5'-V_L-linker-V_H-3' design, which was found suitable for the expression of a variety of single-chain antibodies and their fragments in bacteria (16), although we believe that the converse, 5'-V_H-linker-V_L-3', alignment (15) can be used as well.

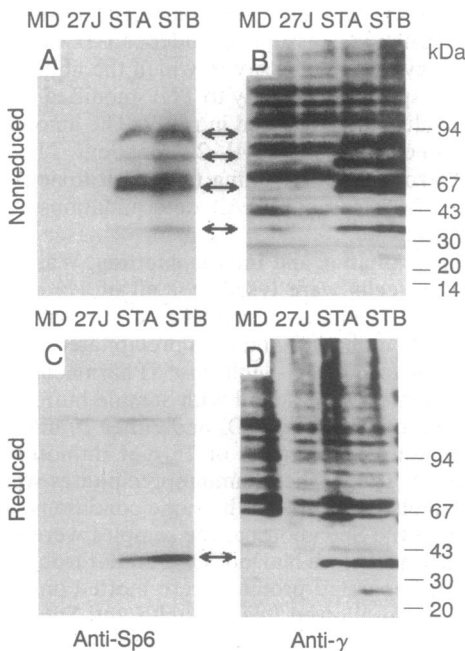


FIG. 3. Immunoblotting analysis of lysates prepared from scFvR γ transfectants and parental hybridomas developed by anti-Sp6 idiotype mAb 20.5 (A and C) and rabbit anti-human γ chain (B and D). Electrophoresis was on four separate gels. The molecular mass scales are related to B and D; the arrows point to the same bands in A and B or C and D.

Introduction of the chimeric scFvR γ gene into the MD.45 murine CTL hybridoma (STA series of transfectants) or its MD.27J TCR α^- mutant, which does not express surface TCR/CD3 complex (STB series), resulted in the expression of the chimeric molecule on the cell surface of selected clones as revealed by staining with the anti-Sp6 idiotypic antibody (Fig. 2). Similar staining was observed for STZ, which was derived by transfecting MD.27J with the scFvR ζ chimeric gene. The surface expression of the scFvR γ or scFvR ζ molecule was independent of the TCR/CD3 complex: it did not restore surface expression of the CD3 in MD.27J transfected STB or STZ cells, and some subclones of the STA that initially expressed both scFvR γ and TCR/CD3 on their surface lost, upon a prolonged culture period, the TCR/CD3 expression without any apparent effect on the scFvR γ expression and function (not shown).

Immunoblotting analysis of cell lysates prepared from representative STA and STB transfectants using either anti-idiotypic mAb 20.5 or polyclonal anti-human γ antibodies revealed four distinct bands of apparent molecular mass of 36, 54–62, 74–80, and 85–90 kDa, which did not appear in the parental cells (Fig. 3 A and B). Under reducing conditions (Fig. 3 C and D) one species, which corresponds to the predicted 36-kDa monomeric form of the scFvR γ , was apparent, indicating the multimeric nature of the molecule. The band with apparent 75-kDa molecular mass corresponds to the homodimeric molecule, and the nature of the 90-kDa species is unknown. It might be a novel γ -associated polypeptide, analogous to the one recently reported (31). This species can be detected only in immunoblots of cell lysates and is not apparent after surface iodination and immunoprecipitation (Fig. 4B), suggesting the intracellular origin of the molecule. The appearance of bands in the range of 54–62 kDa was more pronounced in the STB transfectant. It might

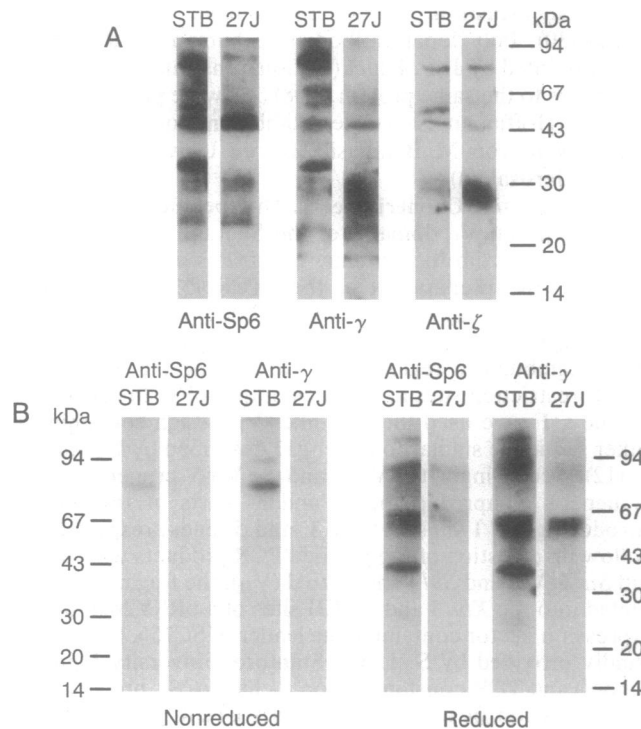


FIG. 4. Composition of the scFvR γ dimers. (A) Immunoblot analysis of anti-Sp6 precipitates prepared from STB (scFvR γ transfectant cells) and their parent (MD.27J hybridoma cells). After electrophoresis under nonreducing conditions and blotting, the blot was allowed to react with anti-Sp6, anti-human γ , or anti-mouse ζ antibodies. (B) Immunoprecipitation of lysates made of surface-iodinated STB cells (scFvR γ transfectant cells) and their parent (MD.27J hybridoma cells).

represent heterodimers between the chimeric scFvR γ chain and endogenous ζ and probably η chains of the CD3 complex. We therefore electrophoresed anti-Sp6 immunoprecipitates made from STB lysates, blotted the gels, and developed the blots with anti-Sp6, anti- γ , or anti-mouse ζ/η antibodies (Fig. 4A). Both the anti-idiotypic and the anti- γ antibodies revealed the four bands from the transfected cells; however, the anti- ζ (which cross-reacts with the mouse η chain) differentially developed only the 60-kDa species. Immunoprecipitation of surface-iodinated proteins with either anti-Sp6 or anti- γ antibodies (Fig. 4B) demonstrated a main species of 75 kDa under nonreducing conditions. This is the homodimer of the chimeric chain.

Expression of scFvR γ/ζ as Functional Receptors. To test whether the chimeric scFvR γ or scFvR ζ can function as an active receptor molecule, we studied the ability of the transfected hybridomas to undergo antigen-specific stimulation. The MD.45 T cell hybridoma can be triggered through its TCR to produce IL-2, IL-3, or granulocyte/macrophage colony-stimulating factor (GM-CSF). It specifically recognizes and responds to H-2^b target cells (29), while its mutant, MD.27J, cannot be stimulated through its TCR due to the absence of an α chain. Upon introduction of the chimeric Sp6-scFvR γ , both of these cells could be specifically triggered to produce IL-2 after incubation with TNP-modified stimulator cells (Fig. 5A) or plastic-immobilized TNP-fowl γ globulin (TNP-F γ G) (Fig. 5B). Nonmodified A.20 cells or F γ G did not activate the transfectants, demonstrating the specificity of the response toward TNP. Stimulation of the various transfectants with immobilized antigen resulted in different degrees of reactivity. While STA responded to plastic-bound TNP-F γ G in consistent manner, STB and STZ (transfected with scFvR γ and scFvR ζ respectively) lost their ability to undergo stimulation with immobilized antigen but not with hapten-modified cells. Such behavior suggests the necessity of additional synergistic signal for these cells. Indeed, costimulation with TNP-F γ G plus either phorbol 12-myristate 13-acetate (PMA) or Ca²⁺ ionophore resulted in enhancement of IL-2 production (data not shown). Incubation with soluble TNP-proteins even at high hapten-to-protein ratios did not result in activation but rather specifically inhibited triggering by immobilized antigen (Fig. 5B) or cell-bound hapten. The activation of GTAE.20, a transfectant expressing a two-chain cTCR (9), was also inhibited by

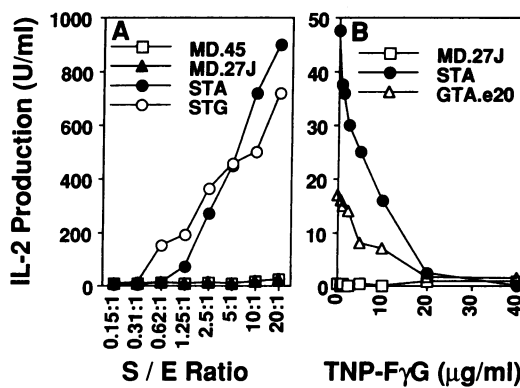


FIG. 5. Transfectants expressing scFvR are stimulated to produce IL-2 after stimulation with TNP-A.20 (A) or plastic-immobilized TNP-F γ G (B). GTAE.20 is an Sp6 double-chain cTCR transfectant from our previous study (9). The scFvR ζ -expressing STZ produced about 200 units (U) of IL-2 per ml after coculture with TNP-A.20 at 8:1 stimulator-to-effector (S/E) cell ratio. Not shown are the responses of the transfectants to nonmodified A.20 or F γ G controls, which were completely negative, exactly like the background responses of the MD.45 and MD.27J cells to TNP-antigen.

soluble TNP-F γ G. Identical concentrations of antigen were needed to cause 50% inhibition (IC₅₀) of STA and GTAE.20 (Fig. 5B), indicating that the single-chain and the double-chain Fv display the same relative affinity to TNP.

Finally, we tested the ability of the chimeric receptors to mediate specific target cell lysis by incubating them with ⁵¹Cr-labeled cells. As shown in Fig. 6, only the cells transfected with the Sp6-scFvR γ or scFvR ζ could lyse TNP-modified target cells in a dose-related fashion. This cytolytic activity was specific to TNP, as soluble TNP-F γ G blocked it (not shown) and unmodified A.20 cells were not affected by the transfectants.

DISCUSSION

In this study we demonstrate that a single-chain Fv of an antibody molecule fused to the γ chain of the immunoglobulin Fc receptor or to the ζ chain of the CD3 complex can be expressed in T cells as an antigen-specific receptor. The chimeric scFvR γ/ζ endowed T cells with antibody-type specificity, transmitted a signal for IL-2 production, and mediated target cell lysis. The demonstration that the scFvR γ/ζ fusion protein could mediate antigen-specific stimulation of T cells not expressing the TCR/CD3 receptor complex [as shown for the STB and STZ transfectants derived from the TCR-negative MD.27J mutant (Figs. 5 and 6)], strongly suggests that the γ and ζ chains are capable of autonomous activation of T cells. Yet, because of the low level of heterodimers between the scFvR γ and the endogenous ζ and η chains (Figs. 3 and 4), we cannot exclude some contribution by the residual ζ (or η) chain in the signaling process. Nonetheless, our results clearly indicate that the TCR chains do not take part in this process, thus confirming and complementing recent observations in which antibody crosslinking through the extracellular domains of CD4, CD8, IL-2 receptor, or CD16 joined to the cytoplasmic tail of either one of the γ/ζ family members resulted in T-cell activation (25–28). Like scFvR γ/ζ , chimeric CD4 or CD16- γ/ζ molecules expressed in cytotoxic lymphocytes could direct specific cytosis against appropriate target cells (25, 28). Interestingly, analysis of mutations within the intracellular 18-residue motif, which has been recently assigned to account for the activity of the γ/ζ chain, revealed that the ability to mediate calcium responsiveness can be separated from the ability to support cytosis (28). This opens new possibilities in which the chimeric chain, composed of scFv and genetically modified ζ or γ chains, can be used not only to direct

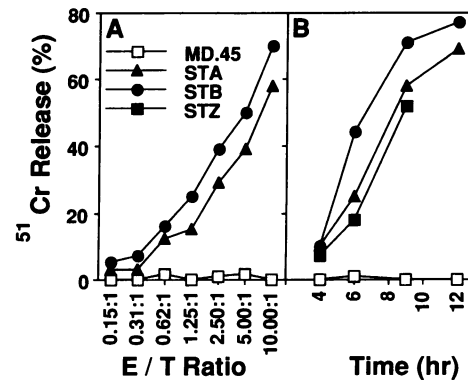


FIG. 6. Specific ⁵¹Cr release of TNP-A.20 cells after incubation with transfectants expressing scFvR. Effector cells were incubated with plastic-immobilized TNP-F γ G for 8 hr before the killing assay. Kinetic assay was done at an effector-to-target (E/T) cell ratio of 10:1; dose-response was determined in a 9-hr assay. Control nonmodified A.20 target cells incubated with the same effector cells in identical conditions did not release more ⁵¹Cr than the spontaneous release (not shown).

specificity but also to dictate the selected reactivity of lymphocytes.

The finding that immobilization of antigen is needed for efficient stimulation through scFvR γ/ζ and that soluble multimeric ligand (such as TNP-protein) did not trigger but rather inhibited receptor-mediated activation through cell- or plastic-bound TNP (Fig. 5B) indicates that mere engagement or even crosslinking of adjacent γ or ζ chains does not result in T-cell activation (as manifested by IL-2 release). The dependence on ligand immobilization for efficient T-cell triggering has been reported also for cTCR-mediated signaling (8, 9), and the mechanisms underlying this are as yet unclear.

Additional potential applications offered by the antibody scFvR design involve retargeting lymphocytes *in vivo*. As manifested by the TNP-specific cytosis of target cells mediated by transfectants expressing the scFvR γ/ζ (Fig. 6), the chimeric protein endowed the CTL hybridomas with MHC-nonrestricted specificity. As we previously suggested for the cTCR, this can be exploited to retarget T cells *in vivo* to tumor cells or to any other target of choice, toward which antibodies can be raised. In this regard, the scFvR design is advantageous over the cTCR one. It requires the expression of only one gene instead of the gene pair required for the cTCR, thereby providing simpler construction and transfection. Second, the scFvR design can be employed to confer antibody specificity on a larger spectrum of signaling molecules composed of only one chain. Third, the scFv maintains both V_H and V_L together in one chain; thus, even upon mixed pairing of chimeric with endogenous chains, the antigen-binding properties of the molecule are conserved. Finally, the fact that γ and ζ constitute the signaling chains of the TCR/CD3, Fc γ RIII, and Fc ϵ RII expands the feasibility of exploiting the chimeric receptor for redirecting other effector cells, such as NK cells, basophils, or mast cells in addition to T cells.

We believe that the chimeric scFvR γ/ζ described here (or any of the simple modifications of it as suggested below) that combines the specificity of an antibody as a continuous single chain and the effector function of cytotoxic T cells and NK cells or regulatory function of helper T cells could offer important consequential development for targeted immunotherapy. This approach exploits the scFv as the antigen-recognition unit and the potent cytotoxic responses of NK cells and T cells and/or the ability of T cells to secrete lymphokines and cytokines upon activation at the target site, thus recruiting, regulating, and amplifying other arms of the immune system. The chimeric scFv receptors can confer on the lymphocytes the following functions: antibody-type specificity toward any predefined antigen; specific "homing" to their targets; specific recognition, activation, and execution of effector function as a result of encountering the target; and specific and controlled proliferation at the target site. Potential receptor or signaling molecules that can be used in the single-chain design are γ , ζ , and η subunits of the TCR/FcR complexes; any of the α , β , γ , or δ of the TCR chains; CD16 α chain of the Fc γ RIII α ; CD2 and CD28 surface molecules; and α , β , and γ chains of the IL-2 receptor as well as any of the chains of the cytokine receptors which take part in stimulation of lymphocyte activation and/or proliferation. Candidate lymphocytes to be endowed with antibody specificity by using this approach are NK cells, lymphokine-activated killer cells (LAK), cytotoxic T cells, helper T cells, and the various subtypes of the above. These cells can execute their authentic natural function and can serve, in addition, as carriers of foreign genes designated for gene therapy, and the chimeric receptor shall serve in this case to direct the cells to their target. Finally, this approach can be applied to anti-idiotypic vaccination by using helper T cells expressing chimeric receptors made of Fv of anti-idiotypic antibodies. Such "designer lymphocytes" will interact and

stimulate idiotype-bearing B cells to produce antigen-specific antibodies, thus bypassing the need for active immunization with toxic antigens.

We are grateful to Drs. G. Köhler, J.-P. Kinet, D. Presky, J. Kochan, and M. Baniyash for providing us with DNA clones and antibodies and Dr. P. Hwu for critically reading this manuscript. This work was supported in part by the Crown Fund. Z.E. is the incumbent of the Marshall and Renette Ezralow Chair in Cellular and Chemical Immunology.

1. Lowder, J. N., Meeker, T. C. & Levy, R. (1985) *Cancer Surv.* 4, 359–375.
2. Waldmann, T. A. (1991) *Science* 252, 1657–1662.
3. Jain, R. K. (1989) *J. Natl. Cancer Inst.* 81, 64–66.
4. Mule, J. J., Shu, S., Schwartz, S. L. & Rosenberg, S. R. (1984) *Science* 225, 1487–1489.
5. Rosenberg, S. A., Spiess, P. & Lafreniere, R. (1986) *Science* 233, 1318–1321.
6. Rosenberg, S. A. (1992) *J. Clin. Oncol.* 10, 180–199.
7. Kuwana, Y., Asakura, Y., Utsunomiya, N., Nakanishi, M., Arata, Y., Itoh, S., Nagase, F. & Kurosawa, Y. (1987) *Biochem. Biophys. Res. Commun.* 149, 960–968.
8. Gross, G., Gorochov, G., Waks, T. & Eshhar, Z. (1989) *Transplant. Proc.* 21, 127–130.
9. Gross, G., Waks, T. & Eshhar, Z. (1989) *Proc. Natl. Acad. Sci. USA* 86, 10024–10028.
10. Becker, M. L. B., Near, R., Mudgett-Hunter, M., Margolies, M. N., Kubo, R. T., Kaye, J. & Hedrick, S. M. (1989) *Cell* 58, 911–921.
11. Goverman, J., Gomez, S. M., Segesman, K. D., Hunkapiller, T., Laug, W. E. & Hood, L. (1990) *Cell* 60, 929–939.
12. Colcher, D., Bird, R., Roselli, M., Hardman, K. D., Johnson, S., Pope, S., Dodd, S. W., Pantoliano, M. W., Milenic, D. E. & Schliom, J. (1990) *J. Natl. Cancer Inst.* 82, 1191–1197.
13. Kuster, H., Thompson, H. & Kinet, J.-P. (1990) *J. Biol. Chem.* 265, 6448–6452.
14. Mosmann, T. (1983) *J. Immunol. Methods* 65, 55–63.
15. Huston, J. S., Levinson, D., Mudgett-Hunter, M., Tai, M.-S., Novotny, J., Margolies, M. N., Ridge, R. J., Brucocieri, R. E., Haber, E., Crea, R. & Oppermann, H. (1988) *Proc. Natl. Acad. Sci. USA* 85, 5879–5884.
16. Bird, R. E., Hardman, K. D., Jacobson, J. W., Johnson, S., Kaufman, B. M., Lee, S.-M., Lee, T., Pope, S. H., Riordan, G. S. & Whitlow, M. (1988) *Science* 242, 423–426.
17. Weissman, A., Frank, S. J., Orloff, D. G., Mercep, M., Ashwell, J. D. & Klausner, R. D. (1989) *EMBO J.* 8, 3651–3656.
18. Bauer, A., McConkey, D. J., Howard, F. D., Clayton, L. K., Novick, D., Koyasu, S. & Reinherz, E. L. (1991) *Proc. Natl. Acad. Sci. USA* 88, 3842–3846.
19. Unkeless, J. C., Scigliano, E. & Freedman, V. H. (1988) *Annu. Rev. Immunol.* 6, 251–281.
20. Ravetch, J. V. & Kinet, J.-P. (1991) *Annu. Rev. Immunol.* 9, 457–492.
21. Wirthmuller, U., Kurosaki, T., Murakami, M. S. & Ravetch, J. V. (1992) *J. Exp. Med.* 175, 1381–1390.
22. Orloff, D. G., Ra, C. S., Frank, S. J., Klausner, R. D. & Kinet, J. P. (1990) *Nature (London)* 347, 189–191.
23. Köhler, G. & Milstein, C. (1976) *Eur. J. Immunol.* 6, 511–519.
24. Vivier, E., Rochet, N., Kochan, J. P., Presky, D. H., Schlossman, S. F. & Anderson, P. (1991) *J. Immunol.* 147, 4263–4270.
25. Romeo, C. & Seed, B. (1991) *Cell* 64, 1037–1046.
26. Irving, B. A. & Weiss, A. (1991) *Cell* 64, 891–901.
27. Letourneau, F. & Klausner, R. D. (1991) *Proc. Natl. Acad. Sci. USA* 88, 8905–8909.
28. Romeo, C., Amiot, M. & Seed, B. (1992) *Cell* 68, 889–897.
29. Kaufmann, Y., Berke, G. & Eshhar, Z. (1981) *Proc. Natl. Acad. Sci. USA* 78, 2502–2506.
30. Rusconi, S. & Köhler, G. (1985) *Nature (London)* 314, 330–334.
31. Schoneich, J., Wilkinson, V. L., Kado-Fong, H., Presky, D. H. & Kochan, J. P. (1992) *J. Immunol.* 148, 2181–2185.
32. Eshhar, Z., Gross, G. & Treisman, J. (1992) in *Practical Approach to Tumor Immunology*, ed. Gallagher, G. (IRL, Oxford), in press.
33. Gross, G. (1991) Ph.D. thesis (Weizmann Institute of Science, Rehovot, Israel).
34. Kabat, E. A., Wu, T. T., Reid-Miller, M., Perry, H. M. & Gottesman, K. S. (1987) *Sequences of Proteins of Immunological Importance* (Department of Health and Human Services, Washington, D.C.), 4th Ed.

Human T-lymphocyte cytotoxicity and proliferation directed by a single chimeric TCR ζ /CD28 receptor

John Maher, Renier J. Brentjens, Gertrude Gunset, Isabelle Rivière, and Michel Sadelain*

Artificial receptors provide a promising approach to target T lymphocytes to tumor antigens. However, the receptors described thus far produce either an activation or a co-stimulatory signal alone, thus limiting the spectrum of functions accomplished by the genetically modified cells. Here we show that human primary T lymphocytes expressing fusion receptors directed to prostate-specific membrane antigen (PSMA) and containing combined T-cell receptor- ζ (TCR ζ), and CD28 signaling elements, effectively lyse tumor cells expressing PSMA. When stimulated by cell-surface PSMA, retrovirally transduced lymphocytes undergo robust proliferation, expanding by more than 2 logs in three weeks, and produce large amounts of interleukin-2 (IL-2). Importantly, the amplified cell populations retain their antigen-specific cytolytic activity. These data demonstrate that fusion receptors containing both TCR and CD28 signaling moieties are potent molecules able to redirect and amplify human T-cell responses. These findings have important implications for adoptive immunotherapy of cancer, especially in the context of tumor cells that fail to express major histocompatibility complex antigens and co-stimulatory molecules.

The induction of potent tumor immunity presents a major challenge for cancer immunotherapy. Tumor cells have many properties that facilitate immune evasion^{1–3}. Most tumor antigens characterized to date are self-antigens and are thus poorly immunogenic^{4,5}. The paucity of target antigens, the difficulty of overcoming tolerance to self-antigens, and impaired antigen presentation also contribute to compromise T-cell priming in cancer-bearing hosts^{1–3,6–10}. Furthermore, malignant cells may escape from tumor-specific effector T cells by downregulating major histocompatibility complex (MHC) and/or antigen expression, or by establishing an immunosuppressive microenvironment^{1–3,11}.

Genetic approaches offer a potential means to enhance immune recognition and elimination of cancer cells. One promising strategy is to genetically engineer T lymphocytes to express artificial TCRs that direct cytotoxicity toward tumor cells^{12,13}. Artificial receptors typically comprise a tumor antigen-specific recognition element derived from a single-chain antibody variable fragment (scFv). When used to reprogram T-cell specificity, such fusion receptors permit MHC-independent recognition of native rather than processed antigen^{12–14}. ScFv-based TCRs are engineered to contain a signaling domain that delivers an activation stimulus (signal 1) only^{12–14}. The TCR ζ cytoplasmic domain, which delivers a potent signal 1 in the absence of the remaining components of the TCR-CD3 complex^{15,16}, is well suited for activating cytolytic functions. The potential clinical utility of this strategy is supported by the demonstration that, despite fears about defective signaling in lymphocytes of tumor-bearing subjects¹⁷, ζ -chain fusion receptors retain potent activity in cancer patient cytotoxic T cells¹⁸.

However, while sufficient to elicit tumoricidal functions, the engage-

ment of ζ -chain fusion receptors may not suffice to elicit substantial IL-2 secretion in the absence of a concomitant co-stimulatory signal¹⁸. In physiological T-cell responses, optimal lymphocyte activation requires the engagement of one or more co-stimulatory receptors (signal 2), the best characterized of which is CD28 (refs 19–22). Provision of signal 1 in the absence of CD28 signaling can result in a very poor T-cell proliferative response or in the induction of anergy or apoptosis^{19–22}. Consequently, it may be extremely valuable to engineer human T cells so that they receive a co-stimulatory signal in a tumor antigen-dependent manner. An important development in this regard has been the successful design of scFv-CD28 fusion receptors that transduce a functional antigen-dependent co-stimulatory signal in human primary T cells, permitting sustained T-cell proliferation when both the endogenous TCR and the chimeric CD28 receptor are engaged²³.

In the present study, we combine activation and co-stimulatory functions within a single receptor by constructing scFv-based receptors that comprise both TCR ζ and CD28 sequences. The function of these dual-fusion receptors was investigated in CD4⁺ and CD8⁺ primary T cells to fully assess proliferative and cytotoxic functions in biologically and therapeutically relevant cell types. These fusion receptors are specific for PSMA, a glutamate carboxypeptidase that is expressed on the surface of normal prostate epithelial cells and is overexpressed in the majority of prostate carcinomas²⁴. PSMA is also present in the neovasculature associated with a broad range of solid tumors²⁵ and is therefore an attractive target for immunotherapy²⁶. Here, we report that when the signaling domain of CD28 is placed proximal to that of TCR ζ , the resultant P28z receptor confers upon human peripheral blood T lymphocytes (PBLs) the ability to produce IL-2, to proliferate,

*Department of Human Genetics/Medicine, Gene Transfer and Somatic Cell Engineering Laboratory, and Immunology Program, Memorial Sloan-Kettering Cancer Center, New York, NY 10021. *Corresponding author (m.sadelain@ski.mskcc.org)*

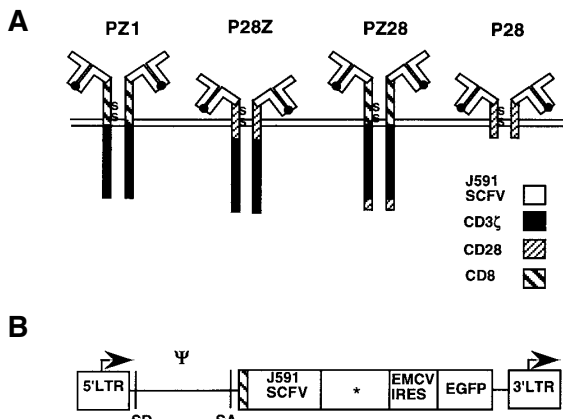


Figure 1. Structure of TCR ζ -CD28 fusion receptors. (A) The PSMA-specific fusion receptors encompass an scFv derived from the J591 hybridoma, joining the V H and V L fragments through a serine/glycine linker (shown as the filled circle). In Pz1, a human CD8 α hinge and transmembrane domain links the scFv to the intracellular domain of human TCR ζ . In P28, the scFv is joined to the intracellular, transmembrane, and much of the extracellular portion of human CD28. In P28z, the intracellular TCR ζ sequence has been joined to the C terminus of P28. Pz28 consists of the intracellular 41 amino acids of CD28 joined onto the Pz1 receptor. (B) All PSMA-specific receptors were expressed using the SFG onco-retroviral vector. The asterisk indicates the site of insertion of cDNA sequences that differed among the PSMA-specific fusion receptors. Bicistronic constructs encoding the receptor cDNA cloned upstream of the EMCV-IRES-eGFP cassette were used for all experiments. The long terminal repeat (LTR) promoter is arrowed, and the splice donor (SD) and splice acceptor (SA) sites flanking the packaging signal (ψ) are indicated.

and to kill in a PSMA-dependent manner. Our data demonstrate that a single molecule can deliver both functional and antigen-specific signals 1 and 2 in human primary T cells.

Results

Transduction and expression of PSMA-specific TCR ζ -CD28 fusion receptors in primary human T lymphocytes. The goal of the present study was to genetically modify primary human T lymphocytes so that they acquire both a TCR-like and a co-stimulatory signal upon interaction with native PSMA. A series of receptors were generated that comprise a PSMA-specific scFv fragment coupled to signaling elements derived from TCR ζ and/or CD28 (Fig. 1A). Pz1 (ref. 18) and P28 are designed to respectively deliver signals 1 and 2 in a PSMA-dependent manner. In P28z, the intracellular portion of TCR ζ has been joined to the C terminus of P28 (ref. 23), while in Pz28, the CD28 signaling domain was added at the C terminus of Pz1. All chimeric complementary DNAs

(cDNAs) were cloned in bicistronic onco-retroviral vectors upstream of enhanced green fluorescent protein (eGFP; Fig. 1B). Three days after transduction of mitogen-activated PBLs, gene transfer efficiency, as assessed by flow cytometry, ranged from 20% to 70% (Fig. 2A). CD4 $^+$ and CD8 $^+$ T-cell subsets were transduced at similar efficiencies (Fig. 2B), as reported elsewhere^{18,19,27}. Expression of ζ -chain containing fusion receptors was also analyzed by western blotting, confirming homodimer formation and little, if any, heterodimerization with endogenous CD8 or CD28 (Fig. 2C).

The P28z and Pz28 fusion receptors promote PSMA-specific cytotoxicity. To confirm that the TCR ζ -CD28 fusion receptors specifically engaged PSMA, cytotoxicity assays were performed three days after transduction. Pz1, which was previously shown to direct specific cytotoxicity against PSMA-positive tumor cells¹⁸, served as positive control. Both P28z and Pz28 receptors, but not P28, mediated specific lysis of fibroblasts expressing human PSMA (Fig. 3A).

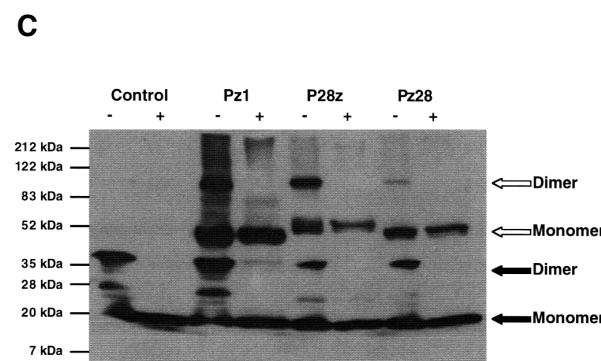
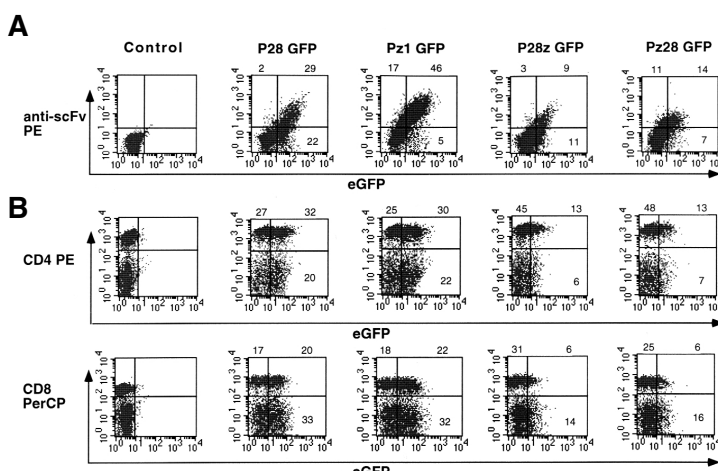


Figure 2. Expression of PSMA-specific TCR ζ -CD28 fusion receptors in primary human T lymphocytes (PBLs). (A) PBLs were transduced with the indicated GFP-containing dicistronic retroviral constructs or an irrelevant control (SFG-c-fms). On day 7, gene transfer efficiency was assessed by flow cytometry, measuring GFP fluorescent emission and by staining with PE-conjugated antisera reactive with the J591-derived scFv. (B) To determine the percentage transduction of T-cell subsets, samples were also stained with CD4 PE and CD8 PerCP antibodies and analyzed by three-color flow cytometry, using GFP emission to identify transduced cells. Quadrants were set using control samples so that 99% of events were negative for the marker of interest. Surface expression of Pz1 was typically greater than that of P28 or either of the TCR ζ -CD28 fusion receptors. Mean fluorescence intensity when Pz1 expression was normalized to 100 was as follows: P28 = 35.1 ± 17.8 ($P < 0.05$); P28z = 29.6 ± 12.2 ($P < 0.01$); Pz28 = 25.9 ± 6.9 ($P < 0.01$) ($n = 3\text{--}4$ experiments). There was no significant difference in expression intensity between P28, P28z, and Pz28. (C) Lysates were prepared under reducing (+) and nonreducing (-) conditions from PBLs following transduction with Pz1 (54% GFP-expressing), P28z (21% GFP-expressing), and Pz28 (20% GFP-expressing). Untransduced PBLs were used as controls. Immunoreactive receptor bands were detected by western blotting using an anti-TCR ζ monoclonal antibody. Filled arrows indicate the monomeric and dimeric forms of the endogenous TCR ζ . Pz1 and P28z are predominantly expressed as homodimers, as would be expected from the design of the hinge regions of these molecules. However, Pz28 was found to dimerize less effectively in T cells and in PG13 cells (data not shown). No bands indicating productive heterodimerization with CD8 α , CD8 β , or CD28 were detected. The additional band seen under that corresponding to dimerized ζ is likely to be a degradation product of this dimer. Empty arrows show the positions of the monomeric and dimeric PSMA-specific fusion receptors. Molecular mass markers are indicated on the left of the panel.



The fusion receptor P28z elicits IL-2 production upon engagement with PSMA. To assay the ability of the different receptors to signal for IL-2 production, transduced PBLs were co-cultivated with NIH3T3 cells expressing PSMA and/or B7.1 (refs 18,19) in medium lacking IL-2 (Table 1). Three receptors (Pz1, P28z, and Pz28) elicited IL-2 secretion in the presence of PSMA and B7.1. In the absence of co-stimulatory ligand, IL-2 production was only observed in cultures of P28z-transduced T cells. IL-2 levels were elevated, ranging within 40–55% of those obtained by co-culturing the same transduced T cells with the monolayer co-expressing PSMA and B7.1.

The P28z fusion receptor promotes proliferation of genetically modified T cells in response to PSMA. To test if P28z could deliver combined and functional signals 1 and 2, transduced PBLs were plated on NIH3T3 cells expressing B7.1, PSMA, PSMA + B7.1, or on unmodified NIH3T3 cells. All cultures declined over one week in the absence of PSMA (Fig. 4A, B).

When stimulated by a monolayer co-expressing PSMA + B7.1 (Fig. 4D), Pz1-transduced PBLs underwent expansion, as did PBLs transduced with P28z or Pz28, further establishing that both TCR ζ -CD28 fusion receptors deliver a TCR-like signal. Control P28-transduced T cells did not expand under these conditions, indicating that neither co-stimulation alone nor adherence to the monolayer enhanced proliferation. When stimulation was provided by NIH3T3

cells expressing PSMA alone (Fig. 4C), T cells expressing Pz1 underwent limited expansion. Pz28-transduced cells also grew poorly, further indicating that this fusion receptor does not deliver a meaningful co-stimulatory signal. By contrast, P28z-transduced T cells consistently proliferated, corroborating observations by Eshhar *et al.* showing that immobilized hapten can induce proliferation in T cells that express a trinitrophenol-specific CD28-Fcγ fusion receptor²⁸. P28z-transduced T cells markedly expanded, showing absolute increases in cell numbers (8.6 ± 5.2-fold over a seven-day period, $n = 8$ experiments). Taken together, these data strengthen the argument that P28z can provide both signals 1 and 2. Importantly, after seven days of co-culture onto a PSMA $^+$ fibroblast monolayer, T cells expressing the P28z fusion receptor retained the ability to specifically lyse PSMA $^+$ targets (Fig. 3B).

The P28z fusion receptor permits sequential re-stimulation of transduced human PBLs in response to PSMA. If P28z can provide co-stimulation in addition to a TCR-like signal, it would be expected that cells expressing this receptor should undergo further expansion upon secondary encounter with PSMA. However, if the co-

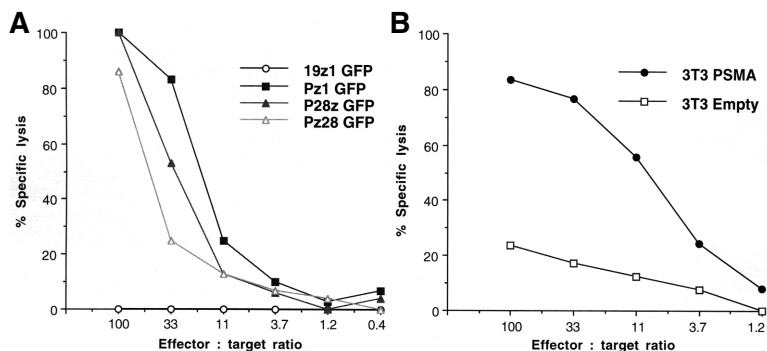


Figure 3. Specific target cell lysis by PSMA redirected T cells. (A) T cells were transduced with 19z1 GFP (control), Pz1 GFP, P28z GFP, or Pz28 GFP. Three days after completion of gene transfer, 4 h CTL assays were established at the indicated ratios using as targets NIH3T3 cells expressing PSMA. No specific lysis was observed using untransduced NIH3T3 cells as control targets. The greater lytic activity of Pz1-transduced cells may reflect the higher cell-surface expression of this receptor, or, more likely, the greater proportion of transduced T cells (46% of T cells, of which 21% are CD8 $^{+}$, compared with 25% P28z-transduced cells, including 12% CD8 $^{+}$ cells, and 20% Pz28-transduced cells, including 10% CD8 $^{+}$ cells). The control 19z1 receptor (specific for CD19; R.J.B. and M.S., unpublished results) did not effect lysis of PSMA-expressing targets, despite the presence of the same TCR ζ chain in this molecule. (B) P28z-transduced T cells were stimulated on NIH3T3 cells expressing PSMA and, after one week, were established in 4 h CTL assays with NIH3T3 cells expressing PSMA or untransduced cells as controls. At this time, the T cells were 62% GFP $^{+}$ (of which 17% were CD8 $^{+}$).

stimulatory potency of this molecule is inadequate, sequential exposure to antigen could result in a poor proliferative response resulting from induction of anergy and/or apoptosis^{20,21}. To test this, transduced PBLs stimulated on the different NIH3T3 monolayers were subjected to secondary re-stimulation after a seven-day interval. Pz1-transduced T cells expanded in response to primary encounter with PSMA. However, re-stimulation with PSMA resulted in a dramatic decline in the number of transduced cells (Fig. 5A, B). Importantly, the same T cells underwent brisk expansion after both primary and secondary stimulation if the fibroblast monolayer co-expressed PSMA and B7.1 (Fig. 5C and D, respectively). In contrast, the absolute number of P28z-transduced CD8 $^{+}$ and CD4 $^{+}$ T cells increased after primary stimulation and underwent further increase after re-stimulation on day 7, irrespective of the presence of B7.1. Expansion was indeed similar in response to PSMA alone or PSMA + B7.1, underscoring the relative potency of the co-stimulatory signal provided by P28z. Re-stimulation of P28z cultures with PSMA yielded a 4.0 ± 2.4-fold expansion in total cell number over a seven-day period ($n = 4$ experiments). Following another re-stimulation under the same conditions, the total cell number increased by more than 2 logs over a three-week interval (Fig. 5E). In this period, a progressive enrichment of transduced over nontransduced cells was observed, in keeping with the selective advantage conferred to cells expressing P28z (Fig. 5F). Together, these data provide conclusive evidence that P28z delivers a functional signal 1 and signal 2 upon interaction with PSMA. Importantly, the same result was obtained with another receptor, 19-28z, which was modeled on P28z. 19-28z-transduced PBLs showed the same ability to be re-stimulated by CD19 $^{+}$ cells and to proliferate (unpublished observations), indicating that proliferative responses were achieved with receptors recognizing unrelated antigens.

P28z-transduced PBLs lyse PSMA $^{+}$ tumor cells and proliferate in response to LNCaP cells. We had previously shown that Pz1-transduced T cells specifically lyse LNCaP cells, a PSMA $^{+}$ human prostate cancer cell

Table 1. Interleukin-2 production by human PBL transduced with different CD3 ζ -CD28 fusion receptors^a

Fibroblast feeder	PSMA-specific receptor			
	P28	Pz1	P28z	Pz28
Unmodified NIH3T3	<50 (-)	<50 (-)	<50 (-)	<50 (-)
B7.1	<50 (-)	<50 (-)	<50 (-)	<50 (-)
PSMA	<50 (-)	<50 (-)	21,900 (1,153)	<50 (-)
PSMA + B7.1	<50 (-)	164,236 (3,285)	52,936 (2,786)	29700 (958)

^aThree days after retroviral transduction, human PBLs expressing the indicated chimeric receptor were plated at 10 6 PBLs/ml on the specified NIH3T3 monolayers. Supernatants were harvested after 24 h and assayed for IL-2 content by ELISA. Data are expressed as mean IL-2 concentrations (pg/ml) from duplicate wells, followed in parentheses, by IL-2 content normalized for gene transfer efficiency. Coefficients of variation between duplicates were all <2.5%. Normalized IL-2 values were determined by dividing the mean IL-2 concentration by the percentage transduced cells in the appropriate culture. Normalized IL-2 content measured in medium conditioned by P28z- and Pz1-transduced lymphocytes were comparable when the stimulus consisted of both PSMA and B7.1. Pz28-transduced T cells also produced readily detectable amounts of IL-2, but, interestingly, the magnitude of this response was consistently lower than that obtained with either Pz1 or P28z. Similar findings were observed in two independent experiments.

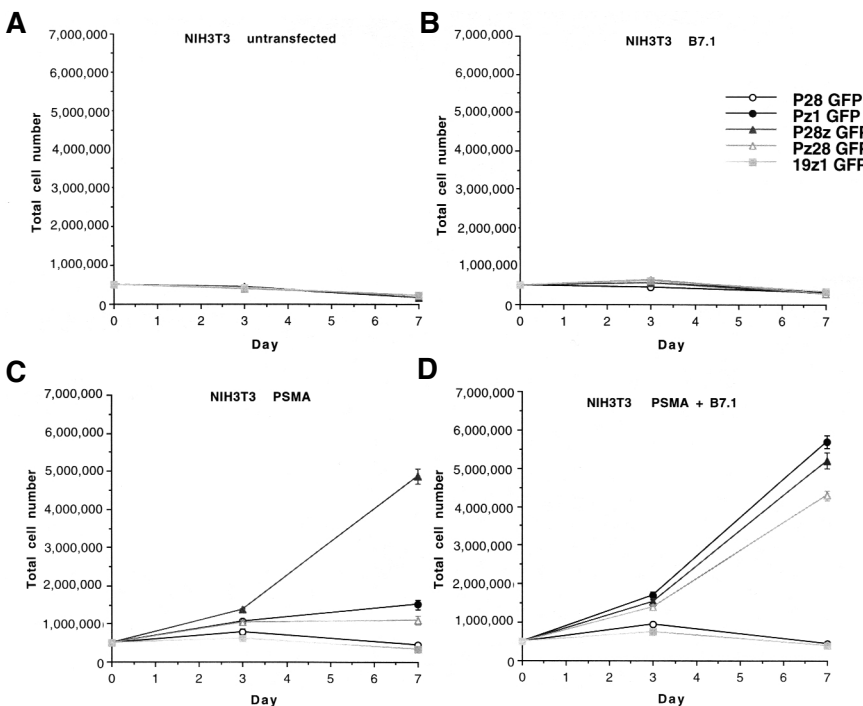


Figure 4. The P28z fusion receptor renders human T lymphocytes capable of PSMA-dependent expansion. Human T cells were transduced with the following retroviral constructs (gene transfer efficiency indicated in parentheses): SFG 19z1 (60%), SFG P28 (53%), SFG Pz1 (68%), SFG P28z (23%), and SFG Pz28 (32%). Three days later, 5×10^5 transduced T cells were co-cultured in 20 U/ml IL-2 with irradiated NIH3T3 feeder cells as follows: (A) unmodified (B) NIH3T3-B7.1 (C) NIH3T3-PSMA, or (D) NIH3T3-PSMA + B7.1. Cell numbers were counted on days 3 and 7, and data presented are mean \pm s.d. of triplicate evaluations. Similar results were obtained in three experiments.

advantage conferred by the receptor. The capacity of P28z to deliver signal 1 is demonstrated by production of IL-2 and induction of cell proliferation upon stimulation with PSMA + B7.1, which are comparable to those obtained in T cells expressing Pz1 (which contains TCR ζ but no CD28 sequences). Specific lysis of PSMA $^+$ targets also reflects functional activation through the TCR pathway. Importantly, the P28z fusion receptor can also provide potent co-stimulation (signal 2). Thus, in the absence of exogenous B7-driven co-stimulation, engagement

of PSMA elicits IL-2 production and proliferation. Under the same conditions, Pz1-transduced cells fail to secrete IL-2 and proliferate, corroborating findings by Finney *et al.* obtained in Jurkat cells³¹.

The relative positions of the TCR ζ and CD28 signaling elements within the fusion receptor proved crucial. In P28z, the hinge, transmembrane, and proximal intracellular portions of the molecule were derived from CD28, followed by the signaling domain of TCR ζ . When CD28 sequences were fused to the C terminus of TCR ζ , as in Pz28, the functional activity was substantially compromised relative to P28z, particularly with regard to sustaining proliferation. This occurred despite comparable cell-surface expression of the two receptors. Pz28 retained the ability to deliver a TCR-like signal upon PSMA binding, as evidenced by cytolytic activity and B7.1-dependent proliferation and IL-2 production. However the co-stimulatory potency of Pz28, as evaluated in the absence of B7.1, was no better than that of Pz1.

One potential explanation for this finding is that the conformational integrity of the fusion receptor is disrupted when the CD28 signaling domain is placed downstream of TCR ζ . It is noteworthy in this regard that western blotting analysis indicated that the Pz28 receptor exhibited less homodimerization in human T cells than either P28z or Pz1. An alternative explanation is that membrane proximity is more critical for CD28 than for TCR ζ . Thus, placement of the CD28 moiety distal to TCR ζ might impair its ability to associate with downstream signaling molecules, such as p56 ek (ref. 32), which reside in very close proximity to the cell membrane. A third possibility is that these fusion receptors differ in their ability to interact with negative regulators, for example, MAP kinase phosphatase-6 (MKP-6)³³. It is plausible that the ability of P28z to bind MKP-6 might be impaired as a result of steric hindrance, thereby enhancing co-stimulatory activity. Conversely, in the case of Pz28, the binding of this phosphatase at the C terminus may adversely affect the signaling potency of this receptor. This hypothesis is supported by findings indicating that Pz28 was not only less active in eliciting IL-2 secretion than P28z, but also less active than Pz1. A final possible explanation for the superior function of P28z is that it contains the CD28 transmembrane domain, unlike Pz28 and Pz1. However, this is unlikely because the cytoplasmic portion of CD28 is sufficient for co-stimulatory activity³⁴.

line, as well as PSMA-transduced PC3 and EL4 cells, which are respectively a human prostate cancer cell line and a murine thymoma¹⁹. Pz1, P28z, and Pz28 directed comparable and elevated cytolytic activity against LNCaP cells (Fig. 6A). Proliferative responses elicited by LNCaP cells expressing B7.1 were also comparable for these receptors (data not shown). Of the three receptors, however, only P28z could induce sustained proliferation during co-cultivation with LNCaP cells (Fig. 6B). The restimulated T cells preserved their tumocidal activity (data not shown), corroborating findings obtained with PSMA $^+$ fibroblasts (Fig. 3B).

Discussion

The expansion of functional tumor-specific T lymphocytes is of central importance in tumor immunity. Whether in the context of *in vivo* immunization or *ex vivo* T-cell expansion, the biological requirements for T-cell priming and amplification have to be met to attain meaningful immune responses. Co-stimulation is crucial in this process^{19–22} and is thus central to the development of effective adoptive immunotherapy of cancer^{19,29}. Here we describe scFv-based chimeric receptors designed to provide both TCR-like and co-stimulatory signals upon binding of the tumor antigen PSMA. To achieve this, the intracellular domains of human TCR ζ and CD28 have been fused in series within a single molecule, thereby recruiting these signaling motifs to the site of antigen engagement at a fixed stoichiometry of 1:1. Most important, our study was performed in human primary T lymphocytes—that is, in biologically and therapeutically relevant cells. The ability to sustain T-cell expansion and tumocidal functions could therefore be evaluated, which is not possible in leukemic cells^{30,31}. We show here that, following contact with cell-bound PSMA, activated human PBLs engineered to express the P28z receptor produce IL-2, undergo sequential rounds of expansion, and maintain thereafter their ability to execute specific lysis of PSMA-expressing target cells.

The most important finding in this study is the demonstration that expression of P28z enables T cells to undergo repeated rounds of antigen-dependent stimulation and expansion. This process was accompanied by a progressive increase in the proportion of transduced T cells within bulk cultures, consistent with the expected selective

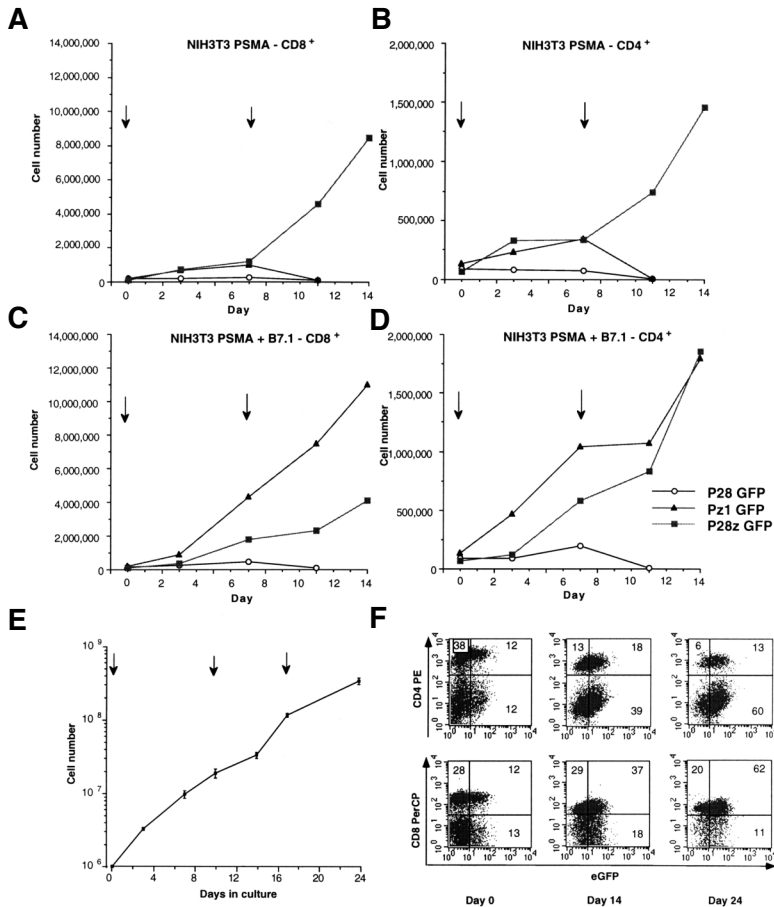


Figure 5. Primary and secondary stimulation of transduced T cells in response to PSMA. Peripheral blood T cells were transduced with the following retroviral constructs (gene transfer efficiency indicated in parentheses): P28 (27%), Pz1 (36%), or P28z (17%). Then the cells were subjected to two rounds of stimulation on NIH3T3 fibroblast feeder layers (indicated by arrows). For the primary stimulation, 1×10^6 transduced T cells were co-cultured in IL-2 (20 U/ml) with irradiated NIH3T3 cells expressing PSMA (panels A and B) or PSMA + B7.1 (panels C and D). On day 7, cultures were re-stimulated by co-culture with a similar monolayer. Absolute numbers of transduced CD8⁺ (panels A and C) and CD4⁺ T cells (panels B and D) were calculated as the product of percentage transduced (determined by flow cytometry) \times total cell count. Co-culture of all transduced PBL populations with B7.1-expressing or unmodified NIH3T3 cells resulted in a progressive decline in total cell number and content of transduced T cells (data not shown). (E) P28z-transduced T cells were expanded by sequential re-stimulation on NIH3T3 PSMA fibroblast feeder layers, as indicated by the arrows. Cultures were maintained in IL-2 (20 U/ml), which was added every three days. The data represent the mean \pm s.d. of six data points (triplicate cell counts from two separate cultures). These cultures were subjected to three-color flow cytometry at intervals to detect transduced (eGFP⁺) cells of the CD4⁺ and CD8⁺ subsets. Similar data were obtained upon analysis of both cultures, and data shown are from one representative example (F).

In summary, we have shown that artificial receptors based upon fusion of the signaling domains of TCR ζ and CD28 can be used to redirect the specificity of primary human T cells to a tumor antigen. The transduced T cells undergo selective expansion following contact with cell-bound PSMA while maintaining the ability to mediate specific lysis of tumor cells. The availability of a single chimeric receptor providing both activation and co-stimulatory functions should greatly facilitate lymphocyte transduction and hence clinical applicability. These findings raise the prospect of a useful approach to cancer immunotherapy based on T cells that are genetically engineered to sustain proliferative and cytotoxic responses against tumor antigens.

Experimental protocol

Recombinant receptors and retroviral vectors. All fusion receptors contain a scFv derived from the J591 hybridoma²⁵ as described¹⁸. To facilitate detection of transduced cells, all constructs contained the encephalomyocarditis virus internal ribosome entry site (EMCV-IRES)³⁷ and the eGFP gene inserted in the SFG vector³⁸. In Pz1, the J591 scFv is coupled through human CD8 α hinge and transmembrane sequences to the intracellular domain of human TCR ζ (ref. 18). P28 comprises a fusion of the J591 scFv to human CD28 as described^{23,39}. To construct P28z, nucleotides 336–660 of CD28 were amplified using primers 1 (5'-GGCGGCCG CAATTGAAGTTATGTATC-3') and 2 (5'-TGCGCTCTGTAACCTCTGGAGCGATAGGCTGCGAAGTCGCG-3'). The intracellular domain of TCR ζ was amplified using primers 3 (5'-AGAGTGAAGTTCAAGCAGGAGCGA-3') and 4 (5'-CTCGAGTGGCTGTAGCGAGG-3'). The products were fused in a separate PCR reaction driven by primers 1 and 4, A-tailed with Taq polymerase, and subcloned as a

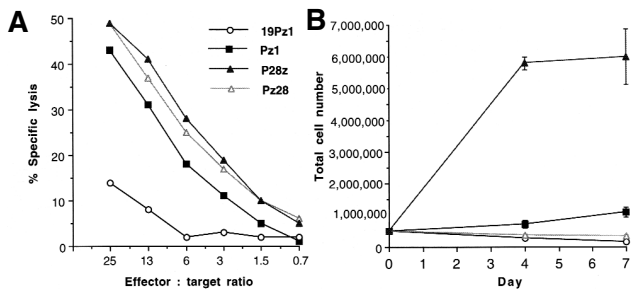


Figure 6. PSMA⁺ tumor cells activate cytolytic and proliferative responses in P28z-transduced PBLs. (A) Specific tumor cell lysis by PSMA-redirected T cells. T cells were transduced with 19z1 (control), Pz1, P28z GFP, and Pz28 GFP. Four days after completion of gene transfer, equivalent numbers of transduced T cells were added to LNCaP human prostate cells. All PSMA-specific T cells (Pz1, P28z, and Pz28) demonstrated cytotoxic activity similar to that demonstrated against NIH3T3 PSMA⁺ fibroblasts. Background cytotoxic activity seen with 19z1 control T cells may be due to alloreactivity (which is not seen with the murine NIH3T3 fibroblasts; Fig. 3). (B) The P28z fusion receptor renders T lymphocytes capable of PSMA-dependent, B7.1-independent expansion following co-cultivation with LNCaP tumor cells. 19z1-, Pz1-, and Pz28-transduced T cells did not expand.

NotI/XbaI fragment into SFG-Pz1. To generate Pz28, the intracellular domain of CD28 was amplified using 5'-GCACTTCACATGCAGGCTCTGCCAC-CTCGCAGGAGTAAGAGGAGCAGGCTCTGCAC-3' and 5'-CGCTC-GAGTCAGGAGCGATAGGCTGCGAAGTCGCGT-3' (two silent mutations introduced to interrupt cytosine repeats are underlined). The resultant PCR product represents a fusion of the distal nine codons of TCR ζ (minus stop codon) to the intracellular domain of CD28 and contains a convenient 5' *Nsi*I site. This fragment was subcloned, digested with *Nsi*I/XbaI, and ligated into SFG-Pz1. SFG-c-fms encodes the human macrophage colony-stimulating factor receptor (J.M. and M.S., unpublished results).

Culture and retroviral transduction of primary human T cells. Peripheral blood mononuclear cells from healthy donors were established in RPMI + 10% (vol/vol) human serum, activated with phytohemagglutinin (2 μ g/ml) for two days, and transferred to non-tissue culture-treated plates (Falcon, Becton Dickinson, Franklin Lakes, NJ) precoated with retinectin (15 μ g/ml; Takara Biomedicals, Shiga, Japan). Gibbon ape leukemia virus envelope-pseudotyped retroviral particles were generated as described^{27,40}. Transduced cells were co-cultivated with NIH3T3 fibroblasts expressing PSMA and/or B7.1 as described^{18,23}. For experiments with LNCaP cells, cells were admixed weekly at a T-cell:tumor cell ratio of 5:1.

Protein analyses. Flow cytometry was carried out using a FACScan cytometer with Cellquest software. Expression of PSMA-specific fusion receptors was directly demonstrated using phycoerythrin (PE)-conjugated goat anti-mouse antiserum¹⁸. CD4-PE and CD8-PerCP antibodies (Becton Dickinson) were used for T-cell subset identification. For western blot analysis, transduced

T-cell samples were prepared as described⁴¹. Briefly, cells were suspended in radioimmunoprecipitation buffer at a concentration of 1×10^7 cells/ml. After 1 h incubation on ice, cells were boiled in 2x loading buffer under nonreducing or reducing conditions with 0.1 M dithiothreitol. Samples were run on 10–20% acrylamide gradient gels and transferred to polyvinylidene fluoride transfer membrane (NEN Life Science Products, Boston, MA). Fusion proteins were detected using the anti-human ζ -chain monoclonal antibody 8D3 (PharMingen, San Diego, CA) as described⁴¹. Immunodetection was performed using the ECL Plus western blotting detection system (Amersham, Buckinghamshire, UK).

Cytotoxicity assays. Cytotoxic T-lymphocyte assays were performed using a nonradioactive cytotoxicity detection kit (lactate dehydrogenase (LDH); Roche Diagnostics, Indianapolis, IN) as described⁴² or ^{51}Cr -release assays performed as described¹⁸.

Statistical analyses. The one-tailed Student's *t*-test was used.

Acknowledgments

We thank P. King and C. Lyddane for critical review of the manuscript. We also thank H. Gallardo and H. Zhu for assistance with T-cell transduction, and J.-B. Latouche for providing NIH3T3-derived feeder cells. This work was supported by the National Institutes of Health, grant CA-59350, the CaP CURE Association, the Jean Shanks Clinical Research Fellowship (Royal College of Pathologists, London, UK), and the Cure for Lymphoma Foundation.

Received 22 September 2001; accepted 22 October 2001

- Gilboa, E. How tumors escape immune destruction and what we can do about it. *Cancer Immunol. Immunother.* **48**, 382–385 (1999).
- Meliet, C.J. et al. Strategies for immunotherapy of cancer. *Adv. Immunol.* **75**, 235–282 (2000).
- Ferrone, S., Finerty, J.F., Jaffee, E.M. & Nabel, G.J. How much longer will tumour cells fool the immune system. *Immunol. Today* **21**, 70–72 (2000).
- Houghton, A.N. Cancer antigens: immune recognition of self and altered self. *J. Exp. Med.* **180**, 1–4 (1994).
- Boon, T., Coulie, P.D. & Van den Eynde, B. Tumor antigens recognized by T cells. *Immunol. Today* **18**, 267–268 (1997).
- Nanda, N.K. & Sercarz, E.E. Induction of anti-self-immunity to cure cancer. *Cell* **82**, 13–17 (1995).
- Sotomayor, E.M., Borrello, I. & Levitsky, H.I. Tolerance and cancer: a critical issue in tumor immunology. *Crit. Rev. Oncog.* **7**, 433–456 (1996).
- Kiertscher, S.M., Luo, J., Dubinett, S.M. & Roth, M.D. Tumors promote altered maturation and early apoptosis of monocyte-derived dendritic cells. *J. Immunol.* **164**, 1269–1276 (2000).
- Almand, B. et al. Increased production of immature myeloid cells in cancer patients: a mechanism of immunosuppression in cancer. *J. Immunol.* **166**, 678–689 (2001).
- Lee, P.P. et al. Characterization of circulating T cells specific for tumor-associated antigens in melanoma patients. *Nat. Med.* **5**, 677–685 (1999).
- Marincola, F.M., Jaffee, E.M., Hicklin, D.J. & Ferrone, S. Escape of human solid tumors from T cell recognition: molecular mechanisms and functional significance. *Adv. Immunol.* **74**, 181–273 (2000).
- Eshhar, Z., Waks, T., Gross, G. & Schindler, D.G. Specific activation and targeting of cytotoxic lymphocytes through chimeric single chains consisting of antibody-binding domains and the gamma or zeta subunits of the immunoglobulin and T-cell receptors. *Proc. Natl. Acad. Sci. USA* **90**, 720–724 (1993).
- Altschmidt, U., Moritz, D. & Groner, B. Specific cytotoxic T lymphocytes in gene therapy. *J. Mol. Med.* **75**, 259–266 (1997).
- Paillard, F. Immunotherapy with T cells bearing chimeric antitumor receptors. *Hum. Gene Ther.* **10**, 151–153 (1999).
- Geiger, T.L., Leitenberg, D. & Flavell, R.A. The TCR ζ -chain immunoreceptor tyrosine-based activation motifs are sufficient for the activation and differentiation of primary T lymphocytes. *J. Immunol.* **162**, 5931–5939 (1999).
- Haynes, N.M. et al. Redirecting mouse CTL against colon carcinoma: superior signaling efficacy of single-chain variable domain chimeras containing TCR- ζ vs FcR γ . *J. Immunol.* **166**, 182–187 (2001).
- Whiteside, T.L. Signaling defects in T lymphocytes of patients with malignancy. *Cancer Immunol. Immunother.* **48**, 346–352 (1999).
- Gong, M.C. et al. Cancer patient T cells genetically targeted to prostate-specific membrane antigen specifically lyse prostate cancer cells and release cytokines in response to prostate-specific membrane antigen. *Neoplasia* **1**, 123–127 (1999).
- Harding, F.A., McArthur, J.G., Gross, J.A., Raulet, D.H. & Allison, J.P. CD28-mediated signalling co-stimulates murine T cells and prevents induction of anergy in T cell clones. *Nature* **356**, 607–609 (1992).
- Lenschow, D.J., Walanus, T.L. & Bluestone, J.A. CD28/B7 system of T cell costimulation. *Annu. Rev. Immunol.* **14**, 233–258 (1996).
- Ward, S.G. CD28: a signalling perspective. *Biochem. J.* **318**, 361–377 (1996).
- Greenfield, E.A., Nguyen, K.A. & Kuchroo, V.K. CD28/B7 costimulation: a review. *Crit. Rev. Immunol.* **18**, 389–418 (1998).
- Krause, A. et al. Antigen-dependent CD28 signaling selectively enhances survival and proliferation in genetically modified activated human primary T lymphocytes. *J. Exp. Med.* **188**, 619–626 (1998).
- Israel, R.S., Powell, C.T., Corr, J.G., Fair, W.R. & Heston, W.D.W. Expression of the prostate-specific membrane antigen. *Cancer Res.* **54**, 1807–1811 (1994).
- Liu, H. et al. Monoclonal antibodies to the extracellular domain of prostate-specific membrane antigen also react with tumor vascular endothelium. *Cancer Res.* **57**, 3629–3634 (1997).
- Gong, M.C., Chang, S.S., Sadelain, M., Bander, N.H. & Heston, W.D.W. Prostate-specific membrane antigen (PSMA)-specific monoclonal antibodies in the treatment of prostate and other cancers. *Cancer Metastasis Rev.* **18**, 483–490 (1999).
- Gallardo, H.F., Tan, C., Ory, D. & Sadelain, M. Recombinant retroviruses pseudotyped with the vesicular stomatitis virus G glycoprotein mediate both stable gene transfer and pseudotransduction in human peripheral blood lymphocytes. *Blood* **90**, 952–957 (1997).
- Eshhar, Z., Waks, T., Bendavid, A. & Schindler, D.G. Functional expression of chimeric receptor genes in human T cells. *J. Immunol. Meth.* **248**, 67–76 (2001).
- Liebowitz, D.N., Lee, K.P. & June, C.H. Costimulatory approaches to adoptive immunotherapy. *Curr. Opin. Oncol.* **10**, 533–541 (1998).
- Alvarez-Vallina, L. & Hawkins, R.E. Antigen-specific targeting of CD28-mediated T cell co-stimulation using chimeric single-chain antibody variable fragment-CD28 receptors. *Eur. J. Immunol.* **26**, 2304–2309 (1996).
- Finney, H.M., Lawson, A.D.G., Bebbington, C.R. & Weir, A.N.C. Chimeric receptors providing both primary and costimulatory signaling in T cells from a single gene product. *J. Immunol.* **16**, 2791–2797 (1998).
- King, P.D. et al. Analysis of CD28 cytoplasmic tail tyrosine residues as regulators and substrates for the protein tyrosine kinases, EMT and LCK. *J. Immunol.* **158**, 580–590 (1997).
- Marti, F. et al. Negative-feedback regulation of CD28 costimulation by a novel mitogen-activated protein kinase phosphatase, MKP6. *J. Immunol.* **166**, 197–206 (2001).
- Stein, P.H., Fraser, J.D. & Weiss, A. The cytoplasmic domain of CD28 is both necessary and sufficient for costimulation of interleukin-2 secretion and association with phosphatidylinositol 3'-kinase. *Mol. Cell. Biol.* **14**, 3392–3402 (1994).
- Hanson, H.L. et al. Eradication of established tumors by CD8⁺ T cell adoptive immunotherapy. *Immunity* **13**, 265–276 (2000).
- Cordaro, T.A. et al. Tumor size at the time of adoptive transfer determines whether tumor rejection occurs. *Eur. J. Immunol.* **30**, 1297–1307 (2000).
- Gallardo, H.F., Tan, C. & Sadelain, M. The internal ribosome entry site of the encephalomyocarditis virus enables reliable coexpression of two transgenes in primary human T lymphocytes. *Gene Ther.* **4**, 1115–1119 (1997).
- Rivière, I., Brose, K. & Mulligan, R.C. Effects of retroviral vector design on expression of human adenosine deaminase in murine bone marrow transplant recipients engrafted with genetically modified cells. *Proc. Natl. Acad. Sci. USA* **92**, 6733–6737 (1995).
- Krause, A., Gong, M., Tan, C. & Sadelain, M. Genetic approaches to sustain the function of tumor-specific T-lymphocytes. *Mol. Ther.* **1**, S260, 713 (2000).
- Rivière, I., Gallardo, H.F., Hagani, A.B. & Sadelain, M. Retroviral-mediated gene transfer in primary murine and human T-lymphocytes. *Mol. Biotechnol.* **15**, 133–142 (2000).
- Jensen, M.C. et al. Human T lymphocyte genetic modification with naked DNA. *Mol. Ther.* **1**, 49–55 (2000).
- Vukmanovic-Stojic, M., Vyas, B., Gorak-Stolinska, P., Noble, A. & Kemeny, D.M. Human Tc1 and Tc2/Tc0 CD8 T cell clones display distinct cell surface and functional phenotypes. *Blood* **95**, 231–240 (2000).

ORIGINAL ARTICLE

Chimeric Antigen Receptor T Cells for Sustained Remissions in Leukemia

Shannon L. Maude, M.D., Ph.D., Noelle Frey, M.D., Pamela A. Shaw, Ph.D.,
 Richard Aplenc, M.D., Ph.D., David M. Barrett, M.D., Ph.D.,
 Nancy J. Bunin, M.D., Anne Chew, Ph.D., Vanessa E. Gonzalez, M.B.A.,
 Zhaohui Zheng, M.S., Simon F. Lacey, Ph.D., Yolanda D. Mahnke, Ph.D.,
 Jan J. Melenhorst, Ph.D., Susan R. Rheingold, M.D., Angela Shen, M.D.,
 David T. Teachey, M.D., Bruce L. Levine, Ph.D., Carl H. June, M.D.,
 David L. Porter, M.D., and Stephan A. Grupp, M.D., Ph.D.

ABSTRACT

BACKGROUND

Relapsed acute lymphoblastic leukemia (ALL) is difficult to treat despite the availability of aggressive therapies. Chimeric antigen receptor-modified T cells targeting CD19 may overcome many limitations of conventional therapies and induce remission in patients with refractory disease.

METHODS

We infused autologous T cells transduced with a CD19-directed chimeric antigen receptor (CTL019) lentiviral vector in patients with relapsed or refractory ALL at doses of 0.76×10^6 to 20.6×10^6 CTL019 cells per kilogram of body weight. Patients were monitored for a response, toxic effects, and the expansion and persistence of circulating CTL019 T cells.

RESULTS

A total of 30 children and adults received CTL019. Complete remission was achieved in 27 patients (90%), including 2 patients with blinatumomab-refractory disease and 15 who had undergone stem-cell transplantation. CTL019 cells proliferated in vivo and were detectable in the blood, bone marrow, and cerebrospinal fluid of patients who had a response. Sustained remission was achieved with a 6-month event-free survival rate of 67% (95% confidence interval [CI], 51 to 88) and an overall survival rate of 78% (95% CI, 65 to 95). At 6 months, the probability that a patient would have persistence of CTL019 was 68% (95% CI, 50 to 92) and the probability that a patient would have relapse-free B-cell aplasia was 73% (95% CI, 57 to 94). All the patients had the cytokine-release syndrome. Severe cytokine-release syndrome, which developed in 27% of the patients, was associated with a higher disease burden before infusion and was effectively treated with the anti-interleukin-6 receptor antibody tocilizumab.

CONCLUSIONS

Chimeric antigen receptor-modified T-cell therapy against CD19 was effective in treating relapsed and refractory ALL. CTL019 was associated with a high remission rate, even among patients for whom stem-cell transplantation had failed, and durable remissions up to 24 months were observed. (Funded by Novartis and others; CART19 ClinicalTrials.gov numbers, NCT01626495 and NCT01029366.)

From the Division of Oncology, Children's Hospital of Philadelphia (S.L.M., R.A., D.M.B., N.J.B., S.R.R., D.T.T., S.A.G.), the Departments of Pediatrics (S.L.M., R.A., D.M.B., N.J.B., S.R.R., D.T.T., S.A.G.), Biostatistics and Epidemiology (P.A.S., R.A.), and Pathology and Laboratory Medicine (J.J.M., B.L.L., C.H.J., S.A.G.), the Division of Hematology–Oncology (N.F., D.L.P.), and Abramson Cancer Center (N.F., A.C., V.E.G., Z.Z., S.F.L., Y.D.M., J.J.M., B.L.L., C.H.J., D.L.P., S.A.G.), Perelman School of Medicine, University of Pennsylvania — all in Philadelphia; and Novartis Pharmaceuticals, East Hanover, NJ (A.S.). Address reprint requests to Dr. Grupp at the Division of Oncology, Children's Hospital of Philadelphia, 3006 Colket Translational Research Bldg., 3501 Civic Center Blvd., Philadelphia, PA 19104, or at grupp@email.chop.edu.

Drs. Maude and Frey contributed equally to this article.

This article was updated on February 18, 2016, at NEJM.org.

N Engl J Med 2014;371:1507-17.

DOI: 10.1056/NEJMoa1407222

Copyright © 2014 Massachusetts Medical Society.

ENGINEERED T-CELL THERAPY IS A NEW strategy for the treatment of relapsed and refractory acute lymphoblastic leukemia (ALL), which is associated with an extremely poor prognosis in adults and remains a leading cause of death from childhood cancer.¹⁻³ In initial proof-of-principle clinical trials involving patients with chronic lymphocytic leukemia (CLL), chimeric antigen receptor-modified T cells that target CD19 produced a durable complete remission in a small number of patients.⁴⁻⁶ Our group and others then extended these findings to relapsed and refractory B-cell ALL, and we found profound responses in a small number of children and adults.^{7,8}

Chimeric antigen receptors are genetically engineered receptors that couple an anti-CD19 single-chain Fv domain to intracellular T-cell signaling domains of the T-cell receptor, thereby redirecting cytotoxic T lymphocytes to cells expressing this antigen. With the use of lentiviral-vector technology for gene transfer and permanent T-cell modification, CTL019 (formerly known as CART19)-engineered T cells express a chimeric antigen receptor in which the T-cell activation signal is provided by the CD3-zeta domain, and the co-stimulatory signal is provided by the CD137 (4-1BB) domain.⁴

We previously reported a high degree of in vivo expansion of CTL019 cells that resulted in complete remission in two children with relapsed and highly refractory B-cell ALL.⁸ However, the rate of complete remission in a larger cohort, long-term persistence of chimeric antigen receptor-modified T cells, and the durability of remission remained unknown. We now report the results of CART19 (A Phase I/IIA Study of Redirected Autologous T Cells Engineered to Contain Anti-CD19 Attached to TCRzeta and 4-1BB Signaling Domains in Patients with Chemotherapy Resistant or Refractory CD19+ Leukemia and Lymphoma) showing the efficacy of CTL019 and provide follow-up of up to 2 years in our expanded cohort of 30 patients with relapsed and refractory ALL. Robust expansion of CTL019 cells rapidly induced complete remission in this cohort of patients who were previously considered to have refractory and incurable disease.

METHODS

TRIAL DESIGN AND OVERSIGHT

We conducted pilot clinical trials at Children's Hospital of Philadelphia and the Hospital of the

University of Pennsylvania that were designed to assess the safety and feasibility of CTL019 T-cell therapy in patients with relapsed and refractory CD19+ cancers; the protocols were approved by the respective institutional review boards. All the authors discussed and interpreted the study results and vouch for the data and analyses. All the patients or their parents provided written informed consent. Enrolled patients received CTL019 infusions between April 2012 and February 2014. Additional details regarding the study design are provided in the Supplementary Appendix, available with the full text of this article at NEJM.org.

Leukapheresis products were stimulated with paramagnetic beads coated with antibodies to CD3 and CD28 and transduced with the CD19-BB-zeta transgene as described previously.^{4,9} After leukapheresis, patients received interim therapy at the discretion of their treating physician. Chemotherapy aimed at depletion of T lymphocytes (Table S1 in the Supplementary Appendix) was administered 1 week before infusion of CTL019 (Table S2 in the Supplementary Appendix), except in three patients who had persistent cytopenias.

PATIENT CHARACTERISTICS

A total of 25 patients, 5 to 22 years of age, were treated at Children's Hospital of Philadelphia (pediatric trial), and 5 older patients, 26 to 60 years of age, were treated at the Hospital of the University of Pennsylvania (adult trial) (Table 1). Of these patients, 26 had B-cell ALL in a first to fourth relapse, 3 had primary refractory B-cell ALL, and 1 had relapsed T-cell ALL that expressed CD19. Eighteen patients had relapsed disease after allogeneic stem-cell transplantation. Three patients (Patients 2, 3, and 20) had disease that was previously shown to be refractory to blinatumomab (a bispecific antibody with one domain that binds to CD3 on T cells and the other that binds to CD19).

RESULTS

OUTCOMES

Twenty-seven of 30 patients (90%) were in a morphologic complete remission at the first assessment 1 month after the infusion of CTL019. A test to detect minimal residual disease by means of multiparametric flow cytometry was negative in 22 patients, positive in 3 patients (the levels of minimal residual disease were 0.1% [and subsequently negative at 3 months], 0.09%, and 0.22%,

respectively), and not performed in 2 patients. A complete remission was achieved in 2 of 3 patients who had previously been exposed to blinatumomab. The 2 patients in whom blast cells were detected in the cerebrospinal fluid at the time of infusion subsequently had no detectable central nervous system (CNS) leukemia as of the most recent follow-up (6 months), and no CNS relapses were observed.

Seven patients who had a complete remission subsequently had a relapse between 6 weeks and 8.5 months after infusion of CTL019 cells. Three relapses developed after early loss of CTL019-modified T cells at 2 weeks to 3 months, and in these patients the relapsed ALL remained CD19-positive. After recovery of normal B cells at 2 to 3 months, one relapse occurred rapidly at 3 months and two relapses were delayed (they occurred at 6 and 8.5 months). Patient 9, who had minimal residual disease (0.22%) at 1 month, had a relapse with CD19-positive ALL at 6 weeks. The disease rapidly progressed, and the patient died from ALL. This patient had highly refractory disease that was in the fourth relapse at the time of infusion and was not eligible for stem-cell transplantation because of coexisting conditions. In three patients, the loss of the expression of CD19 in leukemia cells resulted in a relapse; one of these patients (Patient 2) had received prior blinatumomab therapy. In these patients, CTL019 cells were not lost at the time of relapse.

Of the 27 patients who had a complete remission, 19 remained in remission: 15 patients received no further therapy, and 4 patients withdrew from the study to receive other therapy. In Patient 11, the myelodysplastic syndrome developed during ALL remission, and the patient withdrew from the study to receive other therapy. The median follow-up was 7 months (range, 1 to 24). No deaths were related to the study treatment. Seven patients died after disease progression or relapse, including 1 patient who died from the myelodysplastic syndrome. At 6 months, the event-free survival rate was 67% (95% confidence interval [CI], 51 to 88) and the overall survival rate was 78% (95% CI, 65 to 95) (Fig. 1A and 1B).

IN VIVO EXPANSION AND PERSISTENCE OF CTL019

The CTL019 cells were easily detectable by means of flow cytometry, thus reflecting high *in vivo* proliferation. In 27 patients who had a response, high peak proportions of CTL019-modified T cells were detected by this method (median, 39.8% of

Table 1. Baseline Characteristics of the Patients.*

Characteristic	Pediatric Cohort (N=25)	Adult Cohort (N=5)	Total (N=30)
Sex — no. (%)			
Female	11 (44)	1 (20)	12 (40)
Male	14 (56)	4 (80)	18 (60)
Age at infusion — yr			
Median	11	47	14
Range	5–22	26–60	5–60
Allogeneic transplantation — no. (%)	18 (72)	0	18 (60)
Primary refractory disease — no. (%)	0	3 (60)	3 (10)
Relapse — no. (%)			
1	3 (12)	2 (40)	5 (17)
≥2	22 (88)		22 (73)
Baseline burden of acute lymphoblastic leukemia — no. (%)			
Presence of detectable disease†	20 (80)	4 (80)	24 (80)
Morphologic remission‡		1 (20)	1 (3)
Absence of minimal residual disease	5 (20)		5 (17)
High-risk cytogenetic factors — no.			
BCR-ABL1		2	
IKZF1 deletion		2	
iAMP21		1	
MLL translocation		1	
Hypodiploidy		2	
CNS status — no.§			
CNS-1		23	
CNS-2		2	

* CNS denotes central nervous system, and iAMP21 intrachromosomal amplification of chromosome 21.

† Disease was detected by assessment of bone marrow and cerebrospinal fluid morphologic features and measurement of minimal residual disease.

‡ Minimal residual disease was not measured.

§ CNS status was determined only in the pediatric trial. CNS status was defined as CNS-1 (no detectable blast cells in a sample of cerebrospinal fluid), CNS-2 (blast cells detected in a sample with <5 leukocytes per cubic millimeter and <10 erythrocytes per cubic millimeter), and CNS-3 (blast cells detected in a sample with ≥5 leukocytes per cubic millimeter and <10 erythrocytes per cubic millimeter). The presence of CNS-3 disease was an exclusion criterion.

CTL019-positive cells in CD3-positive cells; range, 4.4 to 69.3), whereas in the 3 patients who did not have a response, 0.2%, 0.6%, and 8.2% of CD3-positive cells, respectively, were CTL019-positive at peak levels. CTL019 cells were detectable in the blood by means of flow cytometry for up to 11 months (Fig. 2A and 2B).

The probability of persistence of CTL019 at 6 months was 68% (95% CI, 50 to 92). CTL019

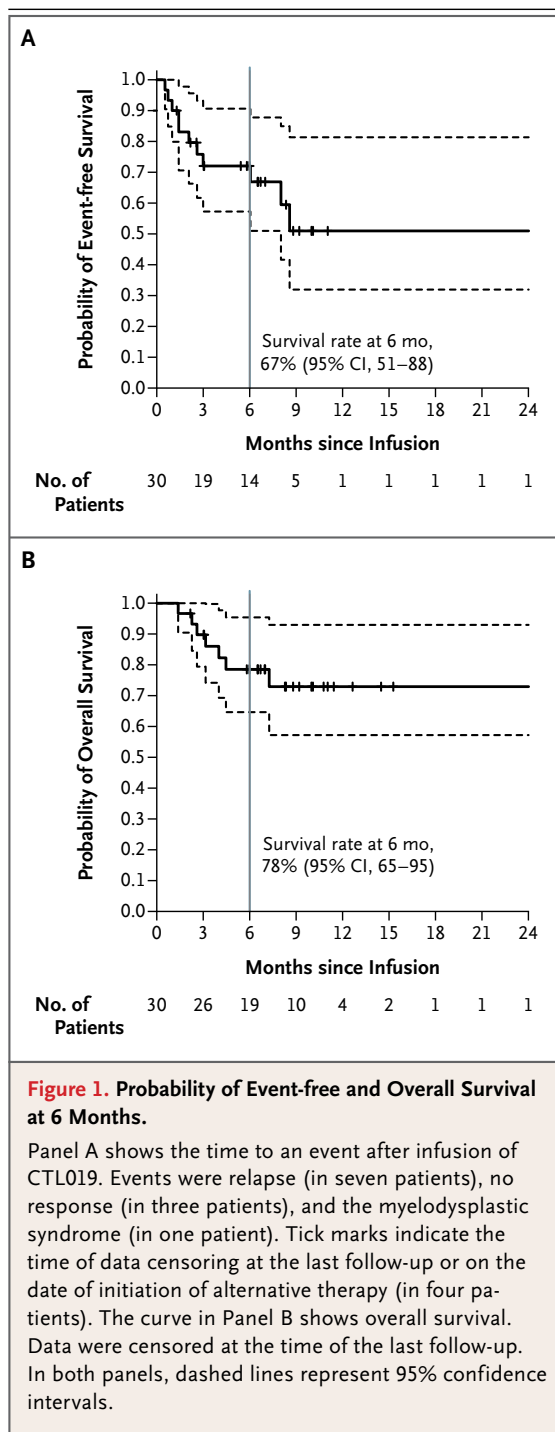


Figure 1. Probability of Event-free and Overall Survival at 6 Months.

Panel A shows the time to an event after infusion of CTL019. Events were relapse (in seven patients), no response (in three patients), and the myelodysplastic syndrome (in one patient). Tick marks indicate the time of data censoring at the last follow-up or on the date of initiation of alternative therapy (in four patients). The curve in Panel B shows overall survival. Data were censored at the time of the last follow-up. In both panels, dashed lines represent 95% confidence intervals.

sequences remained detectable by means of quantitative polymerase-chain-reaction (PCR) assay in patients with sustained remissions until 2 years (Fig. 2C and data not shown). This assay showed very high levels of proliferation of CTL019 cells; all patients had peak levels greater than 5000 copies per microgram of genomic DNA, and 26 patients had peak levels greater than 15,000 copies

per microgram of genomic DNA. One patient (Patient 17) received infusions again at 3 months and 6 months because of early loss of CTL019 cells with B-cell recovery, and this patient subsequently had persistence of CTL019. In the patient with the longest remission (2 years), B-cell aplasia (absence of CD19-positive cells) (Fig. 3) continued for a year after the loss of CTL019 cells detectable by flow cytometry, suggesting functional persistence of CTL019 cells below the limits of detection by flow cytometry, whereas CTL019 remained detectable by means of quantitative PCR. The probability of relapse-free B-cell aplasia at 6 months was 73% (95% CI, 57 to 94).

CTL019 FOR RELAPSE AFTER ALLOGENEIC STEM-CELL TRANSPLANTATION

In the 18 patients who were treated for relapse of disease after allogeneic stem-cell transplantation, the median donor chimerism at the time of leukapheresis was 100% (range, 68 to 100). No graft-versus-host disease was observed after infusion of CTL019. Event-free survival and overall survival did not differ significantly between the patients who had previously undergone stem-cell transplantation and those who had not undergone stem-cell transplantation ($P=0.21$ for event-free survival and $P=0.24$ for overall survival).

THERAPY AFTER ADMINISTRATION OF CTL019

Five patients withdrew from the study after the administration of CTL019 to receive other therapy; three of these patients underwent allogeneic stem-cell transplantation while their disease was in remission, and the disease remained in remission 7 to 12 months after the infusion of CTL019. Patient 12, who had undergone a previous stem-cell transplantation, had a post-transplantation relapse of T-cell ALL that aberrantly expressed CD19, was refractory to two intensive reinduction regimens, and entered a morphologic remission after the infusion of CTL019, but the patient had minimal residual disease (0.09%). She subsequently received bortezomib and an infusion of donor lymphocytes, and the disease remained in remission without minimal residual disease at 11 months. In Patient 11, the myelodysplastic syndrome developed and led to overt acute myeloid leukemia with a monosomy 8 clone that also shared cytogenetic features with the original B-cell ALL.

CYTOKINE-RELEASE SYNDROME

A major toxic effect associated with CTL019 is the cytokine-release syndrome, a systemic inflammatory response that is produced by elevated levels of cytokines; these elevations are associated with T-cell activation and proliferation. The cytokine-release syndrome ranges from mild and self-limiting, with high temperatures and myalgias, to severe and life-threatening, with a clinical course that also includes vascular leak, hypotension, respiratory and renal insufficiency, cytopenias, and coagulopathy. Several aspects of the cytokine-release syndrome mirror those of the macrophage activation syndrome.⁸ All the patients in our studies had the cytokine-release syndrome, which was mild to moderate in 22 of the 30 patients. These patients required hospitalization for febrile neutropenia and received broad-spectrum antibiotics and pain medications. Severe cytokine-release syndrome, which required intensive care with varying degrees of respiratory support (from placement of a nasal cannula to mechanical ventilation), developed in 8 patients (27%), and all these patients required vasopressor support for hypotension. Coagulopathy, with elevated prothrombin and partial-thromboplastin times as well as severe hypofibrinogenemia, was observed in patients who had severe cytokine-release syndrome, although clinical bleeding was rare (observed in 3 patients).

Severe cytokine-release syndrome started a median of 1 day after infusion, whereas cytokine-release syndrome that was not severe started a median of 4 days after infusion ($P=0.005$). Laboratory markers of systemic inflammation, including C-reactive protein and ferritin levels, were elevated in all the patients. Patients who had severe cytokine-release syndrome had higher peak levels of interleukin-6 than did patients who did not have severe cytokine-release syndrome ($P<0.001$) (Fig. 4A); they also had higher peak levels of C-reactive protein ($P=0.02$), ferritin ($P=0.005$), interferon- γ ($P<0.001$), and soluble interleukin-2 receptor ($P<0.001$) (Fig. S2 in the Supplementary Appendix). The baseline disease burden (the percentage of blast cells in bone marrow before infusion) correlated with the severity of the cytokine-release syndrome; a higher disease burden was significantly associated with severe cytokine-release syndrome ($P=0.002$) (Fig. 4B). Patients with severe cytokine-release syndrome also had higher levels of CTL019-positive

CD8 cells ($P=0.012$) and CTL019-positive CD3 cells ($P=0.026$).

We previously found marked elevation of interleukin-6 levels after CTL019 therapy and rapid reversal of severe cytokine-release syndrome with the interleukin-6-receptor blocking antibody tocilizumab⁸; therefore, tocilizumab was incorporated into the management of severe cytokine-release syndrome in this study. Nine patients received tocilizumab, which resulted in rapid defervescence and stabilization of blood pressure, with improvement (weaning from vasopressor support) over a period of 1 to 3 days. Six patients also received short courses of glucocorticoids, and four patients received a second dose of tocilizumab for recrudescence of the cytokine-release syndrome after transient improvement with the first dose. All the patients recovered fully, and there was a complete reversal of symptoms and a normalization of laboratory results. Relapses occurred in two of the nine patients who received immunosuppressive therapy for the cytokine-release syndrome.

ENCEPHALOPATHY

Thirteen patients had neurologic toxic effects, which ranged from delirium during the period of high temperatures to global encephalopathy with one or more of the following: aphasia, confusion, delirium, and hallucinations. Six patients had delayed encephalopathy that occurred after high temperatures had resolved and was independent of the severity of the cytokine-release syndrome and whether the patient had received prior tocilizumab therapy. Symptoms were self-limiting (lasting 2 to 3 days and resolving over 2 to 3 days), and they resolved fully without further intervention or apparent long-term sequelae. One patient with encephalopathy had two seizures that may have been caused by concomitant electrolyte abnormalities. Several patients had normal computed tomographic or magnetic resonance imaging of the head and lumbar puncture that was negative for infection or leukemia.

B-CELL APLASIA

We performed flow cytometry to detect CD19-positive B cells in order to monitor patients for the development of B-cell aplasia, which can be used as a pharmacodynamic measure of CTL019 function (Fig. 3). B-cell aplasia occurred in all

the patients who had a response and persisted for up to 1 year after CTL019 cells were no longer detectable by means of flow cytometry. Patients with B-cell aplasia received immunoglobulin replacement to maintain IgG levels greater than 500 mg per deciliter.

DISCUSSION

The engineering of T lymphocytes to express chimeric antibodies that target tumor antigens has been studied for more than 20 years.^{10,11} Clinical progress had been limited by poor *in vivo* expansion of engineered T cells and failure of these cells to persist after infusion.¹²⁻¹⁶ We and others have documented a high level of proliferation, activity against bulk disease, and long-term persistence of chimeric antigen receptor T cells.^{4-8,17,18}

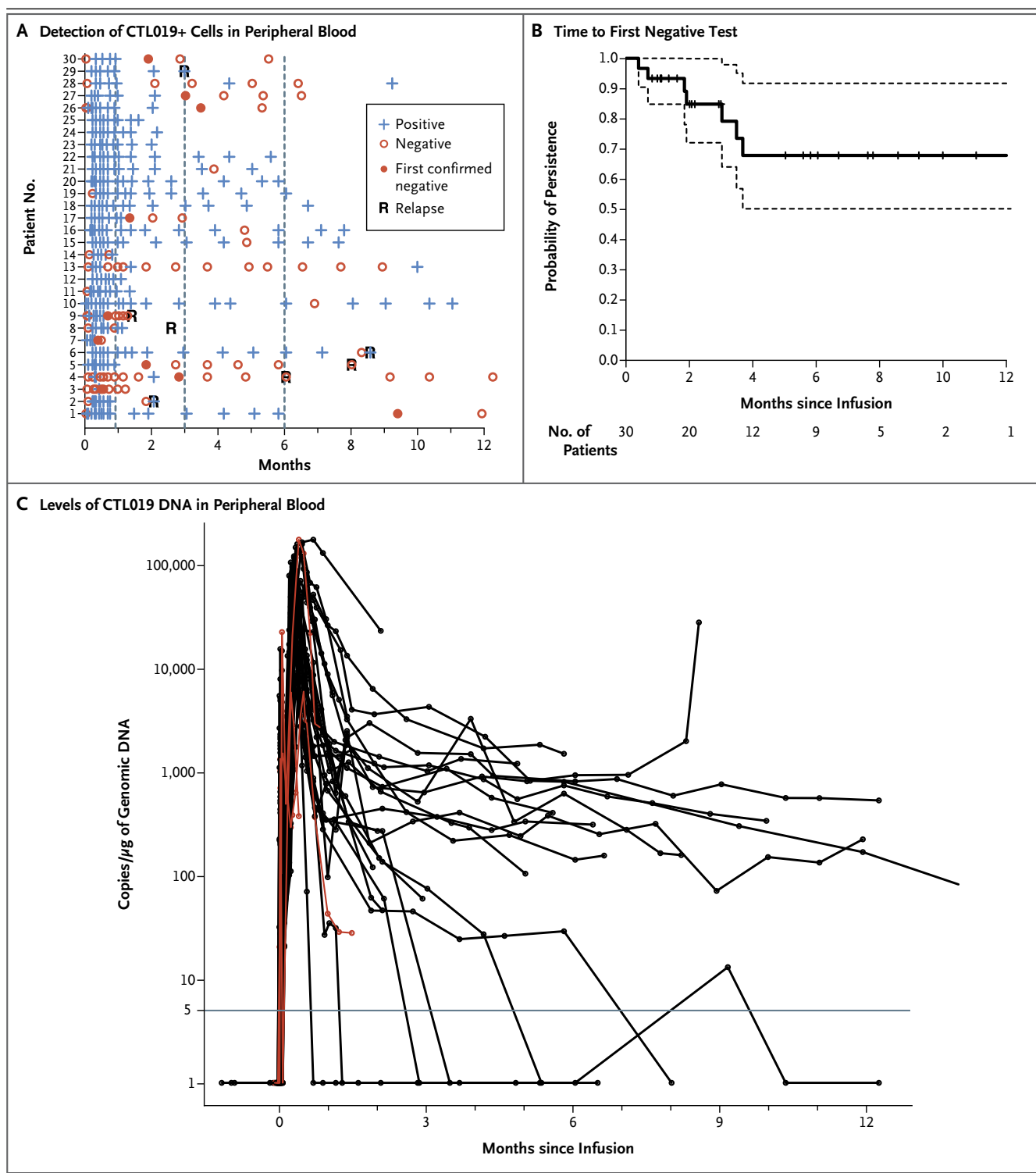
In this study, we found a 90% rate of complete remission among 30 children and adults who received CTL019 for ALL that was relapsed or refractory. With a follow-up period of 2 to 24 months, sustained remissions were observed in 19 patients (15 of whom received no further therapy) and were associated with the persistence of CTL019 and B-cell aplasia that continued beyond 2 to 3 months, suggesting continued effector function. Three patients who were in remission subsequently underwent allogeneic stem-cell transplantation. However, for several reasons (e.g., the lack of a suitable donor, prior stem-cell transplantation, or family choice), most patients did not undergo stem-cell transplantation; this allowed for longer follow-up. The rate of event-free survival at the median follow-up of 6 months was 67% in this heavily pretreated population. Several patients with relapse received salvage therapy, and the rate of overall survival at 6 months was 78%. In comparison, with the use of clofarabine, nelarabine, and liposomal-encapsulated vincristine — the most recently approved drugs for relapsed ALL¹⁹⁻²¹ — the Food and Drug Administration label indicates rates of complete remission of less than 25%, with a median documented duration of response of 4 to 9 weeks.

Davila et al. recently reported results from an expanded cohort of 16 adult patients with B-cell ALL.²² The short-term results were similar to those in our study; the overall complete remission rate was 88% with the use of a CD19 chimeric antigen receptor with the CD28 costimulatory domain. However, the only long-term remissions that

Figure 2 (facing page). Persistence of CTL019.

Panel A shows the results of detection of CTL019-positive T cells detected by means of flow cytometry in peripheral-blood samples. "Confirmed negative" was defined as the first of two consecutive negative measurements (<0.1% CTL019-positive cells in CD3-positive cells). Patients 1 through 25 were participants in the pediatric trial (which included children and young adults 5 to 22 years of age), and Patients 26 through 30 were participants in the adult trial (which included patients 26 to 60 years of age). CTL019-modified T cells were also detected in the cerebrospinal fluid of 17 of 19 patients with specimens that could be evaluated. Panel B shows the Kaplan-Meier curve of the time to the first confirmed negative measurement in peripheral blood and bone marrow. Data were censored at the time of the last follow-up. Dashed lines represent 95% confidence intervals. Panel C shows measurements of CTL019 gene-modified T cells in peripheral blood as assessed by means of quantitative real-time polymerase-chain-reaction (PCR) assay. Genomic DNA was isolated from samples of whole blood obtained at serial time points before and after infusion of CTL019. The horizontal line at 5 copies per microgram of DNA represents the lower limit of quantification of this assay. Data on patients who did not have a response are shown in red. In general, the levels of CTL019 detected by means of quantitative PCR correlated well with the level of CTL019-positive cells detected by means of flow cytometry, with the exception of the levels in 3 patients who did not have a response and whose peak levels measured by means of quantitative PCR (6066, 5982, and 178,481 copies per microgram of genomic DNA, respectively) did not correspond with detection of CTL019 cells by means of flow cytometry or the induction of B-cell aplasia. CTL019 sequences were detected (23 copies of CTL019 cells per microgram of DNA) at month 24 by means of quantitative PCR in the 1 patient who remained in complete remission at the 2-year follow-up. Data at the first time point were obtained before infusion of CTL019 cells. Doses of cells were determined according to the total amount of cells available after manufacturing. The manufacturing goal of 1.5×10^7 to 5×10^9 total cells (3×10^5 to 1×10^8 cells per kilogram of body weight) was achieved in all treated patients (see Table S2 in the Supplementary Appendix). A split-dose strategy was used to determine safety with 0.1×10^8 to 1×10^8 cells per kilogram infused over 1 to 3 days (5×10^8 to 50×10^8 cells in patients who weighed 50 kg or more). The transduction efficiency ranged from 5.5 to 45.3%; this yielded a dose of 0.76 to 20.6×10^6 CTL019 cells per kilogram.

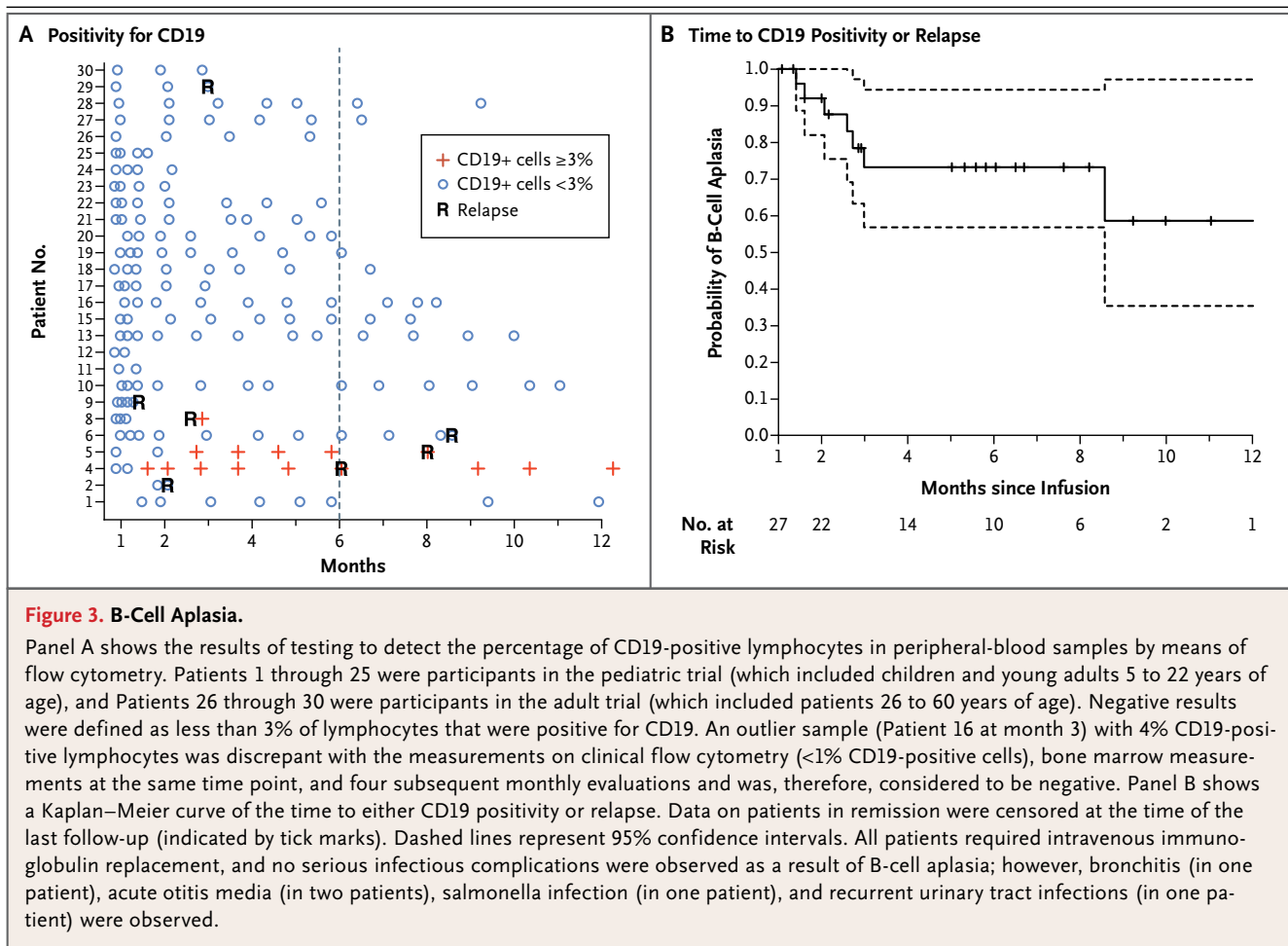
were reported occurred in patients who crossed over to allogeneic stem-cell transplantation. The median duration of persistence of 19-28z chimeric antigen receptor T cells was 30 days (range, 0 to 120). As a bridge to transplantation, high



levels of proliferation with a short duration of persistence is sufficient to achieve remission and eligibility for stem-cell transplantation. However, in patients who are ineligible for stem-cell transplantation, short persistence of chimeric antigen receptor T cells is unlikely to produce long-term

remission. We observed prolonged persistence of CTL019 cells and B-cell aplasia for as long as 2 years in this cohort and for more than 3 years in patients with CLL.⁴

There was no discernible effect of the density of CD19 antigen or cell dose on either efficacy



or toxicity (Table S2 in the Supplementary Appendix), although this study was not powered to investigate these correlations. Both complete remissions and severe cytokine-release syndrome were observed at the lower doses of cells administered. Although there was generally good concordance of CTL019 proliferation as measured by means of flow cytometry and quantitative PCR, in the cases of the three patients who did not have a response, the degree of proliferation of CLT019 cells determined by means of quantitative PCR was matched neither by the detection of cells expressing surface chimeric antigen receptor nor by the induction of B-cell aplasia. The mechanisms underlying this observation, including possible gene silencing of CTL019, are unknown. B-cell aplasia can be used as a pharmacodynamic measure of the persistence of functional CD19-targeted T cells. Continued B-cell aplasia was seen in all patients who had a sustained remission, and none of the patients with B-cell aplasia had a CD19-positive relapse.

Relapses were associated with either lack of CTL019 persistence or CD19 escape variants. In two cases of loss of CTL019, relapse was heralded by recovery of normal B cells, suggesting that monitoring for the return of normal B cells will be important to identify patients at the highest risk for relapse and potentially provide a window for repeat treatment or stem-cell transplantation. Selection of CD19-negative clones or down-regulation of CD19 expression are concerns associated with CD19-directed therapies. Data are lacking to determine the mechanism of CD19-negative relapses.

The most prominent and serious toxic effect of chimeric antigen receptor T-cell therapy is the cytokine-release syndrome, an inflammatory process marked by dramatic elevations of cytokine levels.²³ Because this cytokine release probably both results from and contributes to T-cell activation, some degree of cytokine-release syndrome is probably necessary for efficacy. In the major-

ity of our patients, the cytokine-release syndrome was self-limited, with high temperatures and myalgias that resolved spontaneously in a few days. However, in approximately 30% of the patients in our study, hypotension and respiratory insufficiency associated with this syndrome required treatment in the intensive care unit. The cytokine-release syndrome has been described by several groups in association with CD19 chimeric antigen receptor T-cell therapy,^{8,22} but until recently, management was nonspecific, glucocorticoid-based, and directed primarily toward supportive care. In severely affected patients, glucocorticoids may have a limited effect on toxicity but a substantial negative effect on T-cell proliferation and persistence.^{4,7,8,22}

We previously observed marked elevation of interleukin-6 levels in a patient with severe cytokine-release syndrome after infusion of CTL019, and our study showed the benefit of cytokine-directed therapy.⁸ Tocilizumab, an interleukin-6-receptor blocking antibody, produced a rapid and profound improvement in severe manifestations of the cytokine-release syndrome without an apparent impact on the efficacy of CTL019. We have now incorporated tocilizumab as a first-line agent in the management of severe cytokine-release syndrome. Tocilizumab could blunt maximal T-cell proliferation by interfering with a cytokine feedback loop; therefore, we have limited its use to patients with grade 4, or life-threatening, toxic effects. Despite this theoretical concern, in this study, all the patients who received tocilizumab had robust proliferation of CTL019 cells, a complete remission, and the continued persistence of CTL019 cells. Future studies are needed to determine whether tocilizumab can be used preemptively without compromising efficacy.

We observed that many findings in patients with the cytokine-release syndrome were similar to those in patients with the macrophage activation syndrome or hemophagocytic lymphohistiocytosis.^{8,24,25} Hyperferritinemia is a hallmark of these two conditions, and we observed marked elevations in ferritin levels during the period of maximal T-cell proliferation. The degree of elevation in ferritin and C-reactive protein levels was significantly higher in patients with severe cytokine-release syndrome.

Neurologic toxic effects were seen in a subgroup of patients. Encephalopathy typically occurred after symptoms of the cytokine-release

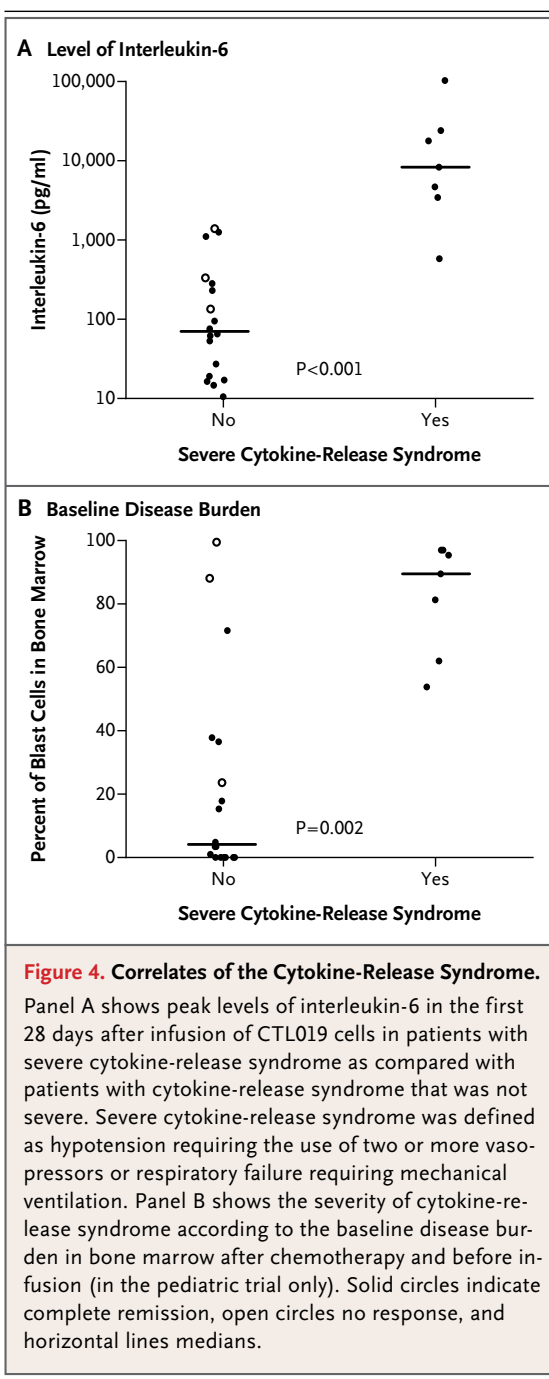


Figure 4. Correlates of the Cytokine-Release Syndrome.

Panel A shows peak levels of interleukin-6 in the first 28 days after infusion of CTL019 cells in patients with severe cytokine-release syndrome as compared with patients with cytokine-release syndrome that was not severe. Severe cytokine-release syndrome was defined as hypotension requiring the use of two or more vaso-pressors or respiratory failure requiring mechanical ventilation. Panel B shows the severity of cytokine-release syndrome according to the baseline disease burden in bone marrow after chemotherapy and before infusion (in the pediatric trial only). Solid circles indicate complete remission, open circles no response, and horizontal lines medians.

syndrome peaked and was self-limited. CNS toxic effects have been associated with other T-cell-activating therapies, including other chimeric antigen receptor-modified T-cell therapies and blinatumomab.^{22,26,27} The pathophysiology of encephalopathy after the use of CTL019 is not known. The mechanism could involve direct T-cell-mediated toxicity or it could be cytokine-mediated. We have observed no clear predictors of neurologic toxic effects. CTL019-modified

T cells were detected in the cerebrospinal fluid of 17 of 19 patients with specimens that could be evaluated. This may have implications for successful surveillance of CNS disease, yet only a fraction of the patients had encephalopathy. The 2 patients (of the 25 patients in the pediatric trial) in whom cerebrospinal fluid leukemic blasts were detected (CNS-2 disease) did not have encephalopathy. Neurologic toxic effects did not obviously correlate with the severity of the cytokine-release syndrome and was not prevented by tocilizumab. Further studies are needed to determine the potential predictors, mechanism, and treatment of neurologic toxicity.

Relapsed ALL is a considerable therapeutic challenge, particularly in patients who do not have a second complete remission or have a relapse after stem-cell transplantation.^{1-3,28,29} Salvage therapy induces remissions in only 40% of children who have had two or more bone marrow relapses, and long-term survival is quite poor.³ This study included patients with multiple relapses or with disease that was refractory to two or more attempts at reinduction, and 18 patients (60%) had had a relapse after allogeneic stem-cell transplantation. Two complete remissions were achieved in 3 patients with disease that was refractory to blinatumomab, a promising CD19-directed bispecific antibody for relapsed ALL,³⁰ suggesting that a lack of response to CD19-directed therapy may not preclude successful therapy with CTL019. The complete remission rate of 90% and sustained remissions of

up to 2 years that were seen in this study are encouraging.

Supported in part by a grant from Novartis (to Dr. June), by grants from the National Institutes of Health (1R01CA165206, to Dr. June; and R01CA102646 and R01CA116660, to Dr. Grupp), the Leukemia and Lymphoma Society, the Jeffrey Jay Weinberg Memorial Foundation, and the Children's Hospital of Philadelphia Hematologic Malignancy Research Fund, a Stand Up to Cancer–St. Baldrick's Pediatric Dream Team translational research grant (SU2C-AACR-DT1113), a St. Baldrick's Foundation Scholar Award (to Dr. Maude), and a Research Scholar Grant from the American Cancer Society (RSG-14-022-01-CDD, to Dr. Teachey).

Disclosure forms provided by the authors are available with the full text of this article at NEJM.org.

We thank Jeff Finklestein, Farzana Nazimuddin, Harit Parakandi, and Marina Bogush for sample processing and flow-cytometric analysis; Irina Kulikovskaya and Minnal Gupta for the quantitative polymerase-chain-reaction assay; Fang Chen for the Luminex assay; Marybeth Helfrich, Gerald Wertheim, and Michele Paessler for assistance with interpretation of the marrow findings; Alexey Bersenev, Anne Lamontagne, Alexander Malykhin, Neel Manvar, Matthew O'Rourke, Megan Suhoski-Davis, and members of the Clinical Cell and Vaccine Production Facility for cell manufacturing and testing; Colleen Callahan, Christine Strait, Brittany Girard, Margaret Tartaglione, Trish Hankins, Brandon Loudon, Christopher Grupp, Maya Mudambi, Laura Motley, Elizabeth Veloso, Lester Lledo, Joan Gilmore, Holly McConville, Christina Jemison, and James Capobianchi for clinical research assistance; Wei-Ting Hwang for statistical support; Michele Sharr and Patricia Wood at Novartis for discussions and protocol support; Children's Hospital of Philadelphia Vector Core (Frasier Wright and Katherine High) for clinical-grade vector production; Kenneth Cornetta and the National Gene Vector Biorepository at the Indiana University School of Medicine for postinfusion testing of the product for replication-competent lentivirus; Bipulendu Jena and Laurence Cooper for provision of the chimeric antigen receptor anti-idiotypic detection reagent; the data and safety monitoring board; our hematology–oncology and critical care faculty for providing clinical support; and the nurses, residents, and fellows at our two institutions. Drs. Dario Campana and Chihaya Imai and others at St. Jude Children's Research Hospital designed, developed, and provided under material transfer agreements the chimeric antigen receptor (CAR) that was used in this study.

REFERENCES

- Bhajwani D, Pui C-H. Relapsed childhood acute lymphoblastic leukaemia. *Lancet Oncol* 2013;14(6):e205-e217.
- Forman SJ, Rowe JM. The myth of the second remission of acute leukemia in the adult. *Blood* 2013;121:1077-82.
- Raetz EA, Bhatla T. Where do we stand in the treatment of relapsed acute lymphoblastic leukemia? *Hematology Am Soc Hematol Educ Program* 2012;2012:129-36.
- Kalos M, Levine BL, Porter DL, et al. T cells with chimeric antigen receptors have potent antitumor effects and can establish memory in patients with advanced leukemia. *Sci Transl Med* 2011;3:95ra73.
- Porter DL, Levine BL, Kalos M, Bagg A, June CH. Chimeric antigen receptor-modified T cells in chronic lymphoid leukemia. *N Engl J Med* 2011;365:725-33.
- Kochenderfer JN, Wilson WH, Janik JE, et al. Eradication of B-lineage cells and regression of lymphoma in a patient treated with autologous T cells genetically engineered to recognize CD19. *Blood* 2010;116:4099-102.
- Brentjens RJ, Davila ML, Riviere I, et al. CD19-targeted T cells rapidly induce molecular remissions in adults with chemotherapy-refractory acute lymphoblastic leukemia. *Science Transl Med* 2013;5:177ra38.
- Grupp SA, Kalos M, Barrett D, et al. Chimeric antigen receptor-modified T cells for acute lymphoid leukemia. *N Engl J Med* 2013;368:1509-18.
- Milone MC, Fish JD, Carpenito C, et al. Chimeric receptors containing CD137 signal transduction domains mediate enhanced survival of T cells and increased antileukemic efficacy in vivo. *Mol Ther* 2009;17:1453-64.
- Irving BA, Weiss A. The cytoplasmic domain of the T cell receptor zeta chain is sufficient to couple to receptor-associated signal transduction pathways. *Cell* 1991;64:891-901.
- Eshhar Z, Waks T, Gross G, Schindler DG. Specific activation and targeting of cytotoxic lymphocytes through chimeric single chains consisting of antibody-binding domains and the gamma or zeta subunits of the immunoglobulin and T-cell receptors. *Proc Natl Acad Sci U S A* 1993;90:720-4.
- Kalos M, June CH. Adoptive T cell transfer for cancer immunotherapy in the era of synthetic biology. *Immunity* 2013;39:49-60.
- Kershaw MH, Westwood JA, Parker LL, et al. A phase I study on adoptive immunotherapy using gene-modified T cells for ovarian cancer. *Clin Cancer Res* 2006;12:6106-15.
- Lamers CH, Sleijfer S, Vulto AG, et al. Treatment of metastatic renal cell carcinoma with autologous T-lymphocytes ge-

- netically retargeted against carbonic anhydrase IX: first clinical experience. *J Clin Oncol* 2006;24(13):e20-e22.
15. Till BG, Jensen MC, Wang J, et al. Adoptive immunotherapy for indolent non-Hodgkin lymphoma and mantle cell lymphoma using genetically modified autologous CD20-specific T cells. *Blood* 2008;112:2261-71.
 16. Savoldo B, Ramos CA, Liu E, et al. CD28 costimulation improves expansion and persistence of chimeric antigen receptor-modified T cells in lymphoma patients. *J Clin Invest* 2011;121:1822-6.
 17. Brentjens RJ, Rivière I, Park JH, et al. Safety and persistence of adoptively transferred autologous CD19-targeted T cells in patients with relapsed or chemotherapy refractory B-cell leukemias. *Blood* 2011;118:4817-28.
 18. Kochenderfer JN, Dudley ME, Carpenter RO, et al. Donor-derived CD19-targeted T cells cause regression of malignancy persisting after allogeneic hematopoietic stem cell transplantation. *Blood* 2013;122:4129-39.
 19. O'Brien S, Schiller G, Lister J, et al. High-dose vincristine sulfate liposome injection for advanced, relapsed, and refractory adult Philadelphia chromosome-negative acute lymphoblastic leukemia. *J Clin Oncol* 2013;31:676-83.
 20. Jeha S, Gandhi V, Chan KW, et al. Clofarabine, a novel nucleoside analog, is active in pediatric patients with advanced leukemia. *Blood* 2004;103:784-9.
 21. Berg SL, Blaney SM, Devidas M, et al. Phase II study of nelarabine (compound 506U78) in children and young adults with refractory T-cell malignancies: a report from the Children's Oncology Group. *J Clin Oncol* 2005;23:3376-82.
 22. Davila ML, Riviere I, Wang X, et al. Efficacy and toxicity management of 19-28z CAR T cell therapy in B cell acute lymphoblastic leukemia. *Science Transl Med* 2014;6:224ra25.
 23. Maude SL, Barrett D, Teachey DT, Grupp SA. Managing cytokine release syndrome associated with novel T cell-engaging therapies. *Cancer J* 2014;20:119-22.
 24. Teachey DT, Rheingold SR, Maude SL, et al. Cytokine release syndrome after blinatumomab treatment related to abnormal macrophage activation and ameliorated with cytokine-directed therapy. *Blood* 2013;121:5154-7.
 25. Risma K, Jordan MB. Hemophagocytic lymphohistiocytosis: updates and evolving concepts. *Curr Opin Pediatr* 2012;24:9-15.
 26. Schlegel P, Lang P, Zugmaier G, et al. Pediatric posttransplant relapsed/refractory B-precursor acute lymphoblastic leukemia shows durable remission by therapy with the T-cell engaging bispecific antibody blinatumomab. *Haematologica* 2014;99:1212-9.
 27. Topp MS, Kufer P, Gökbüget N, et al. Targeted therapy with the T-cell-engaging antibody blinatumomab of chemotherapy-refractory minimal residual disease in B-lineage acute lymphoblastic leukemia patients results in high response rate and prolonged leukemia-free survival. *J Clin Oncol* 2011;29:2493-8.
 28. Nguyen K, Devidas M, Cheng SC, et al. Factors influencing survival after relapse from acute lymphoblastic leukemia: a Children's Oncology Group study. *Leukemia* 2008;22:2142-50.
 29. Poon LM, Hamdi A, Saliba R, et al. Outcomes of adults with acute lymphoblastic leukemia relapsing after allogeneic hematopoietic stem cell transplantation. *Biol Blood Marrow Transplant* 2013;19:1059-64.
 30. Topp MS, Gökbüget N, Zugmaier G, et al. Long-term follow-up of hematologic relapse-free survival in a phase 2 study of blinatumomab in patients with MRD in B-lineage ALL. *Blood* 2012;120:5185-7.

Copyright © 2014 Massachusetts Medical Society.

Nutrient Competition: A New Axis of Tumor Immunosuppression

Madhusudhanan Sukumar,¹ Rahul Roychoudhuri,¹ and Nicholas P. Restifo^{1,*}

¹Center for Cancer Research, National Cancer Institute (NCI), National Institutes of Health Bethesda, MD 20892, USA

*Correspondence: restifo@nih.gov

<http://dx.doi.org/10.1016/j.cell.2015.08.064>

It is thought that cancer cells engage in Warburg metabolism to meet intrinsic biosynthetic requirements of cell growth and proliferation. Papers by Chang et al. and Ho et al. show that Warburg metabolism enables tumor cells to restrict glucose availability to T cells, suppressing anti-tumor immunity.

In the presence of oxygen, most differentiated cells utilize mitochondrial oxidative phosphorylation to generate energy in the form of adenosine triphosphate (ATP) that can be used to sustain cellular processes. In the absence of oxygen, such cells revert to much less efficient glycolysis as a means of ATP production. Cancer cells often utilize glycolysis despite the presence of oxygen (aerobic glycolysis or the "Warburg effect") (Warburg, 1956). While less efficient at producing energy, it is thought that this form of metabolism supports the macromolecular requirements of cell growth and proliferation. Thus, the field has primarily focused on Warburg metabolism as an adaptation that confers intrinsic growth advantages to tumor cells themselves. However, cancer cells may consume nutrients, particularly glucose, in excess of their requirement to sustain proliferation and cell growth (Vander Heiden et al., 2009). This raises the possibility that nutrient consumption serves additional roles to meeting the intrinsic bioenergetic and biosynthetic requirements of cancer cells. In this issue of *Cell*, Ho et al. (2015) and Chang et al. (2015) show that Warburg metabolism provides tumor cells with a cell-extrinsic advantage, promoting depletion of extracellular glucose which renders tumor-infiltrating T cells dysfunctional.

In both studies, glycolysis within tumor cells is shown to cause depletion of extracellular glucose which restricts glucose availability to T cells. Decreased glucose availability causes suppression of glycolytic metabolism within T cells, and this is associated with decreased effector function (Figure 1, left).

Ho et al. identify a mechanism by which glucose metabolism directly controls effector function. The authors find that T cell receptor (TCR)-induced Ca^{2+} flux is markedly dependent upon extracellular glucose and glucose metabolism by T cells. Sarco/endoplasmic reticulum (ER) Ca^{2+} -ATPase (SERCA) is an ATP-dependent Ca^{2+} channel that pumps Ca^{2+} from the cytoplasm into the ER. Extracellular glucose is shown to promote accumulation of the glycolytic metabolite, phosphoenolpyruvate (PEP), which inhibits SERCA-dependent evacuation of Ca^{2+} from the cytosol into the ER, thereby increasing TCR-induced Ca^{2+} flux and effector function (Figure 1, right). This observation adds to a growing list of examples whereby metabolic processes directly control the outcome of T cell activation (Chang et al., 2013; MacLver et al., 2013).

That tumor cell glycolysis directly suppresses T cells raises the possibility that tumor metabolism can be therapeutically manipulated to improve immune function within tumors. Checkpoint blockade immunotherapy with anti-PD-L1 antibodies is thought to work by limiting inhibitory PD-1 signaling received by tumor-specific T cells (Keir et al., 2008). Chang et al. made the surprising observation that PD-1 ligand (PD-L1) expressed by tumor cells provides a constitutive "reverse signal" that promotes tumor cell glycolysis through activation of the AKT/mTOR pathway (Figure 1, left). Treatment of tumor cells with therapeutic anti-PD-L1 antibodies attenuates glycolysis by triggering PD-L1 endocytosis (Figure 1, right). Remarkably, two other check-

point-blockade antibodies, anti-PD-1 and anti-CTLA-4, are also shown to cause changes in extracellular glucose concentrations within tumors, though mechanisms for these observations are unclear. That PD-L1 expression causes constitutive activation of the Akt/mTOR pathway has important implications for understanding tumor cell biology and tumor-host interactions, and it will be important to characterize precise molecular mechanisms by which PD-L1 constitutively activates the Akt/mTOR pathway. Given that immune checkpoint blockade elicits durable clinical responses and improves survival in patients with certain metastatic cancers (Larkin et al., 2015; Topalian et al., 2012), it is relevant to measure the effect of checkpoint blockade antibodies on intratumoral nutrient availability and T cell metabolism in patients and correlate this with clinical outcomes. Further, it will be important to dissect the effects of checkpoint blockade on inhibitory T cell signaling versus tumor cell metabolism.

Instead of manipulating tumor cell metabolism, Ho et al. suggest an alternate approach to improve T cell function by mimicking nutrient availability within transferred T cells during adoptive cell therapy (ACT). Phosphoenolpyruvate Carboxykinase (PCK1) converts oxaloacetate into PEP. By overexpressing Pck1 in transferred T cells, Ho et al. are able to artificially increase PEP levels, restoring TCR-induced Ca^{2+} flux and anti-tumor T cell function despite the presence of low environmental glucose levels within tumors. Intriguingly, blocking glucose

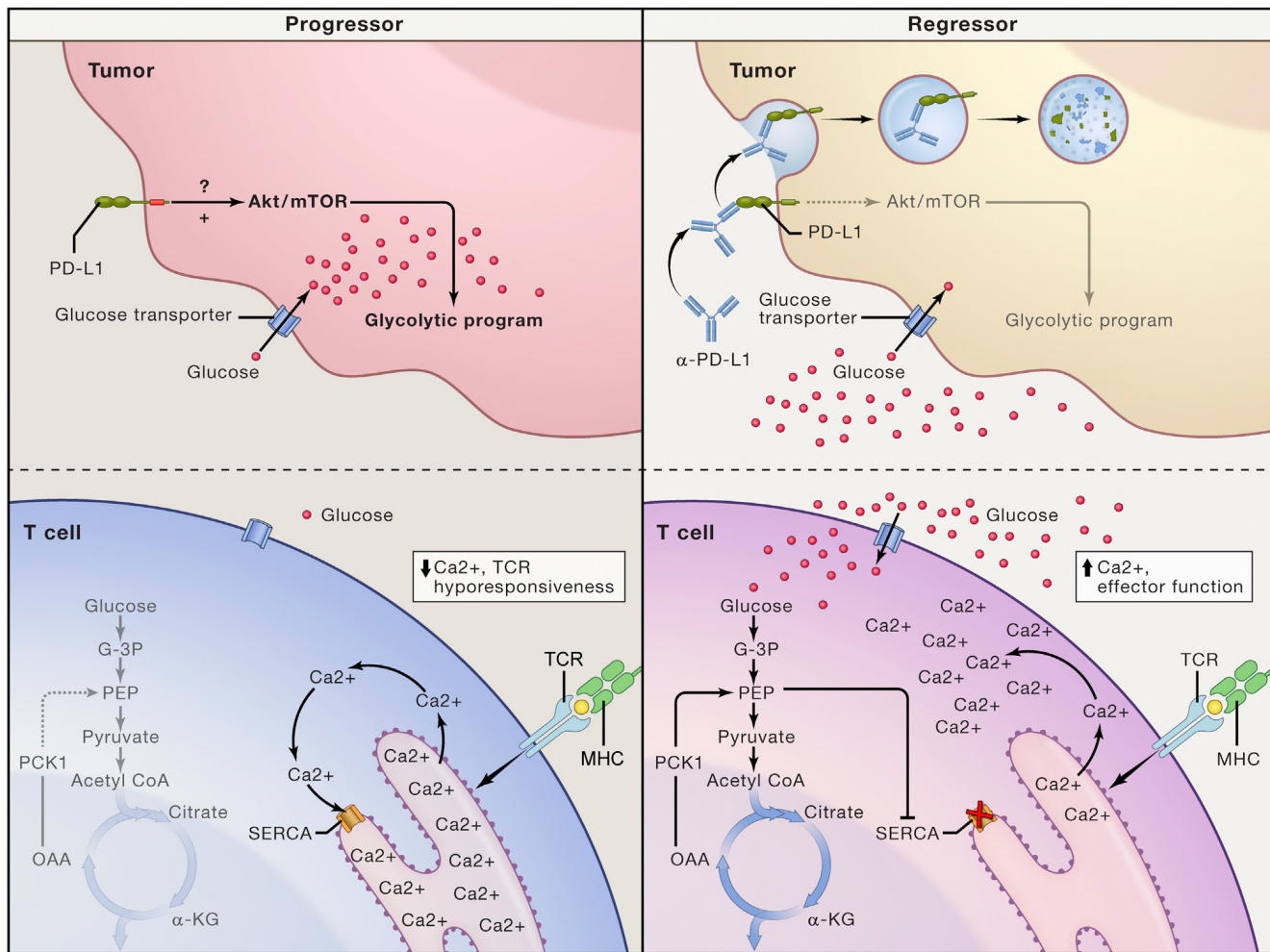


Figure 1. Nutrient Competition between Tumor Cells and T Cells Controls Immune Function within Tumors

Schematic depicting glucose metabolism and cellular signaling in highly glycolytic progressor tumors and regressor tumors undergoing therapy. In the progressor tumor (left), constitutive activation of the Akt/mTOR pathway by PD-L1 expressed on tumor cells causes high levels of tumor cell glycolysis and absorption of extracellular glucose. Decreased extracellular glucose levels causes impaired glycolysis in T cells, wherein depletion of the glycolytic metabolite PEP causes unrestrained SERCA activity, sequestration of cytoplasmic Ca²⁺ into the ER and impairment of TCR-induced Ca²⁺ flux and effector function. In the regressor tumor (right), therapeutic anti-PD-L1 antibodies bind to PD-L1 causing its endocytosis and inactivation. Loss of constitutive PD-L1 signaling leads to decreased activation of the Akt-mTOR pathway decreased tumor cell glycolysis and increased extracellular glucose concentrations. Increased extracellular glucose drives T cell glycolysis, replenishing PEP levels, inhibiting SERCA-dependent sequestration of cytoplasmic Ca²⁺ and promoting TCR-induced Ca²⁺ flux and anti-tumor effector functions. Alternatively, constitutive overexpression of PCK1 in adoptively transferred T cells increases availability of PEP leading to inhibition of SERCA, increased anti-tumor effector function and tumor regression.

metabolism during expansion of T cells for adoptive immunotherapy withholds effector differentiation and promotes differentiation of memory cells which mediate superior tumor clearance (Sukumar et al., 2013). These findings provide striking examples of how modulating T cell metabolism can improve the outcome of adoptive cell therapy for cancer.

Taken together, the two new studies provide compelling evidence that cancer cells subvert the metabolic charac-

teristics of the tumor microenvironment to shape immune responses within tumors. The results also provide an explanation of how nutrient consumption in excess of the bioenergetic and biosynthetic requirements may benefit cancer cells. As Warburg's original observation is revisited in ever new reincarnations, it remains to be seen whether insights from the field of immunometabolism will change the game at this new front in our war against cancer.

REFERENCES

- Chang, C.H., Curtis, J.D., Maggi, L.B., Jr., Faubert, B., Villarino, A.V., O'Sullivan, D., Huang, S.C., van der Windt, G.J., Blagih, J., Qiu, J., et al. (2013). *Cell* 153, 1239–1251.
- Chang, C.-H., Qiu, J., O'Sullivan, D., Buck, M.D., Noguchi, T., Curtis, J.D., Chen, Q., Gindin, M., Guabin, M.W., and van der Windt, G.J.W. (2015). *Cell* 162, this issue, 1229–1241.
- Ho, P.-C., Bihuniak, J.D., Macintyre, A.N., Staron, M., Liu, X., Amezquita, R., Tsui, Y.-C., Cui, G., Miccovic, G., Perales, J.C., et al. (2015). *Cell* 162, this issue, 1217–1228.

- Keir, M.E., Butte, M.J., Freeman, G.J., and Sharpe, A.H. (2008). *Annu. Rev. Immunol.* 26, 677–704.
- Larkin, J., Chiarion-Sileni, V., Gonzalez, R., Grob, J.J., Cowey, C.L., Lao, C.D., Schadendorf, D., Dummer, R., Smylie, M., Rutkowski, P., et al. (2015). *N. Engl. J. Med.* 373, 23–34.
- MacLver, N.J., Michalek, R.D., and Rathmell, J.C. (2013). *Annu. Rev. Immunol.* 31, 259–283.
- Sukumar, M., Liu, J., Ji, Y., Subramanian, M., Crompton, J.G., Yu, Z., Roychoudhuri, R., Palmer, D.C., Muranski, P., Karoly, E.D., et al. (2013). *J. Clin. Invest.* 123, 4479–4488.
- Topalian, S.L., Hodi, F.S., Brahmer, J.R., Getlinger, S.N., Smith, D.C., McDermott, D.F., Powdery, J.D., Carvajal, R.D., Sosman, J.A., Atkins, M.B., et al. (2012). *N. Engl. J. Med.* 366, 2443–2454.
- Vander Heiden, M.G., Cantley, L.C., and Thompson, C.B. (2009). *Science* 324, 1029–1033.
- Warburg, O. (1956). *Science* 123, 309–314.

Single-Cell Analysis: The Differences That Kill

Savaş Tay^{1,2,*}

¹Department of Biosystems Science and Engineering, ETH Zurich, Basel 4058, Switzerland

²Institute for Molecular Engineering, University of Chicago, Chicago 60637, USA

*Correspondence: tays@uchicago.edu

<http://dx.doi.org/10.1016/j.cell.2015.08.053>

Using single-cell RNA sequencing, Avraham et al. investigate how variability in macrophage response to infection is controlled by variability within the pathogen population. They find that heterogeneous expression of the *Salmonella* virulence factor PhoP and subsequent cell-wall modifications lead to the bimodal induction of the interferon-response in infected macrophages.

What exactly happens when pathogens penetrate the outer defenses of tissues and start infecting various cells? Since the dawn of modern biology, the battle between pathogens and immune cells has been a central focus, and thanks to powerful new methods that analyze individual cells, we are taking a fresh look at our understanding of infection and immunity. Unlike what traditional population-averaged analyses show, the outcome of pathogen exposure is vastly more complex at the individual-cell level. For example, some host cells completely avoid infection and survive. Other cells become infected and die, survive with the presence of bacteria inside them, or completely clear the pathogens and function normally afterward. The intricate workings of the molecular pathways determining infection and immunity are largely unclear. In this issue of *Cell*, Hung and colleagues take a new look at this fundamental problem using single-cell analysis and ask whether variability in infection outcomes can be explained by the variability among individual bacteria (Avraham et al., 2015). This is a unique approach as compared to most work in the newly emerging field of single-cell

immunology. In explaining heterogeneous infection outcomes, the field tends to focus on the state of the host and environment (Snijder et al., 2009), rather than pre-existing variability in the pathogen.

Hung's team focus on the infection of macrophages—first responders of the innate immune system—with *Salmonella typhimurium*, a pathogen that causes typhoid fever and food poisoning in humans. Despite a century of antibiotic treatment and improved hygiene, basic pathogens such as *Salmonella* remain a major health problem, especially in the developing world. Even the developed world is at risk from these basic infections, as evidenced by thousands of *salmonella* infections every year in the USA alone and the recent *E. coli* outbreak in Germany that killed 50 people over the course of a few weeks.

Salmonella typhimurium has specialized molecular tools to avoid, resist, and even hijack the mammalian immune system. Macrophages recognize these pathogen-associated factors and mount transcriptional programs to change their physiology and clear the pathogen. Individual *Salmonella* cells can vary in the manner they express virulence factors.

Can the variability in infection outcomes be explained by the variability within the pathogen population? And if so, what virulence factors control this variability? To answer these questions, Avraham et al. first use fluorescent single-cell microscopy to distinguish various infection outcomes: When mixed with *salmonella*, the macrophages could remain uninfected, or become infected with either live or dead bacteria inside. They isolate these single macrophages and use state-of-the-art RNA sequencing (RNA-seq) to determine their transcriptional state by measuring the expression of 535 immune response genes. These genes cluster into distinct groups; however, one cluster shows much higher expression variability between individual cells. These variable genes were related to innate immune recognition of the bacterial virulence factors, including bacterial cell-wall components like lipopolysaccharide (LPS), hinting that the LPS/TLR4 signaling pathway underlies phenotype variability. In particular, Type 1 interferon (IFN) response exhibit bimodal expression in host macrophages, with roughly one third of cells expressing IFN genes at high levels, and the rest at low levels



HHS Public Access

Author manuscript

Curr Opin Immunol. Author manuscript; available in PMC 2018 July 03.

Published in final edited form as:

Curr Opin Immunol. 2017 June ; 46: viii–xi. doi:10.1016/j.coि.2017.06.002.

Editorial overview: Metabolism of T cells: integrating nutrients, signals, and cell fate

Nancie J MacIver and

Departments of Pediatrics, Immunology, and Pharmacology and Cancer Biology, Duke University School of Medicine, Durham, NC, United States

Jeffrey C Rathmell

Vanderbilt Center for Immunobiology, Departments of Pathology, Microbiology, and Immunology, Cancer Biology, Vanderbilt University Medical Center, Nashville, TN, United States

It is an exciting time in the field of immunometabolism. Over the last several years, there has been substantial progress in the understanding of how immune cell metabolism and function are influenced by one another, particularly in regards to lymphocytes. As T lymphocytes (T cells) are critical members of the immune system which orchestrate overall immune response through the production of cytokines and other immune factors, this special section of *Current Opinion in Immunology* highlights some of the key aspects of T cell metabolism. This includes new understanding about the utilization of distinct fuels to determine T cell differentiation and function, the response of T cells to both inadequate and overabundant nutrients, the role of T cell immunometabolism in diseases such as cancer, autoimmunity, and infection, and an improved understanding of the signaling pathways that regulate T cell metabolic changes at the molecular level. Altogether, this series of review articles provides a broad overview of the mechanisms by which T cell metabolism alters immunity in health and disease.

It is now well established that the metabolic properties of T cells are altered upon T cell activation and that different T cell subsets (e.g. naïve, effector, memory, regulatory) have distinct metabolic phenotypes. For the most part, naïve T cells utilize a mixed fuel metabolism dominated by oxidative phosphorylation to promote energy production for immune surveillance, whereas effector T cells (Teff) generally increase glucose and glutamine metabolism, with a predominant increase in aerobic glycolysis, in order to produce ATP quickly and to promote T cell growth and proliferation through the production of biosynthetic precursors [1]. Memory T cells (Tmem) and regulatory T cells (Treg), however, rely largely on oxidative phosphorylation and fatty acid oxidation to fuel immune surveillance and immune suppression, respectively [2-4].

There are, however, nuances in T cell metabolism amongst these broader categories of Teff, Tmem, and Treg. For example, while Teff cells such as Th1, Th2, and Th17 cells generally express high amounts of the glucose transporter Glut1, to promote glucose uptake and utilize a largely glycolytic metabolism, Treg cells usually express low levels of Glut1 and generally utilize oxidative metabolism to fuel suppressive function [2,5]. When cultured *in vitro*, however, Treg cells were shown to engage in both glycolysis and fatty acid oxidation to enhance proliferation, and conditions such as acute infection or inflammation have been

Author Manuscript
Author Manuscript
Author Manuscript
Author Manuscript

shown to provide signals that increase Treg Glut1 expression and glycolytic metabolism such that Treg become more proliferative but less suppressive [6]. Likewise, Teff cells vary in their metabolic programs. In the review by Kidani *et al.*, the authors review recent studies demonstrating that the cholesterol and fatty acid synthesis pathways promote ROR γ activity and IL-17 production in Th17 cells, specifically; however, why fluxes through lipid synthetic pathways promote Th17 differentiation remains unknown.

Despite the findings that T cells alter their metabolic state upon activation, it is not entirely clear how altered nutrient availability and the overall metabolic state of the organism influence T cell function and response to infection. The review by Balmer *et al.* describes how infections disrupt homeostasis and lead to a switch toward catabolic metabolism at the organismal level. That, in turn, leads to increased systemic availability of glucose, fatty acids, and ketone bodies which may disturb immune cell metabolism. For example, increased glucose availability is likely to promote T cell activation in an acute infection response through increased glycolytic metabolism. Increased availability of fatty acids may be utilized by T cells for fuel, for storage of lipid droplets, and for incorporation into membrane lipid rafts. Increased ketone bodies and acetate may be metabolized into acetyl-CoA to fuel the TCA cycle or to generate acetyl-groups for increased acetylation of proteins. Moreover, acetylation of the glycolytic enzyme Glyceraldehyde 3-phosphate dehydrogenase (GAPDH) has been shown to increase GAPDH activity as well as promote glycolysis [7].

Infection response in obesity, however, is likewise disrupted through altered availability of nutrients systemically. As Green *et al.* discuss, the obesity epidemic in the developed world has broad implications for immune response through effects on T cell metabolism and function. Obesity has been shown to impair immune response to select infections such as H1N1 and seasonal influenza by altering and impairing both B cell and T cell response. Moreover, diet-induced obese and genetically obese mice displayed altered metabolomics profiles in many tissues following infection with influenza, in comparison to infected lean mice [8]. The mechanism by which T cell function and infection response are altered in obesity is not entirely clear, yet there is evidence that these changes are downstream to alterations in nutrients, cytokines, and hormones seen in obesity. Indeed the hormone leptin is increased in obesity and has been shown to promote Teff cell response by promoting Teff glycolytic metabolism upon activation and driving the production of inflammatory cytokines IFN- γ and IL-17 [9-11]. Infection response in obesity is, therefore, likely to result in altered T cell metabolism and impaired T cell response, in part, by promoting T cell inflammation and reducing anti-inflammatory immune surveillance and memory formation.

T cell metabolism also plays a key role in immune response in both autoimmune disease and cancer immunosurveillance. The review by Weyand *et al.* highlights the metabolic abnormalities of T cells in rheumatoid arthritis, characterized by a diversion of glucose metabolism toward a synthetic/proliferative phenotype, shifting T cells into a low energy state, diverting ATP production toward the pentose phosphate pathway, and thereby increasing NADPH while consuming reactive oxygen species (ROS). This ATP-low, NADPH-high, ROS-low state of T cells drives T cell proliferation and promotes differentiation into pro-inflammatory Th1 and Th17 subsets [12]. At the same time, these energy-deprived T cells in rheumatoid arthritis lose DNA repair abilities, accumulate

telomeric damage, and enter premature senescence [13]. On the other hand, macrophages in rheumatoid arthritis are characterized by mitochondrial stress, increased glucose uptake and increased glycolytic activity, and over-production of the inflammatory cytokine IL-6, altogether predisposing toward an inflammatory state [14]. In the field of cancer immunology, Ho *et al.* describe how metabolic stresses in the tumor microenvironment (nutrient deprivation, hypoxia, acidosis, etc.) lead to altered T cell metabolism and decreased T cell anti-tumor immunity. Here, the authors suggest that manipulation of the T cell metabolic state to promote tumor-specific memory T cells may be a useful treatment to improve T cell anti-tumor response. Likewise, Sukumar *et al.* also describe recent work demonstrating that modulation of T cell metabolism may improve T cell anti-tumor immunity. In this review, the key metabolic properties of anticancer T cells are described as dynamic, requiring metabolites to promote both T cell effector function and long-term survival. T cells with low mitochondrial membrane potential had phenotypes that promoted memory T cell formation, whereas T cells with high mitochondrial membrane potential were more glycolytic with increased effector gene expression [15]. The authors propose a model for anti-tumor immunity where cells are selected for high metabolic activity during *in vitro* expansion and priming, in order to assume an effector phenotype, followed by a selection of T cells with constrained metabolic activity when applied to the tumor site, in order to promote long-lasting cell survival and persistent antitumor immune response.

It is important to note that many of the factors that influence T cell metabolism (nutrients, cytokines, growth factors, etc.) do so through regulation of key signaling proteins, including the mammalian target of rapamycin (mTOR) and AMPK-activated protein kinase (AMPK). AMPK is a metabolic regulator that senses changes in cellular energy status and functions to maintain energy balance through its ability to promote ATP-producing pathways (e.g. glycolysis, fatty acid oxidation) while inhibiting ATP-consuming pathways (e.g. synthesis of macromolecules such as proteins and fatty acids). Ma *et al.* describe recent work highlighting the role of AMPK in T cells, including the ability of AMPK to respond to changes in T cell nutrient availability, as well as how AMPK influences T cell metabolism to alter Tmem development, Teff cytokine production, and T cell tumor response. Additionally, activation of AMPK negatively regulates mTOR complex 1 (mTORC1) activity in T cells and reduces protein translation. Zeng *et al.* review the role of mTOR in the differentiation and function of Treg, Tmem, and Teff cells, including the unique population of T follicular helper (Tfh) cells which influence B cell differentiation and production. T cell signaling through T cell receptors, costimulatory receptors, and cytokine receptors all activate the PI3K/Akt/mTOR pathway to promote metabolic reprogramming and favor cell growth and proliferation. As the authors of this review discuss, the role that mTOR plays is distinct in various T cell subsets, and therefore understanding the regulation of mTOR in T cells is of critical importance. This is complex, as multiple upstream signals influence mTOR signaling and these signals are contextually dependent.

Interestingly, recent studies have shown that during CD8+ T cell proliferation, there is an asymmetric segregation of metabolic regulators which dictate cell fate. During T cell activation and division, the cell most proximal to the antigen presenting cell (APC) becomes a short-lived Teff cell characterized by increased expression of mTORC1 and the pro-

glycolytic transcription factor Myc, whereas the cell more distal from the APC has low mTORC1 and Myc levels and differentiates into a Tmem cell [16,17].

Lastly, the review by Patel *et al.* suggests approaches by which we may use the above lessons to target T cell metabolism and alter the course of disease. Several drugs have been identified that may target aspects of T cell metabolism. For example, the drug rapamycin can be used to inhibit mTOR activity and promote Treg generation and Teff anergy while enhancing Tmem development. Alternatively, targeting of the mTORC1 inhibitory protein TSC2 may enhance mTORC1 activity and increase Teff function. Modulation of amino acid metabolism may alter Teff/Treg differentiation; as one example of this approach, use of the glutamine antagonist 6-Diazo-5-oxo-L-norleucine (DON) has been shown to disrupt T cell response. The glycolytic inhibitor 2-deoxyglucose (2-DG) has been tested as a therapy to decrease inflammation in mouse models of inflammatory disease, and was found to decrease the Th17/Treg ratio. Other approaches have targeted glucose-derived pyruvate metabolism, fatty acid metabolism, and mitochondrial function. When used alone or together [18], these drugs can selectively alter T cell subsets in ways that may be therapeutically useful in the treatment of a variety of diseases and conditions including autoimmunity, organ or graft rejection, antitumor immunity, and infection response.

Altogether, this series of review papers highlights some of the important work done over the last 5–10 years in the field of T cell metabolism. As is demonstrated in the above reviews, T cells are comprised of a complex group of subsets with varying functional and metabolic phenotypes. Better understanding of these distinct T cell subset properties can enhance our understanding of T cell metabolism and function in health and aid us in the development of immunometabolic targets for the treatment of disease.

References

1. MacIver NJ, Michalek RD, Rathmell JC. Metabolic regulation of T lymphocytes. *Annu Rev Immunol.* 2013; 31:259–283. [PubMed: 23298210]
2. Michalek RD, Gerriets VA, Jacobs SR, Macintyre AN, MacIver NJ, Mason EF, Sullivan SA, Nichols AG, Rathmell JC. Cutting edge: distinct glycolytic and lipid oxidative metabolic programs are essential for effector and regulatory CD4+ T cell subsets. *J Immunol.* 2011; 186:3299–3303. [PubMed: 21317389]
3. Shi LZ, Wang R, Huang G, Vogel P, Neale G, Green DR, Chi H. HIF1alpha-dependent glycolytic pathway orchestrates a metabolic checkpoint for the differentiation of TH17 and Treg cells. *J Exp Med.* 2011; 208:1367–1376. [PubMed: 21708926]
4. van der Windt GJ, Everts B, Chang CH, Curtis JD, Freitas TC, Amiel E, Pearce EJ, Pearce EL. Mitochondrial respiratory capacity is a critical regulator of CD8+ T cell memory development. *Immunity.* 2012; 36:68–78. [PubMed: 22206904]
5. Macintyre AN, Gerriets VA, Nichols AG, Michalek RD, Rudolph MC, Deoliveira D, Anderson SM, Abel ED, Chen BJ, Hale LP, et al. The glucose transporter Glut1 is selectively essential for CD4 T cell activation and effector function. *Cell Metab.* 2014; 20:61–72. [PubMed: 24930970]
6. Gerriets VA, Kishton RJ, Johnson MO, Cohen S, Siska PJ, Nichols AG, Warmoes MO, de Cubas AA, MacIver NJ, Locasale JW, et al. Foxp3 and Toll-like receptor signaling balance Treg cell anabolic metabolism for suppression. *Nat Immunol.* 2016; 17:1459–1466. [PubMed: 27695003]
7. Balmer ML, Ma EH, Bantug GR, Grahlert J, Pfister S, Glatter T, Jauch A, Dimeloe S, Slack E, Dehio P, et al. Memory CD8(+) T cells require increased concentrations of acetate induced by stress for optimal function. *Immunity.* 2016; 44:1312–1324. [PubMed: 27212436]

8. Milner JJ, Rebeles J, Dhungana S, Stewart DA, Sumner SC, Meyers MH, Mancuso P, Beck MA. Obesity increases mortality and modulates the lung metabolome during pandemic H1N1 influenza virus infection in mice. *J Immunol.* 2015; 194:4846–4859. [PubMed: 25862817]
9. Reis BS, Lee K, Fanok MH, Mascaraque C, Amoury M, Cohn LB, Rogoz A, Dallner OS, Moraes-Vieira PM, Domingos AI, et al. Leptin receptor signaling in T cells is required for Th17 differentiation. *J Immunol.* 2015; 194:5253–5260. [PubMed: 25917102]
10. Gerriets VA, Danzaki K, Kishton RJ, Eisner W, Nichols AG, Saucillo DC, Shinohara ML, MacIver NJ. Leptin directly promotes T-cell glycolytic metabolism to drive effector T-cell differentiation in a mouse model of autoimmunity. *Eur J Immunol.* 2016; 46:1970–1983. [PubMed: 27222115]
11. Saucillo DC, Gerriets VA, Sheng J, Rathmell JC, MacIver NJ. Leptin metabolically licenses T cells for activation to link nutrition and immunity. *J Immunol.* 2014; 192:136–144. [PubMed: 24273001]
12. Yang Z, Shen Y, Oishi H, Matteson EL, Tian L, Goronzy JJ, Weyand CM. Restoring oxidant signaling suppresses proarthritogenic T cell effector functions in rheumatoid arthritis. *Sci Transl Med.* 2016; 8:331ra38.
13. Li Y, Shen Y, Hohensinner P, Ju J, Wen Z, Goodman SB, Zhang H, Goronzy JJ, Weyand CM. Deficient activity of the nuclease MRE11A induces T Cell aging and promotes arthritogenic effector functions in patients with rheumatoid arthritis. *Immunity.* 2016; 45:903–916. [PubMed: 27742546]
14. Shirai T, Nazarewicz RR, Wallis BB, Yanes RE, Watanabe R, Hilhorst M, Tian L, Harrison DG, Giacomini JC, Assimes TL, et al. The glycolytic enzyme PKM2 bridges metabolic and inflammatory dysfunction in coronary artery disease. *J Exp Med.* 2016; 213:337–354. [PubMed: 26926996]
15. Sukumar M, Liu J, Mehta GU, Patel SJ, Roychoudhuri R, Crompton JG, Klebanoff CA, Ji Y, Li P, Yu Z, et al. Mitochondrial membrane potential identifies cells with enhanced stemness for cellular therapy. *Cell Metab.* 2016; 23:63–76. [PubMed: 26674251]
16. Pollizzi KN, Sun IH, Patel CH, Lo YC, Oh MH, Waickman AT, Tam AJ, Blosser RL, Wen J, Delgoffe GM, et al. Asymmetric inheritance of mTORC1 kinase activity during division dictates CD8(+) T cell differentiation. *Nat Immunol.* 2016; 17:704–711. [PubMed: 27064374]
17. Verbist KC, Guy CS, Milasta S, Liedmann S, Kaminski MM, Wang R, Green DR. Metabolic maintenance of cell asymmetry following division in activated T lymphocytes. *Nature.* 2016; 532:389–393. [PubMed: 27064903]
18. Lee CF, Lo YC, Cheng CH, Furtmuller GJ, Oh B, Andrade-Oliveira V, Thomas AG, Bowman CE, Slusher BS, Wolfgang MJ, et al. Preventing allograft rejection by targeting immune metabolism. *Cell Rep.* 2015; 13:760–770. [PubMed: 26489460]

Biographies

Nancie J MacIver



Nancie MacIver completed a BA in Mathematics at Johns Hopkins University before getting her MD degree, as well as a PhD in Immunology, from the Mayo Clinic. She then trained in Pediatrics and Pediatric Endocrinology at Duke University and thereafter joined the Duke faculty in 2009. Dr. MacIver is now an Associate Professor at the Duke School of Medicine

with a primary appointment in the Department of Pediatrics and secondary appointments in the Department of Immunology and the Department of Pharmacology and Cancer Biology. Dr. MacIver's laboratory is studying the effects of large nutritional changes (both malnutrition and obesity) on T cell function and metabolism. These studies are applicable to many diseases, including diabetes, autoimmunity, and infection response, in which changes in nutritional status can influence immunity.

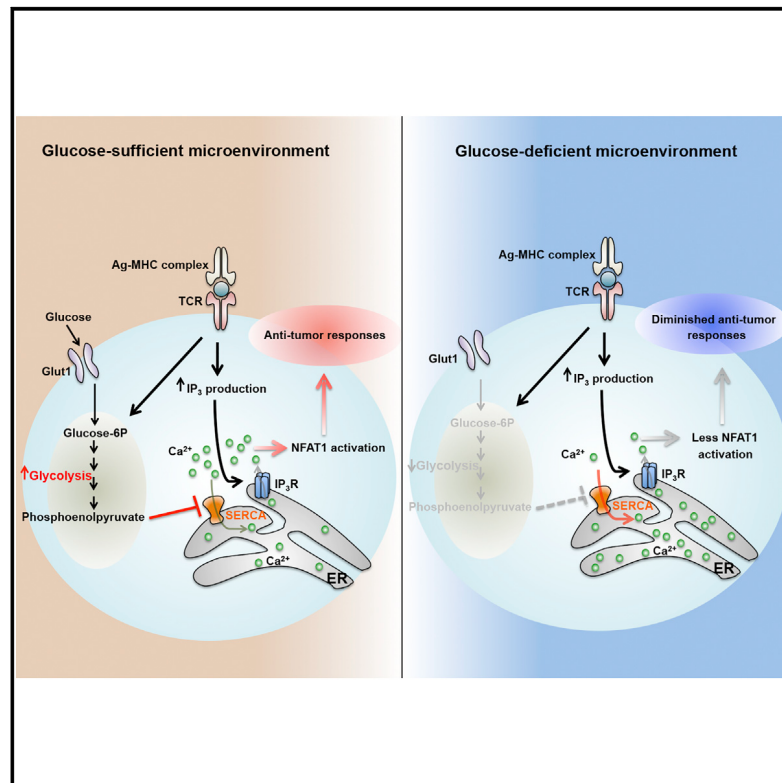
Jeffrey C Rathmell



Jeffrey C. Rathmell, PhD Director, Vanderbilt Center for Immunobiology, Cornelius Vanderbilt Professor of Immunobiology, Department of Pathology, Microbiology, and Immunology, Cancer Biology. He studies mechanisms that influence lymphocyte death and differentiation in inflammatory diseases and cancer. Following undergraduate studies at the University of Northern Iowa, he earned a PhD in Immunology at Stanford University. In postdoctoral studies at the University of Chicago and University of Pennsylvania, he showed that lymphocyte metabolism was dynamically regulated to control cell function and survival in inflammatory diseases and cancer. He began at Duke University in 2003 in the departments of Pharmacology and Cancer Biology and Immunology and moved in 2015 to Vanderbilt University to direct the Vanderbilt Center for Immunobiology and co-leads to Host Tumor Interactions Program of the Vanderbilt Ingram Cancer Center. The ongoing focus on Dr. Rathmell's ongoing work is to understand how metabolic pathways regulate CD4 T cell subsets in inflammatory diseases and how the tumor microenvironment and metabolism impacts anti-cancer responses.

Phosphoenolpyruvate Is a Metabolic Checkpoint of Anti-tumor T Cell Responses

Graphical Abstract



Authors

Ping-Chih Ho, Jessica Dauz Bihuniak, Andrew N. Macintyre, ..., Marcus W. Bosenberg, Jeffrey C. Rathmell, Susan M. Kaech

Correspondence

ping-chih.ho@unil.ch (P.-C.H.), susan.kaech@yale.edu (S.M.K.)

In Brief

High rates of tumor cell glycolysis suppress intratumoral T cell function by depriving T cells of glucose and the downstream metabolite phosphoenolpyruvate (PEP), which is necessary for maximal Ca^{2+} -NFAT signaling in T cells. Metabolic rewiring of T cells to generate PEP in glucose-poor conditions improves their anti-tumor responses.

Highlights

- Glucose deprivation suppresses anti-tumor T cell effector functions
- Glycolytic metabolite PEP sustains Ca^{2+} and NFAT signaling by blocking SERCA
- Ca^{2+} signaling is an integrator of glycolytic activity and TCR signaling
- T cell metabolic reprogramming enhances anti-tumor effector functions

Phosphoenolpyruvate Is a Metabolic Checkpoint of Anti-tumor T Cell Responses

Ping-Chih Ho,^{1,*} Jessica Dauz Bihuniak,² Andrew N. Macintyre,³ Matthew Staron,¹ Xiaojing Liu,⁴ Robert Amezquita,^{1,5} Yao-Chen Tsui,^{1,6} Guoliang Cui,¹ Goran Micevic,⁷ Jose C. Perales,⁸ Steven H. Kleinstein,⁵ E. Dale Abel,⁹ Karl L. Insogna,² Stefan Feske,¹⁰ Jason W. Locasale,⁴ Marcus W. Bosenberg,^{5,7} Jeffrey C. Rathmell,³ and Susan M. Kaech^{1,6,*}

¹Department of Immunobiology, Yale University School of Medicine, New Haven, CT 06519, USA

²Department of Internal Medicine, Yale University School of Medicine, New Haven, CT 06519, USA

³Department of Pharmacology and Cancer Biology, Immunology, Duke Molecular Physiology Institute, Duke University, Durham, NC 27710, USA

⁴Division of Nutritional Sciences, Cornell University, Ithaca, NY 14853, USA

⁵Department of Pathology, Yale University School of Medicine, New Haven, CT 06519, USA

⁶Howard Hughes Medical Institute, Chevy Chase, MD 20815, USA

⁷Department of Dermatology, Yale University School of Medicine, New Haven, CT 06519, USA

⁸Biophysics Unit, Department of Physiological Sciences II, IDIBELL–University of Barcelona, Fexia Llarga s/n 08907, Spain

⁹Fraternal Order of Eagles Diabetes Research Center, Division of Endocrinology and Metabolism, Department of Medicine, Carver College of Medicine University of Iowa, Iowa City, IA 52242, USA

¹⁰Department of Pathology, New York University Langone Medical Center, New York, NY 10016, USA

*Correspondence: ping-chih.ho@unil.ch (P.-C.H.), susan.kaech@yale.edu (S.M.K.)

<http://dx.doi.org/10.1016/j.cell.2015.08.012>

SUMMARY

Activated T cells engage aerobic glycolysis and anabolic metabolism for growth, proliferation, and effector functions. We propose that a glucose-poor tumor microenvironment limits aerobic glycolysis in tumor-infiltrating T cells, which suppresses tumoricidal effector functions. We discovered a new role for the glycolytic metabolite phosphoenolpyruvate (PEP) in sustaining T cell receptor-mediated Ca^{2+} -NFAT signaling and effector functions by repressing sarco/ER Ca^{2+} -ATPase (SERCA) activity. Tumor-specific CD4 and CD8 T cells could be metabolically reprogrammed by increasing PEP production through overexpression of phosphoenolpyruvate carboxykinase 1 (PCK1), which bolstered effector functions. Moreover, PCK1-overexpressing T cells restricted tumor growth and prolonged the survival of melanoma-bearing mice. This study uncovers new metabolic checkpoints for T cell activity and demonstrates that metabolic reprogramming of tumor-reactive T cells can enhance anti-tumor T cell responses, illuminating new forms of immunotherapy.

INTRODUCTION

Host immunity provides wide spectrum protection that serves to eradicate cancerous cells in addition to infectious pathogens. Multiple types of immune cells are involved in tumor immuno-surveillance and of particular importance are the tumor-infiltrating lymphocytes (TILs) (i.e., T cells) (Braumüller et al., 2013; Shiao et al., 2011). In most established tumors, however, the tumoricidal effector functions of TILs such as IFN γ production and cyto-

toxicity are restricted by multiple environmental factors. This includes the accumulation of immunoregulatory cells such as regulatory CD4+ T cells (Tregs), myeloid derived suppressor cells (MDSCs) and tolerogenic antigen-presenting cells (APCs) (Mellman et al., 2011; Shiao et al., 2011). Additionally, alterations in the availability of nutrients (e.g., lactate and tryptophan-related metabolites such as kynureneine) in the tumor microenvironment can limit TIL activity (Yang et al., 2013). Another prominent feature of TILs is the increased expression of inhibitory checkpoint receptors (e.g., programmed cell death protein 1 [PD-1], lymphocyte-activation gene 3 [Lag3], and cytotoxic T-lymphocyte-associated protein 4 [CTLA-4]) that desensitizes T cell receptor (TCR) signaling and contributes to their functional impairment (Baitsch et al., 2012). T cells displaying such properties are commonly referred to as “functionally exhausted” (Wherry, 2011). These discoveries have led to the development of cancer immunotherapies that reawaken exhausted TILs by blocking inhibitory checkpoint receptors such as PD-1 or CTLA-4 or targeting other immunoregulatory cells. Adoptive cell therapy (ACT) of tumor-specific T cells is another promising form of anti-cancer immunotherapy that increases the repertoire of cytotoxic T cells to eradicate established tumors. ACT has the added benefit of permitting genetic modifications of TILs to express proteins that could aide in tumor destruction (Maude et al., 2014). These breakthroughs demonstrate that tumor immunotherapy holds great promise (Callahan et al., 2010; Wolchok et al., 2013), but also present us with challenges to devise additional treatment options in conjunction with those currently available to further increase patient objective responses. To meet these challenges, we must gain a clearer understanding of what causes T cell exhaustion in tumors, and we hypothesize that the metabolic states of the TILs and tumor cells, as well as other cell types in the tumor microenvironment, are principal components of this process.

Deregulated anabolic metabolism and increased rates of aerobic glycolysis (i.e., the Warburg effect), glutaminolysis and fatty acid synthesis are cardinal features of most tumor cells that fuels their growth and proliferation (Hanahan and Weinberg, 2011; Ward and Thompson, 2012). Interestingly, activated T lymphocytes undergo a metabolic switch similar to cancer cells and upregulate aerobic glycolysis and glutaminolysis to permit proliferation and differentiation into specialized effector T cells. Given their similarities in metabolic profiles and nutrient requirements, it is possible that the abnormally high metabolic rates and consumption of nutrients by tumor cells competes with neighboring T cells, which leads to T cell metabolic exhaustion that underlies their functional exhaustion. Supporting this notion, reports have shown that the concentration of extracellular glucose are lower in tumors compared to healthy tissues (Gullino et al., 1964). Thus, limited glucose availability could be an environmental restriction that promotes T cell exhaustion, and if true, it is important to learn how this affects T cell receptor (TCR) signaling and effector functions in tumors. Perhaps, new therapies directed at reprogramming T cell metabolism could be developed to enhance their functional fitness in the tumor microenvironment.

TCR stimulation activates numerous key signaling pathways that coordinately induce anabolic metabolism, aerobic glycolysis, and effector T cell proliferation and differentiation (Smith-Garvin et al., 2009). Increased aerobic glycolysis is essential for the production of biosynthetic precursors that fuel effector T cell proliferation and production of effector molecules like IFN γ , IL-2, and IL-17 and Granzyme B in T cells (Cham et al., 2008; Chang et al., 2013; Finlay et al., 2012; Michalek et al., 2011). Activation of PI3K, Akt, and mTOR triggers the switch to anabolic metabolism by inducing transcription factors such as Myc and hypoxia-inducible factor 1 (HIF1) (MacLver et al., 2013; Wang et al., 2011a). T cells rendered functionally anergic that are unable to activate Ca $^{2+}$ and nuclear factor of activated T cells (NFAT) signaling show diminished rates of aerobic glycolysis and anabolic metabolism following stimulation (Srinivasan and Frauwirth, 2007; Zheng et al., 2009). Similarly, CD8 T cells with increased PD-1 expression fail to fully activate mTOR or aerobic glycolysis following TCR stimulation and conversely, those with hyper-HIF1 α activity and aerobic glycolysis are refractory to functional exhaustion (Doedens et al., 2013; Parry et al., 2005; Staron et al., 2014). The glycolytic enzymes may also serve direct roles in regulating effector functions in T cells because recent work showed that when glycolytic rates are low, the glyceraldehyde phosphate dehydrogenase (GAPDH) binds to and suppresses Ifng mRNA translation in T cells (Chang et al., 2013; Gubser et al., 2013). These findings demonstrate strong interconnections between T cell metabolism and effector functions but little remains known about how metabolic pathways or their metabolites fine-tune T cell activity.

In this study, we found that intratumoral CD4 T cells displayed signs of glucose deprivation and diminished anti-tumor effector functions, suggesting that a glucose-poor tumor microenvironment might contribute to TIL exhaustion. Furthermore, increased expression of hexokinase 2 (HK2) in tumor cells allowed for more efficient evasion of CD4 T cell-mediated immune surveillance indicating that a metabolic competition could exist between TILs and tumor cells. Linking glucose-deprivation to T cell func-

tion, we also discovered that insufficiency of the glycolytic metabolite phosphoenolpyruvate (PEP) led to defects in Ca $^{2+}$ -NFAT signaling and T cell activation by increasing SERCA-mediated Ca $^{2+}$ re-uptake. Most importantly, we provided proof-of-concept evidence that metabolic reprogramming of T cells to increase PEP production could be a promising strategy to elevate T cell mediated anti-tumor immune responses and improve the effects of adoptive T cell transfer immunotherapy.

RESULTS

Glucose Limitation Suppresses Anti-tumor Effector Functions of Intratumoral TH1 CD4 T Cells while Stimulating TGF β Production

To investigate whether limited glucose availability within the tumor microenvironment suppressed aerobic glycolysis and hence, effector functions in TILs, we first compared the concentration of glucose in the interstitial fluid of the spleen, blood, and tumors from melanoma-bearing Tyr-creERT2/BrafV600E/Pten-*lox* (Braf/Pten) mice (Dankort et al., 2009) (Figure 1A) and B16 melanoma-bearing mice (data not shown). As reported in other solid tumors (Gullino et al., 1964), the glucose level of the tumor interstitial fluid (\sim 0.6 mM) was approximately ten times lower than that of the spleen and blood (\sim 9 mM). Additionally, intratumoral CD44hi CD25lo CD4+ T cells (i.e., activated non-Treg CD4+ T cells) failed to take-up glucose as efficiently as their counterparts in the spleen based on intracellular staining with the fluorescent glucose analog 2-NBDG (Figure 1B). We further assessed 2NDBG-uptake in tumor infiltrating non-Treg CD4+ T cells, Tregs, tumor-associated macrophages (TAMs), and MDSCs. This showed that non-Treg CD4+ T cells take-up marginally less 2NDBG than TAMs, but not MDSCs. Unexpectedly, the intratumoral and splenic Tregs demonstrated higher 2NDBG uptake compared to the other cell populations (Figure S1A). Furthermore, co-culturing TH1 CD4+ T cells with Braf/Pten melanoma cells demonstrated that the presence of tumor cells could reduce glucose uptake by TH1 cells (Figure 1C), suggesting that tumor cells may directly restrict glucose availability for TILs. As there is no facile way to directly and specifically measure rates of glycolysis in TILs *in vivo* or *in situ*, we attempted to determine if intratumoral CD4+ T cells express genes induced by glucose deprivation. We identified a “glucose-deprivation transcriptional signature” in CD4+ T cells by comparing the differentially expressed genes of activated TH1 cells cultured in high (10 mM) or low (0.1 mM) glucose concentrations using RNA-sequencing and microarrays (Figure S1B), and observed that intratumoral CD4+ T cells expressed higher levels of the glucose-deprived signature genes than CD4+ T cells in the draining lymph nodes (dLNs) (Figure 1D). This result suggested that some portion of the CD4+ TILs experienced glucose-deprivation within the tumor microenvironment *in vivo*.

Next, we stimulated functional TH1 CD4+ T cells (isolated from lymphocytic choriomeningitis virus (LCMV)-infected animals) in different concentrations of glucose (ranging from 0.1–10 mM) to directly interrogate the effects of glucose deprivation on production of CD40 ligand (CD40L) and IFN γ —two factors critical for maintaining an immunostimulatory microenvironment in the Braf/Pten melanomas (Ho et al., 2014). This showed that

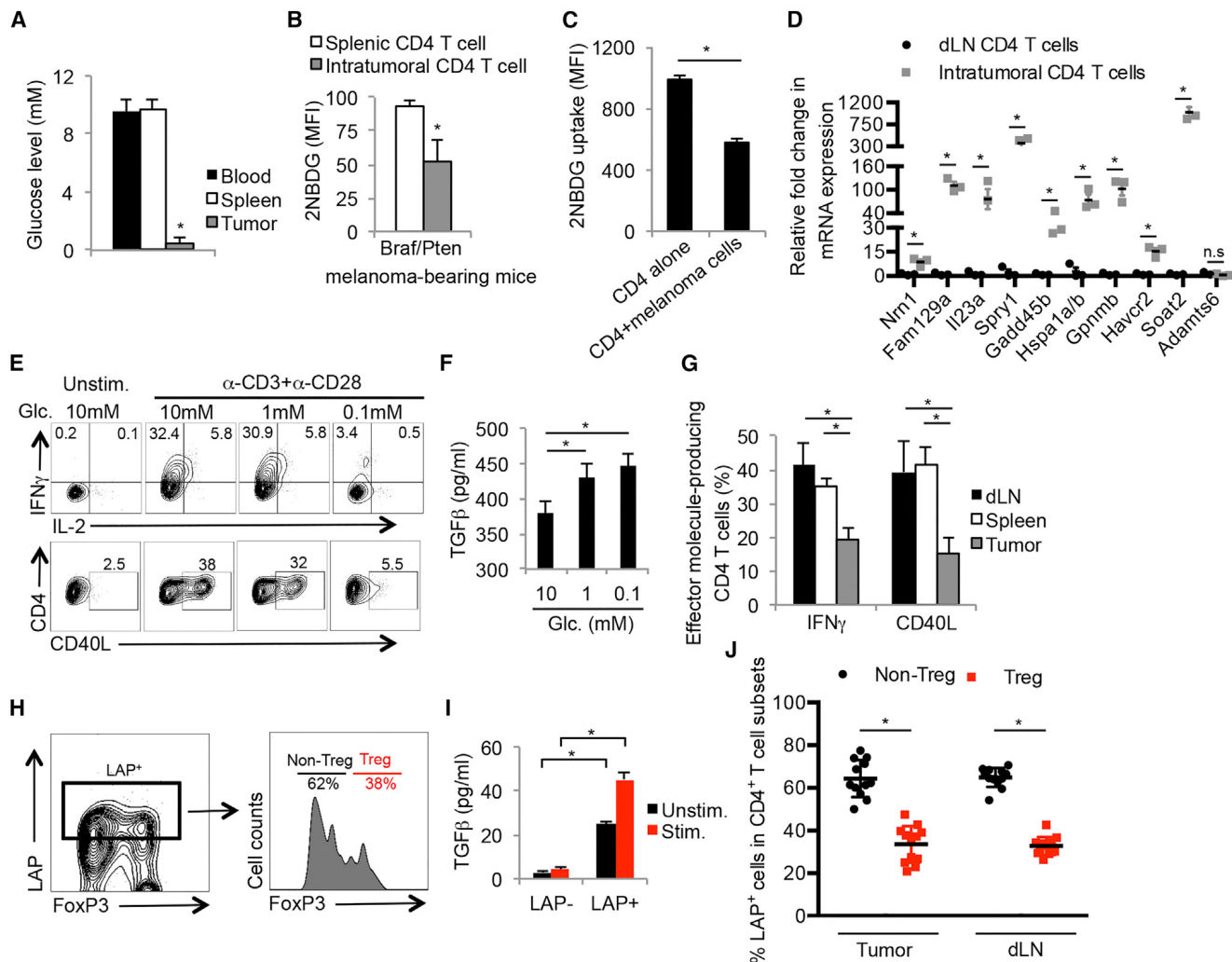


Figure 1. Tumor Microenvironment Deprives Glucose to Infiltrating CD4⁺ T Cells

(A) Bar graphs show the glucose concentration in blood and interstitial fluid of tumors and spleens from Braf/Pten melanoma-bearing mice. (B and C) Glucose uptake in splenic and intratumoral CD44⁺/CD25^{lo} and CD44⁺/CD25^{hi} CD4⁺ T cells (B) or in T_H1 cells cultured with or without Braf/Pten melanoma cells (C) was determined using fluorescent 2-NBDG and measured by flow cytometry. (D) The expression of glucose-deprived signature genes in CD4⁺ T cells isolated from melanomas and draining lymph nodes (dLNs) was determined by qRT-PCR. (E and F) T_H1 CD4⁺ T cells derived from LCMV Armstrong-infected mice were stimulated by anti-CD3/anti-CD28 mAbs in vitro in the indicated glucose concentrations for 5 hr. The expression of IFN γ , IL-2, and CD40L was analyzed by flow cytometry (E), and production of TGF β was determined by ELISA (F). (G) The production of CD40L and IFN γ in CD4⁺ T cells isolated from the dLN, spleen, or tumors in Braf/Pten mice was analyzed by flow cytometry. (H) LAP surface expression was compared between activated FoxP3⁺ (T_{reg}) and FoxP3⁻ (non-T_{reg}) CD4⁺ T cells within melanomas using flow cytometry. (I) Validation of LAP staining as a surrogate for TGF β secreting capability was performed by stimulating purified intratumoral LAP⁺ and LAP⁻ CD44⁺ CD4⁺ T cells with or without anti-CD3/anti-CD28 mAbs for 16 hr and measuring the amount of TGF β in culture supernatants by ELISA. (J) The frequency of LAP⁺ FoxP3⁺ (T_{reg}) and FoxP3⁻ (non-T_{reg}) CD4⁺ T cells within melanomas or dLNs was assessed using flow cytometry. Data shown are cumulative of two (A and B, D, H, I) ($n = 3\text{--}6$ mice/group/experiment) and three (G and J) independent experiments ($n = 3\text{--}4$ mice/group/experiment) or representative of three (C, E and F) independent experiments ($n = 3\text{--}5$ /group). Data are expressed as mean \pm SD and (C) is presented as mean \pm SEM. * $p < 0.05$ by unpaired Student's t test.

these effector functions were suppressed by limited amounts of glucose (Figure 1E). Conversely, glucose deprivation augmented TGF β production in activated CD4⁺ T cells (Figure 1F), suggesting that glucose deprivation can cause CD4⁺ T cells to switch from immuno-supportive to immuno-suppressive states. Importantly, the CD4⁺ T cells isolated directly ex vivo from melanomas displayed similar functional attributes to the in vitro glucose-deprived TH1 cells. For example, the percentage of CD44^{hi}

CD25^{lo} (non-Treg) CD4⁺ T cells that produced IFN γ or CD40L in the tumors was ~50% lower than that in the spleen or dLN (Figure 1G). Additionally, the expression of the TGF β latency associated peptide (LAP), a surrogate marker for cells competent to produce TGF β , was examined on the CD4⁺ T cells (Figures 1H–IJ), and this showed that a greater proportion of non-Treg CD4⁺ T cells expressed elevated LAP compared to the FoxP3⁺ Tregs in both the tumors and dLNs (Figure 1J).

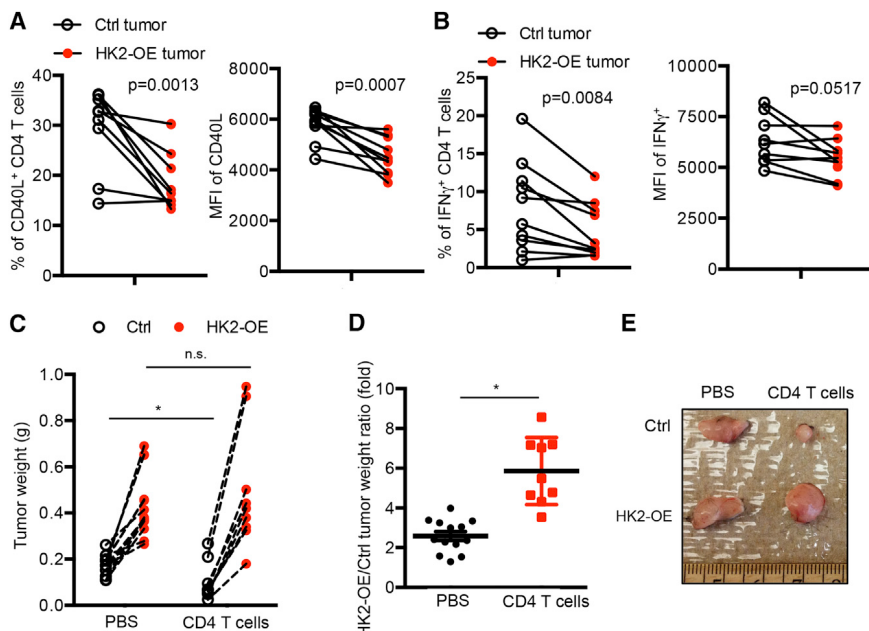


Figure 2. HK2 Overexpression in Melanoma Cells Suppresses CD4⁺ T Cell-Mediated Anti-tumor Responses

(A and B) Control (Ctrl) or HK2-OE Braf/Pten tumors were engrafted into the right and left flanks of C57BL/6 mice. Fourteen days later, the CD4⁺ TILs were isolated, stimulated *in vitro* by anti-CD3/anti-CD28 mAbs for 5 hr and analyzed for CD40L and IFN γ expression by flow cytometry. Left: percentage of CD40L⁺ (A) or IFN γ ⁺ (B); right: mean fluorescence intensity (MFI) of the indicated proteins. (C–E) Ctrl or HK2-OE Braf/Pten tumors were engrafted into the right and left flanks of Rag1-KO mice that were either injected with PBS or reconstituted with CD4⁺ T cells and 14 days later the weight (C and D) and size (E) of tumors was assessed. (C and D) Graphs show tumor weights of the contralateral pairs of ctrl and HK2-OE melanomas collected from same mouse expressed as actual weights (C) or as a ratio (D). Data shown are cumulative of three (A and B) independent experiments ($n = 3\text{--}4$ mice/group) or four (C and D) independent experiments ($n = 2\text{--}4$ mice/group). Data are expressed as mean \pm SD and * $p < 0.05$ by unpaired Student's *t* test.

Collectively, these data demonstrate that CD4⁺ TILs display genetic and functional features associated with glucose-deprivation and suggest that competition between tumor cells and TILs for glucose in the tumor microenvironment could contribute to an immunosuppressive environment.

Increased Rates of Aerobic Glycolysis in Melanoma Cells Suppress CD4⁺ T Cell-Mediated Immunosurveillance

Increased rates of aerobic glycolysis and expression of glycolytic enzymes (e.g., hexokinase 2 [HK2]) are common hallmarks of cancer cells (Hanahan and Weinberg, 2011), and this may lead to glucose-deprivation and T cell dysfunction in tumors as suggested by the data above. To investigate this hypothesis further, we analyzed the expression of effector T cell genes (e.g., *Ifng* and *Cd40lg*) and markers of glycolysis (e.g., *Hk2*) mRNA within the tumors of 384 melanoma patients (data obtained from The Cancer Genome Atlas [TCGA]) (Cerami et al., 2012; Gao et al., 2013). Interestingly, this showed that the amount of *Cd40lg* and *Ifng* mRNA inversely correlated with *Hk2* mRNA (Figure S2A). To more directly test if the glycolytic rates of tumor cells affect tumor immunosurveillance by CD4⁺ T cells, we established stable clones of the Braf/Pten melanoma cell line (YUMM1.7) that expressed either a control vector or one overexpressing HK2 (HK2-OE). As expected, HK2-OE tumor cells had higher rates of aerobic glycolysis than the control cells based on extracellular acidification rates (ECAR) using the Seahorse Extracellular Flux Analyzer (Figure S2B) and HK2-OE tumor cells more efficiently suppressed glucose uptake of TH1 CD4⁺ T cells in the co-culture assay (Figure S2C). Then we engrafted control and HK2-OE melanoma cell lines into the left and right flanks, respectively, of wild-type C57BL/6 mice. Two weeks later, the production of CD40L and IFN γ by CD4⁺ TILs re-stimulated directly *ex vivo* was assessed and compared to CD4⁺

T cells isolated from the control melanomas, those isolated from HK2-OE tumors had lower production of CD40L and IFN γ (Figures 2A and 2B and S2D). This result demonstrated that T cell effector functions could be affected by the rates of tumor cell aerobic glycolysis. Next, we compared the growth rates of control and HK2-OE melanoma cell lines engrafted into the left and right flanks, respectively, of Rag1-KO mice that were either reconstituted with CD4⁺ T cells or not. In accord with higher rates of aerobic glycolysis, the HK2-OE melanomas grew faster compared to the control tumors in both groups of mice (Figure 2C). However, the presence of CD4⁺ T cells potently suppressed the growth of control melanoma cells, but had little effect on the HK2-OE melanoma cells (Figures 2C–E). Taken together, these results support the intriguing model that tumor cells with increased rates of aerobic glycolysis are better able to evade anti-tumor CD4⁺ T cell responses.

Glucose Deprivation Suppresses TCR-Dependent Activation of Ca²⁺ and NFAT Signaling

To better understand how glucose deprivation alters TH1 cell functions, we examined how glycolysis affects TCR signaling after TCR stimulation using several approaches. First, we observed that the induction of the immediate early gene Nur77 (as measured using a Nur77-eGFP reporter that reads out TCR signaling in a Ca²⁺-dependent manner; Moran et al., 2011) was suppressed in glucose-poor conditions or in the presence of 2-DG (Figure 3A). In contrast, the amount of phosphorylated ERK1/2 (pERK1/2) or AKT (pAKTS473 and pAKTT308) was minimally affected following activation of TH1 CD4 T cells in glucose-deprived conditions (Figure S3). The defect in Nur77 induction prompted us to more closely monitor cytoplasmic calcium flux using the ratiometric Ca²⁺-sensitive dyes (Fluo-4 and Fura-Red) and flow cytometry, and this revealed that glucose deprivation profoundly repressed TCR-induced Ca²⁺

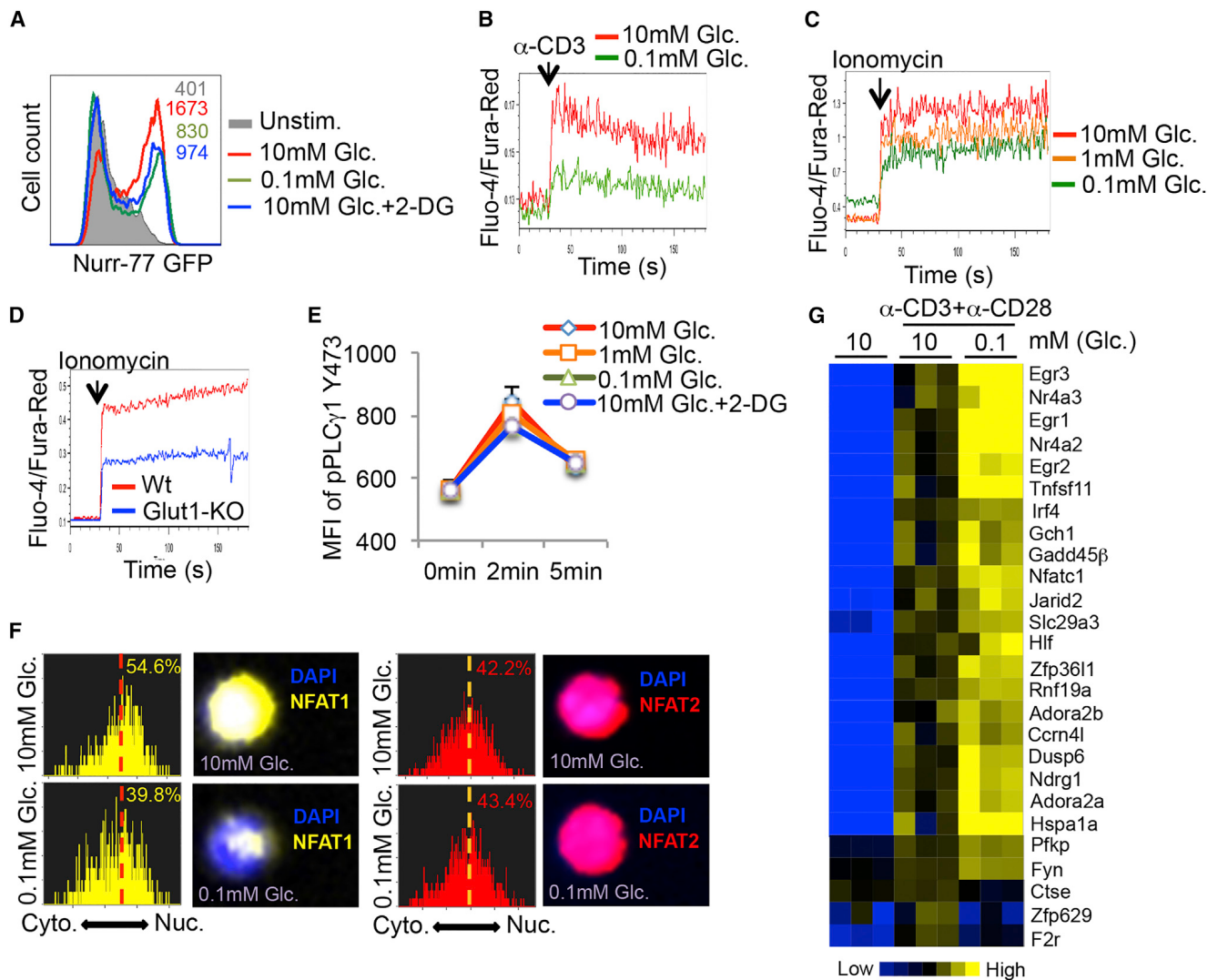


Figure 3. Glycolysis Modulates the Ca^{2+} -NFAT1 Signaling Pathway in CD4+ T Cells

(A) Naive CD4+ T cells from Nur-77-eGFP mice were left unstimulated or stimulated with anti-CD3/anti-CD28 mAbs for 5 hr in the indicated conditions and GFP fluorescence was measured by flow cytometry. Glc.: glucose; 2-DG: 2-deoxy-D-glucose.

(B and C) Intracellular Ca^{2+} levels were measured in Fluo-4- and Fura-Red-labeled TH1 CD4+ T cells cultured in 10 mM glucose or 0.1 mM glucose before and after activation with anti-CD3 crosslinking antibodies (B) or ionomycin (C). The ratio of Fluo-4 and Fura-Red fluorescence was measured using flow cytometry.

(D) Intracellular Ca^{2+} levels were measured as above in naive CD4+ T cells isolated from wild-type (Wt) or GLUT-1-knockout (Glut1-KO) mice.

(E) T_H1 CD4+ T cells were stimulated with anti-CD3/anti-CD28 in the indicated conditions and amounts of phospho-PLC γ 1 were measured by flow cytometry.

(F) T_H1 cells were stimulated with ionomycin in medium containing 10 mM or 0.1 mM glucose for 10 min and the cytoplasmic versus nuclear distribution of NFAT1 and NFAT2 was determined by Amnis Imagestream. Representative histograms and images show the similarity profiles of NFAT1 (yellow, left) or NFAT2 (red, right) with DAPI staining to measure nuclear localization. The percentage of T cells with nuclear NFAT1 or NFAT2 is shown.

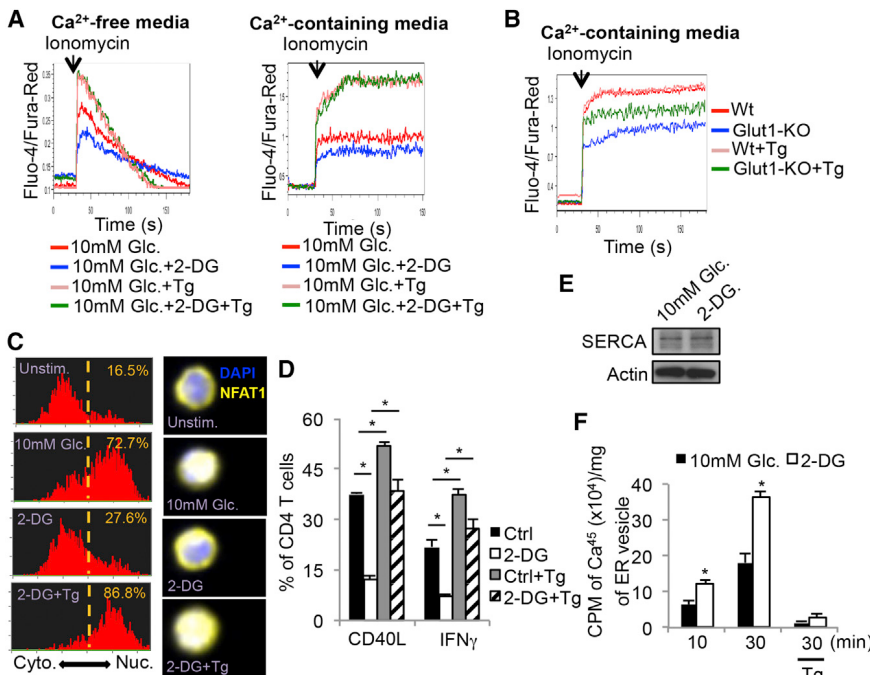
(G) Heat map shows normalized expression of select genes associated with T cell anergy (Safford et al., 2005) in T_H1 cells stimulated for 5 hr with anti-CD3/anti-CD28 mAbs in glucose-sufficient (10 mM) or glucose-deficient (0.1 mM) conditions.

Data shown are representative of two (D and E) and three (A–C, F) independent experiments or cumulative of three (G) independent experiments ($n = 2$ mice/group).

flux in activated TH1 cells (Figure 3B). Moreover, reducing aerobic glycolysis in activated TH1 cells by glucose deprivation or deletion of the glucose transporter 1 (Macintyre et al., 2014) also suppressed ionomycin-induced cytosolic Ca^{2+} accumulation (Figures 3C and 3D). This latter result indicated that the defect in Ca^{2+} flux could be IP3-independent because ionomycin triggers Ca^{2+} efflux from the ER in an IP3-independent manner.

In agreement, glucose deprivation did not affect TCR-induced phosphorylation of PLC γ -1 in TH1 cells (Figure 3E). Altogether, these results suggested that glucose-deprivation dampened the magnitude of TCR-induced Ca^{2+} flux, and consequently CD4+ T cell effector functions.

Interestingly, anergic T cells, which have similar functional defects to those observed with glucose-deprivation, also



(F) Ca^{2+} -uptake using radiolabeled 45CaCl_2 was measured in ER microsomal fractions isolated from Jurkat T cells treated with or without 2-DG for 10 or 30 min. Data shown are representative of two (E and F) and three (A and B, C-E) independent experiments ($n = 3/\text{group}$ in D and F). Data are expressed as mean \pm SD and * $p < 0.05$ by unpaired Student's t test.

display defects in Ca^{2+} signaling (Schwartz, 2003). Other work has shown that the reduced Ca^{2+} signaling in anergic CD8 T cells impairs the nuclear localization of NFAT1, but not that of NFAT2, indicating differential sensitivity to cytosolic Ca^{2+} levels between these two transcription factors (Srinivasan and Frauwrith, 2007). These phenotypes prompted us to examine the cellular distribution of NFAT1 and 2 and expression of anergy-associated genes in glucose-deprived TH1 cells (Safford et al., 2005). In agreement with the prior study (Srinivasan and Frauwrith, 2007), nuclear translocation of NFAT1, but not NFAT2, was severely compromised in glucose-deprived TH1 cells (Figure 3F). Importantly, 5 hr of glucose deprivation led to increased expression of several “anergy” signature genes, including *Egr2*, *Egr3*, *Irf4*, *Hspa1a*, *Gadd45b*, and *Nfatc1* as previously described (Figure 3G, note the augmented expression of some of these genes in TILs in Figure 1D) (Safford et al., 2005). Collectively, these results identified that glycolysis is critical for sustaining high amounts of Ca^{2+} -NFAT signaling in TH1 cells and that glucose-deprivation results in CD4 T cell dysfunction and expression of anergy-associated genes.

Glycolysis Modulates SERCA-Mediated ER Calcium Uptake Activity

Stimulation of the TCR initially triggers Ca^{2+} efflux from the ER, which subsequently induces extracellular Ca^{2+} import via the calcium-release-activated calcium (CRAC) channel (Feske et al., 2012). To distinguish ER Ca^{2+} efflux from extracellular Ca^{2+} influx, we stimulated CD4+ T cells in the presence or absence of 2-DG with ionomycin in Ca^{2+} -free or Ca^{2+} -containing

Figure 4. Glycolysis Sustains Cyttoplasmic Ca^{2+} Accumulation via Modulation of SERCA-Mediated Calcium Reuptake

(A) Intracellular calcium levels were measured in Fluo-4- and Fura-Red-labeled CD4+ T cells cultured in Ca^{2+} -free (left) or Ca^{2+} -containing media (right) in 10 mM glucose or 2-DG with or without thapsigargin (Tg).

(B) Intracellular Ca^{2+} levels were measured as above in naive CD4+ T cells isolated from wild-type (Wt) or GLUT1-knockout (Glut1-KO) mice and cultured in Ca^{2+} -containing media with or without Tg.

(C) Naive CD4+ T cells were left unstimulated or stimulated with ionomycin in the presence of 10 mM glucose, 2-DG or 2-DG plus Tg for 10 min and the cytoplasmic versus nuclear distribution of NFAT1 was determined by Amnis Imagestream. Representative histograms (left) and images (right) show the similarity profiles of NFAT1/DAPI staining to measure NFAT1 nuclear localization. The frequency of T cells with nuclear NFAT1 is shown.

(D) Control or 2-DG treated TH1 cells were stimulated with anti-CD3/anti-CD28 mAbs for 5 hr in the absence or presence of Tg. The expression of CD40L and IFN γ was analyzed by flow cytometry. (E) Western blots showing the amount of SERCA protein in Jurkat T cells treated with or without 2-DG for 30 min.

media and found that 2-DG treatment diminished ionomycin-induced cytosolic accumulation in either condition (Figure 4A, compare red and blue lines in left and right). This suggested that glycolysis is important for maintenance of cytosolic Ca^{2+} levels to support T cell activation. Several Ca^{2+} channels expressed on the plasma membrane (plasma membrane Ca^{2+} ATPase: PMCA), mitochondrial membrane (mitochondrial Ca^{2+} uniporter: MCU), and ER membrane (SERCA) could lower cytosolic Ca^{2+} levels, so we next tested if blocking these Ca^{2+} channels could restore Ca^{2+} flux in glucose-deprived T cells. In contrast to blocking PMCA and MCU channels, treatment with the SERCA inhibitor thapsigargin (Tg) increased Ca^{2+} flux in 2-DG treated or Glut1-KO CD4+ T cells (compare blue and green lines, Figures 4A and 4B and Figure S4). This result suggested that glucose-deprived T cells have increased SERCA activity that suppressed maximal Ca^{2+} flux. Importantly, Tg treatment also restored nuclear translocation of NFAT1 (Figure 4C) as well as IFN γ and CD40L production (Figure 4D) in 2-DG treated TH1 cells. Western blotting of Jurkat T cells showed that 2-DG treatment did not affect the overall amounts of SERCA compared to control cells (Figure 4E), suggesting that the increase in ER Ca^{2+} re-uptake stemmed from increased SERCA activity. Indeed, measurement of radio-labeled Ca^{2+} uptake in ER vesicles isolated from Jurkat T cells revealed that 2-DG treatment increased SERCA-dependent Ca^{2+} uptake by ~2-fold compared to the control cells (Figure 4F). Taken together, these findings strongly indicate that glycolysis suppresses SERCA activity and consequently, glucose deprivation leads to defective Ca^{2+} -NFAT signaling and effector functions in glucose-deprived T cells.

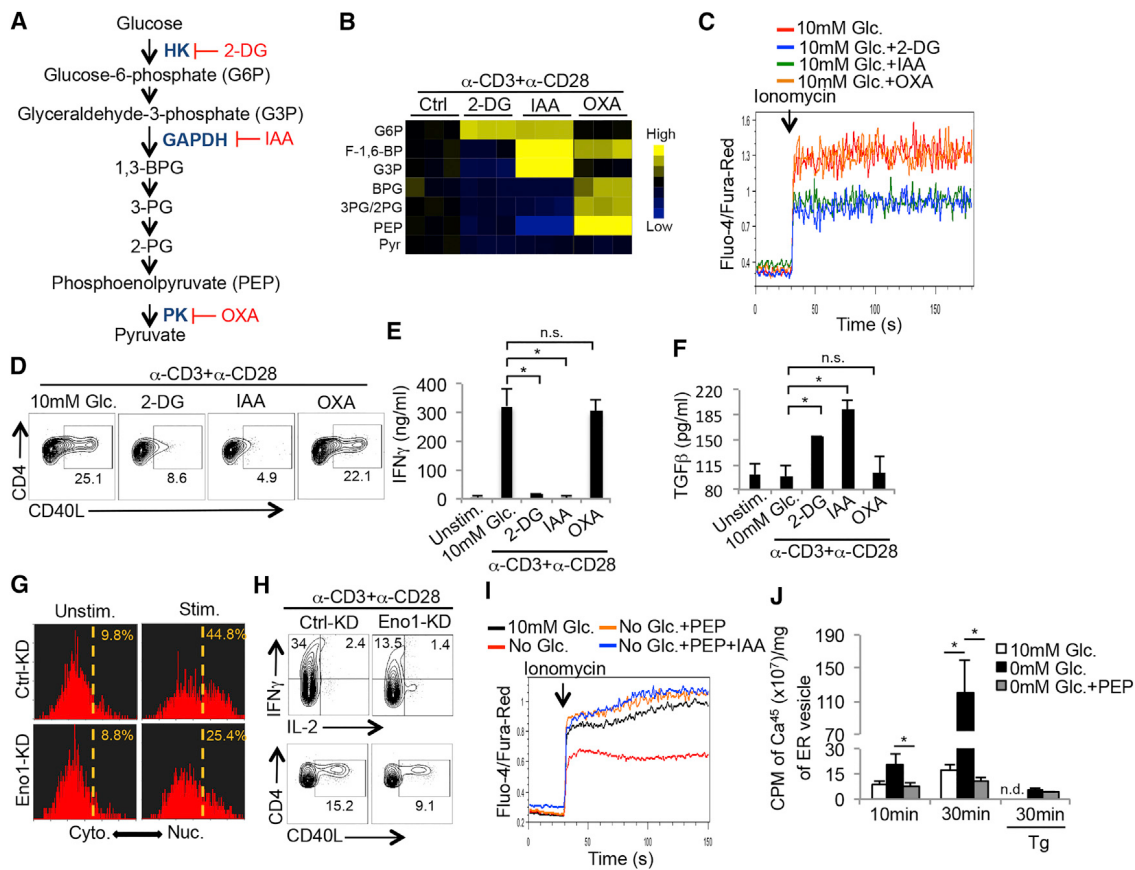


Figure 5. PEP Suppresses SERCA-Mediated ER Calcium Reuptake

(A) Illustration of the glycolysis pathway and the targets of the indicated glycolytic inhibitors. 2-DG: 2-deoxyglucose; IAA: iodoacetate; OXA: oxalate.

(B) Heat map shows the normalized concentrations of the indicated glycolytic metabolites in CD4+ T cells stimulated with anti-CD3/anti-CD28 mAbs for 1 hr in the absence or presence of the glycolytic inhibitors described in (A) as measured by LC-QE-MS.

(C) Intracellular Ca²⁺ levels were measured in Fluo-4- and Fura-Red-labeled T_H1 cells treated with indicated glycolytic inhibitors before and after activation with ionomycin.

(D–F) T_H1 cells were left alone or stimulated with anti-CD3/anti-CD28 mAbs for 5 hr in 10 mM glucose in the absence or presence of indicated glycolytic inhibitors and the expression of CD40L (D), IFN γ (E) and TGF β (F) was measured by flow cytometry (D) or ELISA (E and F).

(G and H) CD4+ T cells were transduced with empty vector control retroviruses (RV, Ctrl-KD) or those expressing enolase-1 shRNAi (eno1-KD). RV-infected T cells were left alone or stimulated with ionomycin for 10 min and the cytoplasmic versus nuclear distribution of NFAT1 was determined by Amnis Imagestream as described in Figure 3F (G), or alternatively were stimulated with anti-CD3/anti-CD28 mAbs in vitro in the presence of 10 mM glucose for 5 hr and the expression of IFN γ , IL-2 and CD40L was analyzed by flow cytometry (H).

(I) Intracellular Ca²⁺ levels in CD4+ T cells that were partially permeabilized and recovered in the absence or presence of PEP were measured as in (C) in the absence or presence of glycolytic inhibitor IAA.

(J) Ca²⁺-uptake assay as described in Figure 4F was performed on ER microsomal fractions isolated from Jurkat T cells cultured in the presence or absence of glucose or exogenous PEP. The addition of Tg served as a specificity control for SERCA-dependent activity.

Data shown are representative of two (H and J) and three (C and D, G and I) independent experiments or cumulative of three (B, E and F) independent experiments. Data are expressed as mean \pm SD and *p < 0.05 by unpaired Student's t test.

The Glycolytic Metabolite Phosphoenolpyruvate Regulates Ca²⁺-NFAT Signaling in TH1 CD4+ T Cells by Inhibiting SERCA Activity

To determine which steps of glycolysis regulate cytoplasmic Ca²⁺ accumulation and T cell effector functions, TH1 cells were treated with 2-DG, iodoacetate (IAA) and oxalate (OXA), to inhibit hexokinase (HK), glyceraldehyde phosphate dehydrogenase (GAPDH), and pyruvate kinase (PK), respectively, at doses that showed comparable inhibition of lactate production (Figure 5A and data not shown). The glycolytic metabolites

were examined by high-resolution liquid-chromatography Q-exactive mass spectrometry (LC-QE-MS) in the CD4+ T cells stimulated in the absence or presence of the inhibitors and as expected, the levels of 3- and 2-phosphoglycerate (3-PG/2-PG), and phosphoenolpyruvate (PEP) were suppressed by 2-DG and IAA, but promoted by OXA (Figures 5B and S5A). Interestingly, 2-DG and IAA, but not OXA, suppressed TH1 cell Ca²⁺ flux after ionomycin stimulation (Figure 5C) and CD40L and IFN γ production after TCR stimulation (Figures 5D and 5E). Likewise 2-DG and IAA, but not OXA, augmented TGF β production

(Figure 5F). These results suggested that a metabolite produced downstream of GAPDH and upstream of PK fine-tunes Ca^{2+} signaling and TH1 effector functions.

We hypothesized that such a metabolite may be PEP because of the above inhibitor studies and because TCR activation increases expression of the less-active M2 isoform of pyruvate kinase (PKM2) (Wang et al., 2011a), which allows the accumulation of several metabolic intermediates, including PEP, in proliferating cells (Vander Heiden et al., 2010). To more rigorously confirm the role of PEP in regulating the Ca^{2+} -NFAT pathway, we knocked down enolase 1 (Eno-1), the glycolytic enzyme that converts 2-PG into PEP (Figure S5B), and analyzed NFAT1 nuclear translocation and expression of IFN γ and CD40L in activated CD4+ T cells. This showed that NFAT1 nuclear translocation and the production of IFN γ and CD40L (Figures 5G and 5H) were impaired by Eno-1 knock down. Additionally, treating TH1 CD4+ T cells with PKM2 activator DASS, which will decrease intracellular PEP levels (data not shown) (Anastasiou et al., 2012), similarly suppressed the production of IFN γ and CD40L (Figure S5C). Finally, supplementation of PEP (1 $\mu\text{g}/\text{ml}$), but not fosfomycin (a structurally related analog), to glucose-deprived CD4+ T cells restored Ca^{2+} flux in the presence of IAA (Figures 5I and S5D). Together these experiments narrowing in on the enzymes regulating PEP metabolism in cells, demonstrate that the accumulation of PEP is critical for sustaining Ca^{2+} -NFAT signaling.

To directly test if PEP can inhibit SERCA-mediated calcium uptake, we repeated the ER Ca^{2+} uptake assay by isolating ER vesicles from Jurkat T cells cultured in the presence or absence of glucose. This showed that glucose deprivation promoted ER Ca^{2+} uptake ability; however, PEP supplementation to the ER vesicle fraction significantly suppressed ER Ca^{2+} uptake indicating that PEP can inhibit SERCA activity (Figure 5J). Given that oxidation of SERCA on cysteine residues (e.g., Cys674 and Cys675) reduces SERCA activity (Sharov et al., 2006), we then examined whether glucose deprivation in T cells affects the redox state of SERCA using fluorescent thiol probes that measure the abundance of reduced cysteine residues on proteins. Jurkat T cells were cultured in glucose-replete or -deplete conditions, and ER vesicles were isolated and labeled with fluorescent probes that covalently bind to free thiols. SERCA was then immunoprecipitated from the ER vesicles and the amount of sample fluorescence measured indicated the abundance of reduced cysteines in SERCA. ER vesicles from glucose-deprived cells treated with H_2O_2 or β -mercaptoethanol (β -ME) served as positive controls for maximal cysteine oxidation and reduction, respectively. These experiments showed that compared to cells cultured in glucose-replete medium, glucose-deprivation increased the abundance of free thiols on SERCA, indicative of a more reduced state (Figure S5E). The addition of PEP, but not fosfomycin, to the ER vesicles decreased thiol abundance on SERCA similar to the amounts observed with H_2O_2 (Figure S5E). This result suggests that PEP likely impairs SERCA activity by promoting cysteine oxidation. To further explore this possibility, we found that treating glucose-deprived CD4+ T cells with H_2O_2 , which suppresses SERCA activity via cysteine oxidation (Qin et al., 2013), could restore their ability to flux Ca^{2+} (Figure S5F). Collectively, these results identify a previously uncharacterized role for the metab-

olite PEP in controlling Ca^{2+} signaling through inhibition, and likely the oxidation, of SERCA in T cells. These findings elucidate a nutrient-sensing mechanism by which T cells integrate their functional states with their metabolic states.

Metabolic Reprogramming of TILs Boosts Tumoricidal Activities in the Glucose-Deprived Tumor Microenvironment

The above findings support a model whereby the hyper-anabolic metabolic states of tumor cells reduce the availability of nutrients, such as glucose, and prevent TILs from sustaining Ca^{2+} -NFAT signaling and effector functions, in part, from PEP insufficiency. If so, it may be possible to metabolically reprogram anti-tumor T cells to increase their fitness and function in the tumor microenvironment. Because the data indicated that PEP was a critical metabolite controlling T cells function, we speculated that overexpression of phosphoenolpyruvate carboxykinase 1 (PCK1), which converts oxaloacetate (OAA) into PEP, could bolster the tumoricidal activity of TILs (Figure 6A). To examine this hypothesis, PCK1 (PCK1-OE) was overexpressed in Trp-1 CD4+ T cells specific for the melanoma antigen gp75/tyrosinase-related protein 1 (TRP-1), and this demonstrated that PCK1-OE specifically boosted PEP levels in T cells cultured in glucose-poor conditions (Figure 6B, compare blue and green bars), but had little effect on the amount of PEP above and beyond that normally found in T cells cultured in glucose-rich conditions. In contrast to control cells, PCK1-overexpression also reversed the effects of glucose-deprivation on Ca^{2+} flux and NFAT1 nuclear localization in CD4+ T cells (Figures 6C and 6D). It is important to note that the effects of glucose deprivation and PCK1-OE on CD8 T cell Ca^{2+} flux and effector functions were very similar to those observed in CD4 T cells. For example, blocking PEP accumulation via glycolytic inhibitors or PKM2 activators also diminished CD8+ T cell IFN γ production (Figures S6A and S6B). Additionally, PCK1-overexpression restored Ca^{2+} flux in glucose-deprived CD8+ T cells (Figure S6C). Thus, PCK1-OE lessened the dependence of both CD4 and CD8 T cells on glucose for Ca^{2+} -NFAT1 signaling in glucose-poor conditions.

Next, we examined whether PCK1-OE could enhance the anti-tumor responses of tumor-infiltrating Trp-1 CD4+ T cells. To this end, PCK1-OE or control Trp-1 CD4+ T cells were adoptively transferred into mice that contained engrafted B16 melanomas. Strikingly, PCK-OE increased Trp-1 CD4+ T cell production of IFN γ and CD40L over that of control cells in the tumors, but not in the spleen or draining lymph nodes where glucose is more abundant (Figure 6E). Additionally, relatively higher amounts of costimulatory ligand (CD86) and MHC class I and II expression were observed on TAMs in mice that received PCK1-OE Trp-1 CD4+ T cells compared to those that received control cells (Figure 6F), suggesting that restored effector functions by PCK1-OE Trp-1 CD4+ T cells promoted the maturation of TAMs. Most importantly, transfer of PCK1-OE Trp-1 CD4+ T cells suppressed melanoma growth (Figure 6G) and prolonged the survival of B16 melanoma-bearing mice (Figure 6H) compared to the control T cells. Of note, a similar suppression in tumor growth was observed in separate experiments when PCK1 was overexpressed in Pmel CD8+ T cells, specific for the melanoma antigen gp100 (Figures S6D and S6E). Taken

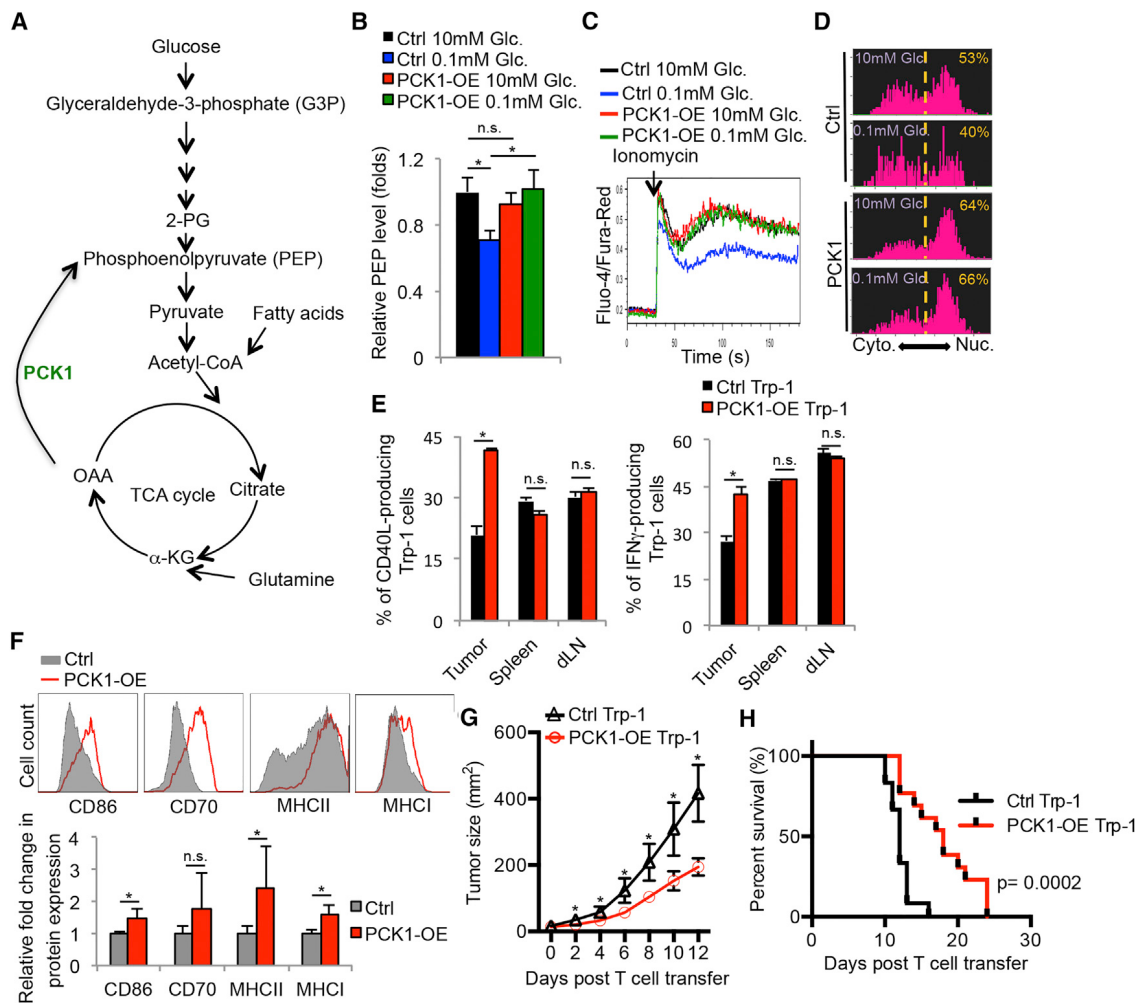


Figure 6. Overexpression of Phosphoenolpyruvate Carboxykinase 1 Boosts Ca²⁺-NFAT Signaling and Tumoricidal Activities of Tumor-Specific CD4⁺ T Cells

(A) Illustration of the metabolic function of PCK1 in converting OAA to PEP.

(B–D) CD4⁺ T cells were transduced with control (Ctrl) or PCK-1 overexpressing (PCK1-OE) RVs. (B) Intracellular PEP levels were measured after culturing the RV-transduced cells for 1 hr in the indicated conditions using a fluorescence-based assay. (C) Intracellular Ca²⁺ levels were measured in the transduced CD4⁺ T cells cultured in 10 mM or 0.1 mM glucose before and after activation with ionomycin.

(D) The cytoplasmic versus nuclear distribution of NFAT1 was determined in the RV-transduced CD4⁺ T cells stimulated with ionomycin in 10 mM glucose or 0.1 mM glucose for 10 min by Amnis Imagestream as described in Figure 5G.

(E–H) Melanoma-specific Trp-1⁺ CD4⁺ T cells transduced with Ctrl or PCK-1-OE RVs were adoptively transferred into B16 melanoma-bearing mice. (E and F) Three days later, the donor Trp-1⁺ CD4⁺ T cells (E) or TAMs (F) were isolated from the indicated tissues and analyzed for expression of the indicated proteins by flow cytometry. Rates of tumor growth (G) and animal survival (H) were determined over time.

Data shown are representative of two (D) and three (C) independent experiments or cumulative of two (F) (n = 2–3 mice/group/experiment), three (B, E) (n = 2–3 mice/group/experiment), and four (G and H) independent experiments (n = 3–4 mice/group/experiment). Data are expressed as mean ± SD (B and F) or mean ± SEM (E) and *p < 0.05 by unpaired Student's t test.

together, our results provide strong evidence that metabolic reprogramming of both CD4 and CD8 T cells is a promising strategy to boost effector functions of tumor-specific T cells in nutrient stressed conditions.

DISCUSSION

It is well appreciated that deregulated metabolism drives tumor cell growth, but it is underappreciated how this affects

the metabolic or functional states of cells that infiltrate tumors (Pearce et al., 2013). Do cancer cells play a “metabolic tug-of-war” with immune cells in tumors? Our work suggests they may because tumors with elevated rates of glycolytic activity were better able to elude T cell immunosurveillance. Further, TILs displayed signs of glucose deprivation, including impaired production of IFN γ and CD40L, but increased expression of TGF β and genes associated with T cell anergy. This led to the discovery that glycolysis controls T cell Ca²⁺-NFAT

signaling and effector functions via the glycolytic metabolite PEP. Importantly, manipulation of this pathway by metabolically reprogramming TILs to increase PEP production yielded stronger anti-tumor responses. This work reveals that a glucose-poor tumor microenvironment can impose immunosuppressive properties on TILs and provides critical proof-of-concept evidence that metabolic reprogramming of tumor-specific T cells can be an adjunct form of immunotherapy.

In addition to other well-known immunosuppressive factors, our work indicates that glucose deprivation is another critical environmental restriction in solid tumors that restrains the tumocidal functions of infiltrating tumor-specific CD4+ T cells. Support for this model also stems from studies showing that tumor-specific T cells regain effector function after being cultured *in vitro* for a short period of time (6–24 hr) in nutrient replete conditions (Wang et al., 2011b). Targeted inhibition of oncogenes, such as *BrafV600E* and *KrasG12D*, can stimulate T cell infiltration and production of IFN γ in tumors, and it is possible that these effects stem from their suppression of tumor cell aerobic glycolysis (Ho et al., 2014; Ying et al., 2012). However, further *in vivo* analyses are required to determine if tumor cells restrict glucose to infiltrating T cells through their own glycolytic activities and if this contributes to an immunosuppressive tumor microenvironment. Given that PD-1 signaling suppresses Akt-mTOR pathway and aerobic glycolysis (Parry et al., 2005; Staron et al., 2014), the therapeutic effects of anti-PD-1 immunotherapy will most certainly rely on TILs re-engaging aerobic glycolysis to regain proliferation and function. Indeed, rapamycin treatment abrogated the therapeutic effects of anti-PDL1 blockade on exhausted CD8 T cells during chronic viral infection (Staron et al., 2014). That both tumor cells and activated T cells share similar requirements for anabolic metabolism raises important considerations for designing drug treatments that combine metabolically targeted therapies with immunotherapy. For example, drugs that suppress tumor cell glycolysis may have poor efficacy long-term because of their unintended effects on TIL function. Therefore, as new treatments are tested, the effects of anti-cancer drugs on the metabolism and function of tumor infiltrating immune cells should be considered and examined.

It is clear that certain metabolic pathways serve as “metabolic checkpoints” to control T cell activation and function, but mechanistically how this occurs is not well understood. Our study uncovers a mechanism through which the glycolytic intermediate PEP regulates the amplitude of Ca²⁺ flux and NFAT activation to fine-tune T cell effector function. Although PEP could inhibit SERCA activity and increase its oxidative state, the precise molecular mechanism(s) by which this occurs remains unknown. Possibly PEP directly conjugates to or oxidizes cysteine residues on SERCA or alternatively PEP could serve as a high-energy phosphate donor to phosphorylate SERCA or other proteins that inhibit its activity (Vander Heiden et al., 2010). Future biochemical studies are needed to precisely characterize which residues in SERCA, if any, are modified by PEP.

Metabolic flexibility allows activated T cells to adapt to changes in glucose availability by utilizing alternative substrates

for energy production (Blagih et al., 2015; Frauwirth et al., 2002). Possibly, TILs become dependent on other carbon sources, such as lactic acid and free fatty acids (FFAs) abundant in the tumor microenvironment, and this not only changes the metabolic activities of TILs, but also their effector functions. Indeed, it is interesting to consider which carbon sources are used by the PCK-1 overexpressing T cells to manufacture PEP when glucose-deprived; our preliminary studies *in vitro* suggest that both lactic acid and FFAs may be involved (data not shown). Future in-depth metabolite profiling of TILs will help to characterize the nutrients they consume and the metabolic pathways they exercise *in vivo*, through which, one may develop more robust methods to harness anti-tumor T cell responses via metabolic manipulation.

Overall, our findings describe a metabolic checkpoint for T cell activity in tumors in which a glycolytic metabolite, PEP, serves as an intracellular sensor for glucose availability in the environment to regulate T cell activation and production of effector molecules. Together with another recent discovery identifying a secondary role for GAPDH in inhibiting IFN γ mRNA translation in T cells (Chang et al., 2013), these finding demonstrate that both metabolites and metabolic enzymes have adopted additional roles as metabolic checkpoint regulators to control specialized functions in T cells. From a therapeutic standpoint, better delineation of the metabolic pathways or enzymes differentially utilized by cancer cells and cancer-specific T cells could reveal vulnerable drug-targets in cancer cells. Additionally, rewiring the metabolic activity of TILs, as demonstrated herein and elsewhere (Doedens et al., 2013), could pose a new strategy for enhancing the potency and durability of ACT.

EXPERIMENTAL PROCEDURES

Mice, Tumor Engraftment, and Tumor Induction

The inducible mouse model of melanoma was previously described (Dankort et al., 2009) and Trp-1 TCR transgenic mice were purchased from Jackson Laboratory (Bar Harbor, ME). For melanoma cell engraftment, 2x105 B16 or *Braf/Pten* melanoma cells were suspended in 50 μ l of PBS and then injected subcutaneously into wild-type C57BL/6 mice (Jackson Laboratory). All mouse experiments were performed according to the approved procedures of the Yale Institutional Animal Care and Use Committee.

ER Vesicle Isolation and Calcium Uptake Assay

Jurkat cells were cultured in glucose-free RPMI with 10% dialyzed FBS in the indicated conditions for 30 min. ER microsomal fractions were then isolated as previously described (Ho et al., 2011). ER vesicles were then analyzed by a calcium uptake assay with 45CaCl₂ as the tracer of calcium uptake, as previously described (Borge and Wolf, 2003). For analysis of the effect of PEP on ER calcium uptake, the calcium uptake assay was performed in the presence of 6 μ M PEP.

Fluorescence Labeling of SERCA Thiol Groups

ER microsomal fractions were then isolated from Jurkat cells cultured in glucose-free RPMI with 10% dialyzed FBS in 10 mM glucose or 0.1 mM glucose for 30 min. Two hundred micrograms of ER microsomal fraction was re-suspended in 20 mM sodium phosphate (pH7.4) buffer and then incubated with control vehicle, 1 μ g/ml PEP, 1 μ g/ml fosphomycin, 5 mM H₂O₂ or 1 mM β -mercaptoethanol for 10 min at 37°C. 200 mM Thiol-fluorescent probe IV (EMD Millipore, Billerica, MA) in the presence of 1% SDS for 30 min at 37°C. Then the reaction mixture was subjected for immunoprecipitation of SERCA or control IgG. The fluorescence intensity of the immunoprecipitates was then determined.

Statistical Analysis

Results were presented as mean \pm SD or mean \pm SEM and statistical significance was examined by an unpaired Student's t test. p value < 0.05 was considered as statistically significant.

ACCESSION NUMBERS

The accession number for the RNA-seq data reported in this paper is SRA: SRP058700.

SUPPLEMENTAL INFORMATION

Supplemental Information includes Supplemental Experimental Procedures and six figures and can be found with this article online at <http://dx.doi.org/10.1016/j.cell.2015.08.012>.

AUTHOR CONTRIBUTIONS

P.-C.H., S.M.K., J.D.B., K.L.I., and A.N.M. designed the research. P.-C.H., J.D.B., A.N.M., X.L., M.S., Y.-C.T., G.C., R.A., G.M., M.W.B. and S.H.K. performed the experiments and bioinformatics analyses. J.C.P. and E.D.A. provided critical reagents. P.-C.H., J.W.L., J.C.R., S. F., and S.M.K. analyzed the results. P.-C.H. and S.M.K. wrote the manuscript.

ACKNOWLEDGMENTS

This study was supported in part by the Yale Cancer Center, Yale SPORE in Skin Cancer (5 P50 CA121974, R. Halaban, PI), Wade F.B. Thompson/Cancer Research Institute-CLIP grant, Howard Hughes Medical Institute, Melanoma Research Alliance (S.M.K.), Melanoma Research Foundation (M.W.B.), National Cancer Center (P.-C.H.), CCFA award (284879, A.N.M.), Alliance for Lupus Research (J.C.R.) and NIH grants R37AI066232 and R01AI074699 to S.M.K., R01HL108006 to J.C.R., R00CA168997 and R01AI110613 to J.W.L.

Received: February 11, 2015

Revised: June 3, 2015

Accepted: July 21, 2015

Published: August 27, 2015

REFERENCES

- Anastasiou, D., Yu, Y., Israelsen, W.J., Jiang, J.K., Boxer, M.B., Hong, B.S., Tempel, W., Dimov, S., Shen, M., Jha, A., et al. (2012). Pyruvate kinase M2 activators promote tetramer formation and suppress tumorigenesis. *Nat. Chem. Biol.* 8, 839–847.
- Baitsch, L., Fuertes-Marraco, S.A., Legat, A., Meyer, C., and Speiser, D.E. (2012). The three main stumbling blocks for anticancer T cells. *Trends Immunol.* 33, 364–372.
- Blagih, J., Coulombe, F., Vincent, E.E., Dupuy, F., Galicia-Vázquez, G., Yurchenko, E., Raissi, T.C., van der Windt, G.J., Viollet, B., Pearce, E.L., et al. (2015). The energy sensor AMPK regulates T cell metabolic adaptation and effector responses in vivo. *Immunity* 42, 41–54.
- Borge, P.D., Jr., and Wolf, B.A. (2003). Insulin receptor substrate 1 regulation of sarco-endoplasmic reticulum calcium ATPase 3 in insulin-secreting beta-cells. *J. Biol. Chem.* 278, 11359–11368.
- Braumüller, H., Wieder, T., Brenner, E., Aßmann, S., Hahn, M., Alkhaled, M., Schilbach, K., Essmann, F., Kneilling, M., Griessinger, C., et al. (2013). T-helper-1-cell cytokines drive cancer into senescence. *Nature* 494, 361–365.
- Callahan, M.K., Wolchok, J.D., and Allison, J.P. (2010). Anti-CTLA-4 antibody therapy: immune monitoring during clinical development of a novel immunotherapy. *Semin. Oncol.* 37, 473–484.
- Cerami, E., Gao, J., Dogrusoz, U., Gross, B.E., Sumer, S.O., Aksoy, B.A., Jacobsen, A., Byrne, C.J., Heuer, M.L., Larsson, E., et al. (2012). The cBio cancer genomics portal: an open platform for exploring multidimensional cancer genomics data. *Cancer Discov.* 2, 401–404.
- Cham, C.M., Driessens, G., O'Keefe, J.P., and Gajewski, T.F. (2008). Glucose deprivation inhibits multiple key gene expression events and effector functions in CD8+ T cells. *Eur. J. Immunol.* 38, 2438–2450.
- Chang, C.H., Curtis, J.D., Maggi, L.B., Jr., Faubert, B., Villarino, A.V., O'Sullivan, D., Huang, S.C., van der Windt, G.J., Blagih, J., Qiu, J., et al. (2013). Post-transcriptional control of T cell effector function by aerobic glycolysis. *Cell* 153, 1239–1251.
- Dankort, D., Curley, D.P., Cartlidge, R.A., Nelson, B., Karnezis, A.N., Damsky, W.E., Jr., You, M.J., DePinho, R.A., McMahon, M., and Bosenberg, M. (2009). Braf(V600E) cooperates with Pten loss to induce metastatic melanoma. *Nat. Genet.* 41, 544–552.
- Doedens, A.L., Phan, A.T., Stradner, M.H., Fujimoto, J.K., Nguyen, J.V., Yang, E., Johnson, R.S., and Goldrath, A.W. (2013). Hypoxia-inducible factors enhance the effector responses of CD8(+) T cells to persistent antigen. *Nat. Immunol.* 14, 1173–1182.
- Feske, S., Skolnik, E.Y., and Prakriya, M. (2012). Ion channels and transporters in lymphocyte function and immunity. *Nat. Rev. Immunol.* 12, 532–547.
- Finlay, D.K., Rosenzweig, E., Sinclair, L.V., Feijoo-Carnero, C., Hukelmann, J.L., Rolf, J., Panteleyev, A.A., Okkenhaug, K., and Cantrell, D.A. (2012). PDK1 regulation of mTOR and hypoxia-inducible factor 1 integrate metabolism and migration of CD8+ T cells. *J. Exp. Med.* 209, 2441–2453.
- Frauwirth, K.A., Riley, J.L., Harris, M.H., Parry, R.V., Rathmell, J.C., Plas, D.R., Elstrom, R.L., June, C.H., and Thompson, C.B. (2002). The CD28 signaling pathway regulates glucose metabolism. *Immunity* 16, 769–777.
- Gao, J., Aksoy, B.A., Dogrusoz, U., Dresdner, G., Gross, B., Sumer, S.O., Sun, Y., Jacobsen, A., Sinha, R., Larsson, E., et al. (2013). Integrative analysis of complex cancer genomics and clinical profiles using the cBioPortal. *Sci. Signal.* 6, pl1.
- Gubser, P.M., Bantug, G.R., Razik, L., Fischer, M., Dimeloe, S., Hoenger, G., Durovic, B., Jauch, A., and Hess, C. (2013). Rapid effector function of memory CD8+ T cells requires an immediate-early glycolytic switch. *Nat. Immunol.* 14, 1064–1072.
- Gullino, P.M., Clark, S.H., and Grantham, F.H. (1964). The Interstitial Fluid of Solid Tumors. *Cancer Res.* 24, 780–794.
- Hanahan, D., and Weinberg, R.A. (2011). Hallmarks of cancer: the next generation. *Cell* 144, 646–674.
- Ho, P.C., Chuang, Y.S., Hung, C.H., and Wei, L.N. (2011). Cytoplasmic receptor-interacting protein 140 (RIP140) interacts with perilipin to regulate lipolysis. *Cell. Signal.* 23, 1396–1403.
- Ho, P.C., Meeth, K.M., Tsui, Y.C., Srivastava, B., Bosenberg, M.W., and Kaech, S.M. (2014). Immune-based antitumor effects of BRAF inhibitors rely on signaling by CD40L and IFN γ . *Cancer Res.* 74, 3205–3217.
- Macintyre, A.N., Gerriets, V.A., Nichols, A.G., Michalek, R.D., Rudolph, M.C., Deoliveira, D., Anderson, S.M., Abel, E.D., Chen, B.J., Hale, L.P., and Rathmell, J.C. (2014). The glucose transporter Glut1 is selectively essential for CD4 T cell activation and effector function. *Cell Metab.* 20, 61–72.
- MacIver, N.J., Michalek, R.D., and Rathmell, J.C. (2013). Metabolic regulation of T lymphocytes. *Annu. Rev. Immunol.* 31, 259–283.
- Maude, S.L., Frey, N., Shaw, P.A., Aplenc, R., Barrett, D.M., Bunin, N.J., Chew, A., Gonzalez, V.E., Zheng, Z., Lacey, S.F., et al. (2014). Chimeric antigen receptor T cells for sustained remissions in leukemia. *N. Engl. J. Med.* 371, 1507–1517.
- Mellman, I., Coukos, G., and Dranoff, G. (2011). Cancer immunotherapy comes of age. *Nature* 480, 480–489.
- Michalek, R.D., Gerriets, V.A., Jacobs, S.R., Macintyre, A.N., MacIver, N.J., Mason, E.F., Sullivan, S.A., Nichols, A.G., and Rathmell, J.C. (2011). Cutting edge: distinct glycolytic and lipid oxidative metabolic programs are essential for effector and regulatory CD4+ T cell subsets. *J. Immunol.* 186, 3299–3303.
- Moran, A.E., Holzapfel, K.L., Xing, Y., Cunningham, N.R., Maltzman, J.S., Punt, J., and Hogquist, K.A. (2011). T cell receptor signal strength in Treg and iNKT cell development demonstrated by a novel fluorescent reporter mouse. *J. Exp. Med.* 208, 1279–1289.

- Parry, R.V., Chemnitz, J.M., Frauwirth, K.A., Lanfranco, A.R., Braunstein, I., Kobayashi, S.V., Linsley, P.S., Thompson, C.B., and Riley, J.L. (2005). CTLA-4 and PD-1 receptors inhibit T-cell activation by distinct mechanisms. *Mol. Cell. Biol.* 25, 9543–9553.
- Pearce, E.L., Poffenberger, M.C., Chang, C.H., and Jones, R.G. (2013). Fueling immunity: insights into metabolism and lymphocyte function. *Science* 342, 1242454.
- Qin, F., Siwik, D.A., Lancel, S., Zhang, J., Kuster, G.M., Luptak, I., Wang, L., Tong, X., Kang, Y.J., Cohen, R.A., and Colucci, W.S. (2013). Hydrogen peroxide-mediated SERCA cysteine 674 oxidation contributes to impaired cardiac myocyte relaxation in senescent mouse heart. *J. Am. Heart Assoc.* 2, e000184.
- Safford, M., Collins, S., Lutz, M.A., Allen, A., Huang, C.T., Kowalski, J., Blackford, A., Horton, M.R., Drake, C., Schwartz, R.H., and Powell, J.D. (2005). Egr-2 and Egr-3 are negative regulators of T cell activation. *Nat. Immunol.* 6, 472–480.
- Schwartz, R.H. (2003). T cell anergy. *Annu. Rev. Immunol.* 21, 305–334.
- Sharov, V.S., Dremina, E.S., Galeva, N.A., Williams, T.D., and Schöneich, C. (2006). Quantitative mapping of oxidation-sensitive cysteine residues in SERCA in vivo and in vitro by HPLC-electrospray-tandem MS: selective protein oxidation during biological aging. *Biochem. J.* 394, 605–615.
- Shiao, S.L., Ganesan, A.P., Rugo, H.S., and Coussens, L.M. (2011). Immune microenvironments in solid tumors: new targets for therapy. *Genes Dev.* 25, 2559–2572.
- Smith-Garvin, J.E., Koretzky, G.A., and Jordan, M.S. (2009). T cell activation. *Annu. Rev. Immunol.* 27, 591–619.
- Srinivasan, M., and Frauwirth, K.A. (2007). Reciprocal NFAT1 and NFAT2 nuclear localization in CD8+ anergic T cells is regulated by suboptimal calcium signaling. *J. Immunol.* 179, 3734–3741.
- Staron, M.M., Gray, S.M., Marshall, H.D., Parish, I.A., Chen, J.H., Perry, C.J., Cui, G., Li, M.O., and Kaech, S.M. (2014). The transcription factor FoxO1 sustains expression of the inhibitory receptor PD-1 and survival of antiviral CD8(+) T cells during chronic infection. *Immunity* 41, 802–814.
- Vander Heiden, M.G., Locasale, J.W., Swanson, K.D., Sharfi, H., Heffron, G.J., Amador-Noguez, D., Christofk, H.R., Wagner, G., Rabinowitz, J.D., Asara, J.M., and Cantley, L.C. (2010). Evidence for an alternative glycolytic pathway in rapidly proliferating cells. *Science* 329, 1492–1499.
- Wang, R., Dillon, C.P., Shi, L.Z., Milasta, S., Carter, R., Finkelstein, D., McCormick, L.L., Fitzgerald, P., Chi, H., Munger, J., and Green, D.R. (2011a). The transcription factor Myc controls metabolic reprogramming upon T lymphocyte activation. *Immunity* 35, 871–882.
- Wang, S.F., Fouquet, S., Chapon, M., Salmon, H., Regnier, F., Labroquère, K., Badoval, C., Damotte, D., Validire, P., Maubec, E., et al. (2011b). Early T cell signalling is reversibly altered in PD-1+ T lymphocytes infiltrating human tumors. *PLoS ONE* 6, e17621.
- Ward, P.S., and Thompson, C.B. (2012). Metabolic reprogramming: a cancer hallmark even warburg did not anticipate. *Cancer Cell* 21, 297–308.
- Wherry, E.J. (2011). T cell exhaustion. *Nat. Immunol.* 12, 492–499.
- Wolchok, J.D., Kluger, H., Callahan, M.K., Postow, M.A., Rizvi, N.A., Lesokhin, A.M., Segal, N.H., Ariyan, C.E., Gordon, R.A., Reed, K., et al. (2013). Nivolumab plus ipilimumab in advanced melanoma. *N. Engl. J. Med.* 369, 122–133.
- Yang, M., Soga, T., and Pollard, P.J. (2013). Oncometabolites: linking altered metabolism with cancer. *J. Clin. Invest.* 123, 3652–3658.
- Ying, H., Kimmelman, A.C., Lyssiotis, C.A., Hua, S., Chu, G.C., Fletcher-Sanikone, E., Locasale, J.W., Son, J., Zhang, H., Coloff, J.L., et al. (2012). Oncogenic Kras maintains pancreatic tumors through regulation of anabolic glucose metabolism. *Cell* 149, 656–670.
- Zheng, Y., Delgoffe, G.M., Meyer, C.F., Chan, W., and Powell, J.D. (2009). Anergic T cells are metabolically anergic. *J. Immunol.* 183, 6095–6101.

Originally published 9 May 2014; corrected 30 May 2014



www.sciencemag.org/content/344/6184/641/suppl/DC1

Supplementary Materials for

Cancer Immunotherapy Based on Mutation-Specific CD4+ T Cells in a Patient with Epithelial Cancer

Eric Tran, Simon Turcotte, Alena Gros, Paul F. Robbins, Yong-Chen Lu, Mark E. Dudley, John R. Wunderlich, Robert P. Somerville, Katherine Hogan, Christian S. Hinrichs, Maria R. Parkhurst, James C. Yang, Steven A. Rosenberg*

*Corresponding author. E-mail: sar@nih.gov

Published 9 May 2014, *Science* **344**, 641 (2014)
DOI: 10.1126/science.1251102

This PDF file includes:

Materials and Methods
Figs. S1 to S7
Tables S1 to S8
References

Correction: An earlier version of the supplementary materials was mistakenly posted. The data and conclusions were not affected.

Materials and Methods

Whole-exomic sequencing

Whole-exomic sequencing of cryopreserved tumor tissue (embedded in OCT) and normal peripheral blood cells was performed by Personal Genome Diagnostics (PGDx, Baltimore, MD) as previously described (27). The average number of distinct high quality sequence reads at each base was 155 and 160 for tumor and normal (PBMC) DNA, respectively.

Patient treatment and generation of TIL for adoptive cell therapy

Patient 3737 was enrolled in the institutional-review board (IRB)-approved protocol: "A Phase II Study Using Short-Term Cultured, Autologous Tumor-Infiltrating Lymphocytes Following a Lymphocyte Depleting Regimen in Metastatic Digestive Tract Cancers" (ClinicalTrials.gov number: NCT01174121), which was designed to evaluate the safety and effectiveness of the adoptive transfer of autologous, ex vivo expanded tumor-infiltrating lymphocytes (TIL) in patients with gastrointestinal cancers.

TIL used for patient's first treatment was generated as previously described (28). Briefly, resected tumors were minced into approximately 1-2 mm fragments and individual fragments were placed in wells of a 24-well plate containing 2 ml of complete media (CM) containing high dose IL-2 (6000 IU/ml, Chiron). CM consisted of RPMI supplemented with 10% in-house human serum, 2 mM L-glutamine, 25 mM HEPES and 10 µg/ml gentamicin. Additionally, a mixed tumor digest was also cultured in CM with high dose IL-2. After the initial outgrowth of T cells (between 2-3 weeks), 5e6 T cells from select cultures were rapidly expanded in gas-permeable G-Rex100 flasks using irradiated allogeneic PBMC at a ratio of 1 to 100 in 400 ml of 50/50 medium, supplemented with 5% human AB serum, 3000 IU/ml of IL-2, and 30 ng/ml of OKT3 antibody (Miltenyi Biotec). 50/50 media consisted of a 1 to 1 mixture of CM with AIM-V media. All cells were cultured at 37°C with 5% CO₂. The cells were rapidly expanded for two weeks prior to infusion. Patient 3737 underwent a non-myeloablative lymphodepleting regimen consisting of cyclophosphamide and fludarabine prior to receiving 42.4 billion total T cells in conjunction with four doses of high dose IL-2 (see Fig. S4 for treatment scheme and details).

TIL used for the patient's second treatment was generated in a similar manner as the first treatment with the following changes. The first treatment product (Patient 3737-TIL) was composed of a combination of 5 individual TIL cultures. These 5 cultures were individually assessed for expression of CD4 and Vβ22, and reactivity against mutated ERBB2IP, and one culture was found to be highly enriched in Vβ22+ ERBB2IP-mutation-reactive CD4+ T cells (data not shown). This one TIL culture (after the initial outgrowth with high dose IL-2) was then rapidly expanded as described above. The patient underwent an identical non-myeloablative lymphodepleting regimen as the first treatment prior to receiving 126 billion total T cells in conjunction with four doses of high dose IL-2.

Generation of tandem minigene (TMG) constructs

The detailed methodology will be published elsewhere, but briefly, for each non-synonymous substitution mutation identified by whole exome sequencing, a "minigene" construct encoding the corresponding amino acid change flanked by 12 amino acids of the wild-type protein sequence was made. Multiple minigenes were genetically fused together to generate a tandem minigene (TMG) construct. These minigene constructs were codon optimized and synthesized as DNA String constructs (Life Technologies). TMGs were then cloned into the pcDNA3.1/V5-His TOPO vector using In-Fusion technology (Clontech). Site-directed mutagenesis was used to generate the nine "wild-type reversion" TMG-1 constructs (Gene Oracle). The nucleotide sequence of all TMGs was verified by standard Sanger sequencing (Macrogen and Gene Oracle).

Generation of autologous antigen presenting cells (APCs)

Monocyte-derived, immature dendritic cells were generated using the plastic adherence method. Briefly, autologous pheresis samples were thawed, washed, set to 5-10e6 cells/ml with neat AIM-V media (Life Technologies) and then incubated at approximately 1e6 cells/cm² in an appropriate sized tissue culture flask and incubated at 37°C, 5% CO₂. After 90 min, non-adherent cells were collected, and the flasks were vigorously washed with AIM-V media, and then incubated with AIM-V media for another 60 min. The flasks were then vigorously washed again with AIM-V media and then the adherent cells were incubated with DC media. DC media comprised of RPMI containing 5% human serum (collected and processed in-house), 100 U/ml penicillin and 100 µg/ml streptomycin, 2 mM L-glutamine, 800 IU/ml GM-CSF and 800 U/ml IL-4 (media supplements were from Life Technologies and cytokines were from Peprotech). On day 3, fresh DC media was added to the cultures. Fresh or freeze/thawed DCs were used in experiments on day 5-7 after initial stimulation. In all experiments, flow cytometry was used to phenotype the cells for expression of CD11c, CD14, CD80, CD86, and HLA-DR (all from BD Bioscience) to ensure that the cells were predominantly immature DCs (CD11c+, CD14-, CD80^{low}, CD86+, and HLA-DR+; data not shown). Antigen presenting B cells were generated using the CD40L and IL-4 stimulation method. Briefly, human CD19-microbeads (Miltenyi Biotec) were used to positively select B cells from autologous pheresis samples. CD19+ cells were then cultured with irradiated (6000 rad) 3T3 cells stably expressing CD40L (3T3-CD40L) at approximately a 1:1 ratio in B-cell media. B-cell media comprised of IMDM media (Life Technologies) supplemented with 7.5-10% human serum (in-house), 100 U/ml penicillin and 100 µg/ml streptomycin (Life Technologies), 10 µg/ml gentamicin (CellGro), 2 mM L-glutamine (Life Technologies), and 200 U/ml IL-4 (Peprotech). Fresh B-cell media was added starting on day 3, and media added or replaced every 2-3 days thereafter. Additional irradiated 3T3-CD40L feeder cells were also added as required. Antigen presenting B cells were typically used in experiments 2-3 weeks after initial stimulation.

Generation of in vitro transcribed RNA (IVT) RNA

Plasmids encoding the tandem minigenes were linearized with the restriction enzyme Sac II. A control pcDNA3.1/V5-His-TOPO vector encoding GFP was linearized with Not I. Restriction digests were terminated with EDTA, sodium acetate and ethanol precipitation. Complete plasmid digestion was verified by standard agarose gel electrophoresis.

Approximately 1 µg of linearized plasmid was used for the generation of IVT RNA using the mmessage mmachine T7 Ultra kit (Life Technologies) as directed by the manufacturer. RNA was precipitated using the LiCl₂ method, and RNA purity and concentrations were assessed using a NanoDrop spectrophotometer. RNA was then aliquoted into microtubes and stored at -80°C until use.

RNA transfections

APCs (DCs or B cells) were harvested, washed 1x with PBS, and then resuspended in Opti-MEM (Life Technologies) at 10-30e6 cells/ml. IVT RNA (4 µg or 8 µg) was aliquoted to the bottom of a 2 mm gap electroporation cuvette, and 50 µl or 100 µl of APCs were added directly to the cuvette. The final RNA concentration used in electroporations was thus 80 µg/ml. Electroporations were carried out using a BTX-830 square wave electroporator. DCs were electroporated with 150 V, 10 ms, and 1 pulse, and B cells were electroporated with 150 V, 20 ms, and 1 pulse. Transfection efficiencies using these settings were routinely between 70-90% as assessed with GFP RNA (data not shown). All steps were carried out at room temperature. Following electroporation, cells were immediately transferred to polypropylene tubes containing DC- or B-cell media supplemented with the appropriate cytokines. Transfected cells were incubated overnight (12-14 h) at 37°C, 5% CO₂. Cells were washed 1x with PBS prior to use in co-culture assays.

Peptide pulsing

Autologous B cells were harvested, washed, and then resuspended at 1e6 cells/ml in B-cell media supplemented with IL-4, and then incubated with 1 µg/ml of a 25-mer peptide overnight (12-14 h) at 37°C, 5% CO₂. After overnight pulsing, B cells were then washed 2x with PBS, and then resuspended in T-cell media and immediately used in co-culture assays. The peptides used were: mutated ERBB2IP (TSFLSINSKEETGHLENGNKYPNLE); wild-type ERBB2IP (TSFLSINSKEETEHLENGNKYPNLE); and, as a negative control, mutated ALK (RVLKGGSVRKLRHAKQLVLELGEEA). The mutated ERBB2IP peptide was purchased from three different sources (GenScript, Peptide 2.0, and SelleckChem) with all yielding the same in vitro results, while the wild-type ERBB2IP and mutated ALK peptides were purchased from Peptide 2.0. For culturing allogeneic EBV-B cells, RPMI media containing 10% FBS, 100 U/ml penicillin and 100 µg/ml streptomycin (Life Technologies), 10 µg/ml gentamicin (CellGro), and 2 mM L-glutamine was used instead of B-cell media.

T-cell sorting, expansion, and cloning

The BD FACSaria IIu and BD FACSJazz were used in all experiments requiring cell sorting. In indicated experiments, sorted T cells were expanded using excess irradiated (4000 rad) allogeneic feeder cells (pool of three different donor leukapheresis samples) in 50/50 media containing 30 ng/ml anti-CD3 antibody (OKT3) and 3000 IU/ml IL-2. Limiting dilution cloning was carried out in 96-well round bottom plates using the above stimulation conditions with 5e4 feeder cells per well and 1-2 T cells per well. Media was exchanged starting at approximately 1 week post stimulation and then every other day or as required. Cells were typically used in assays, or further expanded, at approximately 2-

3 weeks after the initial stimulation.

Co-culture assays: IFN- γ ELISPOT and ELISA, flow cytometry for cell surface activation markers, and intracellular cytokine staining (ICS)

When DCs were used as APCs, approximately 3.5e4 to 7e4 DCs were used per well of a 96-well flat or round-bottom plate. When B cells were used as APCs, approximately 2e5 cells were used per well of a 96-well round-bottom plate. In ELISPOT assays, 1e3 to 1e4 effector T cells were used per well, and in flow cytometry assays, 1e5 effector T cells were used per well. T cells were typically thawed and rested in IL-2 containing 50/50 media (3000 IU/ml IL-2) for two days and then washed with PBS (3x) prior to co-culture assays. All co-cultures were performed in the absence of exogenously added cytokines. For all assays, plate-bound OKT3 (0.1 μ g/ml or 1 μ g/ml) was used as a positive control. In experiments involving HLA blocking antibodies, the following antibodies were used: pan-class-II (clone: IVA12), pan-class-I (clone: W6/32), HLA-DR (clone: HB55), HLA-DP (clone: B7/21), and HLA-DQ (clone: SPV-L3). Cells were blocked with 20-50 μ g/ml of the indicated antibody for 1-2 h at 37°C, 5% CO2 prior to co-culture with T cells. T4 are T cells that have been transduced with an HLA-DR4-restricted TCR that is reactive against an epitope in tyrosinase. DMF5 is an HLA-A2-restricted T-cell line reactive against MART-1. 624-CIITA is a HLA-A2 and HLA-DR4-positive melanoma cell line that stably expresses MHC-II due to ectopic expression of CIITA (class II, major histocompatibility complex, transactivator), and is positive for MART-1 and tyrosinase expression.

For IFN- γ ELISPOT assays, briefly, ELIIP plates (Millipore, MAIPSWU) were pre-treated with 50 μ l of 70% ethanol per well for 2 min, washed 3x with PBS, and then coated with 50 μ l of 10 μ g/ml IFN- γ capture antibody (Mabtech, clone: 1-D1K) and incubated overnight in the fridge. For OKT3 controls, wells were coated with a mixture of IFN- γ capture antibody (10 μ g/ml) and OKT3 (1 μ g/ml). Prior to co-culture, the plates were washed 3x with PBS, followed by blocking with 50/50 media for at least 1 h at room temperature (RT). After 20-24 h of co-culture, cells were flicked out of the plate, washed 6x with PBS + 0.05% Tween-20 (PBS-T), and then incubated for 2 h at RT with 100 μ l/well of a 0.22 μ m filtered 1 μ g/ml biotinylated anti-human IFN- γ detection antibody solution (Mabtech, clone: 7-B6-1). The plate was then washed 3x with PBS-T, followed by a 1 h incubation with 100 μ l/well of streptavidin-ALP (Mabtech, diluted 1:3000). The plate was then washed 6x with PBS followed by development with 100 μ l/well of 0.45 μ m filtered BCIP/NBT substrate solution (KPL, Inc.). The reaction was stopped by rinsing thoroughly with cold tap water. ELISPOT plates were scanned and counted using an ImmunoSpot plate reader and associated software (Cellular Technologies, Ltd).

Expression of the T-cell activation markers OX40 and 4-1BB was assessed by flow cytometry at approximately t=22-26h post-stimulation. Briefly, cells were pelleted, washed with FACS buffer (1X PBS supplemented with 1% FBS and 2 mM EDTA), and then stained with the appropriate antibodies for approximately 30 min, at 4°C in the dark. Cells were washed at least once with FACS buffer prior to acquisition on a BD FACSCanto II flow cytometer. All data were gated on live (PI negative), single cells.

Cytokine production was assessed using intracellular cytokine staining (ICS) and flow cytometry. Briefly, after target and effector cells were combined in the wells of a 96-well plate, both GolgiStop and GolgiPlug were added to the culture (BD Biosciences).

GolgiStop and GolgiPlug were used at 1/2 of the concentration recommended by the manufacturer. At t=6h post stimulation, cells were processed using the Cytofix/Cytoperm kit (BD Biosciences) according to the manufacturer's instructions. Briefly, cells were pelleted, washed with FACS buffer, and then stained for cell surface markers (described above). Cells were then washed 2x with FACS buffer prior to fixation and permeabilization. Cells were then washed with Perm/Wash buffer and stained with antibodies against cytokines for 30 min, at 4°C in the dark. Cells were washed 2x with Perm/Wash buffer and resuspended in FACS buffer prior to acquisition on a FACSCantoII flow cytometer. All flow cytometry data were analyzed using FlowJo software (TreeStar Inc).

IFN- γ in serum samples was detected using a human IFN- γ ELISA kit as directed by the manufacturer (Thermo Scientific).

Flow cytometry antibodies

The following titrated anti-human antibodies were used for cell surface staining: CCR7-FITC (clone: 150503), CD45RO-PE-Cy7 (clone: UCHL1), CD62L-APC (clone: DREG-56), CD27-APC-H7 (clone: M-T271), CD4-eFluor 605NC (clone: OKT4), CD57-FITC (clone: NK-1), CD28-PE-Cy7 (clone: CD28.2), CD127-APC (clone: eBioRDR5), CD3-AF700 (clone: UCHT1), CD4-FITC, PE-Cy7, APC-H7 (clone: SK3), CD8-PE-Cy7 (clone: SK1), V β 22-PE (clone: IMMU 546), V β 5.2-PE (clone: 36213), OX40-PE-Cy7 or FITC (clone: Ber-ACT35), 4-1BB-APC (clone: 4B4-1), and CD107a-APC-H7 (clone: H4A3). All antibodies were from BD Biosciences, except CD4-eFluor605NC (eBioscience), V β 22-PE and V β 5.2-PE (Beckman Coulter), and 4-1BB-APC and OX40-PE-Cy7 (BioLegend). The following optimally titrated anti-human antibodies were used for intracellular cytokine staining: IFN- γ -FITC (clone: 4S.B3), IL-2-APC (clone: MQ1-17H12), TNF-PerCP-Cy5.5 or APC (clone: MAAb11), IL-17-PE (clone: eBio64DEC17), and IL-4-PE-Cy7 (clone: 8D4-8). All ICS antibodies were from eBioscience except IL-4-PE-Cy7 (BD Bioscience). The IO Mark Beta Mark TCR V kit was used to assess the TCR-V β repertoire (Beckman Coulter).

Sequencing of the ERBB2IP mutation

Sanger sequencing was used to validate the *ERBB2IP* mutation found by whole-exomic sequencing. Total RNA was extracted from snap frozen T cells or tumor tissues (OCT block) using the RNeasy Mini kit (Qiagen). Total RNA was then reverse transcribed to cDNA using ThermoScript reverse transcriptase with oligo-dT primers (Life Technologies). Normal and tumor cDNA were then used as templates in a PCR with the following ERBB2IP primers flanking the mutation: ERBB2IP Seq Forward: 5'-TGT TGA CTC AAC AGC CAC AG-3'; and ERBB2IP Seq Reverse: 5'-CTG GAC CAC TTT TCT GAG GG-3'. Phusion DNA polymerase (Thermo Scientific) was used with the recommended 3-step protocol with a 58°C annealing temperature (15 sec) and a 72°C extension (30 sec). PCR products were isolated by standard agarose gel electrophoresis

and gel extraction (Clontech). Products were directly sequenced using the same PCR primers (Macrogen).

Quantitative PCR

Total RNA was extracted from snap frozen T cells or tumor tissues (OCT block) using the RNeasy Mini kit (Qiagen). Total RNA was then reverse transcribed to cDNA using qScript cDNA Supermix (Quanta Biosciences). Gene-specific Taqman primer and probe sets for human β -actin (catalogue #: 401846) and ERBB2IP (catalogue #: 4331182) were purchased from Life Technologies. Quantitative PCR was carried out with TaqMan Fast Advanced Master Mix using the 7500 Fast Real Time PCR machine (both from Applied Biosystems). Specificity of amplified products was verified by standard agarose gel electrophoresis. All calculated threshold cycles (Ct) were 30 or below.

TCR-V β deep sequencing

TCR-V β deep sequencing was performed by immunoSEQ, Adaptive Biotechnologies (Seattle, WA) on genomic DNA isolated from peripheral blood, T cells, and frozen tumor tissue using the DNeasy blood and tissue kit (Qiagen). The number of total productive TCR reads per sample ranged from 279, 482 to 934,672. Only productive TCR rearrangements were used in the calculations of TCR frequencies.

TCR sequencing and construction of the ERBB2IP-mutation reactive TCR

T cells were pelleted and total RNA isolated (RNeasy Mini kit, Qiagen). Total RNA then underwent 5'RACE as directed by manufacturer (SMARTer RACE cDNA amplification kit, Clontech) using TCR-alpha and -beta chain constant primers. Program 1 of the kit was used for the PCR, with a modification to the extension time (2 min instead of 3 min). The sequences of the alpha and beta chain constant primers are: TCR-alpha, 5'—GCC ACA GCA CTG TGC TCT TGA AGT CC—3'; TCR-beta, 5'—CAG GCA GTA TCT GGA GTC ATT GAG—3'. TCR PCR products were then isolated by standard agarose gel electrophoresis and gel extraction (Clontech). Products were then either directly sequenced or TOPO-TA cloned followed by sequencing of individual colonies (Macrogen). For sequencing of known V β 22+ T-cell clones, cDNA was generated from RNA using qScript cDNA Supermix (Quanta Biosciences). These cDNAs then were used as templates in a PCR using the TCR-beta constant primer (above) and the V β 22-specific primer: 5'—CAC CAT GGA TAC CTG GCT CGT ATG C—3'. PCR products were isolated by standard agarose gel electrophoresis and gel extraction (Clontech). Products were directly sequenced (Macrogen) using the nested TCR-beta chain constant primer: 5'—ATT CAC CCA CCA GCT CAG—3'.

Construction of the V β 22+ ERBB2IP-mutation TCR was done by fusing the V β 22+ TCR-alpha V-D-J regions to the mouse TCR-alpha constant chain, and the V β 22+ TCR-beta-V-D-J regions to the mouse TCR-beta constant chains. The alpha and beta chains were separated by a furin SGSG P2A linker. Use of mouse TCR constant regions promotes pairing of the introduced TCR and also facilitates identification of positively transduced T cells by flow cytometry using an antibody specific for the mouse TCR- β chain (eBioscience). The TCR construct was synthesized and cloned into the MSGV1 retroviral vector (Gene Oracle).

TCR transduction of peripheral blood T cells

Autologous pheresis samples were thawed and set to 2e6 cells/ml in T-cell media, which consists of a 50/50 mixture of RPMI and AIM-V media supplemented with 5% in-house human serum, 10 µg/ml gentamicin (CellGro), 100 U/ml penicillin and 100 µg/ml streptomycin, 1.25 µg/ml amphotericin B (Fungizone) and 2 mM L-glutamine (all from Life Technologies). 2e6 cells (1 ml) were stimulated in a 24-well plate with 50 ng/ml soluble OKT3 (Miltenyi Biotec) and 300 IU/ml rhu IL-2 (Chiron) for 2 days prior to retroviral transduction. To generate transient retroviral supernatants, the retroviral vector MSGV1 encoding the V β 22-positive, ERBB2IP-mutation-specific TCR (1.5 µg/well) and the envelope encoding plasmid RD114 (0.75 µg/well) were co-transfected into the retroviral packaging cell line 293GP (1e6 cells per well of a 6-well poly-D-lysine-coated plates, plated the day prior to transfection) using Lipofectamine 2000 (Life Technologies). Retroviral supernatants were collected at 42-48 h after transfection, diluted 1:1 with DMEM media, and then centrifuged onto Retronectin-coated (10 µg/ml, Takara), non-tissue culture-treated 6-well plates at 2,000 g for 2 h at 32°C. Activated T cells (2e6 per well, at 0.5e6 cells/ml in IL-2 containing T-cell media) were then spun onto the retrovirus plates for 10 min at 300 g. Activated T cells were transduced overnight, removed from the plates and further cultured in IL-2 containing T-cell media. GFP and mock transduction controls were included in transduction experiments. Cells were typically assayed 10-14 days post-retroviral transduction.

Fig. S1

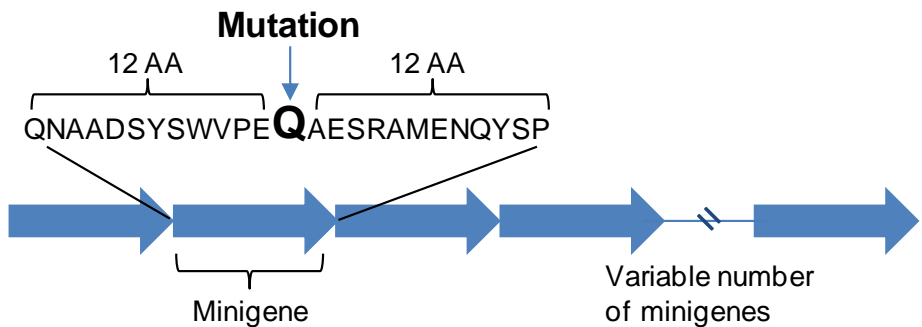


Fig. S1. Basic anatomy of a tandem minigene (TMG) construct. The TMG construct consists of a variable number of minigenes genetically fused together. Each minigene encodes for a mutation flanked by 12 amino acids (AA) from the endogenous protein.

Fig. S2

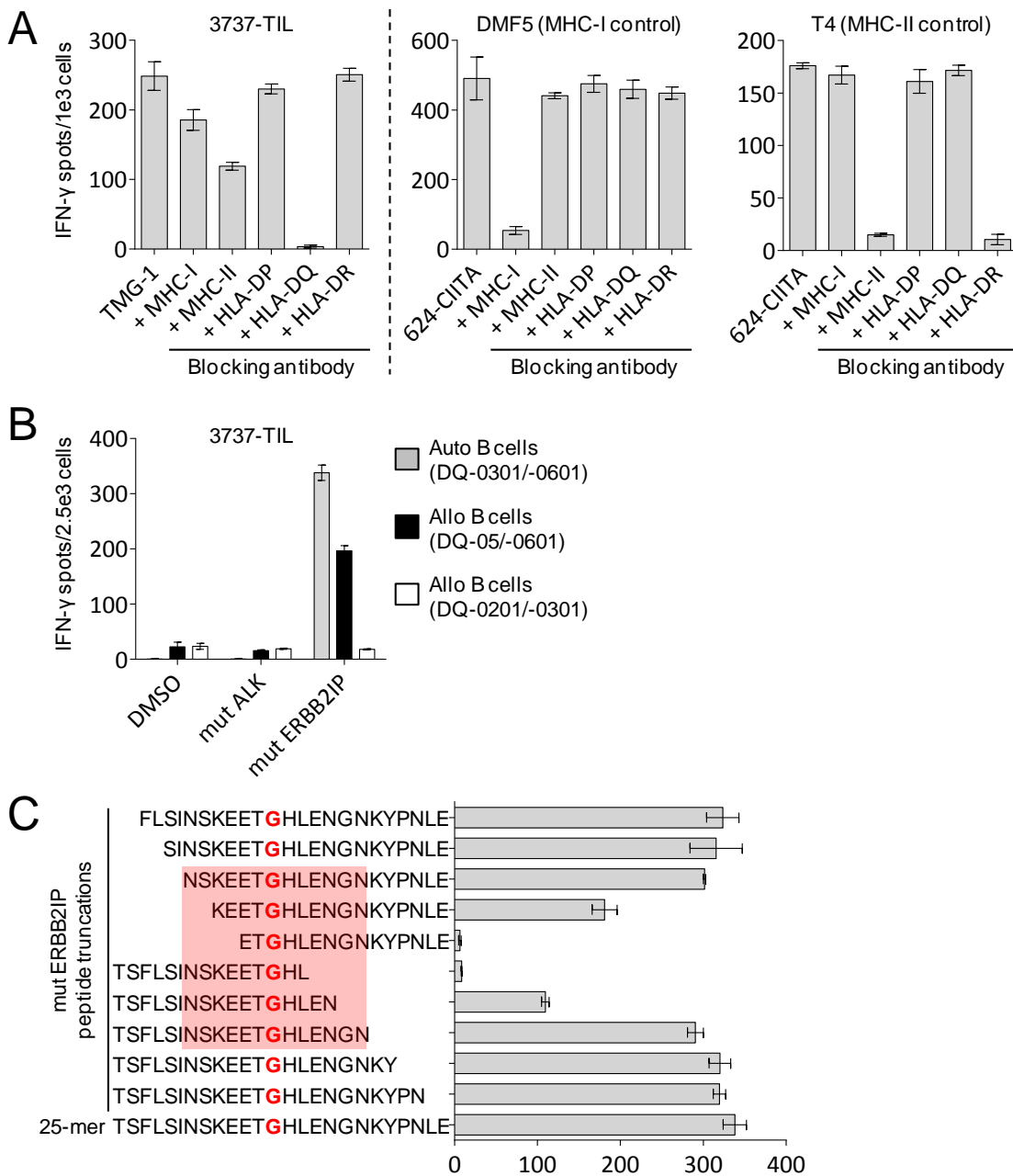


Fig. S2. Molecular characterization of the ERBB2IP-mutation reactive T-cell response. (A) IFN- γ ELISPOT assay at 20 h. Patient 3737-TIL were co-cultured with DCs transfected with TMG-1 that had been pre-incubated with nothing, or the indicated HLA-blocking antibodies (**left**). As controls for antibody blocking, the HLA-A2 restricted MART-reactive T cell DMF5 (**middle**) and the HLA-DR-restricted tyrosinase-reactive T cell T4 (**right**) were co-cultured with the MART and tyrosinase-positive 624-CIITA melanoma cell line that had been pre-incubated with nothing, or the indicated HLA-blocking antibodies. (B) IFN- γ ELISPOT assay at 20 h. Patient 3737-TIL were co-cultured with autologous B cells or allogeneic EBV-B cells partially matched at the

HLA-DQ locus that had been pulsed overnight with DMSO, mutated (mut) ALK or mut ERBB2IP 25-AA long peptides. (C) IFN- γ ELISPOT assay at 20 h. Patient 3737-TIL were co-cultured with autologous B cells that had been pulsed overnight with the mut ERBB2IP 25-AA peptide, or the indicated truncated mut ERBB2IP peptides. All data is representative of 2 independent experiments.

Fig. S3

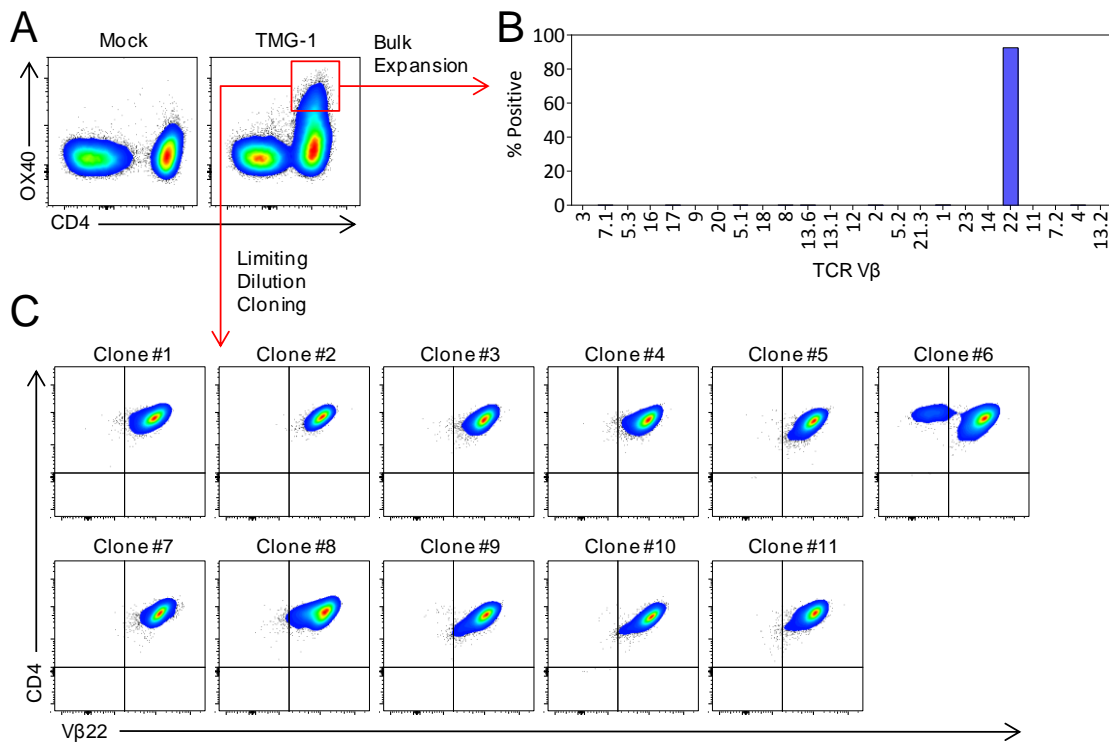


Fig. S3. Assessing clonality of ERBB2IP mutation-reactive CD4+ T cells. (A) Patient 3737-TIL were co-cultured with DCs transfected with nothing (Mock) or TMG-1. CD4+ T cells that upregulated OX40 at t = 24 h (red box) were sorted by FACS and then expanded in bulk (B) or cloned by limiting dilution (C) using irradiated allogeneic feeders in the presence of anti-CD3 antibody (OKT3, 30 ng/ml) and IL-2 (3000 IU/ml). Flow-cytometry based TCR-V β repertoire analysis was performed on (B) and V β 22-specific staining was done on (C). Data are gated on live CD3+ cells.

Fig. S4

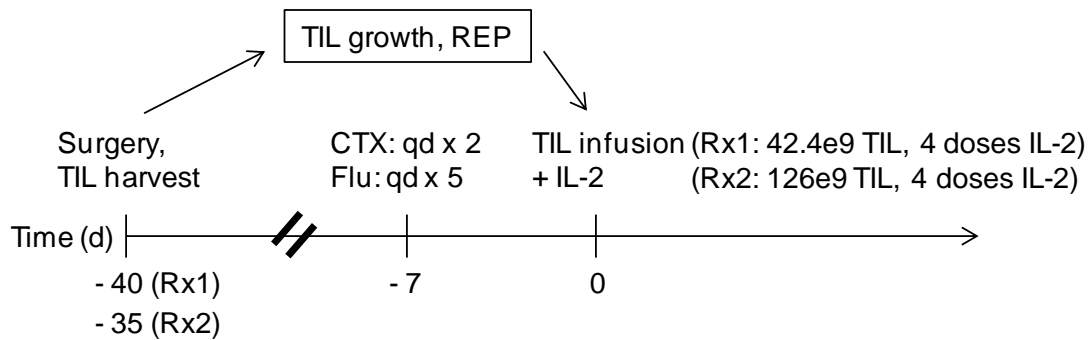


Fig. S4. Patient treatment scheme. For the first treatment (Rx1), Patient 3737 underwent a resection of lung lesions. Tumors were then minced into small fragments and incubated with high dose IL-2 to expand tumor infiltrating lymphocytes (TIL). After an initial expansion in IL-2, select TIL cultures were further expanded for 2 weeks using a rapid expansion protocol (REP) consisting of irradiated allogeneic peripheral blood feeder cells, OKT3 and IL-2. Prior to cell infusion, the patient was pre-conditioned with cyclophosphamide (CTX: 60 mg/kg, once a day for two days) followed by fludarabine (Flu: 25 mg/m² for 5 days). Patient 3737-TIL consisted of 42.4 billion TIL containing over 10 billion (25%) ERBB2IP-mutation reactive T cells, and was administered on day 0, followed by IL-2 (Aldesleukin, 7.2e5 IU/kg) every 8 hours. The patient received a total of 4 doses of IL-2. The second treatment (Rx2) was essentially identical as the first, except that the second cell infusion product consisted of 126 billion TIL containing greater than 120 billion (95%) V β 22+ ERBB2IP-mutation-reactive T cells (derived from the first surgery). For both treatments, the side effects were expected with the administration of high dose IL-2 and included malaise and fluid retention but the patient tolerated the treatments well and was discharged on schedule. See Materials and Methods for more details of the treatment.

Fig. S5

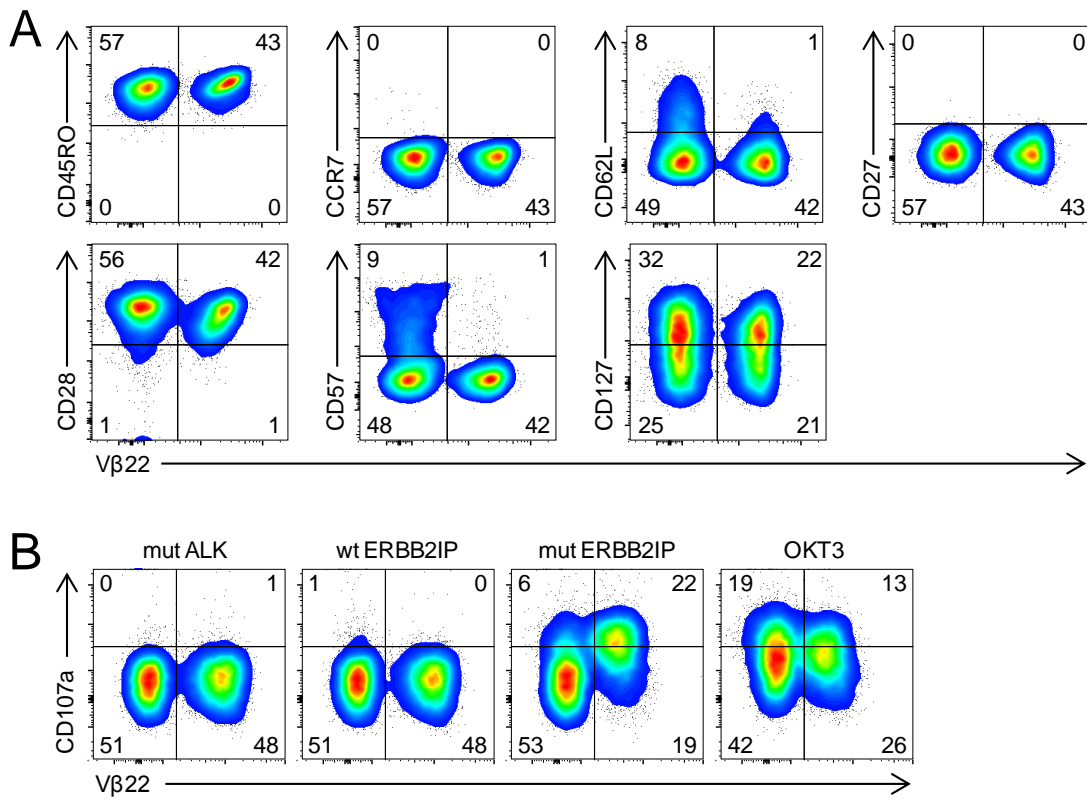


Fig. S5. T-cell differentiation phenotype and cytolytic potential of Patient 3737-TIL.

(A) Patient 3737-TIL were assessed for expression of V β 22 (representing ERBB2IP-mutation-reactive T cells) and the indicated T-cell differentiation markers. Data are gated on live CD3+CD4+ cells. Positive and negative quadrant gates were set using isotype stained or unstained cells. Human peripheral blood cells (containing T cells of all differentiation stages) were included in experiments to ensure that the antibodies were working (data not shown). (B) Patient 3737-TIL were co-cultured for 6 h with autologous B cells pulsed overnight with wild-type (wt) ERBB2IP, or mutated (mut) ALK or mut ERBB2IP 25-AA long peptides. Antibodies specific for the degranulation marker CD107a were added at the beginning of the co-culture. Flow cytometry was used to assess expression of V β 22 and to detect cell surface mobilization of CD107a. Data are gated on the CD4+ population. All data are representative of at least two independent experiments.

Fig. S6

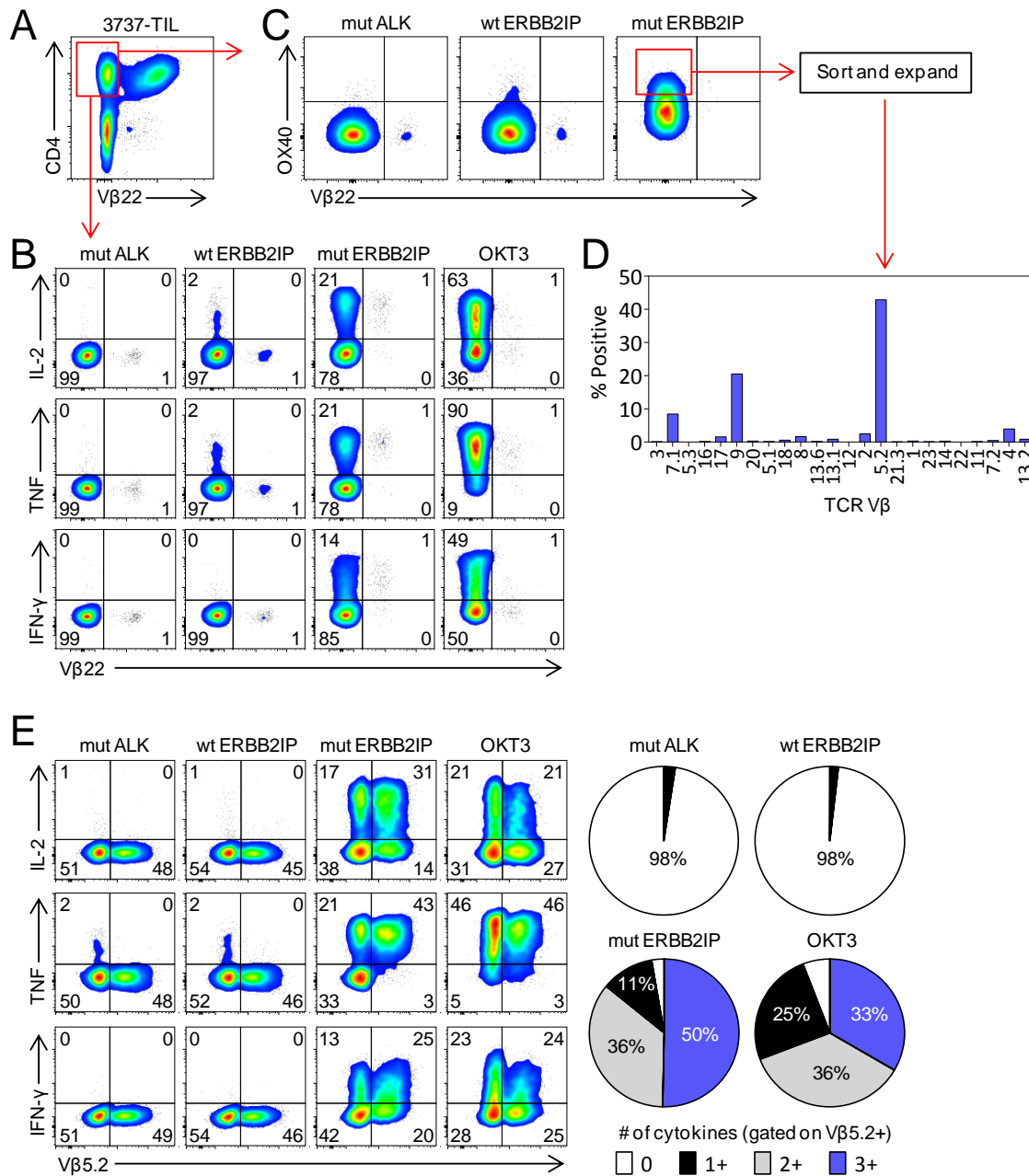


Fig. S6. Patient 3737-TIL contain V β 22-negative ERBB2IP-mutation-reactive T cells. (A) CD4+ V β 22-negative cells present in Patient 3737-TIL were sorted by FACS (red box). (B-C) These cells were then rested in IL-2 containing media for 2 days prior to being co-cultured with autologous B cells pulsed overnight with wild-type (wt) ERBB2IP, or mutated (mut) ALK or mut ERBB2IP 25-AA long peptides. (B) Flow cytometry was used to assess expression of V β 22 and to detect intracellular production of IL-2, TNF, and IFN- γ in the CD4+ population at 6 h post-stimulation. (C) Flow cytometry was used to assess expression OX40 and V β 22 in the CD4+ population at 24 h

post stimulation. Cells that upregulated OX40 were sorted (red box) and expanded, and the TCR-V β repertoire was analyzed by flow cytometry (**D**). Data are gated on live CD4+ cells. (**E**) The sorted cells described in (D) were co-cultured for 6 h with autologous B cells pulsed overnight with wt ERBB2IP, or mut ALK or mut ERBB2IP 25-AA long peptides. Flow cytometry was used to assess expression of V β 5.2 and to detect intracellular production of IL-2, TNF, and IFN- γ in the CD4+ population. Pie charts display the percentage of V β 5.2+ cells that expressed the indicated number of cytokines.

Fig. S7

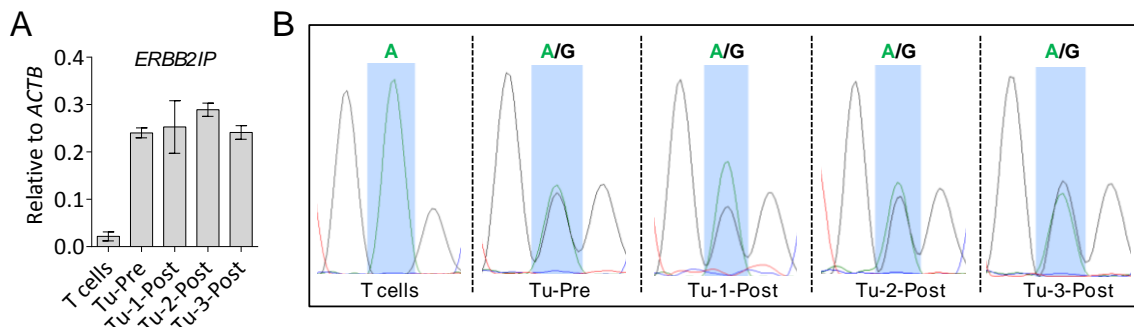


Fig. S7. Expression of wild-type and mutated *ERBB2IP* in normal and tumor tissues. (A) RT-qPCR analysis of *ERBB2IP* expression in Patient 3737-TIL (T cells) and tumors pre-(Tu-Pre) and post adoptive cell transfer. Three separate metastatic lung lesions (Tu-1, -2, -3-Post) were resected approximately 17 months post cell infusion. Data are relative to β -actin (*ACTB*), and are representative of two independent experiments. (B) A 350 bp segment of the *ERBB2IP* gene containing the mutation was PCR-amplified from the cDNA samples described in (A) and Sanger sequenced. The location of the mutation is at nucleotide position 2414 of the coding sequence, corresponding to a change at position 805 of the amino acid sequence.

Table S1. Clinical characteristics of patient 3737

Sex	Age	Primary	Metastatic sites	Prior Therapy	Prior IL-2	Harvest site*	ECOG [†] Status	HLA-I	HLA-II
F	43	Intrahepatic cholangiocarcinoma (poorly differentiated)	Lungs, liver	Cisplatin + gemcitibine, gemcitibine, taxotere	No	Lung	0	A*26 B*38 B*52 C*12	DRB1*0405 DRB1*1502 DQB1*0301 DQB1*0601 DPB1*0401 DPB1*10401

* Harvest site for generation of TIL and for whole exomic sequencing.

† Performance status: ECOG, Eastern Cooperative Oncology Group

Table S2. Somatic mutations identified by whole-exome sequencing of a metastatic lung nodule* from Patient 3737

Gene Symbol	Gene Description	Transcript Accession	Mutation Position Nucleotide (genomic)	Amino Acid (protein)	Mutation Type	Consequence	% Mutant Reads*
ALK	anaplastic lymphoma receptor tyrosine kinase	CCDS33172.1	chr2_29996620-29996620_C_T	137R>H	Substitution	Nonsynonymous coding	30%
AR	androgen receptor	CCDS14387.1	chrX_66858483-66858483_C	NA	Insertion	Frameshift	31%
CD93	CD93 molecule	CCDS13149.1	chr20_23012929-23012929_C_T	634R>Q	Substitution	Nonsynonymous coding	26%
DIP2C	DIP2 disco-interacting protein 2 homolog C (Drosophila)	CCDS7054.1	chr10_365545-365545_C_T	NA	Substitution	Splice site acceptor	25%
ERBB2IP	erbB2 interacting protein	CCDS3990.1	chr5_65385316-65385316_A_G	805E>G	Substitution	Nonsynonymous coding	59%
FCER1A	Fc fragment of IgE; high affinity I; receptor for; alpha polypeptide	CCDS1184.1	chr1_157544227-157544227_G_C	219D>H	Substitution	Nonsynonymous coding	30%
GRXCR1	glutaredoxin; cysteine rich 1	CCDS43225.1	chr4_42590102-42590102_C_T	21A>V	Substitution	Nonsynonymous coding	18%
HLA-D0A	HLA class II histocompatibility antigen, DO alpha chain precursor	CCDS4763.1	chr6_33085209-33085209_C_T	NA	Substitution	Splice site donor	36%
KIF9	kinesin family member 9	CCDS2752.1	chr3_47287859-47287859_T_C	155T>A	Substitution	Nonsynonymous coding	20%
KLHL6	kelch-like 6 (Drosophila)	CCDS3245.2	chr3_184692410-184692413_CAGA	NA	Deletion	Frameshift	20%
LHX9	LIM homeobox 9	CCDS1393.1	chr1_196164923-196164923_A	NA	Deletion	Frameshift	21%
LONRF3	LON peptidase N-terminal domain and ring finger 3	CCDS35374.1	chrX_118007666-118007666_A_C	NA	Substitution	Splice site donor	10%
NAGS	N-acetylglutamate synthase	CCDS11473.1	chr17_39440355-39440355_G_A	412R>H	Substitution	Nonsynonymous coding	29%
NLRP2	NLR family; pyrin domain containing 2	CCDS12913.1	chr19_60186650-60186650_G_T	591S>I	Substitution	Nonsynonymous coding	32%
PDZD2	PDZ domain containing 2	CCDS34137.1	chr5_32124833-32124833_A	NA	Deletion	Frameshift	30%
POU5F2	POU domain, class 5, transcription factor 2	NM_153216	chr5_93102847-93102847_A_C	60V>G	Substitution	Nonsynonymous coding	34%
RAC3	ras-related C3 botulinum toxin substrate 3 (rho family; small GTP binding protein Rac3)	CCDS11798.1	chr17_77584690-77584690_C_A	125T>N	Substitution	Nonsynonymous coding	27%
RAP1GDS1	RAP1; GTP-GDP dissociation stimulator 1	CCDS43253.1	chr4_99532209-99532209_C_A	198L>I	Substitution	Nonsynonymous coding	19%
RASA1	RAS p21 protein activator (GTPase activating protein) 1	CCDS34200.1	chr5_86703757-86703757_C_T	589R>C	Substitution	Nonsynonymous coding	63%
RETSAT	retinol saturase (all-trans-retinol 13,14-reductase)	CCDS1972.1	chr2_85424308-85424308_C_T	553R>K	Substitution	Nonsynonymous coding	11%
SEC24D	SEC24 family; member D (<i>S. cerevisiae</i>)	CCDS3710.1	chr4_119872085-119872085_A_G	901M>T	Substitution	Nonsynonymous coding	18%
SENP3	SUMO1/sentrin/SMT3 specific peptidase 3	ENST00000321337	chr17_7408824-7408824_A_G	292M>V	Substitution	Nonsynonymous coding	33%
SLIT1	slit homolog 1 (Drosophila)	CCDS7453.1	chr10_98753840-98753840_G_C	1280N>K	Substitution	Nonsynonymous coding	45%

TARBP1	TAR (HIV-1) RNA binding protein 1	CCDS1601.1	chr1_232649342-232649342_C_A	655G>V	Substitution	Nonsynonymous coding	18%
TGM6	transglutaminase 6	CCDS13025.1	chr20_2332325-2332325_G_A	398D>N	Substitution	Nonsynonymous coding	51%
TTC39C	tetratricopeptide repeat domain 39C	CCDS32804.1	chr18_19966475-19966475_A_C	503N>T	Substitution	Nonsynonymous coding	24%

* The tumor nodule was estimated to be approximately 70% tumor by pathological analysis of an H&E stained section.

Table S3. Tandem minigene (TMG) constructs

TMG	Mutated Gene	Mutated* Minigene Amino Acid Sequence	TMG Amino Acid Sequence
1	ALK	RVLGGGSVRKLR HAKQLVLELGEEA QNAADSYSWVPE Q AESRAMENQYSP	RVLGGGSVRKLR HAKQLVLELGEEA QNAADSYSWVPE Q AESRAMENQYSP TFSFLSINSKEET G HLENGNKYPN LEFIPLLVVILFAV H TGLFISTQQQVTESDRPRKVRFRIV V SSHSGRVLKEVYEIYNESLFDLLS A LPYVGPSVTPMTG KKLRRDDYLASL H PRLHSIYVSEGYPDIKQELLRCDI I C K GGHSTVTDLQVGTKLDRDDKD N IERLRDKKLAPI
	CD93	QNAADSYSWVPE Q AESRAMENQYSP	
	ERBB2IP	TSFLSINSKEET G HLENGNKYPNLE	
	FCER1A	FIPLLVVILFAV H TGLFISTQQQVT	
	GRXCR1	ESDRPRKVRFRIV V SSHSGRVLKEVY	
	KIF9	EIYNESLFDLLS A LPYVGPSVTPMT	
	NAGS	GKKLRDDYLASL H PRLHSIYVSEGY	
	NLRP2	PDIKQELLRCDI I CKGGHSTVTDLQ	
	RAC3	VGTKLDLRDDKD N IERLRDKKLAPI	
2	RAP1GDS1	VKLLGIHCQNAAI TEMCLVAFGNLANLRKSSPGTSNK	VKLLGIHCQNAAI TEMCLVAFGNLANLRKSSPGTSNK CLRQVSSLVLHIELGRLHPCVMASL K AQSPIPNLYLTG LLPIHTLDVKST T LPAAVRCSESRLMTMDNFGKHYTL K SEAPLYVG MPVHDGPVFAEVNA N YITWLWHEDESROAKEDFS GYDFETRLHVRVIAHALASPAVRPGICPGPD G WRIPLG PLPHF
	RASA1	NLRKSSPGTSNK CLRQVSSLVLHIE	
	RETSAT	LGRLHPCVMASL K AQSPIPNLYLTG	
	SEC24D	LLPIHTLDVKST T LPAAVRCSESRL	
	SLIT1	MTMDNFGKHYTL K SEAPLYVG MPVHDGPVFAEVNA N YITWLWHEDESROAKEDFS GYDFETRLHVRVIAHALASPAVRPGICPGPD G WRIPLG PLPHF	
	TARBP1	AVDVEGMKTQYS V KQRTEVNLRIFL	
	TGM6	HDGPFVFAEVNA N YITWLWHEDESROAKEDFS GYDFETRLHVRVIAHALASPAVRPGICPGPD G WRIPLG PLPHF	
	TTC39C	QAKEDFGYDFE TRLHVRVIAHALAS	
	POU5F2	PAVRPGICPGPD G WRIPLG PLHEF	
3	SENP3	VAQELFQGS D L G V AEAAERPGEKAG	VAQELFQGS D L G V AEAAERPGEKAGGTATTLDLN PL S LTHIRRIVPGAVS D GRMGSWRAPTLS V PASPLT LLQSHFRQQARVRHLSQEFGLQITPP PG I P V H ESTAT L Q H Y S S G W A E K S K I L S R K Q T W K I R T C L R R V R Q K C F T L L S P Q E A G A T K D E G E E A G S R D L R S W V T E E T G M P N K A S K Q G P G S T Q R E G S L E E I P G L T N I Y K L L T S V W G L R L V V W G P A F T C V S E I A M R L
	LHX9	GTATTLDLTNPL LSL	
	KLHL6	THIRRIVPGAVS D GRMGSWRAPTLS VPASPLTLLQSHFRQQARV	
	AR	RHLSQEFGLQITPP PG I P V H ESTATLQ HY S S G W A E K S K I L	
	PDZD2	SPDSKIQMVS S S Q K R A L C L I A L S R K Q T W K I R T C L R R V R Q K C F T L L S P Q E A G S R D L R S W V T E E T G M P N K A S K Q G P G S T Q R E G S L E E I P G L T N I Y K L L T S V W G L R L V V W G P A F T C V S E I A M R L	
	HLA-DOA	TLLSPQEAGATK DE C E G E G A G S R D L R S W V	
	LONRF3	EETGMPN K A S K Q G P G S T Q R E G S L E E P G L T N I Y K L L T S V W G L R L V V W G P A F A F T S C V T S E I A M R L	

*Red and bolded denotes mutated amino acids and neo-sequences encoded by point mutations, or nucleotide insertions or deletions. For splice-site donor mutations (*HLA-DOA* and *LONRF3*), we designed mutant minigene transcripts that continued into the downstream intron until the next stop codon, based on the assumption that the mutations prevented splicing at that site. The splice-site acceptor mutation in *DIP2C* was not assessed.

Table S4. TCR β V-D-J sequences of V β 22-positive ERBB2IP-mutation-reactive T-cell clones

TCR V β	V-D-J nucleotide sequence (CDR3 highlighted)	V-D-J amino acid sequence (CDR3 highlighted)	Number of V β 22 (TRBV2) clones with indicated V-D-J
V β 22 (TRBV2)	GAACCTGAAGTCACCCAGACTCCCAGCCATCAGGT CACACAGATGGGACAGGAAGTGATCTTGCCTGT GTCCCCATCTCTAACTCACTTATACTTCTATTGGTACA GACAAATCTGGGGCAGAAAGTCGAGTTCTGGTT TCCTTTATAATAATGAAATCTCAGAGAAGTCTGAA ATATTGATGATCAATTCTCAGTTGAAAGGCCTGAT GGATCAAATTCACTCTGAAGATCCGGTCCACAAA GCTGGAGGACTCAGCCATGTACTCTGT GCCAGCA GCCTGGGTGACAGGGTAATGAAAAACTGTTTT TGGCAGTGGAACCCAGCTCTGTCTGG	EPEVTQTPSHQVTQMG QEVLRCVPISNHLYFYR QILGQKVEFLVSFYNNES EKSEIFDDQFSVERPDGS NFLKIRSTKLEDSAMYF CASSLGDRGNEKLFFGS GTQLSVL	6/6

Table S5. TCR α V-J sequence of the V β 22+ ERBB2IP-mutation-reactive T-cell clone

TCR V α	V-J nucleotide sequence (CDR3 highlighted)	V-J amino acid sequence (CDR3 highlighted)
TRAV26-2	GATGCTAAGACCACACAGCAAATTCAATGGAG AGTAACGAAGAAGAGCCTGTTCACTGCCTGTA ACCACTCCACAATCAGTGGAACTGATTACATACA TTGGTATCGACAGCTCCCTCCAGGGTCCAGAG TACGTGATTCATGGTCTTACAAGCAATGTGAACA ACAGAATGCCCTCTGGCAATCGCTGAAGACA GAAAGTCCAGTACCTTGATCCTGCACCGTGCTAC CTTGAGAGATGCTGCTGTACTACTGCATCCTG AGACGTCTAACGACTACAAGCTCAGCTTGGAG CCGGAACCACAGTAACTGTAAGAGCAA	DAKTTQPNSMESNEE PVHLP CNHSTISGTDYIH WYRQLPSQ GPEYVIHGLTSNVNNRMA SLAIAEDRKSSTLILHRATLRDA AVYYCILRRLNDYKLSFGAGTT VTVRA

Table S6. Most frequent TCR β V-D-J sequence of V β 22-negative ERBB2IP-mutation-reactive T cells*

TCR V β	V-D-J nucleotide sequence (CDR3 highlighted)	V-D-J amino acid sequence (CDR3 highlighted)	Number of TOPO- TA clones with indicated V-D-J
V β 5.2 (TRBV5-6)	GACGCTGGAGTCACCCAAAGTCCCACACACCTGAT CAAAACGAGAGGAACAGCAAGTGACTCTGAGATGC TCTCCTAAGTCTGGCATGACACTGTGTCCTGGTAC CAACAGGCCCTGGTCAGGGGCCAGTTATCTT TCAGTATTATGAGGAGGAAGAGAGACAGAGAGGC AACTCCCTGATCGATTCTCAGGTACCAGTCCCT AACTATAGCTGAGCTGAATGTGAACGCCCTGTT GCTGGGGGACTCGGCCCTATCTCTGT GCCAGCA GCAAAGGCCGGGAGGCAACTACGAGCAGTACTT CGGGCCGGGACCAAGGCTCACGGTCACAG	DAGVTQSPTHLIKTR GQQVTLRCSPKSGHD TVSWYQQALGQGPQ FIFQYYEEERQRGNF PDRFSGHQFPNYSSE LNVNALLGDSALYLC ASSKGPGGNYEQYF GPGTRLTVT	3/7

* V β 22-negative cells that upregulated OX40 upon stimulation with mutated ERBB2IP were sorted and expanded. RNA from these cells was then isolated and underwent 5'RACE with TCR- β constant chain primers to identify the expressed TCR-V β sequences. TOPO-TA cloning was performed on the PCR products and individual colonies were then sequenced. Flow cytometry demonstrated that 40-50% of these T cells were V β 5.2 (TRBV5-6). By Sanger sequencing, 3/7 TOPO-TA colonies were V β 5.2 (TRBV5-6) with the indicated sequence above.

Table S7. Immunohistochemistry analysis of T-cell infiltrates pre- and post-ACT*

Tumor Nodule	CD3		CD8		CD4	
	Tumor	Stroma	Tumor	Stroma	Tumor	Stroma
Pre-1A	0-1	1	0-1	1	0-1	1
Pre-2A	0-1	1	0-1	1	0	0
Pre-3A	0	0-1	0	0-1	0	0
Pre-3B	0-1	1	0-1	0-1	0-1	1
Post-1A	1	1	1	1	0-1	1
Post-1B	1	2	1-2	2	1	2
Post-2A	0-1	1	0-1	1	0-1	0-1

*Post-ACT tumors were harvested approximately 17 months after the first ACT.

A positive control (tonsil) was included for all stains.

0, no infiltrate

1, rare to few

2, moderately dense

3, very dense

Table S8. Immunohistochemistry analysis of MHC expression on tumors pre- and post-ACT*

Tumor Nodule	HLA-I	HLA-II (HLA-DR)
Pre-1A	1-2, >50%	0
Pre-2A	1-2, >50%	0
Pre-3A	1, >50%	0
Pre-3B	2, >50%	0
Post-1A	2-3, >50%	0
Post-1B	3, >50%	0
Post-2A	2, >50%	0

*Post-ACT tumors were harvested approximately 17 months after the first ACT.

> 50% denotes greater than 50% of the tumor cells were positive.

A positive control (tonsil) was included for all stains.

0, negative

1, weakly positive

2, moderately positive

3, strongly positive

References and Notes

1. B. Vogelstein, N. Papadopoulos, V. E. Velculescu, S. Zhou, L. A. Diaz Jr., K. W. Kinzler, Cancer genome landscapes. *Science* **339**, 1546–1558 (2013). [Medline](#) [doi:10.1126/science.1235122](https://doi.org/10.1126/science.1235122)
2. P. van der Bruggen, V. Stroobant, N. Vigneron, B. Van den Eynde, “Tumor antigens resulting from mutations,” *Cancer Immunity* (2013), <http://cancerimmunity.org/peptide/mutations/>.
3. P. F. Robbins, Y. C. Lu, M. El-Gamil, Y. F. Li, C. Gross, J. Gartner, J. C. Lin, J. K. Teer, P. Cliften, E. Tycksen, Y. Samuels, S. A. Rosenberg, Mining exomic sequencing data to identify mutated antigens recognized by adoptively transferred tumor-reactive T cells. *Nat. Med.* **19**, 747–752 (2013). [Medline](#) [doi:10.1038/nm.3161](https://doi.org/10.1038/nm.3161)
4. N. van Rooij, M. M. van Buuren, D. Philips, A. Velds, M. Toebe, B. Heemskerk, L. J. van Dijk, S. Behjati, H. Hilkmann, D. El Atmioui, M. Nieuwland, M. R. Stratton, R. M. Kerkhoven, C. Kesmir, J. B. Haanen, P. Kvistborg, T. N. Schumacher, Tumor exome analysis reveals neoantigen-specific T-cell reactivity in an ipilimumab-responsive melanoma. *J. Clin. Oncol.* **31**, e439–e442 (2013). [Medline](#) [doi:10.1200/JCO.2012.47.7521](https://doi.org/10.1200/JCO.2012.47.7521)
5. Y. C. Lu, X. Yao, Y. F. Li, M. El-Gamil, M. E. Dudley, J. C. Yang, J. R. Almeida, D. C. Douek, Y. Samuels, S. A. Rosenberg, P. F. Robbins, Mutated PPP1R3B is recognized by T cells used to treat a melanoma patient who experienced a durable complete tumor regression. *J. Immunol.* **190**, 6034–6042 (2013). [Medline](#) [doi:10.4049/jimmunol.1202830](https://doi.org/10.4049/jimmunol.1202830)
6. V. Corbière, J. Chapiro, V. Stroobant, W. Ma, C. Lurquin, B. Lethé, N. van Baren, B. J. Van den Eynde, T. Boon, P. G. Coulie, Antigen spreading contributes to MAGE vaccination-induced regression of melanoma metastases. *Cancer Res.* **71**, 1253–1262 (2011). [Medline](#) [doi:10.1158/0008-5472.CAN-10-2693](https://doi.org/10.1158/0008-5472.CAN-10-2693)
7. J. Huang, M. El-Gamil, M. E. Dudley, Y. F. Li, S. A. Rosenberg, P. F. Robbins, T cells associated with tumor regression recognize frameshifted products of the CDKN2A tumor suppressor gene locus and a mutated HLA class I gene product. *J. Immunol.* **172**, 6057–6064 (2004). [Medline](#)
8. H. Echchakir, F. Mami-Chouaib, I. Vergnon, J. F. Baurain, V. Karanikas, S. Chouaib, P. G. Coulie, A point mutation in the alpha-actinin-4 gene generates an antigenic peptide recognized by autologous cytolytic T lymphocytes on a human lung carcinoma. *Cancer Res.* **61**, 4078–4083 (2001). [Medline](#)
9. S. Mandruzzato, F. Brasseur, G. Andry, T. Boon, P. van der Bruggen, A CASP-8 mutation recognized by cytolytic T lymphocytes on a human head and neck carcinoma. *J. Exp. Med.* **186**, 785–793 (1997). [Medline](#) [doi:10.1084/jem.186.5.785](https://doi.org/10.1084/jem.186.5.785)
10. K. T. Hogan, D. P. Eisinger, S. B. Cupp 3rd, K. J. Lekstrom, D. D. Deacon, J. Shabanowitz, D. F. Hunt, V. H. Engelhard, C. L. Slingluff Jr., M. M. Ross, The

- peptide recognized by HLA-A68.2-restricted, squamous cell carcinoma of the lung-specific cytotoxic T lymphocytes is derived from a mutated elongation factor 2 gene. *Cancer Res.* **58**, 5144–5150 (1998). [Medline](#)
11. V. Karanikas, D. Colau, J. F. Baurain, R. Chiari, J. Thonnard, I. Gutierrez-Roelens, C. Goffinet, E. V. Van Schaftingen, P. Weynants, T. Boon, P. G. Coulie, High frequency of cytolytic T lymphocytes directed against a tumor-specific mutated antigen detectable with HLA tetramers in the blood of a lung carcinoma patient with long survival. *Cancer Res.* **61**, 3718–3724 (2001). [Medline](#)
12. S. Wedén, M. Klemp, I. P. Gladhaug, M. Møller, J. A. Eriksen, G. Gaudernack, T. Buanes, Long-term follow-up of patients with resected pancreatic cancer following vaccination against mutant K-ras. *Int. J. Cancer* **128**, 1120–1128 (2011). [Medline doi:10.1002/ijc.25449](#)
13. Materials and methods are available as supplementary materials on *Science Online*.
14. D. Mumberg, P. A. Monach, S. Wanderling, M. Philip, A. Y. Toledano, R. D. Schreiber, H. Schreiber, CD4(+) T cells eliminate MHC class II-negative cancer cells in vivo by indirect effects of IFN-gamma. *Proc. Natl. Acad. Sci. U.S.A.* **96**, 8633–8638 (1999). [Medline doi:10.1073/pnas.96.15.8633](#)
15. A. Corthay, D. K. Skovseth, K. U. Lundin, E. Røsjø, H. Omholt, P. O. Hofgaard, G. Haraldsen, B. Bogen, Primary antitumor immune response mediated by CD4+ T cells. *Immunity* **22**, 371–383 (2005). [Medline doi:10.1016/j.jimmuni.2005.02.003](#)
16. S. A. Quezada, T. R. Simpson, K. S. Peggs, T. Merghoub, J. Vider, X. Fan, R. Blasberg, H. Yagita, P. Muranski, P. A. Antony, N. P. Restifo, J. P. Allison, Tumor-reactive CD4(+) T cells develop cytotoxic activity and eradicate large established melanoma after transfer into lymphopenic hosts. *J. Exp. Med.* **207**, 637–650 (2010). [Medline doi:10.1084/jem.20091918](#)
17. Y. Xie, A. Akpinarli, C. Maris, E. L. Hipkiss, M. Lane, E. K. Kwon, P. Muranski, N. P. Restifo, P. A. Antony, Naive tumor-specific CD4(+) T cells differentiated in vivo eradicate established melanoma. *J. Exp. Med.* **207**, 651–667 (2010). [Medline doi:10.1084/jem.20091921](#)
18. P. D. Greenberg, D. E. Kern, M. A. Cheever, Therapy of disseminated murine leukemia with cyclophosphamide and immune Lyt-1+,2- T cells. Tumor eradication does not require participation of cytotoxic T cells. *J. Exp. Med.* **161**, 1122–1134 (1985). [Medline doi:10.1084/jem.161.5.1122](#)
19. Z. C. Ding, L. Huang, B. R. Blazar, H. Yagita, A. L. Mellor, D. H. Munn, G. Zhou, Polyfunctional CD4⁺ T cells are essential for eradicating advanced B-cell lymphoma after chemotherapy. *Blood* **120**, 2229–2239 (2012). [Medline doi:10.1182/blood-2011-12-398321](#)
20. K. A. Shafer-Weaver, S. K. Watkins, M. J. Anderson, L. J. Draper, A. Malyguine, W. G. Alvord, N. M. Greenberg, A. A. Hurwitz, Immunity to murine prostatic tumors: Continuous provision of T-cell help prevents CD8 T-cell tolerance and activates tumor-infiltrating dendritic cells. *Cancer Res.* **69**, 6256–6264 (2009). [Medline doi:10.1158/0008-5472.CAN-08-4516](#)

21. N. N. Hunder, H. Wallen, J. Cao, D. W. Hendricks, J. Z. Reilly, R. Rodmyre, A. Jungbluth, S. Gnjatic, J. A. Thompson, C. Yee, Treatment of metastatic melanoma with autologous CD4+ T cells against NY-ESO-1. *N. Engl. J. Med.* **358**, 2698–2703 (2008). [Medline doi:10.1056/NEJMoa0800251](#)
22. H. Braumüller, T. Wieder, E. Brenner, S. Aßmann, M. Hahn, M. Alkhaled, K. Schilbach, F. Essmann, M. Kneilling, C. Griessinger, F. Ranta, S. Ullrich, R. Mocikat, K. Braungart, T. Mehra, B. Fehrenbacher, J. Berdel, H. Niessner, F. Meier, M. van den Broek, H. U. Häring, R. Handgretinger, L. Quintanilla-Martinez, F. Fend, M. Pesic, J. Bauer, L. Zender, M. Schaller, K. Schulze-Osthoff, M. Röcken, T-helper-1-cell cytokines drive cancer into senescence. *Nature* **494**, 361–365 (2013). [Medline doi:10.1038/nature11824](#)
23. Z. Qin, T. Blankenstein, CD4+ T cell—mediated tumor rejection involves inhibition of angiogenesis that is dependent on IFN gamma receptor expression by nonhematopoietic cells. *Immunity* **12**, 677–686 (2000). [Medline doi:10.1016/S1074-7613\(00\)80218-6](#)
24. J. Yuan, S. Gnjatic, H. Li, S. Powel, H. F. Gallardo, E. Ritter, G. Y. Ku, A. A. Jungbluth, N. H. Segal, T. S. Rasalan, G. Manukian, Y. Xu, R. A. Roman, S. L. Terzulli, M. Heywood, E. Pogoriler, G. Ritter, L. J. Old, J. P. Allison, J. D. Wolchok, CTLA-4 blockade enhances polyfunctional NY-ESO-1 specific T cell responses in metastatic melanoma patients with clinical benefit. *Proc. Natl. Acad. Sci. U.S.A.* **105**, 20410–20415 (2008). [Medline doi:10.1073/pnas.0810114105](#)
25. S. A. Rosenberg, J. C. Yang, R. M. Sherry, U. S. Kammula, M. S. Hughes, G. Q. Phan, D. E. Citrin, N. P. Restifo, P. F. Robbins, J. R. Wunderlich, K. E. Morton, C. M. Laurencot, S. M. Steinberg, D. E. White, M. E. Dudley, Durable complete responses in heavily pretreated patients with metastatic melanoma using T-cell transfer immunotherapy. *Clin. Cancer Res.* **17**, 4550–4557 (2011). [Medline doi:10.1158/1078-0432.CCR-11-0116](#)
26. S. Turcotte, A. Gros, K. Hogan, E. Tran, C. S. Hinrichs, J. R. Wunderlich, M. E. Dudley, S. A. Rosenberg, Phenotype and function of T cells infiltrating visceral metastases from gastrointestinal cancers and melanoma: Implications for adoptive cell transfer therapy. *J. Immunol.* **191**, 2217–2225 (2013). [Medline doi:10.4049/jimmunol.1300538](#)
27. S. Jones, T. L. Wang, IeM. Shih, T. L. Mao, K. Nakayama, R. Roden, R. Glas, D. Slamon, L. A. Diaz Jr., B. Vogelstein, K. W. Kinzler, V. E. Velculescu, N. Papadopoulos, Frequent mutations of chromatin remodeling gene ARID1A in ovarian clear cell carcinoma. *Science* **330**, 228–231 (2010). [Medline doi:10.1126/science.1196333](#)
28. J. Jin, M. Sabatino, R. Somerville, J. R. Wilson, M. E. Dudley, D. F. Stroncek, S. A. Rosenberg, Simplified method of the growth of human tumor infiltrating lymphocytes in gas-permeable flasks to numbers needed for patient treatment. *J. Immunother.* **35**, 283–292 (2012). [Medline doi:10.1097/CJI.0b013e31824e801f](#)

Metabolic shift induced by systemic activation of T cells in PD-1-deficient mice perturbs brain monoamines and emotional behavior

Michio Miyajima^{1,9}, Baihao Zhang^{1,2,9}, Yuki Sugiura^{3,9}, Kazuhiro Sonomura^{4,9}, Matteo M Guerrini¹, Yumi Tsutsui¹, Mikako Maruya¹, Alexis Vogelzang¹, Kenji Chamoto², Kurara Honda³, Takatoshi Hikida⁵, Satomi Ito¹, Hongyan Qin⁶, Rikako Sanuki⁷, Keiichiro Suzuki¹, Takahisa Furukawa⁷, Yasushi Ishihama⁸, Fumihiko Matsuda⁴, Makoto Suematsu³, Tasuku Honjo² & Sidonia Fagarasan¹

T cells reorganize their metabolic profiles after being activated, but the systemic metabolic effect of sustained activation of the immune system has remained unexplored. Here we report that augmented T cell responses in *Pdcd1*^{-/-} mice, which lack the inhibitory receptor PD-1, induced a metabolic serum signature characterized by depletion of amino acids. We found that the depletion of amino acids in serum was due to the accumulation of amino acids in activated *Pdcd1*^{-/-} T cells in the lymph nodes. A systemic decrease in tryptophan and tyrosine led to substantial deficiency in the neurotransmitters serotonin and dopamine in the brain, which resulted in behavioral changes dominated by anxiety-like behavior and exacerbated fear responses. Together these data indicate that excessive activation of T cells causes a systemic metabolomic shift with consequences that extend beyond the immune system.

Activated T cells adapt their cellular metabolism to sustain proliferation and effector functions and to maintain immunological memory¹. Quiescent T cells generate energy (ATP) through oxidative phosphorylation, which is fueled by the breakdown of glucose, fatty acids and amino acids. T cell activation is accompanied by a metabolic shift, including substantial induction of aerobic glycolysis. Although glycolysis is less efficient than oxidative phosphorylation in terms of ATP production, it supplies T cells with the metabolic intermediates essential for the synthesis of the proteins, nucleic acids and lipids needed for effector functions².

Engagement of the antigen-specific T cell antigen receptor (TCR) on T cells is essential for the acquisition of effector function, but the duration and strength of a response is the result of the integration of co-receptor signals. PD-1 (encoded by *Pdcd1*) is an inhibitory co-receptor induced after the activation of T cells. Engagement of PD-1 by its ligands (PD-L1 and PD-L2) causes phosphorylation of the cytoplasmic tail of PD-1 and dephosphorylation of signaling molecules induced by activation of the TCR, which ultimately suppresses the proliferation and cytokine production of T cells. Genetic deletion of PD-1 or antibody-mediated blockade of PD-1 leads to the expansion of T cell populations with an activated phenotype and enhanced immunity to infections and

tumors³. However, the accumulation of activated T cells provides an excess of germinal-center-promoting factors and facilitates the selection of antibodies with self-reactive properties^{4,5}. Indeed, PD-1 deficiency in mice and PD-1-blockade immunotherapy in patients has revealed strain- or patient-specific susceptibility to the development of autoimmune diseases such as gastritis, dilated cardiomyopathy, rheumatoid arthritis, systemic lupus erythematosus and Grave's disease³.

Here we investigated whether the metabolic readjustments within activated T cells following activation of the immune system affected systemic metabolism. Using *Pdcd1*^{-/-} mice as a model of systemic activation of T cells, we found that concentrations of free amino acids in the serum of *Pdcd1*^{-/-} mice decreased as a consequence of the accumulation of amino acids in activated T cells in the lymph nodes (LNs). This systemic drop in amino-acid availability downstream of strong activation of the immune system affected biochemical pathways that depend on free amino acids as precursor metabolites. Specifically, reduced availability of tryptophan and tyrosine in the brain of *Pdcd1*^{-/-} mice affected the synthesis of monoamine neurotransmitters, which resulted in increased anxiety-like behavior and fear responses. Thus, sustained activation of T cells can affect emotional behavior through systemic metabolic alteration.

¹Laboratory for Mucosal Immunity, Center for Integrative Medical Sciences, RIKEN Yokohama Institute, Yokohama, Japan. ²Department of Immunology and Genomic Medicine, Kyoto University Graduate School of Medicine, Kyoto, Japan. ³Department of Biochemistry and Integrative Biology, Keio University, Tokyo, Japan.

⁴Center for Genomic Medicine, Kyoto University Graduate School of Medicine, Kyoto University, Kyoto, Japan. ⁵Medical Innovation Center, Kyoto University Graduate School of Medicine, Kyoto, Japan. ⁶Department of Medical Genetics and Developmental Biology, 4th Military Medical University, Xi'an, China. ⁷Laboratory for Molecular and Developmental Biology, Institute for Protein Research, Osaka University, Osaka, Japan. ⁸Department of Molecular and Cellular Bioanalyses, Graduate School of Pharmaceutical Sciences, Kyoto University, Kyoto, Japan. ⁹These authors contributed equally to this work. Correspondence should be addressed to S.F. (sidonia.fagarasan@riken.jp).

Received 23 August; accepted 3 October; published online 23 October 2017; doi:10.1038/ni.3867

RESULTS

Diminished amino acids in serum of *Pdcd1*^{-/-} mice

We performed metabolomic profiling of serum from *Pdcd1*^{-/-} mice, focusing particularly on small, water-soluble molecules that can bridge diverse tissues via the circulation. Partial least-squares discriminant analysis (PLS-DA) of metabolites indicated that *Pdcd1*^{-/-} mice had a systemic metabolome profile different from that of wild-type mice (Fig. 1a), with the most significantly decreased abundance in compounds involved in energy production, such as components of the tricarboxylic acid (TCA) cycle and amino-acid metabolism (Fig. 1b and Supplementary Table 1). Most proteinogenic amino acids, including the essential amino acids (methionine (Met), threonine (Thr), histidine (His), lysine (Lys), tryptophan (Trp), phenylalanine (Phe), leucine (Leu), isoleucine (Ile) and valine (Val)) were 10–30% less abundant in *Pdcd1*^{-/-} mice than in wild-type non-littermate mice (Fig. 1c) or wild-type littermates (Fig. 1d). The reduction in abundance of the aromatic amino acids Trp, tyrosine (Tyr) and Phe in *Pdcd1*^{-/-} mice relative to that in wild-type mice was already significant by 2 months of age (Fig. 1e), and it further decreased by 4–6 months of age and persisted throughout a 1-year monitoring period, unlike results obtained for branched-chain amino acids (Leu, Ile and Val), which were similar in abundance in *Pdcd1*^{-/-} mice to their baseline amounts in wild-type mice at 2 months of age (Fig. 1e). These data indicated alterations in the metabolome of serum from PD-1 deficient mice, relative to that of wild-type mice; in particular, an accelerated decrease in aromatic amino acids.

T cells affect serum biochemistry in *Pdcd1*^{-/-} mice

PD-1 is expressed on activated T cells, although has also been reported to be expressed on some B cells and innate cell subsets^{6,7}. To investigate the contribution of T cells to the systemic metabolomic profile of *Pdcd1*^{-/-} mice, we measured amino acids in serum from 3-month-old *Cd3e*^{-/-} mice, which are deficient in the gene encoding the invariant signaling protein CD3ε and lack T cells, and age-matched *Pdcd1*^{-/-}/*Cd3e*^{-/-} mice. Except for minor changes, such as a 10% increase in Leu and 30% decrease in Thr in *Pdcd1*^{-/-}/*Cd3e*^{-/-} mice relative to their abundance in *Cd3e*^{-/-} mice, all other proteinogenic amino acids were similar in mice of these two genotypes (Fig. 2a). Thus, the reduction in the abundance of serum amino acids observed in the *Pdcd1*^{-/-} mice was largely T cell dependent.

As for the distribution of T cells among lymphoid tissues, by 4–6 months of age, *Pdcd1*^{-/-} mice had accumulated more T cells in the LNs and spleen than wild-type mice had, while the number of T cells in the colon and lamina propria of the small intestine was similar in both groups of mice (Fig. 2b). The absolute number of CD4⁺ T cells, CD8⁺ T cells and activated CD44^{hi} T cells was higher in *Pdcd1*^{-/-} LNs than in the LNs of age-matched wild-type mice at 2, 3 and 4–6 months of age (Fig. 2c); this corresponded to the age-dependent decrease in aromatic amino acids in the serum of *Pdcd1*^{-/-} mice (Fig. 1e). We next investigated whether activated T cells had a greater intracellular abundance of amino acids than that of naive T cells. CD44^{hi} T cells sorted from the LNs of wild-type mice had a greater intracellular abundance (1.5-fold) of Trp and Tyr, on a per-cell basis, than that of naive CD44^{lo} T cells (Fig. 2d). Large neutral amino acid such as Trp or Tyr are transported across the cell membrane by the system L transporter, a heterodimer composed of the heavy chain CD98 (encoded by *Slc3a2*) and the light chain LAT1 (encoded by *Slc7a5*)⁸. Indeed, *ex vivo* flow cytometry of LN cells identified higher surface expression of CD98 on activated CD44^{hi}CD4⁺ and CD44^{hi}CD8⁺ T cells than on naive CD44^{lo} T cells (Fig. 2e).

To further investigate whether the activation of T cells increased their uptake and accumulation of free amino acids intracellularly

despite extensive proliferation, we measured total protein, Trp and Tyr within cells after stimulation. We sorted T cells from the LNs of wild-type and *Pdcd1*^{-/-} mice and stimulated the TCR *in vitro* with antibody to the TCR invariant chain CD3 (anti-CD3) and antibody to the co-receptor CD28 (anti-CD28). We found that this stimulation induced the accumulation of intracellular Trp and Tyr at 48 h (1.5-fold) and at 96 h (2-fold) in activated T cells, relative to their abundance in non-activated T cells (Fig. 2f). The expression of *Slc3a2* and *Slc7a5* transcripts was increased at 24 h after stimulation in both wild-type T cells and *Pdcd1*^{-/-} T cells (Fig. 2g). These results were in line with published findings that stimulation of the TCR upregulates system L amino-acid transporters to sustain clonal expansion and differentiation⁹. As expected, the number of cells and, hence, total protein per well, increased substantially following stimulation with anti-CD3 and anti-CD28, which resulted in twofold more protein, on a per-cell basis, in activated T cells than in unstimulated T cells (Fig. 2h). The uptake of isotope-labeled Trp ([¹³C]Trp), as measured by liquid chromatography and mass spectrometry (LC-MS), was also greater in cells stimulated for 96 h with anti-CD3 and anti-CD28 than in unstimulated cells, and this coincided with less [¹³C]Trp in the culture medium (Fig. 2i). These results indicated that activated LN T cells upregulated their expression of amino-acid transporters and accumulated free intracellular amino acids *in vivo* and *in vitro*.

Effect of IFN-γ and microbiota on *Pdcd1*^{-/-} mice

Activated *Pdcd1*^{-/-} T cells produce the inflammatory cytokine interferon-γ (IFN-γ)¹⁰, which is known to mediate the induction of IDO (indoleamine 2,3-dioxygenase), a rate-limiting enzyme for the degradation of Trp in the kynurenine pathway^{11,12}. To assess whether the IFN-γ-mediated induction of IDO contributed to the decreased abundance of Trp in *Pdcd1*^{-/-} serum, we performed targeted LC-MS analysis of kynurene, kynurenic acid and 3-hydroxy kynurene, all of which are derived from the catabolism of Trp via the kynurene pathway (Supplementary Fig. 1a). Despite a twofold increase in IFN-γ⁺ CD4⁺ T cells and IFN-γ⁺CD8⁺ T cells in *Pdcd1*^{-/-} mice relative to their abundance in age-matched wild-type mice (Fig. 3a), serum kynurene, as well as the kynurene metabolites, were decreased more than 50% in *Pdcd1*^{-/-} mice, relative to their abundance in age-matched wild-type mice (Fig. 3b). In line with the previously described role of IFN-γ in kynurene production, the amount of kynurene in the serum was 20% lower in *Pdcd1*^{-/-}/*Ifng*^{-/-} mice than in *Pdcd1*^{-/-} mice (Fig. 3c). However, the amount of Trp in serum from *Pdcd1*^{-/-}/*Ifng*^{-/-} mice did not differ from that of *Pdcd1*^{-/-} mice (Fig. 3c), and the serum metabolome profile and the abundance of amino acids in *Pdcd1*^{-/-}/*Ifng*^{-/-} mice and *Pdcd1*^{-/-} mice were comparable (Supplementary Fig. 1b,c). These results indicated that the reduction in the abundance of Trp in the serum of *Pdcd1*^{-/-} mice was not due to the increased production of IFN-γ by *Pdcd1*^{-/-} T cells.

PD-1 deficiency is also marked by microbial dysbiosis due to an impairment in the T cell selection of affinity-matured B cells that produce immunoglobulin A (IgA) in the gut⁵. Furthermore, some gut bacteria, particularly certain species of *Clostridia*, can influence Trp catabolism^{13,14}. Thus, we assessed the contribution of the microbiota to the systemic depletion of amino acids in *Pdcd1*^{-/-} mice. PLS-DA of gas chromatography–mass spectrometry (GC-MS) measurements of serum revealed non-overlapping metabolome profiles for germ-free (GF) *Pdcd1*^{-/-} mice and their respective age-matched, GF wild-type mice (Fig. 3d). GF *Pdcd1*^{-/-} mice had significantly less Trp and Tyr in the serum (Fig. 3e), as well as more CD44^{hi} CD4⁺ T cells and CD8⁺ T cells that produced large amounts of IFN-γ (Fig. 3a,f,g), than did GF

wild-type mice. These observations suggested that the microbiota was not the dominant cause of the amino-acid depletion in *Pcd1^{-/-}* mice.

We further assessed the contribution of genetic factors versus environmental factors to the systemic metabolome through the use of

gnotobiotic transfer of wild-type or *Pcd1^{-/-}* specific-pathogen-free fecal microbiota into GF hosts of each genotype. *Pcd1^{-/-}* hosts had less Trp and Tyr in their serum than did wild-type hosts, whether they had received microbiota from wild-type mice or *Pcd1^{-/-}* mice

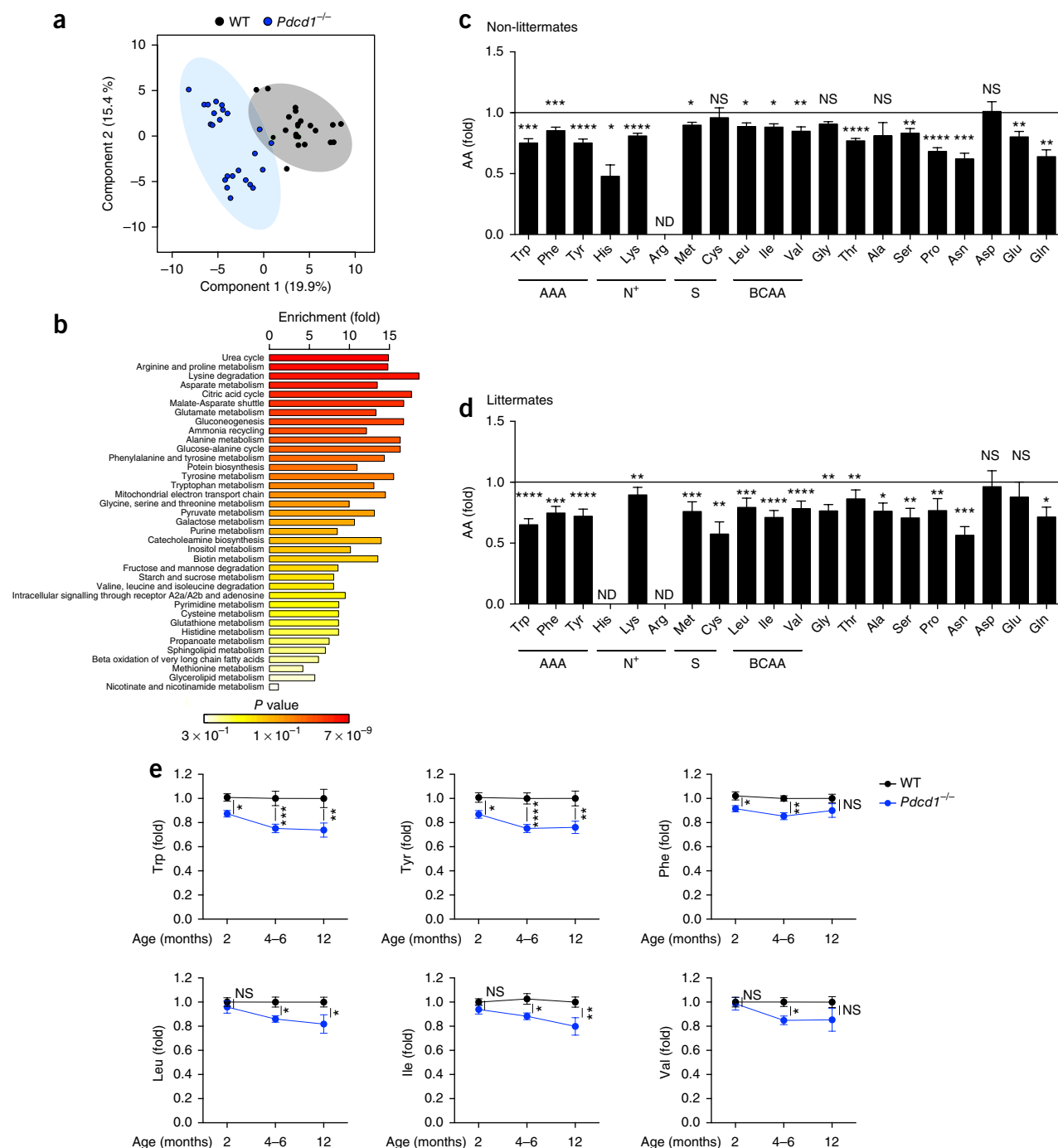


Figure 1 Depletion of amino acids in the serum of *Pcd1^{-/-}* mice. (a) PLS-DA of the serum metabolome of *Pcd1^{-/-}* mice ($n = 24$) and wild-type (WT) mice ($n = 22$). Each symbol represents the result for an individual mouse. (b) Metabolite-set-enrichment analysis of the compounds in each pathway in the data set in a that differ significantly (in abundance) in wild-type mice versus *Pcd1^{-/-}* mice. (c,d) GC-MS of amino acids (horizontal axis), grouped as aromatic amino acids (AAA), basic amino acids (N⁺), sulfur-containing amino acids (S) or branched-chain amino acids (BCAA), in the serum of 4- to 6-month-old *Pcd1^{-/-}* mice ($n = 24$) and wild-type mice ($n = 22$) that were not littermates (c) or were littermates ($n = 7$ –10 mice per group) (d), presented as the ratio of the abundance of each amino acid (AA) in *Pcd1^{-/-}* mice to that in wild-type mice. (e) Abundance of amino acids in the serum of *Pcd1^{-/-}* mice at various ages (horizontal axis: $n = 26$ (2 months), $n = 24$ (4–6 months) and $n = 7$ (12 months)). ND, not detected. NS, not significant ($P > 0.05$); * $P < 0.05$, ** $P < 0.005$, *** $P < 0.0005$ and **** $P < 0.0001$ (two-tailed unpaired Student's *t*-test (c,d) or analysis of variance (ANOVA) (e)). Data are pooled from two or more experiments (mean \pm s.e.m. in c,d, or mean \pm s.e.m. in e).

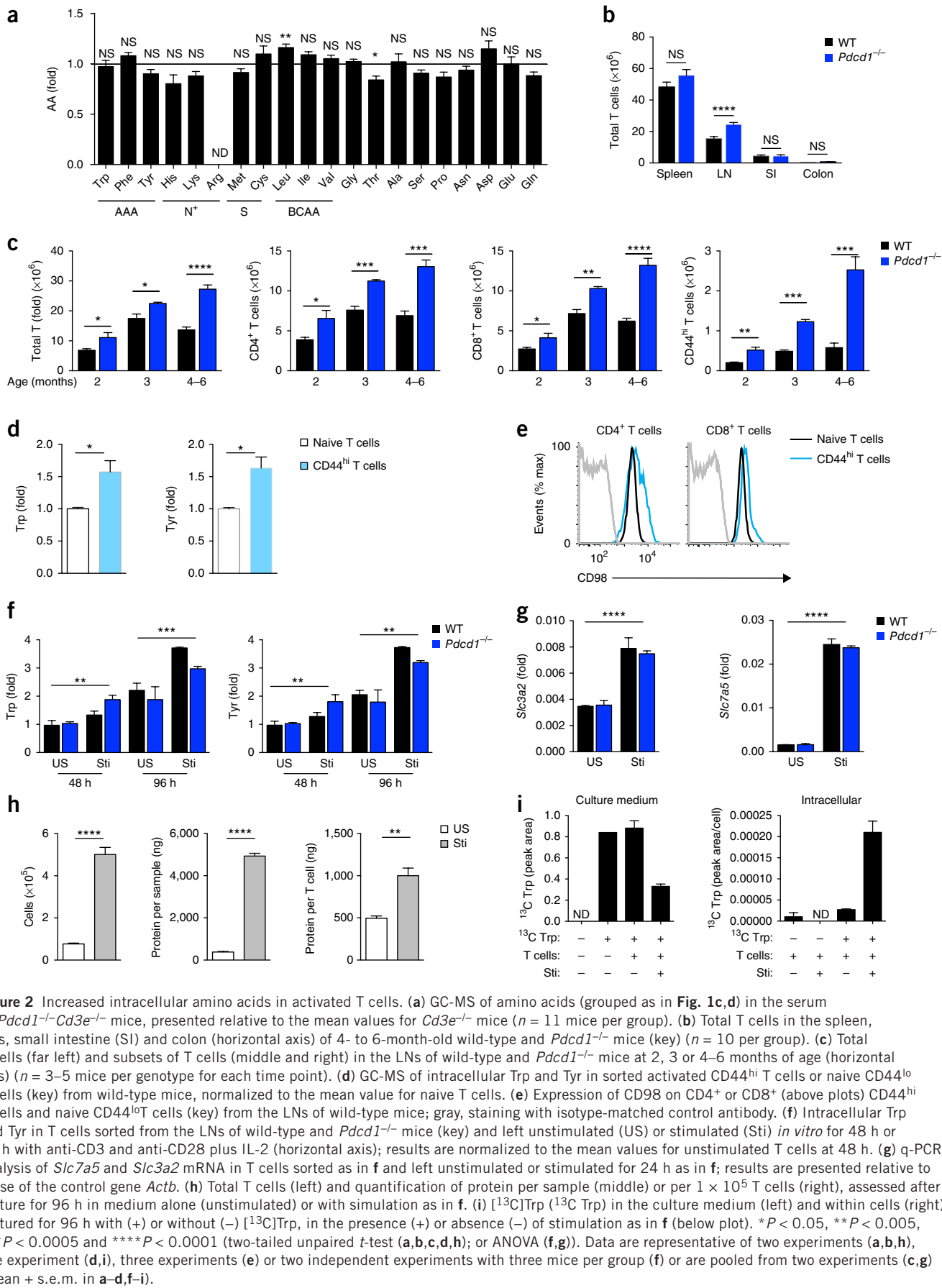


Figure 2 Increased intracellular amino acids in activated T cells. (a) GC-MS of amino acids (grouped as in Fig. 1c,d) in the serum of *Pdcd1^{-/-}Cd3e^{-/-}* mice, presented relative to the mean values for *Cd3e^{-/-}* mice ($n = 11$ mice per group). (b) Total T cells in the spleen, LNs, small intestine (SI) and colon (horizontal axis) of 4- to 6-month-old wild-type and *Pdcd1^{-/-}* mice (key) ($n = 10$ per group). (c) Total T cells (far left) and subsets of T cells (middle and right) in the LNs of wild-type and *Pdcd1^{-/-}* mice at 2, 3 or 4–6 months of age (horizontal axis) ($n = 3$ –5 mice per genotype for each time point). (d) GC-MS of intracellular Trp and Tyr in sorted activated CD44^{hi} T cells or naive CD44^{lo} T cells (key) from wild-type mice, normalized to the mean value for naive T cells. (e) Expression of CD98 on CD4⁺ or CD8⁺ (above plots) CD44^{hi} T cells and naive CD44^{lo} T cells (key) from the LNs of wild-type mice; gray, staining with isotype-matched control antibody. (f) Intracellular Trp and Tyr in T cells sorted from the LNs of wild-type and *Pdcd1^{-/-}* mice (key) and left unstimulated (US) or stimulated (Sti) *in vitro* for 48 h or 96 h with anti-CD3 and anti-CD28 plus IL-2 (horizontal axis); results are normalized to the mean values for unstimulated T cells at 48 h. (g) q-PCR analysis of *Slc7a5* and *Slc3a2* mRNA in T cells sorted as in f and left unstimulated or stimulated for 24 h as in f; results are presented relative to those of the control gene *Actb*. (h) Total T cells (left) and quantification of protein per sample (middle) or per 1×10^5 T cells (right), assessed after culture for 96 h in medium alone (unstimulated) or with simulation as in f. (i) [¹³C]Trp (¹³C Trp) in the culture medium (left) and within cells (right) cultured for 96 h with (+) or without (-) [¹³C]Trp, in the presence (+) or absence (-) of stimulation as in f (below plot). * $P < 0.05$, ** $P < 0.005$, *** $P < 0.0005$ and **** $P < 0.0001$ (two-tailed unpaired t-test (a,b,c,d,h); or ANOVA (f,g)). Data are representative of two experiments (a,b,h), one experiment (d,i), three experiments (e) or two independent experiments with three mice per group (f) or are pooled from two experiments (c,g) (mean + s.e.m. in a-d,f-i).

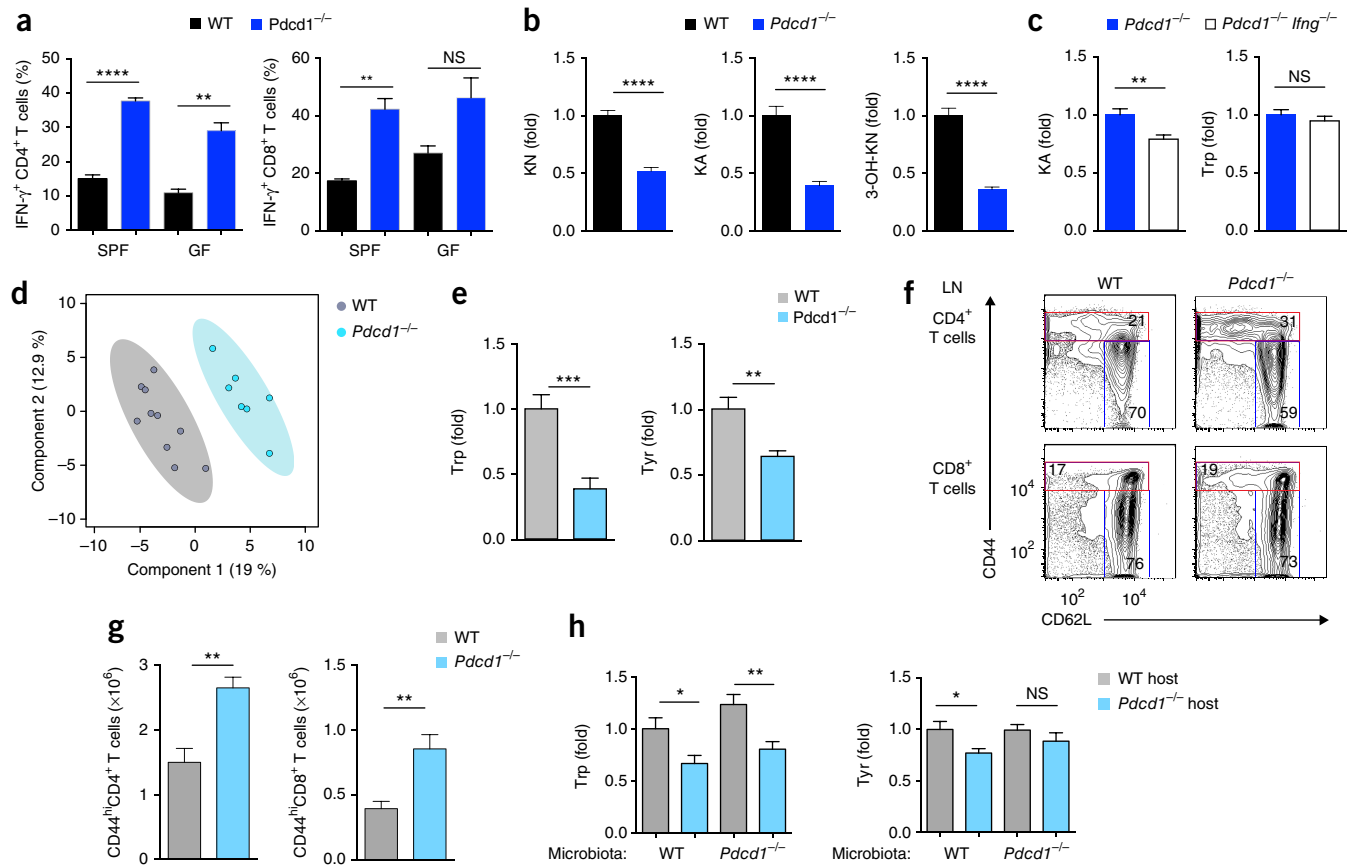


Figure 3 IFN- γ - and microbiota-independent depletion of amino acids in the serum of *Pdcd1^{-/-}* mice. **(a)** Frequency of IFN- γ ⁺ CD4⁺ or CD8⁺ T cells among cells obtained from specific-pathogen-free (SPF) or GF (horizontal axis) wild-type and *Pdcd1^{-/-}* mice (key) ($n = 3$ per group) and stimulated *in vitro* with PMA and ionomycin. **(b)** LC-MS of kynurenine (KN), kynurenic acid (KA) and 3-hydroxy kynurenine (3-OH-KN) in the serum of specific-pathogen-free *Pdcd1^{-/-}* mice ($n = 16$), presented relative to the mean value for wild-type mice ($n = 10$). **(c)** LC-MS of kynurenic acid and Trp in the serum of *Pdcd1^{-/-} Ifng^{-/-}* ($n = 14$), presented relative to the mean value for *Pdcd1^{-/-}* mice ($n = 12$). **(d)** PLS-DA of serum from GF wild-type mice ($n = 10$) and *Pdcd1^{-/-}* mice ($n = 7$). **(e)** Quantification of Trp and Tyr in serum from the mice in **d**. **(f)** Flow cytometry analyzing expression of the activation marker CD44 and memory marker CD62L by total CD4⁺ or CD8⁺ T cells (left margin) from the LNs of GF wild-type and *Pdcd1^{-/-}* mice (above plots). Numbers in outlined areas indicate percent CD44^{hi} (activated) cells (top, red outline) or CD44^{lo}CD62L⁺ (naive) cells (right, blue outline). **(g)** Total CD44^{hi} CD4⁺ or CD8⁺ T cells analyzed as in **g** for $n = 10$ mice per group. **(h)** GC-MS analysis of Trp and Tyr in the serum of gnotobiotic wild-type or *Pdcd1^{-/-}* (key) ($n = 7$ –12 per group) at 8 weeks after gavage of wild-type or *Pdcd1^{-/-}* fecal microbiota (horizontal axis); results are presented relative to those of GF wild-type mice given transplantation of wild-type fecal microbiota. NS, $P < 0.0578$ **(a)**; * $P < 0.05$, ** $P < 0.005$, *** $P < 0.0005$ and **** $P < 0.0001$ (two-tailed unpaired *t*-test). Data are from one of two experiments with similar results **(a)**, are pooled from two experiments **(b,c,g,h)** or are representative of two experiments **(d)** or two independent experiments **(e,f)** (mean \pm s.e.m. in **a–c,e,g,h**).

(Fig. 3h). Thus, the reduction in the abundance of amino acids in the serum of *Pdcd1^{-/-}* mice was due to genetic effects other than excessive IFN- γ production or gut dysbiosis.

Acute T cell activation causes serum amino-acid depletion

We next investigated whether strong stimulation of adaptive immunity had a systemic effect on amino-acid dynamics. For this, we immunized wild-type mice in the footpad with ovalbumin (OVA) in complete Freund's adjuvant or with saline (sham condition), then performed metabolome profiling of serum by LC-MS. At 7 d after immunization, Trp and Tyr were decreased 25% in the serum of OVA-immunized mice relative to their abundance in that of sham-immunized mice (Fig. 4a). In a second experimental system, we induced systemic activation of T cells by intravenous administration of adjuvant-free OVA to OT-I mice or OT-II mice, which have transgenic expression of OVA-specific TCRs on CD8⁺ T cells or CD4⁺ T cells, respectively. Both OT-I mice and OT-II mice underwent rapid depletion of serum Trp by day 5 after immunization (Fig. 4b), which indicated that activation of either the CD8⁺ T cell subset or the CD4⁺ T cell subset

influenced the levels of systemic amino acids, although no change in the amount of Tyr was observed in this model (Fig. 4b).

We also evaluated if serum amounts of amino acids were reduced by acute inhibition of PD-1, a technique used for cancer immunotherapy. We injected MC38 adenocarcinoma cells subcutaneously into 2-month-old wild-type mice, treated the tumor-bearing mice with anti-PD-1 or isotype-matched control antibody and then compared the abundance of amino acids in serum at day 13 after cell injection. Administration of 100 μ g of anti-PD-1 at days 5, 8 and 11 of tumor growth induced a significant reduction in the amount of amino acids in serum (Fig. 4c), to the extent observed in *Pdcd1^{-/-}* mice (Fig. 1c), but the administration of isotype-matched control antibody did not (Fig. 4c). This showed activation of T cells specific for tumor-derived antigens had a substantial effect on the amount of amino acids in serum.

Accumulation of amino acids in activated LNs of *Pdcd1^{-/-}* mice

We next investigated whether the depletion of serum amino acids in *Pdcd1^{-/-}* mice was due to peripheral activation of the immune system, defects in intestinal absorption or a reduction in hepatic biosynthesis.

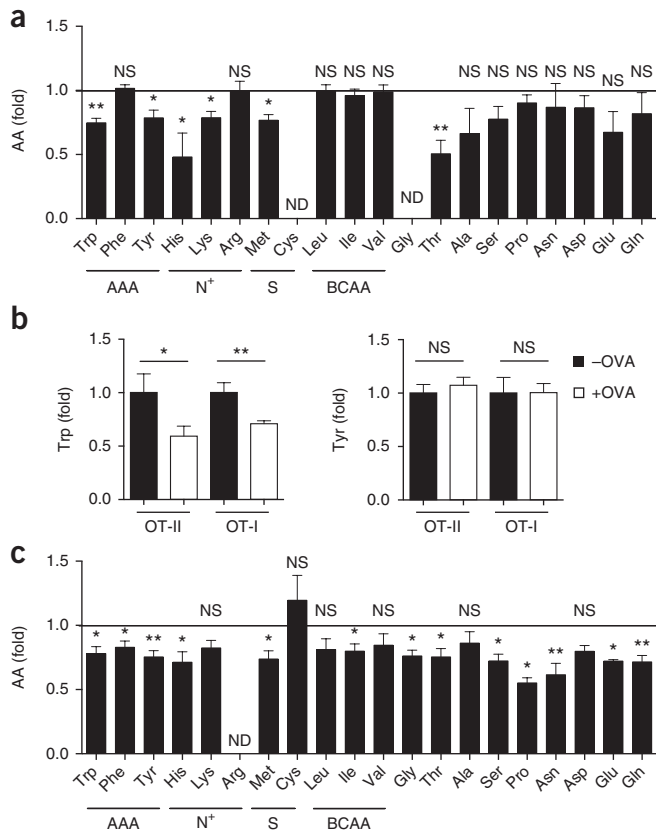


Figure 4 T cell activation depletes serum of amino acids in several models. (a) LC-MS of amino acids (grouped as in Fig. 1c,d) in serum from wild-type mice at 7 d after immunization (in the footpad) with OVA in complete Freund's adjuvant ($n = 7$); results are presented relative to the mean values for sham-immunized mice ($n = 5$). (b) Abundance of Trp and Tyr in serum from OT-II mice ($n = 10$) or OT-I mice ($n = 5$) (horizontal axis) on day 5 after injection of OVA (on days 0 and 3) (+ OVA (key)); results are presented relative to the mean values for OT-II mice ($n = 8$) or OT-I mice ($n = 4$) given injection of PBS (-OVA). (c) GC-MS of amino acids (as in a) in serum of wild-type mice ($n = 5$ per group) inoculated with MC38 tumor cells, then given injection of anti-PD-1 on day 5, 8 and 11 after inoculation and analyzed at day 13; results presented as relative to mean values for MC38-inoculated mice given injection of isotype-matched control antibody. * $P < 0.05$ and ** $P < 0.005$ (two-tailed unpaired t -test). Data are representative of two experiments (a, and b (OT-II)) or one experiment (b (OT-I) and c) (mean + s.e.m. throughout).

Thus, we measured local metabolites in the LNs, spleen, segments of the small and large intestine and liver by non-targeted metabolome analysis (Supplementary Fig. 2) and targeted metabolome analysis (Fig. 5). Principal-component analysis detected a change in metabolite profiles in the LNs of 5-month-old *Pdcd1*^{-/-} mice relative to those in the LNs of age-matched wild-type mice, but not in the gut or liver (Fig. 5a), consistent with the substantial activation of the immune system observed in these mice. The most significant differences between the LN metabolome of *Pdcd1*^{-/-} mice and that of wild-type mice involved amino-acid metabolism, intracellular signaling, transcription and protein synthesis (Fig. 5b). The abundance of aromatic amino acids, including Trp, was twofold greater in the LNs and, to a lesser extent, the spleen of *Pdcd1*^{-/-} mice than in those of wild-type, while the amount of amino acids in gut and liver was comparable in these mice (Fig. 5c and Supplementary Fig. 3). As with the amino acids, the abundance of nucleosides, glycolysis and

TCA-cycle metabolites was significantly greater in the LNs of *Pdcd1*^{-/-} mice than in those of wild-type mice (Fig. 5d-f), indicative of enhanced biochemical processes consistent with considerable, localized activation of the immune system. These results suggested that the depletion of amino acids from the serum was due to their accumulation in LNs to support the metabolic requirements necessitated by the enhanced activation of immune cells in *Pdcd1*^{-/-} mice.

Diminished brain monoamines in *Pdcd1*^{-/-} mice

In addition to being required for protein synthesis and energy generation in lymphocytes, free amino acids are precursors of monoamine neurotransmitters. Tyr and Trp are essential for synthesis of the neurotransmitters dopamine and 5-hydroxytryptamine (5-HT (serotonin)) (Supplementary Fig. 4a,b). Dopamine is critical for processes that drive executive functions, including motor control, motivation, learning and fear responses^{15,16}. 5-HT is thought to regulate many behavioral aspects, including mood, anxiety, aggression and fear-conditioning processes^{17,18}. By measuring whole-brain homogenates by LC-MS after focused microwave fixation, we observed that the amount of Tyr and Trp in the brain was significantly lower in 5-month-old *Pdcd1*^{-/-} mice than in age-matched wild-type mice (Fig. 6a), as were the levels of dopamine and 5-HT, as measured by high-performance liquid chromatography coupled to an electrochemical detector (HPLC-ECD) (Fig. 6a and Supplementary Fig. 4c). Additionally, *in situ* immunostaining showed less 5-HT in tryptophan hydroxylase-positive serotonergic neurons in midbrain raphe nuclei in *Pdcd1*^{-/-} mice than in those of wild-type mice (Fig. 6b). Imaging mass spectrometry also showed a 1.8-fold less dopamine in the striatum and 2.2-fold less 5-HT in the midbrain of *Pdcd1*^{-/-} mice than in that of wild-type mice (Fig. 6c). Similar biochemical changes were also detected in whole-brain homogenates of GF *Pdcd1*^{-/-} mice versus GF wild-type mice (Supplementary Fig. 4d). We observed no difference between *Pdcd1*^{-/-} brain and wild-type brain in the excitatory neurotransmitter glutamate and inhibitory neurotransmitter GABA (4-aminobutyric acid) (Fig. 6a and Supplementary Fig. 4d), which indicated that neurotransmitter-synthesis pathways varied in their sensitivity to diminished precursor availability. To assess extracellular brain metabolites, we performed *in vivo* microdialysis. We found significantly less Tyr and Trp at steady state in freely moving *Pdcd1*^{-/-} mice than in their wild-type counterparts, and less release of 5-HT in response to potassium challenge in the prefrontal cortex of *Pdcd1*^{-/-} mice than in that of wild-type mice (Supplementary Fig. 4e). These data suggested that among the tissues assessed, mainly the brain was affected by the depletion of Trp and Tyr from the serum of *Pdcd1*^{-/-} mice, and this resulted in reduced synthesis of the monoamine neurotransmitters dopamine and 5-HT.

To rule out the possibility that insufficiency in biosynthetic enzymes and/or cofactors contributed to the reduction in the abundance of dopamine and 5-HT in *Pdcd1*^{-/-} mice, we used q-PCR to measure mRNA encoding individual components of monoamine-synthesis pathways (Supplementary Fig. 4a,b). We observed no major difference between *Pdcd1*^{-/-} mice and wild-type mice in the expression of mRNA encoding tyrosine hydroxylase (encoded by *Th*), which is the rate-limiting enzyme for dopamine synthesis, or aromatic L-amino acid decarboxylase (encoded by *Aadc*). Expression of *Tph2*, which encodes the rate-limiting enzyme for 5-HT synthesis, was higher in the raphe nuclei of *Pdcd1*^{-/-} mice than in those of wild-type mice (Fig. 6d). The amount of tetrahydrobiopterin, a cofactor required for the activity of both tyrosine hydroxylase and tryptophan hydroxylase 2, was similar in *Pdcd1*^{-/-} mice and wild-type mice, as measured in whole-brain extracts by LC-MS (Fig. 6e). Thus, the *Pdcd1*^{-/-} brain

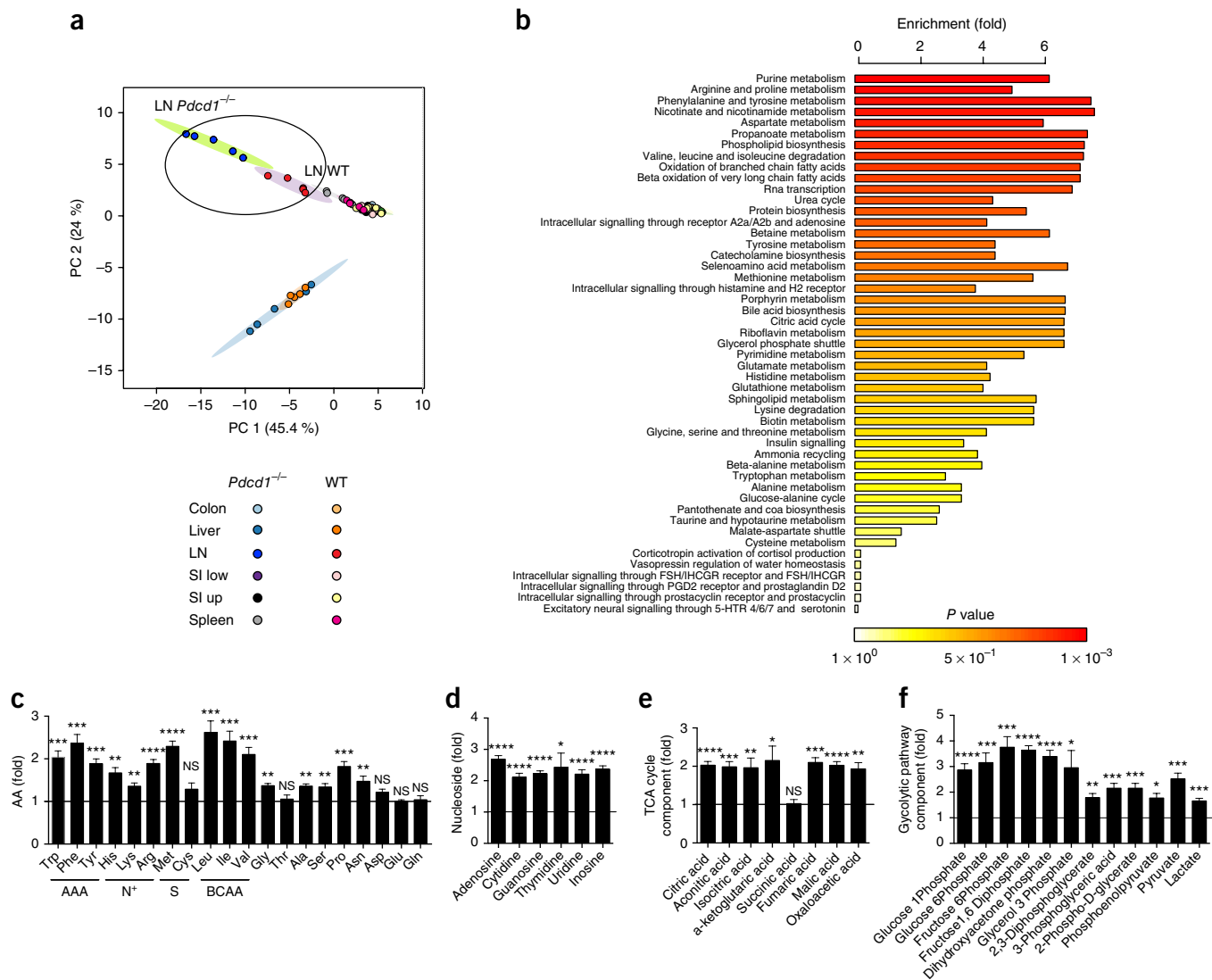


Figure 5 Accumulation of amino acids in the LNs of $Pdcd1^{-/-}$ mice. (a) Principal-component analysis of the metabolome profile of the colon, liver, LNs, upper and lower segments of the small intestine (SI up and SI low, respectively) and spleen of $Pdcd1^{-/-}$ mice and wild-type mice (key); difference between LN-derived $Pdcd1^{-/-}$ samples and LN-derived wild-type samples is outlined. Each symbol represents the result for an individual mouse. (b) Metabolite-set-enrichment analysis (as in Fig. 1a) of the compounds in each pathway in the data set that differ significantly (in abundance) in LNs of $Pdcd1^{-/-}$ mice versus those of wild-type mice. (c–e) LC-MS analysis of amino acids (grouped as in Fig. 1c,d) (c), nucleosides (d) and components of the TCA cycle (e) in the LNs of $Pdcd1^{-/-}$ mice; results are presented relative to the mean values of wild-type mice ($n = 5$ per group). (f) Ion chromatography-tandem mass spectrometry analysis of components of the glycolytic pathway in $Pdcd1^{-/-}$ mice; results are presented relative to the mean values of wild-type mice ($n = 5$ per group). * $P < 0.05$, ** $P < 0.005$, *** $P < 0.0005$ and **** $P < 0.0001$ (two-tailed unpaired t -test). Data are pooled from two experiments (mean + s.e.m. in c–f).

was not deficient in the critical enzymes and cofactors required for monoamine synthesis.

In addition to being caused by limited availability of precursor amino acids, the decrease in brain monoamines could have also been caused by their accelerated degradation. Thus, we measured the catabolites of dopamine and 5-HT in whole-brain extracts by LC-MS. The amount of norepinephrine, of which dopamine is a precursor, was significantly lower in $Pdcd1^{-/-}$ mice than in wild-type mice (Fig. 6f). However, the abundance of other catabolites of dopamine (DOPAC (3,4-dihydroxyphenylacetic acid), 3-MT (3-methoxytyramine) and HVA (homovanillic acid)) and the 5-HT catabolite 5-HIAA (5-hydroxyindole aminoacetic acid) was similar in $Pdcd1^{-/-}$ mice and wild-type mice (Fig. 6f), which might indicate accelerated degradation of dopamine and 5-HT in $Pdcd1^{-/-}$ mice. Thus, decreased

availability of amino-acid precursors and possibly altered catabolism of dopamine and 5-HT in $Pdcd1^{-/-}$ mice resulted in reduced amounts of brain monoamine in these mice.

Behavioral changes in $Pdcd1^{-/-}$ mice

We next assessed whether the reduced levels of monoamines in the brains of $Pdcd1^{-/-}$ mice had an effect on their behavior. When monitored in metabolic chambers, the daily energy expenditure and oxygen consumption of $Pdcd1^{-/-}$ mice were significantly lower than those of wild-type mice (Supplementary Fig. 5a), indicative of a hypoactive phenotype. $Pdcd1^{-/-}$ mice displayed less motility than that of wild-type mice during the first 2 d after transfer into the metabolic chamber (Supplementary Fig. 5a), suggestive of reduced exploratory behavior in a novel environment. We performed a larger

battery of neurological, sensorial and behavioral tests to measure locomotor activity, fear responses, anxiety and social interactions. In the elevated-plus maze test, a behavioral test that measures

anxiety in response to open spaces, *Pcd1*^{-/-} mice spent less time in the open arms or center of the platform and moved less overall than did wild-type mice (Fig. 7a). In the dark-light transition

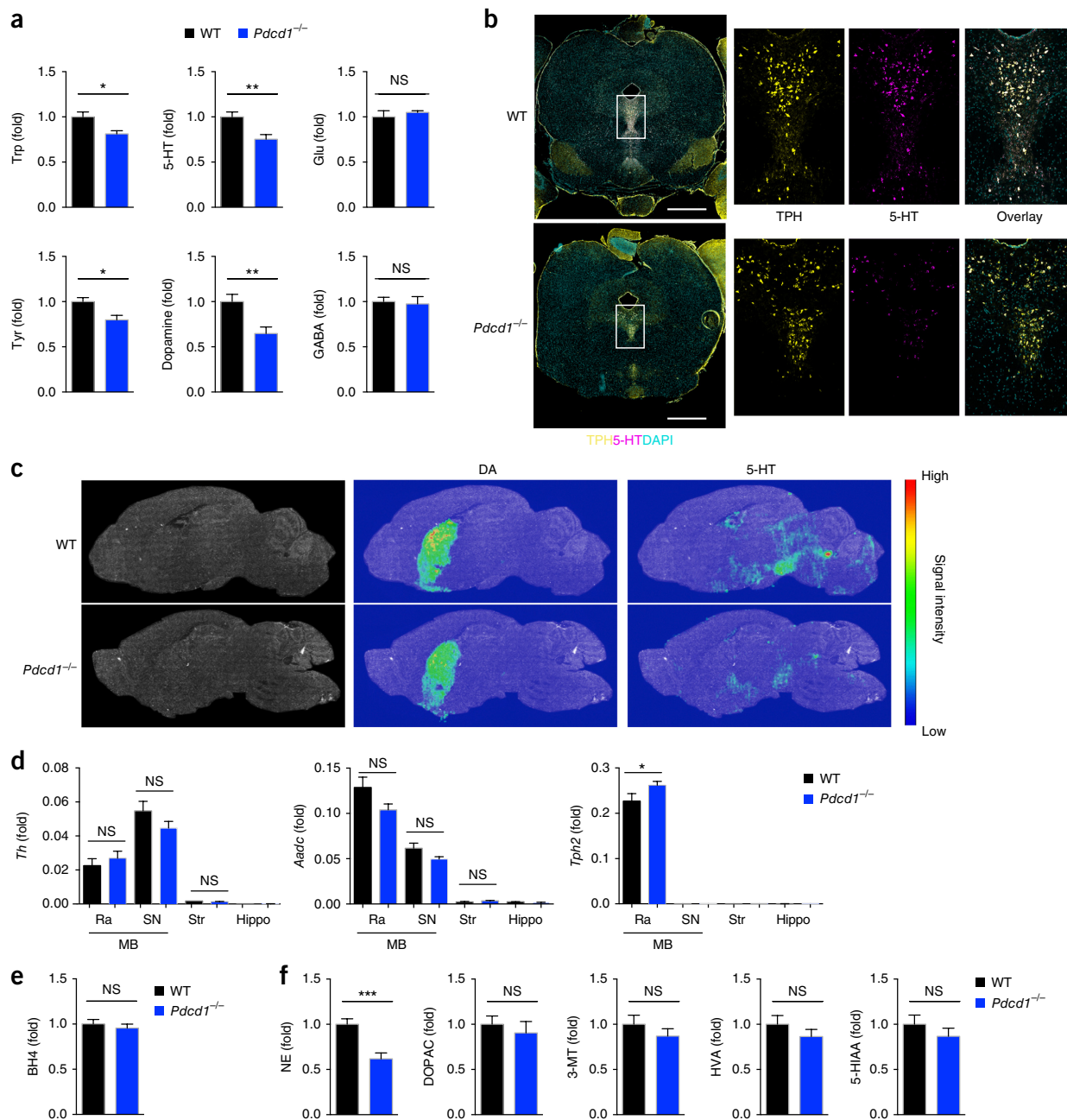


Figure 6 Reduced levels of monoamine neurotransmitters and their amino-acid precursors in the brain of *Pcd1*^{-/-} mice. (a) LC-MS analysis of the amino acids Trp, Glu and Tyr in the brain of wild-type mice ($n = 4$) and *Pcd1*^{-/-} mice ($n = 6$), and HPLC-ECD analysis of the neurotransmitters 5-HT, dopamine (DA) and GABA in the brain of wild-type mice ($n = 10$) and *Pcd1*^{-/-} mice ($n = 11$). (b) Microscopy of coronal brain sections of wild-type and *Pcd1*^{-/-} mice (left margin), stained for tryptophan hydroxylase (TPH), 5-HT and the DNA-binding dye DAPI (left); raphe nuclei (white rectangles at left) are enlarged 10x at right (single-color and overlay images). Scale bars, 1 mm. (c) Imaging mass spectrometry of the distribution and abundance of dopamine and 5-HT (above images) in sagittal sections of brain from wild-type and *Pcd1*^{-/-} mice (left margin): dopamine signal, 207,804,304 pixels (wild-type) and 112,989,802 pixels (*Pcd1*^{-/-}); 5-HT signal, 152,529,424 pixels (wild-type) and 66,408,795 pixels (*Pcd1*^{-/-}). (d) q-PCR analysis of *Th*, *Aadc* and *Tph2* mRNA in the raphe nuclei (Ra) and substantia nigra (SN) of the mid-brain (MB) and the striatum (Str) and hippocampus (Hippo) of wild-type and *Pcd1*^{-/-} mice (key) ($n = 5$ –6 per group (raphe nuclei and substantia nigra) or $n = 2$ per group (striatum and hippocampus)); results presented relative to those of the control gene *Gapdh*. (e,f) Abundance of tetrahydrobiopterin (BH4) (a cofactor of tyrosine hydroxylase and tryptophan hydroxylase 2) (e) and of norepinephrine (NE), DOPAC, 3-MT and HVA (catecholamines of dopamine) and 5-HIAA (5-HT catabolite) (f) in brain extracts from *Pcd1*^{-/-} mice, presented relative to results for wild-type mice ($n = 5$ –6 mice per group). * $P < 0.05$, ** $P < 0.005$ and *** $P < 0.0005$ (two-tailed unpaired *t*-test). Data are pooled from two experiments (a,d), four independent experiments (b) or two experiments with $n = 2$ –3 mice each (c,e,f) (mean + s.e.m. in a,d–f).

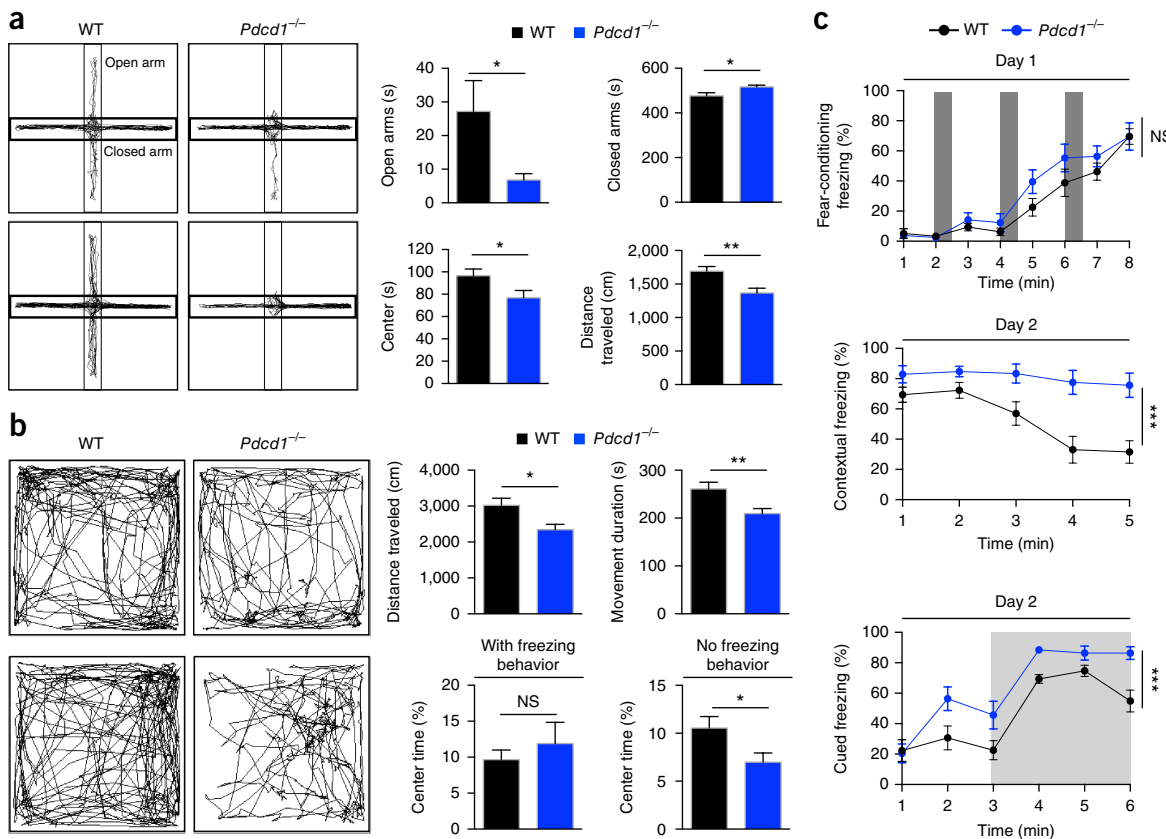


Figure 7 Increased anxiety-like behavior and enhanced fear responses in *Pdcd1*^{-/-} mice. **(a)** Elevated-plus maze results for wild-type mice ($n = 13$) and *Pdcd1*^{-/-} mice ($n = 13$) (left), as well as total time spent in open arms, center or closed arms of the maze (top right) and total distance traveled (bottom right). **(b)** Open-field test results for wild-type mice ($n = 11$) and *Pdcd1*^{-/-} mice ($n = 13$) (left half), as well as total distance traveled (top right), total movement duration (top far right) and percent time spent in center with (bottom far right) or without (bottom right) exclusion of *Pdcd1*^{-/-} mice ($n = 2$) showing a freezing-behavior movement pattern (as in bottom right plot at left). **(c)** Fear responses of wild-type and *Pdcd1*^{-/-} mice ($n = 11$ per group) during a fear-conditioning session on day 1 (top; dark gray areas, duration of the presentation of a pairing of a conditioned stimulus and an unconditioned stimulus), a contextual fear session (middle) and a cued fear session (bottom; light gray area, duration of the conditioned stimulus), both on day 2; results presented as percent time spent in freezing behavior. * $P < 0.05$, ** $P < 0.005$ and *** $P < 0.0005$ (two-tailed unpaired *t*-test (a,b) or ANOVA (c)). Data are representative of at least two experiments with similar results (mean + s.e.m. in a,b and mean \pm s.e.m. in c).

test, which measures the response to mild stressors such as a novel environment and light, *Pdcd1*^{-/-} mice were slower to enter the light zone than were wild-type mice, and they transitioned less between the dark zone and light zone and spent significantly less time in the light zone than did wild-type mice (Supplementary Fig. 5b). In an open-field test, which measures locomotion and anxiety, *Pdcd1*^{-/-} mice showed decreased locomotor activity (reduced distance of travel or movement duration) relative to that of wild-type mice (Fig. 7b). While *Pdcd1*^{-/-} mice generally spent less time in the center of the field than did wild-type mice, some froze there for extended periods (Fig. 7b). There were no significant differences between the groups of mice in the forced-swim test, which measures depression, although there was a trend toward less swimming and greater immobility in *Pdcd1*^{-/-} mice than in wild-type mice (Supplementary Fig. 5c). *Pdcd1*^{-/-} mice did not differ from wild-type mice in social interaction or pain sensitivity (Supplementary Fig. 5d,e). Elevated-plus maze and open-field tests performed on pairs of *Pdcd1*^{-/-} mice and their wild-type littermates produced similar results (Supplementary Fig. 6a,b), which suggested a limited effect of maternal influences or microbiota on the altered behavioral phenotype of *Pdcd1*^{-/-} mice.

To determine whether the long periods of immobility observed during elevated-plus maze and open-field testing in the *Pdcd1*^{-/-} mice

were associated with abnormal fear responses, we used a Pavlovian fear-conditioning test, a behavioral paradigm that explores the learning and reactions to aversive environmental stimuli. Although no major differences between *Pdcd1*^{-/-} mice and wild-type mice were observed during fear acquisition on day 1, both contextual fear responses and cued fear responses, which were tested on day 2, were significantly heightened in *Pdcd1*^{-/-} (Fig. 7c and Supplementary Fig. 6c). In addition, *Pdcd1*^{-/-} mice exhibited impaired extinction of fear memory (Supplementary Fig. 5f). No difference between *Pdcd1*^{-/-} mice and wild-type mice was observed for spatial memory, as evaluated by the alternation rate in a Y-maze test (Supplementary Fig. 5g). Overall, these results showed that *Pdcd1*^{-/-} mice exhibited hypo-locomotion, anxiety-like behavior and enhanced fear responses, relative to the phenotype of wild-type mice.

Pharmacological and dietary intervention ‘rescues’ behavior

We next investigated whether pharmacological supplementation with monoamines could ameliorate the conditioned fear responses of *Pdcd1*^{-/-} mice. Phenelzine and fluoxetine are known to modulate the expression of conditioned fear^{19,20} by altering the amounts of monoamine neurotransmitters in the brain. Selective serotonin-reuptake inhibitors such as fluoxetine act by delaying the reuptake of 5-HT, which leads to longer persistence of 5-HT in the synaptic

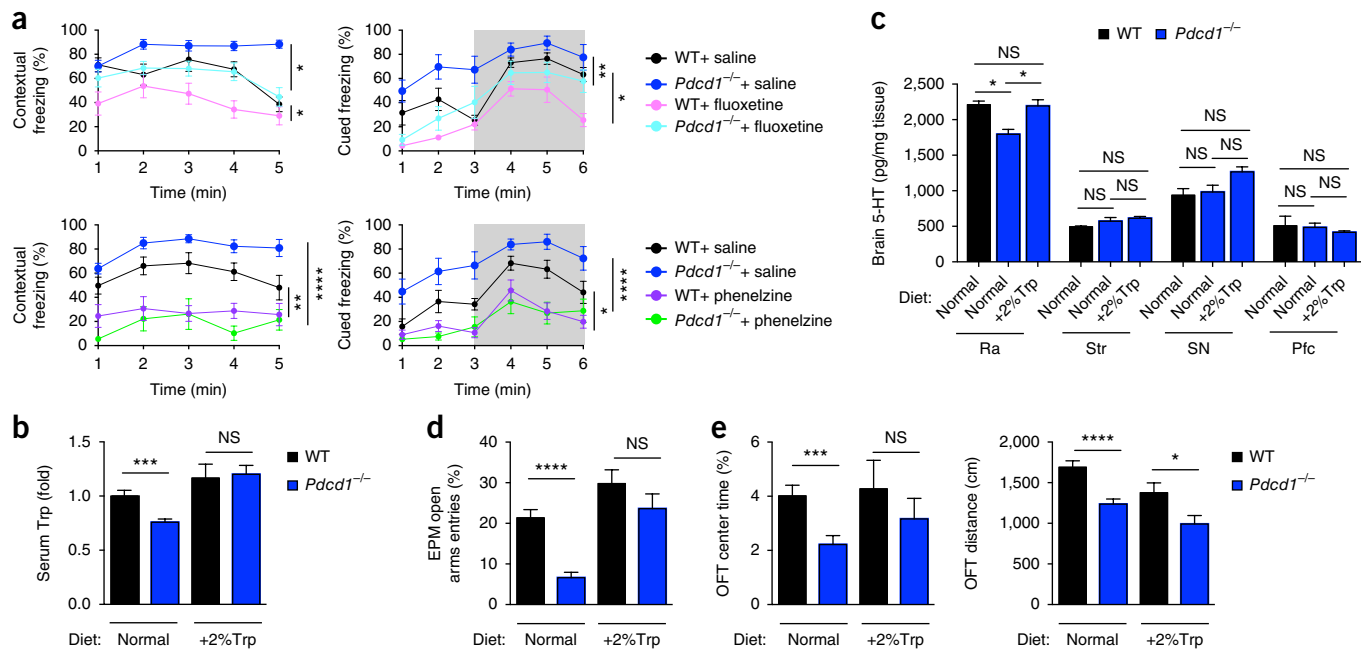


Figure 8 Pharmacological and dietary supplementation ameliorates the behavior of *Pdcd1*^{-/-} mice. **(a)** Fear responses (in contextual and cued tests as in Fig. 7c) of wild-type and *Pdcd1*^{-/-} mice ($n = 6\text{--}9$ per group) given saline (as a control) or fluoxetine (top row) or phenelzine (bottom row) (key) 1 d after a fear-conditioning session (presented as in Fig. 7c). **(b,c)** LC-MS of Trp in the serum (**b**) and of 5-HT in the raphe nuclei, striatum, substantia nigra and prefrontal cortex (Pfc) (**c**) of wild-type and *Pdcd1*^{-/-} mice (key) fed standard chow (Normal) or a diet supplemented with a high percentage of Trp (+2% Trp), for 1 month (below plot). **(d,e)** Anxiety-like behavior phenotype of wild-type and *Pdcd1*^{-/-} mice fed standard chow ($n = 28\text{--}29$ mice per group) or a 2% Trp diet ($n = 14$ mice per group), assessed as percent entries into the open arms in the elevated-plus maze (EPM) (**d**), percent time spent in the center of the open-field test (OFT) (**e**, left), and locomotor activity of those mice, assessed as total distance traveled in the open-field test (**e**, right). * $P < 0.05$, ** $P < 0.005$, *** $P < 0.0005$ and **** $P < 0.0001$ ((ANOVA (**a**) or two-tailed unpaired *t*-test (**b**–**e**)). Data are pooled from two experiments (**a**; mean \pm s.e.m.) or are representative of two independent experiments with similar results (**b**–**e**; mean \pm s.e.m.).

space, while monoamine-oxidase inhibitors such as phenelzine inhibit monoamine-oxidase enzymes and thereby block the degradation of both 5-HT and dopamine²¹.

The administration of fluoxetine before the contextual conditioning normalized the fear responses in *Pdcd1*^{-/-} mice to the levels observed in untreated wild-type mice (Fig. 8a). Phenelzine had a more profound effect and decreased fear responses in both wild-type mice and *Pdcd1*^{-/-} mice, relative to the fear responses of untreated wild-type mice and *Pdcd1*^{-/-} mice (Fig. 8a). However, the possibility of collateral effects of the drugs on the peripheral nervous system could not be entirely excluded, because phenelzine slightly increased the locomotion of both wild-type mice and *Pdcd1*^{-/-} mice in an open-field test (Supplementary Fig. 6d).

We finally evaluated whether restoring the serum concentration of Trp by a diet supplemented with Trp was able to diminish the anxiety-like behavior of *Pdcd1*^{-/-} mice. In specific-pathogen-free mice, consumption of a diet supplemented with 2% (weight/weight) Trp for 1 month increased the amount of Trp in the serum of *Pdcd1*^{-/-} mice to that in the serum of wild-type mice fed standard chow (Fig. 8b) and normalized the expression of 5-HT in the brain, particularly in the raphe nuclei (Fig. 8c). In addition, supplementation with Trp ‘rescued’ the anxiety phenotype of *Pdcd1*^{-/-} mice to that of wild-type mice fed standard chow, as evaluated by the frequency of entry into the open arms in the elevated maze test and time spent in the center in the open field test, but it did not ameliorate the hypoactivity of *Pdcd1*^{-/-} mice (Fig. 8d,e). The results indicated that monoamine deficiency due to limited availability of precursor amino acids was responsible for certain behavioral changes in *Pdcd1*^{-/-} mice.

DISCUSSION

Here we have shown that T cell activation in PD-1-deficient mice induced metabolic changes that could be measured in the blood. The expanded population of CD44^{hi} T cells in the LNs of *Pdcd1*^{-/-} mice underwent intracellular accumulation of amino acids, which caused systemic depletion of those amino acids. Such systemic changes to the ‘aminome’ (the abundance and distribution of amino acids in an organism) were not observed in *Pdcd1*^{-/-} mice that lacked T cells, but this effect was replicated in acute models of T cell activation, at early time points probably preceding B cell activation and germinal-center induction.

Published *in vitro* studies have indicated that intracellular metabolic changes associated with T cell activation, such as increased metabolism of glutamine and glucose, are required for proliferation, survival and cytokine production^{22,23}. Simultaneous stimulation of human T cells via the TCR and PD-1 *in vitro* has been shown to inhibit glycolysis and the metabolism of some amino acids such as glutamine and the branched-chain amino acids²⁴. Our results revealed a strong and unexpected effect of T cell activation on the systemic metabolic profile, reflective of the powerful influence of the immune system on the biochemical networks of the body. Since PD-1 is expressed on all activated T cells, our experiments did not allow us to distinguish the effects of different functional subsets (effector versus central memory; CD4⁺ T cells versus CD8⁺ T cells) on the systemic ‘aminome’. Further studies are needed to delineate the functions of intracellular free-amino-acid stores in activated T cells in immune responses to different kinds of antigens, as well as their relative incorporation rates into downstream metabolism pathways for energy production or protein synthesis.

We further demonstrated that T cell activation diminished the pool of aromatic amino acids in serum, affected the production of neurotransmitters in the brain and induced specific behavioral changes. T cells are essential ‘arbiters’ of protective immune responses to infection and thus they monopolize the systemic amino acids available in the serum to support their effector functions; this reflects a physiological prioritization of immune-system enhancement at the cost of optimal brain function. Indeed, monoamine-neurotransmitter-biosynthesis rates in the brain were sensitive to depletion of Trp and Tyr from the serum in *Pdcd1*^{-/-} mice; this resulted in abnormal behavior that was ameliorated by dietary supplementation with Trp or pharmacological enhancement of the concentration of 5-HT or dopamine in the brain.

We found that activation of T cells driven by tumor-derived antigens and enhanced by blockade of PD-1 had a substantial effect on the amount of amino acids in serum. This raised the possibility that emotional responses might be altered in patients undergoing T cell-boosting immunotherapy or in patients with autoimmune T cell activation or infection. As anti-PD-1 is widely used for cancer treatment, future studies should address the development of affective and behavioral disorders that might be predicted to arise from long-term therapy, in addition to autoimmune manifestations. Further study is needed to confirm whether the distinct serum metabolome pattern of PD-1 inhibition is recapitulated in humans, in which case it might have beneficial application as a method of monitoring the efficacy of immunotherapy.

METHODS

Methods, including statements of data availability and any associated accession codes and references, are available in the [online version of the paper](#).

Note: Any Supplementary Information and Source Data files are available in the [online version of the paper](#).

ACKNOWLEDGMENTS

We thank S. Yamamoto, S. Oonawa and Y. Doi for technical help; S. Kawamoto, T. Chaya, and T. Kozuka for the help with metabolome and brain dissection and preparations; S. Narumiya, T. Sato and K. Tanaka for discussions and suggestion; Y. Iwakura (Tokyo University of Science) and M. Kubo (IMS RIKEN) for *Ifng*^{-/-} mice; B. Malissen (Centre d’Immunologie de Marseille-Luminy) for *Cd3e*^{-/-} mice; and N. Lonberg (Bristol-Myers Squibb) for anti-PD-1. Supported by Japan Agency for Medical Research and Development—Core Research for Evolutional Science and Technology (14532135 to S.F.), Japan Agency for Medical Research and Development (145208 and 16770835 to T.H.) and the Cell Science Foundation (K.C.).

AUTHOR CONTRIBUTIONS

M.Mi. performed most of the *in vivo* experiments; B.Z. performed all *in vitro* experiments and behavioral studies at Kyoto University facility; Y.S., K.So. and K.H. performed all metabolome analyses; M.M.G. performed quantitative PCR and 5-HT staining and collaborated in writing the manuscript; Y.T. and S.I. performed behavioral studies at the RIKEN IMS facility; M.Mi and M.Ma. performed all germ-free and gnotobiotic experiments; A.V. collaborated in the writing and revision of the manuscript; K.C. contributed to tumour and anti-PD-1 blockade experiments; T.Hi. contributed expertise in behavioral studies; H.Q. contributed initial observations of mouse behavior; R.S. performed brain-region dissection; K.Su. contributed to OT-I and OT-II *in vivo* experiments; T.F. Y.I., F.M., M.S. and T.Ho. contributed expertise in metabolome

and behavioral studies and conceptual design; and S.F. conceived of the conceptual design, analyzed the results and wrote the manuscript.

COMPETING FINANCIAL INTERESTS

The authors declare no competing financial interests.

Reprints and permissions information is available online at <http://www.nature.com/reprints/index.html>. Publisher’s note: Springer Nature remains neutral with regard to jurisdictional claims in published maps and institutional affiliations.

- O'Neill, L.A., Kishton, R.J. & Rathmell, J. A guide to immunometabolism for immunologists. *Nat. Rev. Immunol.* **16**, 553–565 (2016).
- Loftus, R.M. & Finlay, D.K. Immunometabolism: cellular metabolism turns immune regulator. *J. Biol. Chem.* **291**, 1–10 (2016).
- Okazaki, T., Chikuma, S., Iwai, Y., Fagarasan, S. & Honjo, T. A rheostat for immune responses: the unique properties of PD-1 and their advantages for clinical application. *Nat. Immunol.* **14**, 1212–1218 (2013).
- Good-Jacobson, K.L. *et al.* PD-1 regulates germinal center B cell survival and the formation and affinity of long-lived plasma cells. *Nat. Immunol.* **11**, 535–542 (2010).
- Kawamoto, S. *et al.* The inhibitory receptor PD-1 regulates IgA selection and bacterial composition in the gut. *Science* **336**, 485–489 (2012).
- Agata, Y. *et al.* Expression of the PD-1 antigen on the surface of stimulated mouse T and B lymphocytes. *Int. Immunol.* **8**, 765–772 (1996).
- Taylor, S. *et al.* PD-1 regulates KLRL1⁺ group 2 innate lymphoid cells. *J. Exp. Med.* **214**, 1663–1678 (2017).
- Hyde, R., Taylor, P.M. & Hundal, H.S. Amino acid transporters: roles in amino acid sensing and signalling in animal cells. *Biochem. J.* **373**, 1–18 (2003).
- Sinclair, L.V. *et al.* Control of amino-acid transport by antigen receptors coordinates the metabolic reprogramming essential for T cell differentiation. *Nat. Immunol.* **14**, 500–508 (2013).
- Iwai, Y., Terawaki, S. & Honjo, T. PD-1 blockade inhibits hematogenous spread of poorly immunogenic tumor cells by enhanced recruitment of effector T cells. *Int. Immunol.* **17**, 133–144 (2005).
- Hayaishi, O., Rothberg, S., Mehler, A.H. & Saito, Y. Studies on oxygenases: enzymatic formation of kynurenone from tryptophan. *J. Biol. Chem.* **229**, 889–896 (1957).
- Takikawa, O., Habara-Ohkubo, A. & Yoshida, R. Induction of indoleamine 2,3-dioxygenase in tumor cells transplanted into allogeneic mouse: interferon-γ is the inducer. *Adv. Exp. Med. Biol.* **294**, 437–444 (1991).
- Wikoff, W.R. *et al.* Metabolomics analysis reveals large effects of gut microflora on mammalian blood metabolites. *Proc. Natl. Acad. Sci. USA* **106**, 3698–3703 (2009).
- Yano, J.M. *et al.* Indigenous bacteria from the gut microbiota regulate host serotonin biosynthesis. *Cell* **161**, 264–276 (2015).
- Palmiter, R.D. Dopamine signaling in the dorsal striatum is essential for motivated behaviors: lessons from dopamine-deficient mice. *Ann. NY Acad. Sci.* **1129**, 35–46 (2008).
- Darvas, M., Wunsch, A.M., Gibbs, J.T. & Palmiter, R.D. Dopamine dependency for acquisition and performance of Pavlovian conditioned response. *Proc. Natl. Acad. Sci. USA* **111**, 2764–2769 (2014).
- Mosienko, V. *et al.* Exaggerated aggression and decreased anxiety in mice deficient in brain serotonin. *Transl. Psychiatry* **2**, e122 (2012).
- Bauer, E.P. Serotonin in fear conditioning processes. *Behav. Brain Res.* **277**, 68–77 (2015).
- Santos, J.M., Martinez, R.C. & Brandão, M.L. Effects of acute and subchronic treatments with fluoxetine and desipramine on the memory of fear in moderate and high-intensity contextual conditioning. *Eur. J. Pharmacol.* **542**, 121–128 (2006).
- Maki, Y. *et al.* Monoamine oxidase inhibitors reduce conditioned fear stress-induced freezing behavior in rats. *Eur. J. Pharmacol.* **406**, 411–418 (2000).
- Anthony, J. & Trevor, B.G.K. Marieke Kruizinga-Hall. Antidepressants. in *Katzung & Trevor's Pharmacology: Examination & Board Review*, 11e. Ch 30 (McGraw-Hill Education, 2015).
- Carr, E.L. *et al.* Glutamine uptake and metabolism are coordinately regulated by ERK/MAPK during T lymphocyte activation. *J. Immunol.* **185**, 1037–1044 (2010).
- Chang, C.H. *et al.* Posttranscriptional control of T cell effector function by aerobic glycolysis. *Cell* **153**, 1239–1251 (2013).
- Patoukis, N. *et al.* PD-1 alters T-cell metabolic reprogramming by inhibiting glycolysis and promoting lipolysis and fatty acid oxidation. *Nat. Commun.* **6**, 6692 (2015).

ONLINE METHODS

Mice. *Pcd1*^{-/-} mice (C57BL/6N), described previously²⁵, were provided by RIKEN Bioresource Center through the National Bio-Resource Project of the MEXT Japan. Heterozygous breeding generated matched wild-type for experiments as needed. *Cd3e*^{-/-} mice and *Ifng*^{-/-} mice (C57BL/6J), described previously^{26,27}, were crossed with *Pcd1*^{-/-} mice. Mice were bred and maintained under specific-pathogen-free (SPF) conditions at IMS RIKEN and in an SPF facility at Kyoto University Graduate School of Medicine. C57BL/6N wild-type mice were purchased from CLEA Japan. *Pcd1*^{-/-} mice and wild-type mice in germ-free (GF) and gnotobiotic conditions were generated and maintained in vinyl isolators at IMS RIKEN. For gnotobiotic experiments, 4-week-old GF wild-type or *Pcd1*^{-/-} mice received a suspension of feces pooled from three wild-type or *Pcd1*^{-/-} mice, administrated orally. Littermates or appropriate age- and sex-matched mice were randomly grouped and used for analyses. For behavioral testing, only male mice were used. All animal experiments were performed in accordance with approved protocols from the Institutional Animal Care at RIKEN and Kyoto University Graduate School of Medicine.

Measurement of metabolic parameters. Energy expenditure and oxygen consumption were measured with a metabolic chamber system, consisting of acrylic metabolic chambers, mass spectrometer (ARCO2000, ARCO SYSTEM) and gas sampler (ARCO2000-GS, ARCO SYSTEM). Animal movements were monitored by an animal movement analyzing system (ACTIMO-100M, SHINFACTORY). Energy expenditure was calculated according to the Lusk formula: $3.815 \times VO_2 + 1.232 \times VCO_2$. VO_2 is the oxygen consumption and VCO_2 is the carbon dioxide exhaustion. Mice were monitored under a normal 12h–12h light–dark cycle for 6 d. Mice were not subjected to acclimation before experiments.

Sample preparation for Serum metabolome. 50 µl of serum was mixed with 250 µl of solvent (methanol: water:chloroform = 2.5:1:1) containing 6 µl of 0.1 mg/ml 2-isopropylmalic acid (Sigma-Aldrich), which was used as an internal standard. The mixture was shaken at 1,200 r.p.m. for 30 min at 37 °C (Maximizer MBR-022UP, Taitec). After centrifugation at 16,000g for 5 min at 25 °C, 150 µl of supernatant was collected and mixed with 140 µl of purified water by a vortex mixer for 5 s. After centrifugation at 16,000g for 5 min at 25 °C, 180 µl and 50 µl of supernatant were collected for GC-MS and LC-MS analysis, respectively, and were then lyophilized. For GC-MS analysis, the lyophilized sample was dissolved in 80 µl of methoxyamine solution (20 mg/ml in pyridine, Sigma-Aldrich) and was shaken at 1,200 r.p.m. for 30 min at 37 °C. 40 µl of N-methyl-N-trimethylsilyl trifluoroacetamide solution (GL Science) were added for trimethylsilyl derivatization, followed by agitation at 1,200 r.p.m. for 30 min at 37 °C. After centrifugation, 50 µl of supernatant was transferred to a glass vial and subjected to GC-MS measurement. For LC-MS analysis, lyophilized sample was dissolved in 30 µl of 0.1% formic acid in water and 5 µl aliquot was injected into the LCMS-8060 (Shimadzu).

GC-MS analysis for serum metabolome. GC-MS analysis was conducted with a GCMS-QP2010 Ultra (Shimadzu). The derivatized metabolites were separated on a DB-5 column (30 m × 0.25 mm id; film thickness ,1.0 mm; Agilent Technologies). The helium carrier gas was set at the flow rate of 39 cm/s. The inlet temperature was 280 °C and the column temperature was first held at 80 °C for 2 min, then raised at a rate of 15 °C/min to 330 °C, and held for 6 min. 1 µl of the sample was injected into the GC-MS in the split mode (split ratio, 1:3). The mass spectra were obtained under following conditions: electron ionization (ionization voltage, 70 eV); ion source temperature, 200 °C; interface temperature, 250 °C; full scan mode in the range of m/z 85–500; scan rate, 0.3 s/scan. Metabolite peaks were manually identified based on retention time and mass spectrum matching with a GC/MS Metabolite Mass Spectral Database (Shimadzu). For semiquantitative analysis, the area of each metabolite peak was calculated and divided by the area of the internal standard peak. Principal component analysis, PLS-DA and metabolite set enrichment analysis were performed using MetaboAnalyst3.0 (available online at: <http://www.metaboanalyst.ca>)²⁸.

LC-MS analysis for serum metabolome. LC separation was conducted on a Shodex RSpak DE-213 column (150 mm × 2.0 mm id, Showa Denko) with a Nexera UHPLC system (Shimadzu). The mobile phase consisted of 0.1% formic acid in water (A) and 0.1% formic acid in acetonitrile (B). The gradient

program was as follows: 0–3 min, 0% B; 3–15 min, linear gradient to 60% B; 15–20 min, 95% B; 20–22.5 min, linear gradient to 0% B; hold for 7.5 min; flow rate, 0.2 ml/min. The column oven temperature was maintained at 40 °C. The LC system was coupled with a triple-quadrupole mass spectrometer LCMS-8060 (Shimadzu). LCMS-8060 was operated with the ESI in positive ion and multiple reaction monitoring (MRM) mode with the following ion transitions: kynurenine, *m/z* 208.90>192.05; kynurenic acid, *m/z* 190.10>144.00; 3-hydroxy-kynurene, *m/z* 225.10>208.20.

Brain metabolome. Brain tissue is sensitive to post-mortem changes in labile metabolites such as adenylates. To minimize autolytic changes, we employed focused microwave irradiation, which suspends metabolic processes by rapidly raising the tissue temperature to inactivate the enzymes within seconds. We used a laboratory microwave instrument (MMW-05 Muromachi-Kikai) designed for euthanasia of laboratory rodents. Mice were placed into a transparent water-jacket holder (MH28- HZ, Muromachi-Kikai). Microwave irradiation at 5 kW for 0.96 s elevates the temperature of the brain up to 80 °C, which is sufficient to inactivate metabolic enzymes, such as acetylcholine esterase²⁹. After microwave irradiation, brains were dissected with a surgical knife at room temperature, and cut into right and left hemisphere blocks for imaging MS and metabolome analyses, respectively. Brain blocks for imaging MS were embedded into a super cryo-embedding medium (SCEM, Section Lab Co.), and both tissue blocks were rapidly frozen in liquid nitrogen and stored at –80 °C.

Sample preparation for brain metabolome analysis. Extraction of metabolites from brain for metabolomics was performed as described previously³⁰. In brief, the frozen tissue block, together with internal control compounds (described below), was homogenized in ice-cold methanol (500 µl) using a manual homogenizer (Finger Masher (AM79330), Sarstedt), followed by the addition of an equal volume of chloroform and 0.4 times the volume of ultrapure water (LC/MS grade, Wako). The suspension was then centrifuged at 15,000g for 15 min at 4 °C. After centrifugation, the aqueous phase was filtered using an ultrafiltration tube (Ultrafree-MC, UFC3 LCC NB, Human Metabolome Technologies). The filtrate was concentrated with a vacuum concentrator (SpeedVac, Thermo). The concentrated filtrate was dissolved in 50 µl of ultrapure water and was analyzed by LC-MS/MS and HPLC-ECD.

Quantification of metabolites by internal and external standards. We used both internal standard compounds (added to the tissue before extraction) and external standard compounds (used to produce calibration curves for each compound) for concentration calculation. The details of the methods are provided below.

Internal standard compounds. We used 2-morpholino ethanesulfonic acid (MES) and 1,3,5-benzenetricarboxylic acid (trimesate) as internal standards for anionic metabolites, as these compounds have no endogenous equivalent in tissues. Loss of endogenous metabolites during sample preparation was corrected for by calculation of the recovery rate (%) for each sample measurement.

External standard compounds. An external calibration curve was used to calculate the absolute abundance of metabolites. Before sample measurement, we measured the mixture of authentic compounds of target metabolites at three different concentrations in ultrapure water to generate calibration curves. Quantification (amount of metabolites, nmol/mg tissue) was performed by comparison of the internal-standard-normalized peak areas against the calibration curves.

Liquid chromatography-tandem mass spectrometry for amino acid measurement. The amount of amino acids in the brain was quantified using liquid chromatography-tandem mass spectrometry. In brief, a triple-quadrupole mass spectrometer equipped with an electrospray ionization (ESI) ion source (LCMS-8040, Shimadzu) was used in the positive- and negative-ESI and multiple-reaction-monitoring (MRM) modes. The samples were resolved on the Discovery HS F5-3 column (2.1 mmI.D. x 150 mmL, 3µm particle, Sigma-Aldrich), using a step gradient with mobile phase A (0.1% formate) and mobile phase B (0.1% acetonitrile) at ratios of 100:0 (0–5 min), 75:25 (5–11 min), 65:35 (11–15 min), 5:95 (15–20 min) and 100:0 (20–25 min), at a flow rate of 0.25 ml/min and a column temperature of 40 °C. The LCMS-8040

was operated with the ESI in MRM mode with the previously reported conditions for amino-acid detection³¹.

Ion chromatography-tandem mass spectrometry for anionic metabolites.

For metabolome analysis focused on glucose metabolic central pathways (glycolysis and the TCA cycle), the anionic metabolites were measured using an orbitrap-type MS (Q-Exactive Focus, Thermo Fisher Scientific) connected to a high-performance ion-chromatography (IC) system (ICS-5000+, Thermo Fisher Scientific) that enables highly selective and sensitive metabolite quantification owing to the IC-separation and Fourier Transfer MS principle³². The IC was equipped with an anion electrolytic suppressor (Thermo Scientific Dionex AERS 500) to convert the potassium hydroxide gradient into pure water before the sample entered the mass spectrometer. The separation was performed using a Thermo Scientific Dionex IonPac AS11-HC, 4-μm-particle-size column. The IC flow rate was 0.25 ml/min supplemented post-column with 0.18 ml/min makeup flow of MeOH. The potassium hydroxide gradient conditions for IC separation were as follows: from 1 mM to 100 mM (0–40 min), 100 mM (40–50 min), and 1 mM (50.1–60 min), at a column temperature of 30 °C. The Q-Exactive Focus mass spectrometer was operated under an ESI negative mode for all detections. Full mass scan (*m/z* 70–900) was used at a resolution of 70,000. The automatic gain control target was set at 3×10^6 ions, and maximum ion injection time was 100 ms. Source ionization parameters were optimized with the spray voltage at 3 kV, and other parameters were as follows: transfer temperature at 320 °C, S-Lens level at 50, heater temperature at 300 °C, sheath gas at 36, and auxiliary gas at 10.

Measurement of dopamine, 5-HT and related metabolites by HPLC with an electrochemical detector (ECD). Metabolites extracted by the protocol described above were injected with an autosampler (M-510, Eicom) into an HPLC unit (Eicom) coupled to an ECD (ECD-300, Eicom). The samples were resolved on the Eicompak SC-5ODS column (φ3.0 × 150 mm, Eicom), using an isocratic mobile phase (5 mg/l EDTA-2Na, 220 mg/l sodium 1-octanesulfonate in acetate/citrate buffer (0.1 M, pH 3.5)/MeOH (83:17, v/v)), at a flow rate of 0.5 ml/min and a column temperature of 25 °C. At the ECD, analytes were subjected to oxidation reactions within the ECD unit with WE-3G graphite electrode (applied potential, +750 mV against an Ag/AgCl reference electrode). The resulting chromatograms were analyzed using the software EPC-300 (Eicom).

Non-targeted metabolome analysis of the liver, lymph nodes, small intestine and colon. For non-targeted analysis, metabolome data obtained by orbitrap-type MS (Q-Exactive focus, Thermo Fisher Scientific, San Jose, CA) connected to a HPLC (Ultimate3000 system, Thermo Fisher Scientific) with the discovery HS F5-3 column or an IC (ICS-5000+, Thermo Fisher Scientific) with the IonPac AS11-HC, 4-μm particle size column were analyzed. A Compound Discoverer 2.0 (Thermo Fisher Scientific) was used for the non-targeted metabolomics workflow as described³³. In brief, this software first aligned the total ion chromatograms of different samples along the retention time. Then, the detected features with an intensity of no less than 100,000 and an S/N larger than 5 in each set of data were extracted and merged into components. The resulting compounds were identified by both (i) formula prediction based on accurate *m/z* value and isotope peak patterns and (ii) MS/MS structural validation. Moreover, formula predicted signals were assigned into candidate compounds by database search (Chempider database; <http://www.chemspider.com/>). The PCA analysis as well as volcano-plotting based on a T-test were performed and are presented.

Preparation of tissue sections for MALDI-imaging analysis. Thin sections were cut with a cryomicrotome (CM3050, Leica Microsystems) and were thaw-mounted on an indium thin oxide-coated glass slide (Bruker Daltonics) at -16 °C. Brain tissues subjected to focused microwave tended to be more fragile than those treated by other methods; however, embedding the tissue with SCEM medium, which did not interfere with the ionization efficiency of metabolites, aided in successful sectioning^{30,34}.

Matrix coating and MALDI-MS Imaging acquisition. We employed on-tissue derivatization of brain neurotransmitters³⁵. Tissue sections were spray-coated manually with 2,4-diphenyl-pyranylum (1.5 mg/ml in 75% MeOH and 0.1% TFA) using an artistic airbrush (Procon Boy FWA Platinum 0.2-mm caliber

airbrush, Mr. Hobby), followed by DHB as a matrix (50 mg/ml, dissolved in 80% ethanol containing saturated ammonium sulfate (AS)). The addition of AS diminished the ion suppression effect of analytes caused by excess derivatization reagent³⁶. MALDI-IMS was performed using a 7T FT-ICR-MS (Solarix Bruker Daltonik) equipped with an Nd:YAG laser. The laser power was optimized to minimize in-source decay of metabolites. Data were acquired in the positive mode with raster scanning using a pitch distance of 80 μm. Each mass spectrum was the result of 300 laser shots at each data point. Signals with an *m/z* between 300 and 500 were collected by use of continuous accumulation of selected ions mode. Image reconstruction was performed using FlexImaging 4.0 software (Bruker Daltonics). Peaks of specific metabolite molecules were assigned by accurate MS analyses. The high mass accuracy provided by FT-ICR-MS allowed selective ion signals for derivatized-monoamine species to be obtained within a mass window of 5 ppm, which enabled identification of the specific elemental composition of compounds by querying of the highly accurate masses against databases³⁷.

In vivo microdialysis. *In vivo* microdialysis for freely moving mice was performed as described elsewhere³⁸. In brief, mice were anesthetized with isoflurane and were implanted stereotactically with a guide cannula (one site per mouse) in the prefrontal cortex (for dialysis probe, A+2 mm, L-0.5 mm, V-0.5 mm, from the bregma and skull) immobilized with dental acrylic. A 2-mm active probe membrane (A-1-4-02, Eicom, Kyoto, Japan) was used. After surgery, the mice were housed individually for at least 1 week before experiments. Approximately 3 h after the start of perfusion, the dialysates were collected using a fraction collector (EFC-82, Eicom). Ringer solution (147 mM Na⁺, 4 mM K⁺, 2.3 mM Ca²⁺ and 155.6 mM Cl⁻) was perfused by use of a micro-infusion pump ESP-32 (Eicom) with gas-tight syringes at rates of 1 μl/min. For the high-potassium challenge, high-potassium Ringer solution (51 mM Na⁺, 100 mM K⁺, 2.3 mM Ca²⁺ and 155.6 mM Cl⁻) was perfused at the same rate. The collected dialysates were injected into the HPLC system for 5-HT quantification as described above.

Antibodies and flow cytometry. The following antibodies were purchased from BD Bioscience: anti-CD8α (1: 100 dilution; clone 53-6.7, #557654), anti-IFN-α (1: 100 dilution; clone XMG1.2, #554412), anti-TCRβ (1: 50 dilution; clone H57-597, #553174) and anti-TCRβ (1: 50 dilution; clone H57-597, #560706). The following antibodies were purchased from eBioscience: anti-CD4 (1: 100 dilution; clone RM4-5, #47-0042-82), anti-CD44 (1: 100 dilution; clone IM7, #12-0441-82), anti-CD62L (1: 3200 dilution; clone MEL-14, #13-0621-82), anti-CD98 (1: 50 dilution; clone RL388, #12-0981-81), anti-B220 (1: 100 dilution; clone RA3-6B2, #11-0452-82) and rat IgG2a-κ isotype control (1: 100 dilution; clone eBR2a, #12-4321-42). The following antibodies were purchased from Biolegend: anti-CD11c (1: 100 dilution; clone N418, #117311), anti-CD11b (1: 100 dilution; clone M1/70, #101219) anti-CD3 (1: 100 dilution; clone 145-2C11, #100321), anti-CD4 (1: 100 dilution; clone RM4-5, #25-0042), anti-CD62L (1: 100 dilution; clone MEL-14, #104426) and CD44 (IM7, #103026). Streptavidin Pacific Blue (1: 200 dilution; #S11222) was purchased from Invitrogen. To measure cytokine production by T cells, spleens were dissected and then single-cell suspensions were maintained in DMEM(H) (KOHJIN BIO) plus 10% FCS and stimulated with PMA plus ionomycin (Sigma) and GolgiStop (BD Bioscience) at 37 °C for 3.5 h before surface and intracellular staining using cytofix/cytoperm (BD Bioscience). Flow cytometry was performed using a BD FACSAria II (BD Bioscience).

Immunofluorescence. For brain immunofluorescence, mice were intracardially perfused with 5 mM EDTA solution in phosphate-buffered saline (PBS) and then with 2% PFA solution in PBS (PBS 2% PFA). The brain was immediately isolated and cut into six regions using an Alto brain matrix (CellPoint Scientific). The sections were post-fixed for 6 h in PBS 2% PFA at 4 °C and were soaked in 30% sucrose in PBS overnight at 4 °C. The sections were then embedded in Tissue-Tek OCT blocks (Sakura). 10-μm coronal sections were cut by cryostat (Leica CM3050S). The appropriate sections were selected on a morphological basis and were stained with the following antibodies: polyclonal goat anti-mouse 5-hydroxytryptamine (1:100 dilution; Immunostar, #20079) and monoclonal anti-mouse Tryptophan Hydroxylase (1:100 dilution clone WH3, which recognizes tryptophan hydroxylase 1 and tryptophan hydroxylase 2, Sigma-Aldrich,

#T0678). The sections were counterstained with DAPI (Sigma-Aldrich, #T0678) and mounted with the Fluoromount-G antifade reagent (Southern Biotech). Images were acquired with BZ-X700 fluorescence microscope (Keyence).

Real-time PCR. Total RNA was isolated from cells using the TRIzol Reagent (Invitrogen). After DNase I treatment (Invitrogen), random hexamers were used for first-strand cDNA synthesis. All procedures were performed according to the manufacturer's instructions (Invitrogen). Quantitative PCR was performed on a LightCycler 480 thermal cycler (Roche Life Science) using the Thunderbird SYBR Green qPCR mix (Toyobo) and analyzed by dedicated software (Roche Life Science). The primers were designed using BEACON DESIGNER software (Premier Biosoft International). All reactions were performed in duplicate. The relative expression of mRNA was normalized on the expression of *Gapdh* or *Actb*. Primers were as follows: *Tph2* forward, TTGACCCAAAGACGACCTGCTT, and reverse, CGAGAAGGGACGGTAATTGACT; *Th* forward, ACCTA TGCACTCACCGAGC, and reverse, AACTGGCAAATGTGCGGTC; *Gapdh* forward, TGTGTCGCTGCTGGATCTGA, and reverse, CCTGCTTCAC CACCTCTTGAT; *Slc7a5* (ref. 9) forward, CTGGATCGAGCTGCTCATC, and reverse, GTTCACAGCTGTGAGGAGC; *Slc3a2* forward, GTTTTTGAATGC CACTGGCA, and reverse, AAAGTCTGCGAGGAGTCCTG; and *Actb* forward, CACCCTGTGCTGCTCACCGA, and reverse, AGTGTGGGT GACCCCGTCTCC.

Behavioral tests. All behavioral testing procedures were approved by the Institutional Animal Care at RIKEN and Kyoto University Graduate School of Medicine and were performed according to manual of Medical Research Support Center, Graduate School of Medicine, Kyoto University.

Elevated-plus maze test. The elevated-plus maze test was conducted as previously described³⁷. The maze (O'Hara&Co.) consists of two open arms (25 cm × 5 cm) and two closed arms of the same size, with transparent walls (15 cm). The arms and center square (5 cm × 5 cm) are made of white plastic plates elevated to a height of 55 cm above the floor. 3-mm-high plastic ledges decrease open arm falls. Individual mice were placed in the center square facing a closed arm, and data were recorded for 10 min.

Open field test. Individual mice were placed in the corner of an enclosed platform (40 cm × 40 cm × 30 cm; Accuscan Instruments). The total distance traveled, movement duration and time spent in the center area (20 cm × 20 cm) were recorded for 10 min. Results obtained from replicate experiments performed in different mouse facilities were the same.

Dark-light transition test. The dark–light transition test was conducted as previously described⁴⁰ using a cage with two sections (of equal size) divided by a partition containing a door (O'Hara&Co.). One 'light chamber' section was brightly illuminated at 390 lux, while the 'dark chamber' emitted 2 lux. Individual mice were placed into the 'dark chamber', and data were recorded as each mouse was allowed to move freely between the two chambers with the door open for 10 min.

Forced-swim test. Individual mice were placed in a Plexiglas cylinders 20 cm high and 10 cm wide filled with water (23 °C), and sessions were recorded for 10 min. Total distance traveled and percentage immobility (time spent without swimming) were measured from the third minute to the sixth minute.

Social-interaction test. The social interaction test was conducted as previously described⁴¹. Two mice of the same genotype but different home cages were placed into a box together. Data were recorded as mice interacted freely for 10 min.

Hot-plate test. The hot-plate test was used to evaluate pain sensitivity. Individual mice were placed on a hot plate at 55.0 ± 0.3 °C (Columbus Instruments), and latency to the first hind-paw response (foot shake or paw lick) was measured.

Y-maze test. The Y-maze consisted of three arms (A, B and C) made of matte gray plastic joined in the middle to form a Y shape (O'Hara&Co,

30 mm × 400 mm × 120 mm). Individual mice were placed into one of the arm of the maze (start arm, A) and were allowed to explore freely in the three arms of the maze for 5 min. Spontaneous alternation rate was calculated using following formula: (number of successive three times for entry into different arm) / (total entry number – 1) × 100.

Contextual and cued fear conditioning test. The contextual and cued fear-conditioning test was conducted as previously described⁴². Individual mice were placed in a test chamber (26 cm × 34 cm × 29 cm) inside a sound-attenuated square chamber (O'Hara&Co.) and received three pairings of conditioned stimulus (CS) and unconditioned stimulus (US) for fear conditioning. 30 s of white noise at 55 dB served as the CS. CS terminated together with a foot shock (2 s and 0.35 mA), which served as the US (interstimulus interval, 1.5 min). For the contextual test, at 24 h after conditioning, each mouse was again placed in the same chamber without CS and US for 5 min. 1–2 h later, the cued test was performed using a triangular chamber (35 cm × 35 cm × 40 cm), which was located in a different room. In cued testing, each mouse was habituated to the chamber over a period of 180 s before presentation with continued CS (180 s).

Fear-extinction test. The fear-extinction test procedure was as previously described⁴³ with slight modifications. On conditioning day 1, each mouse was placed in a square conditioning chamber as in contextual and cued fear-conditioning test above. After 2 min of acclimation, fear conditioning was delivered by three pairings of CS (white noise at 55 dB) and US (foot shock for 2 s at 0.35 mA). CS was presented for 30 s and was terminated together with a foot shock with an interstimulus interval of 30 s. On days 2–5 of extinction sessions, mice were trained to fear extinction in the triangular chamber used for cued test by presentation, five times, of CS with an interstimulus interval of 30 s. After the final CS-US, behavior was recorded for 1 min. Fear-extinction indices were calculated with the following formula: freezing percentage = (CS1 + CS2 at day 2) – (CS4 + CS5 at day 5).

Behavioral-image analysis. The acquisition and analysis of behavioral data were performed automatically using Image software developed by T. Miyakawa (O'Hara&Co.) based on the NIH Image program (NIH, Bethesda, MD, available at <http://rsb.info.nih.gov/nih-image/>) and ImageJ (Imagejdev.Org, available at <http://imagejdev.org/>).

Drugs and diet. Fluoxetine and phenelzine (Sigma-Aldrich) were dissolved in 0.9% saline (Otsuka) and were administered at doses of 20 mg/kg (fluoxetine) or 40 mg/kg (phenelzine). Mice were given intraperitoneal injection of either saline or drugs in a volume of 10 ml/kg at 1 h (fluoxetine) or 4 h (phenelzine) before the contextual test or open-field test. High-tryptophan diet supplementation contained 2% L-tryptophan (w/w) (Funabashi Farm) provided *ad libitum* for 4 weeks before behavior testing.

In vivo T cell activation by tumor or exogenous antigen. Mouse MC38 colon cancer cells (5×10^5) were injected intradermally into the right flank (day 0). Mice were treated intraperitoneally with 100 µg of monoclonal antibody to PD-1 (clone 4H2, Bristol-Myers Squibb) on days 5, 8 and 11. Serum was harvested on day 13 for metabolite measurement by GC-MS. The experiments were performed in accordance with approved protocols from the Institute of Laboratory Animals, Graduate School of Medicine, Kyoto University. OT-I mice⁴⁴ and OT-II mice⁴⁵ were bred in SPF facility at Graduate School of Medicine, Kyoto University. Mice were treated intravenously with 200 µg OVA (Sigma) on day 0 and day 3, and serum was harvested on day 5 for metabolite measurement by GS-MS. For footpad immunization, wild-type mice were immunized with complete Freund's adjuvant and OVA (1:1) in the left footpad (20 µg/mouse), and serum from 7 d after immunization underwent metabolite measurement as above.

T cell purification and *in vitro* activation. For *ex vivo*-sorting of T cells, LNs (axillary, brachial and inguinal) were pooled and disrupted to form a single-cell suspension. CD44^{hi} T cells (CD11c[−], CD11b[−], B220[−], CD4⁺ or CD8⁺, and CD44^{hi}) or naive T cells (CD11c[−], CD11b[−], B220[−], CD4⁺ or CD8⁺, CD44^{lo}, CD62L⁺) T cells were sorted using a FACSaria II cell sorter (BD Bioscience),

with replacement of FACSFlow (BD Bioscience) with PBS to avoid metabolite contamination. 1×10^6 sorted cells were washed with PBS and were rapidly frozen in liquid nitrogen for metabolite analysis.

LN T cells purified using a MagniSort mouse T cell enrichment kit (Invitrogen) were cultured for 48 or 96 h at a density of 1×10^6 cells per ml in 96-well plates bound to anti-CD3e (2.5 µg/ml; 145-2C11; BD Pharmingen) in the presence of anti-CD28 (2 µg/ml; 37.51; BD Pharmingen) and IL-2 (20 ng/ml; R&D system)). RPMI-1640 medium (Wako) supplemented with 10% (v/v) FBS, 1× MEM non-essential amino acids, 10 mM HEPES, 50 µM 2-mercaptoethanol, 1 mM sodium pyruvate, 100 U/ml penicillin and 100 U/ml streptomycin was used for culture. For [^{13}C]Trp-uptake assays, the medium was supplemented with 12 µM L-tryptophan- ^{13}C (TAIYO NIPPON SANSO) or L-tryptophan- ^{12}C (Sigma).

Statistical analysis. PRISM (Graphpad) was used for statistical analysis. Analyses were conducted using the two-tailed unpaired Student's *t*-test or analysis of variance (ANOVA). No statistical methods were used to predetermine sample size.

A Life Science Reporting Summary for this paper is available.

Data availability. The data that support the findings of this study are available from the corresponding author upon reasonable request. Methods are available in the online version of the paper. All supplementary information and source data files are available in the online version of the paper.

25. Nishimura, H., Minato, N., Nakano, T. & Honjo, T. Immunological studies on PD-1 deficient mice: implication of PD-1 as a negative regulator for B cell responses. *Int. Immunol.* **10**, 1563–1572 (1998).
26. Malissen, M. *et al.* Altered T cell development in mice with a targeted mutation of the CD3-epsilon gene. *EMBO J.* **14**, 4641–4653 (1995).
27. Tagawa, Y., Sekikawa, K. & Iwakura, Y. Suppression of concanavalin A-induced hepatitis in IFN- $\gamma^{-/-}$ mice, but not in TNF- $\alpha^{-/-}$ mice: role for IFN- γ in activating apoptosis of hepatocytes. *J. Immunol.* **159**, 1418–1428 (1997).
28. Xia, J., Sinelnikov, I.V., Han, B. & Wishart, D.S. MetaboAnalyst 3.0—making metabolomics more meaningful. *Nucleic Acids Res.* **43**, W1, W251–W257 (2015).
29. Moroji, T., Takahashi, K., Ogura, K., Toishi, T. & Arai, S. Rapid microwave fixation of rat brain. *J. Microwave Power.* **12**, 273–286 (1977).
30. Sugiura, Y., Honda, K., Kajimura, M. & Suematsu, M. Visualization and quantification of cerebral metabolic fluxes of glucose in awake mice. *Proteomics* **14**, 829–838 (2014).
31. Oka, M. *et al.* Arl8b is required for lysosomal degradation of maternal proteins in the visceral yolk sac endoderm of mouse embryos. *J. Cell. Sci.* <http://dx.doi.org/10.1242/jcs.200519> (2017).
32. Hu, S. *et al.* Targeted metabolomic analysis of head and neck cancer cells using high performance ion chromatography coupled with a Q exactive HF mass spectrometer. *Anal. Chem.* **87**, 6371–6379 (2015).
33. Zhou, Z. Non-target impurity profiling of marketplace Cetirizine using high-resolution mass spectrometry and multivariate data analysis. *Rapid Commun. Mass Spectrom.* **30**, 1941–1950 (2016).
34. Morikawa, T. *et al.* Hypoxic regulation of the cerebral microcirculation is mediated by a carbon monoxide-sensitive hydrogen sulfide pathway. *Proc. Natl. Acad. Sci. USA* **109**, 1293–1298 (2012).
35. Sharifiatgorji, M. *et al.* Direct targeted quantitative molecular imaging of neurotransmitters in brain tissue sections. *Neuron* **84**, 697–707 (2014).
36. Sugiyama, E., Masaki, N., Matsushita, S. & Setou, M. Ammonium Sulfate Improves Detection of Hydrophilic Quaternary Ammonium Compounds through Decreased Ion Suppression in Matrix-Assisted Laser Desorption/Ionization Imaging Mass Spectrometry. *Anal. Chem.* **87**, 11176–11181 (2015).
37. Marshall, A.G., Hendrickson, C.L. & Jackson, G.S. Fourier transform ion cyclotron resonance mass spectrometry: a primer. *Mass Spectrom. Rev.* **17**, 1–35 (1998).
38. Benveniste, H. & Hansen, A.J. Practical aspects of using microdialysis for determination of brain interstitial concentrations. In: Robinson, T.E., Jr., J.B.J. & Huston, J.P. (eds). *Microdialysis in the neurosciences*. Elsevier: New York, USA, 1991, pp 81–97.
39. Komada, M., Takao, K. & Miyakawa, T. Elevated plus maze for mice. *J. Vis. Exp.* **22**, e1088 (2008).
40. Takao, K. & Miyakawa, T. Light/dark transition test for mice. *J. Vis. Exp.* **1**, e104 (2006).
41. Miyakawa, T. *et al.* Conditional calcineurin knockout mice exhibit multiple abnormal behaviors related to schizophrenia. *Proc. Natl. Acad. Sci. USA* **100**, 8987–8992 (2003).
42. Koshimizu, H. *et al.* Adenomatous polyposis coli heterozygous knockout mice display hypoactivity and age-dependent working memory deficits. *Front. Behav. Neurosci.* **5**, 85 (2011).
43. Pattwell, S.S. *et al.* Altered fear learning across development in both mouse and human. *Proc. Natl. Acad. Sci. USA* **109**, 16318–16323 (2012).
44. Hogquist, K.A. *et al.* T cell receptor antagonist peptides induce positive selection. *Cell* **76**, 17–27 (1994).
45. Barnden, M.J., Allison, J., Heath, W.R. & Carbone, F.R. Defective TCR expression in transgenic mice constructed using cDNA-based alpha- and beta-chain genes under the control of heterologous regulatory elements. *Immunol. Cell Biol.* **76**, 34–40 (1998).

Life Sciences Reporting Summary

Corresponding author(s): Sidonia Fagarasan

 Initial submission Revised version Final submission

Nature Research wishes to improve the reproducibility of the work that we publish. This form is intended for publication with all accepted life science papers and provides structure for consistency and transparency in reporting. Every life science submission will use this form; some list items might not apply to an individual manuscript, but all fields must be completed for clarity.

For further information on the points included in this form, see [Reporting Life Sciences Research](#). For further information on Nature Research policies, including our [data availability policy](#), see [Authors & Referees](#) and the [Editorial Policy Checklist](#).

► Experimental design

1. Sample size

Describe how sample size was determined.

No sample size calculation was performed. For statistic analyses more than 3 samples were used and the number of samples were indicated in the figure legends.

2. Data exclusions

Describe any data exclusions.

Infrequently, mice showed signs of inflammation even in normal SPF condition. Therefore, when sacrificed, mice were routinely checked for the inflammation status and samples from mice showing severe inflammation status (splenomegaly and colitis) were excluded. And, Pdcd1^{-/-} mice generally spent less time in the center of the field than wild-type mice, but some froze there for extended periods. When animals displaying this confounding behaviour were excluded (Fig. 7b and Supplementary Fig. 6a).

3. Replication

Describe whether the experimental findings were reliably reproduced.

For each experiment, all attempts at replication were successful.

4. Randomization

Describe how samples/organisms/participants were allocated into experimental groups.

Samples were randomly allocated into experimental groups.

5. Blinding

Describe whether the investigators were blinded to group allocation during data collection and/or analysis.

We were not blinded to group allocation during data collection and analysis.

Note: all studies involving animals and/or human research participants must disclose whether blinding and randomization were used.

6. Statistical parameters

For all figures and tables that use statistical methods, confirm that the following items are present in relevant figure legends (or in the Methods section if additional space is needed).

n/a Confirmed

- The exact sample size (n) for each experimental group/condition, given as a discrete number and unit of measurement (animals, litters, cultures, etc.)
- A description of how samples were collected, noting whether measurements were taken from distinct samples or whether the same sample was measured repeatedly
- A statement indicating how many times each experiment was replicated
- The statistical test(s) used and whether they are one- or two-sided (note: only common tests should be described solely by name; more complex techniques should be described in the Methods section)
- A description of any assumptions or corrections, such as an adjustment for multiple comparisons
- The test results (e.g. P values) given as exact values whenever possible and with confidence intervals noted
- A clear description of statistics including central tendency (e.g. median, mean) and variation (e.g. standard deviation, interquartile range)
- Clearly defined error bars

See the web collection on [statistics for biologists](#) for further resources and guidance.

Software

Policy information about [availability of computer code](#)

7. Software

Describe the software used to analyze the data in this study.

Flowjo software were used for FACS analysis. BZ-X analyzer software was used for analysis of photomicrograph. Compound Discoverer 2.0 software was used for non-target analysis of mass spectrometry data. FlexImaging 4.0 software was used for Imaging mass spectrometry. MetaboAnalyst was used for analysis of metabolome data. PRISM software was used for statistical analysis.

For manuscripts utilizing custom algorithms or software that are central to the paper but not yet described in the published literature, software must be made available to editors and reviewers upon request. We strongly encourage code deposition in a community repository (e.g. GitHub). [Nature Methods guidance for providing algorithms and software for publication](#) provides further information on this topic.

Materials and reagents

Policy information about [availability of materials](#)

8. Materials availability

Indicate whether there are restrictions on availability of unique materials or if these materials are only available for distribution by a for-profit company.

No unique materials were used.

9. Antibodies

Describe the antibodies used and how they were validated for use in the system under study (i.e. assay and species).

Data was provided in the manuscript.

10. Eukaryotic cell lines

a. State the source of each eukaryotic cell line used.

No eukaryotic cell lines were used.

b. Describe the method of cell line authentication used.

No eukaryotic cell lines were used.

c. Report whether the cell lines were tested for mycoplasma contamination.

No eukaryotic cell lines were used.

d. If any of the cell lines used are listed in the database of commonly misidentified cell lines maintained by [ICLAC](#), provide a scientific rationale for their use.

No commonly misidentified cell lines were used.

► Animals and human research participants

Policy information about [studies involving animals](#); when reporting animal research, follow the [ARRIVE guidelines](#)

11. Description of research animals

Provide details on animals and/or animal-derived materials used in the study.

WT (C57BL/6N), PD-1-/- (C57BL/6N), PD-1-/- IFNg-/- (C57BL/6), PD-1-/- CD3-/- (C57BL/6), CD3-/- (C57BL/6), OT-I (C57BL/6J) and OT-II (C57BL/6J) mice were used in this study. Both male and female mice were used. 2 Mo-12 Mo old mice were used in this study.

Policy information about [studies involving human research participants](#)

12. Description of human research participants

Describe the covariate-relevant population characteristics of the human research participants.

This study did not involve human research participants.

Flow Cytometry Reporting Summary

Form fields will expand as needed. Please do not leave fields blank.

► Data presentation

For all flow cytometry data, confirm that:

1. The axis labels state the marker and fluorochrome used (e.g. CD4-FITC).
2. The axis scales are clearly visible. Include numbers along axes only for bottom left plot of group (a 'group' is an analysis of identical markers).
3. All plots are contour plots with outliers or pseudocolor plots.
4. A numerical value for number of cells or percentage (with statistics) is provided.

Methodological details

5. Describe the sample preparation.

The cells were collected from spleen, lymph nodes, small intestine or colon. Spleen and lymph nodes were mechanically smashed and filtered with strainer and used for flow cytometry. Small intestine and colon were prepared by classical EDTA-treatment followed by collagenase digestion, filtration of cells, staining and flow cytometry.

6. Identify the instrument used for data collection.

FACSAria II cell sorter (BD Bioscience) was used for data collection.

7. Describe the software used to collect and analyze the flow cytometry data.

FlowJo software was used for analysis.

8. Describe the abundance of the relevant cell populations within post-sort fractions.

The purity of the samples was not determined.

9. Describe the gating strategy used.

Gating strategies are provided in the manuscript.

Tick this box to confirm that a figure exemplifying the gating strategy is provided in the Supplementary Information.